ABSTRACT

Inhibitors of Tubulin, Nitric Oxide Synthase, and HIF-1 Alpha; Synthesis, Biological, and Biochemical Evaluation

John J. Hall, Ph.D.

Mentors: Kevin G. Pinney, Ph.D.; Mary Lynn Trawick, Ph.D.

Vascular disruption is an innovative method for treating cancer. By selectively altering the endothelial cells of tumor vasculature, the tumor can be destroyed by oxygen deprivation and starvation. The combretastatin (CA) family of small molecules has shown great effectiveness as vascular disrupting agents (VDAs). Structure activity relationship (SAR) studies were continued for the combretastatin family by placement of a 3,4,5-trifluoro substituted A-ring, and 2- or 3-nitro/amine substitutions on the B-ring. Indole scaffolds that are similar to the CA analogues and Oxi8006 were also prepared. The VDAs were tested for cancer cytotoxicity and their ability to inhibit tubulin polymerization. The 3′-amino stilbene **15** was the most effective of the fluoro-nitro stilbenes synthesized, having a tubulin IC_{50} of 2.9 μM, and a cell cytotoxicity of 0.0093 μg/mL against NCI H460 lung cancer carcinoma.

Though VDAs have been effective against a variety of tumor cells, there are cancers, such as human oral squamous cell (SaS), that are resistant to combretastatin A4 phosphate (CA4P). It is believed the SaS resistance results from an increase in nitric

oxide (NO) production, which can increase tumor blood supply and vascular tone. CA4P co-salts with the nitric oxide synthase (NOS) inhibitors L-NMMA and L-NAME have been shown to increase drug sensitivity. As such, L-NMMA and L-NAME co-salt formulations with Oxi8007 were prepared to increase drug sensitivity

CA4 and CA1 were coupled with aromatic bioreductive triggers to increase drug response in hypoxic areas that are resistant to chemotherapeutics. These nitro-aromatic triggers are expected to only release upon reduction within the hypoxic environment, and increase drug specificity to these areas.

The transcription factor HIF-1α has been labeled as a primary target in treating the hypoxic areas of tumors. Drugs that are effective at inhibiting HIF-1α may be better suited for treating hypoxic tumor cells. Approximately 20 compounds were analyzed for their ability to inhibit HIF-1α preservation. Benzosuberene **96** and benzophenone **37** were the most effective at inhibiting HIF-1α preservation. The tubulin IC_{50} activity of compound **96** is > 40 μM, suggesting that it is inhibiting HIF-1α preservation by a means other than microtubule disruption.

Inhibitors of Tubulin, Nitric Oxide Synthase, and HIF-1 Alpha; Synthesis, Biological, and Biochemical Evaluation

by

John J. Hall, B.S.

A Dissertation
Approved by the Department of Chemistry and Biochemistry

_____

David E. Pennington, Ph.D., Interim Chairperson

Submitted to the Graduate Faculty of
Baylor University in Partial Fulfillment of the
Requirements for the Degree
of

Doctor of Philosophy

Approved by the Dissertation Committee

_____

Kevin G. Pinney, Ph.D., Chairperson

_____

Mary Lynn Trawick, Ph.D., Chairperson

_____

Robert R. Kane, Ph.D.

_____

Charles M. Garner, Ph.D.

_____

Carlos E. Manzanares, Ph.D.

_____

Erich J. Baker, Ph.D.

Accepted by the Graduate School
May 2008

_____

J. Larry Lyon, Ph.D., Dean

TABLE OF CONTENTS

LIST OF FIGURES

LIST OF SCHEMES

LIST OF TABLES

ACKNOWLEDGMENTS

There are many people who deserve my appreciation and a nomination of sainthood for guiding my education and professional development these past five years. I am grateful to my advisors Dr. Kevin G. Pinney and Dr. Mary Lynn Trawick for allowing me the opportunity to work in their laboratories. Dr. Pinney and Dr. Trawick gave me the opportunity to learn a variety of techniques from many projects, and allowed me to receive a broad education relevant to my future education in medicine. Furthermore, Dr. Pinney has helped me mold my once spirited personality into a more professional and academically focused demeanor. I consider Dr. Pinney and Dr. Trawick, not only academic advisors, but personal friends.

I also thank my committee members, Dr. Bob Kane, Dr. Charles Garner, Dr. Carlos Manzanares, and Dr. Erich Baker for assisting, and offering advice for my dissertation. I appreciate the valuable time my committee has taken from their schedules to ensure my success in future academia.

I thank former and current Pinney and Trawick group members for their support and friendship. I am deeply grateful to Madhavi Sriram for her constant guidance and friendship. I am also grateful to Benson Nguyen and Freeland Ackley, who were not only excellent colleagues, but dedicated friends. I thank Dr. Guddneppanavar, Dr. Kishore Gaddale Devanna, Abishek Dogra, Dr. Raj Tanpure, Dr. Ming Zhou, Dr. Bennon Mugabe, Dr. Graciela Miranda, Gerardo, Lindsay, Clinton, Milenka, Amanda, Gustavo and Sam for their continued support and friendship. I also thank Nick Martinez, Caroyln

Kienstra, Ann Lilly, Clark Damon, Jordan Lamb, Candice Allen, and Matthew Lee, who were all phenomenal undergraduates that added tremendously to my research.

I thank Nancy Kallus, Adonna Cook, Corrie Harris, Andrea Johnson, and Patricia Diamond for their continued hard work and support over the past five years.

I thank the Department of Chemistry and Biochemisty, Baylor University, the Welch Foundation, and Oxigene Inc. for their generous financial support.

I thank my family for being supportive of me these past five years. I especially thank my wife Rebecca, who has stood strong by me. Whenever I was filled with self doubt she was always there to pick me up, comfort me, show me the positives in my life, and help me move forward. I am both humbled and honored to have her as my life-long companion.

LIST OF ABBREVIATIONS

^{o}C	Degree Celsius
Ac_2O	Acetic anhydride
AcOH	Acetic Acid
CA	Combretastatin
CA1	Combretastatin A-1
CA1P	Combretastatin A-1-Phosphate
CA4	Combretastatin A-4
CA4P	Combretastatin A-4-Phosphate
CH_2Cl_2	Dichloromethane
Conc.	Concentration
DBP	Dibenzylphophite
DCC	Dicyclohexyl carbodiimide
DDQ	5,6-Dichloro-2,3-dicyanoquinone
DHN	Dihydronaphthalene
DIPEA	N,N-Diisopropylethylamine
DMAP	4-(N,N-dimethylformamide
DMSO	Dimethyl sulfoxide
DNA	Deoxyribonucleic acid
DU-145	Prostate Carcinoma
EtOAc	Ethyl acetate
GI_{50}	Concentration where 50% of cell growth is inhibited

GDP	Guanosine diphosphate
GTP	Guanosine triphosphate
h	Hour
HIF-1α	Hypoxia inducible factor 1 alpha
HPLC	High Pressure Liquid Chromatography
Hz	Hertz
IC_{50}	Concentration where 50% of protein activity is inhibited
LDA	Lithium diisopropylamide
MeLi	Methyl Lithium
MHz	Mega hertz
min	Minutes
µg/mL	Micrograms/milliliter
µM	Micromolar
mL	Milliliter
mM	Millimolar
mmol	Millmole
MT	Microtubule
n-BuLi	n-butyllithium
NCI	National Cancer Institute
NCI H460	Lung cancer carcinoma
NCS	N-chlorosuccinamide
nM	Nanomolar
NMR	Nuclear Magnetic Resonance Spectrocopy

ODB	*o*-Dichlorobenzene
PCC	Pyridinium chlorochromate
ppm	Parts per million
p-TSA	Para-Toluenesulfonic acid
RNA	Ribonucleic Acid
r.t.	Room temperature
Rf	Retention Factor
SRB	Sulforhodamine B
TBAF	Tetrabutylammonium fluoride
TBSCl	*tert*-Butyldimethylsilyl chloride
TMEDA	Tetramethylethylenediamine
TMSBr	Trimethylsilyl bromide
TMSCl	Trimethylsilyl chloride
UV	Ultraviolet
VDA	Vascular disrupting agent
VTA	Vascular Targeting Agent
Z	*cis*-isomer

DEDICATION

To my brother
Jason Christopher Hall

CHAPTER ONE

Background and Research Rationale

Brief History of Cancer Therapy and Cancer Biology

Cancer is the generic name for any malignant tumor.[1] Hippocrates is credited with naming the disease *carcinos*, which is Greek for crab because of the tumor's crablike appearance. Later, *carcinos* was translated into the Latin word *cancer*. Treatment for cancers within these early years, 460-370 B.C., was based on the humor theory of four body fluids: blood, phlegm, black bile, and yellow bile. Early physicians believed that an imbalance of any one of the four fluids was the cause of illness. Cancer treatment in the Hippocratic era was focused on elixirs and balms from herbal plants, bloodletting, and diet.[2] Humor theory remained popular until the 19th century when Campell De Morgan argued that cancer was the result of external factors as well as genetic predisposition. De Morgan is also credited with discovering cancer metastasis.[3] In the 19th century, sterile surgical techniques developed by Joseph Lister drastically increased the survival rate for surgery. Until the invention of radiation and chemotherapy, surgical removal of tumors was the primary means of treating cancer.

Scientific research has elucidated the physiology, cause, and treatment of cancer. In recent terminology, cancer describes a series of diseases in which abnormal cells uncontrollably divide, invade other tissues, and can spread throughout the body using the lymph or circulatory systems. While there are more than 100 different types of cancer, there are five major categories:[4,5]

(1) Carcinoma is cancer that begins in the tissues that line organs.

(2) Sarcoma is cancer that begins in bone, cartilage, muscle, or other connective tissue.

(3) Leukemia is cancer that starts in blood-forming tissue.

(4) Lymphoma and myeloma are cancers of the immune system.

(5) Central nervous system cancers effect the brain and spinal cord.

Cancer is caused by a series of mutations to cellular DNA that disrupts the balance between cell proliferation and programmed death (Figure 1). In normal tissues, a damaged cell undergoes apoptosis; however, if multiple mutations to cellular DNA occur,

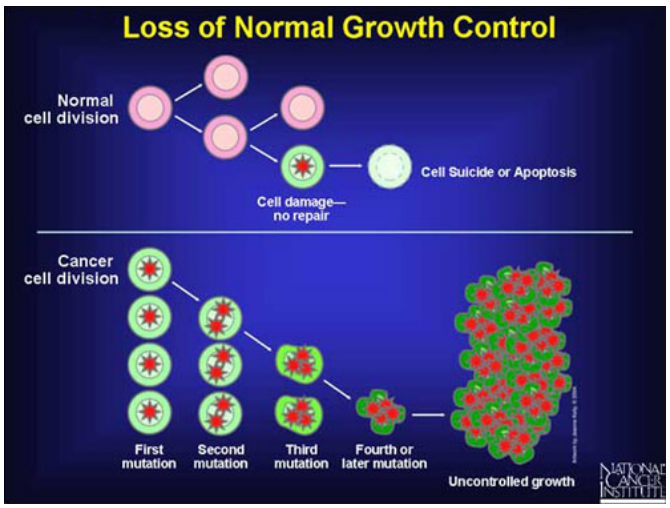

Figure 1. Formation of malignant tumors. Taken from Ref. 4.

the tumor cell may grow and proliferate uncontrollably. The uncontrolled growth may be the result of both the up-regulation of mitotic inducing proteins and the inhibition of tumor suppresser proteins such as p53. Over-expressed genes may become oncogenes which increase the transcription of factors responsible for uncontrolled cell growth and

proliferation. Examples of oncogene proteins include growth factors, tyrosine kinases like vascular endothelial growth (VEGF), and transcription factors. By controlling the rate of mitotic division and protein synthesis, therapeutics have been shown to control tumor growth, or eradicate malignant cells.

Chemotherapeutic agents target the carcinogenic sequence, generally exploiting the rapid progression of cancer cells throughout the cell cycle. Within the cell cycle, there are four phases: the G1 (gap 1) phase in which the cell synthesizes RNA necessary for DNA synthesis; the S (synthesis) phase in which the cell constructs proteins, RNA, and DNA; the G2 (gap 2) phase in which more RNA and protein synthesis occurs; and the M (mitotic) phase in which the cell divides.[6] Unlike normal cells, malignant cells are in a constant state of mitosis. Because malignant cells divide more rapidly than normal cells, disrupting their mitotic state has a higher impact on tissue death. An example of an effective FDA approved chemotherapeutic that targets tumor cell mitosis is vincristine. Vincristine, isolated from *Catharanthus roseus* (Figure 2), disrupts tumor cell proliferation by binding tubulin and disrupting microtubule function.

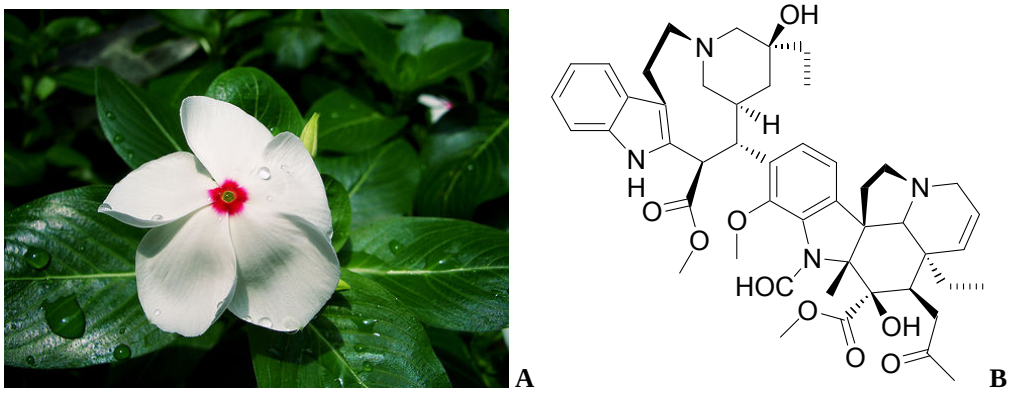

Figure 2. (A) Picture of *Catharanthus roseus.* Taken from http://www.flickr.com/photos/nagarazoku/33863363/. (B) Structure of clinically approved anti-mitotic cancer chemotherapeutic vincristine.

The major disadvantages to chemotherapy are the side effects caused by the non-selective nature of the compounds. Recent cancer research has tried to identify biochemical differences between normal and malignant cells in hopes of increasing chemotherapeutic selectivity. Several important differences have been identified; most significant to the research presented within this dissertation are the cytoskeletal abnormalities of tumor vascular endothelial cells.

A classification of drugs called vascular disrupting agents (VDAs) is at the center of the research presented here. The projected VDA chemotherapeutics may have the ability to behave in an antimitotic capacity; however, the group of tubulin colchicine site binding drugs designed here selectively disrupts tumor vasculature and starves the tumor's nutrient supply by disrupting tumor vasculature. VDAs were coupled with anti-cancer bioreductive agents to increase their anti-cancer activity in hypoxic areas. The drugs were also co-crystallized with anti-angiogenic nitric oxide synthase (NOS) inhibitors to increase overall tumor necrosis. The drugs were tested for their ability to inhibit tubulin polymerization and for their ability to inhibit tumor cell growth using the SRB cytotoxicity assay. The binding enthalpies of CA1, CA4, and a potent benzophenone derivative **37** were evaluated using isothermal titration calorimetry. Selected VDA molecules synthesized in the Pinney lab were also evaluated for their ability to inhibit the function of HIF-1α, a protein responsible for increasing tumor viability in hypoxic environments.

Tumor Vasculature

One of the most notable differences between tumors and normal tissue is the vasculature (Figure 3). Healthy tissue is fed by organized vasculature that is engineered to meet the needs of the individual cells. Vasculature for normal tissue is efficient; however, tumor vasculature is generally chaotic and physiologically inadequate. The physiological differences between normal and tumor vasculature suggests that there may be biological differences that can be exploited for chemotherapy. Erratic branching, shunts, and occlusions obstruct blood flow within tumors, creating an environment that is

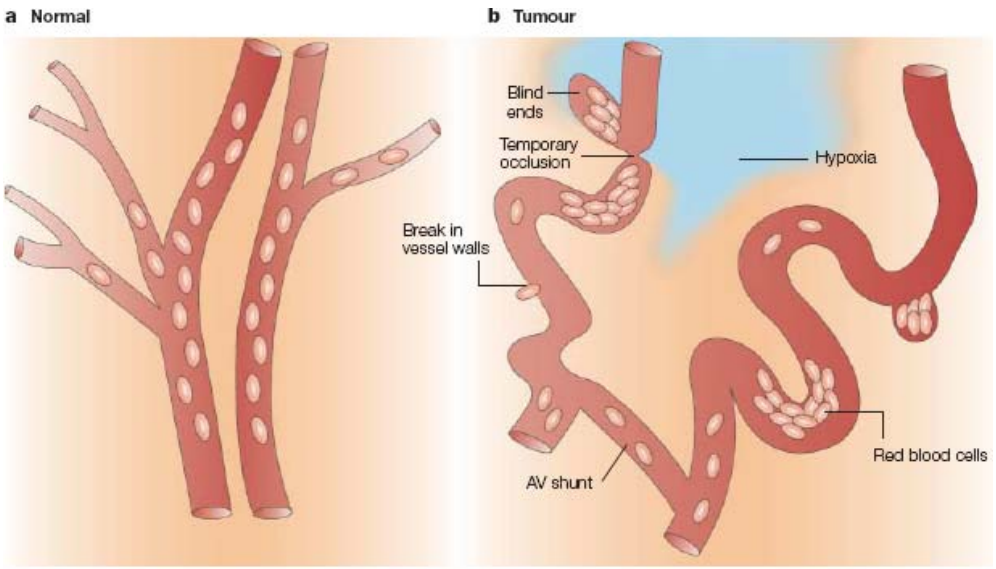

Figure 3. Differences between normal and tumor vasculature. Normal vasculature (a) is well organized and efficient, were as tumor vasculature (b) is chaotic and inefficient. Figure taken from Ref. 74 with permission.

poor in nutrients and oxygen.[74] The vascular framework of healthy tissues is supported by a scaffold of microtubules and actin that is considered stable, whereas tumor vascular

endothelial cells are maintained by microtubules that are undergoing higher rates of polymerization and disassembly. Tumor endothelial cells also express different antigens on the cell surface. The abnormal arrangement and phenotype of tumor vasculature has made the tumor vascular network a target for the development of antitumor agents.[7]

Vascular Targeting Agents (VTAs)

Anti-cancer agents that work by targeting tumor vasculature are labeled Vascular Targeting Agents (VTAs). There are two subsets of VTAs: vascular disrupting agents (VDAs) and anti-angiogenic drugs (Figure 4). Angiogenesis is the formation of new vasculature. Proangiogenic factors like plasminogen activator, growth factors, and adhesion molecules signal vascular endothelial cells to undergo angiogenesis. One of the most studied proangiogenic factors is VEGF, a tyrosine kinase that is involved in transphosphorylation mechanisms. Binding to VEGF receptors induce the growth of new tubular structures composed of endothelial cells. Angiogenic inhibitors target these growth factors in order to prevent neovascularization.[73,75] By inhibiting angiogenesis, tumor growth would be arrested; however, these treatments would only effect complete tumor necrosis if used in conjunction with radiation therapy or other chemotherapeutic agents. Anti-angiogenic drugs are considered cytostatic, which means that they hinder tumor growth, but the existing tumor cells and vasculature are not destroyed.[7] No new anti-angiogenic drugs were synthesized in this work; however, the anti-angiogenic drugs L-NMMA and L-NAME were used in conjunction with a variety of VDA analogues to increase overall tumor necrosis.[47]

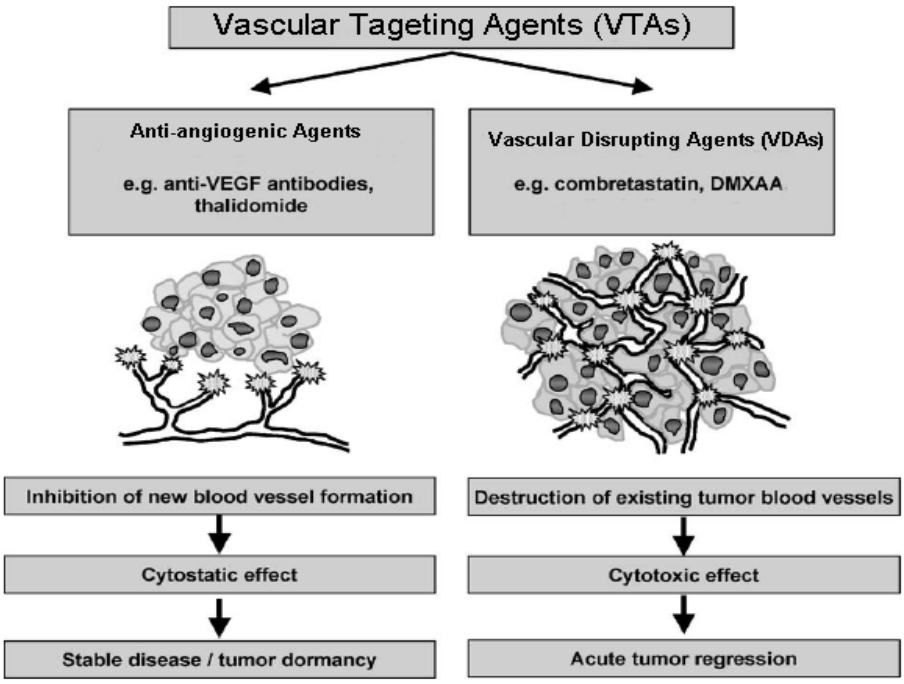

Figure 4. Different approaches to vascular targeted therapy. Modified from Ref. 75 with permission.

Vascular Disrupting Agents (VDAs)

The other branch of vascular targeting focuses on vascular disrupting agents (VDAs) which also target the tumor vasculature, but are considered cytotoxic because they disrupt existing neovasculature of growing tumors and produce a rapid occlusion of blood flow. The blockage of blood flow deprives the tumor of oxygen and nutrients (Figure 5). Prolonged occlusion of the tumor vasculature may cause substantial tumor necrosis. The two current approaches to vascular disruption involve either biological agents or small molecules, both of which are capable of destroying ~95% of the tumor.[7,75] The biological agents use either antibodies or peptides to directly target molecules, like VEGF receptors, that have been upregulated on the surface of the tumor's endothelial cells. Binding of the VDA biological agents may result in host attack on tumor

endothelium, change in endothelial cell shape, or direct thrombosis of tumor blood vessels.[7,75] The molecules synthesized within this work are small molecular VDAs.

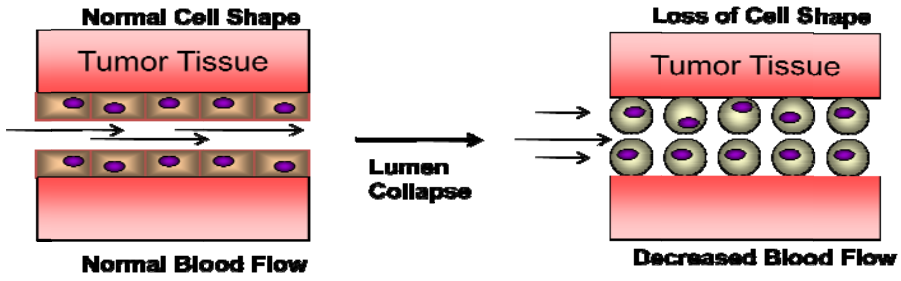

Figure 5. Mechanism of blood vessel occlusion by VDAs.

The small molecular VDAs exploit the pathological differences between tumor and normal endothelial cells and stimulate occlusion of the tumor vasculature. Though Colchicine was the first small molecular discovered to behave as a VDA. Colchicine showed antitumor effectiveness when given orally, intravenously, when injected directly into the tumor, and when used in conjunction with radiotherapy; however, treatment was stopped because of its high toxicity.[7,132] VDA research is still expanding and is divided into two classes: flavone acetic acids and tubulin binding agents.[7]

Taxanes, colchicine, vincristine, and vinblastine are all classified as tubulin binding agents. Each drug binds to specific sites located on the tubulin dimer: colchicine binds to the colchicine binding site; vincristine and vinblastine bind to the vinca alkaloid site, and taxanes bind to the taxoid binding domain. A vast number of compounds have been designed to mimic colchicine's tubulin binding anti-tumor vascular activity. Researchers desire to find an anticancer drug with the tubulin binding capabilities of colchicine, but without its toxicity.

Combretastatins

Professor George R. Pettit discovered a series of small molecule inhibitors of tubulin polymerization that were grouped as combretastatins because of their isolation from the African bushwillow tree *Combretum caffrum* Kuntze (Combretaceae).[8,122-130] Combretastatin A1 (CA1), and combretastatin A4 (CA4), and their corresponding phosphate salt prodrugs CA1P and CA4P, (Figure 6) have been the most studied combretastatins to date.

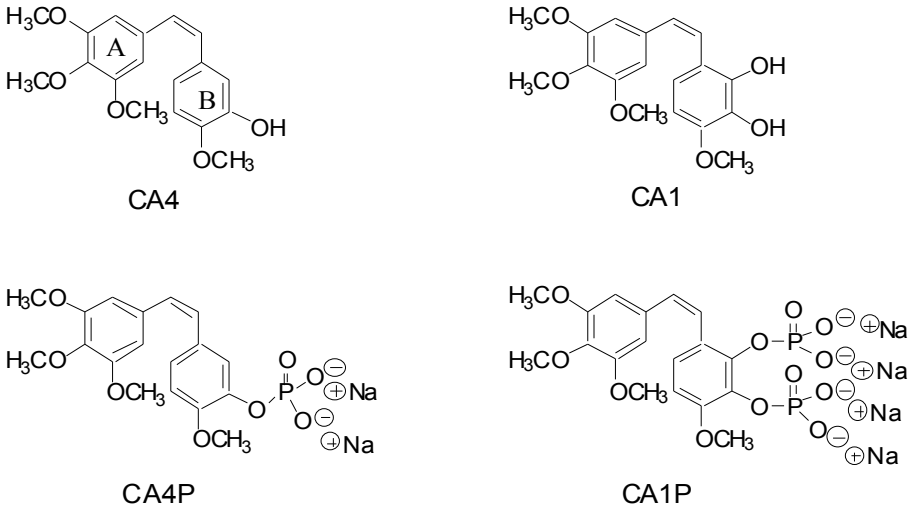

Figure 6. Structures of CA4, CA4P, CA1, and CA1P.

The combretastatin family of drugs is the central focus for the work presented here. The relatively simple structure of the combretastatins not only facilitates ease of synthesis, but they have also been shown through the past two decades to be selective in their ability to occlude tumor vasculature. Understanding the role of CA4P and CA1P in chemotherapy, understanding how these compounds bind to tubulin (in non-prodrug form), and synthesizing drugs analogous of the combretastatin scaffold are key in

developing a thorough structure activity relationship (SAR) for the map of the colchicine binding site on β-tubulin. By expanding the known SAR surrounding the colchicine binding site, improved VDA chemotherapeutics may be synthesized in the future.

The combretastatin A (CA) family is structurally similar to colchicine, because they contain two aryl rings that are tilted 50-60^{o} (Figure 7) relative to one another.[9,130] The aryl rings are attached to each other by an ethene bridge. The two phenyl rings are generally identified as the A-ring, which has the 3,4,5-trimethoxy motif, and the B-ring,

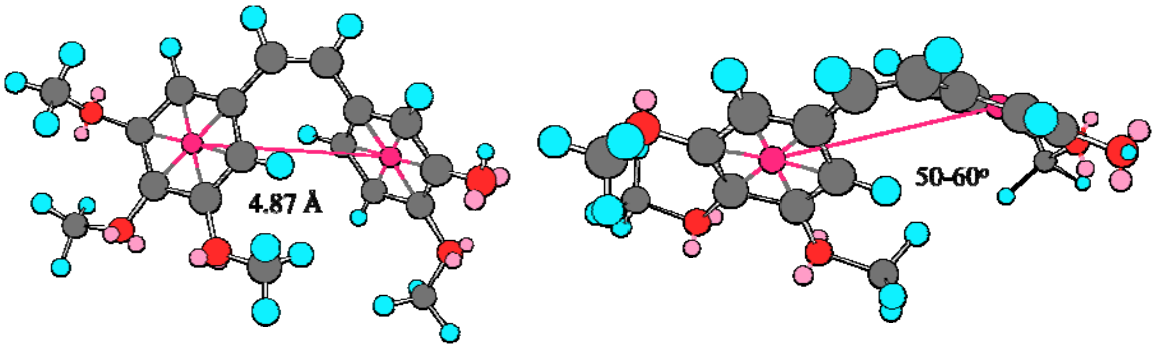

Figure 7. Three dimensional model of CA4.

which has a 3′-hydroxy 4′-methoxy phenyl attachment using the CA4 construct (Figure 6). The limited water solubility of CA1 and CA4 led to the development of CA1P and CA4P which are water soluble analogues.[9] CA1P and CA4P are considered pro-drugs in that they do not interact with the tubulin; rather, the phosphate is cleaved by a phosphatase, converting it into the parent drug, where it then enters the cell and disrupts the microtubule network.[10] Evidence for the prodrug phosphorolysis to the corresponding drug is reflected in the lack of tubulin binding capability of the prodrug.[76] The tubulin binding assay is performed devoid of all other proteins except tubulin. The

drug CA4 has an IC_{50} value of 1.2 μM; however, the prodrug CA4P has an IC_{50} value of >40 μM, meaning the prodrug does not inhibit tubulin polymerization.[10,76] Comparison of the cell cytotoxicity assays show that CA4P is approximately as cytotoxic against the same cancer cell lines as CA4 (Table 1).

Table 1. Biological and Biochemical evaluation of CA1, CA1P, CA4, and CA4P.

Compound	Tubulin Inhibition IC_{50} (μM)	Leukemia P388 GI_{50} (μg/mL)	Pancreas BXPC-3 GI_{50}(μg/mL)	Breast MCF-7 GI_{50} (μg/mL)	CNS SF268 GI_{50}(μg/mL)	Lung-NSC NCI-H460 GI_{50} (μg/mL)	Colon KM20L2 GI_{50} (μg/mL)	Prostate DU-145 GI_{50} (μg/mL)
CA4	1.2[a]	0.0003[b]	0.39[b]	-	<0.001[b]	0.0006[b]	0.061[b]	0.0008[b]
CA4P	>40	0.0004[b]	-	-	0.036[b]	0.029[b]	0.034[b]	-
CA1	1.9[a]	0.25 [b]	4.4[b]	-		0.74[b]	0.061[b]	0.17[b]
CA1P	>40	<0.01[b]	1.5[b]	0.024[b]	0.036[b]	0.038[b]	0.53[b]	0.034[b]

[a] taken from Ref.[10]
[b] taken from Ref.[76]

Both CA4P (Zyberstat®) and the CA1P phosphate salt prodrug Oxi4503 show promising effects on blocking tumor profusion. Salmon and co-workers[11] treated KHT rodent sarcoma growths with either 100 mg/kg CA4P or 25 mg/kg Oxi4503 and monitored the tumor perfusion at 4 h, 24 h, and 48 h. Immediately following treatment with the combretastatin drugs, the tumor perfusion dropped to ~23% with CA4P and 20% with Oxi4503. After 48 h, the tumor perfusion had regained to 75% for CA4P and to 63% for Oxi4503.[11]

Mechanism of CA4P Activity and Cell Signaling

The microtubule network that VDAs disrupt, are responsible for coordinating many cellular processes including cell contraction. Contraction of the cell can lead to

gap formation and increased permeability in the endothelial monolayers. The cell signaling pathway associated with CA4P involves the activation of GTPase Rho and Rho kinase. The first action in the cell signal cascade involves the de-phosphorylation of CA4P by an indiscriminate phosphatase to CA4.[10] The CA4 then enters the cell and interacts with microtubules, causing their depolymerization. Some guanine exchange factors (GEFs) interact with microtubules, and are possibly activated by the disassembly of the tubulin network. GEFs activate RhoA by catalyzing the exchange of GDP for GTP. In turn RhoA is responsible for the phosphorylation of a number of downstream effectors. Activation of RhoA kinase by RhoA results in the phosphorylation of myosin light chain kinase (MLCK). MLCK is can phosphorylate myosin light chain (MLC) which activates actinomyosin interactions and myosin adenosine triphosphatase (ATPase), and leads to increased contraction. Also, Rho-kinase phosphorylates the myosin binding site of MLC phosphatase, which prevents MLC dephosphorylation. The stress activated protein kinase (SAPK), also interact with the cytoskeletal proteins. The SAPK-2/p38 interaction can cause changes in actin dynamics, and lead to stress fiber formation. The rearrangements of the cytoskeleton can induce apoptosis and membrane blebbing (Figure 8).[131]

VDA Research Design

The potency of CA1 and CA4 have inspired numerous synthetic chemists to advance SAR studies of the combretastatin family of tubulin binding drugs. Groups have tested the positions and necessity of the methoxy substituents located on the A-ring, as well as the position and importance of the phenolic groups of the B-ring.[10,98,100,107,116,117]

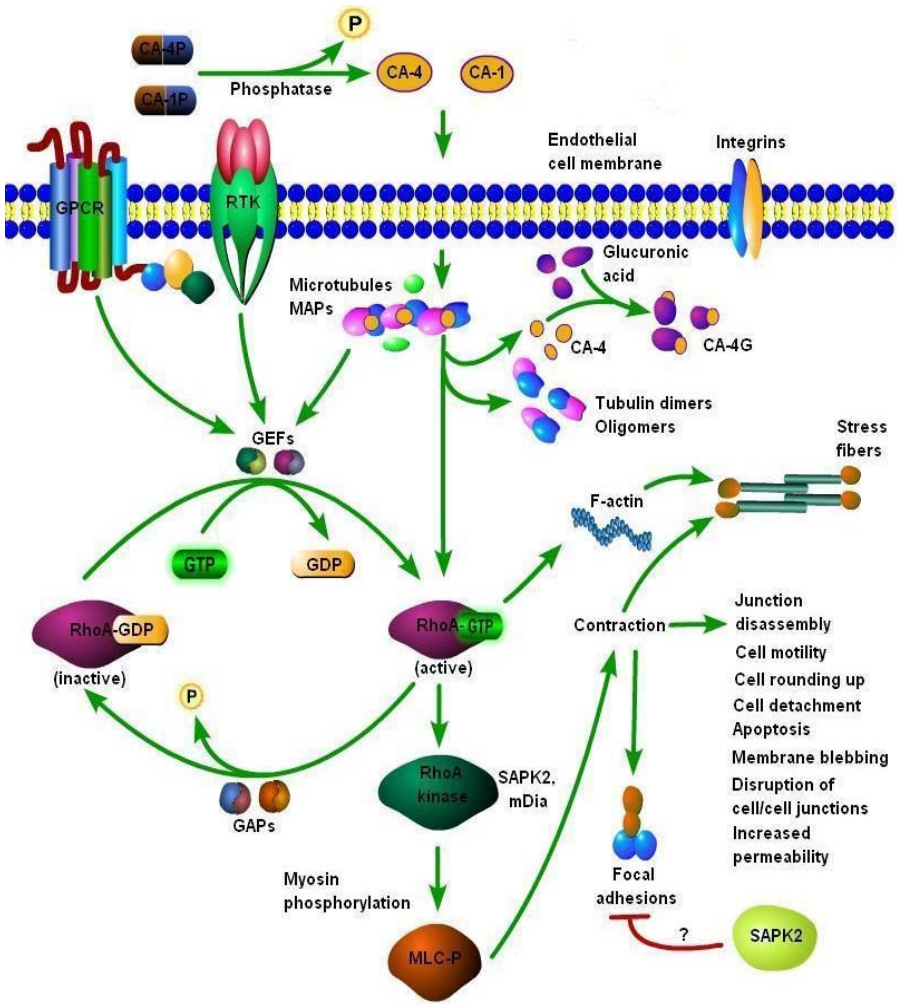

Figure 8. Mechanism of CA4P induced cell signaling pathways. Reproduced from Dr. Benon Mugabe, Ref. 80 with permission..

Other cyclic and heterocyclic scaffolds that have some structural resemblance to colchicine and combretastatin have been synthesized in hopes of furthering the SAR relationship of tubulin colchicine binding site drugs.[12]

Molecular modeling has given some insight into the requirements for the efficient binding of a variety of different tubulin colchicine binding site drugs. Nguyen and co-workers[13] modeled 15 different suspected colchicine binding site drugs to look for similarities between drug binding profiles. Nguyen found that similarities of binding do

exist within 7 different pharmacophoric points (Figure 9). Points A1 (red), A2 (pink), and A3 (yellow) are all hydrogen bond acceptors; therefore, an atom capable of accepting an H-bond would be desirable in this location.

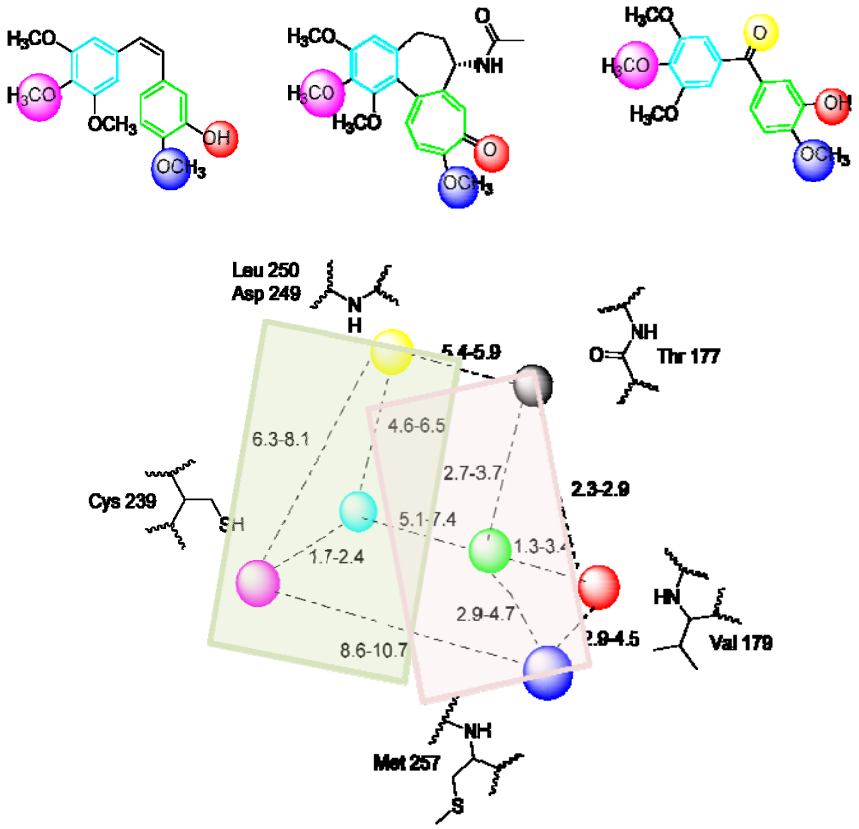

Figure 9. Common pharmacophoric points of a variety of different suspected tubulin colchicine binding site drugs identified with molecular modeling by Nguyen and co-workers. Modified from Ref. 13.

The synthesized VDAs within this research contain H-bond acceptors in these regions; however, the theory that these locations must contain H-bond acceptors will be also be tested by incorporating fluorines onto the 4-position of the combretastatin A-ring. The region labeled D1 (grey) is a hydrogen bond donor, so phenols, amines, and sulfides should be within this vicinity. The D1 pharmacophore is found in the synthesized indole

derivatives, and since the Pinney group has determined the importance of this hydrogen bond donator within the indole scaffold,[14] the validity of this pharmacophore was not tested. H1 (blue) and H2 (cyan line) are hydrophobic centers, and R1 (green line) is planar, so aromatic cycles would be ideal in these locations. All of the proposed compounds are aromatic in nature and will therefore fulfill the planar/hydrophobic spatial requirement.[13]

As mentioned previously, Pinney group members have found other heterocyclic scaffolds to be effective at inhibiting tubulin polymerization, and they share some of the pharmacophoric necessities described by Nguyen. Benzo[*b*]thiophene, benzo[*b*]furan, and indole drugs have shown to inhibit tubulin polymerization with IC_{50} values in the 0.5-2.0 μM.[14-16] These heterocyclic scaffolds are of interest to this work because of the similar aryl A-B centroid-to-centroid distances of the combretastatins and indoles, 4.87 Å and 4.88 Å respectively (Figure 10).[17]

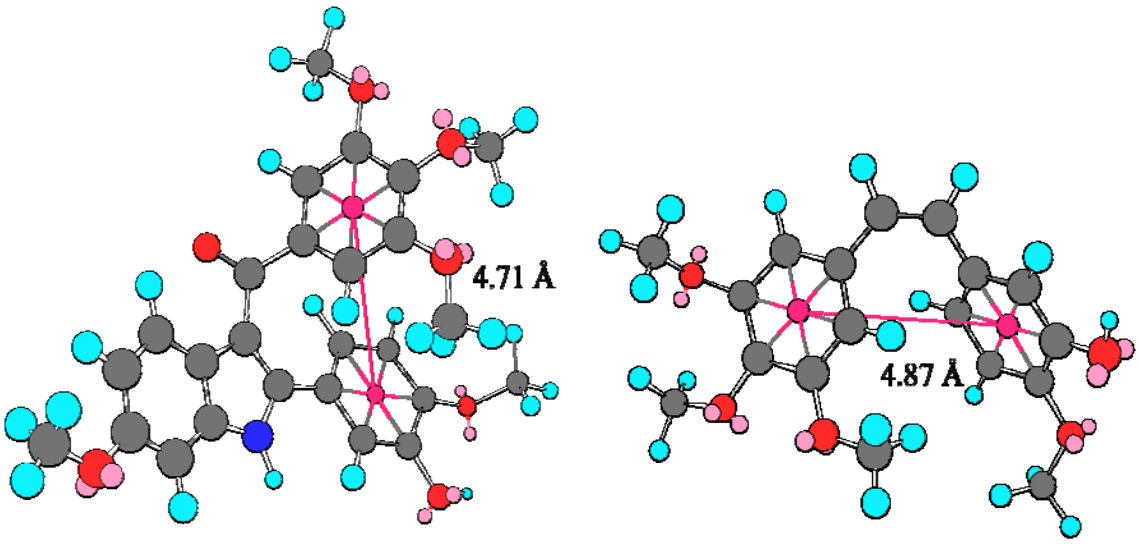

Figure 10. Centroid-centroid distances of indole Oxi8006 are similar to CA4

The discovery of equally potent heteroaromatic scaffolds is important in combretastatin research because combretastatins are well known for their ability to spontaneously convert from the active Z- isomer to the relatively inactive E-isomer. This isomerization is believed to result from the resonance donators located in the ortho- or para- positions of the aryl ring. By donating a lone pair of electrons into the aromatic ring, a lone pair is pushed to one of the ethene carbons, forming a carbanion. The freedom of rotation gained from the loss of the double bond allows the stilbene to reform in the lower energy *E*- conformation (Figure 11). This effect is more prevalent with resonance donators located at the 4′- position.[17] Combretastatin analogues that are not able to be isolated in the *Z* configuration were mimicked using the indole heterocyclic scaffold. The functional group placement for isomerizing combretastatins was tested using the indole scaffold because the aryl-aryl distances are similar to the combretastatin analogues.

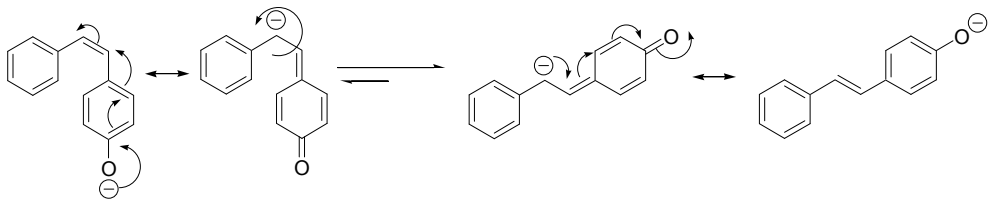

Figure 11. Possible mechanism for stilbene *Z* to *E* isomerization. Modified from Ref. 17.

The VDA synthetic research presented in this dissertation started with a 3′,4′-dihydroxy 5′-methoxy combretastatin derivative. Indole and phenstatin derivatives with the same A-B ring configuration were also synthesized . Indole and combretastatin derivatives that have a trifluoro-A ring, and nitro or amine B-ring moieties were also

synthesized. Several group projects involving the synthesis of dihydronaphthalenes, indoles, and radiolabeled combretastatins will also be discussed. Figure 12 contains a complete list of tubulin binding ligands synthesized within this work.

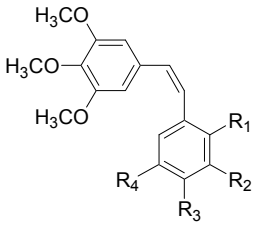

	R1	R2	R3	R4
7	H	OH	OH	OCH_3
25	OH	OH	OCH3	H
27	OPO_3HK	OPO_3HK	OCH3	H

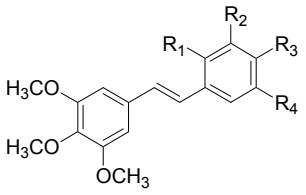

	R1	R2	R3	R4
8	H	OH	OH	OCH_3
35	OH	OH	OCH3	H

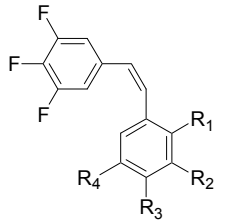

	R1	R2	R3	R4
10	H	OH	OH	OCH_3
13	H	NO_2	OCH_3	H
15	H	NH_2	OCH_3	H
17	NO_2	H	OCH_3	H
19	NH_2	H	OCH_3	H

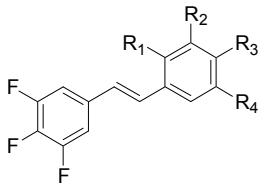

	R1	R2	R3	R4
11	H	OH	OH	OCH_3
14	H	NO_2	OCH_3	H
16	H	NH_2	OCH_3	H
18	NO_2	H	OCH_3	H
20	NH_2	H	OCH_3	H

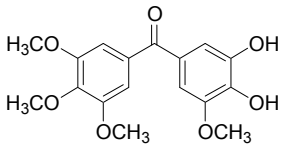

37

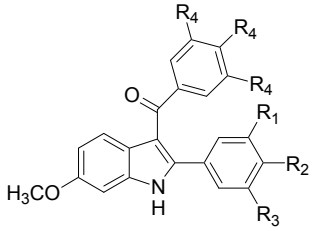

	R1	R2	R3	R4
44	OCH_3	OH	OH	OCH_3
47	OCH_3	OH	OH	F
55	H	OCH_3	OH	F
62[14]	H	OCH_3	OTBS	OCH_3

Figure 12. Structures of tubulin binding agents synthesized within this work.

Microtubule Function

Vascular disrupting agents are suspected to arrest mitosis by hindering tubulin assembly into microtubules (Figure 13). Microtubules are involved in cell shape, motility, transport, and division. The cell cycle is largely dependent on microtubules. During prophase of mitosis, centrioles appear and migrate to opposite ends of the cell.

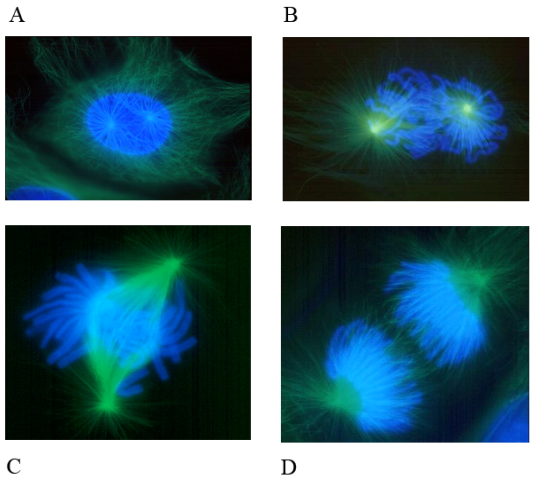

Figure 13. Cell mitosis. Structures labeled green are microtubules while those labeled blue are chromosomes. (A) prophase, (B) prometaphase, (C) metaphase, (D) anaphase. Figures taken from www.wadsworth.org.

A spindle apparatus of microtubules forms and becomes organized by the centrioles. Four to seven microtubules attach to the individual chromosomes at their kinetochores, then align at the equator of the spindle during metaphase. Shortening of the microtubules during anaphase separates the sister chromatids. Once the chromatids are separated, the spindle dissolves and the steps that occur during prophase reverse to produce two individual cells. Without microtubule formation, the cells cannot divide.[18]

Microtubules are involved in many functions other than cell division: they aid in locomotion, they aid in intracellular transport of substances, and they help maintain cell shape. Studies with colchicine have confirmed that microtubules are important structural components for cell morphology. When cells, such as HeLa cells, are exposed to colchicine, the microtubules depolymerize and the cells lose their morphology (Figure 14).[19] When the tumor endothelial cells lose their shape *in vivo*, blood-flow to the tumor is stopped, depriving the tumor of nutrients and oxygen.

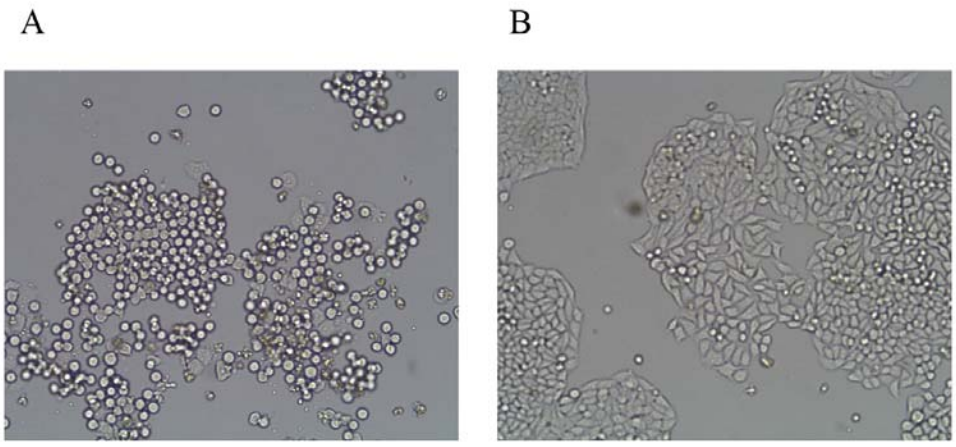

Figure 14. Effects of colchicine on HeLa cell morphology. (A) Colchicine treated cells are rounded. (B) Untreated cell appear flat. Figure by John Hall.

Microtubule Structure and Formation

To effectively design VDA compounds that disrupt microtubule dynamics one must have a good understanding of microtubule structure and formation. Microtubules are hollow tube structures formed from the lateral association of thirteen protofilament strands. The microtubules have an outer circumference of 25 nm, an internal circumference of 15 nm, and reach lengths of 25 μm. The noncovalently bound

protofilaments are composed of tubulin. Tubulin is a globular heterodimer protein composed of an α- and a β- subunit whose amino acid residues are ~50% identical. Each tubulin subunit has a mass of 50 KDa.[20] The dimer interface has a non-exchangeable GTP (N-site) within the α-subunit. There is an exchangeable GTP (E-site) at the β-tubulin that sits at the top surface of the dimer.[21] Polymerization of the tubulin dimers results in the E-site GTP envelopment at the dimer-dimer interface and allows the hydrolysis of GTP (tubulin is a GTPase) by residues of the α-tubulin, which promotes polymerization. The hydrolysis of the γ-phosphate most likely involves Glu254 of the α-subunit. Glu254 is approximately 4 Å from the GTP γ-phosphate when the tubulin dimers are assembled. Studies have shown that Glu254 significantly increases the rate of GTP hydrolysis in tubulin polymerization.[79]

The GTP hydrolysis may also be important in forming strong lateral interactions between the protofilament. Cryo-electron microscopy studies have shown that depolymerizing microtubules are peeling protofilaments which lead to ring structures and are similar to the self-assembled GDP-containing tubulin dimers (Figure 15). A well accepted model of tubulin suggests that tubulin may exist in two different conformations depending on the nucleotide bound at the E-site. If GTP is bound, then the tubulin is in a straight conformation, allowing it to assemble into straight protofilaments, which in turn form straight microtubules. If GDP is bound at the tubulin E-site, then the dimer is bent, and results in curved protofilaments or rings that do not form microtubules. The subunits located within the microtubule are locked into a straight conformation because of structural constraints of the microtubule, and these subunits will remain linear so as long

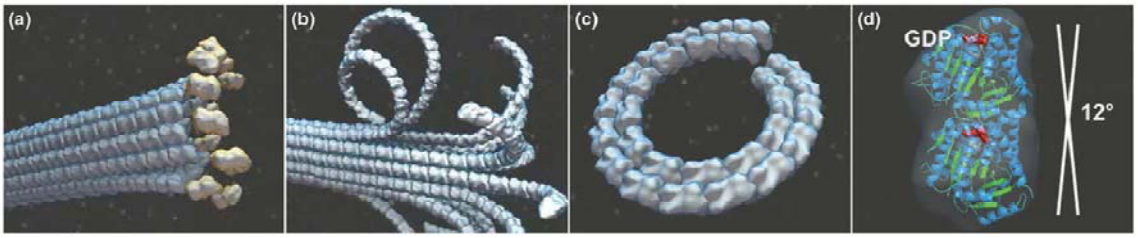

Figure 15. The loss of the GTP cap results in microtubule disassembly. (a) GTP cap loss; (b) peeling of the protofilament; (c) disassembled ring intermediate; (d) bent configuration of GDP tubulin dimer. Taken from Ref. 21 with permission.

as there is a GTP-cap. When the GTP cap is lost, the microtubule depolymerizes rapidly to the low energy curved protofilament state.[21]

The structure of tubulin is known,[22] and there are some key features that allow for microtubule assembly. The C-terminals are acidic and disordered. The N-terminal nucleotide binding domain contains residues 1-206 and is formed from the alternating parallel beta strands S1-S6 and the helices H1-H6. The pocket that contains the nucleotide is made by loops T1-T6 that connect the beta-strands and helices (Figure 16), and the terminal end of helix H7. After the core helix (H7), there is a second domain made of helices H8-H10 and mixed beta sheet S7-S10. Two helices (H11 and H12) that cross over the other two domains form the C-terminal region.[22]

The C-terminal helices of the tubulin form the outer apex of the protofilaments. Most likely, helices H11 and H12 are involved with binding to motor proteins and microtubule associated proteins (MAPS) and may be important for microtubule formation. The protofilament lateral contact is the result of the M-loop (residues 279-

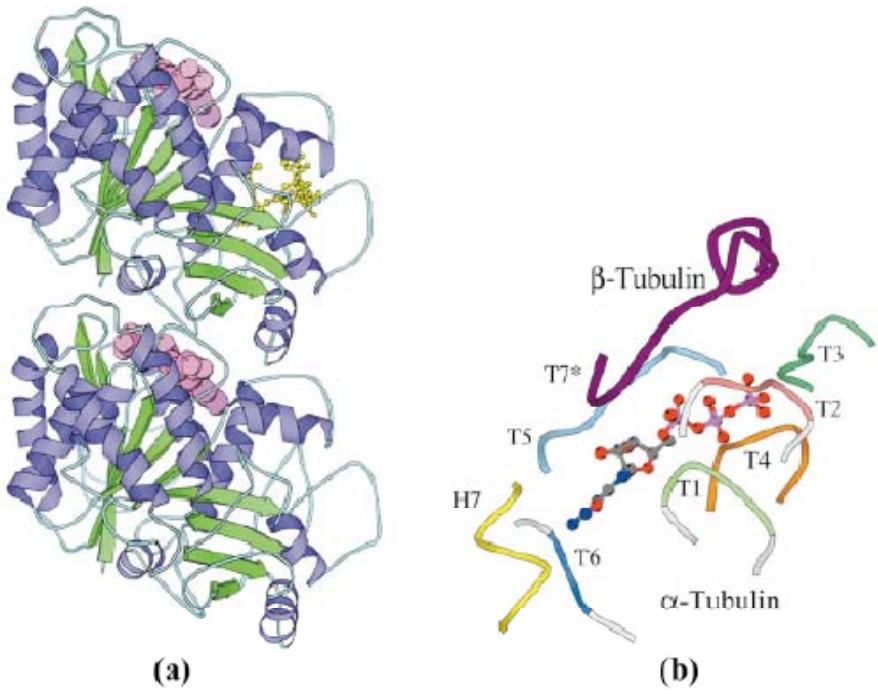

Figure 16. Structure of Tubulin (a) Electron crystallography structure of the tubulin dimer. Taxol is shown in yellow, and GTP in pink. (b) The structural elements that surround the N-site GTP. T1-T6 are from α-tubulin; T7 from β-tubulin. Taken from Ref. 22 with permission.

287) interactions with the loop H1-S2, as well as associations with helix H3 (Figure 17). Loop T3 binds to the γ-phosphate of the E-site nucleotide. It is hypothesized that GTP hydrolysis could occur from a conformational change of H3 that is transmitted from the T3 loop.[22] M-loop lateral interactions are stabilized in the α-subunit by the S9-S10 loop. The β-subunit M-loop stabilization may be of similar origin, but there is a lack of crystallographic evidence. The M-loop sequence is the most divergent section between α- and β- tubulin, and is believed to be the source of preferential lattice formation. The preferred lateral interactions are α-α and β-β, which form an overall B-lattice; however, in the microtubule there is a seam consisting of α-β lateral interactions. The seam may also be responsible for microtubule stability and MAP recognition.[22]

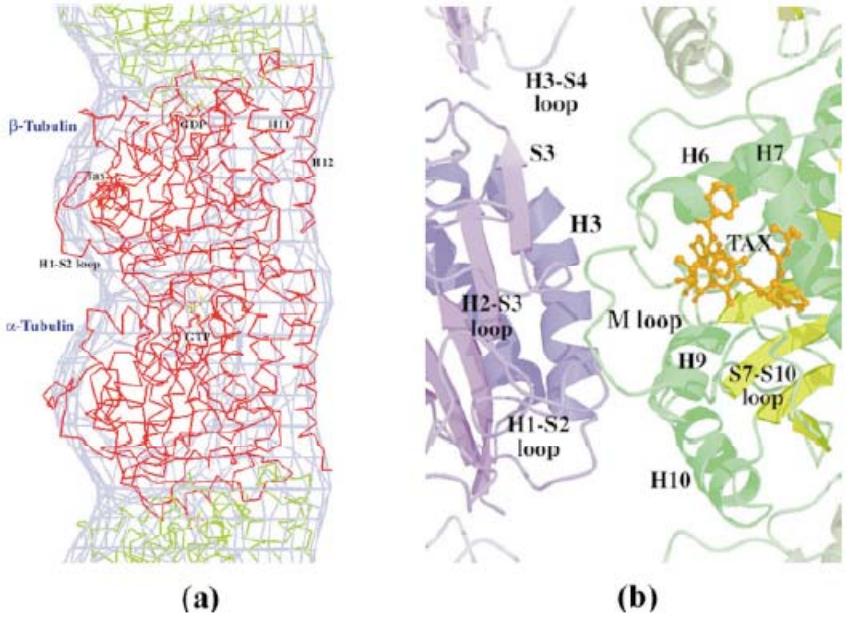

Figure 17. Tubulin Dimer Interactions (a) Side view of a protofilament. The inside of the microtubule is the left side of the protofilaments and is dominated by the H1-S2 loop. The outside is C-terminal helices. (b) Lateral contacts between β-tubulin subunits in two adjacent protofilaments, are dominated by the M loop and H3. Taken from Ref. 22 with permission.

Microtubule Dynamics

The fragile and reversible nature of microtubules has been identified as the source for their dynamic instability (Figure 18). This dynamic instability is crucial to the effectiveness of the VDAs. Microtubules are thought to be in a variable state of polymerization and depolymerization. In normal tissue, tubulin is relatively stable; however, in the endothelium that feed tumor tissue, the rate of microtubule formation and deformation is 100 times faster. The growing end of a microtubule is called the plus (+) end, and the minus (-) end is generally the site of nucleation. When the microtubules are rapidly depolymerized, they are in a state of catastrophe. Recovery is the rapid transition from depolymerization to polymerization. There is also a mechanism for treadmilling, in which there is a net flow of tubulin from the (+) ends to the (-) ends without a net change

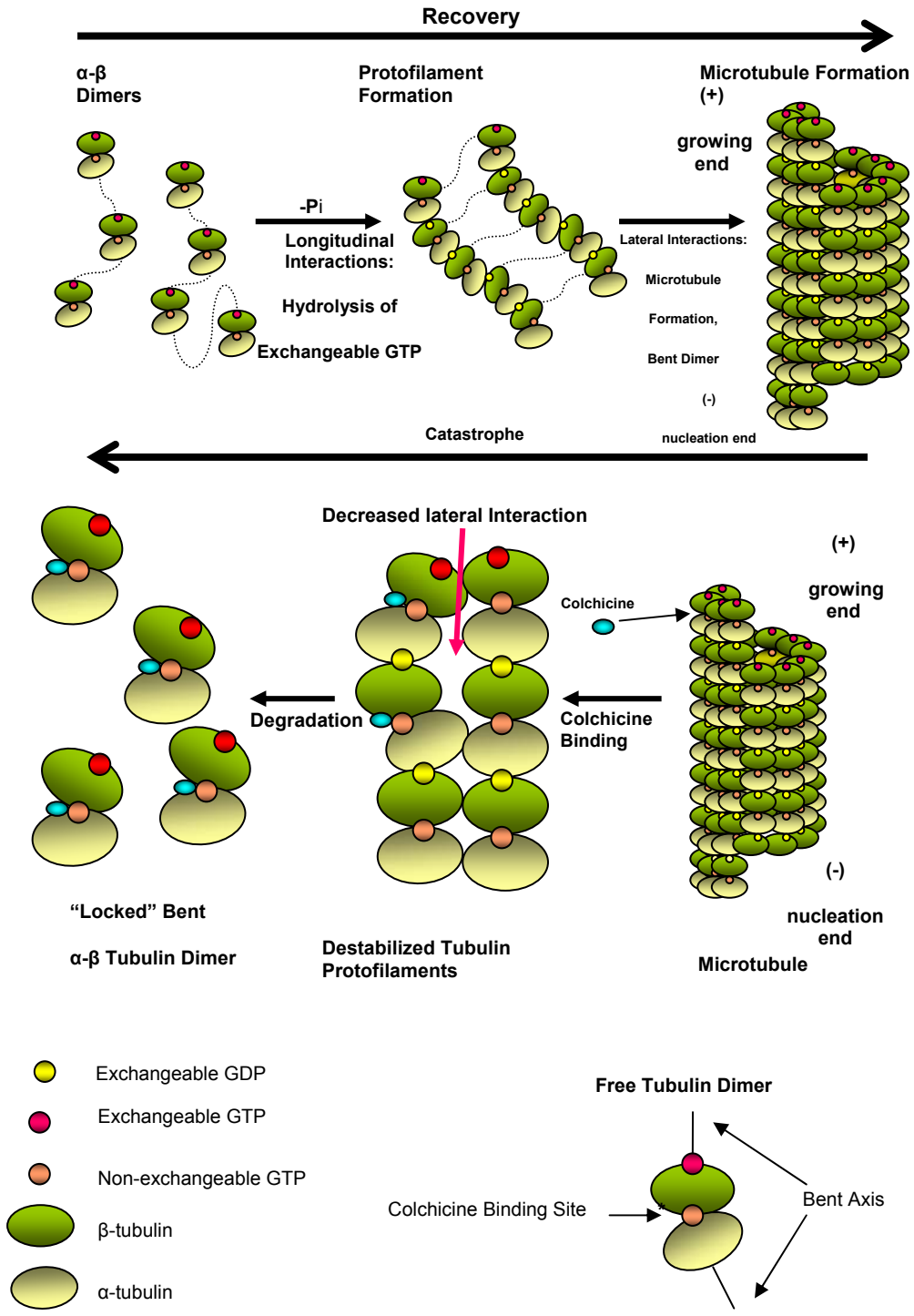

Figure 18. Microtubule dynamic model.

in microtubule length. The frequency that the microtubules grow or shrink is determined by many factors, such as tubulin concentration, assembly proteins, and co-factors. Increasing the concentration of the tubulin dimer raises the rate of polymerization and decreases the frequency of catastrophe. Mg^{2+} induces a 2-fold increase in polymerization rate. The dynamic instability of the minus ends of microtubules is not generally physiologically relevant since they are usually capped with other proteins; however, the minus ends of microtubules of purified tubulin exhibit dynamic instability similar to the plus ends. The drugs synthesized here are proposed to bind dimeric tubulin, preventing their assembly into microtubules, and therefore hinder the tubulin polymerization dynamics.[20]

Tubulin Binding Sites

There are three major classes of tubulin binding drugs; colchicine analogues, vincas, and taxanes. Each drug type is identified by the location of its respective binding site on tubulin (Figure 19). The taxol binding site is located at the boundary between the nucleotide-binding domain and the middle domain on the luminal side of the microtubule. Drugs that bind the taxol site are known to stabilize the microtubule structure. Taxol stabilization of microtubules is thought to result from placing the M-loop in a conformation that is more favorable to lateral contacts. The vinca domain is so named from the discovery of vinblastine, which binds to that region of the tubulin protein. The vinca domain is located at the plus end of the tubulin dimer.[74] Vinblastine binding essentially poisons the growing end of the microtubule, and inhibits elongation.[19] The VDAs synthesized in this work are proposed to bind to the colchicine site.

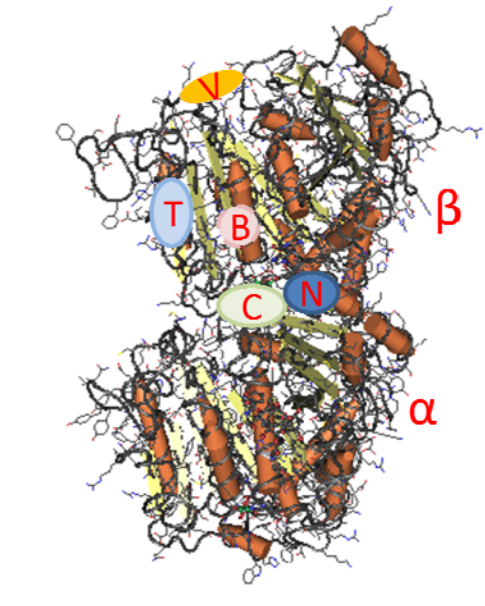

Figure 19. Summary of tubulin drug binding sites. The Taxol site (T) is the site associated with most tubulin stabilizing drugs. The colchicine site (C) is located at the intra-dimer interface. There is a possible benzimidazole site (B). The vinca domain (V) is at the surface of the (+) end of the tubulin. The exchangeable nucleotide site is represented by (E) and the non-exchangeable site is (N). Modified from Ref. 19

Colchicine Binding Site

Colchicine was the first drug discovered to bind to tubulin, and it is known to inhibit the dynamic stability of microtubules. In 2004, a 3.5 Å electron crystallography structure of tubulin bound with *N*-deacetyl-*N*-(2-mercaptoacetyl)-colchicine (DAMA-colchicine) elucidated the specifics of the colchicine binding site (Figure 20). The colchicine site is located in the intermediate domain of the β-subunit, caged by strands S8, S9, loop T7, and helices H7 and H8. Colchicine also interacts with the T5 loop of the adjacent α-subunit (Figure 18). It is also important to note the movement of the T7 loop and the H8 helix in the tubulin-colchicine complex when compared to the structure of the protofilament tubulin because, the movement of T7 and H8 allows more space for colchicine binding.[23]

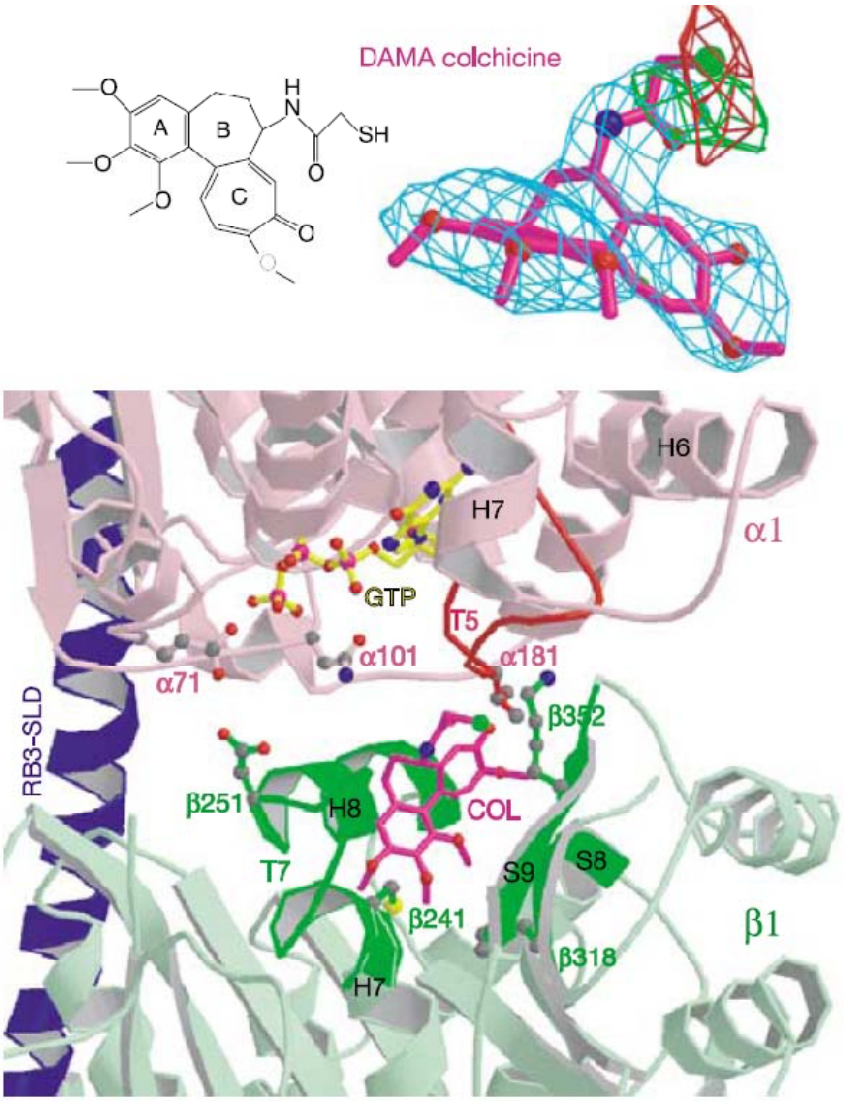

Figure 20. Structure of DAMA colchicine, and its binding to the Colchicine site of tubulin. Taken from Ref. 23 with permission.

Colchicine is known to hinder microtubule growth at low concentrations and depolymerize microtubules at high concentrations. Colchicine's effect on microtubules lies in its ability to obstruct lateral and longitudinal interactions between tubulin dimers. The M-loops of the tubulin subunits are important in lateral interactions of the tubulin subunits. Colchicine binding of tubulin causes the M-loop to be displaced by 9 Å in order to remove the steric clash of colchicine with the α-subunit (Figure 21). This kinked

structure lessens the lateral contacts of the tubulin dimers and hinders tubulin polymerization. It is believed that our colchicine site binding drugs will have the same deleterious effects on tubulin polymerization.

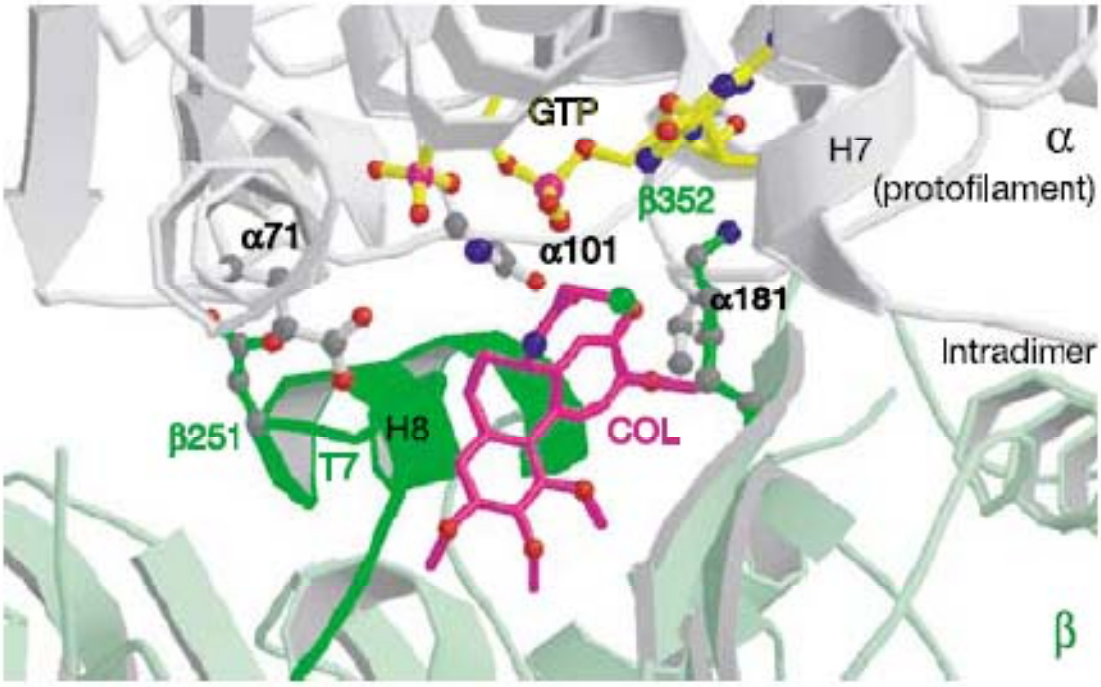

Figure 21. The interface between colchicine binding and the straight conformation of tubulin. The α subunit is kept from this position because steric hindrance of colchicine and residues α101, α181, and GTP. Colchicine also moves the T7 loop, H8 helix, and Lys β352 side chain to an interfering location with the α tubulin. Taken from Ref. 24 with permission.

Nguyen and co-workers[13] were able to further characterize the tubulin colchicine binding site using molecular modeling techniques with 15 compounds in conjunction with the X-ray data presented by Ravelli and co-workers.[23] Nguyen noted that Cys β239 of helix 7 is important in colchicine binding. Also, Thr α177 and Val α179, of sheet 5 and helix 5 respectively, may form hydrogen bonds with colchicine site inhibitors (CSIs). The width of the colchicine site is 4-5 Å which probably contributes to the tight binding

of the inhibitors. There are also two planes of binding with a ~45^{o} tilt that conform to the colchicine site, and it was noted that even inhibitors not having a biaryl structure adhere to the biplanar architecture. In all of the compound binding models, hydrogen bonding occurred with the thiol of Cys β239; hydrogen bonding occurred with the backbone nitrogen of Val α179 in 11 of 15 compounds; in eight of the compounds ordered water or conformational changes lead to hydrogen bonding with the backbone nitrogens of Ala β248, Asp β249, and Leu β250; in four compounds hydrogen bonding occurred with the backbone carbonyl oxygen of Thr α177 (Figure 7).[13] These aspects of the colchicine binding site were taken into consideration when designing the VDAs in this work.

Tubulin Purification

In vitro testing of suspected tubulin binding analogues is achieved with a tubulin binding assay. The *in vitro* testing requires a considerable amount of purified tubulin. Fortunately, Hamel and co-workers[24] have established an effective means of tubulin isolation. Dr. Mary Lynn Trawick has adapted the tubulin purification protocol to be suitable to our facilities (Figure 22).[80]

Using the following general procedure tubulin was isolated from bovine brain. Grey matter of brain tissue contains a high amount of microtubules, and was therefore separated from white matter, meninges, blood vessels, and blood clots. The brain tissue was then homogenized in a stabilizing solution containing 4M glycerol and other stabilizing components. Because tubulin can be polymerized with GTP at 37^{o}C and depolymerized at 0 ^{o}C, the protein was purified by a series of polymerizations and depolymerizations. Once polymerized, the solid tubulin can be separated by

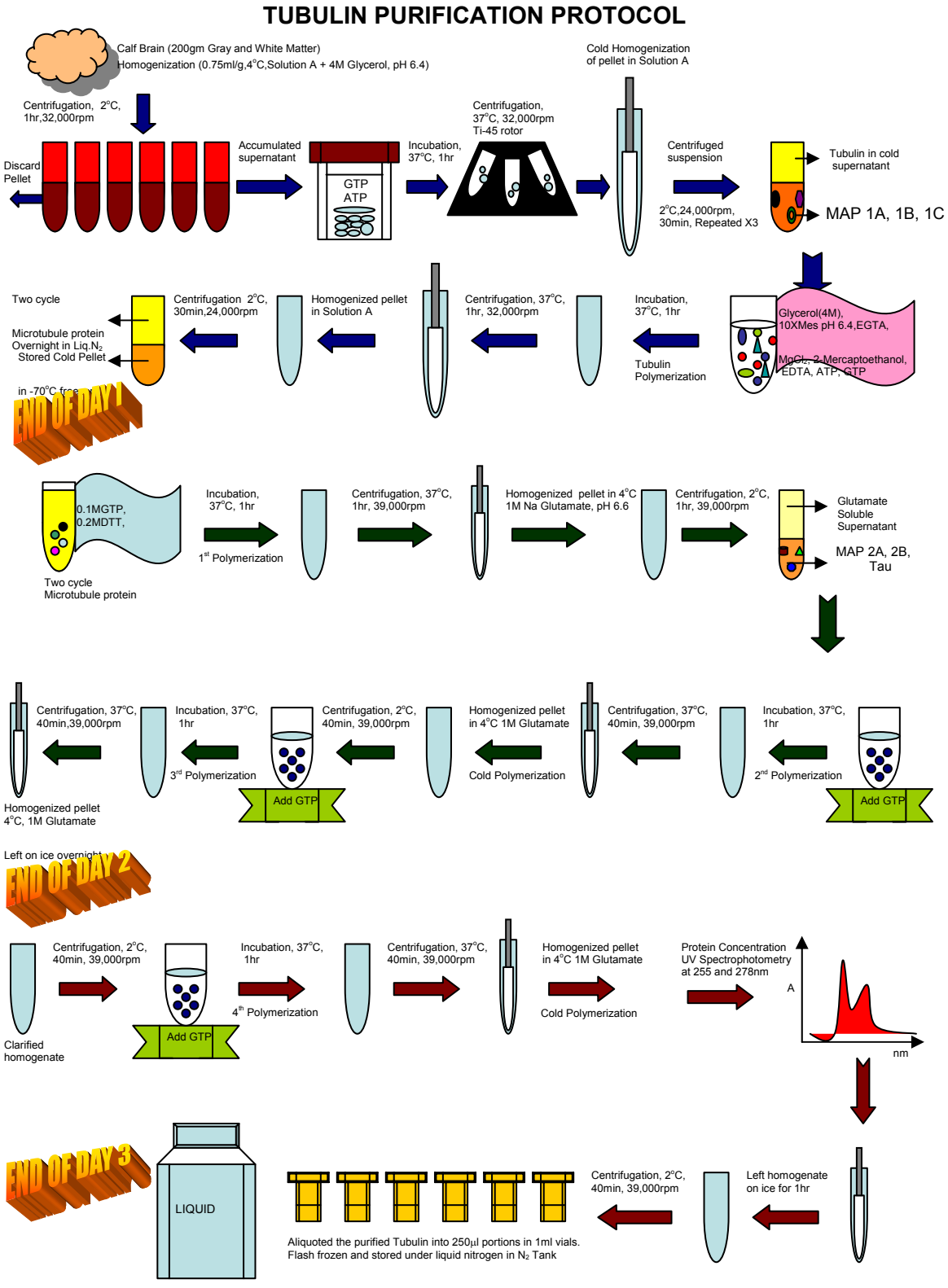

Figure 21. Schematic for tubulin purification. Tubulin isolated from bovine brain, and purified by a series of polymerization and depolymerizations. Reproduced from Dr. Benon Mugabe,[80] with permission.

centrifugation, forming a pellet of tubulin. The remaining proteins are in the supernatant and are discarded. The pellet is then homogenized in a suspension solution and depolymerized by cooling to 0 ^{o}C. Once the tubulin is depolymerized and soluble, ultracentrifugation was used to precipitate insoluble proteins and other material. The cold supernatant contains the depolymerized tubulin dimers, and is therefore saved for further polymerization/depolymerization purification cycles. Hamel has shown that a series of five polymerization/depolymerization cycles purified tubulin completely.[24] For our analysis, we also purified tubulin by five cycles. These five cycles yield very high purity tubulin that is necessary for reproducibility and accuracy of the tubulin assay.

The tubulin concentration should be determined for use in the polymerization assays. While there are many ways to determine protein concentration, Barbier and co-workers developed a method for high purity tubulin using UV spectrophotometry. By measuring the absorbance at 255 for the nucleotide and 278 nm for the protein, the approximate concentration of tubulin can be determined by using the following relationship:

Absorbance at 278nm = 1.20X + 7.66Y

Absorbance at 255nm = 0.65X + 12.17Y

X is the concentration of tubulin in mg/mL, and Y is the concentration of GTP-GDP in mg/mL. Multiplying X by the dilution factor gave the concentration of tubulin in the solution.[25] The purified tubulin was then used for microtubule polymerization assays and isothermal calorimetric (ITC) experiments. The tubulin was stored at a concentration of 10 mg/mL for ease and consistency when used for the tubulin polymerization assay and ITC.

In Vitro Evaluation of Vascular Disrupting Agents
Via Inhibition of Tubulin Polymerization

The tubulin polymerization assay is the most effective method for finding inhibitors of tubulin polymerization. *In vitro* testing is usually the first step in drug evaluation because of its laboratory practicality and cost effectiveness. The tubulin assay is an *in vitro* analysis used to determine the ability of a compound to inhibit the assembly of tubulin into microtubules. An IC_{50} value is the concentration of a drug that is required to inhibit 50 % of the enzymes activity.[6]

IC_{50} values for tubulin inhibitors are usually obtained from turbidity studies. Turbidity is the measurement of scattered light. These turbidity measurements are useful to follow the assembly and disassembly of microtubules *in vitro*. When microtubules are assembled, they scatter light at a frequency of 320-600 nm. The amount of scattered light is proportional to the concentration of microtubules formed in solution. The relationship between microtubule concentration and the amount of scattered light allows a means for quantification of the overall polymerization because the higher the amount of tubulin polymerization, the more light that is scattered.[26,27]

Compounds that bind tubulin and either inhibit or promote its polymerization can be quantified using turbidity measurements. Tubulin assays are most often performed with wavelength absorbance at 350 nm. Monomeric tubulin dimers and most ligands/cofactors do not absorb light at 350 nm. There are many advantages to using turbidity in monitoring tubulin assembly. First, relatively low amounts of tubulin are needed for turbidity studies, usually only 1mg/ml is required. Second, the system can be monitored without perturbing the interaction. Third, polymerization and depolymerization can be monitored continuously.[28]

Purified tubulin can be polymerized into microtubules with a 1M glutamate solution simply by adding GTP, warming to 37 ^{o}C, and then subsequently depolymerized by cooling to below 15 ^{o}C. The polymerization study is usually performed in a sodium glutamate solution. Sodium glutamate stabilizes tubulin by inducing hydration of the protein. This fact has been attributed to the decrease in the protein surface area that is accompanied by tubulin polymerization. High glutamate salt solutions increase the hydration and aggregation of tubulin. By self assembling, the tubulin decreases the total protein surface area, becoming thermodynamically more stable.[29]

When the tubulin polymerizes, it scatters light. The amount of scattered light per time can be recorded. If a compound inhibits the polymerization of the tubulin, then the total amount of light absorbed or scattered is diminished. There is an inhibitor concentration dependence on tubulin polymerization: a minimum inhibitor concentration in which 100% polymerization occurs, and a maximum concentration where 0% polymerization occurs (Figure 23). Evaluation of the tubulin polymerization data for a series of inhibitor concentrations is used to obtain an IC_{50} value for the drug.[26]

A pre-incubation time of the tubulin with the ligand has been found useful for increased accuracy of the tubulin assay. A pre-incubation at 30 ^{o}C for 15 min. is useful for maximum interaction between compounds that are weakly binding to tubulin. Pre-incubation is still preferred because it maximizes the potential for detecting drug-tubulin interaction and also gives more consistent data for slow binding ligands. The colchicine site tubulin binding drug 3-chloroacetyl-2-demethyl thiocolchicine has shown a decrease in its IC_{50} from 8 μM to 3 μM by pre-incubating with tubulin at 37 ^{o}C for 15 minutes. After incubation of the tubulin-ligand at 30 ^{o}C for 15 min., the system should be placed

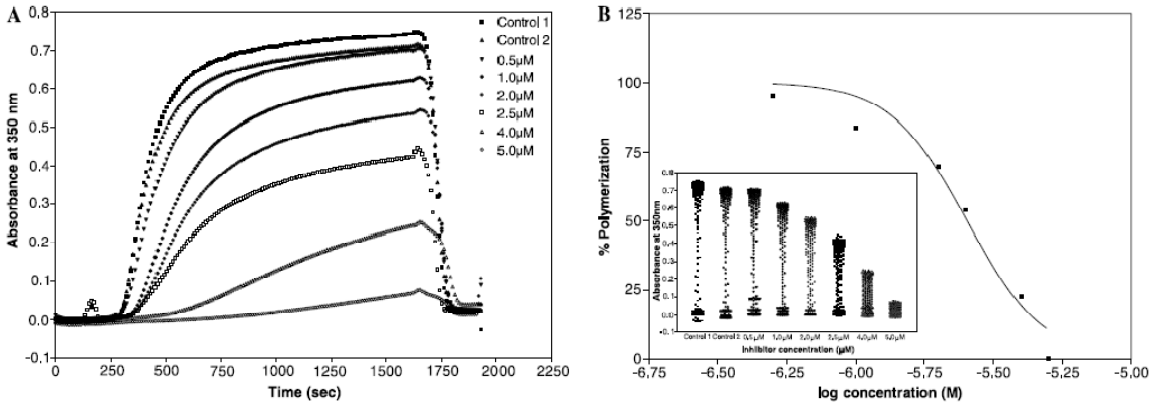

Figure 23. Inhibition of tubulin polymerization. (A) Turbidity study with varying concentrations of a potent tubulin polymerization inhibitor. (B) Logarithmic manipulation of the turbidity study. The anti-log of the concentration at 50% represents the IC_{50} value. Taken from Ref. 10 with permission.

on ice for 15 min. to allow the solution to cool before addition of GTP, which would result in polymerization.[26]

GTP purity and concentration consistency are crucial for accurate and precise polymerization measurements because GDP is a powerful inhibitor of tubulin polymerization. As little as 10 % GDP relative to GTP in solution will significantly inhibit polymerization. Optimal GTP concentrations are between 0.5-1.0 mM, and concentrations of GTP below 0.5 mM give slow, incomplete polymerizations. Using higher concentrations of GTP will increase IC_{50} values. By using 98 % pure GTP instead of 90 % pure GTP (contains 10% GDP), IC_{50} values measured for 3-chloroacetyl-2-demethyl thiocolchicine decreased from 2.1 μM to 0.63 μM.[26]

A variety of suspected tubulin binding agents from the Pinney group were analyzed for their ability to inhibit tubulin polymerization. Data was collected via turbidity studies at 350 nm, with 0.8 M glutamate buffer and 1.0 mM GTP. Compounds were pre-incubated with tubulin for 15 min at 37°C, then again at 0°C for 15 min. The

data was analyzed using a nonlinear regression via Prism software (GraphPad). The log IC_{50}, Hillslopes, R^2, and IC_{50} values of each analogue were determined from a plot of fractional polymerization against the log ligand concentration using the following relationship:

$$Y = \text{Bottom} + \left[\frac{(\text{Top} - \text{Bottom})}{1 + 10^{(\text{X-logIC50}) \text{ Hillslope}}} \right]$$

where X is the log ligand concentration, Y is percent polymerization, bottom is the lowest depolymerization absorbance value, Top is the highest polymerization absorbance value, Hillslope is the pitch of the slope, and IC_{50} is the X value when polymerization is halfway between Bottom and Top. The results of this study were used as a primary screening for potential VDAs to be used in further anti-cancer studies.

Thermodynamic Studies of CA-1 and CA-4 Binding Using Isothermal Titration Calorimetry (ITC)

ITC and Ligand Binding Parameters

The importance of characterizing the thermodynamic interactions of ligand binding to protein is gaining attention as an essential role in drug design rationale. Through understanding the thermodynamic interaction of ligand to protein, structure-activity relationships (SAR) can be hypothesized and therefore lead to more efficient drug design. By discovering the enthalpies of binding between two compounds of equal affinity, drug manufacturers may be able to select which compound should be used for further development.[31] Isothermal titration calorimetry (ITC) has the unique ability to measure binding interactions as a function of changes in heat. ITC is the only technique

that directly measures the enthalpy of binding (ΔH^o) and can be used to indirectly measure the association constant (K_a), stoichiometry (n), free energy (ΔG^o), and entropy (ΔS^o) of binding.[32] ITC is therefore a potentially valuable tool for the tubulin binding research presented here because it may help design more efficient drugs.

By using ITC, one can distinguish between different binding mechanisms of ligands with the same binding affinity. Hydrophobic additions to the ligand would increase the negative value of ΔG and $-T\Delta S$, while having positive ΔH values. An addition of a hydrogen bonding substituent would lead to an increase in the negative for ΔG and ΔH, but also positively results in a more positive shift in the $T\Delta S$. Ligands that undergo a conformational change upon binding are shown to have positive $-T\Delta S$ values and largely negative ΔH values (Figure 24).[33]

As previously mentioned, ITC is the only calorimetric procedure that directly measures the observed molar enthalpy (ΔH_{obs}). Without the use of ITC, an investigator would need to use the van't Hoff relationship, a time consuming process involving the plotting of the equilibrium constant as a function of temperature. The van't Hoff relationship can be expressed by two equations:

$$\text{(i)} \quad \frac{d \ln K}{dT} = \frac{\Delta_r H^\theta}{RT^2} \qquad \text{(ii)} \quad \frac{d \ln K}{d(1/T)} = \frac{-\Delta_r H^\theta}{R}$$

For an exothermic reaction under standard conditions, equation (i) shows that $d \ln K/dT<0$. A negative slope in equation (i) means K decreases as the temperature increases, and from equation (ii) the slope should be linear. The practicality of this method is unreliable and indirect.[33] Most thermodynamic data for tubulin binding

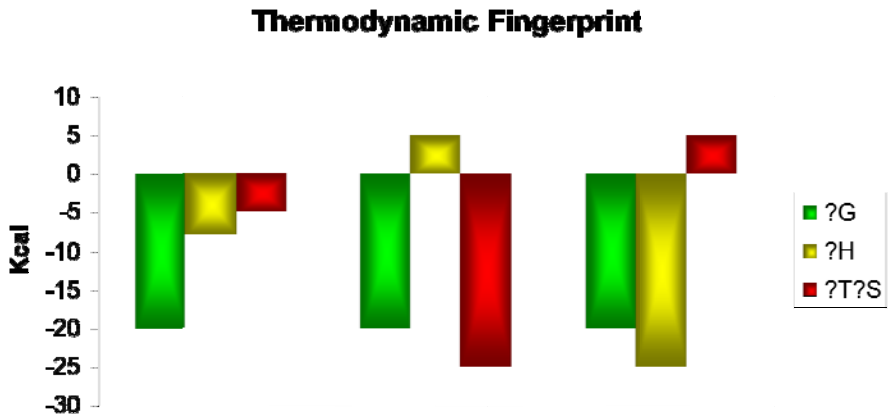

Figure 24. Thermodynamic fingerprints of different inhibitor binding modes.

ligands presented in the literature use the van't Hoft relationship for speculation of ΔH. We wish to directly measure the ΔH values for CA1 and CA4 binding to tubulin. Whereas, the enthalpy of binding can be measured by a single experiment, ITC can also offer K_b, and n values by calculation. In order for accurate calculations of n and K_b to be achieved, the binding constants must lie within the measurable range of 10^2-10^9 M^{-1}.[32] Titrations that lose their curvature cannot be accurately measured, because the K_b is derived from the slope of the curve. As such, experiments need to be chosen carefully. Correct protein/ligand concentrations must be found for accurate K_b determination. Molecules that are weak binding give almost horizontal curves that provide little information on ΔH or K_a. If the slope is too steep, information is provided about ΔH and n, but no information about K_a. For accurate K_a values to be achieved, the protein concentration should be the approximately the K_d value ($1/K_a$). Appropriate experimental design yields high quality data, with initial points giving information on the

magnitude of ΔH, points on the slope indicating affinity and stoichiometry, and final points indicating dilution and mixing effects.[32]

The heat evolved or absorbed from each injection is proportional to the change in concentration of bound ligand:

$$q = V \cdot \Delta H^{o} \cdot [L]_{bound}$$

where V is the volume of the reaction vessel and ΔH^{o} is the enthalpy of binding. The most common binding model is for a single set of identical binding sites and has been adopted for described experiments involving ligand binding to the tubulin colchicine binding site.[32] The binding of ligand to the tubulin colchicine binding site is stoichiometrically represented by one ligand binding per protein, or:

$$M + L_n \rightleftharpoons ML_n$$

The system is defined as the contents of the sample cell plus the ligand to be injected. The equation used to find the heat observed for the i^{th} injection is:

$$q_i = (\Delta H)_i C_i V_i + (\Delta H)_{i+1} C_{i+1} V_{i+1} + (\Delta H)_{inj} C_{inj} V_{inj}$$

where C is the concentration of the protein and V is the volume of the sample cell. Through a series of mathematical manipulations, the following equation can be formulated:

$$Q = V \bullet \Delta H \bullet \left([L] + \frac{1+[M] \bullet n \bullet K - \{(1+[M] \bullet n \bullet K - [L] \bullet K)^2 + 4 \bullet K \bullet [L]\}^{1/2}}{2 \bullet K} \right)$$

where ΔH is the enthalpy of binding, K is the binding constant, n is the number of binding sites, V is the volume of the cell, [L] is the total ligand concentration, and [M] is the protein concentration. By fitting to the Q vs. $[L]_{total}$, an estimation of n, K_a, and ΔH^o can be made.

The familiar sigmoid curve that is associated with ITC is performed by plotting the incremental heat signal (1st derivative of Q with respect to $[L]_{total}$) against the molar ratio ($[L]_{total}/[M]_{total}$). With the ΔH and K_b values known, the free energy (ΔG) and entropy (ΔS) can be calculated using the following equation:

$$\Delta G = -R \bullet T \bullet \ln K_b \qquad \Delta S = \frac{(\Delta H - \Delta G)}{T}$$

Tubulin Binding Agents and ITC

Tubulin binding agents are known to interfere with microtubule assembly and disassembly. Colchicine is a well studied inhibitor of mitosis, binding to tubulin at the colchicine binding site with high affinity for K_b at 1.6×10^7, a ΔH of -20.9 $kJmol^{-1}$ and a ΔS of +64.8 $J K^{-1}$.[34] The tubulin/colchicine binding pathway involves a two step mechanism with a fast initial and reversible bimolecular binding reaction, followed by a slow monomolecular binding reaction shown below.[35-37]

$$\text{Tubulin Col.} \underset{}{\overset{k_1}{\rightleftharpoons}} \text{Tubulin•Col.} \underset{k_{-2}}{\overset{k_2}{\rightleftharpoons}} \text{(Tubulin•Col)'}$$

To date, enthalpies of binding for colchicine have been obtained through indirect means such as radiolabeling or competitive binding assays. Here the ΔH values were determined directly.

Thermodynamic profiles of antimitotic sulfonamides were reported by Banerjee and coworkers in 2005.[41] They used ITC as the method for obtaining thermodynamic values. While these small molecules do not resemble colchicine, they are still known to bind the colchicine-binding site of tubulin with high affinity, having IC_{50} values of 2-4 μM.[38-40] By using ITC, Banerjee and coworkers[41] were able to determine which of the compounds were binding with higher heats of enthalpy and which were driven by entropic rearrangement. Their reported standard deviations were within experimental error, suggesting that ITC is a sensible method for measuring small molecule binding thermodynamics to the tubulin colchicine binding site.[41]

Unfortunately, during the course of our work, Rappl and co-workers[42] reported the thermodynamic properties of combretastatin A-4 using ITC. Before running the ITC measurements, the group wanted to ensure that no tubulin self association was occurring. By using analytical ultracentrifugation, Rappl compared the sedimentation coefficients of 0.25 mg/mL tubulin alone (5.47 S) with tubulin in the presence of excess CA4 (5.51 S). The similarity of the sedimentation coefficients reflected the lack of self-association of the tubulin dimers. Rappl's ITC experiment was performed with a MicroCal MCS titration calorimeter. The ligand was titrated as 5μL aliquots at a concentration of 0.36 x 10^{-3} M into a 1.34 mL calorimeter cell containing tubulin at a concentration of 1.5-2.0 x 10^{-5} M. To avoid solubility issues with the hydrophobic compounds, all experiments were done in PG buffer with 10% DMSO.[42]

Rappl reported very clean ITC profiles of CA4 binding to tubulin. Using these data, Rappl and co-workers calculated the K_a of CA4 binding = (1.88 ± 0.23) x 10^6 M^{-1}, with the number of binding sites = 1.0 ± 0.1.[42] The exothermic heat exchange was

measured directly as $\Delta H = -37.2 \pm 3.3$ kJ/mol.[42] The calculated entropy was slightly negative ($T\Delta S = -1.7 \pm 3.3$ kJ/mol) and is therefore unfavorable in the formation of the tubulin compound complex.[42] CA4 binding to tubulin is apparently enthalpically driven. Because the thermodynamic parameters for CA4 have been obtained, it was evaluated utilizing ITC experiments for comparative reasons. A benzophenone derivative was also evaluated through ITC against tubulin to determine the differences in binding parameters between combretastatin and phenstatin derivatives.

ITC Research

Difficulties in using tubulin for ITC studies might be a contributing reason for the lack of literature in the area. According to Banerjee, the tubulin concentration for the reported sulfonamides was ~2.2 mg/mL. The typical ITC cell is between 0.5 mL and 1.5 mL, meaning that 1-3 mg of tubulin is used per ITC run. Considering that many runs may be necessary for achievement of an acceptable curve, thousands of dollars worth of tubulin may be used to obtain data for a single compound. This cost is overcome by the isolation of tubulin previously described. Another factor affecting results of perceived ITC experiments is tubulin polymerization/depolymerization, which might lead to excess heat evolution/absorption. This error is negated by two precautions. All GTP is removed from the system by dialysis into PEM buffer containing GDP. The lack of GTP should hinder the polymerization of tubulin dimers into polymers, as GTP is necessary for tubulin polymerization. It is also possible that dilution of the tubulin from the titration could lead to changes in enthalpy. This error can be circumvented by running a blank titration of tubulin and buffer. Protein interactions caused by dilution can then be

subtracted from subsequent titrations of PEM into tubulin buffer. This same logic is used for blanks of ligand into buffer, and is then subtracted from ligand-tubulin titrations.

ITC was employed to determine the ΔH, K, and n values for CA1, CA4, and benzophenone **37** (Figure 25). Because ITC directly measures ΔH, the values recovered from experimentation are more accurate than those recovered when using the Van't Hoff relationships. All ITC experiments were determined in PEM buffer as in reported literature,[41] with ligand/protein concentrations adjusted to obtain the most informative thermodynamic curves. The thermodynamic values of binding for each molecule were recorded and compared.

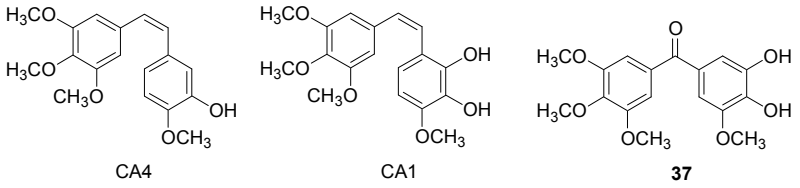

Figure 25. Compounds evaluated by ITC.

Vascular Disrupting Nitric Oxide Synthase Inhibiting Co-Salt Formulations

Physiological Role of Nitric Oxide

Nitric oxide (NO) is an important cell-signaling molecule that is responsible for a variety of biological processes including blood vessel tone and fluidity, neurotransmission, and immunity. Because NO is a small molecule, it diffuses the cell membrane rapidly and is metabolized quickly. Most of the cell-signaling activities involve the synthesis of the secondary messenger cyclic GMP (cGMP), which is in turn responsible for vasorelaxation within smooth muscle cells. NO controls angiogenesis by

increasing the mitotic index of microvascular endothelium. Also, because NO up-regulates cGMP, pro-angiogenic factors such as VEGF and FGF-2 are over expressed which also facilitates angiogenesis.[43] Angiogenesis works against VDA action by forming new vasculature, and NO re-establishes disrupted tumor vasculature. By combining into one compound entity elements of CA4P and Oxi8007 may be accentuated when administered with NOS inhibitors.

NO Production

Nitric Oxide is synthesized by nitric oxide synthase (NOS), a heme-containing metalloenzyme. NOS converts L-arginine to L-citrulline and NO via a 5-electron NADPH-dependent oxidation. There are three identified NOS enzymes within mammalian systems: neuronal NOS (nNOS), inducible NOS (iNOS), and endothelial NOS (eNOS). The three isozymes are >50% homologous, and all are homodimeric proteins of 125-160 kD. The functional NOS enzyme is a homodimer; however, each dimer contains a reductase domain that binds NADPH, FAD, and FMN, and an oxygenase domain that binds tetrahydrobiopterin (H_4B), arginine, and O_2. The oxygenase domain is ~500 residues and catalyzes both steps in the conversion of arginine to citrulline and NO. The reductase domain NADPH is suspected to transmit electrons to the FAD, then to the FMN, then to the heme in the oxidase domain. The heme iron is coordinated with a cysteine.[78]

L-Arginine binds near heme on the side opposite the cysteine with its nitrogen atom to be hydroxylated pointing toward the heme. Oxygen is well known to react with heme; therefore, it probably binds between the heme iron and the N to be oxidized on the L-arginine.[78] Unlike the function of heme, the role of H_4B is not known. Within each

dimer lies a calmodulin (CAM) binding site that is responsible for calcium binding and NOS regulation.[6,44] Hydroxylation of an arginine amidine is the first step in the NOS mechanism to form NO. The hydroxylation uses one equivalent of NADPH and O_2. Presumably one of the oxygen atoms from the elemental molecule forms the N-hydroxyl amine (NHA), though this theory has never been proven.[44] The following steps in the conversion of the NHA to citrulline are less clear (Figure 26). An additional half equivalent of NADPH and another equivalent of O_2 are required. Most NOS models are reproduced from an aromatase P450 and involve a Fe^{III}-OO^-. In the third step, NHA provides one electron, while the other comes from the reductase NADPH. NO and citrulline formation follow the reaction of the ferric peroxide on the guanido carbon (Figure 26).[78]

NOS Inhibitors

Tumor growth has been associated with NO overproduction, and most tumor masses generate NO. Metastasis of tumors has been linked with angiogenesis which NO overproduction facilitates by increasing vascular tone and increasing vascular growth factors. Increasing the levels of NO within colon adenocarcinoma gave an increase in tumor growth and vasculature because of an up-regulation in VEGF. Wild type cancer cells with low levels of NO did not exhibit the same increase in growth.[43]

A variety of NOS inhibitors have been synthesized to battle the deleterious effects of NO overproduction. These inhibitors can be categorized into six different groups: drugs hindering cellular L-arginine uptake, compounds that limit the amount of cofactors necessary for the oxidation of L-arginine, compounds that interfere with the heme moiety, inhibitors of NOS expression, competitors of L-arginine/NOS binding, and compounds

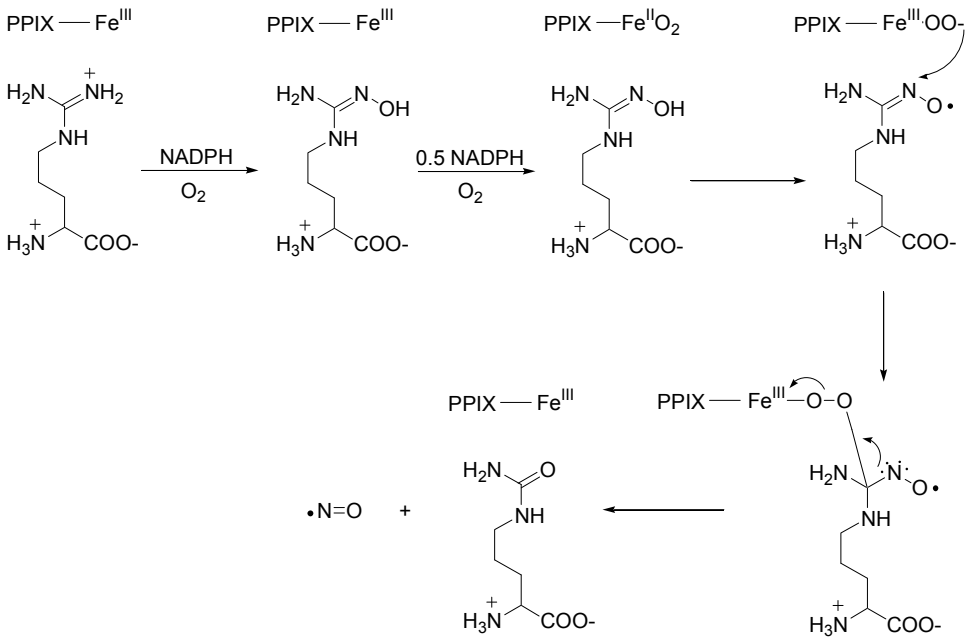

Figure 26. NOS synthesis of L-citrulline and NO from L-arginine.[78]

that scavenge NO. The L-arginine derivative to be first reported as an inhibitor of NOS was L-NMMA (L-N^G-monomethyl arginine), which was shown to reduce NO formation.[45] Compounds like L-NMMA are reversible competitive inhibitors (Figure 27). The methyl ester of L-NNA (L-N^{ω}-nitro arginine) L-NAME (L-N^{ω}-nitro arginine methyl ester) has also proven effective at inhibiting NO levels of tumor tissues and is already FDA approved for lowering NO levels in non-tumor tissues studies.[45]

Use of NOS Inhibitors in Conjunction with CA4P

Though preclinical trials have shown that vascular disrupting agents are effective against a wide variety of solid tumor types, one model, SaS round cell sarcoma in Carter Bagg Albino (CBA) mice, is resistant to CA4P.[46] This cancer cell line produces high

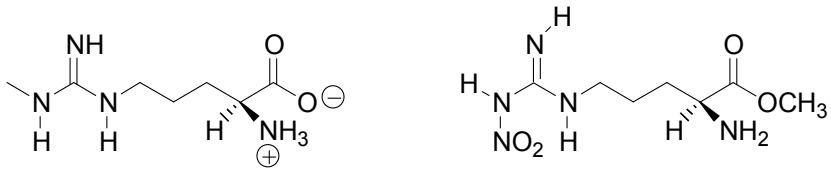

L-NMMA L-NAME

Figure 27. Structures of potent NOS inhibitors L-NMMA and L-NAME.

levels of NO. High levels of NO protect tumor vasculature against the effects of CA4P, presumably through NO's pro-angiogenic activity.[46] Administration of L-NAME and L-NMMA in conjunction with CA4P has not only been shown to decrease CA4P drug resistance among certain cancer cell lines, but also increases the potency of the CA4P against CaNT tumors.[46,47] L-NNA, the drug form of L-NAME, when used in conjunction with CA4P, increased the necrosis scores of CA4P treated SaS tumors from 1 to 9, or from 0% to >81% (Figure 28).[47] There is also a massive decrease in vascular volume (Figure 29) within CaNT tumors when CA4P is used in conjunction with an NOS inhibitor in a 2:1 ratio (NOS inhibitor: CA4P).[47]

NOS inhibitor	Dose (mg/kg)	Without CA4P (*n*)	With CA4P (*n*)
None		1 (20)	1 (6)
L-NNA	10	1 (3)	9 (3)*
L-NMMA	10	ND	2 (5)
L-NMMA	50	1 (3)	8 (3)*
L-NIO	10	1 (3)	4 (3)*
L-NIL	10	1 (3)	5 (3)
S-MTC	50	1 (3)	5 (3)
S-EIT	10	1 (3)	8 (3)*
AMT	10	1 (3)	9 (3)*
L-TC	50	1 (3)	7 (3)*

Figure 28. Necrosis scores of SaS tumors treated with CA4P (500 mg/kg) and NOS inhibitors. Taken from Ref. 47 with permission.

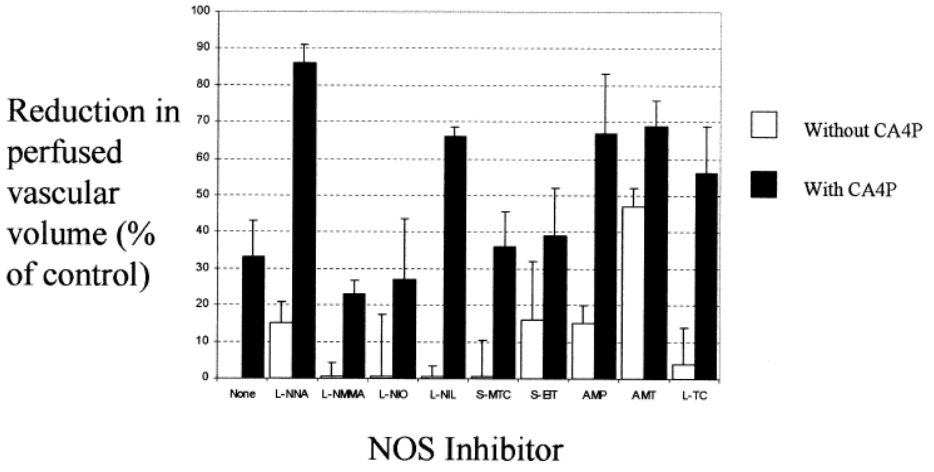

Figure 29. Reduction in tumor vasculature by NOS inhibitors (10 mg/kg) with and without CA4P (25 mg/kg) in CaNT tumor. Taken from Ref. 47 with permission.

NOS/VDA Salt Research

In an effort to continue clinical research on these potent formulations, scale-up reactions of CA4P/L-NMMA, and CA4P/L-NAME (Figure 30) were carried out. Within the Pinney group, several biologically relevant VDA salts have been made.[14-17,113,115] Formulations of these VDA salt prodrugs, like Oxi8007, were made with L-NAME

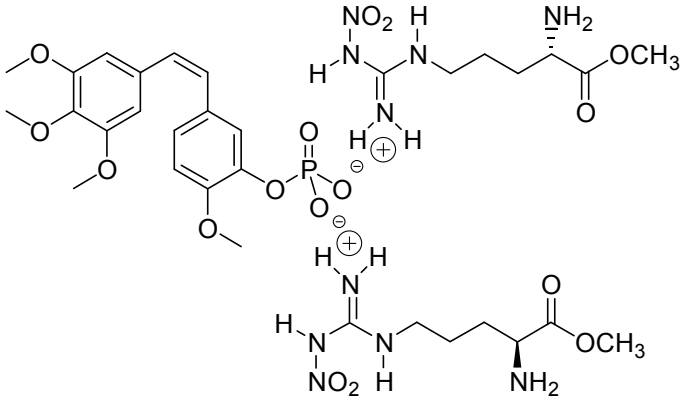

Figure 30. Possible structure of CA4P/L-NAME co-salt formulation in 2:1 ratio.

and L-NMMA in an effort to increase their anti-tumor vascular activity and decrease their drug resistance. The L-NMMA free base is no longer available for commercial purchase, so it was be synthesized, as was the free acid of CA4P.

Screening of Potential Inhibitors of Hypoxia Inducible Factor (HIF-1) Alpha

Research Rationale

If a drug can reduce the amount of intracellular HIF-1α, then the tumor will have less chance of survival in hypoxic regions. Mammals consume more oxygen (O_2) than any other organic or inorganic substance.[48] Oxygen can only diffuse 100-180 μm away from the capillaries before it is completely metabolized, so any cell further from than 180 μm from a capillary will be in areas of low oxygen, called hypoxic locations.[48] When tissue levels are ~2-21 % O_2 (pO_2 15 mmHg-159 mmHg), they are in normoxic conditions and convey normal phenotypic cellular functions,[49] but when O_2 levels are ~1 % O_2 ($pO_2 \leq 10$ mmHg), the region is considered hypoxic and shows an abnormal phenotype.[60] Hypoxia within the tumor microenvironment gives chemotherapeutic resistance to tumor cells and is associated with metastasis and poor survival.[50] HIF-1α is a protein that is responsible for tumor survival in hypoxic areas, as well as chemotherapeutic drug resistance. Screening the Pinney group drug library[14-17,113,115] for compounds that can inhibit HIF-1α allowed us to find chemotherapeutics that are effective at inhibiting HIF-1α accumulation.

Physiological Role of HIF-1α

Nature has battled hypoxia by incorporating a hypoxia response element (HRE) into seemingly all mammalian systems.[49,51] HRE is the enhancer region for over thirty hypoxia-inducible genes, and when activated it is responsible for the up-regulation of many proteins designed to cope with cellular stress. The HIF effector genes encode for vascular endothelial growth factor (VEGF), glucose transporters, erythropoietin (EPO), and various other proteins that are connected to cellular metabolism (Figure 31). HRE

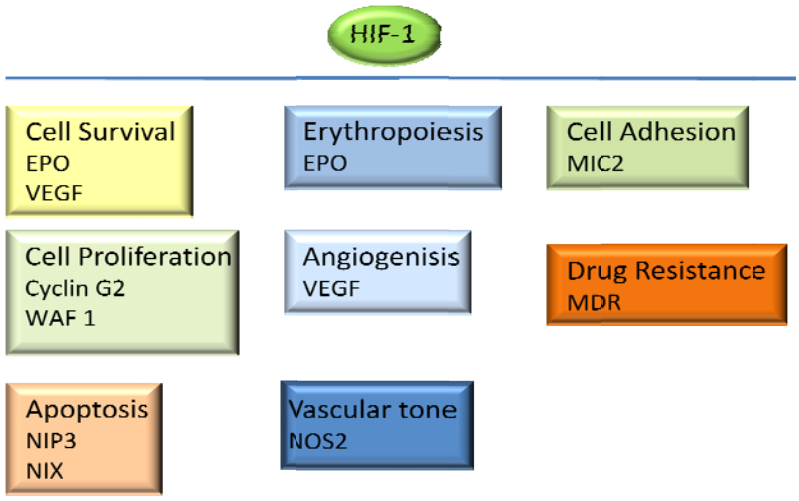

Figure 31. HIF-1α effector proteins. HIF-1α is responsible for up-regulating various genes that are responsible for increased cell proliferation, cell survival, vascular tone, drug resistance, etc. Modified from Ref. 54.

was initially identified as the 50-base pair sequence in the 3′ region of the EPO gene. The core HRE DNA binding element is the 5-bp unit 5′-ACGTC-3′, and is used to denote the DNA binding location of the HIF protein. Hypoxia-inducible Factor 1 (HIF-1) is the transcription protein utilized in binding the 5′-ACGTC-3′ element region and activating gene expression.[52] HIF-1α over expression has been reported in 70% of tumors. Cancers

that have higher amounts HIF-1α experience increased rates of metastasis when compared to normal tissues.[52] Because HIF-1α is up-regulated by a variety of different mechanisms, and its expression is so widely distributed among cancer cell lines, HIF-1α is an important target in anticancer therapy.[50]

HIF-1α Enzymology

HIF-1 is a heterodimer of HIF-1α and HIF-1β. Both subunits are of the basic helix-loop-helix (bHLH) family containing PER-ARNT-SIM (PAS; where PER is the *Drosphilia* period clock protein, ARNT is aryl hydrocarbon receptor nuclear translocator, and SIM is the *Drosphilia* single-minded protein); however, the HIF-1α subunit is 120 kDa, whereas the HIF-1β subunit is 91-94 kDa. The bHLH domain of each subunit is located near the N-terminus preceding the PAS domain and is important for the protein binding to DNA. The N-terminal half of the PAS domain is responsible for protein dimerization and binding to DNA. The two transcriptionally active domains in HIF-1α are the N-terminal activation domain (NAD) and the C-terminal activation domain (CAD). The HIF-1α domain also contains an oxygen dependent degradation domain (ODD) that controls the protein's stability and is the regulating subunit of the heterodimer. The ODD domain overlaps the NAD domain (Figure 32).[53]

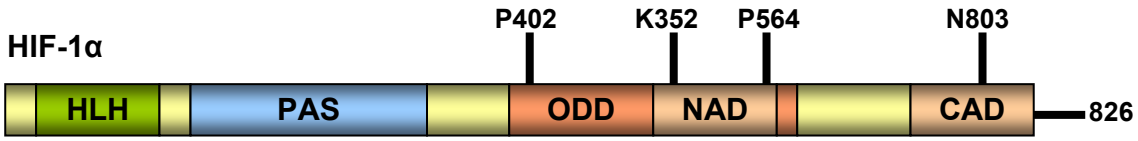

Figure 32. The domain structure of HIF-1α with relative positions of ODD, NAD, and CAD. Proline residues 402 and 564, as well as lysine 352 are important for HIF/VHL interactions. Figure modified Ref 49.

HIF-1α Activation

Activation of HIF can occur by several different pathways, but hypoxia is the physiological pathway. Co^{2+}, Ni^{2+},and Mn^{2+} divalent cations can be used to induce HIF activation, as can iron chelation. The term "hypoxia inducible factor" is deceptive because it implies an up-regulation HIF; however, HIF production is not increased, HIF degradation is decreased, causing an increase in overall HIF activity.[53] Oxygen is responsible for the main regulatory effects for HIF-1α. In the presence of oxygen, HIF-1α has a half-life of <5 minutes. Low oxygen levels increase the half-life and the transcriptional impact of HIF-1α within the cell.[53]

HIF-1α Degradation

The normoxic degradation of HIF-1α occurs through an ubiquitin-proteosome degradation pathway that targets the ODD domain. The Von Hippel-Lindau protein plays an important role in HIF-1α degradation. Cells that have lost the Von Hippel-Lindau (VHL) tumor suppressor gene exhibit higher HIF-1α accumulation. VHL protein binds with elongin B, elongin C, and cullin to convert VHL to an E3 ubiquitin ligase for HIF-1α polyubiquitination. The binding of VHL protein to HIF-1α requires the ODD, because the deletion of the ODD has shown that HIF-1α is stable in the presence of VHL.[53] The VHL labels the HIF-1α with ubiquitin, which marks it for proteolysis by 26S proteasome (Figure 33).[52,53]

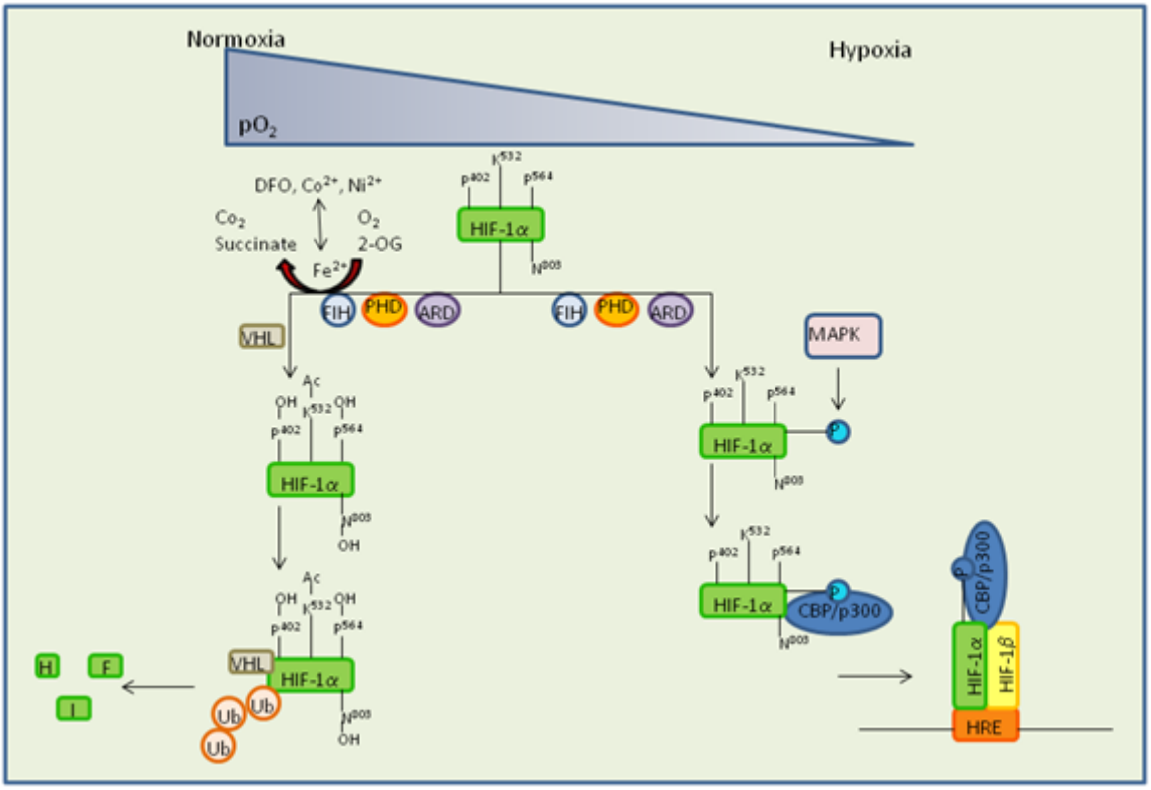

Figure 33. HIF-1α regulation pathways. Under normoxic conditions HIF-1α is oxidized by VHL, then marked via ubiquitin and degraded. In hypoxic conditions the lack of oxygen hinders VHL function. MAPK can then phosphorylate HIF-1α, which can then bind CBP/p300 and HIF-1β and carry out transcription functions. Modified from Ref. 49 and Ref. 53.

VHL Protein Binding To HIF-1α

VHL binds the 530-650 amino acids of HIF-1α. Proline 564, proline 402, and Lysine 532 are the most important residues for VHL binding to HIF-1α.[53] Under normoxic conditions, the two proline residues are hydroxylated by a family of prolyl-4-hydroxylases. The lysine residue is acetylated. VHL/HIF-1α interactions occur because VHL has a single hydroxyproline binding pocket for HIF-1α.[53] The prolylhydroxy domains (PHDs) require Fe^{2+}, O_2, and ascorbate for the proline hydroxylation. During the hydroxylation process, one oxygen is transferred to the proline, and the other reacts with the 2-oxoglutarate to form succinate and CO_2 (Figure 34).[35] The iron is coordinated

with two histidine residues, and one aspartic acid residue within the PHD active site and forms a 2-histidine-1-carboxylate coordination motif. The ascorbate is necessary to maintain iron in the ferrous (Fe^{2+}) state, which is important for PHD. Iron chelators and certain divalent metal cations such as Co^{2+}, Ni^{2+} , and Mn^{2+} are able to stabilize HIF-1α by either diminishing the amount of Fe^{2+} or substituting the iron from within the PHD binding site, which renders the protein inactive.[49,52,53] Fe^{2+} was substituted with Co^{2+} in order to decrease the VHL activity and increase the amount of intracellular HIF-1α.[56]

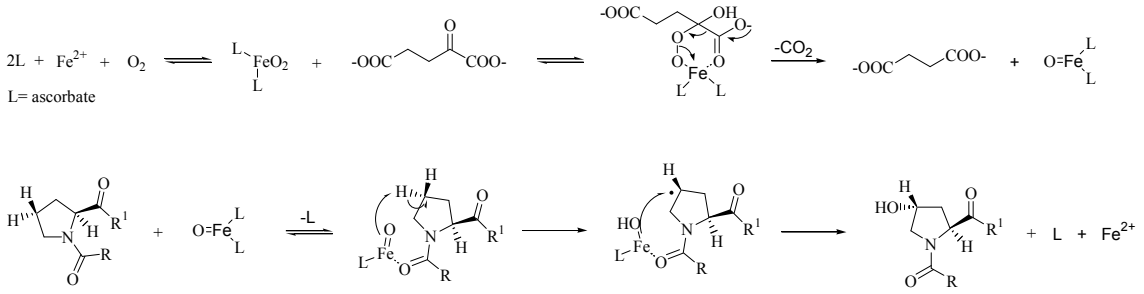

Figure 34. Mechanism for the hydroxylation of proline by prolyl hydroxylase. Modified from Ref. 61.

After the proline residues are hydroxylated, pVHL binds to HIF-1α via a surface pocket that is specific for the HIF-1α hydroxyproline. The pVHL then coordinates with elongin C, elongin B, cullin-2, and Rbx1 to form a VCB-CUl2 E3 ligase, which causes the polyubiquitination of HIF-1α. The pVHL E3 ligase is found in a variety of tissues, and though the ligase is found mainly in the cytoplasm, it also has the ability to migrate into the nucleus.[49]

While the hydroxylation of proline 564 and 402 are most important in regulating HIF-1α activation, other amino acids have been implicated in HIF-1α regulation. Arrest-deffective-1 (ARD1), an acetyl transferase, is responsible for the acetylation of lysine 532

which is located with the ODD domain. The acetylation of Lys532 supports the coordination or HIF-1α and pVHL, which destabilizes HIF-1α. The acetylation of Lys532 is not controlled by oxygen.[49]

Other Mechanisms of HIF-1α Regulation

The second key method for HIF-1α regulation involves manipulation of the CAD and NAD domains, which are responsible for interacting with CBP/p300, SRC-1, and TIF2.[53] In normoxic conditions, asparagine 803 (Asn803) located within the CAD domain of the HIF-1α, is hydroxylated by factor inhibiting HIF-1 (FIH-1). The hydroxylation of Asn803 prevents the interaction of HIF-1α with CBP/p300, which inhibits transcription of target genes.[53] Hypoxic conditions prevent the hydroxylation of Asn803 and allow HIF-1α activation. FIH-1 is another example of a 2-OG-dependent dioxygenase that requires iron and ascorbate cofactors. Since FIH-1 uses O_2, it is the second oxygen sensor for HIF-1α regulation.[49,52]

Phosphorylation of HIF-1α is also important in its regulation and is controlled by mitogen-activated protein kinase (MAPK) p42/44. The exact site of phosphorylation has yet to be identified; however, threonine 796 is the most likely target within HIF-1α.[53] In addition, cytokines, growth factors, external stimuli, and various other signaling pathways are expected to control HIF-1α by activation of MAPK, whereby they migrate from the cytosol into the nucleus where they can phosphorylate HIF-1α.[49]

HIF-1α Regulation and Microtubule Dynamics

Most recent attempts at unraveling mechanisms of HIF-1α activation have focused on microtubule disruption. Microtubule disruption with 2-methoxyestradiol

(2ME2) slows tumor growth and decreases angiogenesis, presumably by inhibiting HIF-1α activity.[55]

Escuin and co-workers wanted to clarify whether HIF-1α inhibition by 2ME2 was specific for the compound, or if the HIF-1α inhibitory effects were a property of all microtubule disrupting agents.[50] A variety of tubulin binding drugs including taxol, vincristine, epothilone B, colchicine, and discodermolide were used for their known microtubule disrupting ability. Human ovarian 1A9 and breast MDA-MB-231 cancer cell lines were treated with varying concentrations of the selected drug panel, and the HIF-1α content was revealed using western blot techniques. Throughout the panel, HIF-1α was inhibited in a dose-dependent manner, regardless of whether the drug was a microtubule stabilizing or destabilizing agent. To determine if the drug panel prevents HIF-1α synthesis or if the drug increases HIF-1α degradation, Escuin and coworkers co-incubated the cells with the desired microtubule disrupting agent and MG-132, a known inhibitor of HIF-1α degradation. In this case, the synthesis rate of the protein can be assumed because the proteosomal degradation of HIF-1α is impaired. It was shown that 25 nmol/L vincristine and epothilone B in the presence of MG-132 resulted in lower HIF-1α accumulation, suggesting that the different microtubule disrupting agents all down regulate HIF-1α synthesis.[50]

Mabjeesh and co-workers have raised an interesting hypothesis concerning the interaction between microtubule disruption, mRNA localization, and HIF-1α knockdown.[55] Several mRNA species require microtubule assemblies for transport and localization within the eukaryotic cell. By using PC-3 cells double labeled with antibodies against α-tubulin and HIF-1α, then treated with 2ME2, Mabjeesh and

coworkers wanted to identify if there was a link between the 2ME2 effects on HIF-1α and microtubules. As seen from Figure 35, there was a 2ME2 dose dependent depolymerization of the microtubule network. No depolymerization of microtubules within the hypoxic control cells was observed. HIF-1α was scarcely detected in the normoxic control cells, but was detected in nucleus the hypoxic control cells. Administration of 2ME2 decreased the nuclear

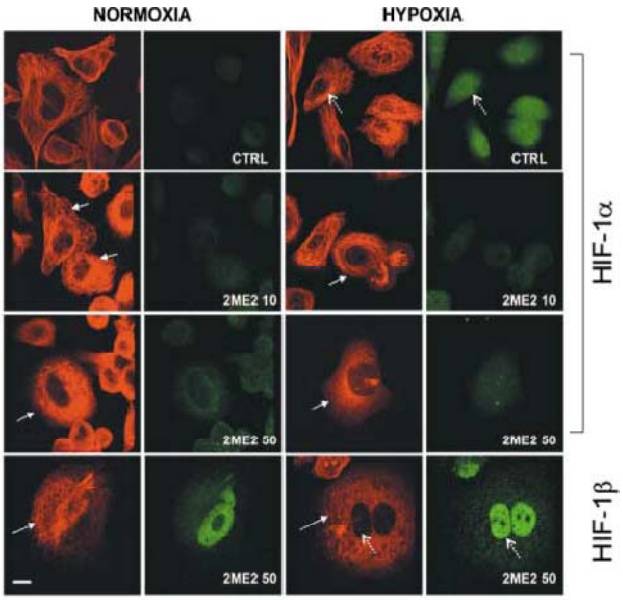

Figure 35. 2ME2 effects on HIF-1α. PC-3 cells were incubated in either normoxic, or hypoxic conditions with indicated concentrations of 2ME2. Taken from Ref. 55 with permission.

accumulation of HIF-1α in the hypoxic cells, suggesting that the microtubule network is necessary for relocating HIF-1α from the cytoplasm to the nucleus before it is degraded.[55]

Mabjeesh and coworkers were curious as to whether microtubule stabilization also would inhibit HIF-1α within the nucleus. In a separate experiment, they once again labeled tubulin and HIF-1α within PC-3 cells, but treated them with 10μM taxol (a

known microtubule stabilizer) or 10μM vincristine (a known potent microtubule depolymerizer). Interestingly, from Figure 36, taxol also inhibited the migration HIF-1α into the nucleus. The similarity of microtubule stabilizers and destabilizers in relevance to HIF-1α migration led Mabjeesh and coworkers to the hypothesis that disruption of the microtubule dynamic is a mechanism of HIF-1α regulation.[55]

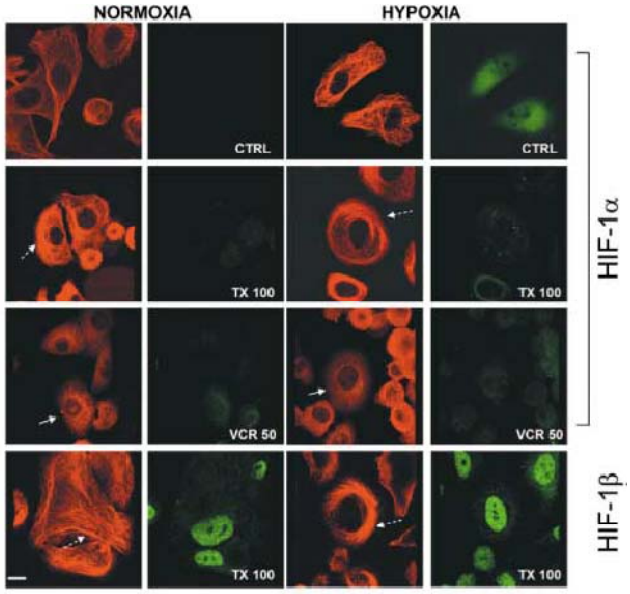

Figure 36. Effects of Taxol and vincristine on HIF-1α. PC-3 cells were incubated in either normoxic, or hypoxic conditions with indicated concentrations of taxol or vincristine. Taken from Ref. 55 with permission.

The results submitted by Mabjeesh and coworkers suggest that the disruption of the microtubule dynamics will lead to HIF-1α inactivation. This result is in correlation with a previous publication by Escuin and co-workers, in which 2ME2 and drugs within the taxane family proved to inhibit HIF-1α activity though disruption of microtubules.[50]

The relationship between microtubule disruption and HIF-1α is not universally supported throughout the literature. Jung and coworkers discovered that vincristine

increased HIF-1α by an NFkB-dependent pathway via microtubule disruption.[82] Jung dosed A549 cells with vinblastine, colchicine, nocodazole, or the microtubule stabilizer paclitaxel, and monitored the HIF-1α produced. All cells treated with microtubule disrupting agents increased the amount of HIF-1α extracted from the nucleus. These results were obtained after the cells were incubated with the MDAs for 4 h. Jung and coworkers investigated the effects of vinblastine over longer periods of time. The initial HIF-1α response is lessened after a period of 5 h.[82]

HIF-1α Research

With such contrasting data available in the literature, more research must be done to elucidate the link between microtubule disruption and HIF-1α, if such a link exists. The Pinney group has made numerous tubulin inhibitors that have a wide range of cell line activity within the past decade.[14-17,113,115] The Tubulin binding agents also have varying tubulin IC_{50} values. Because the literature information available is contradictory in regards to HIF-1α activity and microtubule disruption, the Pinney and Trawick groups may be able to use their compound library and analytic biochemistry techniques to relate corresponding microtubule depolymerization activity with HIF-1α inactivation. By correlating the tubulin activity IC_{50} values with HIF-1α inhibition, the relationship between microtubules and HIF-1α may be elucidated.

Of the many cell lines that can be used in determining HIF-1α inhibition, HeLa cells may be the most appropriate for the HIF study. HeLa stands for the first two letters of the first and last name of Henrietta Lacks, the woman whose cancer cells were immortalized within the laboratory by Dr. George Grey in the 1950's.[55] The robustness of this cell line makes it laboratory compatible. Furthermore, HeLa cells have been

shown to produce markedly elevated levels of HIF-1α expression when dosed with $CoCl_2$. Exposure to $CoCl_2$ produces maximal HIF-1α detection limits in four hours, presumably by inhibiting the prolyhydroxylase from hydroxylating P564 and P402 thereby inhibiting VHL binding to HIF-1α.[56]

Because HeLa cells are so easily grown, and because they have a dramatic response to $CoCl_2$, they were chosen as the cell line used in the study of HIF-1α inhibition by microtubule disruption. HIF-1α antibodies are now readily available, and though most groups use western blot techniques to quantify HIF-1α production, ELISA kits are now offered and are a better source for high throughput drug screening applications. The Panomics HIF-1α kit is a moderately affordable all inclusive ELISA assay. The ELISA assay works by the following series of procedures. First, the nuclear extracts are incubated with the HIF-1α consensus DNA that is bound to biotin, allowing HIF-1α to bind to the DNA. The HIF-1α/DNA complex is then fixed to a plate coated with streptavidin, which has a very high binding affinity for biotin ($K_d \sim 10^{-15}$ mol/L). The biotin binds to the streptavidin coated plate, thus locking the HIF-1α to the plate surface. Once bound, all other nuclear proteins are removed by washing the plate with phosphate buffered saline solution (PBS). The plate is then treated with a solution containing an anti- HIF-1α antibody which can bind to HIF-1α. The plate is then washed with a HRP-labeled 2^o antibody that binds specifically to the 1^o antibody. The plate is then exposed to a solution containing 3,3′,5,5′-tetramethylbenzidine (TMB), which becomes deep blue upon oxidation by horse radish peroxidase, then yellow when exposed to an acidic peroxide stop solution. The blue coloration is the result of the charge transfer complex between the diimine oxidation product, and the parent diamine. Addition of the

acidic peroxide solution stabilizes the diimine product which has a yellow coloration, and is stable in acidic conditions.[119] Quantification of the amount of TMB oxidized is performed with absorbance at 655 nm.

We treated HeLa cells with a variety of compounds synthesized by the Pinney research group.[13-17, 113, 115] The tubulin IC_{50} values for the compound library varied from 1 to >40 μM, to give a range of tubulin binding properties. HeLa cells were grown in Debulco's modified eagles medium (DMEM) with high glucose, and supplemented with 10% fetal bovine serum and 1x penicillin/streptomycin, as prescribed by Dr. Diane Wycuff.[133] Once the plates have reached near 1 x 10^7 cells, the drug was added for a final concentration of 1 μM and incubated for 16 h at 37 ^oC under normoxic conditions.[57] Literature has shown that 125 μM $CoCl_2$ is optimal for maximizing HIF-1α isolation, as higher concentrations lead to significant cell death and decreased nuclear extract concentrations.[54,58] After the cells were incubated with the drug for 16 h, we incubated the cells for 4 hours with 125 μM $CoCl_2$ to induce maximal possible HIF-1α isolation. Nuclear proteins were extracted using standard protocol and reagents provided by Panomics. The nuclear protein concentrations were determined using a standard Bradford assay.[120] The relative amount of HIF-1α contained in the nuclear extract was determined using the Panomics ELISA kit and normalized by dividing by the nuclear protein concentration. The relative HIF-1α/total protein ratio was determined and allowed a method to compare results among the various drugs. Data obtained from the nuclear extracts screened in the HIF-1α ELISA assay were confirmed by western blot analysis.

Bioreductive Drug Targeting

Bioreductive Research Rational

Combretastatin analogues have the ability to function in anti-vascular and antimitotic capacities. While the antivascular action of the combretastatins occurs quickly via microtubule disruption of the tumor endothelial cells, the antimitotic function requires prolonged exposure to the tumor environment. The antimitotic activity of combretastatins is generally not observed in living systems because the drug is rapidly degraded *in vivo*.[63] Studies have also shown that disruption of tumor vasculature only kills ~95% of the malignant tissue.[77] Tumor cells that line the barrier between cancerous and normal tissue are sustained by a constant supply of nutrients from the surrounding tissue. The sustained group of malignant cells creates a viable rim that is seemingly impervious to VDA therapies.[77] Research has provided a series of bioreductive drugs that may increase the overall effectiveness of radiation and VDA therapies.[74,75] By incorporating bioreductive drug triggers with VDAs, both the normoxic and hypoxic cells of the tumor may be eradicated by not only disrupting the tumor vasculature, but also increasing the VDA *in vivo* life of combretastatins so that they may function in an antimitotic capacity as well.[63] The trigger fragments may also act as DNA intercalators or may re-sensitize the hypoxic region to radiation.[106]

Tumor Hypoxia and Bioreductive Drugs

The hypoxic tumor microenvironment creates an alternative atmosphere to which affected cells must adapt to. Proteins such as HIF-1α are responsible for increasing cell viability. By up-regulating proteins such as VEGF, NOS2, and NADPH/cytochrome

P450, effected cells are able to cope with low oxygen and nutrient-poor environments and are therefore less influenced by VDA therapy (Figure 37).[77] New families of bioreductive drugs have been designed to selectively target areas of tumor hypoxia. There are three major divisions of bioreductive drugs: quinones, N-oxides, and nitroaromatics.[64]

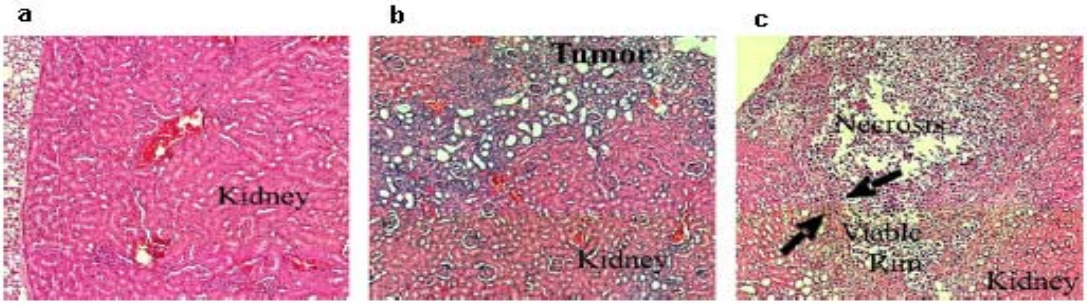

Figure 37. Tumor viable rim. (a) Normal kidney tissue. (b) Normal and malignant kidney tissue. (c) Necrotic tumor tissue with a viable rim of cancerous cells. Taken from Ref. 77 with permission

The first bioreductive drugs to undergo extensive research in the 1970s were a group of nitroimidazoles.[65] Metronidazole, misonidazole, and etanidazole could mimic the effects of oxygen and resensitize hypoxic cells to radiation. Radiation kills cells by forming radicals in DNA. The DNA radical is either oxidized by oxygen, which damages the DNA, or reduced by –SH, which essentially fixes the DNA.[65] The absence of oxygen decreases the amount of DNA damage and the overall effectiveness of radiation therapy. The nitroimidazoles resensitize the hypoxic cells to radiation by forming NO● radicals; however, the drugs were too toxic for clinical use.[65] Nitroaromatic derivatives are still of interest because of their ability to form free radicals in hypoxic environments, their

ability to intercalate DNA, and their ability to act as bioreductive triggers for drugs that would be metabolized before reaching the viable rim.[74]

Nitroaromatic Compounds as Bioreductive Triggers

Nitroaromatics can be reduced by two types of nitroreductase enzymes; oxygen sensitive (type I) and oxygen insensitive (type II) nitroreductases (Figure 38).[65] The oxygen dependent enzymes reduce nitro functional groups via a series of one-electron reductions. The oxygen-insensitive nitroreductases metabolize nitroaromatic compounds by a series of two electron reductions to give nitroso and hydroxylamine intermediates as well as amine products.[65]

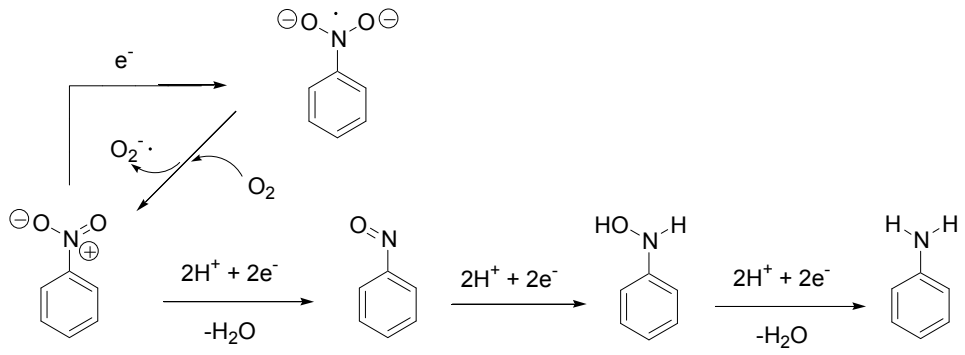

Figure 38. Nitroaromatic reduction pathways via type I and type II nitroreductases. Modified from Ref. 65.

Compounds such as misonidazole and other 2-nitroimidazole derivatives have proven to be potent anticancer drugs, and they also portray selectivity for the hypoxic tumor microenvironment.[64] These nitroaromatic compounds are proposed to alkylate DNA, which may prevent protein synthesis and block mitosis within the cancer cell. Of more interest is the idea of using these reducible drugs to not only alkylate DNA within

cancer cells, but to release other drugs. The nitro functional group is a strong electron-withdrawing substituent that pulls electron density away from the aromatic ring. Once the nitro group is reduced to the amine, a strong resonance donating group, the amine may donate a pair of electrons into the aromatic system, which may cause a cascade of electron movement that results in the release of a suitable drug (Figure 39).[66] Once the prodrug is fragmented, each component can carry out its respective anticancer function.[66]

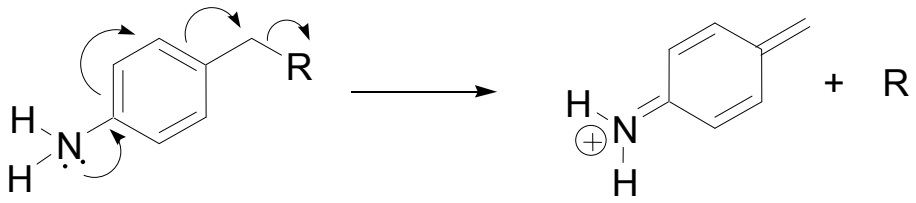

Figure 39. Mechanism of bioreductive prodrug fragmentation. Modified from Ref. 66.

Peter Davis and co-workers were the coupled combretastatin to nitroaromatics, forming VDA bioreductive drug triggers.[68] It is generally accepted that combretastatin analogues do not exhibit antimitotic activity *in vivo* because they are metabolized too rapidly to allow long term exposure.[63] Thompson and co-workers wanted to increase the exposure time of the combretastatin to the tumor by linking CA4 to various reducible nitroaromatics that would fragment upon reduction.[63] Using known Mitsunobu reaction conditions, CA4 was tethered to the nitroaromatic species via an ether linkage (Figure 40).[63,68]

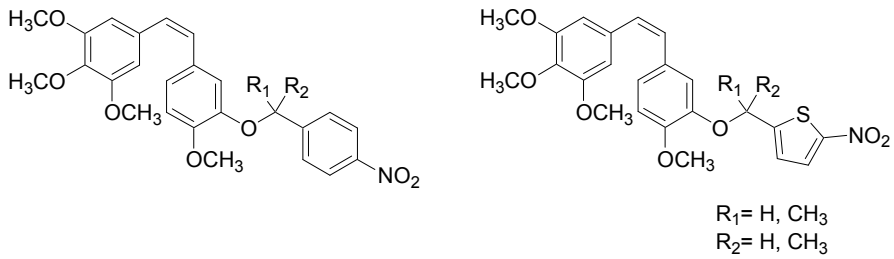

Figure 40. Combretastatin bioreductive drug triggers. Modified from Ref. 63, 67.

Thompson noted that the gem-dimethyl species of the bioreductive prodrug fragmented more rapidly than the unsubstituted derivatives and was the preferred reduction substrate within the series for cytochrome P450R.[63] Even more striking is the formation of CA4 from the gem-dimethyl thiophene prodrug trigger when exposed to hypoxic A549 cells.[63] Within two hours of hypoxic exposure, the concentration of CA4 increased to 4.5 μM, while no appreciable increase in CA4 for normoxic cells treated with the bioreductive prodrug was observed.[63]

Combretastatin Bioreductive Drug Triggers

Within the Pinney group, several potent tubulin polymerization inhibitors are receiving further clinical consideration.[14-17,113,115] It may prove that these new compounds are metabolized too quickly to allow antimitotic function or that they are ineffective in killing cells within hypoxic locations of the tumor. By forming bioreductive triggers, the compounds may be able to affect not only cancer cells near the tumor vasculature, but also cells that are within the hypoxic area of the tumor. Combretastatin analogues CA1 and CA4 and the dihydronaphthalene derivative Oxi6196 were linked with a variety of bioreductive nitroaromatics via Mitsunobu coupling (Figure 41).

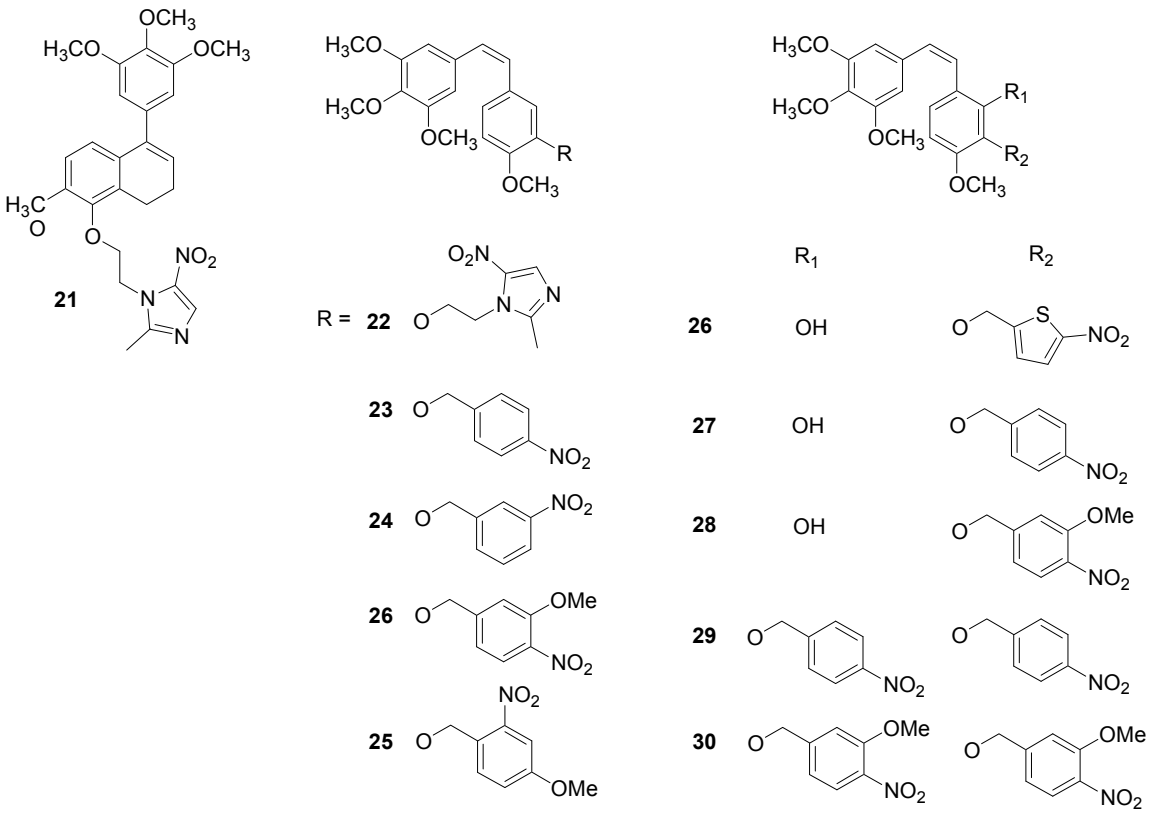

Figure 41. Bioreductive compounds synthesized within this work.

Sulforhodamine B (SRB) Colorimetric Assay

Utilization of the SRB Assay

In April of 1990, the National Cancer Institute (NCI) developed the In Vitro Cell Line Screening Project (IVCLSP) to support the Developmental Therapeutics Program (DTP) which is responsible for screening potential anticancer drugs.[134] Since its original development for the IVLSP project, the SRB assay has become widely used as a standard cytotoxicity assay. The NCI is capable of screening 3,000 compounds annually against 60 cancer cell lines.[69] The goal of this screening is to prioritize synthetic and natural

products that show selective toxicity against individual cell lines for further development.[69]

The ease and practicality of the SRB assay has made it popular with laboratory testing. The SRB assay uses the ability of sulforhodamine B to bind proteins of cells adhered to culture plates with trichloroacetic acid (TCA). The binding of the SRB is considered stoichiometric; therefore, the staining is proportional to cell mass, allowing quantification of cell growth.[70] It is believed that SRB binds basic cellular proteins electrostatically.[71] The structure of SRB is shown in Figure 42.

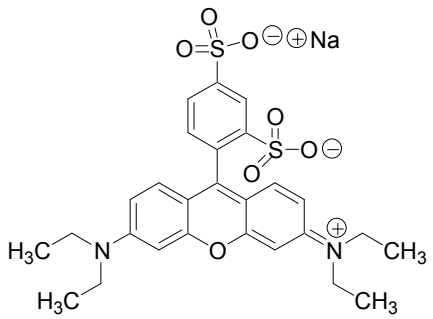

Figure 42. Structure of Sulforhodamine B

The results of the SRB assay are comparable to the tetrazolium dye 3-(4,5-dimethylthiazol-2-yl)-2,5-diphenyltetrazolium bromide (MTT) method in that cell cytotoxicity GI_{50} values can be found from dose dependent linear trends. The main difference is that the MTT requires the cell to metabolize the MTT dye to a purple-colored formazan dye, thereby detecting only viable cells rather than staining all cellular proteins from both live and dead cells. Despite the differences in the two assays, experimentation has shown that MTT and SRB data correlate well; however, the SRB GI_{50} values are generally higher than that of the MTT assay.[70] The SRB GI_{50} values are

generally higher than MTT values because the SRB dye also detects the proteins of dead cells. The main advantage to the SRB assay over the MTT is that there are fewer steps that require optimization in the SRB assay.[70]

SRB Procedure

The SRB assay can be performed in a 96-well plate with cell densities ranging from 1000-180,000 cells/well to give linear responses. Once, fixed and dried, the plates are considered stable and may be stored indefinitely without hindering the accuracy of the results.[70]

The NCI has made its protocol available and gives recommendations for cell loading densities.[135] The protocol requires that two plates be started for the assay. One plate (blank plate), is fixed with TCA after 24 h of incubation, while the second plate (sample plate) is dosed with the desired compounds and incubated for 48 h. The sample plate cells are then fixed with TCA, dyed, and dissolved with tris-base so that absorbance measurements at 550 nm can be determined. The data is calculated using the following equation:[70]

$$\%\ \text{cell growth inhibition} = \frac{(\text{ODsample} - \text{ODblank})}{(\text{ODnegative control} - \text{ODblank})} \times 100$$

The % cell growth inhibition is plotted against the Log of the compound concentration. A linear fit is given, and the IC_{50} is determined as the concentration at 50% cell growth inhibition (NCI) (Figure 43).[70]

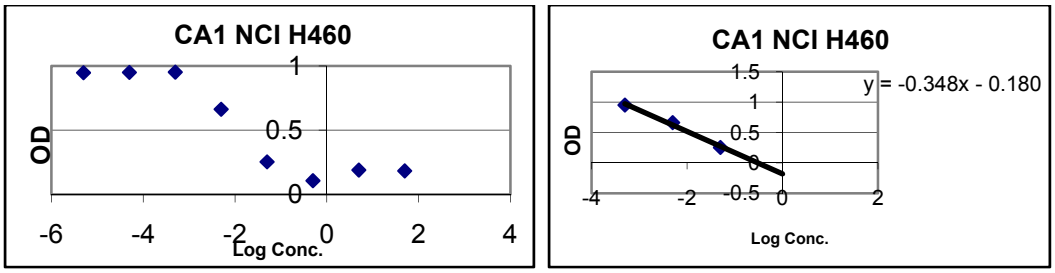

Figure 43. CA1 SRB curves for NCI H460 cells.

SRB Cytotoxicity Screening

The standard protocol as prescribed by NCI[135] was followed for cytotoxic screening with one exception. TCA is used as a fixative because it acidifies proteins and renders them insoluble. This insolubility causes the protein to adhere them to the 96-well plate. Vichai[70] states in the Nature protocol that using 100 µL of a 10% TCA solution is adequate.

Compounds were screened against DU-145 prostate cancer and NCI H460 lung carcinoma cell lines. The cells were dosed with drug concentrations ranging from 50 µg/mL to 0.005 ng/mL. The GI_{50} values for the drugs were recorded and compared. Drugs that showed good cytotoxicity against the cancer cell lines were considered for further evaluation.

CHAPTER TWO

Materials and Methods for Synthesis of Tubulin Polymerization Inhibitors

General Section

Chemicals were purchased from Aldrich Chemical Company, ACROS Organics, Lancaster, Alfa Aesar, A.G. Scientific, or VWR. Dimethyl formamide, o-dichlorobenzene, acetone, ethyl acetate, hexane, and other solvents were dried and purified using standard organic procedures. Methylene chloride (CH_2Cl_2) was dried before each use by distillation from calcium hydride. All reactions were performed in an inert nitrogen atmosphere, and were monitored by TLC with glass plates purchased from VWR that were pre-coated with silica gel 60 F254 with a 0.25 mm layer thickness. Flash column chromatography with silica gel (200-400 mesh, 60 Å) from MP EcoChrom Co or Silicycle was used for chemical separation and purification unless otherwise noted. Samples freeze dried were done so utilizing a Virtic Lyo-Centre 6.6 L lyophilizer.

Organic analysis was achieved with proton (^{1}H), carbon (^{13}C), phosphorous (^{31}P), and fluorine (^{19}F) nuclear magnetic resonance (NMR) at 300MHz, 75 MHz, 90 MHz, and 282 MHz respectively. Deuterated $CDCl_3$ (with 0.03% TMS as an internal standard) was the common NMR solvent used unless otherwise noted. Chemical shifts are expressed in ppm (δ) with peaks patterns listed as singlet (s), broad singlet (b), doublet (d), triplet (t), quartet (q), or multiplet (m), with coupling constants (J) measured in Hz.

The purity of isolated phosphate salts were analyzed by HPLC using a Hewlett Packard HP series 1050 HPLC system. The reversed phase column used in the HPLC

was a Supelco Discovery C18 HPLC column 12.5 cm x 4.6 mm, 5 µm, along with a Supelco Discovery C18 guard column 2 cm x 4 mm. Detection was performed using U.V. at 264 nm. HPLC grade solvents, CH_3CN, H_2O, trifluoroacetic acid, and TBAB, were purchased from Aldrich Chemical Co. Detection of pH was performed with a SevenEasy Meters, Mettler Toledo, Number 20: S20, using an Inlab 409 Ceramic Junction Combination pH electrode.

Tubulin protein isolation was performed using a Beckman Coulter Optima LE-80K Ultracentrifuge, using type 45Ti rotor at appropriate rpms and temperatures. Tubulin protein quantifications were performed using an Agilent 8453 UV/Vis spectrophotometer at 255 nm and 278 nm wavelengths.

Synthesis of Combretastatin Analogues

3,4,5-Trimethoxybenzyl bromide **1**[83]

To a solution containing 3,4,5-trimethoxybenzyl alcohol (20.83 g, 105.1 mmol) in dichloromethane (50mL) at 0°C was added PBr_3 (21.07g, 7.317 mL, 77.85 mmol). The reaction stirred for 3.5 h then was poured over 150 mL of ice water, and neutralized with $NaHCO_3$. The product was extracted three times with CH_2Cl_2 (50 mL). The organic phase was then rinsed with brine, dried with $MgSO_4$, and concentrated to give the bromide product (23.83 g, 91.27 mmol) of pure white product at an 84% yield.

^{1}H NMR ($CDCl_3$, 300 MHz) δ 6.59 (2H, s, Ar*H*), 4.43 (2H, s, benzylic *H*), 3.83 (6H, s, OCH_3), 3.81 (3H, s, OCH_3).

3,4,5-Trimethoxy triphenylphosphine benzyl bromide **2**[84]

Benzyl bromide **1** (12.4 g 47.5 mmol) and triphenyl phosphine (12.5 g 47.5 mmol) were dissolved in CH_2Cl_2 (50 mL) and refluxed for 16 h. The solvent was removed under reduced pressure, and the resulting white solid was flushed with ether until there was no UV absorbent spot by TLC. The resulting white solid was dried under vacuum to give the phosphate bromide salt (19.8 g, 37.8 mmol, 80%).

^{1}H NMR ($CDCl_3$, 300 MHz) δ 7.75 (9H, m, Ar*H*), 7.58 (6H, m, Ar*H*), 6.46 (2H, d, J = 2.5 Hz, Ar*H*), 5.37 (2H, d, J = 14.1 Hz, CH_2), 3.72 (3H, s, OCH_3), 3.46 (6H, s, OCH_3).

^{31}P NMR ($CDCl_3$, 90 MHz) δ 23.40.

3,4-Dihydroxy-5-methoxy benzaldehyde **3**[85]

A mixture of 5-bromovanillin (5.00 g, 21.6 mmol), NaOH (5.83 g, 145 mmol), and copper powder (0.0242 g, 0.380 mmol) in water (100 mL) was refluxed for 27 h. Then, sodium hydrogen phosphate (0.930 g, 0.762 mmol) was added and the mixture refluxed for another hour. The reaction was cooled, filtered to remove the cupric hydrogen phosphate, and acidified with concentrated HCl. The product was extracted with ethyl acetate, washed with aqueous EDTA, brine, dried with $MgSO_4$, concentrated under reduced pressure, and purified by flash column chromatography to give the desired diphenol (2.98 g, 17.7 mmol, 82%) as a tan powder.

^{1}H-NMR ($CDCl_3$, 300 MHz) δ 9.80 (1H, s CO*H*), 7.15 (1H, d, J = 1.7 Hz, Ar*H*), 7.09 (1H, d, J = 1.7 Hz, Ar*H*), 5.91 (1H, s, O*H*), 5.38 (1H, s, O*H*), 3.97 (3H, s, OCH_3).

3,4-Bis-(tert-butyl-dimethyl-silyloxy)-5-methoxy-benzaldehyde **4**

To a solution of benzaldehyde **3** (8.17 g, 48.6 mmol) in DMF (50 mL) at 0°C, was added TEA (25.0 mL, 148 mmol), followed by TBS-Cl (16.6 g, 110 mmol). The reaction proceeded for one hour, then was quenched with water. The organic phase was washed with copious amounts of water. The water phase was extracted with EtOAc, the organic phases were combined, dried with sodium sulfate, and condensed under vacuum to give the diprotected benzaldehyde (14.8 g, 37.4mmol, 77%) as an off-white solid.

^{1}H-NMR ($CDCl_3$, 300 MHz) δ 9.77 (1H, s, CO*H*), 7.07 (1H, d, J = 1.9 Hz, Ar*H*), 7.02 (1H, d, J = 1.9 Hz, Ar*H*), 3.84 (3H, s, OCH_3), 0.993 (9H, s, SiC(CH_3)$_3$), 0.985 (9H, s, SiC(CH_3)$_3$), 0.23 (6H, s, Si(CH_3)$_2$), 0.16 (6H, s, Si(CH_3)$_2$).

^{13}C-NMR ($CDCl_3$, 75 MHz) δ 191.0, 152.5, 148.0, 142.9, 129.2, 117.2, 104.5, 55.3, 26.0, 25.8, 25.7, 18.8, 18.6, -3.8, -4.0, -4.4.

(Z) + (E)-2-(3',4'-Bis-tertbutyl-dimethyl-silyloxy-5'-methoxyphenyl)-1-(3,4,5-trimethoxyphenyl) ethene **5** *and* **6**

A solution containing anhydrous CH_2Cl_2 (20 mL) and NaH (0.604 g, 25.2 mmol), was cooled to 0 °C. The triphenyl phosphate bromide salt **2** (1.321 g, 2.52 mmol) was dissolved in dichloromethane (4 mL) and added to the reaction. After 10 min TBS-protected benzaldehyde **4** (1.00 g, 2.52 mmol) was dissolved in CH_2Cl_2 (4 mL) and added slowly. After 20 min water was added, and the products were extracted with EtOAc, washed with brine, dried with sodium sulfate, condensed onto silica under reduced pressure, and separated by column chromatography to give the *Z*-isomer (0.440 g, 0.785 mmol, 31%) as a white solid, and *E*-isomer (0.850 g, 1.52 mmol, 60%).

(**5**) ^{1}H-NMR ($CDCl_3$, 300 MHz) δ 6.52 (2H, s, C*H*=C*H*), 6.51 (1H, s, Ar*H*), 6.46 (2H, s, Ar*H*), 6.39 (1H, d, J = 1.27 Hz, Ar*H*), 3.62 (3H, s, OCH_3), 3.61 (3H, s, OCH_3), 3.32 (3H, s, OCH_3), 0.91 (9H, s, SiC(CH_3)$_3$), 0.82 (9H, s, SiC(CH_3)$_3$), 0.07 (6H, s, Si(CH_3)$_2$), 0.00 (6H, s, Si(CH_3)$_2$).

(**6**) ^{1}H-NMR ($CDCl_3$, 300 MHz) δ 7.1 (1H, d, J = 16.26 Hz, C*H*=CH), 7.0 (1H, d, J = 16.26 Hz, C*H*=CH), 6.9 (1H, d, J = 2.0 Hz, Ar*H*), 6.86 (2H, s, Ar*H*), 6.7 (1H, d, J = 1.9 Hz, Ar*H*), 3.85 (9H, s, OCH_3), 3.72 (3H, s, OCH_3), 1.01 (18H, s, SiC(CH_3)$_3$), 0.25 (6H, s, Si(CH_3)$_2$), 0.15 (6H, s, Si(CH_3)$_2$).

(Z) + (E)-2-(3',4'-dihydroxy-5'-methoxyphenyl)-1-(3,4,5-trimethoxyphenyl) ethene **7** *and* **8**

Compound **5** (1.80 g, 3.22 mmol) was dissolved in of DMF (30 mL). To the mixture was added 1.00 g of anhydrous KF followed by 48% HBr (1.0 mL). The reaction was sonicated for 2 hours, after which 6M HCl (30 mL) was added. The products were extracted with EtOAc, washed with copious amounts of water, brine, dried with sodium sulfate, concentrated, and purified by flash column chromatography. *Z*-isomer **7** (0.414 g, 1.25 mmol, 39%) was collected as a white solid. The remainder of the product was *E*-isomer **8** (0.653 g, 1.96 mmol, 61% yield). (R_f = 0.3; 50:50; Hexanes:EtOAc). m.p. = 115-117 ^{o}C. Anal. Calcd for $C_{18}H_{20}O_6 \bullet H_2O$: C, 61.71; H, 6.33. Found: C, 61.83; H, 6.33.

(**7**) ^{1}H-NMR ($CDCl_3$, 300 MHz) δ 6.61 (1H, d, Ar*H*, J = 1.8 Hz), 6.54 (2H, s, C*H*=C*H*), 6.43 (2H, s, Ar*H*), 6.41 (1H, d, Ar*H*, J = 1.8 Hz), 3.83 (3H, s, OCH_3), 3.72 (6H, s, OCH_3), 3.69 (3H, s, OCH_3).

(**8**) ^{1}H-NMR ($CDCl_3$, 300 MHz) δ 6.88 (2H, s, C*H*=C*H*), 6.79 (1H, d, J = 1.6 Hz, Ar*H*), 6.71 (2H, s, Ar*H*), 6.64 (1H, d, J = 1.7 Hz, Ar*H*), 5.42 (1H, s, O*H*), 5.28 (1H, s, O*H*), 3.94 (3H, s, OCH_3), 3.92 (6H, s, OCH_3), 3.87 (3H, s, OCH_3).

3,4,5-Trifluoro triphenylphosphine benzyl bromide (**9**)[17]

Triphenylphosphine (1.282 g, 4.889 mmol) was dissolved in CH_2Cl_2 (20 mL). To the mixture was added 3,4,5 trifluorobenzyl bromide (1.000g, 4.445 mmol). The solution was refluxed overnight, then cooled to room temperature, and quenched with water (20 mL). The organic layer was separated, and the water layer was extracted three times with CH_2Cl_2 (20 mL). The organic layers were combined and condensed under vacuum to give a white powder. The solid was flushed with Et_2O until no $P(Ph)_3$ was detected by TLC. The resulting white powder was pure phosphine bromide salt (1.56 g, 3.20 mmol, 72%).

(**9**) ^{1}H-NMR ($CDCl_3$, 300 MHz) δ 7.98 (10H, m, Ar*H*), 7.76 (5H, m, Ar*H*), 7.16 (2H, m, Ar*H*), 5.84 (2H, d, J = 15.3 Hz, CH_2).

(Z)+(E)-2-(3',4'-dihydroxy-5'-methoxyphenyl)-1-(3,4,5-trifluorophenyl) ethene **10** and **11**[17]

Sodium hydride (0.302 g, 12.6 mmol) was dissolved in CH_2Cl_2 (20 mL) cooled to 0 ^{o}C. Phosphine bromide **9** (0.615 g, 1.26mmol) was dissolved in dichloromethane (5 mL) and added to the reaction flask and allowed to stir for 10 min. Benzaldehyde **4** (0.500 g, 1.26 mmol) was dissolved in CH_2Cl_2 (5 mL) and added to the reaction. After 30 min, water (20 mL)was added, and the products were extracted with CH_2Cl_2. The organic layers were combined, dried, and the products were purified by flash column chromatography to give 0.570 g of product as a white solid. The *E* and *Z* isomers where

not able separable by flash column chromatography so they were deprotected at the same time.

The two isomers where dissolved in DMF (10 mL), followed by addition of potassium fluoride(0.500 g). An aqueous solution of 48% HBr (0.5 mL) was added and the solution was sonicated for 2 h. The reaction was quenched with 6 M HCl (30 mL), and the organics were separated with EtOAc. The combined organic layers were rinsed with water, brine, condensed, and isomers separated by flash column chromatography to give the *Z*-isomer (0.157 g, 0.530 mmol, 42%), and the *E*-isomer (0.861 g, 0.291 mmol, 30%). **11** (R_f = 0.2; 70:30; Hexanes:EtOAc). m.p. = 159-161 ^oC. Anal. Calcd for $C_{15}H_{13}F_3O_3 \bullet 0.3H_2O$: C, 59.61; H, 3.89. Found: C, 59.84; H, 4.11.

(**10**) ^{1}H-NMR ($CDCl_3$, 300 MHz) δ 6.89 (2H, d, J = 6.87 Hz, Ar*H*), 6.86 (2H, d, J = 6.86 Hz, Ar*H*), 6.53 (1H, d, J = 12.12 Hz, C*H*=CH), 6.49 (1H, d, J = 1.44 Hz, Ar*H*), 6.33 (1H, d, J = 1.51 Hz, Ar*H*), 6.30 (1H, d, J= 12.16 Hz, C*H*=CH), 5.78 (2H, b, O*H*), 3.71 (3H, s, OCH_3).

(**11**) ^{1}H-NMR ($CDCl_3$, 300 MHz) δ 7.06 (1H, d, J = 6.5 Hz, Ar*H*), 7.03 (1H, d, J = 6.5 Hz, Ar*H*), 6.87 (1H, d, J = 16 Hz, C*H*=CH), 6.76 (1H, d, J = 1.6 Hz, Ar*H*), 6.75 (1H, d, J = 16.2 Hz, C*H*=CH), 6.60 (1H, d, J = 1.9 Hz, Ar*H*), 5.47 (1H, s, O*H*), 5.30 (1H, s, O*H*), 3.92 (3H, s, OCH_3).

2-(3',4'-Dihydroxy-5'-methoxyphenyl)-1-(3,4,5-trifluorophenyl) ethane (**12**)

Stilbene **11** (0.081 mg, 0.27 mmol) was dissolved in CH_2Cl_2 (15 mL). Palladium (5%) on carbon (0.080 mg) was added, and the reaction vessel was fitted with a hydrogen balloon. The reaction was allowed overnight, and was then filtered through a short pad of silica. Removal of the solvent by vacuum gave pure product (0.033 mg, 0.11 mmol,

40%) as a white solid. (R_f = 0.2; 70:30; Hexanes:EtOAc). m.p. = 101-104 ^oC. Anal. Calcd for $C_{15}H_{13}F_3O_3$: C, 60.40; H, 4.39. Found: C, 60.39; H, 4.38.

^{1}H-NMR ($CDCl_3$, 300 MHz) δ 6.75 (2H, t, J = 7.2 Hz, Ar*H*), 6.41 (1H, s, Ar*H*), 6.21 (1H, s, Ar*H*), 5.26 (2H, s, O*H*), 3.84 (3H, s, OCH_3), 2.79 (4H, m, CH_2).

^{13}C-NMR ($CDCl_3$, 75 MHz) δ 151.00 (ddd, J_{C-F} = 247.6, 9.8, 4.1 Hz), 146.79, 143.88, 138.13 (dt, J_{C-F} = 247.4, 15.5), 138.13 (td, J_{C-F} = 7.2, 4.8 Hz), 132.59, 130.74, 112.43 (d, J_{C-F} = 6.2 Hz), 112.24 (d, J_{C-F} = 6.1 Hz), 108.55, 103.40, 56.17, 37.3, 37.2.

(Z)+(E)-2-(4'-Methoxy-3'-nitrophenyl)-1-(3,4,5-trifluorophenyl) ethene **13** and **14**

Sodium hydride (0.264 g, 11.0 mmol) was dissolved in dry CH_2Cl_2 (10 mL) and cooled to 0 ^oC. Phosphonium bromide **9** (0.538 g, 1.10 mmol) was dissolved in dry CH_2Cl_2 (3 mL)and added to the reaction. After 10 min. 4-methoxy-3-nitro benzaldehyde (0.200 g, 1.10 mmol) was dissolved in CH_2Cl_2 (5 mL) and added to the reaction. After 30 min. the reaction was quenched with water and the products were extracted with CH_2Cl_2. The organic layers were combined, condensed, and the products were separated by flash column chromatography. The *Z* isomer (**13**) was collected as a pale yellow solid (0.157 g, 0.508 mmol, 46%), and the *E* isomer (**14**) was isolated as a bright yellow solid (0.042 g, 0.136 mmol, 12%). **13** (R_f = 0.33; 70:30; Hexanes:EtOAc). m.p. = 74-76 ^oC. Anal. Calcd for $C_{15}H_{10}F_3NO_3$: C, 58.26; H, 3.26; N, 4.53. Found: C, 58.12; H, 3.17; N, 4.40. **14** (R_f = 0.3; 70:30; Hexanes:EtOAc). m.p. = 177-179 ^oC.

(**13**) ^{1}H-NMR ($CDCl_3$, 300 MHz) δ 7.69 (1H, d, J = 2.2 Hz, Ar*H*), 7.35 (1H, dd, J = 8.8, 2.2 Hz, Ar*H*), 6.98 (1H, d, J = 8.7 Hz, Ar*H*), 6.83 (1H, d, J = 7.8 Hz, Ar*H*), 6.80 (1H, d, J = 8.06 Hz, Ar*H*), 6.58 (1H, d, J = 12.1 Hz, C*H*=CH), 6.48 (1H, d, J = 12.1 Hz, C*H*=CH), 3.95 (3H, s, OCH_3).

(**13**) ^{19}F-NMR ($CDCl_3$, 282 MHz) δ -134.03 (2F, d, J = 19.74 Hz), -161.01 (1H, t, J = 19.74 Hz).

(**13**) ^{13}C-NMR ($CDCl_3$, 75 MHz) δ 152.33, 151.22 (ddd, J_{C-F} = 250.2, 10.1, 4.2 Hz), 139.50, 139.01 (dt, J_{C-F} = 252.9, 15.4 Hz), 134.33, 132.47 (td, J_{C-F} = 7.9, 5.8 Hz), 129.48, 128.28, 126.06, 113.59, 112.88, 112.69, 56.59.

(**14**) ^{1}H-NMR ($CDCl_3$, 300 MHz) δ 7.99 (1H, d, J = 2.27 Hz, Ar*H*), 7.64 (1H, dd, J = 8.75, 2.33 Hz, Ar*H*), 7.10 (2H, d, J = 8.67 Hz, Ar*H*), 7.08 (1H, d, J = 8.69 Hz, Ar*H*), 6.99 (1H, d, J = 16.3 Hz, C*H*=CH), 6.87 (1H, d, J = 16.1 Hz, C*H*=CH), 4.00 (3H, s, OCH_3).

(**14**) ^{19}F-NMR ($CDCl_3$, 282 MHz) δ -134.07 (2F, d, J = 19.7 Hz), -160.53 (1F, t, J = 19.7 Hz).

(**14**) ^{13}C-NMR ($CDCl_3$, 75 MHz) δ 152.71, 151.51 (ddd, J_{C-F} = 249.7, 10.3, 4.1 Hz), 139.91, 139.31 (dt, J_{C-F} = 253.1, 15.7 Hz), 132.97 (td, J_{C-F} = 7.9, 4.8 Hz), 132.17, 129.16, 128.90 (d, $J_{C-F.}$= 2.5 Hz), 126.50 (dd, J_{C-F} = 5.2, 2.6 Hz), 123.45, 113.90, 110.24 (dd, J_{C-F} = 14.7, 6.7 Hz) 56.72.

(Z)+(E)-2-(4'-methoxy-3'-aminophenyl)-1-(3,4,5-trifluorophenyl) ethene **15** *and* **16**

An unseparated mixture of nitro-stilbenes **13** and **14** (0.060 g, 0.194 mmol) was dissolved in toluene (5 mL). Powdered iron (0.200 g, 3.58 mmol), and glacial acetic acid (1 mL) was added, and the reaction was refluxed for 1 h. The reaction was then cooled, and filtered through a short pad silica. The solvent was removed, and the products were purified by flash column chromatography to give the desired amine *Z*-stilbene **15** (0.0057 g, 0.0204 mmol, 11%), and the *E*-isomer **16 (**0.0110 g, 0.0393 mmol, 20%).

(**15**) ^{1}H-NMR ($CDCl_3$, 300 MHz) δ 6.88 (1H, d, J = 8.9 Hz, Ar*H*) 6.67 (1H, d, J = 8.8 Hz, Ar*H*), 6.59 (1H, d, J = 2.0 Hz, Ar*H*), 6.57 (1H, d, J = 2.0 Hz, Ar*H*), 6.55 (1H, d, J = 11.8 Hz, C*H*=CH), 6.27 (1H, d, J = 12.2 Hz, C*H*=CH), 3.85 (3H, s, OCH_3), 3.75 (2H, b, NH_2).

(**15**) ^{19}F-NMR ($CDCl_3$, 282 MHz) δ -135.27 (2F, d, J = 22.6), -162.51 (1F, t, J = 19.74).

(**15**) ^{13}C-NMR ($CDCl_3$, 75 MHz) δ 150.98 (ddd, J_{C-F} = 251.8, 13.1, 7.3 Hz), 147.07, 138.61 (dt, J_{C-F} = 252.8, 15.4 Hz), 136.10, 133.31 (td, J_{C-F} = 10.1, 4.5 Hz), 132.59, 128.75, 119.28, 114.99, 112.91, 112.71 (d, J_{C-F} = 6.3 Hz), 110.25, 55.50.

(**16**) ^{1}H-NMR ($CDCl_3$, 300 MHz) δ 7.06 (1H, d, J = 9.0 Hz, Ar*H*), 7.04 (1H, d, J = 9.0 Hz, Ar*H*), 6.88 (3H, m, Ar*H*), 6.81 (1H, d, J = 16.0 Hz, C*H*=CH), 6.74 (1H, d, J = 15.8 Hz, C*H*=CH), 3.88 (3H, s, OCH_3), 3.86 (2H, b, NH_2).

(**16**) ^{19}F-NMR ($CDCl_3$, 282 MHz) δ -134.89 (2F, d, J = 22.6 Hz), -162.39 (1F, t, J = 19.74 Hz).

(**16**) ^{13}C-NMR ($CDCl_3$, 75 MHz) δ151.43 (ddd, J_{C-F} = 248.7, 10.3, 4.3 Hz), 147.94, 138.67 (dt, J_{C-F} = 251.4, 15.7 Hz), 136.46, 134.19 (td, J_{C-F} = 7.8, 4.6 Hz), 131.1, 129.37, 123.30 (d, J_{C-F} = 2.5 Hz), 118.20, 112.24, 110.40, 109.83 (dd, J_{C-F} = 14.7, 6.6 Hz), 55.95.

(Z)+(E)-2-(4'-methoxy-2'-nitrophenyl)-1-(3,4,5-trifluorophenyl) ethene **17** and **18**

Sodium hydride (0.146 g, 9.2 mmol) has dissolved in anhydrous dichloromethane (10 mL), and cooled to 0 ^{o}C. Phosphonium bromide **9** (0.300 g, 0.616 mmol) was dissolved in CH_2Cl_2 (5 mL) and added to the sodium hydride mixture. After 10 min. 4-methoxy-2-nitro benzaldehyde (0.111 g, 0.620 mmol) was dissolved in CH_2Cl_2 (5 mL)

and added to the reaction mixture. After 30 min. the reaction was quenched with water. The organics were extracted with CH_2Cl_2. The organic layers were combined, washed with brine, dried with sodium sulfate, condensed, and separated by flash column chromatography. The *Z*-isomer (**17**) was recovered as a pale yellow solid (0.0656 g, 0.212 mmol, 34%), and the *E*-isomer (**18**) was collected as a yellow solid (0.0424 g, 0.137 mmol, 22%). **17** (R_f = 0.48; 70:30; Hexanes:EtOAc). m.p. = 99-100 ^oC. Anal. Calcd for $C_{15}H_{10}F_3NO_3$: C, 58.26; H, 3.26; N, 4.53. Found: C, 58.19; H, 3.22; N, 4.39. Found: C, 58.00; H, 3.21; N, 4.37.. **18** (R_f = 0.33; 70:30; Hexanes:EtOAc). m.p. = 205-207 ^oC. Anal. Calcd for $C_{15}H_{10}F_3NO_3$: C, 58.26; H, 3.26; N, 4.53.

(**17**) ^{1}H-NMR ($CDCl_3$, 300 MHz) δ 7.29 (1H, t, J = 8.04 Hz, Ar*H*), 6.99 (1H, d, J = 8.4 Hz, Ar*H*), 6.74 (2H, t, J = 7.4 Hz, Ar*H*), 6.62 (1H, d, J = 12.1, C*H*=CH), 6.57 (1H, d, J = 12.2 Hz), 3.93 (1H, s).

(**17**) ^{19}F-NMR ($CDCl_3$, 282 MHz) δ 134.37 (2F, d, J = 22.6 Hz), -160.57 (1F, t, J = 19.7 Hz)

(**17**) ^{13}C-NMR ($CDCl_3$, 75 MHz) δ 151.18, 10.97 (ddd, J_{C-F} = 249.7, 10.0, 4.1 Hz), 139.23 (dt, J_{C-F} = 253.3, 15.5 Hz), 131.69 (td, J_{C-F} = 9.7, 2.1 Hz), 131.15, 130.33, 125.24, 121.37, 113.13 (d, J_{C-F} = 6.7 Hz), 112.93 (d, J_{C-F} = 6.8 Hz), 111.97, 56.46.

(**18**) ^{1}H-NMR ($CDCl_3$, 300 MHz) δ 7.43 (1H, t, J = 8.0 Hz, Ar*H*), 7.27 (1H, t, 2.49 Hz, Ar*H*), 7.09 (1H, d, J = 6.6 Hz, Ar*H*), 7.06 (1H, d, J = 6.7 Hz, Ar*H*), 6.99 (1H, d, J = 9.1 Hz, Ar*H*), 6.98 (1H, d, J = 14.9 Hz, C*H*=CH), 6.83 (1H, d, J = 16.0 Hz, C*H*=CH), 3.92 (3H, s, OCH_3).

(**18**) ^{19}F-NMR ($CDCl_3$, 282 MHz) δ -133.79 (2F, d, J = 19.7 Hz), -159.37 (1F, t, J = 19.7 Hz)

(**18**) ^{13}C-NMR ($CDCl_3$, 75 MHz) δ151.49 (ddd, J_{C-F} = 250.1, 10.5, 4.3 Hz), 151.09, 139.79 (dt, J_{C-F} = 254.2, 13.8 Hz), 132.38 (td, J_{C-F} = 14.5, 2.2 Hz), 131.12 (d J_{C-F} = 2.6 Hz), 130.99, 129.75, 122.95 (d, J_{C-F} =2.4 Hz), 117.82, 111.96, 110.96 (d, J_{C-F} = 6.8 Hz), 110.76 (d, J_{C-F} = 6.7 Hz), 56.5.

(Z)-2-(4'-methoxy-2'-aminophenyl)-1-(3,4,5-trifluorophenyl) ethene **19**

Nitrostillbene **17** (0.020 g, 0.065 mmol) was dissolved in toluene (5 mL). Powdered iron (0.10 g, 1.8 mmol), and glacial acetic acid (1 mL) was added, and the reaction was refluxed for 1 h. The reaction was then cooled, and filtered through a short pad silica. The solvent was removed, and the products were purified by preparative TLC (EtOAc/Hexane 40:60) to give 0.011 g (0.039 mmol, 61%) of the desired amine stilbene product.

^{1}H-NMR ($CDCl_3$, 300 MHz) δ 6.85 (1H, d, J = 6.8 Hz, Ar*H*), 6.81 (1H, d, J = 6.6 Hz, Ar*H*), 6.75 (1H, dd, J = 6.31, 3.17 Hz, Ar*H*), 6.67 (1H, d, J = 7.8 Hz), 6.64 (1H, d, J = 3.28 Hz, Ar*H*), 6.61 (1H, d, J = 11.81 Hz, C*H*=CH), 6.47 (1H, d, J = 12.0 Hz, C*H*=CH), 3.90 (2H, s, NH_2), 3.88 (3H, s, OCH_3).

^{19}F-NMR ($CDCl_3$, 282 MHz) δ -135.17 (2F, d, J = 19.7 Hz), -161.44 (1F, t, J = -19.7 Hz).

^{13}C-NMR ($CDCl_3$, 75 MHz) δ 150.00 (ddd, J_{C-F} = 248.5, 14.5, 4.2 Hz), 147.37, 138.81 (dt, J_{C-F}= 251.48, 17.3 Hz), 133.76, 132.73 (td, J_{C-F} = 10.9, 4.7 Hz), 128.62, 121.43, 121.05, 117.89, 112.75 (d, J_{C-F} = 6.6 Hz), 112.55 (d, J_{C-F} = 6.5 Hz), 109.58, 55.60.

(E)-2-(4'-methoxy-2'-aminophenyl)-1-(3,4,5-trifluorophenyl) ethene **20**

Compound **18** (0.020 g, 0.065 mmol) was dissolved in toluene(5 mL). Powdered iron (0.10 g, 1.8 mmol), and glacial acetic acid (1 mL) was added, and the reaction was refluxed for 1 h. The reaction was then cooled, and filtered through a short pad silica. The solvent was removed, and the products were purified by preparative TLC (EtOAc/Hexane 40:60) to give 0.012 g (0.043 mmol, 66%) of the desired product.

^{1}H-NMR ($CDCl_3$, 300 MHz) δ 7.12 (1H, d, J = 4.6 Hz, Ar*H*), 7.09 (1H, d, J = 2.24 Hz, 7.07 (1H, d, J = 4.0 Hz, Ar*H*), 7.02 (1H, t, J = 4.3 Hz), 6.84 (1H, d, J = 16.1 Hz, C*H*=CH), 6.78 (1H, s, Ar*H*), 6.76 (1H, d, J = 1.3 Hz, Ar*H*), 4.04 (2H, b, NH_2), 3.88 (3H, s, OCH_3).

^{19}F-NMR ($CDCl_3$, 282 MHz) δ -134.58 (2F, d, J = 19.7 Hz), -161.75 (1F, t, J = 19.7 Hz).

^{13}C-NMR ($CDCl_3$, 75 MHz) δ 153.43 (ddd, J_{C-F} = 249.1, 10.2, 4.3 Hz), 147.72, 138.92 (dt, J_{C-F} = 252.0, 15.7 Hz), 134.36, 134.00 (td, J_{C-F} =7.6, 4.2 Hz), 126.85 (d, J_{C-F} = 2.6 Hz), 126.46, 122.55, 119.05, 118.24, 110.07 (d, J_{C-F} = 6.6 Hz), 109.88, 55.71.

Synthetic Route for Radiolabeled CA1P Dipotassium Salt (Ox16C)

4-Hydroxy-3,5-dimethoxy benzaldehyde (**21**)[86]

3,4,5-trimethoxy benzaldehyde (5.00 g, 25.5 mmol) was dissolved in CH_2Cl_2 (50 mL). After 10 minutes of stirring, 10.2 g (76.5 mmol, 3 eq.) aluminum trichloride was added in portions. The reaction was allowed for 18 h after which water(160 ml) was added. The organic products were extracted with CH_2Cl_2, washed with brine, and dried

using $MgSO_4$. Solvent removal gave the desired benzaldehyde (4.77 g) as pure product as a tan solid for a quantitative yield.

^{1}H-NMR ($CDCl_3$, 300 MHz) δ 9.81 (1H, s, C*H*O), 7.16 (2H, s, Ar*H*), 6.35 (1H, s, O*H*), 3.97 (6H, s, OCH_3).

4-(tert-Butyl-dimethyl silyloxy)-3,5-dimethoxy-benzaldehyde (**22**)[86]

Benzaldehyde **21** (19.7 g, 108 mmol) was dissolved in 75 mL DMF. Di-isopropyl ethyl amine (22.6 mL, 130 mmol), and DMAP (1.98 g, 16.2 mmol) were added, and the reaction was cooled to 0^{o}C. After 10 min. TBS-Cl (19.7 g, 130 mmol) was added in portions. The reaction was allowed for 12 h at room temperature, and was then quenched with 60 ml water. The products were extracted with EtOAc. The combined organic layers were then washed with copious amounts of water to remove all DMF. The organic layer was then washed with 5% NaOH, brine, and dried over Na_2SO_4. After condensing, the final product was purified using flash column chromatography (70:30 hexane:ethyl acetate) to give the protected benzaldehyde (24.5 g, 82.7 mmol, 99%) as a yellow solid.

^{1}H-NMR ($CDCl_3$, 300 MHz) δ 9.81 (1H, s, C*H*O), 7.09 (2H, s, Ar), 3.86 (6H, s, OCH_3), 1.01 (9H, s, SiC(CH_3)$_3$), 0.15 (6H, s, Si(CH_3)$_2$).

Tert-Butyl-{4-[2-(2',3'-diisopropoxy-4'-methoxy-phenyl-vinyl]-2,6-dimethoxyphenoxy}-dimethyl-silane **23**[86]

(2,3,diisopropoxy-4-methoxybenzyl)-triphenylphosphonium bromide 18.8 g (32.4 mmol) was dissolved in 150 mL dry THF. The mixture was cooled to -10^{o}C and 11.9 mL of n-BuLi (2.5M in hexane, 29.7mmol, 1.1 eq) was added dropwise. The solution turned deep red, and was allowed to stir for 10 min. In another flask benzaldehyde **22** (8.00 g, 27.0 mmol) was dissolved in 10 mL THF, and was added drowise to the phosphorous

ylide solution. After two hours the reaction was quenched with 30 mL of water. The THF was removed by evaporation and the organics were extracted with CH_2Cl_2 (3 x 50 mL). The combined organic layers were washed with brine, dried with sodium sulfate, and condensed onto silica. The products were purified by flash column chromatography (Hexane: EtOAc 98:2) to give the desired *Z*-combretastatin (6.89 g 49%) as a white solid.

^{1}H-NMR ($CDCl_3$, 300 MHz) δ 7.25 (1H, d, J = 8.5 Hz, Ar*H*), 6.91 (1H, d, J = 12.2 Hz, C*H*=CH), 6.45 (4H, m), 4.68 (1H, sep, J = 6.3 Hz, C*H*$(CH_3)_2$), 4.42 (1H, sep, J = 6.0 Hz, C*H*$(CH_3)_2$), 3.82 (3H, s, OC*H*$_3$), 3.58 (6H, s, OC*H*$_3$), 1.28 (12H, d, CH(C*H*$_3)_2$), 0.99 (9H, s, SiC(C*H*$_3)_3$), 0.10 (6H, s, Si(C*H*$_3)_2$).

(Z)-1-(2',3'-diisopropoxy-4'-methoxy)-2-(3,4,5-trimethoxyphenyl)-ethene **24**[86]

TBS protected stilbene **23** (1.51 g, 2.92 mmol) was dissolved in 20 mL dry acetonitrile. The solution was cooled to 0^{o}C and TBAF (10.4 mL 1M, 10.4 mmol) was added. After adding methyl iodide (2.4 mL,37.9 mmol), the reaction stirred for 30 min. Water was added and the organics were extracted with EtOAc (3 x 50ml). The organic phases were combined, washed with brine, and dried with magnesium sulfate. The products were purified by flash column chromatography (Hexane:EtOAc, 70:30) to give the methylated stilbene (0.755 g, 1.81 mmol, 62%) of product as a white solid.

^{1}H-NMR ($CDCl_3$, 300 MHz) δ 6.93 (1H, d, J = 6.6Hz, Ar*H*), 6.62 (1H, d, J = 12.1 Hz, C*H*=CH), 6.49 (1H, d, J = 8.7, Ar*H*), 6.48 (2H, s), 6.42 (1H, d, J = 12.1, C*H*=CH), 4.69 (1H, sep, J = 6.2 Hz, C*H*$(CH_3)_2$), 4.42 (1H, sep, J = 6.2 Hz, C*H*$(CH)_2$), 3.81 (3H, s, OC*H*$_3$), 3.79 (3H, s, OC*H*$_3$), 3.64 (6H, s, OC*H*$_3$), 1.29 (6H, s, CH(C*H*$)_3$), 1.27 (6H, s, CH(C*H*$)_3$).

(Z)-3'-Methoxy-6-[2-(3,4,5-trimethoxy-phenyl)-vinyl]-benzene-1',2'-diol (CA1) **25**[86]

Isopropyl protected **24** (0.755 g, 1.81 mmol) was dissolved in 2 mL CH_2Cl_2. The mixture was cooled to 0°C and $TiCl_4$ (0.5 mL, 4.53 mmol, 2.5 eq) was added dropwise. A dark substance solidified and was promptly disrupted by sonication for 3 min. after which time the reaction was determined complete by TLC. Water (10 mL) was used to quench the reaction, and the products were extracted with 50 mL EtOAc. The water layer was extracted twice more with 20 mL of ethyl acetate. The combined organic layers were washed with water (4 x 20 mL) until the pink coloration of the mixture disappeared. The organic layer was then washed with brine, dried with sodium sulfate, and condensed to give a light tan solid as the desired CA1 product (0.567 g, 1.70 mmol, 94% yield).

^{1}H-NMR ($CDCl_3$, 300 MHz) δ 6.77 (1H, d, J = 8.7 Hz, Ar*H*), 6.60 (1H, d, J = 12.3 Hz, C*H*=CH), 6.53 (1H, d, J = 11.9 Hz, C*H*=CH), 6.38 (1H, d, J = 8.7 Hz, Ar*H*), 5.39 (2H, s, O*H*), 3.94 (3H, s, OCH_3), 3.83 (3H, s, OCH_3), 3.67(6H, s, OCH_3).

2',3'-O-Di[bis-benzylphosphoryl]-combretastatin A-1 **26**[86]

N-chlorosuccinamide (0. 602 g, 4.52 mmol.) was dissolved in acetonitrile (5 mL). The mixture was heated to 40°C for 10 min. then cooled to r.t. Di-benzylphosphite (1.19 g, 4.52 mmol) was then added and the reaction stirred for 2 h. TLC confirmed completeness of bromination. In a separate round bottom flask the following were dissolved in acetonitrile (3 mL): CA1 (0.500 g, 1.50 mmol), DMAP (0.0183 g, 0.150 mmol). The reaction was cooled to 0°C and triethylamine (0.63 ml, 4.52 mmol) was added. The reaction was allowed for 10 min. The phosphate products from the first flask were then added to the CA1 mixture dropwise, and the reaction was allowed for 17 h.

The acetonitrile was removed by reduced pressure, and the resulting solid was azeotroped twice with 20 mL of toluene. Ethyl acetate (20 mL) was added, and the resulting solid was filtered and washed with EtOAc (3 x 20 mL). The combined organic layers were then washed with 0.5 M KH_2PO_4 (4 x 20 mL). The aqueous KH_2PO_4 layer was extracted EtoAc (2 x 40 mL). The combined organic layers were washed with 0.5M NaOH (4 x 10 mL), brine, dried with sodium sulfate, condensed onto silica, and purified using flash column chromatography. The desired dibenzyl phosphate stilbene product was recovered as a clear oil (0.323 mg, 0.378 mmol, 25%).

^{1}H-NMR ($CDCl_3$, 300 MHz) δ 7.25 (20H, m, Ar*H*), 7.00 (1H, d, J = 8.8 Hz, Ar*H*), 6.67 (1H, d, J = 8.4 Hz, Ar*H*), 6.64 (1H, d, J = 12.1 Hz, C*H*=CH), 6.50 (1H, d, J = 11.9 Hz, C*H*=CH), 6.45 (2H, s, Ar*H*), 5.18 (2H, s, benzylic CH_2), 5.16 (2H, s, benzylic CH_2), 5.09 (2H, d, J = 1.2 Hz, benzylic CH_2), 5.07 (2H, d, J = 1.8 Hz, benzylic CH_2), 3.79 (3H, s, OCH_3), 3.77 (3H, s, OCH_3), 3.62 (6H, s, OCH_3).

^{31}P-NMR ($CDCl_3$, 122 MHz) δ 5.32, 5.426.

Di-potassium salt of CA1-(Ox16C) **27**[86,87]

The dibenzylphosphate stilbene **26** (0.323 g, 0.378 mmol) was dissolved in acetonitrile (4.5 mL) and cooled to -10^{o}C. TMS-Br (0.25 mL, 1.89 mmol), was added dropwise. Completion of this step was confirmed with TLC using. In a separate flask sodium methoxide (0.265 g, 3.78 mmol, 10 eq.), was dissolved in 4.5 mL dry methanol and cooled to -10^{o}C. The TMS phosphate product from the first flask was then added to the sodium methoxide solution. The reaction was allowed to reach room temperature and stirred for 3 h. Removal of the solvent gave a pale solid. Water (2 mL) was added to the solid. The pH was carefully titrated to pH 4.8 using 1 M HCl. The solution was filtered

and the filtrate rinsed with 2 mL water. Addition of 7 mL anhydrous ethanol to the solution resulted in formation of a white solid. This white solid was filtered, and dried. NMR confirmed the white solid is pure Oxi16C (100.6mg, 45% yield).

^{1}H NMR (D_2O, 300 MHz) δ 6.87 (1H, d, J = 8.7 Hz, Ar*H*), 6.74 (1H, d, J = 11.6 Hz, C*H*=CH), 6.68 (1H, d, J = 7.53 Hz, Ar*H*), 6.67 (2H, s, Ar*H*), 6.64 (1H, d, J = 15.18 Hz, C*H*=CH), 3.83 (3H, s, OCH_3), 3.73 (3H,s, OCH_3), 3.68 (6H, s, OCH_3).

^{13}C-NMR (D_2O, 75 MHz) δ 152.0, 151.7, 143.6, 143.4, 135.6, 134.3, 133.7, 129.9, 126.0, 125.1, 124.0, 108.2, 106.6, 60.8, 56.1, 55.9.

^{31}P-NMR (D_2O, 122 MHz) δ -3.00, -3.78

HPLC: Retention time: 17.26 minutes.

Alternative Synthetic Route for Radiolabeled CA1P (Ox16C)

3,4,5-Trimethoxybenzaldehyde* **28**[76]

Benzaldehyde **21** (4.77 g, 26.2 mmol) was dissolved in anhydrous DMF (50 mL). Anhydrous potassium carbonate (7.24 g, 52.4 mmol.) and methyl iodide (3.3 mL, 52.4 mmol) was added to the reaction. The reaction was refluxed 16 h, and then quenched with 60 mL water. The products were extracted with ethyl acetate (3 x 80 mL). The combined organic layers were washed with copious amounts of water, 1 M NaOH (50 mL), brine, dried with sodium sulfate, and condensed. The resultant solid was re-crystallized in a EtOAc and hexane mixture to give the methylated benzaldehyde (3.30 g 16.8 mmol, 64%) as white crystals. (*) is used to identify position of a radiolabeled carbon.

^{1}H-NMR ($CDCl_3$, 300 MHz) δ 9.87 (1H, s, C*H*O), 7.13 (2H, s, Ar*H*), 3.94 (3H, s, OCH_3), 3.93 (6H, s, OCH_3).

4-Methoxy-[2,3-di-(tert-buty-dimethyl-silyloxy)] benzaldehyde **29**[88]

DMAP (1.08 g, 8.85 mmol) and 2,3-dihydroxy-4-methoxy benzaldehyde (5.00 g, 29.7 mmol) were dissolved in 20 mL DMF. Once cooled to 0 ^{o}C, DIPEA (12.4 mL, 71.0 mmol,) DIPEA was added and the reaction was stirred for 10 min. TBS-Cl (10.7 g, 71.0 mmol) was added in portions and the reaction was stirred at room temperature for 16 h. Water (200 mL) was added and the products were extracted with EtOAc until no UV active molecules were separated. The combined organic layers were washed with 10 x 200 mL water, rinsed with brine, dried with sodium sulfate, and condensed. The products were separated with flash column chromatography (Hexanes: EtOAc; 80:20) to give the protected benzaldehyde (11.0 g, 27.7, 94%) as an off white solid.

^{1}H-NMR ($CDCl_3$, 300 MHz) δ 10.22 (1H, s, C*H*O), 7.48 (1H, d, J = 8.8 Hz, Ar*H*), 6.62 (1H, d, J = 8.8 Hz, Ar*H*), 3.84 (3H, s, OCH_3), 1.04 (9H, s, SiC(CH_3)$_3$), 0.99 (9H, s, SiC(CH_3)$_3$), 0.13 (12H, s, Si(CH_3)$_2$).

[2,3-di-(tert-butyl-dimethyl-silyloxy)-4-methyoxy-phenyl]-methanol **30**

Benzaldehyde **29** (11.0 g, 27.7 mmol) was dissolved in anhydrous ethanol (50 mL) and cooled to 0^{o}C. To this stirring mixture sodium borohydride (1.16 g, 30.5 mmol) was added in portions. The reaction was allowed for 30 min, at which point 30 mL water was added. The ethanol was removed, and the organics were extracted with ethyl acetate (3 x 50 mL). The combined organic layers were washed with brine, dried with sodium

sulfate, and condensed to give the desired benzyl alcohol (10.0 g, 25.1 mmol, 91%) as an off white solid.

^{1}H-NMR ($CDCl_3$, 300 MHz) δ 6.88 (1H, d, J = 8.4 Hz, Ar*H*), 6.51 (1H, d, J = 8.4 Hz, Ar*H*), 4.60 (2H. d, J = 6.2 Hz, C*H*$_2$OH), 3.76 (3H, s, OC*H*$_3$), 1.83 (1H, t, J = 6.2, O*H*), 1.03 (9H, s, SiC(C*H*$_3$)$_3$), 0.98 (9H, s, SiC(C*H*$_3$)$_3$), 0.14 (6H, s, Si(C*H*$_3$)$_2$), 0.10 (6H, s, Si(C*H*$_3$)$_2$).

1-Bromomethyl-2,3-di-(tert-butyl-dimethyl-silyloxy)-4-methoxy-benzene **31**

Benzyl alcohol **30** (10.0 g, 25.1 mmol) was dissolved in dry CH_2Cl_2 (40 mL) and cooled to 0^{o}C. To this mixture PBr_3 (1.8 mL, 18.8 mmol) was added. The reaction ran for three hours after which it was poured onto 150 mL ice, neutralized with sodium bicarbonate, and extracted with CH_2Cl_2 (3 x 50 mL). The combined organic layers were washed with brine, dried with sodium sulfate and condensed. The resultant orange solid was recrystallized in hexanes to give the desired benzyl bromide (10.1 g, 21.9 mmol, 87%) as a white solid.

^{1}H-NMR ($CDCl_3$, 300 MHz) δ 6.94 (1H, d, J = 8.5 Hz, Ar*H*), 6.5 (1H, d, J = 8.6 Hz, Ar*H*), 4.53 (2H, s, benzylic C*H*$_2$), 3.76 (3H, s, OC*H*$_3$), 1.07 (9H, s, SiC(C*H*$_3$)$_3$), 0.97 (9H, s, SiC(C*H*$_3$)$_3$), 0.14 (6H, d, J = 0.4 Hz, Si(C*H*$_3$)$_2$), 0.11 (6H, d, 0.5 Hz, Si(C*H*$_3$)$_2$).

[2,3-di-(tert-butyl-dimethyl-silyloxy) 4-methoxyl]-triphenylphosphonium benzyl bromide **32**

Benzyl bromide **31 (**10.09 g, 21.9 mmol), and triphenyl phosphine (6.32 g, 24.1 mmol) were dissolved in CH_2Cl_2 (50 mL). The reaction was refluxed 4 h. The dichloromethane was then removed, and the addition of ethyl acetate formed a white precipitate. The solid was filtered and rinsed with di-ethyl ether until no UV active spot

was detected in the filtrate. The solid was dried to give the desired phosphonium salt (14.5 g, 20.0 mmol, 91 %) as a white powder.

^{1}H-NMR ($CDCl_3$, 300 MHz) δ 7.50 (15H, m, Ar*H*), 6.60 (1H, dd, J = 8.7, 2.8 Hz, Ar*H*), 6.28 (1H, d, J= 8.8 Hz, Ar*H*), 5.11 (2H, d, J = 14.2 Hz, benzylic CH_2), 0.93 (9H, s, $SiC(CH_3)_3$), 0.80 (9H, s, $SiC(CH_3)_3$), 0.10 (6H, s, $Si(CH_3)_2$), -0.06 (6H, s, $Si(CH_3)_2$).

^{31}P-NMR ($CDCl_3$, 122) δ 21.22.

(Z)-1-[2',3'-di-(tert-butyl-dimethyl-silyloxy)-4'-methoxy]-2-(3,4,5-trimethoxyphenyl)-ethane **33**[84]

The phosphonium salt **32** (12.2 g, 16.8 mmol) was dissolved in dry THF (100 mL) and cooled to 0 ^{o}C. N-butyl lithium (6.7 mL 2.5M in hexanes, 15.3 mmol) was added and the mixture was stirred for 10 min. Benzaldehyde **28** (3.00 g, 15.3 mmol) was dissolved in 10 mL dry THF and added to the reaction. The reaction was stopped after 2 h with addition of 100 mL water. The THF was removed and the organic products were extracted with ethyl acetate. Separation by flash column chromatography gave the desired *Z*-stilbene (1.04 g, 1.78 mmol, 11%) as a white solid.

^{1}H-NMR ($CDCl_3$, 300 MHz) δ 6.91 (1H, d, J = 8.64 Hz, Ar*H*), 6.62 (2H, s, Ar*H*), 6.59 (1H, d, J = 12.2, C*H*=CH), 6.38 (1H, s, Ar*H*), 6.36 (1H, d, J = 11.8 Hz, C*H*=CH), 3.82 (3H, s, OCH_3), 3.74 (3H, s, OCH_3), 3.67 (6H, s, OCH_3), 1.04 (9H, s, $SiC(CH_3)_3$), 1.00 (9H, s, $SiC(CH_3)_3$), 0.19 (6H, s, $Si(CH_3)_2$), 0.11 (6H, s, $Si(CH_3)_2$).

3'-Methoxy-6-[2-(3,4,5-trimethoxy-phenyl)-vinyl]-benzene-1',2'-diol (CA1) **25**[84]

TBS protected stilbene **33** (1.00 g, 1.78 mmol), and KF (0.52 g, 8.90 mmol) KF, were dissolved in DMF (10 mL). To the solution 50% HBr (1 mL) was added, and the mixture was sonicated for 2 h. Water (50 mL) was added and the products were

extracted with ethyl acetate (3 x 50 mL). The combined organic layers were washed with water (10 x 50 mL), brine, dried with magnesium sulfate, and condensed to give the desired CA1 (0.659 g, 1.98 mmol) in >95% purity for a quantitative yield.

^{1}H-NMR ($CDCl_3$, 300 MHz) δ 6.76 (1H, d, J = 8.7 Hz, Ar*H*), 6.20 (1H, d, J = 12.06 Hz, C*H*=CH), 6.52 (2H, s, Ar*H*), 6.51 (1H, d, J = 11.7 Hz, C*H*=CH), 5.39 (2H, s, O*H*), 3.94 (3H, s, OCH_3), 3.83 (3H, s, OCH_3), 3.67(6H, s, OCH_3).

Synthesis of trans-CA1

(E)-1-(2',3'-diisopropoxy-4'-methoxy)-2-(3,4,5-trimethoxyphenyl)-ethene **34**

2,3-diisopropoxy-4-methoxybenzyl-triphenylphosphonium bromide (14.2 g, 24.5 mmol) was dissolved in THF (50 mL) and cooled to 0 ^{o}C. n-BuLi (9.0 mL, 22.44 mmol, 1.1 eq, 2.5M in hexanes) was added, and the reaction stirred for 10 min. Benzaldehyde **28** was dissolved in 5 mL of THF and added to the reaction. After 30 minutes the reaction was quenched with water. The organics were extracted with EtOAc. The combined organic layers were dried with magnesium sulfate, and condensed. The desired *E*-stilbene crashed out of solution. Recrystalization (Hexanes: EtOAc, 70:30) gave the *E*-stilbene (3.20 g, 7.68 mmol, 37%) as a white solid.

^{1}H-NMR ($CDCl_3$, 300 MHz) δ 7.32 (1H, d, J = 16.14 Hz, C*H*=CH), 7.29 (1H, d, J = 9.4 Hz, Ar*H*), 6.91 (1H, d, J = 16.5 Hz, C*H*=CH), 6.74 (2H, s, Ar*H*), 6.70 (1H, d, J = 8.8 Hz, Ar*H*), 4.62 (1H, sep, J = 6.2 Hz, C*H*(CH_3)$_3$), 4.47 (1H, sep, J = 6.1 Hz, C*H*(CH_3)$_3$), 3.91 (6H, s, OCH_3), 3.87 (3H, s, OCH_3), 3.86 (3H, s, OCH_3), 1.34 (6H, d, J = 2.0 Hz, CH(CH_3)$_3$), 1.29 (6H, d, J = 2.0 Hz, CH(CH_3)$_3$).

(Z)-3'-Methoxy-6-[2-(3,4,5-trimethoxy-phenyl)-vinyl]-benzene-1',2'-diol (CA1) **35**[84]

Stilbene **34** (2.00 g, 4.80 mmol) was dissolved in CH_2Cl_2 (5 mL) and cooled to 0°C. $TiCl_4$ (1.3 mL, 12.0 mmol) was added to the reaction. The mixture was sonicated for three minutes. The reaction was quenched with 20 mL water, and the products were extracted with EtOAc (3 x 50 mL). The combined organic layers were washed with water until there was no pink coloration in the water layer. The organic layer was then washed with brine, dried with sodium sulfate, and condensed to give trans-CA1 (1.36 g, 4.1 mmol, 86%) as a tan solid.

^{1}H-NMR ($CDCl_3$, 300 MHz) δ 7.23 (1H,d , J = 16.4 Hz, C*H*=CH), 7.05 (1H, d, J = 16.3 Hz, C*H*=CH), 7.05 (1H, d, J = 8.7 Hz, Ar*H*), 6.49 (1H, d, J = 8.7 Hz, Ar*H*), 5.81 (1H, s, O*H*), 5.63 (1H, s, O*H*), 3.89 (6H, s, OCH_3), 3.87 (3H, s, OCH_3), 3.86 (3H, s, OCH_3).

Synthesis of Phenstatin Derivatives

[3', 4'-Bis-(tert-butyl-dimethyl-silyloxy)-5'-methoxy-phenyl]-(3,4,5-trimethoxy-phenyl)-methanone **36**

3,4,5-trimethoxybenzyl bromide (1.43 g, 5.79 mmol) was dissolved in anhydrous ether (4 mL). The flask was then purged with nitrogen and cooled to -78°C. N-butyllithium (3.62 mL 1.6 M in hexane, 5.79 mmol) was then added slowly. The reaction mixture was allowed to warm to -30 °C. The TBS-protected aldehyde **4** (1.00 g, 2.24 mmol) was dissolved in 5 mL anhydrous ether and transferred slowly to the bromide/butyl lithium reaction. The reaction was allowed to warm to room temperature for one hour after then was quenched with de-ionized water. The phases were separated,

and the aqueous layer was then extracted with CH_2Cl_2. The organic layers were combined, dried with Na_2SO_4, and concentrated under reduced pressure. Crude product (0.63 g) was carried onto the next step without further purification. The 0.63 g of crude product was dissolved in 5 mL of anhydrous dichloromethane, cooled to 0 ^oC. Celite (3 g) was added followed by PCC (0.264 g, 1.23 mmol) and the reaction proceeded for 10 h. The volatiles were then removed under reduced pressure and compound was purified by flash column chromatography (20:80 Ethyl acetate: Hexanes) to give the protected benzophenone (0.154 g, 0.274 mmol, 24%) as pure white crystals.

^{1}H-NMR ($CDCl_3$, 300 MHz) δ 7.06 (1H, d, J = 2.0 Hz, Ar*H*), 6.98 (2H, s, Ar*H*), 6.95 (1H, d, J = 2.0 Hz, Ar*H*), 3.93 (3H, s, OCH_3), 3.88 (6H, s, OCH_3), 3.82 (3H, s, OCH_3), 1.00 (9H, s, Si(CH_3)$_3$), 0.95 (9H, s, Si(CH_3)$_3$), 0.19 (6H, s, Si(CH_3)$_2$), 0.18 (6H, s, Si(CH_3)$_2$).

(3',4'-dihydroxy-5'-methoxy-phenyl)-(3,4,5-trimethoxy-phenyl)-methanone **37**

Benzophenone **36** (0.154 g, 0.274 mmol) was dissolved in DMF (10 mL). Anhydrous KF (0.25 g, 4.30 mmol) was added to the solution followed by 48% HBr (0.25 mL). The solution was then sonicated for 2 h. HCl (20 mL, 6 M) and ether (20 mL) was then added. The organic layer was separated, washed with brine, dried with sodium sulfate and condensed to give the deprotected benzophenone (0.0433 g, 0.130 mmol, 47%) as a white solid. (R_f = 0.25; 50:50; Hexanes:EtOAc). m.p. = 164-166 ^oC. Anal. Calcd for $C_{17}H_{18}O_7$: C, 61.07; H, 5.43. Found: C, 60.97; H, 5.45.

^{1}H-NMR ($CDCl_3$, 300 MHz) δ 7.09 (2H, d, J = 0.9, Ar*H*), 7.02 (2H, s, Ar*H*), 5.82 (1H, s, O*H*), 5.36 (1H, s, O*H*), 3.96 (3H, s, OCH_3), 3.94 (3H, s, OCH_3), 3.89 (6H, s, OCH_3).

^{13}C-NMR ($CDCl_3$, 75 MHz) δ 194.7, 152.8, 146.8, 143.1, 141.72, 136.7, 133.1, 129.5, 112.5, 107.5, 105.6, 77.2, 61.0, 56.4, 30.9.

Synthesis of Indole Derivatives

1-[3,4-Bis-(tert-butyldimethylsilyloxy)-5-methoxy-phenyl]-ethanol **38**

TBS protected benzaldehyde **4** (14.8 g, 37.4 mmol) was dissolved in anhydrous ether (100 mL) and cooled to 0 ^{o}C. Methyl lithium (48.1 mL 1.6 M in ether, 77.7 mmol) was added to the reaction slowly. After 4 h the reaction was quenched with water. The organic phase was separated, dried with sodium sulfate, and concentrated under reduced pressure to give the benzyl alcohol (15.5 g, 37.6 mmol, quantitative) as a yellow oil. The product was taken to the next step without further purification.

^{1}H-NMR ($CDCl_3$, 300 MHz) δ 6.53 (1H, d, J = 2.0 Hz, Ar*H*), 6.48 (1H, d, J = 2.0 Hz, Ar*H*), 4.74 (1H, m, C*H*OH), 3.81 (3H, s, OCH_3), 2.03 (1H, s, O*H*), 1.43 (3H, d, J = 6.4 Hz), 0.99 (9H, s, SiC(CH_3)$_3$), 0.97 (9H, s, SiC(CH_3)$_3$), 0.19 (6H, s, Si(CH_3)), 0.11 Si(CH_3)).

1-[3,4-Bis-(tert-butyldimethylsilyloxy)-5-methoxy-phenyl]-ethanone **39**

Benzyl alcohol **38** (25.46 g , 61.69 mmol) was dissolved in anhydrous dichloromethane (100 mL) and cooled to 0 ^{o}C. Celite (~10 g) was added to the reaction. PCC (14.62 g, 67.86 mmol) was added and the reaction stirred at room temperature for 18 h. The mixture was then passed through a short bad of silica and flushed with dichloromethane until no UV active products were detected. The combined organics were dried with sodium sulfate and condensed under reduced pressure to give the desired acetophenone (25.33 g, 61.68 mmol, quantitative) as a yellow solid.

^{1}H-NMR ($CDCl_3$, 300 MHz) δ 7.16 (1H, d, J = 2.0 Hz, Ar*H*), 7.14 (1H, d, J = 2.0 Hz, Ar*H*), 3.83 (3H, s, OCH_3), 2.52 (3H, s, COCH_3), 0.99 (18H, s, SiC(CH_3)$_3$), 0.23 (6H, s, Si(CH_3)$_2$), 0.11 (6H, s, Si(CH_3)$_2$).

1,2-Bis-(tert-butyldimethylsilyloxy)-3-methoxy-5-(1-trimethylsiloxy-vinyl)-benzene **40**

A LDA solutions was prepared by combining di-isopropyl amine (6.52 mL, 46.5 mmol) with n-butyllithium (18.6 mL 2.5 M in ether) in anhydrous ether (100 mL) and cooled to 0 ^{o}C. Acetophenone **39** (12.7 g, 30.9 mmol) was dissolved in 5 mL ether and added slowly to the LDA solution. After 5 min, TMS-Cl (5.94 mL, 46.5 mmol) was added. The reaction proceeded for 3 h,and was then neutralized with 10% sodium bicarbonate. The products were extracted with hexanes, dried with sodium sulfate, and concentrated under reduced pressure to give the enol ether (14.8 g, 30.6 mmol, 99%) as a yellow oil. The product was not purified further.

^{1}H-NMR ($CDCl_3$, 300 MHz) δ 6.78 (1H, d, J = 6.78 Hz, Ar*H*), 6.73 (1H, d, J = 2.1 Hz), 4.75 (1H, d, J = 1.6 Hz, CH_2), 4.33, (1H, d, J = 1.6 Hz, CH_2), 3.78 (3H, s, OCH_3), 0.99 (9H, s, SiC(CH_3)$_3$), 0.97 (9H, s, SiC(CH_3)$_3$), 0.26 (9H, s, SiC(CH_3)$_3$), 0.21 (6H, s, Si(CH_3)$_2$), 0.07 (6H, s, Si(CH_3)$_2$).

1-[3,4-Bis-(tert-butyldimethylsilyloxy)-5-methoxy-phenyl]-2-bromo-ethanone **41**

TMS enol ether **40** (14.8 g, 30.6 mmol) and anhydrous potassium carbonate (1 g) were dissolved in CH_2Cl_2 (60 mL) and cooled to 0 ^{o}C. Bromine (1.37 mL, 0.0267 mmol) was dissolved in CH_2Cl_2 (5 mL) and added to the reaction slowly. The reaction was allowed for 20 min then was quenched with a saturated sodium thiosulfate solution. The organic phase was separated, dried with sodium sulfate, condensed onto silica gel, and

purified by flash column chromatography. The desired bromo ethanone **41** (7.48 g, 15.3 mmol, 41%) was collected as an orange solid.

^{1}H-NMR ($CDCl_3$, 300 MHz) δ 7.19 (1H, d, J = 2.1 Hz, Ar*H*), 7.18 (1H, d, J = 2.1 Hz, Ar*H*), 4.34 (2H, s, CH_2), 3.83 (3H, s, OCH_3), 0.99 (18H, s, SiC(CH_3)$_3$), 0.25 (6H, s, Si(CH_3)$_2$), 0.16 (6H, s, Si(CH_3)$_2$).

2-[3',4'-Bis-tert-butyl-dimethyl-silyloxy)-5'-methoxy-phenyl]-6-methoxy-1H-indole **42**

DMF (5.0 mL) and m-anisidine (0.546 mL, 4.89 mmol) were combined in a two neck flask and heated to 90 ^{o}C. Bromo ethanone **42** (1.12 g, 2.30 mmol) was dissolved in DMF (4 mL) and added to the mixture. The reaction was refluxed for 18 h, then cooled and quenched with water. The products were extracted with ethyl acetate, washed with copious amounts of water, dried with sodium sulfate, condensed under vacuum, and purified by flash column chromatography. The indole producte **42** (0.244 g, 0.475 mmol, 31%) was collected as pink crystals.

^{1}H-NMR ($CDCl_3$, 300 MHz) δ 8.05 (1H, b, N*H*), 7.47 (1H, d, J = 8.6 Hz, Ar*H*), 6.91 (1H, d, J = 2.3 Hz), 6.78 (1H, dd, J = 8.6, 2.3 Hz, Ar*H*), 6.74 (2H, s, Ar*H*), 6.60 (1H, dd, J = 2.1, 0.8 Hz, Ar*H*), 3.87 (3H, s, OCH_3), 3.85 (3H, s, OCH_3), 1.01 (18H, s, SiC(CH_3)$_3$), 0.25 (6H, s, Si(CH_3)$_2$), 0.16 (6H, s, Si(CH_3)$_2$).

^{13}C-NMR ($CDCl_3$, 75 MHz) δ 156.4 152.5, 148.0, 137.5, 137.4, 136.2, 125.1, 123.8, 120.9, 110.9, 109.9, 102.0, 98.9, 94.6, 55.6, 55.3, 26.1, 26.0, 25.6, 18.7, 18.6, -3.6, -3.8, -4.1.

{2-[3',4'-Bis-(tert-butyl-dimethyl-silyloxy)-5'-methoxy-phenyl]-6-methoxy-1H-indole-3-yl}-(3'',4'',5''-trimethoxy-phenyl)-methanone **43**

Indole **42** (0.150 g, 0.292 mmol) was dissolved in o-dichlorobenzene (3.0 mL). The solution was heated to 130 ^{o}C, and 3,4,5-trimethoxy benzoyl chloride (0.101 g, 0.443 mmol) was added. The reaction was refluxed for 18 h, then cooled and quenched with saturated sodium sulfate, condensed onto celite, and the products were purified by flash column chromatography. The benzoylated indole **43** (0.120 g, 0.169 mmol, 62%) was recovered as a yellow solid.

^{1}H-NMR ($CDCl_3$, 300 MHz) δ 8.77 (1H, s, N*H*), 7.93 (1H, d, J = 9.5 Hz, Ar*H*), 7.01 (2H, s, Ar*H*), 6.91 (1H, d, J = 2.2 Hz, Ar*H*), 6.88 (1H, s, Ar*H*), 6.53 (1H, d, J = 2.0 Hz), 6.49 (1H, d, J = 1.9 Hz, Ar*H*), 3.80 (6H, s, OCH_3), 3.66 (6H, s, OCH_3), 3.56 (3H, s, OCH_3), 0.95 (9H, s, SiC(CH_3)$_3$), 0.92 (9H, s, SiC(CH_3)$_3$), 0.12 (6H, s, SiC(CH_3)$_2$), 0.06 (6H, s, SiC(CH_3)$_2$).

^{13}C-NMR ($CDCl_3$, 75 MHz) δ 191.6, 157.4, 152.5, 152.1, 147.8, 141.7, 141.5, 137.4, 136.3, 134.4, 124.2, 123.4, 122.5, 114.1, 112.8, 111.7, 107.3, 106.4, 94.5, 60.9, 56.0, 55.7, 26.0, 25.8, 18.6, 18.4, -3.9, -4.2.

[2-(3',4'-Dihydroxy-5'-methoxy-phenyl)-5-methoxy-1H-indol-3-yl]-(3'',4'',5''-trimethoxy-phenyl)-methanone **44**

TBS-protected indole **43** (0.197 g, 0.295 mmol) was dissolved dichloromethane (5 mL). TBAF (0.89 mL of 1M) was then added and the reaction stirred 4 h. Water was then added and the phases were separated. The aqueous layer was extracted with dichloromethane. The organic layers were combined, dried with sodium sulfate, and concentrated under reduced pressure to give the desired deprotected indole **44** (71.5 mg,

0.149 mmol, 50%). (R_f = 0.08; 50:50; Hexanes:EtOAc). m.p. = 142-144 ^oC. Anal. Calcd for $C_{26}H_{25}NO_8 \bullet 0.5H_2O$: C, 63.39; H, 5.36; N, 2.87. Found: C, 63.42; H, 5.24; N, 2.81.

^{1}H-NMR ($CDCl_3$, 300 MHz) δ 8.40 (1H, b, N*H*), 8.00 (1H, d, J = 8.9 Hz, Ar*H*), 6.93 (4H, m, Ar*H*), 6.72 (1H, s, Ar*H*), 6.24 (1H, s, Ar*H*), 5.40 (1H, s, O*H*), 5.38 (1H, s, O*H*), 3.88 (3H, s, OCH_3), 3.79 (3H, s, OCH_3), 3.70 (6H, s, OCH_3), 3.59 (3H, s, OCH_3).

^{13}C-NMR ($CDCl_3$, 75 MHz) δ 192.6, 157.2, 152.4, 146.7, 143.9, 143.5, 141.0, 136.4, 135.0, 133.3, 123.5, 122.9, 122.2, 112.4, 111.7, 108.9, 107.2, 105.7, 94.7, 60.8, 55.9, 55.8, 55.6.

3-Methoxy-5-(6-methoxy-1H-indol-2-yl)-benzene-1,2-diol **45**

TBS protected indole **42** (0.150 g, 0.292 mmol) was dissolved in dichloromethane (5 mL). TBAF (0.878 mL of 1M) was added and the reaction ran for 4 h. Water was added and the phases were separated. The aqueous layer was extracted with dichloromethane. The combined organic layers were dried with sodium sulfate, and concentrated under reduced pressure to give the desired unprotected indole **45** (41.7 mg, 0.146 mmol, 50%).

^{1}H-NMR ($CDCl_3$, 300 MHz) δ 8.28 (1H, b, N*H*), 7.45 (1H, d, J = 8.6 Hz, Ar*H*), 6.84 (2H, s, Ar*H*), 6.78 (1H, dd, J = 8.6, 2.2 Hz, Ar*H*), 6.73 (1H, s, Ar*H*), 6.61 (1H, s, Ar*H*), 5.73 (2H, b, O*H*), 3.90 (3H, s, OCH_3), 3.82 (3H, s, OCH_3).

^{13}C-NMR ($CDCl_3$, 75 MHz) δ 156.4, 147.4, 144.3, 137.4, 137.1, 132.2, 125.0, 123.6, 120.9, 110.0, 105.6, 100.6, 98.9, 94.6, 56.2, 55.7.

[2-(3',4'-Dihydroxy-5'-methoxy-phenyl)-5-methoxy-1H-indol-3-yl]-(3'',4'',5''-trifluoro-phenyl)-methanone **46**

Indole **42** (0.500 g, 0.973 mmol) was dissolved in o-dichlorobenzene (10.0 mL). The reaction was heated to 130 ^{o}C and 3,4,5-trifluoro benzoyl chloride (0.280 g, 1.46 mmol) was added. The Reaction was refluxed for 18 h, then cooled and quenched with saturated sodium sulfate, condensed onto celite, and the products were purified by flash column chromatography. The benzoylated indole **46** (0.583 g, 0.868 mmol, 89%) was recovered as a yellow solid.

^{1}H-NMR ($CDCl_3$, 300 MHz) δ 9.09 (1H, b, N*H*), 8.03 (1H, d, J = 8.7 Hz, Ar*H*), 7.28 (1H, d, J = 4.4 Hz, Ar*H*), 7.23 (1H, d, J = 7.6 Hz, Ar*H*), 6.94 (1H, dd, J = 8.7, 2.3 Hz, Ar*H*), 6.90 (1H, d, J = 2.2 Hz), 6.49 (1H, d, J = 2.0 Hz, Ar*H*), 6.39 (1H, d, J = 2.0 Hz, Ar*H*), 3.83 (3H, s, OCH_3), 3.62 (3H, s, OCH_3), 0.98 (9H, s, SiC(CH_3)$_3$), 0.97 (9H, s, SiC(CH_3)$_3$), 0.17 (6H, s, Si(CH_3)$_2$), 0.11 (6H, s, Si(CH_3)$_2$).

^{13}C-NMR ($CDCl_3$, 75 MHz) δ 189.2, 157.6, 152.1, 149.8 (dd, J_{C-F} = 10.2, 3.2 Hz), 147.9, 144.23, 144.2 (t, J_{C-F} = 15.4 Hz), 140.8 (t, J_{C-F} = 16.0 Hz), 137.7, 136.5, 135.8, 123.6, 122.7, 122.2, 114.7, 113.8 (d, J_{C-F} = 6.5 Hz), 113.6 (d, J_{C-F} = 6.5 Hz), 112.03, 106.4, 94.8, 55.9, 55.1, 25.9, 25.7, 18.6, 18.4, -4.0, -4.4.

^{19}F-NMR ($CDCl_3$, 282 MHz) δ -133.80 (2F, d, J = 19.7 Hz), -154.66 (1F, t, J = 22.6 Hz)

[2-(3',4'-Dihydroxy-5'-methoxy-phenyl)-5-methoxy-1H-indol-3-yl]-(3'',4'',5''-fluoro-phenyl)-methanone **47**

TBS-protected indole **46** (0.283 g, 0.425 mmol) was dissolved DMF (10 mL) and cooled to 0 ^{o}C . TBAF (1.35 mL of 1M, 1.35 mmol) was then added and the reaction stirred 4 h. Water was then added and the phases were separated. The aqueous layer was

extracted with dichloromethane. The organic layers were combined, dried with sodium sulfate, and concentrated under reduced pressure to give the desired deprotected indole **47** (82 mg, 0.185 mmol, 44%). (R_f = 0.33; 50:50; Hexanes:EtOAc). m.p. = 230-232 ^oC. Anal. Calcd for $C_{26}H_{25}NO_8 \bullet 1.0H_2O$: C, 59.87; H, 3.93; N, 3.04. Found: C, 61.20; H, 3.84; N, 3.12.

^{1}H-NMR ($CDCl_3$, 300 MHz) δ 9.07 (1H, s, N*H*), 7.89 (1H, d, J = 8.7 Hz, Ar*H*), 7.30 (2H, t, J = 7.3 Hz, Ar*H*), 6.93 (1H,d , J = 2.2 Hz, Ar*H*), 6.85 (1H, dt, J = 8.7, 1.6 Hz, Ar*H*), 6.44 (1H, t, J = 0.8, Ar*H*), 6.31 (1H, d, J = 1.9 Hz, Ar*H*), 3.80 (3H, s, OCH_3), 3.61 (3H, s, OCH_3).

^{13}C-NMR ($CDCl_3$, 125 MHz) δ 188.7, 157.2, 148.4, 146.9, 146.2, 137.3, 135.7, 122.8, 122.13, 122.1, 114.31, 114.3, 114.1, 112.2, 111.2, 111.1, 106.7, 95.5, 56.4, 56.0.

^{19}F-NMR ($CDCl_3$, 282 MHz) δ -135.7 (2F, d, J = 25.4 Hz), -158.45 (1F, t, J = 22.6 Hz)

3-(Isopropoxy)-4-methoxybenzaldehyde **48**[14]

Isovanillan (11.0 g, 72.3 mmol), was dissolved in DMF (150 mL) and heated to 80 ^oC. Potassium carbonate (20.0 g, 145 mmol) was added and the mixture was heated to 90 ^oC. 2-bromopropane (13.6 mL, 145 mmol) was added and the reaction refluxed for 8 h. The mixture was then cooled, and quenched with water. The products were extracted with ethyl acetate. The combined organic layers were washed with copious amounts of water, dried with sodium sulfate, condensed under reduced pressure, and purified by flash column chromatography. The desired isopropyl protected isovanillan **48** (11.5g, 59.3 mmol, 82%) was recovered as a tan solid.

^{1}H-NMR ($CDCl_3$, 300 MHz) δ 9.80 (1H, s, C*H*O), 7.41 (1H, d, J = 1.9 Hz, Ar*H*), 7.38 (1H, q, J = 1.9 Hz, Ar*H*), 6.94 (1H, d, J = 8.1 Hz, Ar*H*), 4.50 (1H, sep, J = 6.1 Hz, C*H*(CH_3)), 3.89 (3H, s, OCH_3), 1.36 (3H, s, CH(CH_3)$_2$), 1.34 (3H, s, CH(CH_3)$_2$).

^{13}C-NMR ($CDCl_3$, 75 MHz) δ 190.8, 155.5, 147.7, 129.9, 126.4, 112.6, 110.8, 71.2, 56.0, 21.8.

3-(Isopropoxy)-1-(1-hydroxyethyl)-4-methoxybenzene **49**[14]

Aldehyde **48** (11.5 g, 59.3 mmol) was dissolved in ether (20 mL) and cooled to 0 ^{o}C. Methyl lithium (84.7 mL 1.4 M in ether, 119 mmol) was added slowly, and the reaction was stirred at room temperature for 2 hours. The solution was cooled to 0 ^{o}C, and was slowly quenched with water. The organic phase was separated, dried with sodium sulfate and condensed under reduced pressure to give the benzyl alcohol **49** (12.2 g, 58.1 mmol, 98%) as a yellow oil.

^{1}H-NMR ($CDCl_3$, 300 MHz) δ 6.90 (1H, d, J = 1.9 Hz, Ar*H*), 6.83 (1H, ddd, J = 8.23, 2.0, 0.4 Hz, Ar*H*), 6.77 (1H, d, J = 8.3 Hz, Ar*H*), 4.72 (1H, q, J = 6.4 Hz, C*H*OH), 4.49 (1H, sep, J = 6.2 Hz, C*H*(CH_3)$_2$), 3.78 (3H, s, OCH_3), 2.58 (1H, b, O*H*), 1.40 (3H, d, J = 6.4 Hz, CHCH_3), 1.34 (3H, s, CH(CH_3)$_2$), 1.30 (3H, s, CH(CH_3)$_2$).

3-(Isopropoxy)-4-methoxyacetophenone **50**[14]

Celite (10 g) was suspended in dry dichloromethane (60 mL) and cooled to 0 ^{o}C. Benzyl alcohol **49** (12.2 g, 58.1 mmol), was dissolved in the mixture. PCC (13.8 g, 63.9 mmol) was added to the reaction, which was then stirred for 16 h at room temp. The solvent was removed under reduced pressure and the products were separated by flash

column chromatography. The desired acetophenone **50** (10.1 g, 48.6 mmol, 84%) was isolated as a yellow solid.

^{1}H-NMR ($CDCl_3$, 300MHz) δ 7.56 (1H, d, J = 2.1 Hz, Ar*H*), 7.53 (1H, td, J = 2.1, 0.4 Hz, Ar*H*), 13.74 (1H, d, J = 8.1 Hz, Ar*H*), 4.61 (1H, sep, J = 6.2 Hz, C*H*$(CH3)_2$), 3.90 (3H, s, OCH_3), 2.53 (3H, s, COCH_3), 1.37 (3H, s, CH(C$H_3)_2$), 1.33 (3H, s, CH(C$H_3)_2$).

1-[(3-Isopropoxy-4-methoxy)-phenyl]-1-trimethylsilylethene **51**[14]

An LDA solution was prepared by dissolving diisopropylamine (10.2 mL, 72.9 mmol) in ether (50 mL) and cooled to 0 ^{o}C. N-butyllitium (29.2 mL 2.5 M in ether, 72.9 mmol) was then added and the solution stirred for 5 min. Acetophenone **50** was dissolved in ether (50 mL) and added slowly to the LDA solution. The resulting reaction was stirred at room temp. for 18 h. The mixture was then quenched slowly with water. The products were extracted with hexanes. The combined organic layers were dried with magnesium sulfate, and concentrated under pressure to give the TMS enol ether **51** (13.6 g, 48.6 mmol, quantitative) as a red oil.

^{1}H-NMR ($CDCl_3$, 300 MHz) δ 7.19 (1H, d, J = 2.1 Hz, Ar*H*), 7.16 (1H, s, Ar*H*), 6.81 (1H, dd, J = 7.8, 0.9 Hz, Ar*H*), 4.78 (1H, d, J = 1.6 Hz, C=CH_2), 4.53 (1H, sep, J = 6.1 Hz, C*H*$(CH_3)_2$), 4.34 (1H, d, J = 1.6 Hz, C=CH_2), 3.83 (3H, s, OCH_3), 1.38 (3H, s, CH(C$H_3)_2$), 1.36 (3H, s, CH(C$H_3)_2$), 0.26 (6H, s, Si(C$H_3)_2$).

3-(Isopropoxy)-4-methoxy-2-bromoacetophenone **52**[14]

TMS enol ether **51** (14.6 g, 51.9 mmol) was dissolved in dichloromethane (250 mL). Potassium carbonate (9.40 g, 68.0 mmol) was added and the mixture was cooled to 0 ^{o}C. Bromine (2.32 mL, 45.2 mmol) was added and the reaction was allowed until no

acetophenone **50** was observed by TLC. The reaction was then quenched with 10% sodium thiosulfate (100 mL). The products were extracted with dichloromethane. The combined organic layers were with magnesium sulfate, and condensed under reduced pressure. The products were separated by flash column chromatography (80:20; Hexane:EtOAc) to give the bromoactophenone **52** (6.53 g, 22.7 mmol, 44%).

^{1}H-NMR ($CDCl_3$, 300 MHz) δ 7.59 (1H, dd, J = 8.4, 2.1 Hz, Ar*H*), 7.54 (1H, d, J = 2.1 Hz, Ar*H*), 6.90 (1H, d, J = 8.4 Hz), 4.62 (1H, sep, J = 7.2 Hz), 4.40 (2H, s, CH_2Br), 3.92 (3H, s, OCH_3), 1.38 (3H, s, CH(CH_3)$_2$), 1.36 (3H, s, CH(CH_3)$_2$).

2-[(3'-Isopropoxy-4'-methoxy)-phenyl]-6-methoxyindole **53**[14]

m-Anisidine (5.2 mL, 46.0 mmol) was dissolved in DMF (3.5 mL) brought to 170 ^{o}C. Bromoacetophenone **52** (3.99 g, 13.9 mmol) was dissolved in DMF (5 mL) and added to the refluxing m-anisidine mixture. The reaction refluxed for 12 h, then was cooled, and quenched with water. The products were extracted with ethyl acetate. The combined organic layers were dried with sodium sulfate, and condensed under reduced pressure. The products were purified using flash column chromatography to give the desired indole **53** (2.94 g, 9.44 mmol, 21%).

^{1}H-NMR ($CDCl_3$, 300 MHz) δ 8.18 (1H, b, N*H*), 7.48 (1H, d, 8.6 Hz, Ar*H*), 7.19 (1H, dd, J = 5.7, 2.1 Hz, Ar*H*), 7.15 (1H, d, J = 2.1 Hz, Ar*H*), 6.93 (1H, d, J = 8.3 Hz, Ar*H*), 6.89 (1H, d, J = 2.3 Hz, Ar*H*), 6.79 (1H, dd, J = 8.6, 2.3 Hz), 6.63 (1H, dd, J = 2.1, 0.8 Hz, Ar*H*), 4.62 (1H, sep, J = 6.1 Hz, C*H*(CH$_3$)$_2$), 3.89 (3H, s, OCH_3), 3.86 (3H, s, OCH_3), 1.42 (3H, s, CH(CH_3)$_2$), 1.40 (3H, s, CH(CH_3)$_2$).

^{13}C-NMR ($CDCl_3$, 75 MHz) δ 156.4, 150.2, 147.6, 137.4, 137.1, 125.8, 123.7, 120.9, 117.8, 113.4, 112.4, 109.9, 98.8, 94.6, 71.8, 56.1, 55.7, 22.2.

2-[(3'-Isopropoxy-4'-methoxy)-phenyl]-3-[(3'',4'',5''-trifluoro)-benzoyl]-6-methoxyindole **54**

Indole **53** (1.07 g, 3.43 mmol) was dissolved in o-dichlorobenzene (5 mL) and heated to 130 ^{o}C. Trifluoro benzoyl chloride (1.00 g, 5.14 mmol) was added dropwise. The reaction was allowed to reflux for 4 h, then was cooled. The products were absorbed onto celite, then purified by flash column chromatography. The benzoylated indole **54** (0.968 g, 2.06 mmol, 60%) was collected as a yellow solid.

^{1}H-NMR ($CDCl_3$, 300 MHz) δ 8.57 (1H, b, N*H*), 7.92 (1H, d, J = 8.6 Hz, Ar*H*), 7.28 (2H, m, Ar*H*), 6.92 (3H, m, Ar*H*), 6.77 (2H, m, Ar*H*), 4.31 (1H, sep, J = 6.1 Hz, C*H*(CH_3)$_2$), 3.87 (3H, s, OC*H*$_3$), 3.82 (3H, s, OC*H*$_3$), 1.29 (3H, s, CH(C*H*$_3$)$_2$), 1.27 (3H, s, CH(C*H*$_3$)$_2$).

^{13}C-NMR ($CDCl_3$, 75 MHz) δ 189.0, 157.6, 151.4, 147.2, 143.6, 136.3, 124.1, 122.5, 122.3, 122.25, 117.0, 114.0, 113.8, 112.1, 112.07, 111.8, 94.7, 72.1, 56.0, 55.7, 21.9.

^{19}F-NMR ($CDCl_3$, 282 MHz) δ -133.98 (2F, d, J = 22.6 Hz), 155.11 (1F, t, J = 19.7 Hz).

2-[(3'-Hydroxy-4'-methoxy)-phenyl]-3-[(3'',4'',5''-trifluoro)-benzoyl]-6-methoxyindole **55**

Protected indole **54** (0.600 g, 1.28 mmol) was dissolved in dichloromethane (5 mL). Aluminum trichloride (0.511 g, 3.83 mmol) was added and the reaction stirred at room temperature for 45 min. Water was added, and the organic layer was separated, washed with brine, and dried with sodium sulfate. The desired indole **55** (0.408 g, 0.957 mmol, 75%) was collected as a yellow green solid. (R_f = 0.33; 70:30; Hexanes:EtOAc).

m.p. = 263-265 ^{o}C. Anal. Calcd for $C_{23}H_{16}F_3NO_4$: C, 64.64; H, 3.77; N, 3.28. Found: C, 64.03; H, 3.86; N, 3.23.

^{1}H-NMR (DMSO-d_6, 300 MHz) δ 12.04 (1H, b, N*H*), 9.14 (1H, s, O*H*), 7.86 (1H, d, J = 8.7 Hz, Ar*H*), 7.56 (2H, m, Ar*H*), 6.95 (2H, d, J = 2.1 Hz, Ar*H*), 6.84 (2H, m, Ar*H*), 6.72 (2H, m, Ar*H*), 3.82 (3H, s, OCH_3), 3.74 (3H, s, OCH_3).

^{13}C-NMR (DMSO-d_6, 75 MHz) δ 187.9, 156.5, 148.1, 146.0, 145.4, 136.6, 124.1, 121.9, 121.4, 121.1, 116.7, 113.6, 113.3, 111.7, 111.5, 110.7, 94.8, 55.7, 55.2.

^{19}F-NMR (DMSO-d_6, 282 MHz) δ -135.5 (2F, dd, J = 14.1, 8.5 Hz), -158.6 (1F, tt, J = 28.2, 8.5 Hz).

3-(tert-Butyldimethylsilyloxy)-4-methoxybenzaldehyde **56**[14]

Isovanillan (15.3 g, 100 mmol) was dissolved in CH_2Cl_2 (200 mL). TEA (15.4 mL, 110 mmol) was added to the solution, followed by addition of DMAP (1.22 10.0 mmol). The mixture was cooled to 0 ^{o}C and TBS-Cl (16.6 g, 110 mmol) was added. The reaction stirred for 16 h, then was quenched with water. The organic phase was collected, dried with sodium sulfate, and concentrated under reduced pressure to give the TBS-protected benzaldehyde **56** (25.8 g, 97%) as a yellow oil.

^{1}H-NMR ($CDCl_3$, 300 MHz) δ 9.84 (1H, s, C*H*O), 7.49 (1H, dd, J = 8.1, 2.1 Hz, Ar*H*), 7.48 (1H, d, J = 2.1 Hz, Ar*H*), 6.98 (1H, d, J = 8.2 Hz, Ar*H*), 4.04 (3H, s, OCH_3), 1.03 (9H, s, SiC(C*H*)$_3$), 0.20 (6H, s, SiC(CH_3)$_2$).

3-(tert-Butyldimethylsilyloxy)-1-(1'-hydroxyethyl)-4-methoxybenzene **57**[14]

TBS protected benzaldehyde **57** (26.6 g, 100 mmol) was dissolved in anhydrous ether (250 mL). The solution was cooled to 0 ^{o}C and methyl lithium (150 mL 1.4 M in

ether, 210 mmol) was added slowly. The reaction stirred at room temp. for 16 h. Water was added and the organic phase was separated, dried with sodium sulfate, and concentrated to give the benzyl alcohol **57** (25.9 g, 92.0 mmol, 92%) as a yellow oil.

^{1}H-NMR ($CDCl_3$, 300 MHz) δ 6.85 (2H, m, Ar*H*), 6.78 (1H, d, J = 9.5 Hz, Ar*H*), 4.75 (1H, q, J = 5.3 Hz, C*H*OH), 3.76 (3H, s, OCH_3), 1.42 (3H, d, J = 5.3 Hz, CHCH_3), 0.97 (9H, s, SiC(CH_3)$_3$), 0.13 (6H, s, Si(CH_3)$_2$).

3-(tert-Butyldimethylsilyloxy)-4-methoxyacetophenone **58**[14]

Celite (50 g) and the benzyl alcohol **57** (114 g, 405 mmol), were dissolved in dichloromethane (800 mL) and cooled to 0 ^{o}C. PCC (96.0 g, 446 mmol) was added to the mixture and allowed to stir at room temperature for 16 h. The solution was then passed through a short pad of silica and celite. The products were separated by flash column chromatography to give the desired acetophenone **59** (106 g, 0.377 mmol, 93 %) as a yellow solid.

^{1}H-NMR ($CDCl_3$, 300 MHz) δ 7.49 (1H, dd, J = 8.4 Hz, 2.1 Hz, Ar*H*), 7.38 (1H, d, J = 2.1 Hz, Ar*H*), 6.77 (1H, d, J = 8.4 Hz, Ar*H*), 3.77 (3H, s, OCH_3), 2.43 (3H, s, CH_3), 0.91 (9H, s, SiC(CH_3)$_3$), 0.08 (6H, s, Si(CH_3)$_2$).

1-[(3-Isopropoxy-4-methoxy)-phenyl]-1-trimethylsilylethene **59**[14]

An LDA solution was prepared by dissolving diisopropylamine (7.5 mL, 53.5 mmol) in ether (100 mL) at 0 ^{o}C, followed by addition of n-butyllithium (41.2 mL 2.6 M in ether, 53.5 mmol). Acetophenone **58** (10.0 g, 35.7 mmol) was added to the solution followed by addition of TMS-Cl (6.8 mL, 53.5 mmol). The reaction was allowed to stir at room temp. for 16 h, then was quenched with 10% sodium bicarbonate. The organic

layer was separated, dried with sodium sulfate, and condensed to give the TMS enol-ether **58** (14.5 g, 41.1 mmol, 76%).

^{1}H-NMR ($CDCl_3$, 300 MHz) δ 7.17 (1H, dd, J = 8.4, 2.2, Ar*H*), 7.11 (1H, d, J = 2.2 Hz, Ar*H*), 6.78 (1H, d, J = 8.4 Hz, Ar*H*), 4.77 (1H, d, J = 1.6 Hz, C=CH_2), 4.33 (1H, d, J = 1.6 Hz, C=CH_2), 3.80 (3H, s, OCH_3), 1.02 (9H, s, SiC(CH_3)$_3$), 0.26 (9H, s, Si(CH_3)$_3$), 0.16 (6H, s, Si(CH_3)$_2$).

3-(tert-Butyldimethylsilyloxy)-4-methoxy-2-bromoacetophenone **60**[14]

TMS enol-ether **58** (23.0 g, 65.2 mmol) was dissolved in anhydrous dichloromethane (250 mL). Anhydrous potassium carbonate (6.00 g) was added and the mixture was cooled to 0 ^{o}C. Bromine (4.4 mL, 87.3 mmol) was added and the reaction stirred for until no acetophenone **58** was observed by TLC. The reaction was quenched with 10% sodium thiosulfate, and the organic layer was separated. The water layer was extracted with dichloromethane. The combined organic layers were dried with sodium sulfate, and concentrated under reduced pressure. The resulting solid was recrystalized in hexanes to give bromoacetophenone **60** (14.4 g, 40.1, 62%).

^{1}H-NMR ($CDCl_3$, 300 MHz) δ 7.62 (1H, dd, J = 8.5, 2.2 Hz, Ar*H*), 7.49 (1H, d, J = 2.2 Hz, Ar*H*), 6.89 (1H, d, J = 8.5 Hz, Ar*H*), 4.38 (2H, s, CH_2Br), 3.87 (3H, s, OCH_3), 1.00 (9H, s, SiC(CH_3)$_3$), 0.17 (6H, s, Si(CH_3)$_2$).

2-[(3'-tert-Butyldimethylsilyloxy-4'-methoxy)-phenyl]-6-methoxyindole **61**[14]

m-Anisidine (3.32 mL, 27.3 mmol), was dissolved in of n,n-dimethylaniline (11.2 mL), and brought to refluxing termp. Bromoacetophenone **60** (4.66 g, 12.8 mmol) was dissolved in EtOAc (16.6 mL) and added to the reaction. The mixture refluxed for 4 h,

then was cooled and quenched with water. The organic phase was separated, and the aqueous layer was extracted with EtOAc. The organic layers were combined, dried with sodium sulfate, and concentrated under reduced pressure. The products were separated by flash column chromatography to give the desired indole **61** (1.78 g, 4.67 mmol, 17%).

^{1}H-NMR ($CDCl_3$, 300 MHz) δ 8.11 (1H, s, N*H*), 7.46 (1H, d, J = 8.5 Hz, Ar*H*), 7.16 (1H, dd, J = 8.3, 2.2 Hz, Ar*H*), 7.12 (1H, d, J = 2.2 Hz, Ar*H*), 6.78 (1H, dd, J = 8.6, 2.2 Hz, Ar*H*), 6.60 (1H, d, J = 2.0 Hz, Ar*H*), 3.85 (3H, s, OCH_3), 3.84 (3H, s, OCH_3), 1.02 (9H, s, SiC(CH_3)$_3$), 0.19 (6H, s, Si(CH_3)$_2$).

2-[(3'-tert-Butyldimethylsilyloxy-4'-methoxy)-phenyl]-3-[(3'',4'',5''-trimethoxy)-benzoyl]-6-methoxyindole **62**[14]

Indole **61** (3.00 g, 7.81 mmol) was dissolved in o-DCB(60 mL). 3,4,5-Trimethylbenzoyl chloride (2.72 g, 11.8 mmol) was added and the reaction was heated to 120 ^{o}C for 3 h. The mixture was cooled, absorbed onto celite, and the products were purified by flash column chromatography to give the benzoylated indole **62** (2.66 g, 4.6 mmol, 59%).

^{1}H-NMR ($CDCl_3$, 300 MHz) δ 8.58 (1H, s, N*H*), 7.93 (1H, d, J = 9.4 Hz, Ar*H*), 6.99 (2H, s, Ar*H*), 6.90 (3H, m, Ar*H*), 6.77 (1H, d, J = 2.1 Hz, Ar*H*), 6.68 (1H, d, J = 8.4 Hz, Ar*H*), 3.85 (3H, s, OCH_3), 3.79 (3H, s, OCH_3), 3.73 (3H, s, OCH_3), 3.67 (6H, s, OCH_3), 0.93 (9H, s, SiC(CH_3)$_3$), 0.03 (6H, s, Si(CH_3)$_2$).

3-Hydroxy-4-methoxy-2-nitro-benzaldehyde **63**[90]

Isovanillan (1.00 g, 6.53 mmol) and CH_3NO_2 (14.0 ml, 264 mmol) were dissolved in CH_2Cl_2 (33.0 mL). The mixture was cooled to -40 ^{o}C and NO_2BF_4 (0.960 g, 7.26 mmol) was added. The reaction was stirred 4 h at -40 ^{o} C, after which the reaction was

quenched with water and extracted with ether. The organic layer was washed with brine, dried with Mg_2SO_2, and concentrated onto silica under reduced pressure. The products were separated by flash chromatography using (30:70, EtOAc:Hexanes), to give the desired 2-nitro isovanillan **63** as an orange solid (0.369g, 1.87 mmol, 29%).

^{1}H NMR (Acetone d_6, 300 MHz) δ 10.79 (1H, b, O*H*), 9.75 (1H, s, C*H*O), 7.57 (1H, d, J = 8.4 Hz, Ar*H*), 7.34 (1H. d, J = 8.5 Hz), 3.98 (3H, s, OCH_3).

3-Acetoxy-4-methoxy-2-nitrobenzaldehyde **64**[90]

2-nitro-benzaldehyde **63** (1.33 g, 6.74 mmol), acetic anhydride (15.5 ml, 164 mmol), and sodium acetate (0.100 g, 1.22 mmol) were combined and refluxed for 3 h. The reaction was then cooled to room temp and quenched with 10 ml of water. The products were extracted with ether (3 x 20 ml), washed with brine, dried with magnesium sulfate and condensed under reduced pressure. The products were separated by flash column chromatography to give the acetyl-protected nitro benzaldehyde **64** (1.305 g, 80.9%) as a white solid.

^{1}H NMR (CD_3Cl, 300 MHz) δ 9.86 (1H, s, C*H*O), 7.86 (1H, d, J = 8.7 Hz, Ar*H*), 7.20 (1H, d, J = 8.7 Hz, Ar*H*), 3.98 (3H, s, OCH_3), 2.32 (3H, s, CCH_3).

3-Acetoxy-4-methoxy-2,β-dinitrostyrene **65**[90]

Nitromethane (0.66 mL, 12 mmol) was dissolved in THF (5 mL) and cooled to –78 ^{o}C. Potassium bis(trimethylsilyl)amide (6 mL, .5 M solution in toluene, 3 mmol) was added slowly under an argon atmosphere. Acetyl-protected nitrobenzaldehyde **64** (600 mg, 3 mmol) dissolved in THF (4 mL) was added to the reaction and stirred for 2 h at room temperature, then was quenched with water. The products were extracted with

ether, washed with brine, dried with Na_2SO_4, and concentrated to give a red oil (~700 mg). This crude product was dissolved in CH_2Cl_2 (5 mL) and cooled to 0 ^oC. Triethylamine (0.25 mL, 1.79 mmol) was added, followed by the addition of methanesulfonyl chloride (0.30 mL, 3.88 mmol). The reaction was stirred at room temperature for 2 h, then was quenched with water. The products were extracted with ether, washed with brine, dried with Na_2SO_4, and concentrated under reduced pressure. The product was purified by flash column chromatography to to give the desired di-nitrostyrene **65** (226 mg, 0.791 mmol, 26%) as a yellow solid.

^1H NMR (CD_3Cl, 300 MHz) δ 7.90 (1H, d, J = 13.6 Hz, Ar*H*), 7.53 (1H, d, J = 8.9 Hz, Ar*H*), 7.46 (1H, d, J = 13.6 Hz, Ar*H*), 7.16 (1H, d, J = 8.9 Hz, Ar*H*), 3.96 (3H, s, OCH_3), 2.33 (3H, s, OCH_3).

7-Acetoxy-6-methoxyindole **66**[90]

Dinitrostyrene **65** (0.226 g, 0.791 mmol), silica gel (1.8 g), reduced iron powder (680 mg, 12 mmol), glacial acetic acid (1.9 mL, 32.9 mmol), and toluene (4 mL) were combined and to 90 ^oC under nitrogen atmosphere with mechanical stirring for 10 min. The mixture was the filtered through celite and washed with EtOAc. The organic layer was washed with water, brine, dried with Na_2SO_4, and concentrated under reduced pressure. The product was purified by flash column chromatography to give indole **66** (28.4 mg, 0.141 mmol, 18%) as a white crystalline product

^1H NMR (MeOD, 300 MHz) δ 8.04 (1H, b, N*H*), 7.43 (1H, d, J = 8.6 Hz, Ar*H*), 7.10 (1H, dd, J = 3.2, 2.3 Hz, Ar*H*), 6.89 (1H, d, J = 8.6 Hz, Ar*H*), 6.49 (1H, dd, J = 3.2, 2.1 Hz, Ar*H*), 3.89 (3H, s, OCH_3), 2.4 (3H, s, CCH_3).

7-Hydroxy-6-methoxy-1H-indol-3-yl)-(3',4',5'-trimethoxy-phenyl)-methanone **67**

Indole **66** (28.4 mg, 0.141 mmol) was dissolved in o-dichlorobenzene (10mL). 3,4,5-Trimethoxy benzoyl chloride (32.4 mg, 0.141 mmol) was added and the reaction was refluxed for 4 h. The reaction was then quenched with water and the products were extracted with ethyl acetate. The combined organic layers were dried with sodium sulfate, and condensed onto silica. After separation by flash column chromatography it was discovered that no desired benzoylated indole **67** was recovered.

CA4 Free Phosphate Acid/L-NMMA Salts

L-N ^{G}-monomethyl- arginine (L-NMMA) free base **68**[91]

N,S-dimethyl isothiouronium iodide (25.0 g, 108 mmol) was added to a solution of L-(+)-ornithine (9.08 g, 53.8 mmol) in aqueous 1M (108 mL) sodium hydroxide. The reaction was refluxed for 5 h. The reaction then was cooled and brought to pH 4 using concentrated HCl. Purification used an Ion exchange resin. The Amberlite 120H resin was rinsed with water until the elutant reached a pH of 7, then was washed with pH 4 aqueous solution, and finally re-rinsed with water. The reaction mixture was loaded onto the Amberlite column, and flushed with water until the elutant was pH 7, then the product was eluted with 0.2 N ammonium hydroxide. The ammonium elutant was concentrated first by rotary evaporation, then by lyophilization to give L-NMMA free base **68** (3.51 g, 18.6 mmol, 35% yield) as off white solid.

^{1}H NMR (CD_3OD, 300 MHz) δ 3.26 (1H, b, C*H*NH_2 .), 3.17 (2H, b, CH_2C), 2.80 (3H, s, NCH_3), 1.59 (4H, b, CH_2N).

^{13}C NMR (CD_3OD, 75 MHz) δ 182.4, 156.4, 55.4, 40.7, 31.3, 27.3, 24.5.

CA4 Free Phosphate Acid **69**[92]

CA4P disodium phosphate salt (1.00 g, 2.27 mmol) was dissolved in 5 mL of water. 2M HCl was added until the solution was pH 1.5. The aqueous layer was then extracted with ethyl acetate (3x20mL). The ethyl acetate layer was dried with sodium sulfate, and condensed to give the free phosphate acid **69** as a pure pink solid (0.6184 g, 1.57 mmol, 69%).

^{1}H NMR (CD_3OD, 300 MHz) δ 7.25 (1H, s, Ar*H*), 7.05 (1H, d, J = 8.4 Hz, Ar*H*), 6.93, (1H, d, J = 8.5Hz, Ar*H*), 6.55 (2H, s, Ar*H*), 6.48 (2H, s, Ar*H*), 3.87 (3H, s, OCH_3), 3.75 (3H, s, OCH_3), 3.66 (6H, s, OCH_3).

^{13}C NMR (CD_3OD, 75 MHz) δ 152.8, 150.4, 150.3, 140.3, 136.9, 132.8, 131.0, 130.1, 129.3, 128.5, 125.8, 121.6, 121.6, 112.3, 106.0, 59.8, 55.1, 55.6.

^{31}P NMR (CD_3OD, 90 MHz) δ -4.7

CA4P free acid/ LNMMA free base co-salt **70**[92]

CA4 free phosphate acid **69** (600 mg, 1.52mmol) and L-NMMA free base **68** (572 mg, 3.04 mmol) were dissolved in 20 mL DI water and stirred for 2 h. The water was then removed by lyophilization to give the desired product **70** (1.18 g, 1.53 mmol, quantitative) as a white solid.

^{1}H NMR (CD_3OD, 300 MHz) δ 7.32 (1H, s, Ar*H*), 6.82 (1H, d, J = 9.3, Ar*H*), 6.57 (2H, s, Ar*H*), 6.41 (1H, d, J = 11.3, Ar*H*), 4.04 (3H, s, OCH_3), 3.79 (3H, s, OCH_3), 3.62 (6H, s, OCH_3), 3.11 (4H, b, CH_2C), 2.73 (6H, s NCH_3), 1.85 (4H, b, CH_2N), 1.60 (4H, b, CH_2N), 1.16 (1H, b, C*H*NH), 0.75 (1H, b, C*H*NH).

^{13}C NMR (CD_3OD, 75 MHz) δ 174.4, 156.3, 152.0, 149.3, 149.3, 142.74 135.8, 133.5, 130.1, 130.0, 128.7, 123.0, 121.3, 112.4, 106.4, 60.9, 55.9, 55.8, 54.2, 40.6, 40.37, 29.4. 27.5, 27.2, 24.4. 23.8.

^{31}P NMR (CD_3OD, 90 MHz) δ -0.29.

CA4P/L-NMMA **71**[92]

CA4P (0.020 g, 0.045 mmol) and L-NMMA (0.023 g, 0.091 mmol) were dissolved in 1 mL water. The solution was stirred for 2 h at room temp. The water was removed by lyophilization to give the desire CA4P/LNMMA co-salt **71** (0.043 g, 0.045 mmol, quantitative) as a white solid. m.p. = 168-172^{o}C

^{1}H NMR (D_2O, 300 MHz) δ 7.24 (1H, s, Ar*H*), 6.80 (1H, d, J = 8.7 Hz, Ar*H*), 6.76 (1H, d, J = 8.6 Hz, Ar*H*), 6.55 (2H, s, Ar*H*), 6.52 (1H, s, J = 12.4 Hz, C*H*=CH), 6.40 (1H, s, J = 12.1 Hz, C*H*=CH), 3.70 (3H, s, OCH_3), 3.63 (3H, s, OCH_3), 3.56 (6H, s, OCH_3), 3.06 (4H, t, J = 6.9 Hz, CH_2N), 2.66 (6H, s, OCH_3), 1.74 (10H, m), 1.52 (5H, m).

CA4P/L-N^{G}-nitro arginine methyl ester (L-NAME) **72**[92]

CA4P (7.00 g, 15.9 mmol) and L-NAME (8.58 g, 31.8 mmol) were dissolved in 50 mL water. The solution was stirred for 2 h at room temp. The water was removed by lyophilization to give the desire CA4P/LAME co-salt **72** (15.5 g, 15.9 mmol, quantitative) as a white solid.

^{1}H NMR (D_2O, 300 MHz) δ 7.23 (1H, s, Ar*H*), 6.85 (1H, d, J = 8.6 Hz, Ar*H*), 6.81 (1H, d, J = 8.5 Hz, Ar*H*), 6.58 (2H, s, Ar*H*), 6.54 (1H, s, J = 12.3 Hz, C*H*=CH), 6.44 (1H, s, J = 12.2 Hz, C*H*=CH), 3.99 (2H, t, J = 6.0 Hz, C*H*NH_2), 3.78 (9H, b, OCH_3,

NCH_3), 3.66 (3H, s, OCH_3), 3.60 (6H, s, OCH_3), 3.21 (4H, t, J = 7.1 Hz, NHCH_2CH$_2$), 1.90 (4H, m, CH$_2$CH_2CH), 1.62 (4H, m, CH$_2$CH_2CH$_2$).

Oxi8007/L-NMMA co-salt **73**

Oxi8007 (0.100 g, 0.170 mmol) and L-NMMA (84.5 mg, 0.341 mmol) were dissolved in 1 mL of water. The solution stirred at room temp. for 2 h. The water was then removed by lyophilization to give the desired Oxi8007/L-NMMA co-salt **73** (0.191 g, 0.176 mmol, quantitative) as a yellow solid. m.p. = 149-153^{o}C.

^{1}H NMR (D$_2$O, 300 MHz) δ 7.75 (1H, d, J = 8.9 Hz, Ar*H*), 7.39 (1H, s, N*H*), 6.92 (1H, d, J = 2.4 Hz, Ar*H*), 6.76 (1H, dd, J = 8.8, 2.2 Hz, Ar*H*), 6.62 (2H, s, Ar*H*), 6.39 (2H, s, Ar*H*), 3.74 (3H, s, OCH_3), 3.57 (3H, s, OCH_3), 3.53 (6H, s, OCH_3), 3.52 (3H, s, OCH_3), 3.00 (4H, t, J = 6.9 Hz, NCH_2CH$_2$), 2.61 (6H, s, NCH_3), 1.73 (10H, m), 1.49 (6H, m).

Oxi8007/L-NAME co-salt **74**

Oxi8007 (0.200 g, 0.341 mmol) and L-NAME (0.183 mg, 0.681 mmol) were dissolved in 2 mL of water. The solution stirred at room temp. for 2 h. The water was then removed by lyophilization to give the desired Oxi8007/L-NAME co-salt **74** (0.332 g, 0.176 mmol, 86%) as a yellow solid.

^{1}H NMR (D$_2$O, 300 MHz) δ 7.74 (1H, d, J = 8.8 Hz, Ar*H*), 7.36 (1H, s, N*H*), 6.89 (1H, d, J = 2.2 Hz, Ar*H*), 6.74 (1H, dd, J = 8.9, 2.2 Hz, Ar*H*), 6.60 (2H, s, Ar*H*), 6.38 (2H, s, Ar*H*), 3.92 (2H, t, J = 6.3 Hz, CH$_2$C*H*), 3.73 (3H, s, OCH_3), 3.86 (6H, s, COOCH_3), 3.56 (3H, s, OC*H*3), 3.53(6H, s, OCH_3), 3.52 (3H, s, OCH_3), 3.10 (4H, b, NHCH_2), 1.78 (4H, b, CH_2CHN), 1.55 (4H, b, CH$_2$CH_2CH).

1-{2-[2-Methoxy-5-(3',4',5'-trimethoxy-phenyl)-7,8-dihydro-naphthalen-1-yloxy]-ethyl}-2-methyl-5-nitro-1H-imidazole **75**

Oxi6196 (100 mg, 0.292 mmol) of 6196, metronidazole (55.0 mg (0.322 mmol), and azodicarbonyldipiperidine (81.0 mg, 0.322 mmol) were dissolved in dry benzene (3 mL). After 5 minutes of stirring, tributylphosphine (0.79 mL, 0.322 mmol) was added and the reaction allowed for 48 h. The reaction was then condensed onto silica under reduced pressure, and separated by flash column chromatography with (60:40, EtoAc:Hexane), to give desired dihydropaphthalene **75** (0.950 mg, 0.192 mmol, 65%) as a pale yellow solid. (R_f = 0.13; 50:50; Hexanes:EtOAc). m.p. = 76-78 ^oC.

^{1}H-NMR ($CDCl_3$, 300MHz) δ 8.02 (1H, s, C*H*N), 6.76 (1H, d, J = 8.6 Hz, Ar*H*), 6.58 (1H, d, J = 8.6 Hz, Ar*H*), 6.50 (2H, s, Ar*H*), 5.92 (1H, t, J = 4.6 Hz, C=C*H*), 4.71 (2H, t, J = 4.7 Hz, CH_2N), 4.24 (2H, t, J = 4.8 Hz, OCH_2), 3.86 (3H, s, OCH_3), 3.81 (6H. s, OCH_3), 3.68 (3H, s, OCH_3), 2.63 (3H, s, CCH_3), 2.57 (2H, t, J = 7.56 Hz, CH_2CH_2), 2.26 (2H, td, J = 8.2, 4.8 Hz, CH_2CH).

^{13}C-NMR ($CDCl_3$, 75 MHz) δ 152.9, 152.1, 151.5, 143.6, 139.3, 138.4, 137.1, 136.4, 133.1, 130.3, 128.7, 125.1, 122.1, 108.8, 105.8, 71.0, 60.8, 60.3, 56.0, 55.4, 46.8, 22.7, 21.0, 20.5, 14.8, 14.1.

1-(2-{2-Methoxy-5-[2-(3',4',5'-trimethoxy-phenyl)-vinyl]-phenoxy}-ethyl)-2-methyl-5-nitro-1H-imidazole **76**

CA4 (0.100 g, 0.316 mmol), metronidazole (0.060 g, 0.35 mmol), and azodicarbonyldipiperidine (0.088 g, 0.35 mmol) were dissolved in dry benzene (3 mL). Tributylphosphine (0.086 mL) was added slowly and the reaction stirred for two days.

The solvent was then removed under reduced pressure, and products purified by flash column chromatography (60:40, EtOAc:Hexanes). The CA4 imidazole **76** (99.5 mg, 0.211 mmol, 66%) was recovered as a pale yellow solid. (R_f = 0.13; 50:50; Hexanes:EtOAc). m.p. = 136-138 ^oC. Anal. Calcd. for $C_{25}H_{29}N_3O_6$: C, 61.4; H, 5.80; 8.95. Found: C, 61.5; H, 5.80; N, 8.95.

^{1}H-NMR ($CDCl_3$, 300MHz) δ 7.95 (1H, s, C*H*N), 6.89 (1H, dd, J = 8.3, 1.9 Hz, Ar*H*), 6.72 (2H, d, J = 3.3 Hz, Ar*H*), 6.70 (1H, d, J = 3.1 Hz, Ar*H*), 6.5 (2H, s, C*H*=CH), 6.44 (2H, s, Ar*H*), 4.66 (2H, t, J = 4.6 Hz, CH_2N), 4.14 (2H, t, J = 4.8 Hz, CH_2O), 3.84 (3H, s, OCH_3), 3.74 (3H, s, OCH_3), 3.69 (6H, s, OCH_3), 2.63 (3H, s, CCH_3) .

^{13}C-NMR ($CDCl_3$, 75 MHz) δ 153.1, 152.5, 148.8, 147.0, 137.4, 133.3, 132.9, 130.0, 129.33, 129.31, 123.3, 114.4, 111.5, 106.1, 67.9, 61.1, 56.1, 55.8, 46.2, 14.6.

1-(4'-methoxy-3'(3-methoxy-4-nitrophenyl)methyloxy)phenyl-2-(3,4,5-trimethoxy)phenyl-Z-ethene **77**

CA4 (0.100 g 0.316 mmol), 3-methoxy-4-nitro-benzyl alcohol (64 mg, 0.35 mmol), and azodicarbonyldipiperidine (88 mg, 0.35 mmol), were dissolved in dry benzene (3 mL). Tributylphosphine (87 µL, 70 mg, 0.35 mmol) was added slowly, and the reaction stirred for 48 h. Upon completion, the reaction was condensed onto silica under reduced pressure, and separated by flash column chromatography (30:70, EtOAc:Hexane) to give the desired CA4 analogue **77** (151.4 mg, 0.3137 mmol, 98%) as yellow oil.

^{1}H-NMR ($CDCl_3$, 300MHz) δ 7.80 (1H, d, J = 8.3 Hz, Ar*H*), 7.09 (1H, s, Ar*H*), 6.90 (2H, m, Ar*H*), 6.81 (1H, d, J = 8.3 Hz, Ar*H*), 6.76 (1H, d, J = 1.9, Ar*H*), 6.47 (2H, s,

C*H*=C*H*), 6.43 (2H, s, Ar*H*), 4.92 (2H, s, CH_2), 3.94 (3H, s, OCH_3), 3.88 (3H, s, OCH_3), 3.83 (3H, s, OCH_3), 3.69 (6H, s, OCH_3).

^{13}C-NMR ($CDCl_3$, 75 MHz) δ 153.3, 153.0, 148.8, 147.0, 144.4, 138.7, 137.0, 133.1, 129.8, 129.4, 128.9, 126.0, 123.4, 117.9, 114.6, 111.5, 111.3, 105.8, 69.9, 60.8, 56.5, 55.9.

1-(4'-methoxy-3'(4-nitrophenyl)methyloxy)phenyl-2-(3,4,5-trimethoxy)phenyl-Z-ethene **78**

CA4 (100 mg, 0.32 mmol), 4-nitrobenzyl alcohol (54 mg, 0.35 mmol), and azodicarbonyldipiperidine (88 mg ,0.35mmol) were dissolved in dry benzene(3 mL). Tributylphosphine (86 µL, 0.35 mmol) was added slowly, and the reaction was allowed for 48 h. The mixture was then condensed onto silica and separated by flash column chromatography (30:70, EtOAc:Hexane) to give the desired CA4 analogue (125.3 mg, 0.2769 mmol, 87%) as yellow solid. (R_f = 0.23; 70:30; Hexanes:EtOAc). m.p. = 89-90 ^oC

^{1}H-NMR ($CDCl_3$, 300 MHz) δ 8.17 (2H, dt, J = 9.2, 2.3 Hz, Ar*H*), 7.44 (2H, d, J = 8.7Hz, Ar*H*), 6.89 (1H, dd, J = 8.3, 1.9 Hz, Ar*H*), 6.81 (1H, d, J = 8.3 Hz, Ar*H*), 6.75 (1H, d, J = 1.9 Hz, Ar*H*), 6.46 (2H, s, C*H*=C*H*), 6.41 (2H, s, Ar*H*), 4.98 (2H, 2, CH_2), 3.87 (3H, s, OCH_3), 3.84 (3H, s, OCH_3), 3.69 (6H, s, OCH_3).

^{13}C-NMR ($CDCl_3$, 75 MHz) δ 153.0, 148.8, 147.4, 146.9, 144.4, 137.0, 133.0, 129.7, 129.3, 128.9, 127.2, 123.7, 123.3, 114.4, 111.5, 105.8, 69.7, 60.8, 55.9.

1-(2'-Hydroxy-4'-methoxy-3'-(2-nitrophenyl)methyloxy)phenyl-2-(3,4,5-trimethoxy)phenyl-Z-ethene **79**[93]

CA4 (100 mg, 0.32 mmol), 2-nitro-benzylalcohol (53.3 mg, 0.348 mmol), and azodicarbonyldipiperidine (87.8 mg, 0.348 mmol) in 5 mL anhydrous benzene. Tributylphosphine (0.086 mL, 0.35 mmol) was added slowly and the reaction stirred for

48 h. The reaction was then condensed onto silica and separated by flash column chromatography (30:70, EtOAc:Hexane) to give the desired CA4 **79** analogue (53.2 mg, 0.118 mmol, 37%) as a pale yellow solid. (R_f = 0.23; 70:30; Hexanes:EtOAc). m.p. = 84-86 ^oC

^{1}H-NMR ($CDCl_3$, 300MHz) δ 8.11 (1h, dd, J = 8.2, 1.3 Hz, Ar*H*), 7.86 (1H, d, J = 7.4 Hz, Ar*H*), 7.64 (1H, td, J = 7.5, 1.0 Hz, Ar*H*), 7.46 (1H, tdd, J = 8.1, 1.3, 0.5 Hz, Ar*H*), 6.93 (1H, dd, J = 8.3, 1.9 Hz, Ar*H*), 6.83 (1H, s, Ar*H*), 6.81 (1H, d, J = 6.7 Hz, Ar*H*), 6.47 (1H, d, J = 13.3 Hz, C*H*=CH), 6.45 (2H, s, Ar*H*), 6.41 (1H, d, J = 12.1 Hz, C*H*=CH), 5.38 (2H, s, CH_2), 3.88 (3H, s, OCH_3), 3.81 (3H, s, OCH_3), 3.68 (3H, s, OCH_3).

^{13}C-NMR ($CDCl_3$, 75 MHz) δ 152.9, 149.0, 147.3, 146.8, 137.1, 134.0, 133.9, 132.6, 130.2, 129.3, 128.5, 128.3, 124.9, 122.9, 115.2, 111.7, 105.9, 68.1, 60.9, 56.0, 55.9.

1-(2'-Hydroxy-4'-methoxy-3'-(3-nitrophenyl)methyloxy)phenyl-2-(3,4,5-trimethoxy)phenyl-Z-ethene **80**

CA4 (100 mg, 0.316 mmol), 3-nitro-benzylalcohol (53.3 mg, 0.348 mmol), and azodicarbonyldipiperidine (88 mg, 0.348 mmol) were dissolved in anhydrous benzene (5 mL). Tributylphosphine (0.086 mL, 0.35 mmol) was added slowly, and the reaction stirred for 48 h. The reaction was then condensed onto silica and separated by flash column chromatography (30:70, EtoAc:Hexane) to give the CA4 analogue **80** (53.2 mg, 0.259 mmol, 37%) as pale yellow oil.

^{1}H-NMR ($CDCl_3$, 300MHz) δ 8.24 (1H, s, Ar*H*), 8.13 (1H, d, J = 8.1 Hz, Ar*H*), 7.62 (1H, dd, J = 7.5, 0.6 Hz, Ar*H*), 7.49 (1H, t, J = 8.0 Hz, Ar*H*), 6.91 (1H, dd, J = 8.4,

1.8 Hz, Ar*H*), 6.83 (1H, s, Ar*H*), 6.81 (2H, d, J = 6.2 Hz, Ar*H*), 6.47 (2H, s, C*H*=C*H*), 6.44 (2H, s, Ar*H*), 4.99 (2H, s, CH_2), 3.88 (3H, s, OCH_3), 3.83 (3H, s, OCH_3), 3.69 (6H, s, OCH_3).

^{13}C-NMR ($CDCl_3$, 75 MHz) δ 152.9, 149.0, 148.4, 147.1, 139.2, 137.1, 132.9, 132.8, 129.8, 129.5, 129.3, 129.0, 123.2, 122.8, 121.9, 114.9, 111.5, 105.9, 69.9, 60.9, 55.94, 55.9.

1-(2'-Hydroxy-4'-methoxy-3'-(4-nitrophenyl)methyloxy)phenyl-2-(3,4,5-trimethoxy)phenyl-Z-ethene **81**; *1-(2'-Hydroxy-4'-methoxy-di-3'-(4-nitrophenyl)methyloxy)phenyl-2-(3,4,5-trimethoxy)phenyl-Z-ethene* **82**

CA1 (100 mg, 0.30 mmol), 4-nitro-benzylalcohol (51 mg, 0.33 mmol), and azodicarbonyldipiperidine (87 mg, 0.33mmol) were dissolved in anhydrous benzene (5 mL). Tributylphosphine (0.082 mL, 0.33 mmol) was added slowly, and the reaction stirred for 48 h. The reaction was then condensed onto silica and separated by flash column chromatography (30:70, EtoAc:Hexane) to give the CA1 analogue **81** (26.6 mg, 0.0589 mmol, 20%), as pale yellow solid, and the di-substituted CA1 analogue **82** (24.4 mg, 0.0404 mmol, 13%) as a yellow oil. **81** (R_f = 0.2; 70:30; Hexanes:EtOAc). m.p. = 108-110 ^{o}C

81 ^{1}H-NMR ($CDCl_3$, 300MHz) δ 8.23 (2H, dt, J = 6.9, 2.2 Hz, Ar*H*), 7.62 (2H, d, J = 8.6 Hz, Ar*H*), 6.97 (1H, d, J = 8.7 Hz, Ar*H*), 6.56 (1H, d, J = 12.1 Hz, C*H*=CH), 6.51 (1H, d, J = 12.1 Hz, C*H*=CH), 6.51 (2H, s, Ar*H*), 6.39 (1H, d, J = 8.8 Hz), 5.75 (1H, s, O*H*), 5.17 (2H, s, CH_2), 3.84 (3H, s, OCH_3), 3.83 (3H, s, OCH_3), 3.67 (6H, s, OCH_3).

81 ^{13}C-NMR ($CDCl_3$, 300MHz) δ 152.9, 151.5, 147.8, 147.1, 144.5, 137.3, 134.1, 132.6, 130.2, 128.5, 125.1, 123.8, 123.7, 117.5, 105.9, 103.6, 73.7, 60.9, 55.94, 55.88.

82 ^{1}H-NMR ($CDCl_3$, 300MHz) δ 8.18 (2H, d, J = 7.2 Hz, Ar*H*), 8.15 (2H, d, J = 7.2 Hz, Ar*H*), 7.59 (2H, d, J = 8.3 Hz, Ar*H*), 7.52 (2H, d, J = 8.3 Hz, Ar*H*), 7.04 (1H, d, J = 8.7 Hz, Ar*H*), 6.63 (1H, d,J = 8.8 Hz, Ar*H*),6.55 (1H, d, J = 12.1 Hz, C*H*=CH), 6.48 (1H, d, J = 12.1 Hz, C*H*=CH), 6.42 (2H, s, Ar*H*), 5.12 (4H, s, CH_2), 3.84 (3H, s, OCH_3), 3.82 (3H, s, OCH_3), 3.64 (3H, s, OCH_3).

82 ^{13}C-NMR ($CDCl_3$, 300MHz) δ 153.0, 152.9, 150.3, 144.8, 144.6, 140.9, 132.3, 130.6, 128.5, 128.3, 128.2, 125.7, 124.6, 124.5, 123.8, 123.6, 107.9, 106.1, 74.1, 74.0, 60.9, 56.1, 55.9.

Synthesis of 1-(2'-Hydroxy-4'-methoxy-3'-(3-methoxy-4-nitrophenyl)methyloxy)phenyl-2-(3,4,5-trimethoxy)phenyl-Z-ethene **83**, *1-(2'-Hydroxy-4'-methoxy-di-3'-(3-methoxy-4-nitrophenyl)methyloxy)phenyl-2-(3,4,5-trimethoxy)phenyl-Z-ethene* **84**

CA1 (100mg ,0.30 mmol), 3-methoxy-4-nitro-benzylalcohol (60mg ,0.33 mmol), and azodicarbonyldipiperidine (87 mg , 0.33 mmol) in anhydrous benzene (5 mL). Tributylphosphine (0.086 mL, 0.33 mmol) was added slowly, and the reaction stirred for 48 h. The reaction was then condensed onto silica and separated by flash column chromatography with (30:70, EtoAc:Hexane) to give the monosubstituted CA1 analogue **83** (13.4 mg, 0.269 mmol, 9%) and the disubstituted analogue **84** (35.0mg, 0.528 mmol, 18% yield) bothe as pale yellow oils.

83 ^{1}H-NMR ($CDCl_3$, 300MHz) δ 7.87 (1H, d, J = 8.3 Hz, Ar*H*), 7.22 (1H, d, J = 1.2 Hz, Ar*H*), 7.05 (1H, dd, J = 8.3, 1.6 Hz, Ar*H*), 6.98 (1H, d, J = 8.7 Hz), 6.54 (2H, s, C*H*=C*H*), 6.51 (2H, s, Ar*H*), 6.39 (1H, d, J 8.8 Hz), 5.74 (1H, s, O*H*), 5.12 (2H, s, CH_2), 3.97 (3H, s, OCH_3), 3.85 (3H, s, OCH_3), 3.82 (3H, s, OCH_3), 3.67 (3H, s, OCH_3).

83 ^{13}C-NMR ($CDCl_3$, 75 MHz) δ 153.3, 152.9, 151.5, 147.1, 144.4, 139.2, 137.3, 134.2, 132.6, 130.3, 126.0, 125.1, 123.6, 119.1, 117.6, 112.6, 105.9, 103.6, 73.9, 60.9, 56.6, 56.0, 55.9.

84 ^{1}H-NMR ($CDCl_3$, 300MHz) δ 7.82 (2H, d, J = 6.4 Hz, Ar*H*), 7.79 (1H, d, J = 6.5 Hz, Ar*H*), 7.25(1H, d, J = 1.05 Hz, Ar*H*), 7.11 (1H, s, Ar*H*), 7.04 (2H, dd, J = 8.7, 2.2 Hz, Ar*H*), 6.99 (1H, dd, J = 8.4, 1.6 Hz, Ar*H*), 6.63 (1H, s, J = 8.8 Hz, Ar*H*), 6.56 (1H, d, J = 11.5 Hz, C*H*=CH), 6.49 (1H, d, J = 12.2 Hz, C*H*=CH), 6.42 (2H, s, Ar*H*), 5.08 (2H, s, CH_2), 5.07 (2H, s, CH_2), 3.88 (3H, s, OCH_3), 3.85 (6H, s, OCH_3), 3.81 (3H, s, OCH_3), 3.63 (3H, s, OCH_3).

84 ^{13}C-NMR ($CDCl_3$, 75 MHz) δ 153.0, 152.9, 150.3, 147.6, 144.8, 144.6, 140.9, 132.3, 130.6, 128.5, 128.3, 128.2, 125.7, 124.6, 124.5, 123.8, 123.6, 107.9, 106.1, 74.1, 74.0, 60.9, 56.1, 55.9.

Synthesis of (5-Nitro-thiophen-2-yl)-methanol **85**[67]

5-nitro-thiophen-2-carbaldehyde (1.5 g, 9.6 mmol) was dissolved in dry methanol (20 mL) and cooled to 0 ^{o}C. Sodium borohydride (0.903 g, 23.8 mmol) was added and the reaction stirred for 2 h. The reaction was then poured over ice and acidified with 3M HCl. The product was extracted with ethyl acetate, dried with sodium sulfate, condensed under reduced pressure and purified by column to give the desired thiophene **85** (0.901 g, 5.66 mmol, 59%), as a dark oil.

^{1}H-NMR ($CDCl_3$, 300MHz) δ 7.80 (1H, d, J = 4.2 Hz, C=C*H*), 6.92 (1H, d, J = 4.2 Hz, C=C*H*), 4.87 (2H, s, CH_2), 2.64 (1H, b, O*H*).

^{13}C-NMR ($CDCl_3$, 75MHz) δ 153.5, 128.8, 123.4, 60.2.

Synthesis of 1-(5-Nitro-thiophen-2-yl)-ethanol **86**[67]

1-(5-Nitro-thiophen-2-yl)-ethanone (1.5 g, 8.8mmol) was dissolved in dry methanol (20 mL) and colled to 0 ^{o}C. Sodium borohydride (0.83 g, 21.9 mmol) was added and the reaction was stirred for 2 h.. The reaction was then poured over ice and acidified with 3M HCl. The product was extracted with ethyl acetate, the organic layer was dried with sodium sulfate, condensed under reduced pressure, and purified by flash column chromatography to give the desired thiophene alcohol **86** (0.9613 g, 5.56 mmol, 63%) as a red oil.

^{1}H-NMR ($CDCl_3$, 300MHz) δ 7.79 (1H, d, J = 4.2 Hz, C=C*H*), 6.89 (1H, q, J = 4.2, 0.9 Hz, C= C*H*), 5.12 (1H, q, J = 6.6 Hz, C*H*CH_3), 2.48 (1H, b, O*H*), 1.60 (3H, d, J = 10.0 Hz, CHCH_3).

^{13}C-NMR ($CDCl_3$, 300MHz) δ 159.1, 128.7, 122.1, 66.5, 25.3.

1-(2'-Hydroxy-4'-methoxy-3'-(5-nitrothiene-2-yl)methyloxy)phenyl-2-(3,4,5-trimethoxy)phenyl-Z-ethene **87**

CA1 (100 mg, 0.30 mmol), thiophene **85** (53 mg, 0.33 mmol), and azodicarbonyldipiperidine (87 mg, 0.33 mmol) were dissolved in dry THF (3 mL) and cooled to 0 ^{o}C. Tributylphosphine (0.082mL, 0.33mmol) was then added slowly. The reaction was allowed for 2 days, at which time it was condensed onto silica and separated by flash column chromatography (40:60, EtoAC: Hexanes). The desired CA1 thiophen derivative **87** (98.0 mg, 0.207 mmol, 69%) as a light brown oil.

^{1}H-NMR (CDCl3, 300MHz) δ 7.78 (1H, d, J = 4.1Hz, SC=C*H*), 6.89 (1H, dd, J = 4.1, 0.4 Hz, SC=C*H*), 6.75 (1H, d, J = 8.6 Hz, Ar*H*), 6.58 (1H, d, J = 12.2 Hz, C*H*=CH), 6.511 (2H, s, Ar*H*), 6.51 (1H, d, J = 12.0 Hz, C*H*=CH), 6.38 (1H, d, J = 8.6 Hz, Ar*H*),

5.54 (1H, s, O*H*), 4.84 (2H, s, CH_2), 3.84 (3H, s, OCH_3), 3.80 (3H, s, OCH_3), 3.65 (6H, s, OCH_3).

^{13}C-NMR ($CDCl_3$, 75 MHz) δ 153.6, 152.7, 146.4, 141.6, 137.1, 132.6, 132.6, 130.2, 128.7, 124.1, 123.3, 120.3, 117.9, 106.0, 103.0, 60.9, 60.2, 56.2, 56.1, 55.8.

5-Acetoxy-6-methoxy-1,2,3,4-tetrahydronaphthalene **88**[94]

5-hydroxy-6-methoxy-1,2,3,4-tetrahydronapthalene (5.292, 29.7 mmol) was dissolved in dichloromethane (50 mL). DMAP (0.362 g, 2.96 mmol), and triethyl amine (6.20 mL, 44.5 mmol) were added followed by the addition of acetic acid (4.20 mL, 44.5 mmol). The reaction stirred for 12 h, then was condensed onto silica. The product was purified by flash column chromatography to give the acetate protected dihydronaphthalene **88** (4.33 g, 19.6 mmol, 66%).

^{1}H-NMR (CDCl3, 300MHz) δ 6.93 (1H, d, J = 8.4 Hz, Ar*H*), 6.76 (1H, d, J = 8.4 Hz, Ar*H*), 3.80 (3H, s, OCH_3), 2.72 (2H, m, CH_2), 2.57 (2H, m, CH_2), 2.33 (3H, s, COCH_3), 1.75 (4H, m, CH_2).

5-Acetoxy-6-methoxy-1-tetralone **89**[94]

Dihydronaphthalene **88** (4.33 g, 19.6 mmol), was dissolved in a 40 mL of a water-dioxane solution (5:95). DDQ (8.95 g, 39.4 mmol) was dissolved in dioxane (40 mL) and added to the reaction. The solution stirred 16 h. The solids where filtered and washed with ethyl acetate. The elutant was concentrated under reduced pressure, and saturated sodium bicarbonate (100 mL) was added. The products were then extracted with ether. The combined ether was dried with magnesium sulfate and concentrated

under reduced pressure. The products were purified by flash column chromatography to give the tetralone **89** (3.94 g, 16.8 mmol, 85%) as a white solid.

^{1}H-NMR (CDCl3, 300MHz) δ 7.99 (1H, d, J = 8.8 Hz, Ar*H*), 6.93 (1H, d, J = 8.8 Hz), 3.89 (3H, s, OCH_3), 2.78 (2H, t, J = 6.1 Hz, CH_2), 2.60 (2H, s, J = 5.9 Hz, CH_2), 2.35 (3H, s, OCH_3), 2.09 (2H, m, CH_2).

5-Hydroxy-6-methoxy-1-tetralone **90**[94]

Acetate protected tetralone **89** (3.94 g, 16.7 mmol) was dissolved in methanol (100 mL). Anhydrous sodium bicarbonate (2.81 g, 33.4 mmol) was added followed by 5 mL water. The reaction stirred for 16 h, then the solvent was removed by reduced pressure, and saturated $NaHCO_3$ was added. The solution was acidified with concentrated HCl, and the products were extracted with CH_2Cl_2. The combined organic phases were dried with sodium sulfate, and concentrated under reduced pressure to give the deprotected tetralone **90** (2.89g, 15.0 mmol, 90%) as a tan solid.

^{1}H-NMR ($CDCl_3$, 300MHz) δ 7.68 (1H, d, J = 8.6 Hz, Ar*H*), 6.84 (1H, d, J = 8.6 Hz, Ar*H*), 5.74 (1H, s, O*H*), 3.95 (3H, s, OCH_3), 2.92 (2H, t, J = 6.1 Hz, CH_2), 2.60 (2H, t, J = 6.0 Hz, CH_2) 2.11 (2H, m, CH_2).

5-(tert-Butyldimethylsilyl)-oxy-6-methoxy-1-tetralone **91**[95]

Tetralone **91** (2.89 g, 15.0 mmol) was dissolved in anhydrous DMF (60 mL). Triethyl amine (4.01 mL, 22.5 mmol), and DMAP (0.366 g, 3.00 mmol) were added and the solution stirred for 5 min. TBSCl (2.53 g, 16.8 mmol) was added, and the reaction stirred 16 h. The reaction was quenched with water. The products were extracted with EtOAc. The combined organic layers were washed with brine, dried with sodium sulfate

and purified by flash column chromatography to give the TBS-protected tetralone **91** (3.60 g, 11.7 mmol) as a light oil.

^{1}H-NMR ($CDCl_3$, 300MHz) δ 7.70 (1H, d, J = 8.7 Hz, Ar*H*), 6.80 (1H, d, J = 8.7 Hz, Ar*H*), 3.82 (3H, s, OCH_3), 2.89 (2H, t, J = 6.0 Hz, CH_2), 2.55 (2H, t, J = 6.0 Hz, CH_2), 2.05 (2H, m, CH_2), 0.99 (9H, s, SiC(CH_3)$_3$), 0.16 (6H, s, Si(CH_3)$_2$).

Purification of Tubulin From Calf Brain[24]

All chemicals for tubulin purification were purchased from Sigma Aldrich unless otherwise noted.

1M 2-Mercaptoethanol

2-Mercaptoethanol (0.039 g, 0.499 mmol) was dissolved in 0.465 mL ultrapure water.

1M (2-[N-morpholino]ethanesulfonic acid) (Mes)

Mes acid (7.77 g, 36.4 mmol), and Mes base (13.9 g, 65.2 mmol) were dissolved in enough ultrapure water to make 100 mL. The pH was adjusted to 6.4.

100 mM Guanisine Triphosphate (GTP)

GTP (26.16 mg, 0.05000 mmol) was dissolved in 0.5 ml ultrapure water.

Preparation of Solution A + 4 M Glycerol

EGTA (0.190 g, 0.499 mmol), EDTA (0.0186 g, 0.0500 mmol), $MgCl_2$ (0.102 g, 0.502 mmol), MES (50 mL of 1M Mes), and Glycerol (184.2 g, 2.000 mol) were dissolved in 300 mL of ultrapure water. The pH was adjusted to 6.4, and made up to 500

mL with ultrapure water. On the day of the preparation, GTP (0.5 mL of 100 mM GTP) and 2-mercaptoethanol (0.5 mL of 1M 2-mercaptoethanol) were added.

Preparation of Solution A

Mes acid (7.77 g, 36.4 mmol), and Mes base (13.9 g, 65.2 mmol) were dissolved in 1L of ultrapure water. The pH was adjusted to 6.4. EGTA (0.380 g, 1.00 mmol), EDTA (37.2 mg, 0.100 mmol), and $MgCl_2$ (0.203 g, 0.100 mmol) were added. On the day of the preparation GTP (35 µL of 0.1M GTP) and 2-mercaptoethanol (35 µL of 0.1M 2-mercaptoethanol) was added to 35 mL of solution A.

1M Glutamate, pH 6.6

L-Glutamic acid sodium salt monohydrate (37.4 g, 0.200 mol) (purchaced from USB) is dissolved in 80 mL ultrapure water. The pH was adjusted to 6.6 using 1M HCl. The solution was then made to 100 mL using ultrapure water to give a 2M stock solution. From this 10 mL is dissolved in 10 mL of ultrapure water for a 1M Glutamate solution.

Saline Solution 0.8% w/v

NaCl (8.00 g, 0.136 mol) was dissolved in 1 L of ultrapure water.

10X High Mes Solution

Mes acid (7.77 g, 36.4 mmol), and Mes base (13.9 g, 65.2 mmol) were dissolved in 100 mL of ultrapure water. The pH was adjusted to 6.4. EGTA (0.380 g, 1.00 mmol), EDTA (37.2 mg, 0.100 mmol), and $MgCl_2$ (0.203 g, 0.100 mmol) were added. On the day of the high Mes polymerization ATP (27.5 mg, 0.0499 mmol), GTP (7.90 mg, 0.0151

mmol), and 2-mercaptoethanol (50 μL, of 1 M 2-mercaptoethanol) were added to 5 mL of the high Mes stock.

0.2 M DTT

DTT (30.9 mg, 0.200 mmol) was dissolved in 1 mL ultrapure water.

Purification of Tubulin[24]

Blood vessels, meninges, blood clots and brain stems were removed from the calf brain. The grey matter was separated from the white matter, weighed, and rinsed with saline. The grey matter (280 g) was homogenized for 1 min. in solution A + 4 M glycerol (375 mL) using a Waring blender at 4 ^{o}C. The homogenate was then centrifuged at 32,000 rpm for 1h at 4 ^{o}C. The supernatant (~152 mL) was collected and the pellet was discarded. GTP (23.9 mg, 0.0457 mmol) and ATP (83.8 mg, 0.0152 mmol) was added to the supernatant, which was then incubated at 37 ^{o}C for 40 min. The solution was centrifuged at 32,000 rpm at 37 ^{o}C for 1 h. The supernatant is discarded, and the pellet was homogenized in 12 mL of solution A at 4 ^{o}C using a Potter-Elvehjem tissue homogenizer. The suspension is incubated on ice for 30 min. The solution is then centrifuged at 24,000 rpm for 30 min. at 2 ^{o}C. The supernatant was saved, and the pellet is rehomogenized in 6 mL solution A at 4 ^{o}C then centrifuged at 24,000 rpm. The supernatant is saved, and the pellet is rehomogenized in 6 mL solution A at 4 ^{o}C then centrifuged at 24,000 rpm. The supernatants were combined. Glycerol (4.4 mL, 4 M glycerol), 10X Mes (1 mL), water (0.2 mL), ATP (to a final conc. Of 1.0 mM), and GTP (final conc. 0.3 mM) were added, and the solution was incubated at 37 ^{o}C for 1 h. The solution was then centrifuged for 1 h at 32,000 rpm and 37 ^{o}C. The pellet was

homogenized in 6.2 mL of solution A and incubated on ice for 30 min. The solution was then centrifuged at 24,000 rpm for 30 min at 2 ^{o}C. The solution was adjusted to 27.5 mg/mL protein concentration with solution A. GTP (130 µL, 0.1M GTP), DTT (130 µL, 0.2M DTT), Mes base (3.66 g, 16.8 mmol), and Mes acid (0.565 g, 2.65 mmol). The solution was incubated at 37 ^{o}C for 1 h, and was then centrifuged at 39,000 rpm for 1 h at 37^{o}C. The pellets were then homogenized in 5 mL of cold 1 M glutamate, then left on ice for 1 h. The solution was centrifuged at 39,000 rpm for 1 h at 37 ^{o}C. GTP (60 µL, 0.1 M GTP, final concentration of 1 mM) was added to the supernatant (6 mL), and was then incubated at 37 ^{o}C for 1 hr. The solution was then centrifuged for 40 min at 39,000 rpm and 37 ^{o}C. The pellet was homogenized in 2.5 mL of 1 M glutate and left on ice for one hour. The solution was then centrifuged at 39,000 rpm for 40 min at 2 ^{o}C. The supernatant was collected. GTP (35 µL, of 0.1M GTP) was added and the solution was incubated at 37 ^{o}C for 1 h. The solution was centrifuged at 39,000 rpm for 40 min at 37 ^{o}C. The pellet was then homogenized in 2.25 mL of 1 M glutamate, and left on ice for 1 h. The solution was centrifuged at 39,000 rpm at 2 ^{o}C for 40 min. The supernatant was collected, and GTP (30 µL of 0.1 M GTP) was added. The solution was incubated at 37 ^{o}C for 1 h, then was centrifuged at 39,000 rpm for 40 min at 37 ^{o}C. The pellet was then homogenized in 1 mL of 1 M glutamate and left on ice for 1 h. The solution was then centrifuged for 40 min at 39,000 rpm and 2^{o}C. The supernatant was collected and the protein concentration was determined. The concentration was adjusted to 10.0 mg/mL using 1M glutamate. Typical tubulin isolations are between 70-200 mg of tubulin.

Determination of Tubulin Purity by SDS-PAGE[96]

All chemicals were purchased from Invitrogen unless otherwise noted. Tubulin (10 μL of 10 μM) and NuPAGE LDS sample buffer (2.5 μL, 4X) and water (6.5 μL) were combined and incubated at 70°C for 10 min. The tubulin mixture (10 μL) and multi-colored MultiMark protein standard were loaded onto the NuPage Bis-Tris 12% pre-casted mini-gels. The gels were run for 40 min at 200V with a current of 80-130 mA. The gels were stained with Simply Blue SafeStain. Protein bands were visualized against a protein standard with protein bands at 260, 110, 80, 60, 50, 40, 20, 15, 10 3.5 kDa.

Determination of Tubulin Concentration[25]

Tubulin concentration was determined using a UV analysis on an Agilent 8453 spectrophotometer with UV-Vis Chemstation software. The absorption was measured at 255 and 278 nm. The extinction coefficients are 1.2 L $g^{-1}cm^{-1}$ at 278 nm and 0.65 L g^{-1} cm^{-1} at 255 nm for tubulin, and 7.66 x 10^3 M^{-1} cm^{-1} at 278 nm and 12.17 x 10^3 M^{-1} cm^{-1} at 255 nm for GTP.[25] Three samples of purified tubulin (20 μL) were diluted to a ratio of 1:20 using 1M glutamate to obtain an average tubulin concentration. The absorbance of the protein solution was taken at 255 and 278 nm. The tubulin concentration was determined using the following equations:

Absorbance at 278nm = 1.20X + 7.66Y

Absorbance at 255nm = 0.65X + 12.17Y

X is the concentration of tubulin in mg/mL, and Y is the concentration of GTP-GDP in mg/mL. Multiplying X by the dilution factor gave the concentration of tubulin in the solution.

Inhibition of Tubulin Polymerization Assay[80]

Tubulin polymerization assays were performed using an Agilent 8453 spectrophotometer with UV-visible Chemstation software. A background reading with 1M glutamate was taken at 350 nm. Tubulin (18.4 µL of 10 mg/mL) was diluted with 1M sodium glutamate (165.6 µL). Drug solution (8 µL) was added such that the final concentration was between 0-40 µM. The tubulin/drug mixture was then incubated at 37°C for 15 min, then on ice for 15 min. GTP (8 µL, 10mM) was added and the mixture was placed in a 200 µL cuvette, and transferred to a jacketed cell holder that was at 2°C. A baseline absorbance 350 nm was recorded for 100 s at 2 °C. At 100 s, polymerization was initiated by increasing the temperature of the cuvette to 35°C. The polymerization is allowed to continue for 1600 s, then is cooled rapidly to 2 °C. The tubidity of tubulin solution was measured at 350 nm every 10 s. The turbidity was plotted against time in seconds. Data analysis was performed using Prism software and fitting to a non-linear regression:

$$Y = \text{Bottom} + \left[\frac{(\text{Top} - \text{Bottom})}{1 + 10^{(\text{X-logIC50}) \text{ Hillslope}}} \right]$$

where X is the log ligand concentration, Y is percent polymerization, bottom is the lowest depolymerization absorbance value, Top is the highest polymerization absorbance value, Hillslope is the pitch of the slope, and IC_{50} is the X value when polymerization is halfway between Bottom and Top. Using this relationship, IC_{50}, Hillslopes, R^2, and Log IC_{50} values for the various drugs were determined using % polymerization vs Log drug concentration plots.

Enthalpies of Tubulin Binding Using Isothermal Titration Calorimetry[80]

50 mM PEM (PIPES, EGTA, $MgCl_2$) Buffer with 0.1 mM GDP (pH 7.0)

PEM buffer (50 mM PIPES [1,4-piperazinediethanesulfonic acid], 1.0 mM EGTA, 0.5 mM $MgCl_2 \bullet 6H_2O$, pH 7.0, and 0.1mM GDP). PIPES free acid (1.06 g, 3.5 mmol), PIPES sodium salt (2.08 g, 6.4 mmol), EGTA (76 mg, 1.0 mmol), $MgCl_2 6H_2O$ (20.2 mg, 0.5 mmol) were dissolved in 180 mL water. The pH was adjusted to 7.0. The volume was then brought to 200 mL. GDP (8.86 g, 0.10 mmol) was added.

Preparation of Ligands for ITC

CA1 (9.3 mg, 0.028 mmol) was dissolved in DMSO (0.280 mL) for a 0.1M stock solution. The 1M stock was then diluted to 0.33 mM. Phenstatin derivative **37** was made to a 0.1M stock in DMSO solution then diluted to 0.4 mM in PEM buffer.

Preparation of Tubulin Samples for ITC

Tubulin (10 mg/mL in 1M glutamate) was dialyzed in PEM buffer for 24 h at 4 ^oC using Spectra/Por dialysis membrane (MWCO:3,500). Protein concentrations were determined by UV spectrophotometry. Tubulin was diluted to 2.59 mg/mL for samples run with CA1, and 4.53 mg/mL for scans with (3,4-dihydroxy-5-methoxy-phenyl)-(3',4',5'-trimethoxy-phenyl)-methanone **37**.

Measurement of Binding Enthalpies by ITC

ITC experiments were performed with a CSC 4200 Isothermal Titration Calorimeter (Provo, Utah). Tubulin was degassed for 5 min under reduced pressure then loaded into the sample cell. PEM buffer was degassed under reduced pressure, and

loaded into the reference cell. Ligand was degassed and taken into a 250 μL syringe fitted with an 11.25" 22 gauge needle. The sample cell was mixed with a mechanical stirrer at 300 rpm. The ITC experiment consisted of a series of 25 injections (10 μL) at 25 ^{o}C. The total heat of binding was measured for each injection. The samples were blanked against a series (25 X 10 μL) of PEM buffer injections into tubulin. The standard equilibration time was 200 s and the interval between injections was 200 s. The data was analyzed using BindWorks 1.1 software. A single binding model with an independent set of multiple binding sites was used for the non-linear regression. The enthalpy of binding (ΔH), the binding constant (K_b), and the number of binding sites (N) were obtained by the BindWorks 1.1 software using the independent model. The free energy (ΔG) and entropy (ΔS) were obtained using the following equation:

$$\Delta G = -RT \ln K_b = \Delta H - T\Delta S$$

Screening of Compounds for HIF-1α Inhibition of Accumulation

Reagents

2-Methoxyestradiol was purchased from Aldrich. Wash buffer, binding buffer, nuclear extraction buffer, were all supplied by Panomics. All other compounds were synthesized by members of the Pinney group.

Cell Culture[62]

HeLa (Human cervical cancer cell line obtained from Baylor College of Medicine) were cultured in DMEM (Dulbecco's modified eagles medium) with 4500 mg glucose, and L-glutamine (Sigma). Media was supplemented with 10 % fetal bovine

serum (FBS) and 5% penicillin/streptomycin. Cells were cultured in a humidified atmosphere with 5% CO_2 in air at 37°C.

Treatment of Cells[62]

Cells were seeded into 100 mm culture dishes and grown to 70% confluence. The medium was replaced with either new medium only for controls 1 and 2, or new medium containing 1.00 μM of the desired drug. The cells were incubated for 16 h at 37°C. Cobalt chloride (final conc. 125 μM) was then added to Control 2 and the cultures treated with drug to inhibit HIF-1α degradation.

Nuclear Extraction[62]

All nuclear extraction materials were obtained from Panomics. The cells were washed with 10 mL of 1X phosphate buffered saline solution (PBS) twice. The plates were then treated with 1.00 mL of Buffer A (10 mM HEPES; 10 mM KCl; 10 mM EDTA; 10 mM DTT, 2.5% IGEPAL(octyl phenoxylpolyethanoxyethanol); and Panomics Protease Cocktail Inhibitor; pH 7.9). The plates were placed on ice and rocked at 150 rpm for 10 min. Cells were then disrupted by scraping and pipetting, then centrifuged at 15,000 x g for 3 min at 4°C. The supernatant (cytosolic fraction) was saved. The pellet (nuclear fraction) was resuspended in 150 μL of Buffer B (20 mM HEPES; 0.4 M NaCl; 1 mM EDTA; 10 % Glycerol; 20 mM DTT, Panomics Protease Cocktail Inhibitor; pH 7.9), and then agitated on ice at 200 rpm for 2 h. The suspension was then centrifuged at 15,000 x g for 5 min at 4°C. The supernatant (nuclear extract) was collected and protein concentrations were determined by Bradford assay. The nuclear extract was then stored at -78°C until needed further.

Preparation of Wash Buffer[62]

Wash buffer from Panomics (10 mL, 10X), was diluted with 90 mL of ultrapure water.

Preparation of Binding Buffer[62]

Binding buffer (10 μL, 5X), consensus HIF DNA (2.5 μL), and Poly d(IC) (1 μL 0.5 μg/μL) were diluted with 26.5 μL of ultrapure water.

General ELISA Protocol[62]

Binding buffer (40 μL) was added to the wells of a v-bottom 96 well plate supplied by Panomics. Diluted nuclear extract (10 μL of 20:80 nuclear extract:dilution buffer) were added to each well. Nuclear extract dilution buffer (10 μL) was added to the blank well. The plate was incubated for 30 min at room temperature with mild agitation. The 96-well assay plate was prepared by washing 3 times with wash buffer (200 μL, 1X). The nuclear extract/consensus DNA solution (45 μL) was transferred from the v-bottom plate to the ELISA plate, and was agitated at room temperature for 1 h. The assay plate was then washed 3 times with wash buffer (200 μL, 1X). Diluted HIF-1α antibody (100 μL, 1:200 dilution in 1X antibody dilution buffer) was added to each well and the plate was agitated at room temperature for 1 hr. The plate was then rinsed 3 times with wash buffer (200 μL, 1X). Anti-mouse HRP antibody (100 μL, 1:1000 dilution in 1X antibody dilution buffer) was added to each well and the plate was incubated at room temperature for 1 h with mild agitation. The plate was then rinsed 3 times with wash buffer (200 μL, 1X). Substrate solution (100 μL) was added to each well and was developed at room temperature for 5 min. Stop solution (100 μL) was added to each well. The absorbance

of each well was measured at 450 nm using a ThermoLabsystems Ospys MR microplate reated with Ospys MR Revelation QuickLink software.

Determination of HIF-1α/Total Protein

The absorbance observed for each drug using the ELISA kit was divided by the protein concentration of the respective nuclear extract to determine the amount of HIF-1α/total nuclear protein.

$$\text{Relative HIF} = \frac{\text{Abs.450 nm}}{\text{Nuclear extract total protein conc.}}$$

Preparation of 1X Running Buffer[96]

NuPage MES SDS running buffer (50 mL, 20X) was diluted to 1X with ultrapure water (950 mL).

Protein Separation[96]

Nuclear extracts were adjusted to 1 mg/mL concentrations by dilution in Panomics nuclear extract dilution buffer. The nuclear extract (5 µL, 1 mg/mL) was then incubated at 70^{o}C for 10 min, with ultrapure water (6.5 µL), and NuPage LDS sample buffer (2.5 µL, 4X). The protein solution (10 µL) was then loaded onto Invitrogen NuPage 10% Bis-Tris Gels (1.0 mm X 10 well). The protein was then separated (200 V, 35 min) using a Hoefer miniVe vertical electrophoresis system with a BioRad Power Pac 300 power source.

Western Blot Immunodetection Confirmation[97]

Reagents were purchased from VWR unless otherwise noted. Primary HIF-1α (C-term) polyclonal antibody was purchased from Cayman Chemical, and donkey anti-

rabbit (HRP) secondary antibody was purchased from Affinity BioReagents (ABR) Three extra thick Bio-Rad Protein blot paper was presoaked in transfer buffer (25mM tris, pH 10.4, 10% (v/v) methanol). Millipore Immobilon-P^{sq} PVDF transfer membrane was presoaked in 50% (v/v) methanol. One piece of presoaked blotting pad was placed onto the anode of the semi-dry blotting system. The PVDF membrane was placed on top of the pad followed by the gel, and then two pieces of presoaked blotting pads. Air bubbles were rolled out from between the layers. The cathode was then placed on top of the stack, and the proteins were blotted using the Bio-Rad trans-Blot SD semi-dry transfer cell with a Bio-Rad PowerPac 300 (20V, 30 min). The blot was placed in a blocking solution (1% (w/v) bovine serum albumin, 0.05% tween-20) and agitated for 1 h. The blot was rinsed with PBS (10 mM sodium phosphate, pH 7.2, 0.9% (w/v) NaCl, 0.1% Tween-20), then incubated with the primary HIF-1α antibody (1:1000 dilution in BSA blocking solution) for 1 h. The blot was then agitated in PBS 3 times for 10 min each. The blot was then incubated with the secondary antibody (1:2500 dilution in BSA blocking solution). The blot was then rinsed in PBS 5 times for 10 min each, then with water 3 times for 10 min each. The blot was visualized using an Upstate Visualizer Western Blot Detection Kit by mixing detection reagent A and detection reagent B in a 1:2 ratio, then incubating with the blot for 5 min. The luminescence was recorded using and Ultra-Lum Gel-reader, with a Hamamatsu digital camera, and Ultraquant software.

Determination of Cancer Cell Cytotoxicity Using an SRB Assay
Compound Preparation[70]

Compound was dissolved to a 10 mg/mL concentration in either DMSO or water depending on solubility. 10 μL of the 50 mg/mL was dissolved in 990 μL of media for a

final concentration of 100 μg/mL. A series of dilutions are done to give the final concentrations: 10 μg/mL, 1 μg/mL, 0.1 μg/mL, 0.01 μg/mL, 0.001 μg/mL, 0.0001 μg/mL, and 0.00001 μg/mL. The compounds (100 μL) were added to the cell plates to give dose concentrations of: 50 μg/mL, 5 μg/mL, 0.5 μg/mL, 0.05 μg/mL, 0.005 μg/mL, 0.0005 μg/mL, 0.00005 μg/mL, 0.000005 μg/mL.

Cell Thawing Procedure

Media, and 1X PBS was warmed to 37 ^{o}C. Cells were rapidly thawed to 37 ^{o}C using a water bath. PBS (10 mL) was added to a 14 mL centrifuge tube, followed by cells (1 mL), and then the suspension was mixed by inverting the conical tube several times. The cells were then centrifuged at 1000 rpm for 10 min. The supernatant was removed, and the cells were resuspended in the desired media (10 mL). The cells (10 mL) were then added to a 100 mm cell culture appropriate Petri dish.

Cell Culture for DU 145

Du 145 prostate cancer cell line was purchased from ATCC. The were grown in Dubulco Minimum Eagles Medium (DMEM), supplemented with 5 % Fetal Bovine Serum (FBS), 1% Penstrep, and supplemented with 2 mM L-glutamine. The cells were grown in 5% CO_2 at 37^{o}C.

Cell Culture for NCI-H460

NCI H460 lung cancer carcinoma cells were cultured in RPMI 1640 media with 2 mM L-glutamine, 1.5 g/L sodium bicarbonate, 4.5 g/L glucose, 10 mM HEPES, 1.0 mM sodium pyruvate, 5% FBS, and 1% Penstrep. The cells were grown in 5% CO_2 at 37^{o}C.

SRB Assay Using DU-145 or NCI H460 Cell Lines[70]

Two 96-well culture dishes were plated with 10,000-15,000 cells. The culture was allowed for 16 h. The cells of one plate are adhered with TCA (10% w/v, 100 μL) at 2°C for 3 h. The second 96-well plate was treated with the desired compound at varying concentrations, and then incubated for 48 h. The cells were then treated with TCA (10% w/v, 100 μL) and incubated at 2 °C for 3 h. The plate was washed with an acetic acid solution (1% v/v, 3 x 200 μL). The plate was stained with SRB dye (0.4% w/v in 1% acetic acid, 100 μL). The plate was then washed with 1% acetic acid (3 x 100 μL). The dye was resuspended in a 10 mM Tris base solution (200 μL, pH 10.5). The absorbance at 550 nm was then taken using a ThermoLabsystems Ospys MR microplate reader with Ospys MR Revelation QuickLink software. Manipulation of the data is performed using the following equation:[70]

$$\%\ \text{cell growth inhibition} = \frac{(\text{ODsample-ODblank})}{(\text{ODnegative control-ODblank})} \times 100$$

The % cell growth inhibition was plotted against the Log of the compound concentration using Excel. A linear regression is then fitted, and the IC_{50} is determined as the concentration at 50% cell growth inhibition.

CHAPTER THREE

Results and Discussion

The focus of this research was to investigate structure activity relationships for combretastatin and indole based tubulin binding agents, increase combretastin drug effectiveness in hypoxic regions, and determine if compounds synthesized within the Pinney group were effective at inhibiting the preservation of HIF-1α. The effectiveness of the VDAs synthesized were determined by a tubulin polymerization inhibition assay, as well as their cytotoxicity against DU-145 prostate cancer and NCI H460 lung carcinoma cell lines. The development of methodology for the synthesis of radiolabeled CA1 was also performed, as were scale up synthesis of the indole derivative OXi8006, and dihydronaphthalene derivative OXi6196.

Synthesis of Combretastatin Derivatives

Synthesis of (Z) + (E)-2-(3′,4′-dihydroxy-5′-methoxyphenyl)-1-(3,4,5-trimethoxyphenyl) ethane **7** and **8**

The clinical success of CA1 created interest into research of its 3′,4′-dihydroxy-5′-methoxy derivative. The synthesis of **7** may give another effective anti-cancer agent in the combretastatin family, but more importantly, its synthesis will give valuable information for colchicine binding site drugs. The synthesis of the combretastatin analogue **7** was attempted using methods previously established within the Pinney Group shown in Scheme 1.[84,85,98] Synthesis of combretastin **7** started with the bromination of 3,4,5-trimethoxy benzyl alcohol using PBr_3 to 3,4,5-trimethoxy benzyl bromide **1** in an

85% yield. The benzyl bromide **1** was then converted to the 3,4,5-trimethoxy triphenylphosphonium benzyl bromide Wittig salt **2**(80% yield). The other component to the Wittig reaction was prepared starting with the formation of 3′,4′-dihydroxy-5′-methoxy benzaldehyde **3** from 3-bromo-4-hydroxy-5- methoxybenzaldehyde using

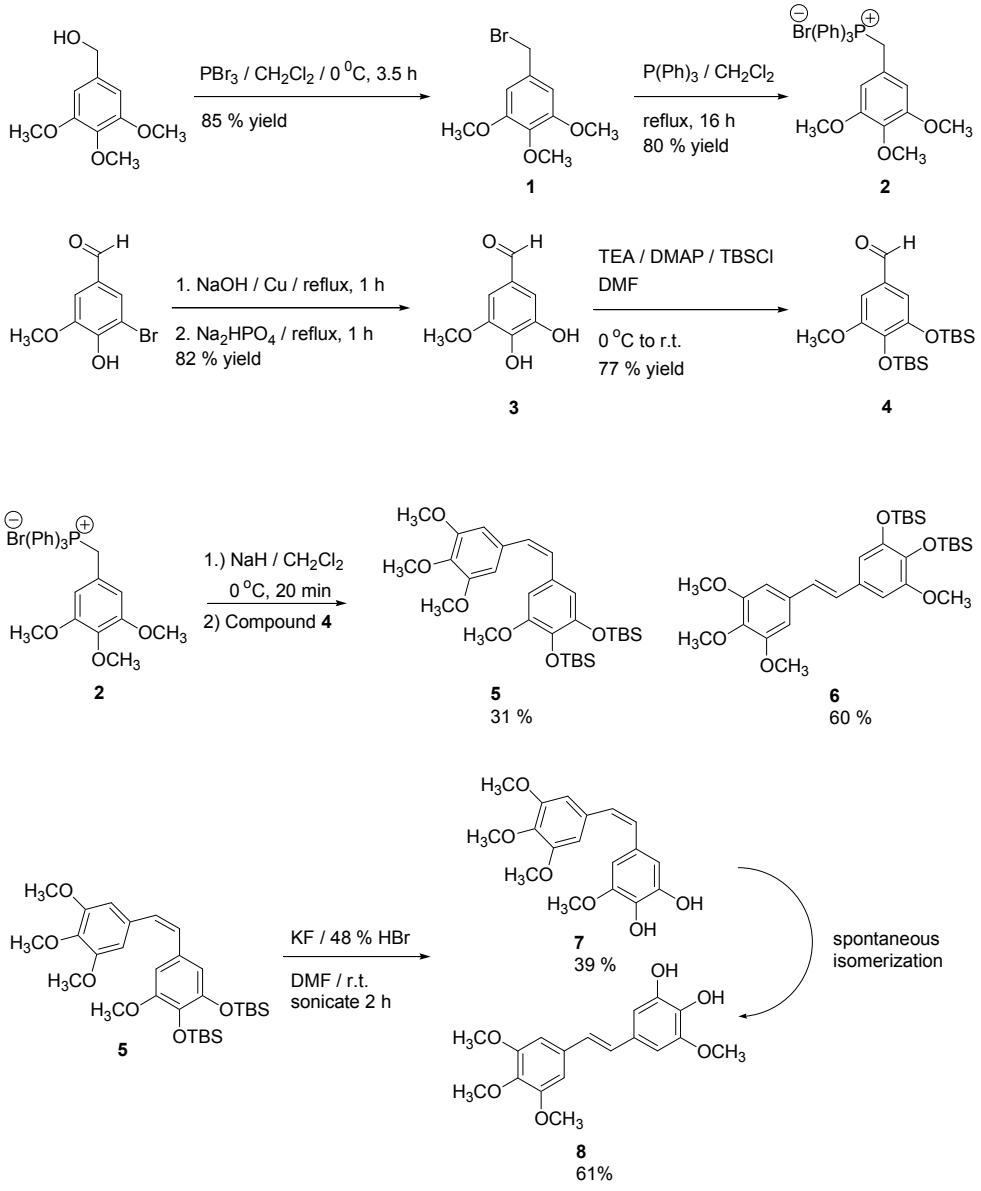

Scheme 1. Synthesis of combretastatin analogues **7** and **8**.

NaOH and Cu in a modified Ullmann synthetic method (82% yield).[85] The benzaldehyde diol **3** can be purchased from Sigma Aldrich, however, it is relatively expensive. Though the formation of aldehyde **3** was reported to undergo a modified Ullmann synthesis, a reaction was run without Cu^0, and the desired diphenol **3** was still recovered in a 60% yield. This suggests that nucleophilic aromatic substitution is also occurring. Aldehyde **3** was then protected using TBSCl, TEA, and DMAP in DMF to form the 3,4-di-[(*tert*-butyl-dimethyl-silanyl)oxy]-5-methoxybenzaldehyde **4** in a 77% yield. The Wittig reaction was accomplished by first forming the phosphorous ylide by reacting salt **2** with NaH at 0 ^oC then adding aldehyde **4**. The TBS-protected combretastatin **5** (31% yield) and *E*-isomer **6** (60% yield) were isolated after purification by flash column chromatography on silica gel. *Z*-combretastin **5** was deprotected using KF and 48% HBr with sonication for 2 h. The desired *Z*-isomer **7** was recovered in a 39% yield; however, a great amount of *E*-isomer was also recovered (61% yield). Despite numerous purification attempts, trace amounts of the *E*-isomer **8** was always recovered with the *Z*-combretastatin **7**. Furthermore, recovery of the amount of *E*-isomer **8** increased with every purification step. It was decided the *Z*-stilbene **7** spontaneously isomerized to *E*-combretastatin **8**. This conversion process was almost immediate in any polar solvent. To monitor the isomerization of combretastatin **7** to **8,** the *Z*-isomer was taken into $CDCl_3$ and monitored by NMR. The solution was slightly acidified to pull the electron density away from the aromatic system to slow the isomerization process. Integrations of the vinyl C-H NMR signal for the *Z*-isomer **7** was taken at 6.61 ppm and compared to corresponding vinyl C-H integrations for the E-isomer **8** taken at 6.64 ppm. The integrations were compared to each other by taking the percent *Z*-isomer at times 0, 16,

27, 38, 101, and 198 min. The amount of the *Z*-isomer **7** in solution decreased with time, and the amount of E-isomer **8** increased (Figure 44). The rate of isomerization was not determined because not enough data points were collected to give an accurate best fit line.

A.

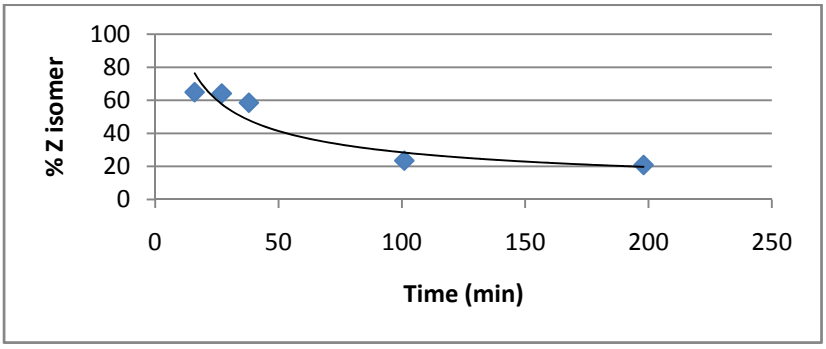

B.

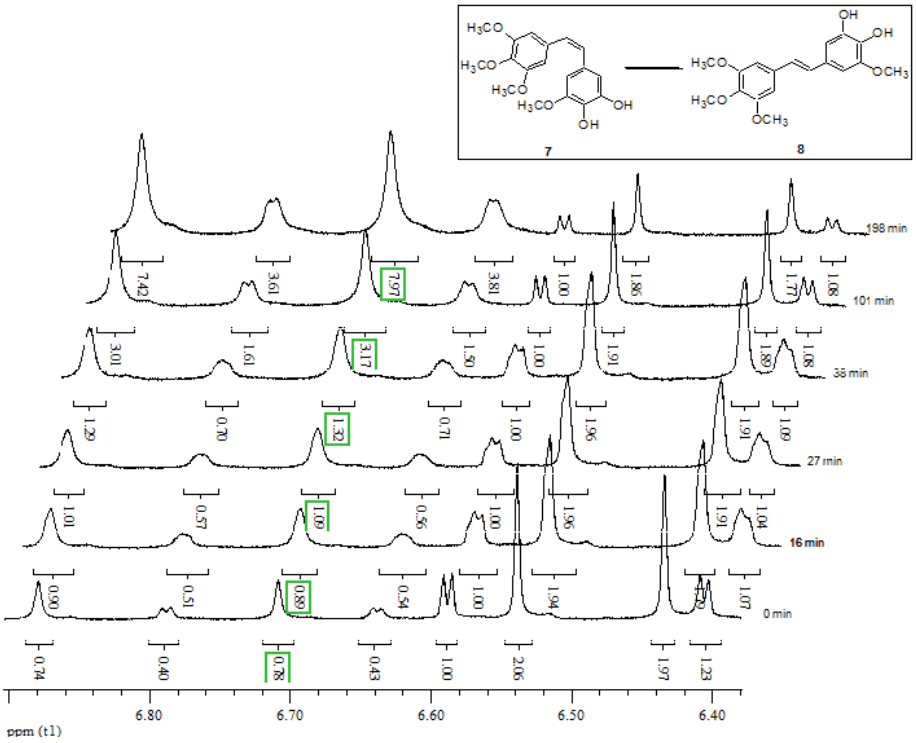

Figure 44. Conversion of **7** to **8.** A) Plot of **7** converting to **8**. B) ^{1}H NMR overlay of **7** isomerizing to **8** in $CDCl_3$.

Synthesis of Fluoro-containing Combretastatin Derivatives **10**, **11**, **12**

The common pharmacophores described by Nguyen and co-workers describes hydrogen bonding with the 4-methoxy of the combretastatin and Cys 239 of the colchicine binding site.[13] Replacement of the methoxy substituent at the 4-position with a fluorine allowed us to further evaluate this hypothesis. The Wittig reaction was used in the synthesis of the fluoro combretastatin analogues, and utilized the same procedures described previously.[84,98] The stilbenes were prepared by first reacting the commercially available 3,4,5-trifluorobenzyl bromide with triphenylphosphine to form the Wittig salt **9** (Scheme 2).

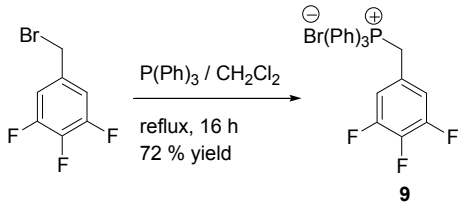

Scheme 2. Synthesis of 3,4,5-trifluoro triphenylphosphine benzyl bromide **9**.

The Wittig salt **9** was then reacted with aldehyde **4** to afford (*Z*)+(*E*)-2-{(3′,4′-di-(*tert*-Butyl silyl)oxy]}-5′-methoxyphenyl-1-(3,4,5-trifluorophenyl) ethene. This stilbene *Z* and *E* mixture was unable to be separated by either flash column chromatography or preparative TLC because the retention times of the isomers were too similar. The *Z* and *E* mixture was deprotected using KF and 48% HBr in DMF with sonication for two hours to give a mixture of *Z*–stilbene **10** and the E-stilbene **11** (Scheme 3). The deprotected stilbenes **10** and **11** were separated by flash column chromatography, giving overall yields for the formation of the *Z*- and *E*-isomers as 42% and 30 % respectively. The

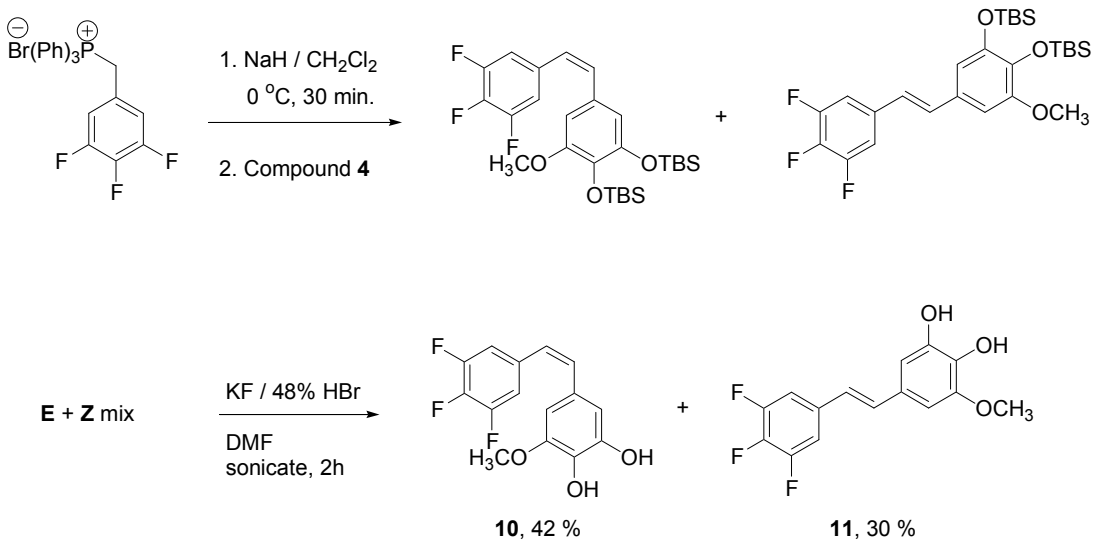

Scheme 3. Synthesis of Z and E fluoro combretastatins derivatives **10** and **11**.

isomerization of **10** to **11** was also observed to occur in the same fashion as its trimethoxy analogues **7** and **8**. NMR studies of the conversion of **10** to **11** were not performed.

Freedom of rotation about the ethane bridge was hypothesized by Dr. Kevin Pinney to possibly allow better tubulin binding. To allow freedom of rotation around the stilbene backbone, the *E*-fluoro stilbene **11** was reacted with Pd (5%) and H_2 to generate the dihydro stilbene **12** in a 40 % yield (Scheme 4).

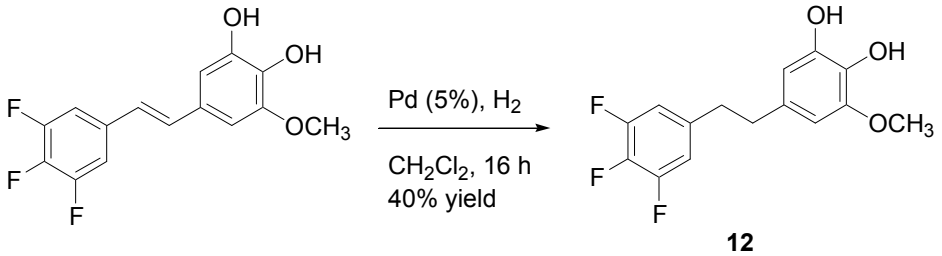

Scheme 4. Synthesis of 2-(3′,4′-dihydroxy-5′-methoxyphenyl)-1-(3,4,5-trifluorophenyl) ethane **12**.

Synthesis of Nitro and Amino Trifluoro-Combretastatins Analogues **13-20**

The synthesis of nitro-CA4 derivatives has been described by the Pinney research group previously.[84,98] To continue the SAR studies of substituted stilbenes, the synthesis of several tri-fluoro combretastatin analogues were accomplished. The formation of the fluoro-nitro combretastatins also utilized a Wittig reaction as a key step in the synthesis. Wittig salt **9** was reacted with commercially available 4-methoxy-3-nitrobenzaldehyde to form *E* and *Z*-stilbenes **13** and **14** in 46% and 12% yields, or with 4-methoxy-2-nitrobenzaldehyde to create *E*- and *Z*-combretastatins **17** and **18** in 34% and 22% yields respectively (scheme 5). The formation of stilbenes **13**, **14**, **17**, and **18** proceeded smoothly, as did the separation of the *Z* and *E*-isomers. Reduction of the nitro substituents was accomplished with Fe and acetic acid,[82] a technique that selectively reduces nitro-substituents. A mixture of stilbenes **13** and **14** was reduced simultaneously to give amino stilbenes **15** and **16** in respective 11% and 20% yields. Reduction of *Z*-nitro stilbene **17** to *Z*-amino stilbene **19** occurred in a 61% yield, whereas the reduction of *E*-nitro combretastatin **18** to the E-amino combretastatin **20** proceeded in a 66% yield (Scheme 5).

Synthetic Methodology Capable of Incorporating a Radio Isotope Into CA1P Dipotassium Salt (OX16C) **27**[86,87]

To monitor the metabolism of OX16C within living systems, a radiolabeled derivative is needed. This project established a method for potentially radiolabeling OX16C for further preclinical studies, and was carried out as a team effort with other Pinney group members, as well as, research associates following previously established procedures.[86,87,136] For identification of key intermediates, the following terminology has

been utilized: cold-precursor refers to the di-protected CA1 in which a TBS protected phenol is located on the 4-position of the A-ring, and the 2, 3-hydroxy substituents on the B-ring are isopropyl protected; hot-CA1 refers to CA1 where a C13 methyl substituent has been added to the 4-position of the A-ring. In development of the synthetic strategy for radiolabeled OX16C, *CH_3 is used to denote the location of the potential C14 methylated carbon; however, only C12 methylation was used in this synthesis. The synthesis of the cold precursor started with the demethylation of 3,4,5-trimethoxybenzaldehyde with $AlCl_3$ at room temperature. The 4-hydroxy-3,5-

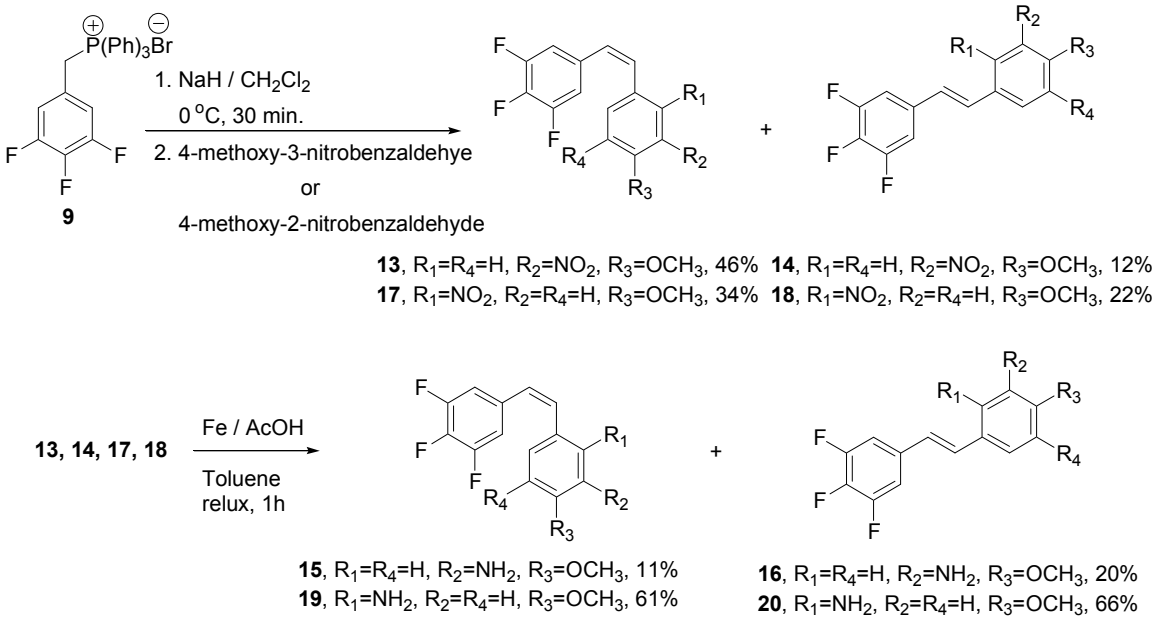

Scheme 5. Synthesis of E-and Z-nitro stilbenes **13**, **14**, **17**, and **18**, and amine analogues **15**, **16**, **19**, and **20**.

dimethoxybenzaldehyde **21** was obtained in quantitative yield. Phenol **21** was protected as its corresponding TBS ether utilizing TBSCl/Et_3N/DMAP in DMF at room temperature. The *cis*-CA1 cold precursor was achieved via a Wittig reaction as described

previously; however, n-BuLi was used in place of NaH. The 2,3-diisopropoxy-4-methoxytriphenylphosphine benzyl bromide obtained from Benson Nguyen, a fellow graduate student in the Pinney research group, was reacted with aldehyde **22** to form a mixture *E* and *Z*-isomers of cold CA1 precursors. The separation of the isomers was difficult. Gravity column chromatography with a solvent mixture of EtOAc:Hexane (1:99) afforded the *Z*-cold precursor **24** in a 49% yield (Scheme 6).

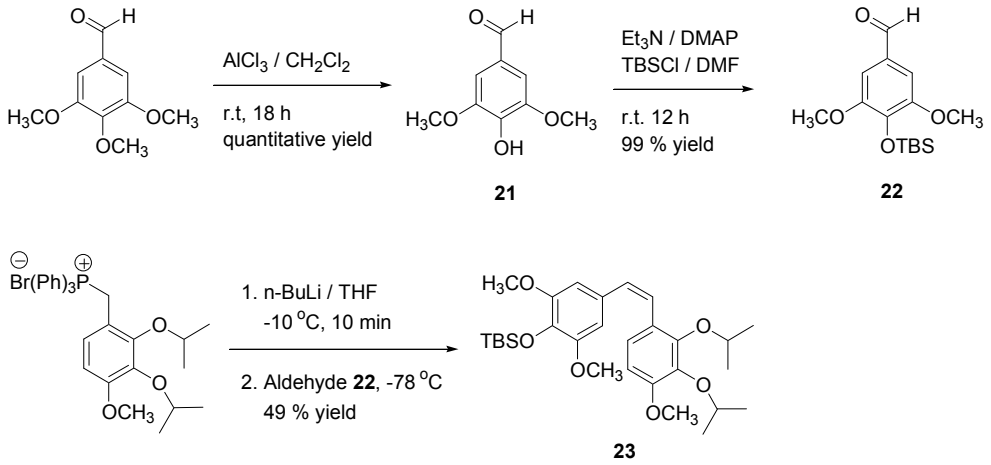

Scheme 6. Synthesis of *cis*-cold precursor **23**.

Formation of the hot CA1 from the cold precursor involved two reactions. In the first step cold precursor was deprotected with TBAF while simultaneously methylating with methyl iodide to form stilbene **24** in a 62% yield (Scheme 7,*C indicates the location C-14 labeled CH_3 would be introduced if this reaction was carried out with C-14 MeI rather than the C-12 MeI that was used to establish this methodology). After methlyation the isopropyl groups were deprotected with 2.5 eq of $TiCl_4$ in CH_2Cl_2 with sonication for 3 min to give the hot CA1 **25** in a 94% yield. Previous work in the Pinney

group for this method of deprotection used 4 eq. of $TiCl_4$ and took 40 min to reach yields of 62%. There were also workup and isomerization problems associated with the higher amounts of titanium in the reaction. Emulsions formed in separation attempts, and CA1 **25** isomerized to the *trans*-isomer **35** when high amounts of $TiCl_4$ were used. Titanium oxide can bind with phenols.[121] If the titanium disrupts the aromaticity of the combretastatin structure, then isomerization can take place as described previously. The sonication method developed here is much more efficient than previous methods established for this reaction in the Pinney group (Scheme 7).

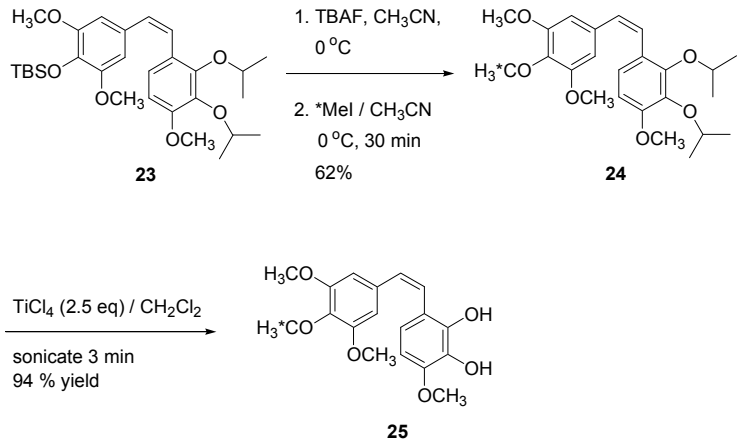

Scheme 7. Formation of hot-CA1 **25**.

The method utilized for the synthesis of OX16C was previously established by other Pinney group members and research associates.[136] Following the reported procedure by Evotec,[87] NCS and DBP were used to form the dibenzyl phosphate CA1 intermediate **26** (25% yield). This procedure eliminated the use of CCl_4, which was previously utilized with DIPEA and DBP to form the same intermediate. Freshly distilled TMSBr (over CaH_2) was used to remove the benzyl substituents of tetrabenzyl

phosphate **26** to form the *tetra*-O-TMS-phosphate intermediate (scheme 8). A reverse quench of the *tetra*-O-TMS phosphate intermediate with a solution of KOMe (10 eq) at -10 ^{o}C gave the tetra-potassium phosphate salt of *cis*-CA1 **25**. Titration of the tetra-potassium phosphate salt with 1M HCl to a pH of 4.75 to 4.85 gave the desired di-potassium salt OX16C **27**. OX16C was easily formed from the tetra-benzyl phosphate CA1 **26** (45% yield), without any isomerization problems (Scheme 8).

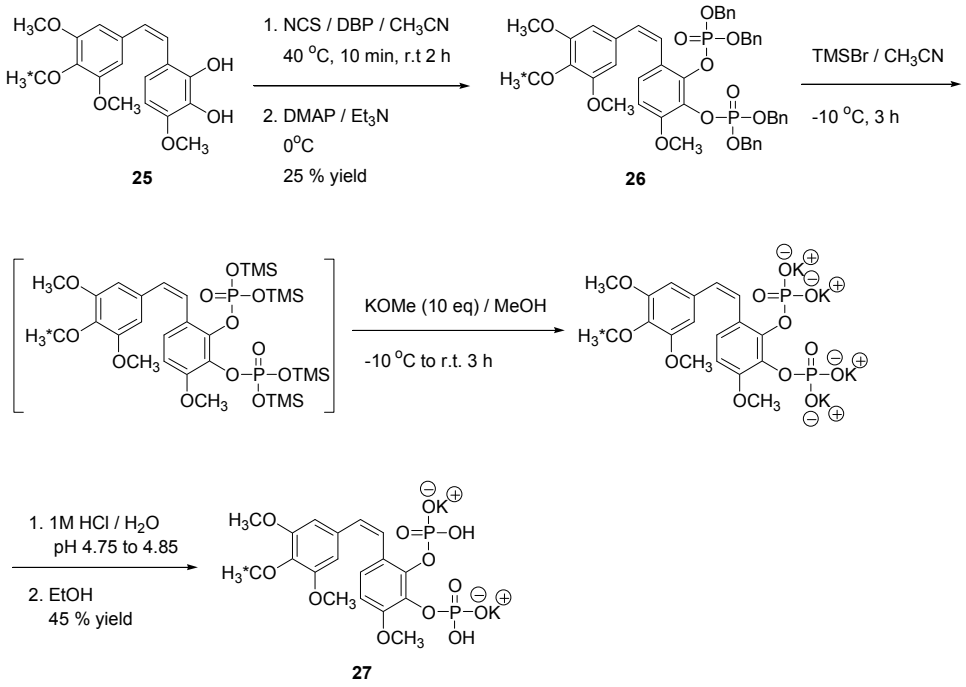

25 **26** **27**

Scheme 8. Synthesis of hot OX16C **27**.

Alternative Synthetic Route to OX16C **27**[86,87]

Previous synthesis of OX16 by Pinney group members and research associates sometimes resulted in isomerization during the formation of the di-potassium phosphate CA1 **27**. It was hypothesized that titanium oxide formed from the excess $TiCl_4$ could be

carried over in the reactions, coordinate with the CA1, and result in isomerization. A route that could be used to form the radiolabeled OX16C was established that did not use $TiCl_4$.

The first step in this alternative route involved the methylation of 4-hydroxy-3,5-dimethoxybenzaldehyde **21**. Aldehyde **21** was methylated by first deprotonating the phenol with aluminum trichloride then methylating with methyl iodide to form the 3,4*,5-trimethoxybenzaldehyde in a 64% yield (Scheme 9). Again 4* is used to identify the location of the potentially radiolabeled CH_3. No C-14 labeled reactants were used in this synthesis.

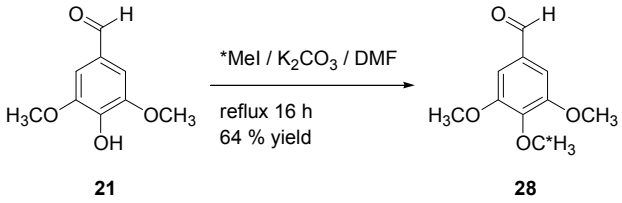

21 **28**

Scheme 9. Synthesis of the 3,4,5-trimethoxybenzaldehyde **28**.

The second part for the alternative synthetic route to potentially achieve a radiolabeled Ox16C involved the formation of the TBS protected Wittig salt **81** (Scheme 10). The 2,3-dihydroxy-4-methoxybenzaldehyde (synthesized by Benson Nguyen, a fellow Pinney group graduate student) was protected with TBS to form aldehyde **29** in a 94% yield. Aldehyde **29** was reduced with $NaBH_4$ to form the benzyl alcohol **30** (91%), which was brominated with PBr_3 to form benzyl bromide **31** in an 87% yield. The Wittig salt was formed by refluxing benzyl bromide **31** with triphenylphosphine to create the triphenylphosphonium benzyl bromide salt **32** in a 91% yield.

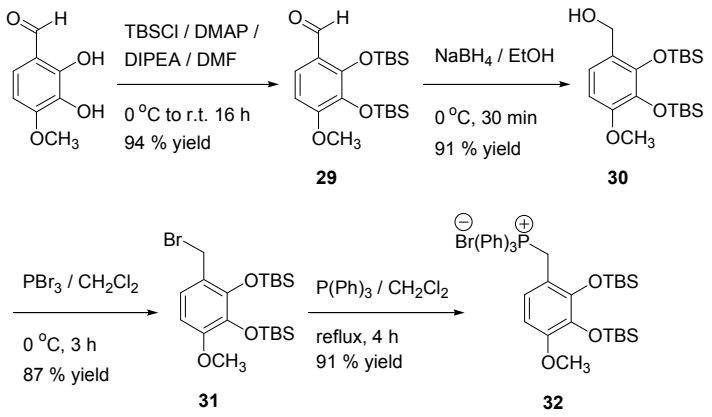

Scheme 10. Synthesis of the 2,3-di-*tert*-butylsilyloxy-3-methoxy-triphenylphosphonium benzyl bromide Wittig Salt **32**.

With both components synthesized, the Wittig reaction between **32** and **28** **(**Scheme 11) using n-BuLi was run as described previously (Scheme 6). The desired TBS-protected CA1 **33** was obtained in an 11% yield. The intermediate **33** was then deprotected by sonication in the presence of KF and 48% HBr in DMF for 2 h. The desired CA1 **25** was purified by recrystallization and obtained in a quantitative yield (Scheme 11). CA1 **25** was then taken to OX16C using the same methods as described

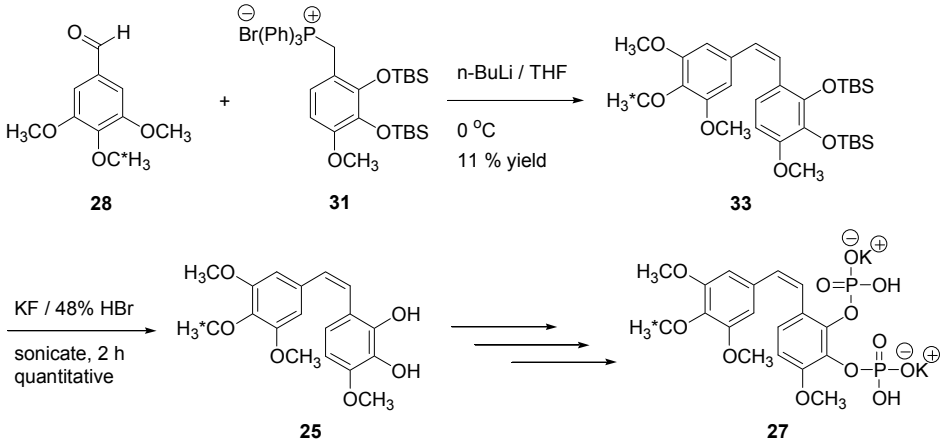

Scheme 11. Synthesis of CA1 **25** via an alternative route that does not use $TiCl_4$.

previously for the first route to OX16C synthesis (see Scheme 8). No problems in regards to isomerization were observed in formation of OX16C using this alternative route.

Synthesis of trans-CA1 **35**

In an attempt to form a large amount of CA1 **25** an effective method of forming *trans*-CA1 was achieved serendipitously. In this route, aldehyde **28** underwent a Wittig reaction with 2,3-diisopropoxy-3-methoxy triphenylphosphonium benzyl bromide (from Benson Nguyen a fellow Pinney group graduate student) using n-BuLi. Only the *E*-isomer, intermediate **34,** was isolated; however, the yield was low (37%). The isopropyl protected CA1 **34** was easily purified by recrystallization in a mixture of hexane and ethyl acetate (70:30), then subsequently deprotected by sonication with $TiCl_4$ in CH_2Cl_2 to afford the desired *trans*-CA1 **35** (86% yield) (Scheme 12). Purification of *trans*-CA1 **35** was performed by recrystallization in hexanes and ethyl acetate. Perhaps the overall yield could have been increased had flash column chromatography had been used for purification rather than recrystallization.

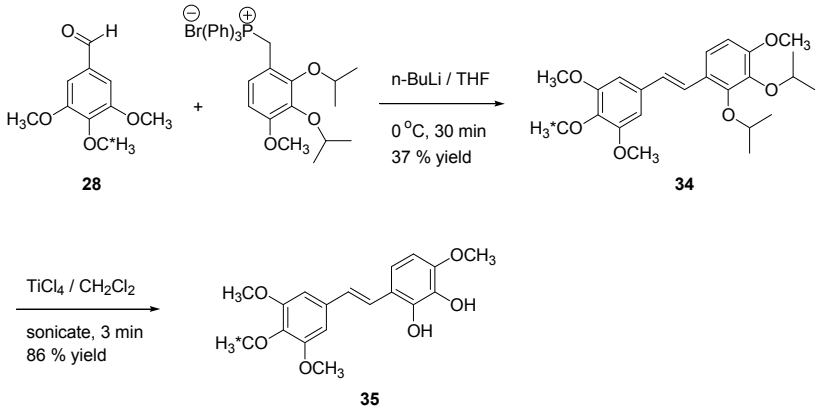

Scheme 12. Formation of trans-CA1 **35**.

Synthesis of a Phenstatin Derivative **37**[99,100]

Because the *Z*-isomer of CA1 analogue **7** spontaneously isomerized to the corresponding *E*-isomer **8** (Scheme 1), the effectiveness of having a 3′,4′-dihydroxy-5′-methoxy substituent placement on a *Z*-stilbene could not be effectively quantified for either tubulin polymerization inhibition or cell line toxicity. Phenstatin is a small molecule known to bind the colchicine binding site and inhibit tubulin polymerization and also structurally resembles CA4 in aryl-aryl centroid-to-centroid distances.[99] Because the biological effectiveness and resemblance of phenstatin to CA4, a benzophenone derivative of combretastatin analogue **7** was synthesized to help determine the effects of having a 3′,4′-dihydroxy-5′-methoxy moiety on the B-ring.[100]

The main reaction in the synthesis of **37** was the coupling of 3,4,5-trimethoxy-1-bromo benzene with aldehyde **4**. A lithium metal exchange took place upon treatment of 3,4,5-trimethoxybromo benzene with n-BuLi. Once the halogen metal exchange was complete, aldehyde **4** was dissolved in anhydrous ether and added to the reaction. Care was taken to ensure that a minimal amount of n-BuLi was used. Excess n-BuLi may react with aldehyde **4** to form the 1-phenylpentanol analogue. The resulting secondary alcohol intermediate was not easily purified, and appeared to potentially decompose on silica gel so the crude mixture was taken to the next step without further purification. The crude secondary alcohol mix was oxidized to the corresponding benzophenone **36** with PCC, and purified by flash column chromatography to give the product in an overall 24% yield. Phenstatin analogue **36** was deprotected to afford to desired benzophenone analogue **37** by sonication with KF and 48% HBr in DMF in a 47% yield (Scheme 13).

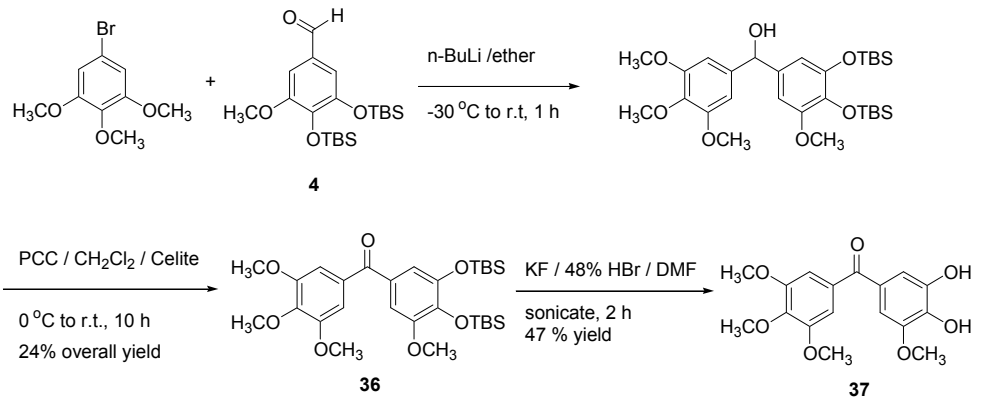

Scheme 13. Synthesis of benzophenone **37**.

A trifluoro analogue of compound **37** was attempted; however, the halogen metal exchange resulted in a mixture of indeterminable products.

Synthesis of Indole Derivatives

Synthesis of Indoles **44** *and* **47**[14,101]

Indole scaffolds have also shown to be good inhibitors of tubulin polymerization. As previously discussed, the A-B aryl-aryl centroid-to-centroid distance is comparable to *Z*-stilbenes (Figure 10). Also, the synthesis of additional indole derivatives would add to the SAR understanding of how these compounds interact with the tubulin colchicine binding site. The indole derivative of the unstable *Z*-stilbene **7** was synthesized using methods previously established within the Pinney group.[14,101] The TBS protected 3,4-dihydroxy-5-methoxybenzaldehyde **4** was converted to the secondary benzyl alcohol **38** in a quantitative yield by a methyl addition reaction with methyllithium (Scheme 14). The secondary alcohol **38** was then oxidized with PCC to the acetophenone **39** in a quantitative yield. Celite was used in the oxidation as an abrasive to keep the stir bar freely rotating. Ketone **39** was placed in an LDA solution to generate the enolate *in situ*,

which was then trapped with the addition of TMSCl thus forming the TMS-enol ether **40** (99% yield). The TMS-enol ether **40** was not purified further because silica gel has the potential to convert **40** back to the acetophenone analogue **39**. The TMS-enol ether **40** was subject to an addition reaction with bromine to form bromoacetophenone **41** (41% yield). Care was taken to not run the reaction for too lengthy a period of time, as a dibromo substituted by-product can result. Also, the bromination reaction was monitored by TLC. Once no acetophenone **39** starting material was observed, then all TMS-enol ether **40** was consumed. Bromoacetophenone **41** was dissolved in DMF, followed by the addition of *m*-anisidine, and then refluxed for 18 h to give cyclized indole **42** in a 31% yield. Several products are formed during the cyclization reaction; however, the indole products can be identified on TLC by treating with iodine. The indole derivatives had a green coloration on TLC when treated with iodine. Solvent effects are also important to the indolization. DMF was used in place of N,N-dimethylaniline serendipitously; however, the use of DMF as the solvent increases the yield of the cyclization by ~20%. The cyclization process involves a substitution reaction followed by an acylation, loss of water, and a phenyl shift. DMF is a more polar solvent than N,N-dimethyl aniline (DMA). When using DMA as the solvent in this reaction, addition of ethyl acetate is required to dissolve a polar tar that forms. When using DMF, this tar never forms. It may be that DMF is better at dissolving the tar organics, or it may be the result of DMF having a lower boiling point than DMA. If the tar components are thermally decomposed organic compounds lowering the temperature of the reaction would decrease the formation of undesirable products. Indole **42** was then refluxed in *o*-dichlorobenzene (ODB) with 3,4,5-trimethoxybenzoly chloride to give the benzoylated indole **43** in a 62%

yield, and with 3,4,5-trifluorobenzoyl chloride to give compound **46** in a 44% yield. Treatment of either trimethoxy indole **43** or trifluoro indole **46** with TBAF at 0 ^{o}C for 4 h, results in complete deprotection in 50% and 44% yields respectively (Scheme 14). Indole analogue **42** was also deprotected with TBAF to **45** in order to compare the tubulin polymerization inhibition capabilities of the benzoylated product to the unbenzoylated material.

Synthesis of Fluorinated Indole **55**[14,101]

The synthesis of a fluorinated derivative of Oxi8006 **55** underwent the same overall reaction sequence; however, an isopropyl protecting group was utilized in place of TBS. Isovanillin was dissolved in DMF and refluxed with 2-bromopropane to obtain the isopropyl protected aldehyde **48** in an 82% yield (Scheme 15). The protected isovanillin **48** was methylated to the secondary benzyl alcohol **49** (98% yield), then oxidized to acetophenone **50** (84% yield). Addition of compound **50** to a LDA solution followed by addition of TMSCl resulted in the formation of an enolate followed by its capture as the TMS-Enol ether **51** in a quantitative yield. This enol ether was brominated with Br_2 in CH_2Cl_2 to afford bromoacetophenone **52 (**44% yield). Indole **53** was formed in a 21% yield by refluxing compound **52** with m-anisidine in DMF for 12 h. The benzoylation with 3,4,5-trifluorobenzoyl chloride gave the fluorinated indole product **54**. Deprotection of **54** was achieved with $AlCl_3$ in CH_2Cl_2 to give the desired fluorinated

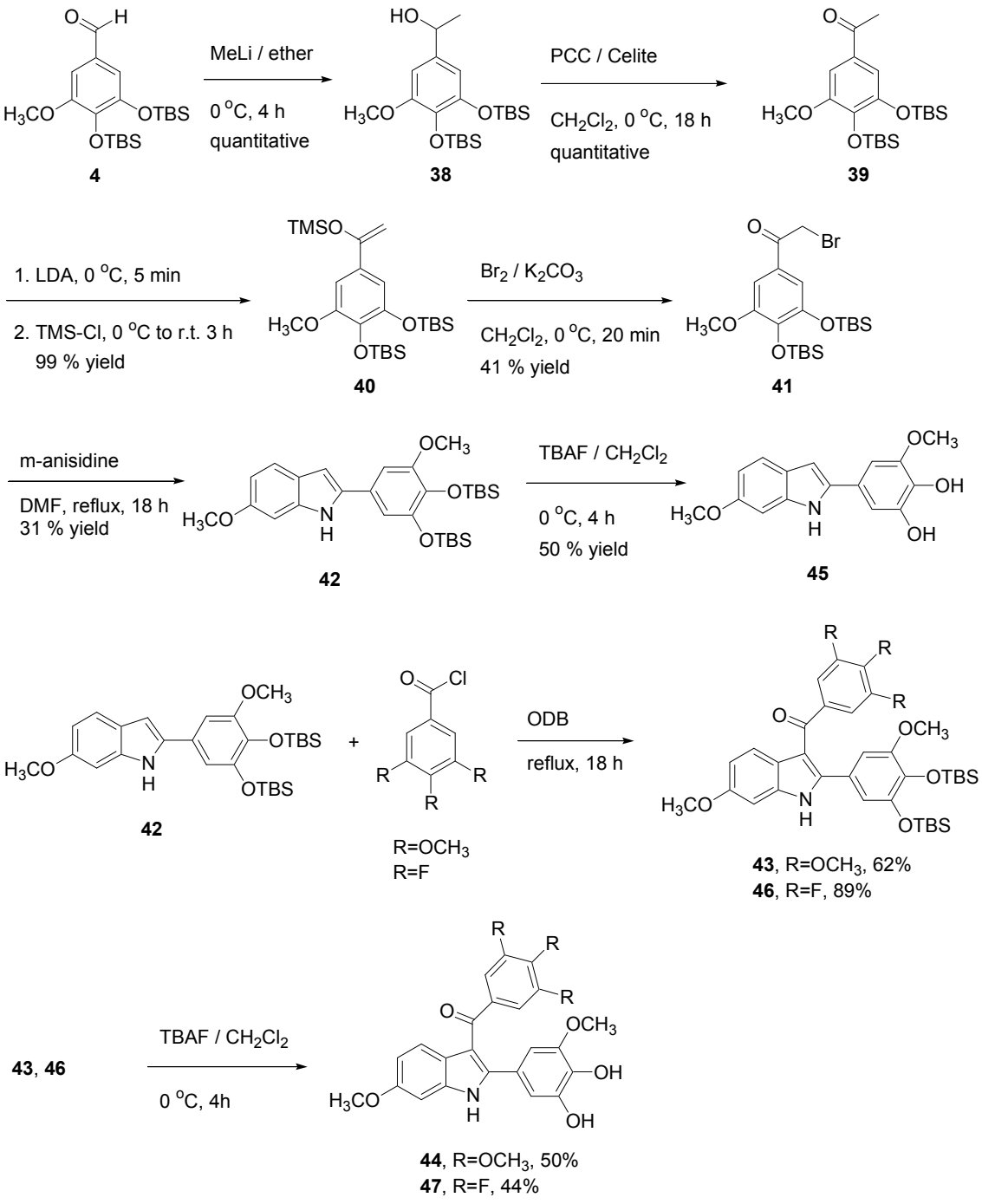

Scheme 14. Synthesis of indoles **44**, **45**, and **47**.

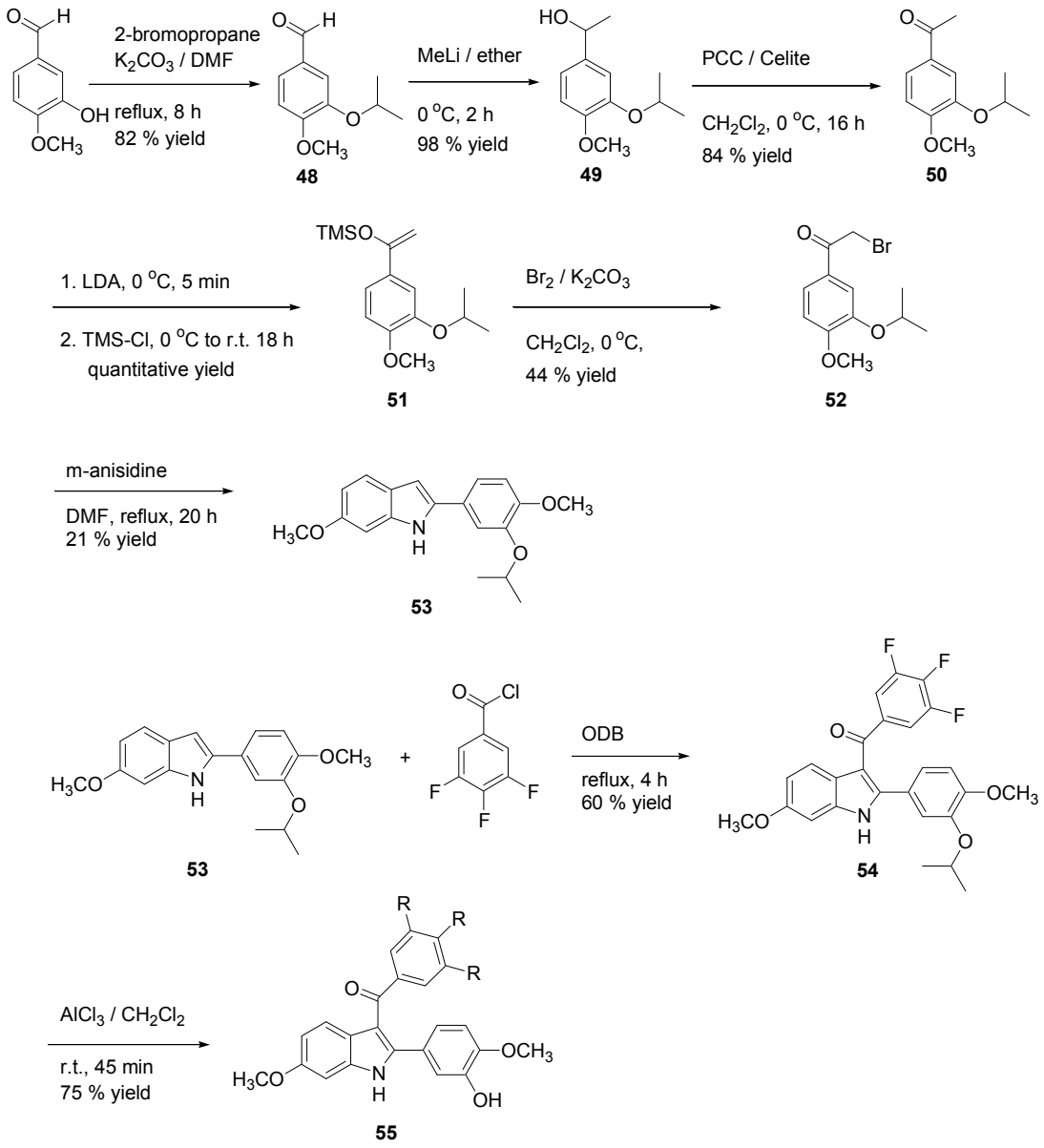

Scheme 15. Synthesis of fluorinated Oxi8006 derivative **55**.

indole **55** as green solid in a 75% yield (Scheme 15). The total synthesis of indole **55** was also attempted with TBS-protected intermediates; however, when the final product was deprotected with TBAF no recognizable products were recovered. The isopropyl protected synthetic route gave much better results.

Synthesis of Indole Oxi8006 **62**[14,101, 136]

The indole Oxi8006 (Figure 10) is an important compound undergoing further biological research. Oxi8006 was first synthesized by Dr. Mallinath Hadimani and Dr. Anjan Ghatak, former members of the Pinney labs.[14] Scale-up syntheses of active compounds are occasionally done as group projects within our team to ensure stockpiles of active compounds are always available for further biochemical and biological testing.

The scale up synthesis of Oxi8006 followed synthetic routes discussed previously.[14,101,136] The Oxi8006 synthesis started with protection of commercially available isovanillin with a TBS group to afford aldehyde **56** in a 97 % yield, which subsequently underwent a methyl addition to give the secondary benzyl alcohol **57** as a yellow oil (92% yield, Scheme 16). Oxidation of the secondary alcohol **57** with PCC gave the acetophenone analogue **58** (93% yield), which was then treated with an LDA solution followed by the addition of TMSCl to give the TMS-enol ether **59** (76% yield). The enol ether **59** was brominated using Br_2 at 0 ^{o}C to give the bromoacetophenone analogue **60** in a 62% yield. The bromoacetophenone analogue **60** was cyclized to indole **61** (17% yield) then benzoylated with 3,4,5-trimethoxybenzoyl chloride to afford compound **62** (59% yield) (Scheme 16). Deprotection and purification of the final product, OXi8006, was carried out by other Pinney group team members.

Synthesis of A-ring Indole **67**[90,101]

The structures of the indoles synthesized in the Pinney group are similar to *Z*-stilbenes in the centroid-to-centroid distances of the aryl rings; however, the indoles benzoylated at the 3-position have the ability to freely rotate, thereby having numerous

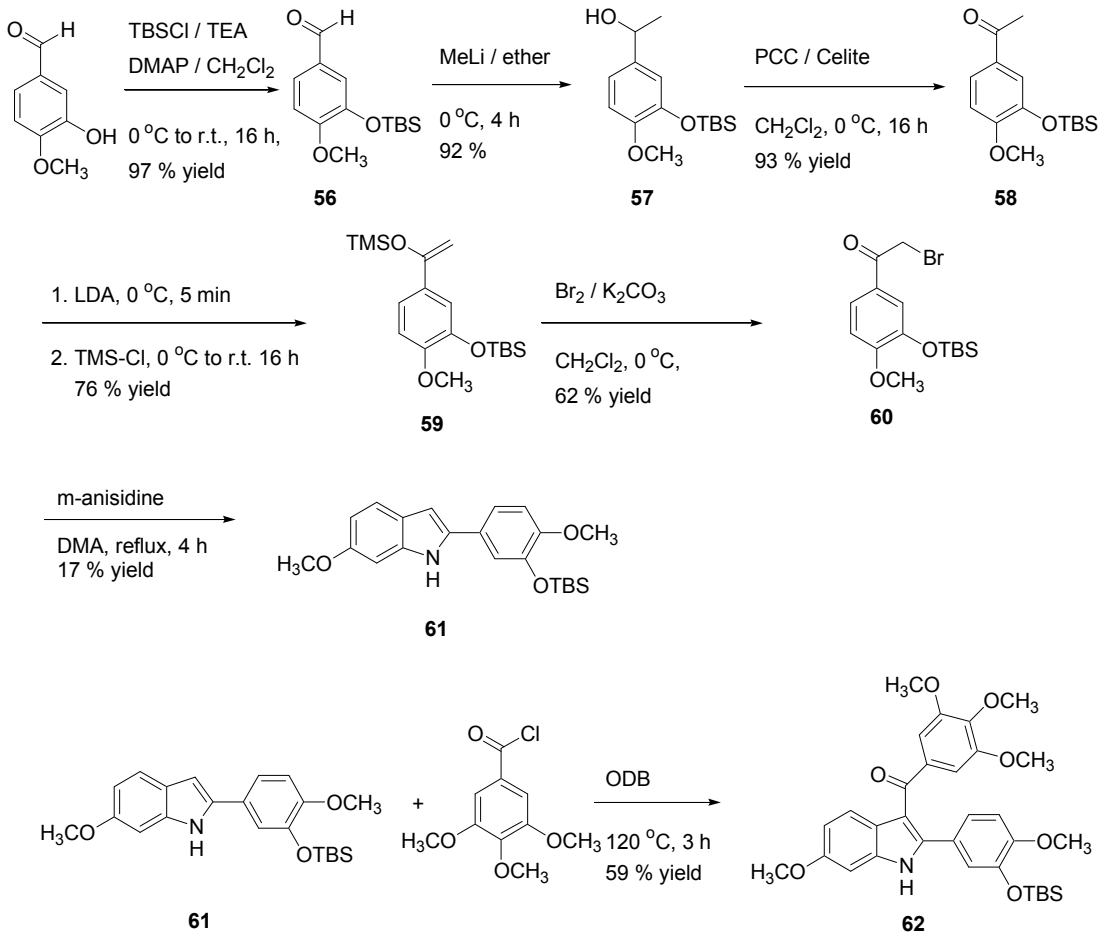

Scheme 16. Synthesis of TBS protected Oxi8006 **62**.

potential conformational modes of binding. The binding of the indoles may be the result of the A and C rings of the scaffold. As such, the synthesis of an indole derivative of Oxi8006 was devised such that a phenol was placed in the 7-position and the B-ring was removed altogether. The synthesis of the A-ring indole largely followed a synthetic route described by Fukuyama and co-workers.[90]

The first step in the formation of the A-ring indole was the nitration of isovanillin with NO_2BF_4 in CH_3NO_2 and CH_2Cl_2 to give the 2-nitroisovanillin **63** (29% yield, scheme 17). The 6-nitro isovanillin regioisomer was obtained in larger yields (52%).

Solid NO_2BF_4 should be used in the nitration. A solution of NO_2BF_4 in sulfolane (0.5 M) was used in several nitration attempts, but were unsuccessful. The phenol **63** was then protected by refluxing with acetic anhydride for 3 h to give the acetate protected aldehyde analogue **64** in an 81% yield. Other protecting groups were attempted, including isopropyl, benzyl, and TBS; however, use of any protecting group other than acetate hindered the ability to form the indole in later cyclization reactions. Nitro methane was added slowly to a solution of $KN(TMS)_2$ dissolved in THF at -78^oC. This resulted in the formation the nitromethane carbanion which then underwent a nucleophilic addition to aldehyde **64** to form the corresponding secondary alcohol. Elimination of the crude product after mesylation gave nitrostyrene **65** in a 26% overall yield (Scheme 17). Reduction of the nitro groups resulted in the spontaneous cyclization and loss of ammonia, forming the desired indole **66** in an 18% yield.[90] Attempts to benzoylate **66** with 3,4,5-trimethoxybenzene resulted in decomposition of the indole. Perhaps replacement of the acetate with another protecting group would be beneficial before the benzoylation. Protection of the indole –NH may also lower the amount of side products formed in this reaction. Further synthetic attempts in formation of indole **67** should be attempted. Liou and co-workers have synthesized a library of indoles in which the B ring has been deleted, some of which , have cell line toxicity in sub-nanomolar concentrations.[111] Furthermore, their synthetic schemes show that protection of the indole amine is necessary to prevent N-benzoylation from being the primary reaction in the coupling of the trimethoxy ring.[111]

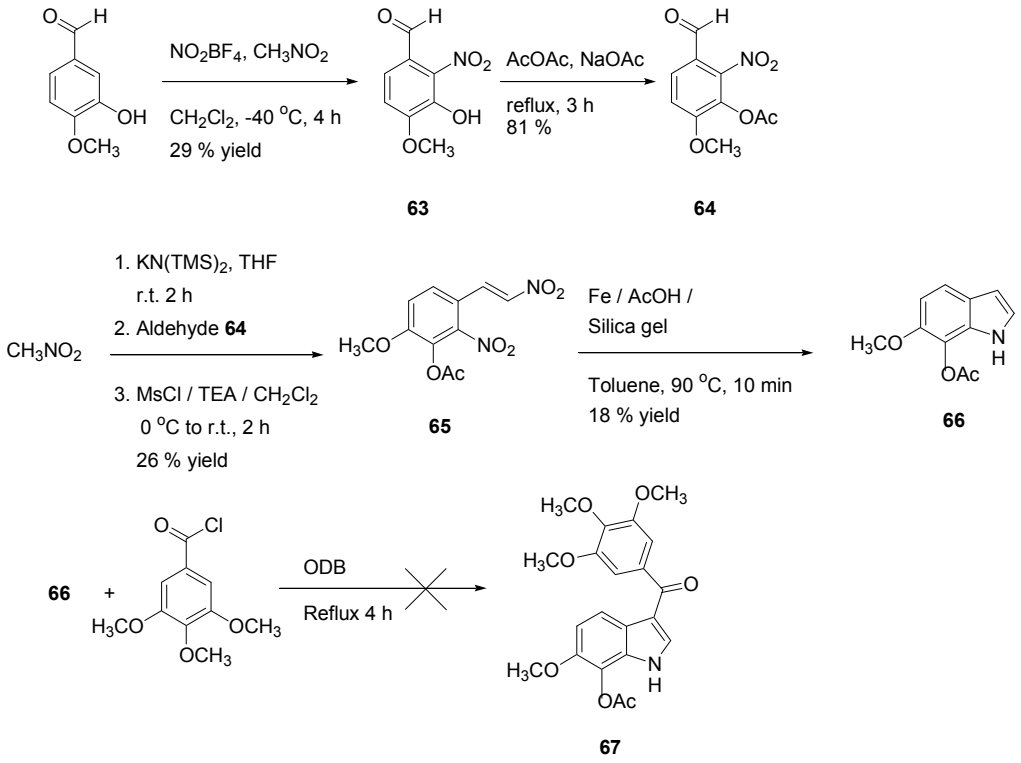

Scheme 17. Attempted synthesis of A-ring indole **67**.

Formulation of VDA / NOS Inhibitor Co-salts **70-74**

Some tumors have shown increased resistance to combretastatin drugs because of the high amounts of nitric oxide nitric oxide (NO) produced *in vivo*.[46] NO behaves as a proangiogenic factor that works in opposition to VDAs.[102] Drugs such as L-NMMA and L-NAME are well known compounds that inhibit NOS.[93] Davis and co-workers have shown that co-salts of CA4P with L-NMMA and L-NAME increased the overall necrosis of tumors treated with the drugs, and also increased the sensitivity of tumors resistant to CA4P.[47] The scale up synthesis of CA4P/L-NMMA and CA4P/L-NMMA was performed to provide reasonable amounts of these compounds for further biological and biochemical evaluation. The free base of L-NMMA is no longer commercially available,

and was therefore synthesized. N,S-dimethyl isothiouronium iodide was reacted with commercially available L-(+)-ornithine in a 1M NaOH solution to form L-NMMA **68** as a freebase in a 35% yield. LNMMA was purified on Amberlite ion exchange resin (Scheme 18).[92]

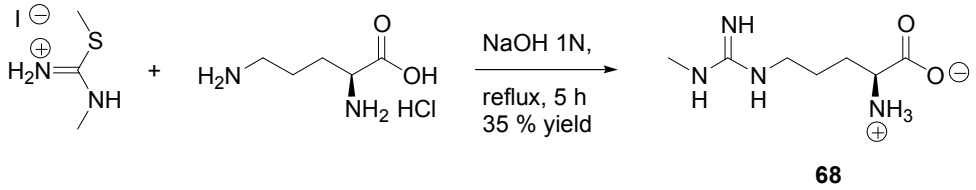

68

Scheme 18. Synthesis of the free base of L-NMMA **68**.

The free acid of CA4P was also synthesized as it is not commercially available. Davis and co-workers have reported a method for the formation of CA4P, though attempts through this route were unsuccessful.[47] Thus to prepare the CA4P free acid, CA4P was dissolved in water and the pH was adjusted to ~1.5 with HCl (Scheme 19). Extraction with EtOAc afforded organic acid **69** (69% yield, Scheme 19). The CA4P free-phosphate acid was very hydroscopic. If exposed to the atmosphere it will pick up moisture and convert from a white powder to a tacky pink solid.

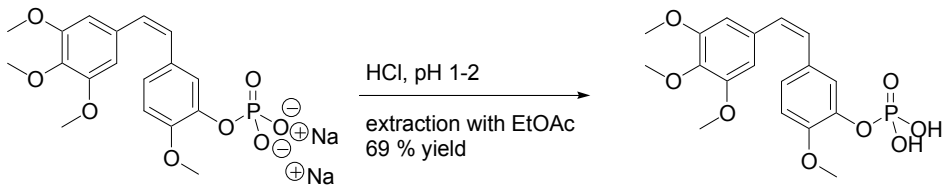

69

Scheme 19. Formation of CA4P free phosphate acid **69**.

The desired CA4P free acid/L-NMMA free base formulation was prepared simply by combining phosphate acid **69** (1 molar equivalent) with L-NMMA **68** (2 molar equivalents) in water for two hours. Lyophilization removed the water leaving the desired salt formulation **70** in a quantitative yield (Scheme 20).[47]

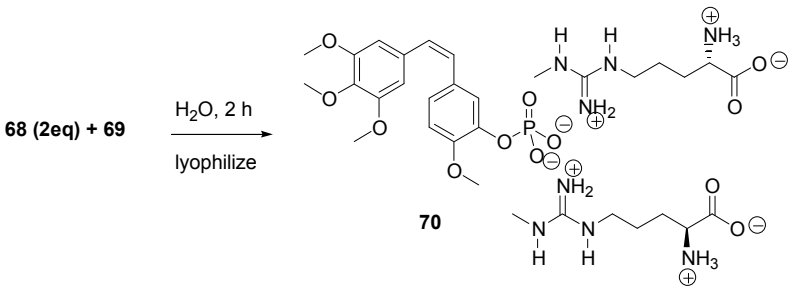

Scheme 20. Formation of CA4P free acid L-NMMA free base co-salt **70**.

The L-NMMA acetic acid salt and L-NAME hydrochloride salt are commercially available. It seemed important to compare the CA4P NOS inhibitors with the commercially available acetate NOS salts. Accordingly, CA4P was treated with each of these salts to form **71** and **72** respectively, each containing 2 equivalents of NaOAc or NaCl. In addition, Oxi8007 was also treated with these salts to form **73** and **74**. (Scheme 21).[47]

Synthesis of Bioreductive Prodrugs

In order to increase the effectiveness Oxi6196, CA4, and CA1 in hypoxic areas, they were attached to bioreductive drugs, and bioreductive drug triggers. Once the drugs reach areas of hypoxia they may be selectively reduced. The reduction may trigger an electron cascade that results in fragmentation of the parent tubulin polymerization inhibitor, and a DNA intercalating hydroxyl amine fragment (Scheme 40).

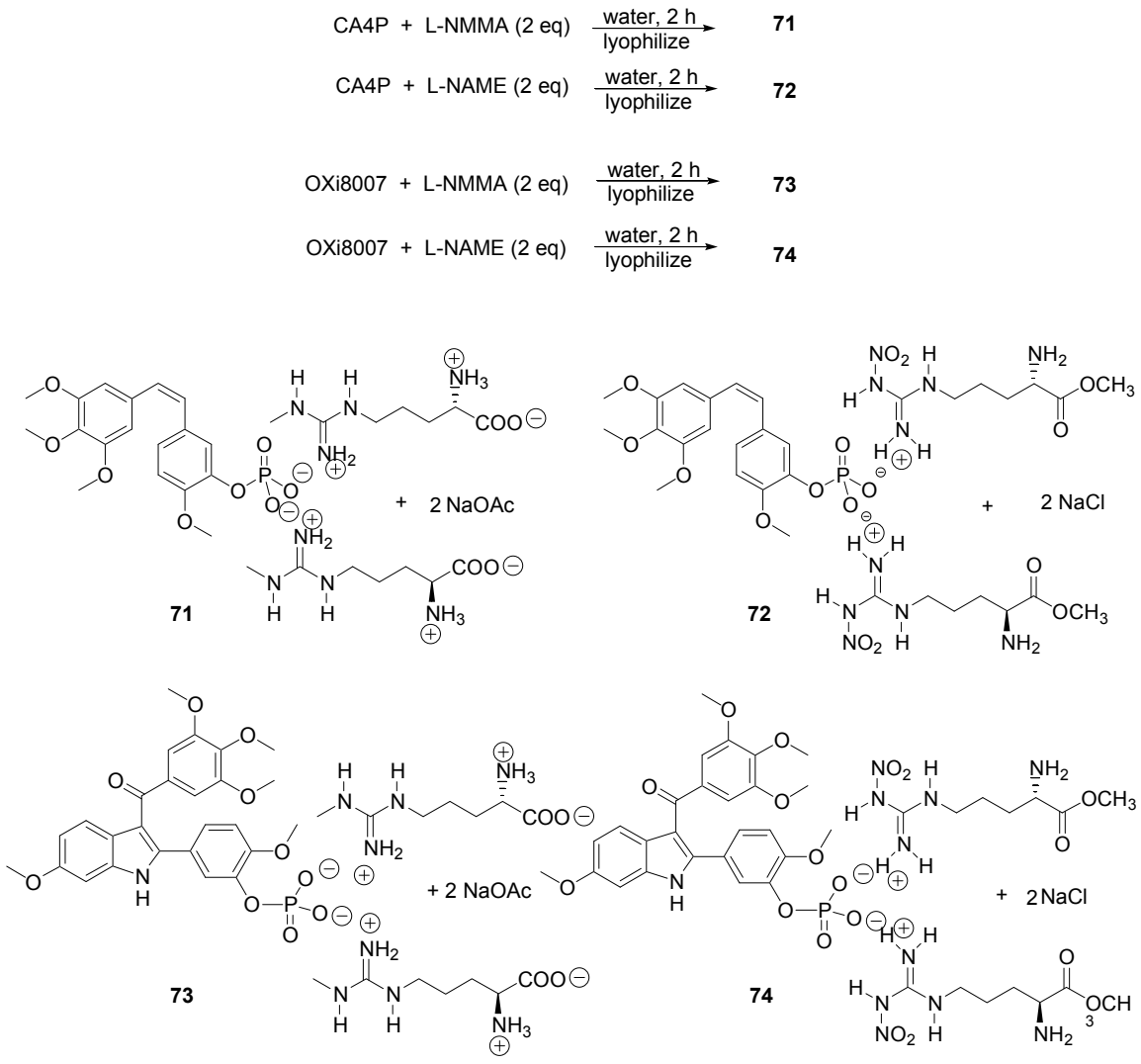

Scheme 21. Formulation of CA4P L-NMMA and L-NAME co-salts **71** and **72**, and formulation of Oxi8007 L-NMMA and L-NAME co-salts **73** and **74**.

Metronidazole Bio-reductive Drugs

The drug metronidazole is known to behave as a bioreductive drug.[103] The dihydronaphthalene derivative Oxi6196 has shown good tubulin binding activity, but has a limited therapeutic index in SCID mice (unpublished data).[139] Oxi6196 was coupled with metronidazole using standard Mitsunobu coupling conditions in anhydrous benzene to give the bioreductive drug candidate **75** in a 65% yield (Scheme 22).[104] Anhydrous

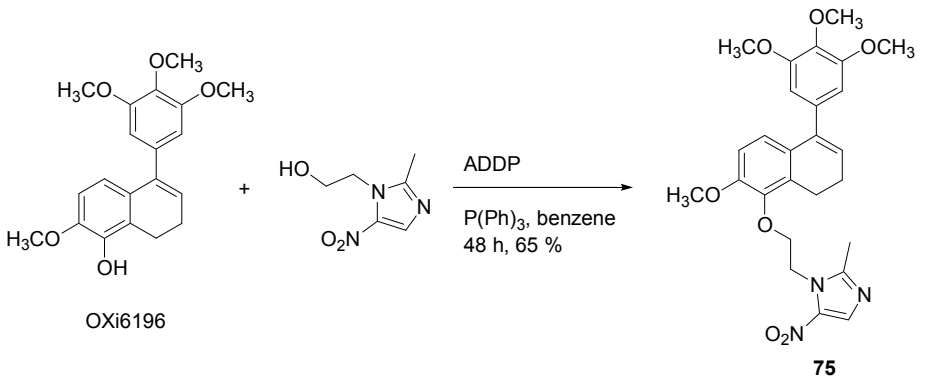

Scheme 22. Synthesis of bioreductive drug candidate **75**

benzene gave better yields than dry THF. The triphenylphosphine byproduct is also easily removed by filtration when benzene is used as the solvent.

CA4 was coupled with metronidazole using Mitsunobu coupling conditions in benzene with azodicarbonyldipiperidine and tributylphosphine (ADDP) to give the CA4 bioreductive product **76** in a 66% yield (Scheme 23).[104]

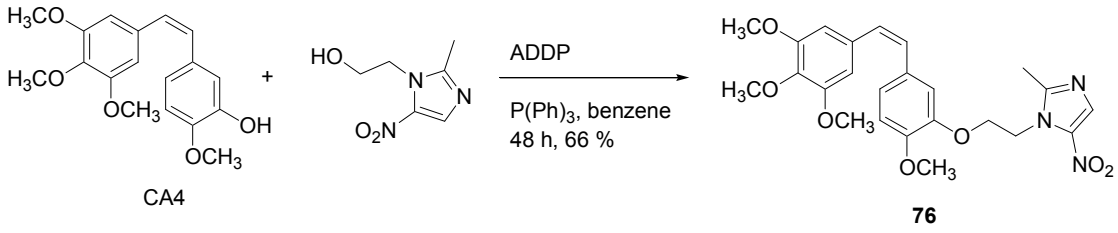

Scheme 23. Synthesis of bioreductive drug candidate **76**

It is instructive to note that analogues **75** and **76** are not designed to undergo fragmentation and release the parent compound (OXi6196 or CA4 respectively), but rather should be viewed as a conjugate molecule potentially capable of being bioreductively activated along with functioning through a tubulin binding mechanism.

Synthesis of CA4 Nitrobenzyl Derivatives **77-80**[104,105]

CA4 and CA1 were coupled with nitro-aromatics that may behave as triggers allowing release of the parent compound (CA4 or CA1 respectively) upon reduction. The first of these compounds was prepared in an attempt to determine the drug release efficiency when another electron donating group is present on the nitro aromatic ring. CA4 was coupled with 3-methoxy-4-nitrobenzyl alcohol via Mitsunobu coupling with tributylphosphine and ADDP to give bioreductive CA4 analogue **77** in a 98% yield. To test the effectiveness of nitro placement on the aromatic trigger *o*-, *m*-, and *p*-nitro benzyl alcohols were coupled with CA4. Coupling of CA4 with 4-nitrobenzyl alcohol by the same Mitsunobu conditions gave the CA4 analogue **78** (87% yield). Similarly, coupling of CA4 with 2-nitrobenzyl alcohol afforded bioreductive candidate **79** (37% yield).[104,105] Electron movement during the nitro reduction should allow fragmentation in the case where the nitro substituent is in the *ortho*- or *para*- position. However, placing the nitro group in the *meta* position the electron flow should not allow fragmentation of the parent drug. To test this hypothesis CA4 was coupled via a Mitsunobu reaction with 3-nitrobenzyl alcohol to give compound **80** in a 37% yield (Scheme 24).

Synthesis of CA1 Nitrobenzyl Derivatives **81-84**

CA1 was also coupled with nitro aromatics to for CA1 bioreductive drug triggers using the Mitsunobu conditions described previously. The coupling reactions with CA1 were less efficient than those from CA4. There are two possible phenolic points of

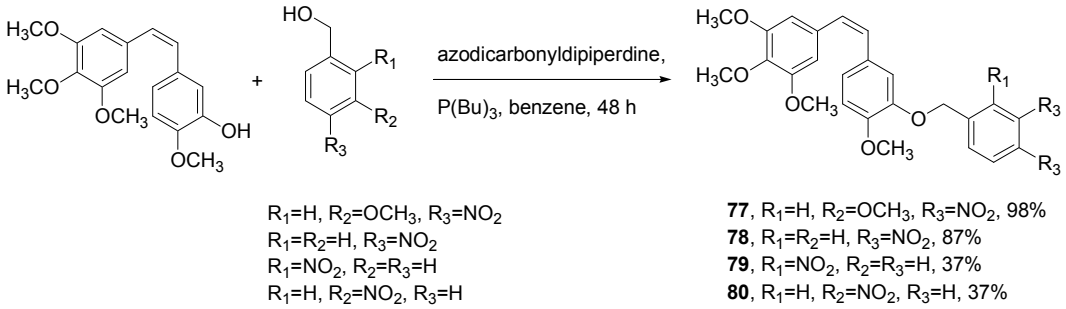

Scheme 24. Synthesis of CA4 bioreductive drugs **77**, **78**, **79**, **80**.

attachment in CA1; therefore there are three possible products that can be formed. In the actual reaction two products were obtained, a mono-coupled and a di-coupled analogue. CA1 was first coupled with 4-nitrobenzyl alcohol to give the mono coupled CA1 derivative **81** (20 % yield), and the di-substituted analogue **82** (13% yield, Scheme 25). Crystallographic analysis was not possible since the prodrugs were obtained as oils, so the linkage to the 2′ products is assumed. CA1 was also coupled with 3-methoxy-2-nitrobenzene to give the mono-coupled product **83 (**9% yield) and the di-substituted product **84** (18% yield) (Scheme 25).

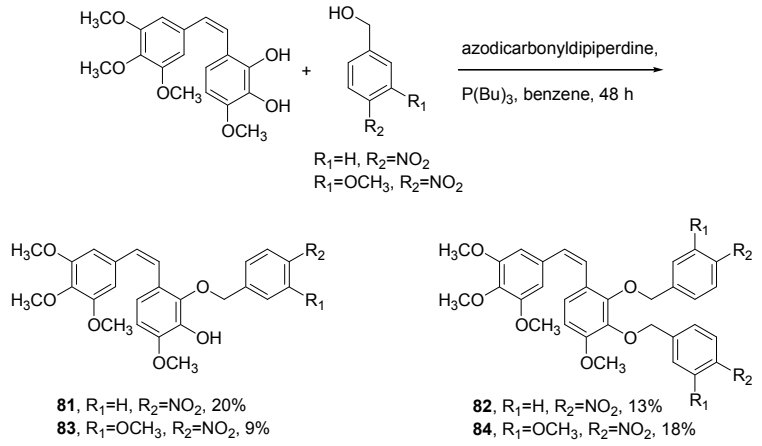

Scheme 25. Synthesis of CA1 bioreductive drug candidates **81**, **82**, **83**, and **84**.

Synthesis of CA1 Nitrothiophene Bioreductive Drugs Candidates **85-87**

The coupling of nitrothiophene derivatives to CA4 as bioreductive drug triggers has shown promising results for increasing drug effectiveness in hypoxic areas.[63] Thiophene derivatives of CA1 were synthesized with an ultimate goal of evaluating their effects on hypoxic cancer cells. First, the nitrothiophene alcohols were formed. Reduction of 5-nitrothiophen-2-carbaldehyde to afford the corresponding alcohol **85** (59% yield) was performed with $NaBH_4$. Similarly the secondary alcohol **86** was formed by reduction of 1-(5-nitrothiophen-2-yl)-ethanone **86** in a 63% yield (Scheme 26).[106]

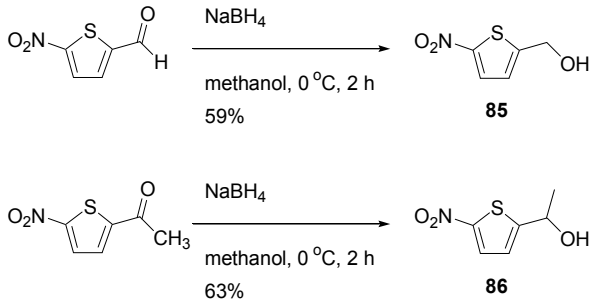

Scheme 26. Synthesis 1-(5-nitrothiophen-2-yl)-methanol **85**, and 1-(5-nitrothiophen-2-yl)-ethanol **86**.

Synthesis of the corresponding tertiary alcohol was attempted several times using procedures established in the literature (treatment with MeLi of MeMgBr); however, they were unsuccessful in our hands.[106] Addition of either methylating reagent to a solution of the starting material resulted in a color change, indicating a reaction had taken place; however, workup of the reaction mixture and product isolation only resulted in the recovery of starting material. Observation of a brilliant red color suggests enolate formation by a competing pathway (Scheme 27).

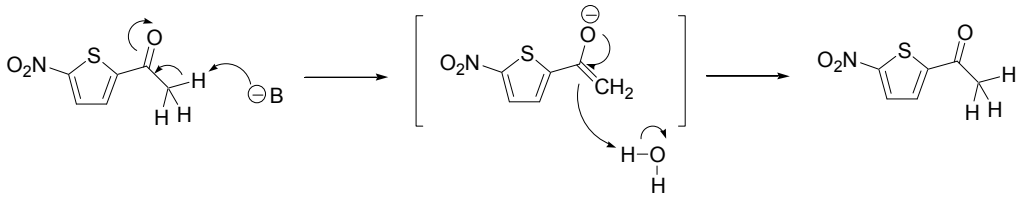

Scheme 27. Competing reaction of 1-(5-nitrothiophen-2-yl)-ethanone with appropriate methylating agents.

The Mitsunobu coupling of CA1 to any of the nitrothiophenes proved difficult in our hands. Most reactions with the thiophenes resulted in decomposition of the nitrothiophene, and nearly quantitative recovery of all CA1. In only one reaction did the Mitsunobu coupling give the desired product. Accordingly, CA1 was coupled under Mitsunobu conditions with ADDP and tributylphosphine in THF to give the desired CA1 nitrothiophene **87** in a 69% yield (Scheme 28).[106]

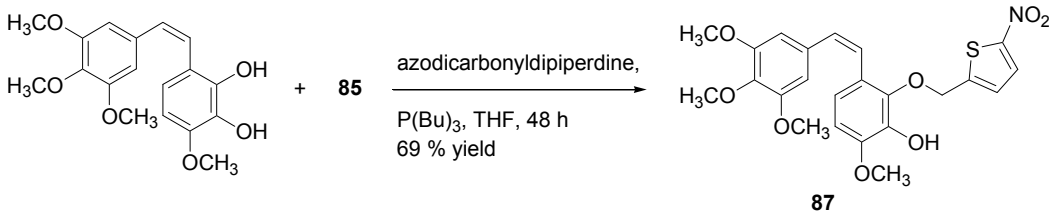

Scheme 28. Synthesis of CA1 nitrothiophene bioreductive drug candidate **87**.

Dihydronaphthalene Oxi6196 Intermediate **91**[94,95]

The dihydronaphthalene Oxi6196 has undergone extensive biochemical and biological testing.[94,95] Because of its importance, a large scale synthesis of the drug was carried out as a group project in the Pinney lab.[137] 5-Hydroxy-6-methoxy-1,2,3,4-tetrahydronaphthalene was synthesized by Benson Nguyen (a Pinney group graduate

student). The phenolic moiety was protected as previously described[94] with acetate using acetic anhydride, TEA, and DMAP in CH_2Cl_2 to obtain the acetate-protected tetrahydronaphthalene **88** in a 66% yield (Scheme 29). The protected compound **88** was then oxidized with DDQ and dioxane to form tetralone **89** in an 85% yield.[94] The acetate was deprotected with sodium bicarbonate in CH_2Cl_2 to form hydroxytetralone **90** in a 90% yield. The phenol analogue **90** was then reprotected with a TBS group using TBSCl, TEA, and DMAP in DMF.[94] The TBS protected tetralone **91** was isolated in a 78% yield (Scheme 29). Pinney group team members completed the synthesis of OXi6196 from intermediate **91**.[94,95]

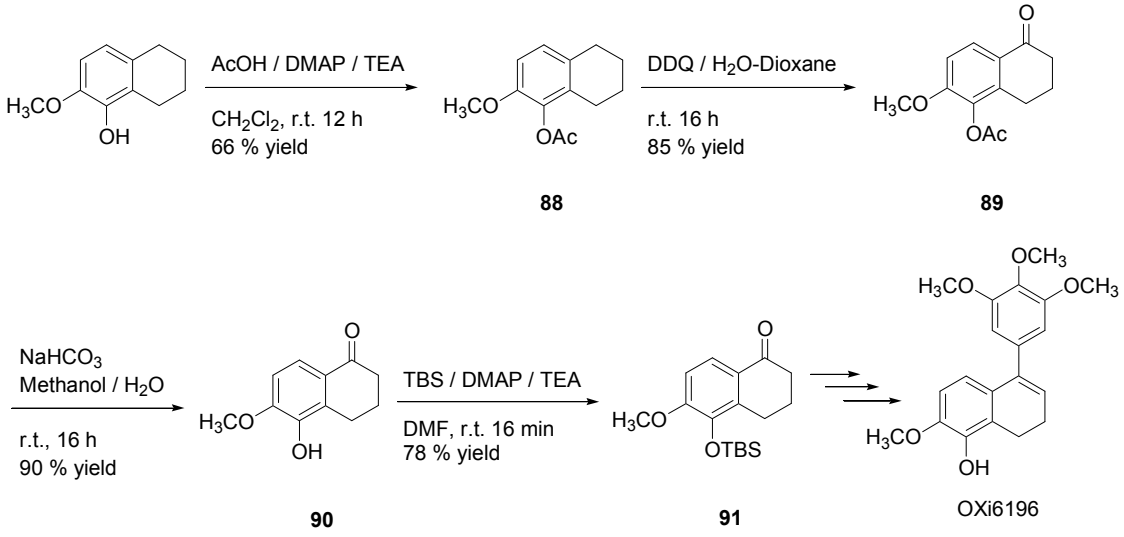

Scheme 29. Synthesis of Oxi6196 intermediate **91**.

Biological Evaluation

Isolation and Purification of Tubulin

Tubulin was purified by a series of five selective polymerizations at 37 ^{o}C in the presence of GTP, and five depolymerizations at 2 ^{o}C. Tubulin was purified from calf brain using a standard protocol created by Hamel and adapted to our lab by Dr. Trawick.[24,80] The purification process involves a series of five polymerization and depolymerization cycles. The brain sample is gathered and all blood clots, meningis, blood vessels, etc. were removed. It was found that removal of white matter was effective for increasing the total amount of tubulin purified during the preparation. The brain was homogenized in Solution A with 4M glycerol at 4^{o}C. One preparation consists of approximately 300 mL of the homogenate. It was found that up to four preparations can be performed without having deleterious effects on the purity of the tubulin isolated. Using GTP, tubulin can be polymerized into microtubules upon heating to 37 ^{o}C, and can be subsequently depolymerized upon cooling to 0 ^{o}C. A series of five polymerization and depolymerization cycles was shown to purify the tubulin to electrophoretic homogeneity and remove MAPS and other proteins. The tubulin is flash frozen and stored at approximately 10 mg/mL in a 1M glutamate solution in liquid nitrogen. A high concentration of glutamate solution stabilizes the tubulin dimer, and promotes polymerization. The concentration of purified tubulin was determined by a UV technique and the purity of the isolated tubulin was confirmed by gel electrophoresis (Figure 45).[25,96] Overall amount of tubulin isolated was 70-110 mg if two preparations were performed, and 200 mg was isolated when 4 preparations were performed.

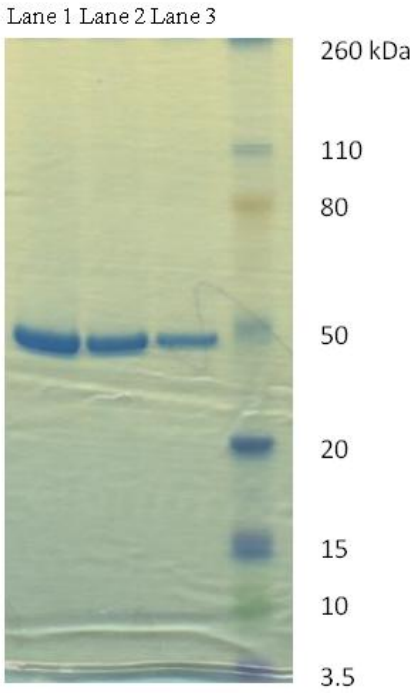

Figure 45. Gel electrophoresis of tubulin isolated from bovine brain. Tubulin concentrations are as follows: Lane 1 2.0 mg/mL, Lane 2 1 mg/mL, Lane 3 0.5 mg/mL.

Tubulin Polymerization Inhibition Assay

The purified tubulin was used in a variety of biochemical evaluations. The tubulin polymerization assay was used to determine the effectiveness of compounds synthesized by Pinney group members at inhibiting tubulin polymerization. To perform the assay, the tubulin was incubated with the drug at the desired concentration for 15 min at 35 ^{o}C then was cooled to 0 ^{o}C for 15 min.[10,26,80] Incubation at 37 ^{o}C insures maximum protein/ligand interaction. GTP is then added and the absorbance due to microtubule formation was measured at 350 nm. A baseline absorbance was measured at 100 s at 2 ^{o}C, then the sample was heated to 35 ^{o}C to induce polymerization until 1600 s when the sample was cooled to 2 ^{o}C. The absorbance difference between the data acquired at 100 s

and 1600 s was calculated. The data obtained for a drug at concentration X was compared to a control, in which tubulin was polymerized in the presence of 8 μM DMSO only. Using the IC_{50} Hillsope equation with prism software, the IC_{50} values of compounds for tubulin polymerization inhibition was determined (Figure 46).

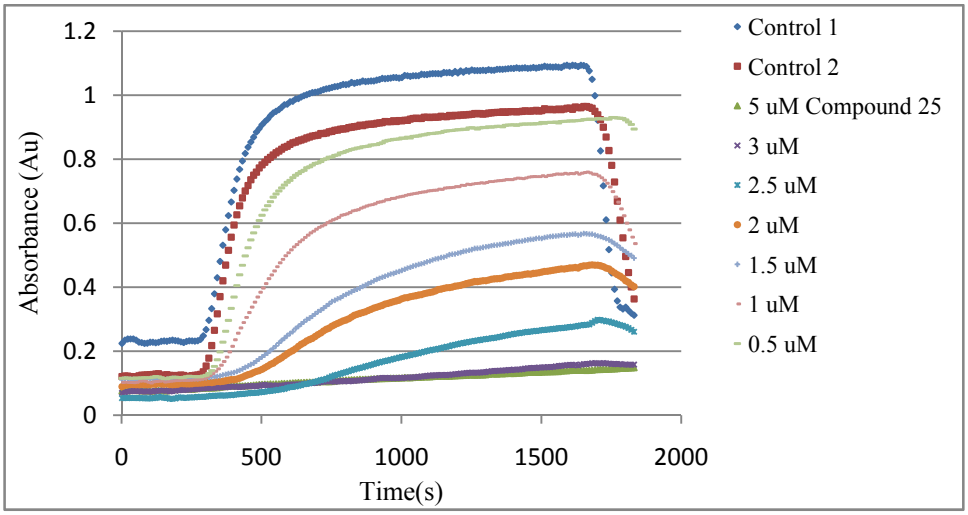

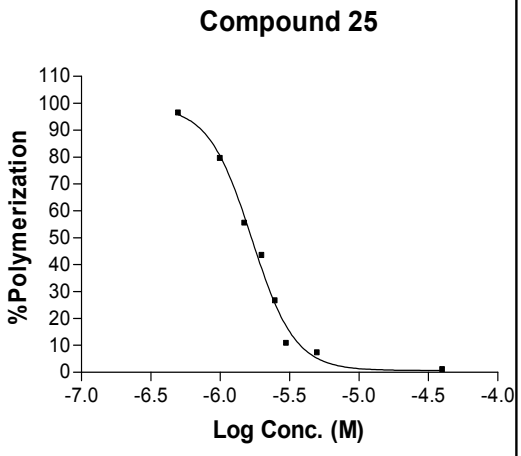

Sigmoidal dose-response (variable slope)	
Best-fit values	
BOTTOM	0.6939
TOP	98.90
LOGEC50	-5.773
HILLSLOPE	-2.790
EC50	1.685e-006
Std. Error	
BOTTOM	3.745
TOP	5.865
LOGEC50	0.03076
HILLSLOPE	0.4762
95% Confidence Intervals	
BOTTOM	-9.703 to 11.09
TOP	82.61 to 115.2
LOGEC50	-5.859 to -5.688
HILLSLOPE	-4.112 to -1.468
EC50	1.384e-006 to 2.051e-006
Goodness of Fit	
Degrees of Freedom	4
R^2	0.9910
Absolute Sum of Squares	77.84
Sy.x	4.411
Data	
Number of X values	8
Number of Y replicates	1
Total number of values	8
Number of missing values	0

Figure 46. Determination of tubulin polymerization assay by CA1 **25**.

Tubulin Polymerization Inhibition Assay by Oxirane derivatives **92**, **93**, **94**, and **95**[113]

Rogelio Siles had synthesized four nitro-combretastatin derivatives that contain an epoxide bridge.[113] Two of the epoxides were mono-nitro derivatives having a 4′-methoxy-3′-nitro structure **92** and a 4′-methoxy-2′-nitro scaffold **93**. The remaining two epoxides were di-nitro containing combretastatin epoxides with a 4′-methoxy-3′,5′-dinitro moiety **94** and a 4′-methoxy-2′,5′-dinitro attachment **95**. The oxiranes **92**, **93**, and **95** all contain S,S stereocenters, while oxirane **94** has an S, R configuration. All of the oxiranes **92-95** have IC_{50} values of > 40 μM (Table 2). Comparison of the IC_{50} for the parent nitro-CA4 derivative reported by Dr. Pettit and co-workers[107] to oxirane **92**, shows that the loss of the ethene bridge and conjugation decreases the effectiveness of tubulin binding. The reported IC_{50} value for the 3-nitro CA4 is 2.6±0.5 μM,[107] which is much more active than the corresponding oxirane **92**. No comparison could be made for oxirane **93**. Comparison of oxiranes **94** and **95** to their corresponding *Z*-dinitro CA1 derivatives show no difference in activity. The 3′,5′-dinitro, and 2′,5′-dinitro *Z*-CA1 analogues have IC_{50} values > 40 μM which is equivalent to oxiranes **94** and **95**. The oxirane derivatives are less active than their *Z*-combretastatin parent compounds (Table

Table 2. Tubulin polymerization inhibition of oxirane analogues **92-95.**[113]

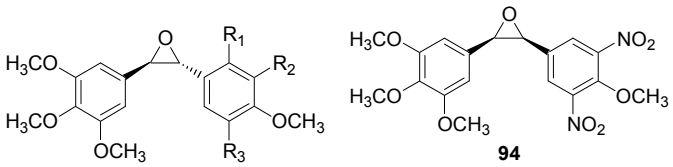

94

Compound	R_1	R_2	R_3	Tubulin Inhibition IC_{50} (μM)
92	H	NO_2	H	> 40
93	NO_2	H	H	> 40
94	H	NO_2	NO_2	> 40
95	NO_2	H	NO_2	> 40

2). The decrease in activity may be the result of change in the angle and distance between the A and B rings. Loss of overall conjugation may not be deleterious to tubulin binding as several compounds including 2ME2 are not entirely planar but have excellent tubulin binding.[108] In the case of oxirane **92**, the synthesis of SS, an RS, and SR derivatives may help conclude the effects of an epoxide bridge on tubulin binding site effectiveness. Stereochemistry may be a factor, so the synthesis of all possible stereoisomers would provide adequate information for the determination of stereocenter effects on oxirane binding to tubulin.

Tubulin Polymerization Inhibition Data for trans-Combretastatin Derivatives **8**, **11**, **35**, **112**

CA1 **25** and its *trans*-isomer **35** were analyzed for their tubulin binding ability. CA1 data is well reported in the literature,[10] and we obtained an IC_{50} value of 1.7 μM for CA1 which is within the accepted range.[10] The *trans*-CA1 IC_{50} value was not reported in the literature, and was found to have a value of 30-35 μM. Synthetic routes for several *cis*-CA1 analogues were attempted with the 3′,4′-dihydroxy-5′-methoxy moiety. Both trimethoxy analogue **7** and trifluoro analogue **10** spontaneously isomerized to the corresponding *trans*-isomers **8** and **11**.[109] Because the *cis*-isomers **7** and **10** were not isolated their tubulin polymerization inhibition data was not collected; however, the *E*-isomers **8** and **11** were analyzed for tubulin inhibition by Hamel. The trimethoxy moiety **8** had a tubulin polymerization inhibition IC_{50} value > 40 μM, which was not surprising as most *E*-combretastatins have poor tubulin polymerization inhibition IC_{50} values; however, the trifluoro derivative **11** had an IC_{50} value of 10-20 μM. Perhaps the fluorines are less sterically bulky and allow the *E*-stilbene to fit within the tubulin

colchicine binding site. Phyllis Athasery synthesized a *trans*-CA1[112] derivative in which the methoxy substituent was removed the 4′- position **112**[112] and had a moderate IC_{50} of 27.4 μM.

Table 3. Tubulin polymerization inhibition of trans-CA1 analogues **8**, **11**, **35**, and **112.**

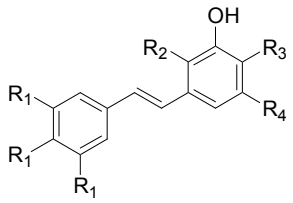

Compound	R_1	R_2	R_3	R_4	Tubulin Inhibition IC_{50} (μM)
CA1					1.7
8	OCH_3	H	OH	OCH_3	> 40[a]
11	F	H	OH	OCH_3	10-20[a]
35	OCH_3	OH	OCH_3	H	30-35
112	OCH_3	OH	H	H	27.4

[a] Evaluated by Earnest Hamel

Tubulin Polymerization Inhibition Data for the Z-nitro and Z-amino Stilbene Derivatives **13**, **15**, **17**, **19**, **97**, *and* **99 104**, **105**, **106**

A series of trimethoxy and trifluoro nitrated *Z*-combretastatin derivatives were synthesized. Trifluorinated nitro-combretastatins **13**, **17** had tubulin polymerization inhibition IC_{50} values of > 40 μM. In the case of **13**, the lack of activity was surprising because the trimethoxy analogue reported by Pettit and co-workers had an IC_{50} value of 2.6 ± 0.5 μM.[107] The fluorinated nitro-stilbenes are hydrophobic so perhaps compound **13** aggregates in solution which would lessen its interaction with the tubulin protein and account for the lowered tubulin polymerization inhibition. The 2′,5′-dinitro combretastatin **97** synthesized by Mallinath Hadimani also had an IC_{50} value > 40 μM.[10,14] The 2,4-dimethoxy-3-nitro *cis*-combretastatin **99** serendipitously made by

Table 4. Tubulin polymerization inhibition of *Z*-nitro and amino combretastatin analogues **13**, **15**, **17**, **19**, **97**, **99**, **104-106**.

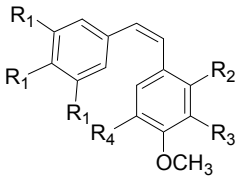

Compound	R_1	R_2	R_3	R_4	Tubulin Inhibition IC_{50} (μM)
CA1					1.7
13	F	H	NO_2	H	> 40
15	F	H	NH_2	H	2.9
17	F	NO_2	H	H	> 40
19	F	NH_2	H	H	> 40
97	OCH_3	NO_2	H	NO_2	> 40[a]
99	OCH_3	OCH_3	NO_2	H	3.3
104	OCH_3	NH_2	H	NO_2	~ 31[a]
105	OCH_3	NO_2	H	NH_2	> 40[a]
106	OCH_3	NH_2	NH_2	H	2.8[a]

[a] Ref. 98

Graciela Miranda had an excellent IC_{50} value of 3.3 μM (Table 4).[110] Placement of a methoxy substituent in the 2′ does not hinder tubulin binding.

It was hypothesized that the reduction of the nitro substituents of the synthesized *Z*-nitro combretastatins would increase their water solubility, thereby increase their affinity to the colchicine binding site. The amino stilbene **15** has an excellent tubulin IC_{50} of 2.9 μM; however, the 2′-analogue **19** had a poor tubulin polymerization inhibition of > 40 μM. For amino-fluoro stilbenes the amine in the 3′ position is preferred. Freeland Ackley synthesized nitro-amine and diamine derivatives of CA1 **104**, **105**, and **106**.[98] Of interest is the difference in activity between stilbene analogues **104** and **105**. The 2′-amino-5′-nitro analogue had an IC_{50} value of ~31 μM, whereas the 2′-nitro-5′-amino analogue had an IC_{50} value >40 μM.[10] An amine in the 2′ position is advantageous over having a nitro substituent in the 2′ position for better interaction within the tubulin

binding site. The 2,3-diamine CA1 **106** has an excellent IC_{50} value of 2.8 μM (Table 6).[10] Having an amine is advantageous over nitro substituents in the design of CA1 analogues. Also, substituents other than hydrogen in the 5′-position decrease the ability of stilbene derivatives to inhibit tubulin polymerization.

Tubulin Inhibition Data for trans-Nitro- and Amino-Stilbene Derivatives **14**, **16**, **18**, **20**, **98**, and **103**

The *trans*-isomers of several nitro- and amino-stilbene derivatives were also analyzed for their ability to inhibit tubulin polymerization. Usually, *trans*-combretastatins have poor tubulin polymerization inhibition capabilities. The fluorinated *E*-nitro combretastatins **14** and **18** have IC_{50} values > 40 μM which was not surprising as their *cis*-analogues **13** and **18** were also inactive. The 2′,3′-dinitro and the 3′,5′-dinitro derivatives of *trans*-CA1 synthesized by Freeland Ackley both had poor IC_{50} values of > 40 μM (Table 5).[98] Nitro containing *trans*-combretastatins are poor inhibitors of tubulin polymerization. The reduction of nitro-stilbenes **14** and **18**, to amino-stilbenes **16** and **20**, had little effect at increasing the ability of the compound to inhibit tubulin polymerization. Di-nitro stilbenes **98** and **103** were also inactive.[10]

Tubulin Polymerization Inhibition Data for Indole Analogues **44**, **45**, **47**, *and* **55**

Several indole compounds were synthesized. The indole Oxi8006 is effective at inhibiting tubulin polymerization with an IC_{50} value of 1-2 μM.[14,101] Trimethoxy and trifluoro indole analogues **44**, **47**, and **55** were evaluated for their ability to inhibit tubulin polymerization. The indole diol **44** had a good IC_{50} value of 2.8 μM. The fluorinated indoles had relatively poor IC_{50} values. Hamel recorded an IC_{50} value of ~20 μM for compound **55**. Hamel speculated that the hydrophobic nature of indole **55** led to

Table 5. Tubulin polymerization inhibition of *E*-nitro and *E*-amino combretastatin analogues **14**, **16**, **18**, **20**, **98**, **103**.

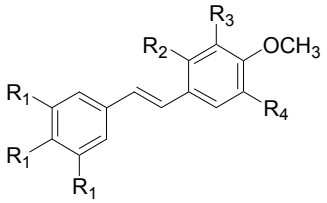

Compound	R_1	R_2	R_3	R_5	Tubulin Inhibition IC_{50} (μM)
CA1					1.7
14	F	H	NO_2	H	> 40
16	F	H	NH_2	H	> 40
18	F	NO_2	H	H	> 40
20	F	NH_2	H	H	> 40
98	OCH_3	NO_2	NO_2	H	> 40[a]
103	OCH_3	H	NO_2	NO_2	> 40[a]

[a] Ref. 98

aggregation of the molecule in solution which resulted in the decreased effectiveness of the compound to inhibit tubulin polymerization. The hydrophobic nature of the fluorinated indole **47** may have also affected the ability of the compound to inhibit tubulin polymerization. Indole **47** had an IC_{50} value of > 40 μM. Not unexpectedly, the unbenzoylated indole **45** had a poor IC_{50} value of 40 μM (Table 6). Within the indole scaffolds tested, a trimethoxy moiety is preferred over the trifluorinated analogue due to solubility concerns.

Tubulin Inhibition Data for Benzosuberenes Derivatives **96**, **101**, **107**, **110** *and Dihydronaphthalene Analogue* **102**[114,115]

A Pinney group colleague, Madhavi Sriram, has synthesized a new class of potential VDA's called benzosuberenes.[114] Neither the benzosuberene diol **96** nor the mono-phenol **101** showed good tubulin polymerization inhibition with IC_{50} values at > 40 μM each. The reduction of benzosuberene **96** to **110** increased the tubulin polymerization

Table 6. Tubulin polymerization inhibition of indole derivatives **44**, **45**, **47**, **55**.

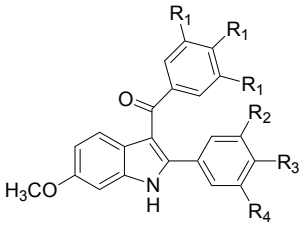

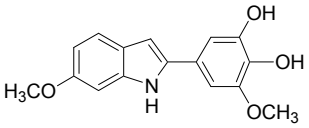

45

Compound	R_1	R_2	R_3	R_4	Tubulin inhibition IC_{50} (μM)
Oxi8006	OCH_3	OH	OCH_3	H	1-2[a]
44	OCH_3	OH	OH	OCH_3	2.8
45	-	-	-	-	> 40
47	F	OH	OH	OCH_3	> 40
55	F	OH	OCH_3	H	~20[b]

[a] Ref. 14
[b] Evaluated by Earnest Hamel

inhibition capabilities greatly from > 40 μM to 6.9-8.1 μM.[115] The benzosuberene analogue **107** also has an excellent tubulin polymerization inhibition with an IC_{50} of 1.7 μM.[115] Having a methanone linkage in the benzosuberene is deleterious to the molecules ability to inhibit tubulin polymerization. Also, the B-ring is preferred in direct attachment to the benzosuberene scaffold. The dihydronaphthalene analogue **102** had a moderate tubulin inhibition with an IC_{50} of 24 μM (Figure 47).[115]

Tubulin Polymerization Inhibition Data for Benzo[a]fluorene Derivative **111**[115] *and Benzophenone Analogue* **37**

The benzo[a]fluorene **111** was synthesized by Madhavi Sriram serendipitously during the reduction of **96**.[115] Compound **111** showed poor tubulin binding activity with an IC_{50} value of > 40 μM.[115] The phenstatin derivative **37** was developed to study the effects of the 3′,4′-dihydroxy-5′-methoxy motif. The benzophenone analogue **37** had

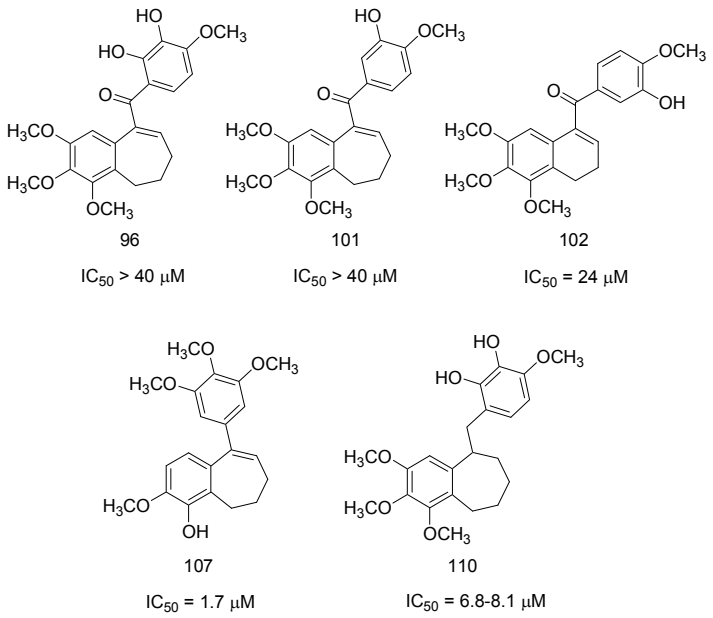

Figure 47. IC_{50} values for benzosuberene derivatives **96**, **101**, **107**, **110** and dihydronaphthalene analogue **102**.[114,115]

an excellent tubulin polymerization inhibition value of 2-4 μM reported by Hamel Figure (52). The 2′,3′-dihydroxy-4′-methoxy derivative, phenstatin, was synthesized by Dr. Pettit and was reported to have an IC_{50} value of 0.82 μM. The shift in connectivity in compound **37** does not significantly decrease the tubulin binding ability when compared to phenstatin (Figure 48).[100]

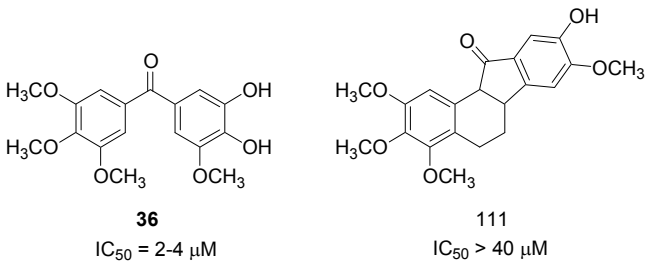

Figure 48. Tubulin polymerization inhibition IC_{50} of phenstatin derivative **36** and benzo[a]fluorene analogue **111.**

Tubulin Polymerization Inhibition of CA1 Glucuronide 1 **108** *and CA1 Glucuronide 2* **109**

Two CA1 glucuronide derivatives were tested for tubulin polymerization inhibition. While the exact structures of each cannot be disclosed, they differ in connectivity. In one case a glucuronide substituent is attached to the 2′-position of CA1, and in the other moiety the glucuronide substituent is attached to the 3′-position. Interestingly CA1 glucuronide 1 **108** was better at inhibiting tubulin polymerization than the CA1 glucuronide 2 **109**. CA1 glucuronide 1 **108** had an IC_{50} value of 11.0 μM while the IC_{50} value for glucuronide 2 **109** was > 40 μM.

Tubulin Polymerization Inhibition of Potential Bioreductive Compounds **76**, **78**, **79**, **81**

The bioreductive compounds were synthesized to activate under hypoxic conditions after fragmenting. Even so, we were interested in determining if several of the bioreductive drugs had any effect on tubulin polymerization. CA4 bioreductive drugs **76**, **78**, and **79** were tested for their ability to inhibit tubulin polymerization. None of compounds **76**, **78**, or **79** had IC_{50} values less than 40 μM. The CA1 bioreductive **81** was also poor at inhibiting tubulin polymerization with an IC_{50} > 40 μM (Figure 49). Substituents attached to CA1 or CA4 hinders the ability to inhibit tubulin polymerization presumably through exclusion from the colchicine binding site.

Screening of Compounds for Cytotoxicity Against DU145 and NCI H460 Cell Lines

Drugs synthesized within the Pinney group were screened against DU-145 prostate cancer and NCI H460 lung cancer carcinoma cell lines using a standard SRB assay. Doxorubicin and CA4 were analyzed for cytotoxicity as references in parallel to

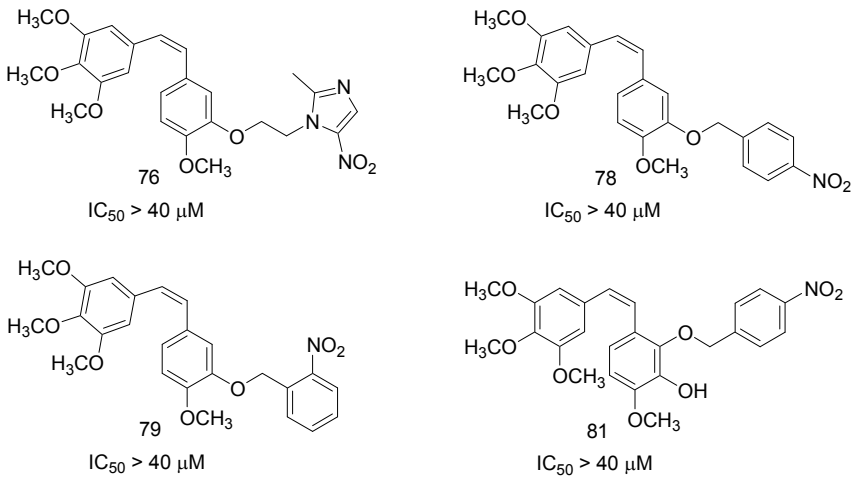

Figure 49. Tubulin polymerization inhibition IC_{50} of bioreductive compounds **76**, **78**, **79**, **81**.

all other compounds. The SRB protocol is available from NCI and is widely used. Several key observations were noted in successfully running an SRB assay.[70] For rapidly dividing cells such as NCI H460, cell plating should be around 10,000 cells per well. High cell counts resulted in decreased sensitivity of the assay. Also, the assay gave decreased sensitivity if the cell media was supplemented with 10% FBS rather than 5%. The excess protein in the FBS adhered to the 96 well plate, and gave incorrectly high GI_{50} values. As such all SRB cells were grown in an appropriate medium that contained 5% FBS. The maximum tested concentration was 50 μg/mL; however, inactive compounds were reported as > 5 μg/mL.

DU-145 and NCI H460 Cell Cytotoxicity for Combretastatin Analogues **8***,* **11***,* **25***, and* **35**

Four combretastatin analogues were analyzed for their ability to inhibit the cell growth of DU-145 and NCI H460 cell lines. Of the four combretastatins, two were also analyzed for growth inhibition of P388 mouse leukemia, BxPC-3 human pancreatic adenocarcinoma, MCF-7 breast cancer, SF-268 CNS (central nervous system), and KM

20L2 colon cancer cell lines by Dr. Pettit at Arizona State University. Of the combretastatin analogues tested, none were as potent as CA4 which had GI_{50} values of 0.0006 μg/mL and 0.0022 μg/mL for DU-145 and NCI H460 cell lines respectively (table 7). CA1 **25** was also active with GI_{50} values of 0.138 μg/mL for DU 145 cells and 0.127 μg/mL for NCI H460 cells. CA1 and CA4 were frequently used as controls in SRB experiments and fell within the accepted literature values[10] The *trans*-CA1 **35** derivative had much less activity with GI_{50} values of > 5 μg/mL for both NCI H460 and DU-145 cell lines. CA1 derivative **8** and the trifluorinated derivative **11** were relatively inactive (Table 7).

Table 7. Cell line cytotoxicity for combretastatin analogues CA1, CA4, **8**, and **11**.

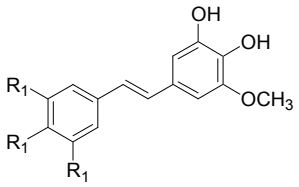

Compound	R_1	P388 GI_{50} (μg/mL)	BxPC-3 GI_{50} (μg/mL)	MCF-7 GI_{50} (μg/mL)	SF-268 GI_{50} (μg/mL)	NCIH460 GI_{50} (μg/mL)	KM20L2 GI_{50} (μg/mL)	DU-145 GI_{50} (μg/mL)
CA4		-	-	-	-	0.0022	-	0.0006
CA1		-	-	-	-	0.138	-	0.127
t-CA1		-	-	-	-	> 10	-	> 10
8	H	> 10[a]	3.3[a]	2.7[a]	5.2[a]	3.9[a]	4.9[a]	3.8[a]
11	F	2.6	2.3	1.6[a]	1.6[a]	1.8[a]	2.9[a]	2.0[a]

[a] From Dr. Pettit's labs.

DU-145 and NCI H460 Cell Cytotoxicity for Combretastatin Analogues **13** *and* **14** *and Amino Stilbenes* **15** *and* **19**

Two fluorinated nitro CA4 derivatives **13** and **17** were evaluated for DU-145 and NCI H460 cell line toxicity, and did not have high cancer cytotoxicity with GI_{50} values of

Table 8. DU-145 and NCI H460 cell line cytotoxicity of nitro combretastatin analogues **13**, and **14.**

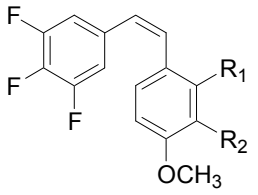

Compound	R_1	R_2	NCIH460 GI_{50} (μg/mL)	DU-145 GI_{50} (μg/mL)
CA4	-	-	0.0013	0.004
13	H	NO_2	> 5	> 5
15	H	NH_2	0.0093[a]	-
17	NO_2	H	> 5	> 5
19	NH_2	H	> 5[a]	-

[a] from Gustavo Chavaria

> 5 μg/mL for both DU-145 and NCI H460 cell lines (Table 8). By reducing **13** to **15** the GI_{50} was dramatically decreased to 0.0093 μg/mL. Reduction of **14** to **19** did not significantly increase the cell line cytotoxicity.

DU-145 and NCI H460 Cell Cytotoxicity for Indole Derivatives **45**, **47**, *and* **55**

Three Oxi8006 derivatives were analyzed for cancer cell cytotoxicity. One indole **47** was analyzed in our lab against DU-145 and NCI H460 cell lines. Indoles **45** and **55** were tested against the six cell lines in Dr. Pettit's lab. Of the three compounds none were as active as Oxi8006.[14] The fluorinated Oxi8006 derivative **55** was more active than its diol counterpart **47** (Table 9). Fluorines on the indole ring had a deleterious effect on the overall activity of the indoles, and are probably the result of solubility problems.

Table 9. Cell line toxicity of indoles **45**, **47**, and **55**.

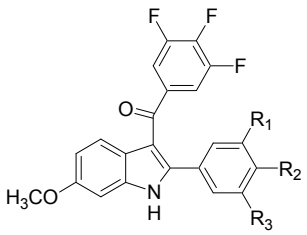

45

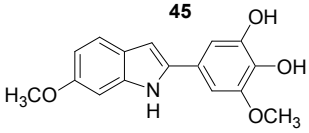

Compound	R_1	R_2	R_3	P388 GI_{50} (μg/mL)	BxPC-3 GI_{50} (μg/mL)	MCF-7 GI_{50} (μg/mL)	SF-268 GI_{50} (μg/mL)	NCIH460 GI_{50} (μg/ mL)	KM20L2 GI_{50} (μg/mL)	DU-145 GI_{50})
Oxi8006				-	0.046[a]	0.0023[a]	0.0055[a]	0.0027[a]	0.0043[a]	0.001[a]
45				>10	3.8	2.2	3.8	5.5	12.9	3.3
47	OH	OH	OCH_3	-	-	-	-	>5	-	2.2
55	OH	OCH_3	H	>10	0.74	0.38	0.33	0.35	19.6	0.32

[a] Data acquired by Dr. Pettit.

DU-145 and NCI H460 Cell Cytotoxicity for Oxi8007/ NOS Inhibitor Salts **73** *and* **74**

The Oxi8007 NOS inhibitor co-salts **73** and **74** were tested against the six cell lines in the Pettit labs. Expectedly, the salts were approximately as active as Oxi8007 (Table 10). For the SF-268 cell line the GI_{50} values were decreased to 31.5 nM and 34.7 nM for **73** and **74** respectively. Addition of the NOS inhibiting salts to the Oxi8007 indole is effective at increasing the sensitivity of SF-268 CNS cancer cells. A noticeable increase in cell line cytotoxicity was also observed for the NCI H460 lung cancer carcinoma when treated with either **73** or **74** (Table 11).

DU-145 and NCI H460 Cell Cytotoxicity for Combretastatin Analogue **12** *and Benzophenone Derivative* **37**

Two compounds, **12** and **37**, were analyzed against six cancer cell lines by Dr. Pettit. Combretastatin analogue **12** is a hydrogenated derivative of tri-fluoro combretastatin **11**. Stilbene analogue **12** had little activity against any of the cell lines.

Table 10. Cell line cytotoxicity of Oxi8007 NOS salts **73** and **74**.

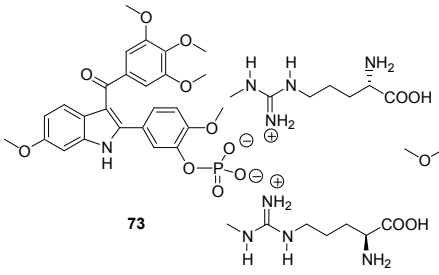

73

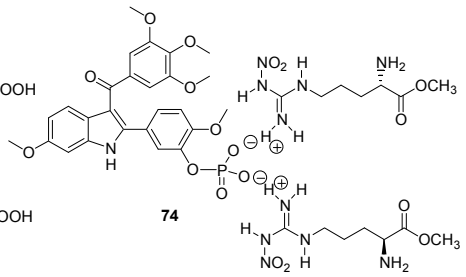

74

Compound	P388 GI_{50} (nM)	BxPC-3 GI_{50} (nM)	MCF-7 GI_{50} (nM)	SF-268 GI_{50} (nM)	NCIH460 GI_{50} (nM)	KM20L2 GI_{50} (nM)	DU-145 GI_{50} (nM)
Oxi8007	-	47.2[a]	26.2[a]	59.4[a]	48.9[a]	24.5[a]	<1.7[a]
73	27.2[a]	58.7[a]	33.7[a]	31.5[a]	31.5[a]	30.4[a]	27.2[a]
74	41.6[a]	109[a]	45.6[a]	34.7[a]	30.7[a]	30.7[a]	35.7[a]

[a] Data acquired by Dr. Pettit.

Phenstatin derivative **37** showed activity across the entire panel, and had greatest activity for the SF-268 and NCI H460 cells with GI_{50} values of 0.038 μg/mL and 0.031 μg/mL respectively (Table 11). Benzophenone **37** had better cell line cytotoxicity than reported for phenstatin.[100]

Table 11. Cell line cytotoxicity of combretastatin derivative **12**and phenstatin analogue 37.

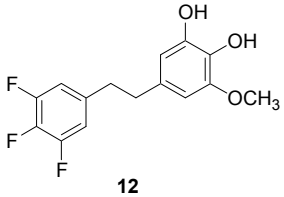

12

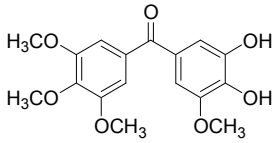

37

Compound	P388 GI_{50} (μg/mL)	BxPC-3 GI_{50} (μg/mL)	MCF-7 GI_{50} (μg/mL)	SF-268 GI_{50} (μg/mL)	NCIH460 GI_{50} (μg/mL)	KM20L2 GI_{50} (μg/mL)	DU-145 GI_{50} (μg/mL)
CA1	0.3[b]	4.4[b]			0.74[b]	0.061[b]	0.17[b]
12	>10[a]	6.4[a]	1.6[a]	2.6[a]	4.3[a]	>10[a]	1.8[a]
37	0.18	0.64[a]	0.094[a]	0.038[a]	0.31[a]	1.8[a]	0.033[a]

[a] Data acquired by Dr. Pettit.
[b] Ref. 100.

DU-145 and NCI H460 Cell Cytotoxicity for Benzosuberenes 96, **101**, **110**, **114**, *and Benzo[a]fluorene* **111**[114,115]

Madhavi Sriram synthesized four benzosuberene analogues **96**, **101**, **110**, **114**, and a benzo[a]fluorene derivative **111** that were analyzed against DU145 and NCI H460 cell lines.[114,115] A dihydronaphthalene **102** was also analyzed against DU145 and NCI H460 cells.[115] The benzosuberene diol analogue **96**, and its mono-phenol analogue **101** did not have significant cytotoxixity. The dihydronaphthalene derivative **102** had moderate activity against DU-145 and NCI H460 cells with GI_{50} values of 1.1 μg/mL and 2.2 μg/mL respectively.[115] While the reduced benzosuberene **110** was active at inhibiting tubulin polymerization, it did not show significant biological activity with GI_{50} values of > 5 μg/mL for both cell lines.[115] Of the benzosuberene compounds tested, compound **114** was the most cytotoxic for DU-145 and NCI H460 Cell lines with GI_{50} values of 0.14 μg/mL, and 0.16 μg/mL respectively (Figure 50).[115]

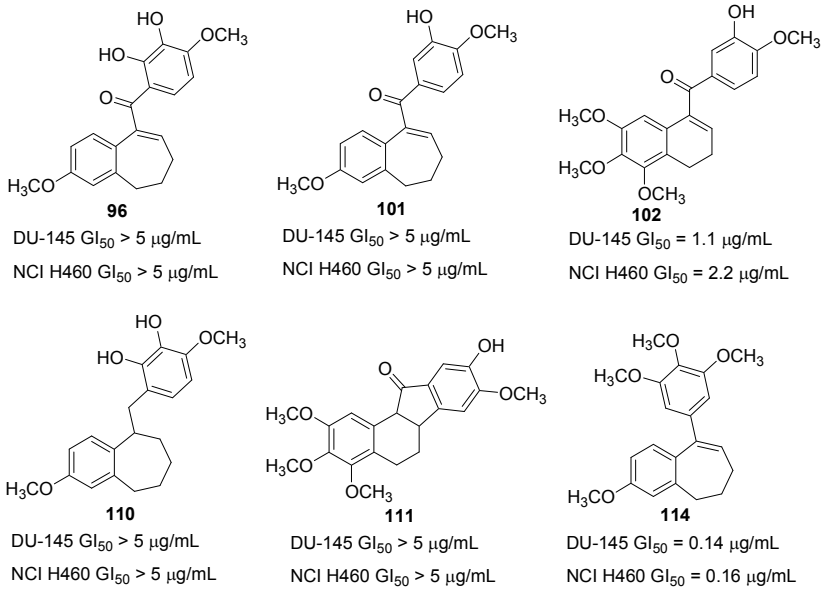

Figure 50. NCI H460 and DU 145 cell line cytotoxicity for benzosuberenes **96**, **101**, **110**, and **114**, dihydronaphthalene **102**, and the benzo[a]fluorene **111**.

DU-145 and NCI H460 Cell Cytotoxicity for Potential Bioreductive Compounds **75**, **76**, **78**

Several potential bioreductive drug triggers were analyzed for cell line cytotoxicity. The bioreductive compounds were proposed to only be active under hypoxic conditions; therefore, we did not expect the drugs to show remarkable cell line cytotoxicity under normoxic conditions. The dihydronaphthalene nitroimidazole **75** showed little cytotoxicity for the DU-145 and NCI H460 cell lines with GI_{50} values of ~ 5 μg/mL for each. Of the two combretastatin bioreductive triggers analyzed, **76** and **78**, only **78** showed high cytotoxicity for either cell line, with GI_{50} values of 0.27 μg/mL and 0.49 μg/mL for DU-145 and NCI H460 cell lines respectively (Figure 51). The cytotoxicity of compound **78** was surprising as the compound is to be active under hypoxic conditions only. To effectively evaluate these bioreductive compounds, their cytotoxicity should be measured in hypoxic conditions and compared to the normoxic values.

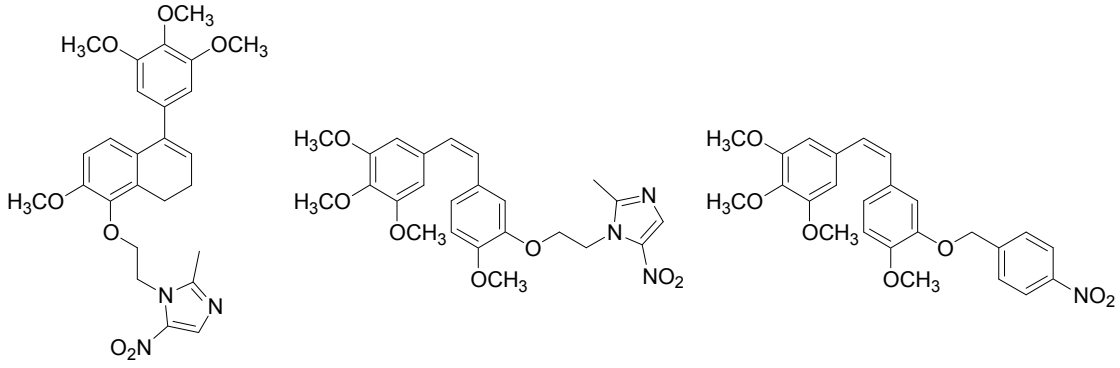

75
DU-145 GI_{50} ~ 5 μg/mL
NCI H460 GI_{50} > 5 μg/mL

76
DU-145 GI_{50} ~ 5 μg/mL
NCI H460 GI_{50} > 5 μg/mL

78
DU-145 GI_{50} = 0.27 μg/mL
NCI H460 GI_{50} = 0.46 μg/mL

Figure 51. DU-145 and NCI H460 cell line cytotoxicity of bioreductive drug triggers **75**, **76**, and **78**.

DU-145 and NCI H460 Cell Cytotoxicity for Bioreductive Analogues **115-122**

Kishore Gaddale Devanna, a postdoctoral member of the Pinney group, submitted 8 potential bioreductive compounds that were also tested for DU-145 and NCI- H460 cell line cytotoxicity in normoxic conditions. Of the nitroimidazole aziridine compounds, **115-117**, only compounds **116** and **117** were moderately active. The tosylated aziridine **116** had GI_{50} values of 2.7 μg/mL and 1.7 μg/mL, while bioreductive analogue **117** had GI_{50} values of 2.9 μg/mL and 2.9 μg/mL for DU-145 and NCI H460 cell lines respectively. The mesylated intermediate **118** and nitro-imidazoles **119-122** were all ineffective at hindering cell growth for DU-145 and NCI H460 cell lines with GI_{50} values of > 5 μg/mL for both cell lines. The cytotoxic effects of compounds **115-122** may be increased if the cell lines are tested under hypoxic conditions (Figure 52).

Isothermal Titration Calorimetry

ITC of combretastatin analogues for tubulin binding proved to be a difficult task. Tubulin dimer association would have been disastrous for data collection because ITC is a sensitive technique that would detect the heats of association between dimers. To best ensure that no protein-protein interactions occurred, stock tubulin in glutamate was centrifuged at 24,000 rpm for 40 min at 2^{o}C to precipitate any denatured protein. The tubulin was then dialyzed in PEM buffer for 24 h at 4^{o}C. The tubulin was dialyzed in PEM buffer to remove glutamate buffer, and replace any GTP bound tubulin in solution with GDP. The tubulin was then recentrifuged at 24,000 rpm for 40 min at 2^{o}C to further remove any denatured protein. Freshly isolated tubulin was also beneficial over older tubulin in running successful ITC experiments

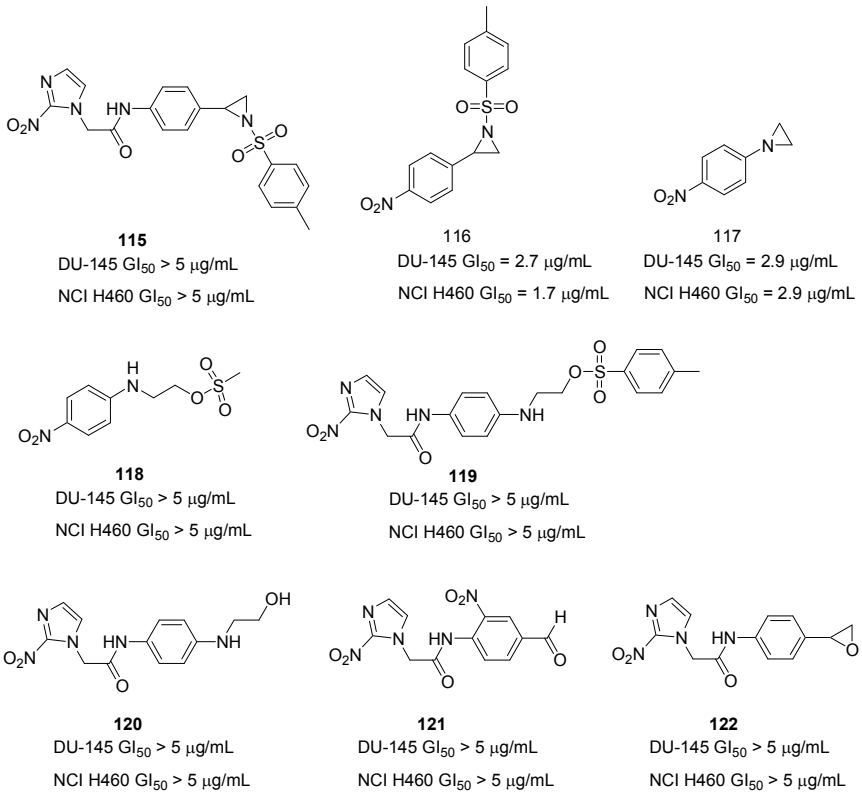

Figure 52. DU-145 and NCI H460 cell line cytotoxicity for bioreductive compounds **115-122**.

Thermodynamic Interaction of Combretastatin A1 with Tubulin

ITC was used to find the thermodynamic binding properties of CA1 binding to the tubulin colchicine binding site. Raw data of the microcalorimetric titrations of CA1 to tubulin are recorded as power (μW) versus time. The area under each peak is proportional to the amount of heat evolved from the binding of CA1 to the tubulin colchicine site. For effective titrations CA1 was injected in 10 μL aliquots at a concentration of 33 μM into tubulin (25.8 μM). Three independent studies with CA1 gave consistent results, Figures 53-55. From the figures we can see that the ITC experiments gave exotherms that were appropriate for calculating the thermodynamic parameters of CA1. Each injection gave an exotherm that decreased consecutively.

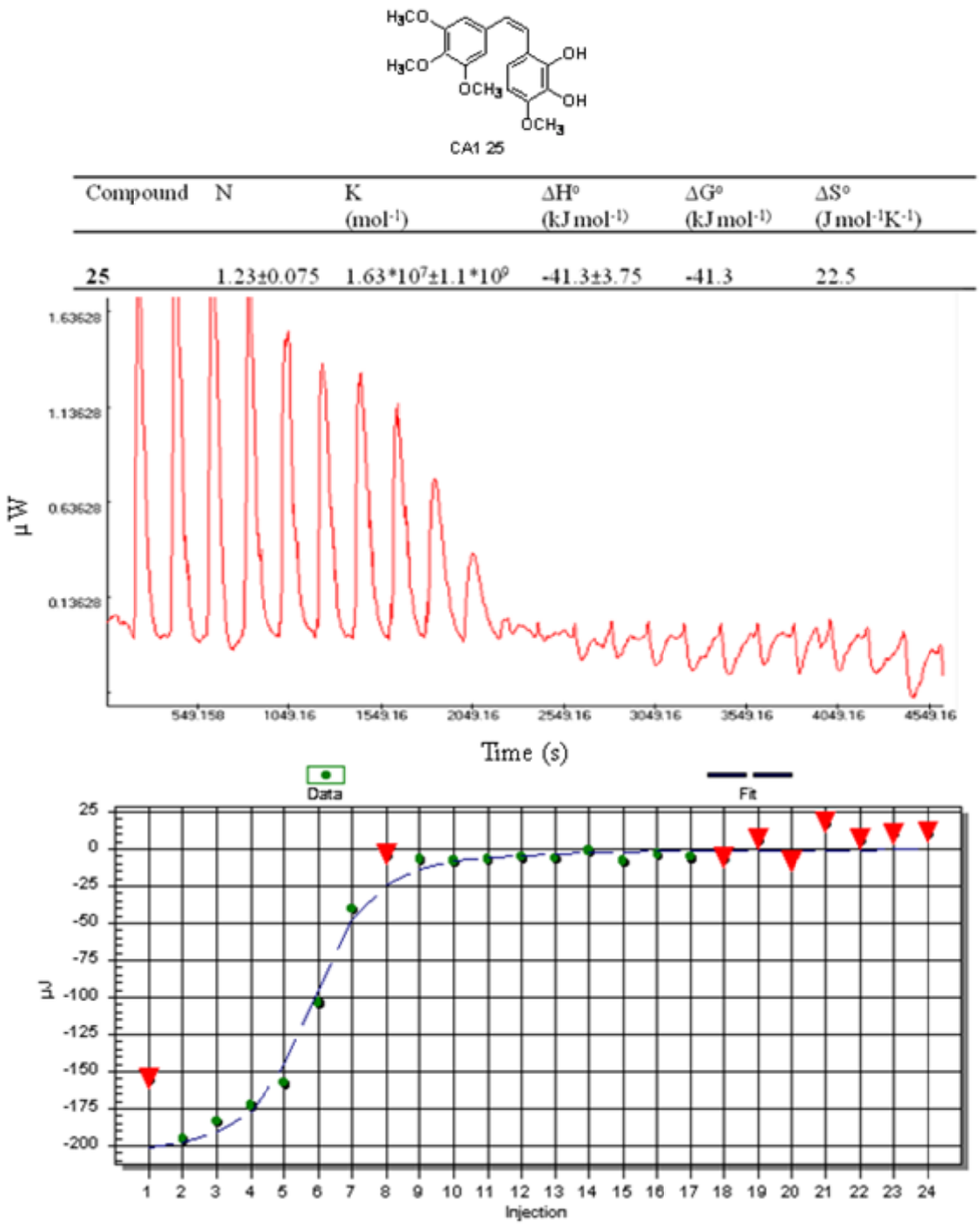

Figure 53. ITC experiment 1 of CA1 binding to tubulin. Top figure represents the thermodynamic values obtained, middle figure represents the power output per injection, and the bottom figure represents the exothermic output per injection.

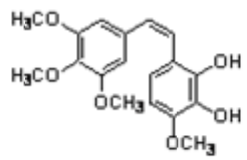

CA1 25

Compound	N	K (mol^{-1})	ΔH° ($kJ\,mol^{-1}$)	ΔG° ($kJ\,mol^{-1}$)	ΔS° ($J\,mol^{-1}K^{-1}$)
25	0.97±0.061	$1.05*10^{7}$±$3.0*10^{7}$	-32.9±2.60	-40.2	24.6

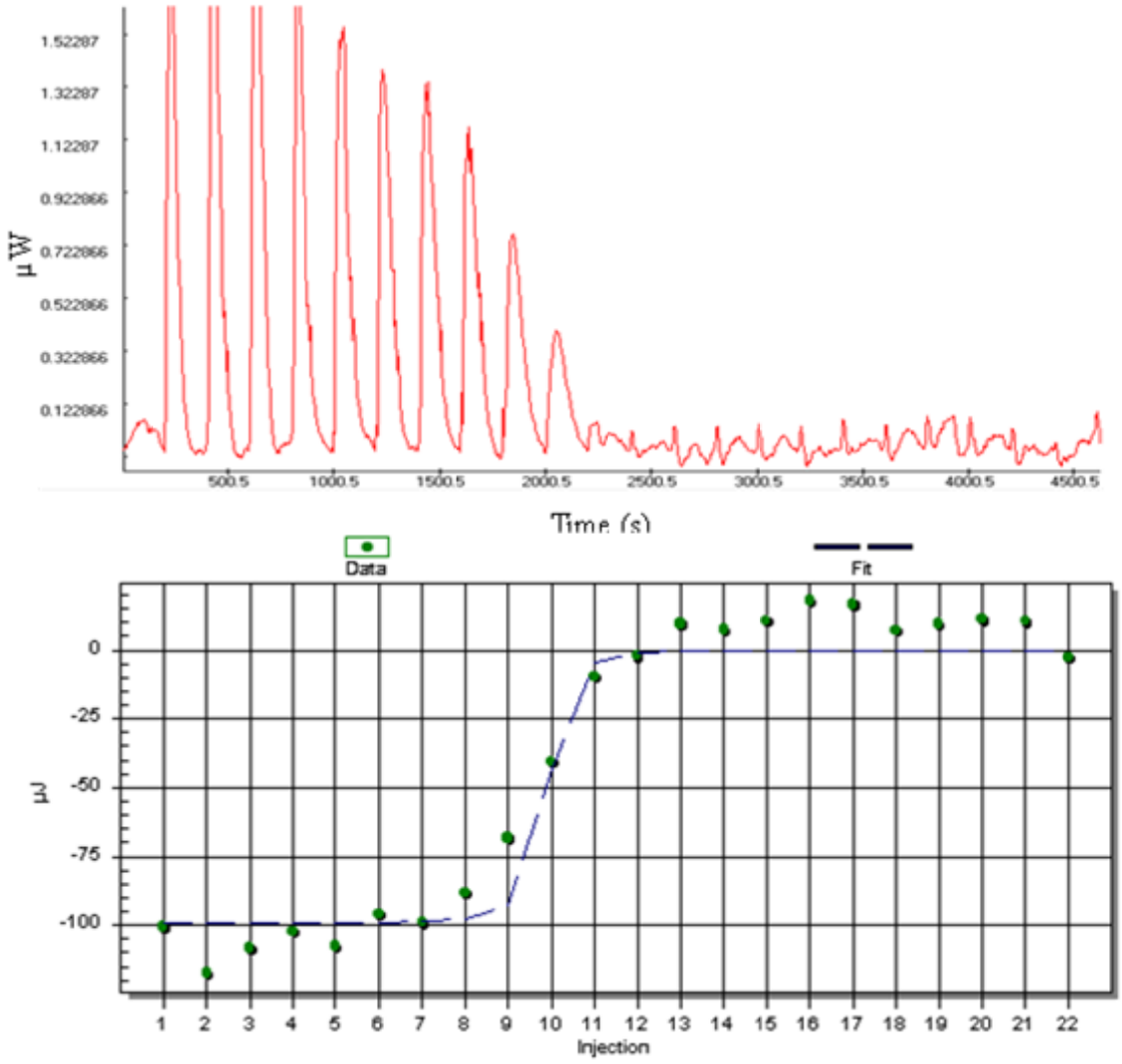

Figure 54. ITC experiment 2 of CA1 binding to tubulin. Top figure represents the thermodynamic values obtained, middle figure represents the power output per injection, and the bottom figure represents the exothermic output per injection.

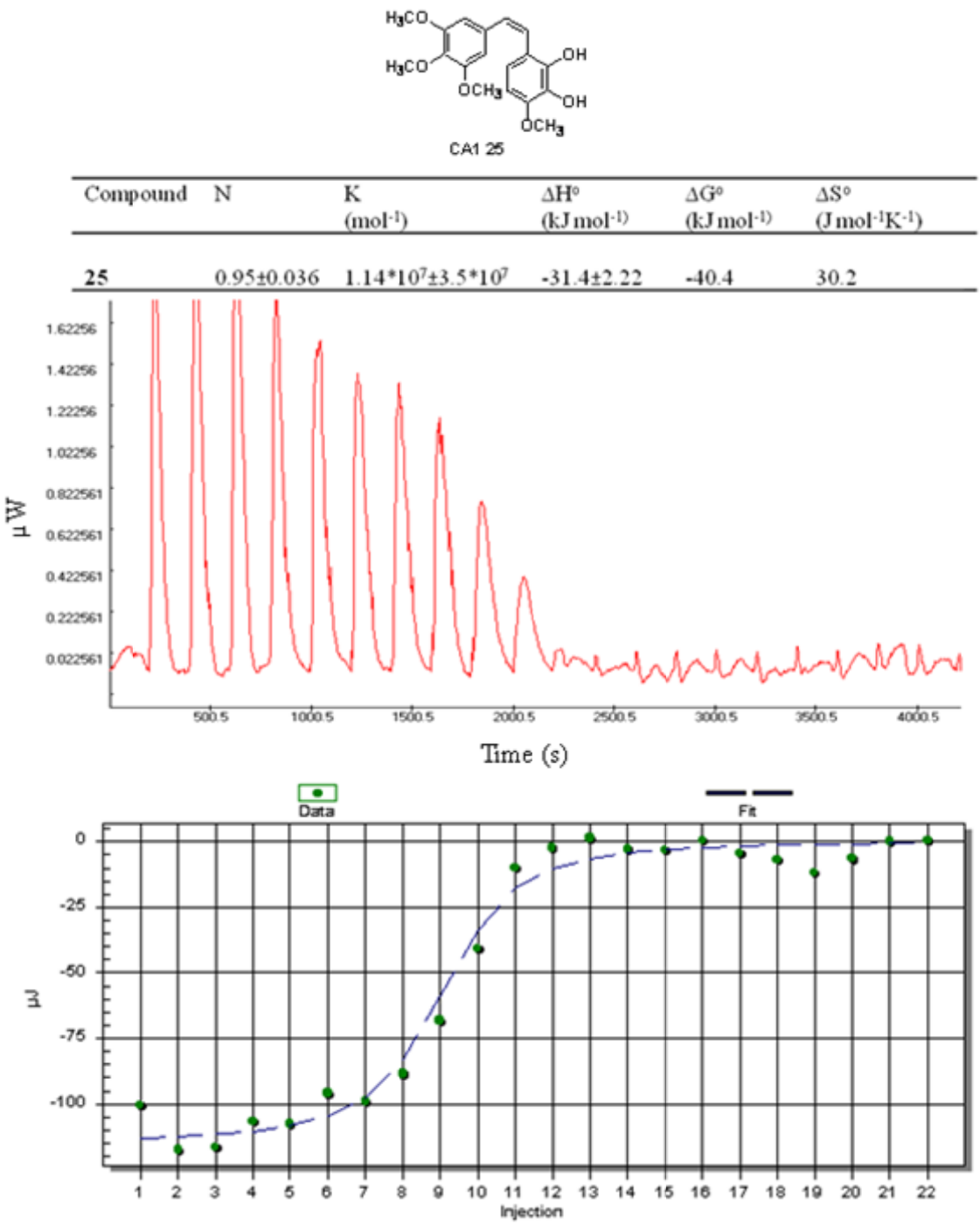

Figure 55. ITC experiment 3 of CA1 binding to tubulin. Top figure represents the thermodynamic values obtained, middle figure represents the power output per injection, and the bottom figure represents the exothermic output per injection.

Exotherms at the end of the experiment are the heats of dilution for the ligand CA1 into the ITC cell. Isotherms were generated by plotting heat (μJ) vs. the molar ratio. The thermodynamic properties of CA1 were averaged to give an N value of 1.05 ± 0.1, a ΔH of -35.2±-3.80 (kJ mol^{-1}), a K value of 1.27 x 10^{7} ± 0.223 x 10^{7} (mol^{-1}), ΔG-40.6 ±0.433 (kJ mol^{-1}), and a ΔS value 25.8±3.27 (J mol^{-1} K^{-1}).

The K_b for CA1 is remarkably high, and is a tight binder of tubulin. The binding is also exothermic and therefore thermodynamically favorable. By graphing the ΔG, ΔH, and –TΔS found for CA1 the thermodynamic binding parameters can be compared to known models.[33,35] The CA1 binding most directly represented a compound that is hydrophobic and can form hydrogen bonds with the protein (Figure 56).[32,33] Considering the CA1 contains 2 phenolic, and 4 methoxy substituents, it had the ability to form hydrogen bonds, but was still binding with hydrophobic interactions because of its aromatic and conjugated system.

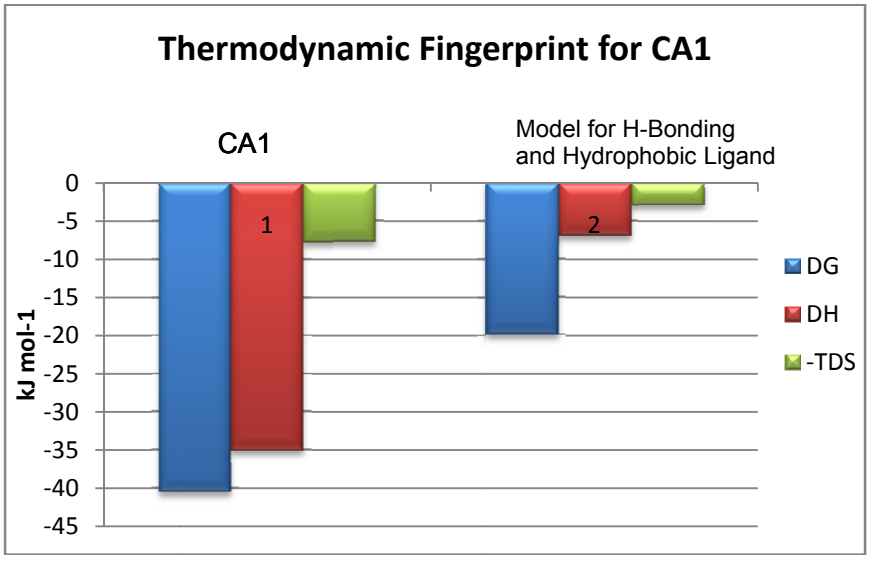

Figure 56. Thermodynamic fingerprint for CA1. Comparison of CA1 thermodynamic parameters to a model of compounds that H-bond and are also hydrophobic.[33,35]

Thermodynamic Interaction of Combretastatin A4 and Colchicine with Tubulin

Significant problems were observed when using tubulin that was more than 1 year old. Several scans of CA4 and colchicine were taken; however, no scan gave data that could be effectively analyzed. It was originally believed that the hydrophobic nature of CA4 and colchicine kept the drugs from being completely dissolved in the PEM buffer at high concentrations. To circumvent the insolubility of CA4 in PEM buffer, the ligand buffer was supplemented with 10% DMSO.[42] While the drugs were completely dissolved, ITC experiments still gave incalculable results. It is possible that aggregation was occurring at these higher concentrations of drug in solution. It was then decided to use a more water soluble molecule.

Thermodynamic Interaction of Benzophenone **37** *with Tubulin*

The thermodynamics of the phenstatin derivative **37** were also evaluated by ITC. One scan of compound **37** was obtained. Benzophenone **37** was able to be scanned effectively when 40 μM of the phenstatin derivative was injected in 10 μL aliquots into buffer at a 38.8 μM tubulin concentration. The scan gave an N value of 0.47±0.042, a K value of $5.3 \times 10^5 \pm 3.5 \times 10^5$ (kJ mol^{-1}), a ΔH of -73.4±11.1 (kJ mol^{-1}), ΔG of -32.7 (kJ mol^{-1}), and a very large ΔS of -136.2 (J mol^{-1} K^{-1}) (Figure 57). This molecule is apparently forming multiple hydrogen bonds with the tubulin given the large enthalpy. The N value is a bit low for **37**; however the stoichiometric coefficient carries the most uncertainty when using ITC. The largely negative ΔS indicates that the binding of the ligand to tubulin is entropically unfavorable. This sort of binding is indicative of a protein-drug interaction that is involved in a conformation shift (Figure 58). More scans of this compound should be performed to validate the data collected.

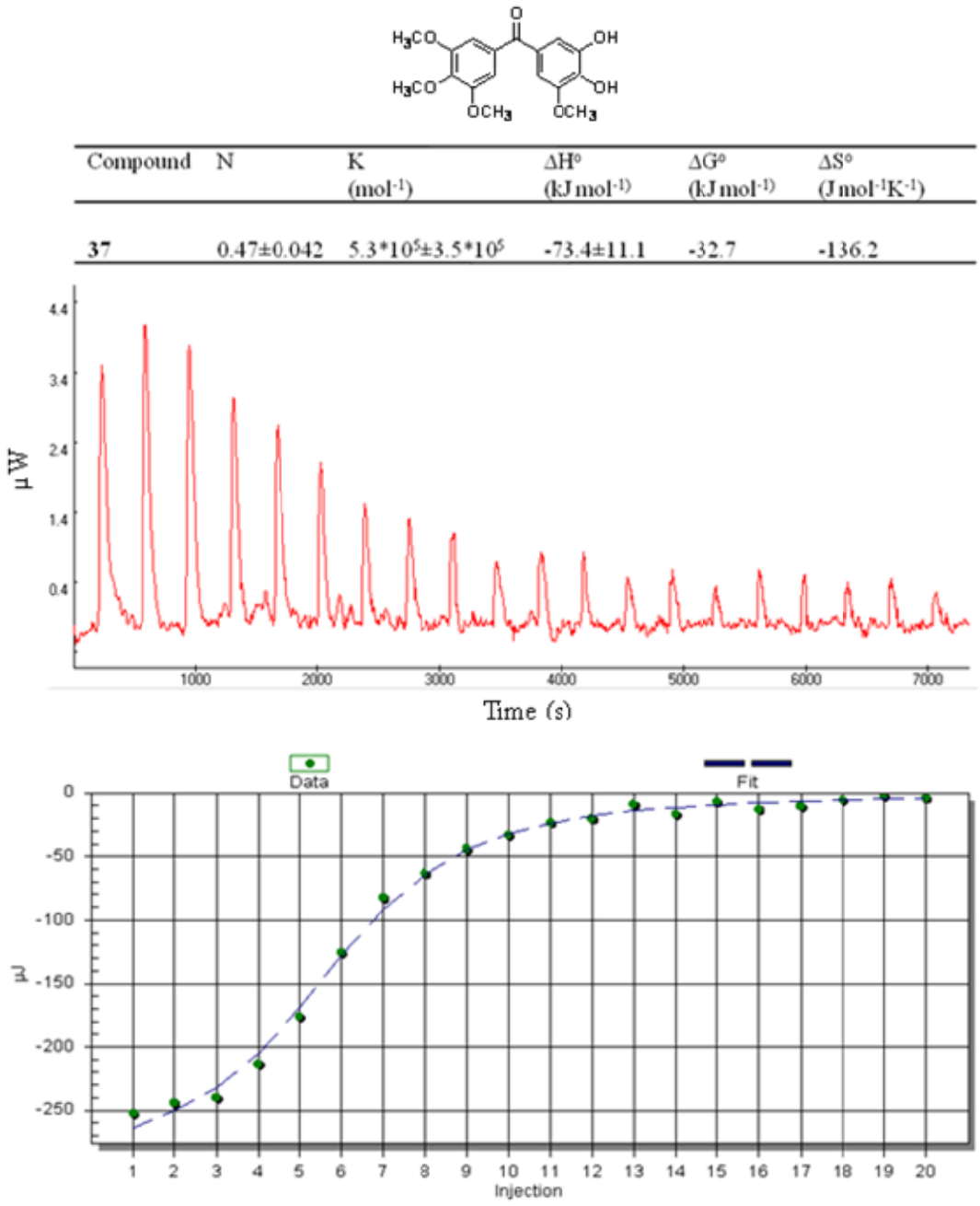

Figure 57. ITC of benzophenone **37**. Top figure represents the thermodynamic values obtained, middle figure represents the power output per injection, and the bottom figure represents the exothermic output per injection.

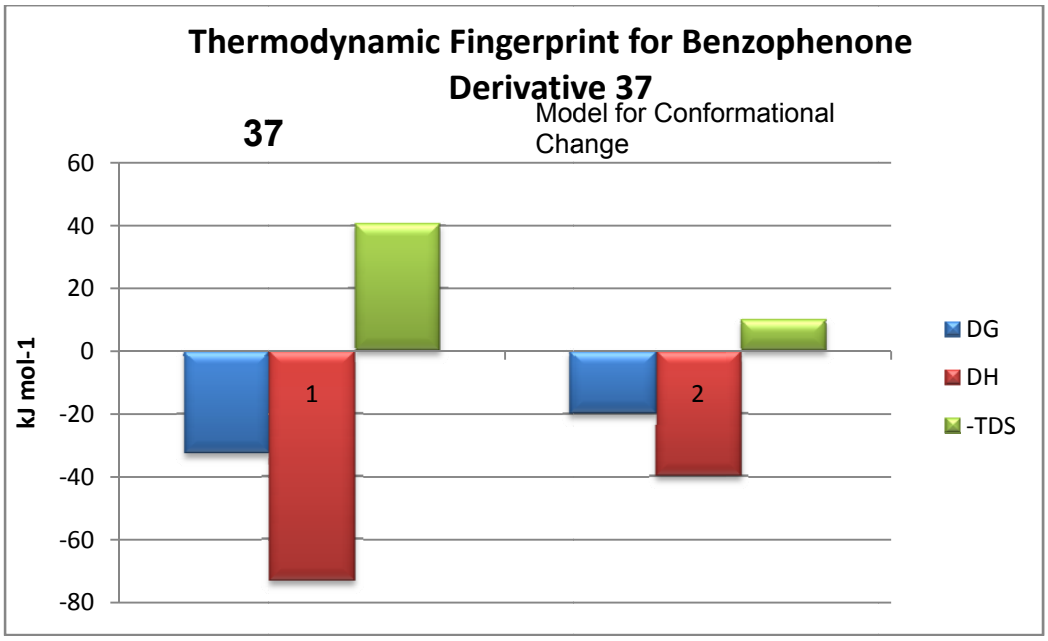

Figure 58. Thermodynamic fingerprint for phenstatin analogue **37**. Comparison of benzophenone **37** to a model for a system that undergoes a conformation change.[33,35]

Screening of Compounds for the Ability to Inhibit HIF-1α

HIF-1α has been shown to up-regulate many proteins that help cancer cells cope with low oxygen environments.[54] Because microtubules translocate HIF-1α from the cytoplasm to the nucleus, tubulin-tubulin interactions may also be partially responsible for the preservation of HIF-1α.[55] The Pinney group has synthesized many compounds that are able disrupt the microtubule framework. Approximately 20 were screened compounds for their effectiveness at inhibiting HIF-1α preservation. HeLa cells were treated with 1μM of the desired compound for 16 h (Figure 59). This allowed maximum drug-protein interaction. The cells were then treated with 125 μM $CoCl_2$ for 4 h. Co^{2+} exchanges with Fe^{2+} in the

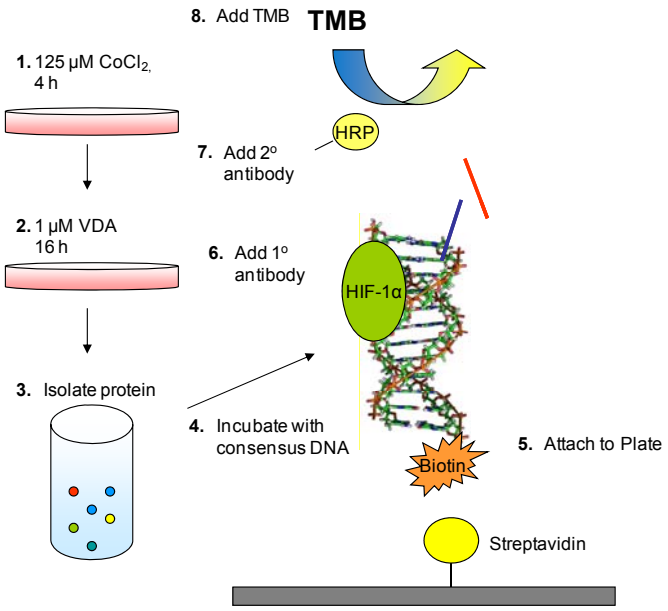

Figure 59. Protein isolation and HIF-1α quantification using an ELISA protocol.

prolyl hydroxylase, hindering its ability to initiate HIF-1α degradation.[49,52,53] Cobalt replaces iron in the prolyl hydroxylase, and renders the catalytic site inactive. The nuclear extracts were then collected via a protocol provided by Panomics.[62] The nuclear extract was screened for HIF-1α using an ELISA assay purchased from Panomics. Western blots were used to confirm the results of the ELISA assay.[97]

The first of the compounds that were tested were the well known inhibitors of tubulin polymerization CA1, CA4, Colchicine, Oxi8006, Oxi6196, and indole **44**.[14,84,116,117] From Figure 60, we can see that treatment of the HeLa cells with 1 μM of each VDA was effective at changing the cell morphology by methods described previously (Figure 8). This change in morphology can be identified by the spherical nature of the cells in Figure 60 C-H. Cells that retain their original morphology appear flat and trapezoidal in appearance (Figure 60 A and B).

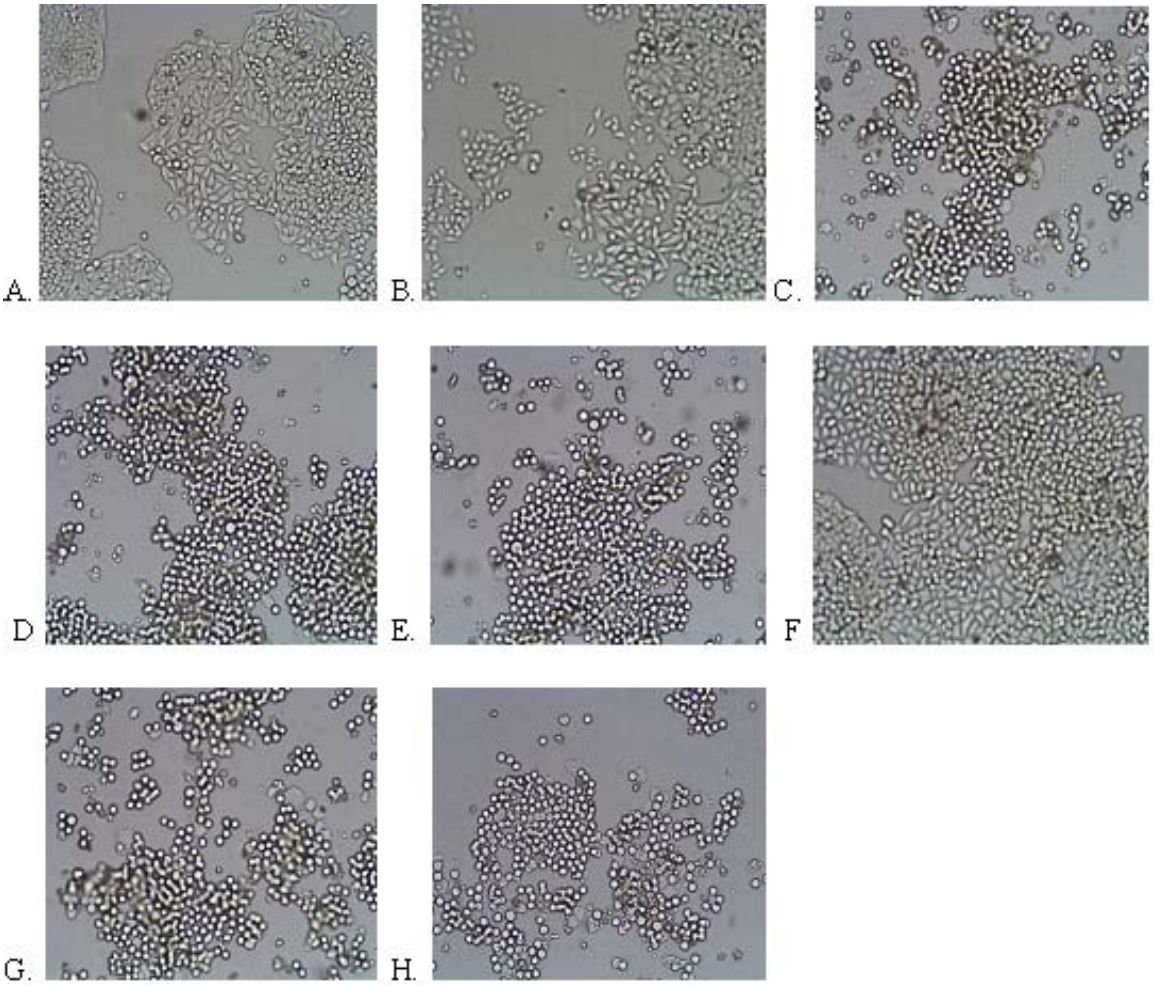

Figure 60. Changes in HeLa cell morphology caused by treatment with drug. A.) no compound, B.) 100 µL DMSO, C.) Colchicine (1 µM), D.) Oxi6196 (1µM), E.) Oxi8006 (1 µM), F.) Indole **44**, G.) CA1 (1 µM), H.) CA4 (1 µM).

indicates that the treatment of HeLa cells with 1µM of the respective drug is appropriate for disrupting the microtubule network. Figure 60 A shows HeLa control cells, which were flat, and adhered well to the plate. Addition of DMSO (Figure 60B) did not affect the cell morphology; however, Figure 61 C-E, G, and H pictures cells that have rounded and are loosely attached to the cell culture plate. Interestingly, indole **44** did not change the cell morphology though it had a tubulin IC_{50} of 2.8 µM, which is comparable to the other VDAs tested.

The amount HIF-1α isolated from each nuclear extract was determined by an ELISA assay acquired from Panomics (Figure 59).[62] Control 1 contained no compound and no $CoCl_2$, and it showed the lowest amount of HIF-1α in the isolated nuclear extract which was expected (Figure 61 A). Treatment of the HeLa cells with $CoCl_2$ showed a remarkable increase in the HIF-1α isolated (Figure 61 B, Control 2). All of the cells treated with both VDA and $CoCl_2$ also showed an increase in the amount of HIF-1α isolated. Of the individual drugs tested, colchicine seemed to be the most effective at reducing the amount of HIF-1α. Oxi6196 and indole **44** also reduced the amount of HIF-1α isolated, but not as effectively as colchicine. The error associated with each sample seemed to vary greatly. For control 1, the error was relatively small; however, for every other sample the deviation was substantial. Preservation of HIF-1α with $CoCl_2$ may be the reason for this deviation. Also of interest, was the observation that compounds that imposed a morphological change on the cell through microtubule disruption such as CA1 and Oxi8006 were less able to decrease the amount of HIF-1α isolated than indole **44,** which did not have an effect on cell morphology. Perhaps another mechanism of HIF-1α regulation is occurring with indole **44**.

Sixteen other compounds were tested for their ability to inhibit the amount of HIF-1α isolated from the nuclear extracts of HeLa cells (Figures 62 and 63).[14,115] In Figures 62 and 63 the western blot of the nuclear extracts is shown at the top, followed by the data obtained from the ELISA assay. The structures of each compound are also shown for convenience. The compounds were selected to have a diversity of tubulin IC_{50} values as

A.

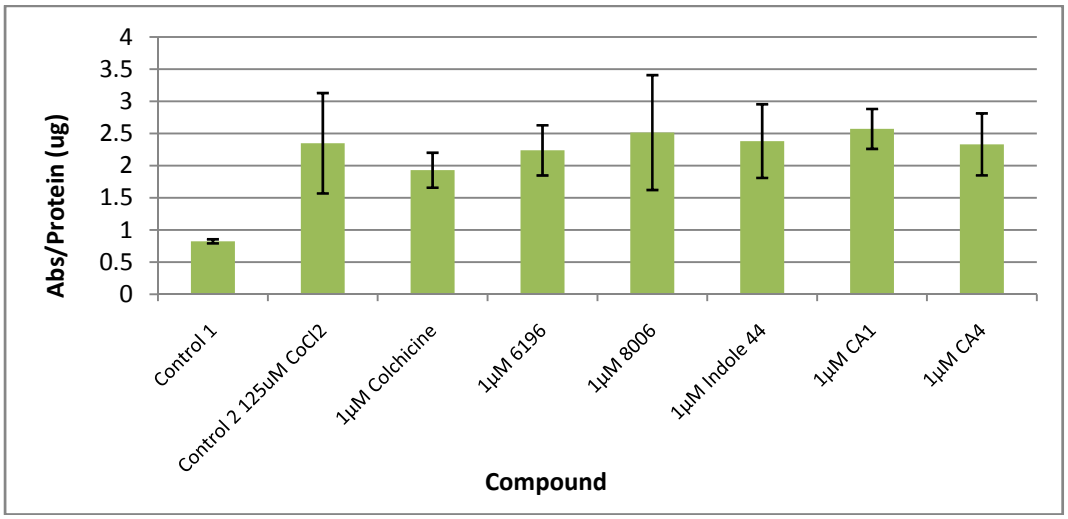

B.

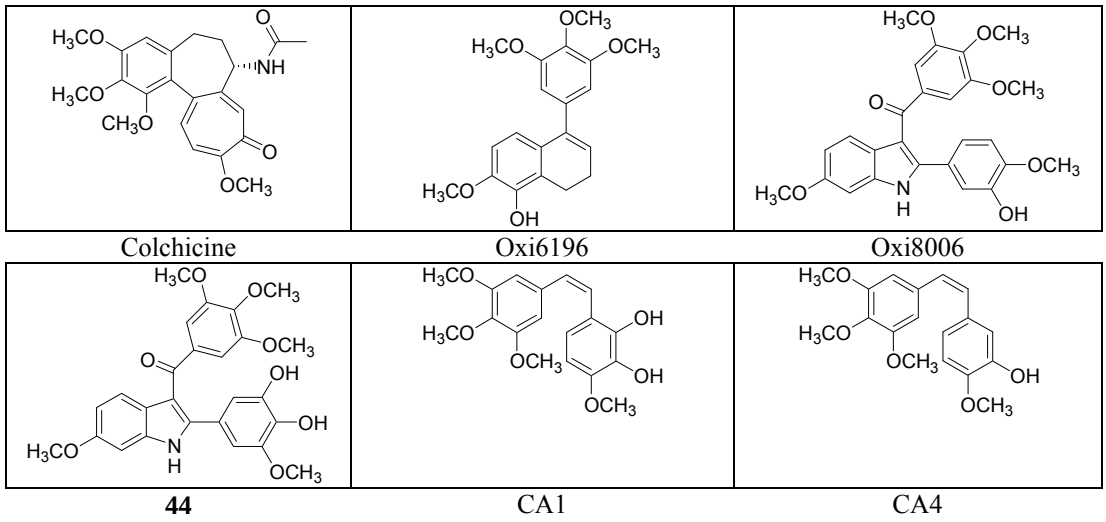

Figure 61. A.) HIF-1α accumulation in HeLa cells treated with 1μM colchicine, Oxi6196, Oxi8006, indole **44**, CA1, and CA4. B.) Structures of colchicine, Oxi6196, Oxi8006, indole **44**, CA1, and CA4.

well as to have a variety of analogue types. Once again HeLa cells were treated with 125 μM $CoCl_2$ to increase HIF-1α preservation. 2ME2 (Figure 62, structure c) was used as a positive control, since it is well known in the literature to decrease amounts HIF-1α within cells.[118] All of the compounds tested decreased the amount of HIF-1α isolated in

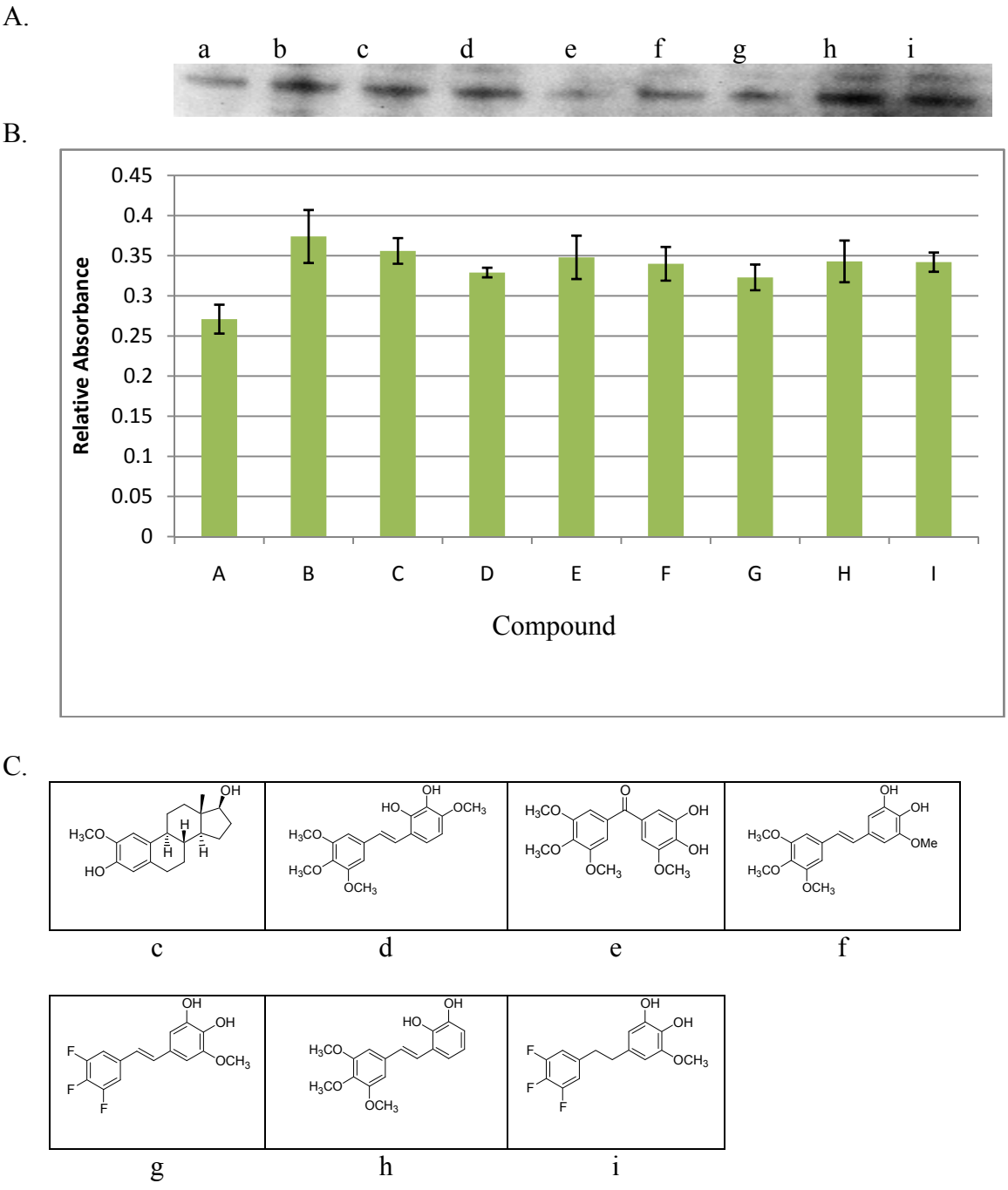

Figure 62. A) Western Blot and B) ELISA immunoassay for HIF-1α detection in HeLa cells treated with (C) compounds: (a) no compound no $CoCl_2$; (b) no compound 125 μM $CoCl_2$; (c) 2ME2 (1 μM), and 125 μM $CoCl_2$; (d) trans-CA1 **35** (1 μM), and 125 μM $CoCl_2$; (e) 3′,4′-dihydroxy-5′-methoxy-phenyl)-(3,4,5-trimethoxy-phenyl)-methanone **37** (1 μM), and 125 μM $CoCl_2$; (f) (*E*)-2-(3′,4′-dihydroxy-5′-methoxyphenyl)-1-(3,4,5-trimethoxyphenyl) ethene **8** (1 μM), and 125 μM $CoCl_2$; (g) (E)-2-(3′,4′-dihydroxy-5′-methoxyphenyl)-1-(3,4,5-trifluorophenyl) ethene **11** (1 μM), and 125 μM $CoCl_2$; (h) (Z)-2-(2′,3′-dihydroxy-5′-methoxyphenyl)-1-(3,4,5-trimethoxyphenyl) ethene **112** (1 μM), and 125 μM $CoCl_2$; (i) (E)-2-(3′,4′-dihydroxy-5′-methoxyphenyl)-1-(3,4,5-trifluorophenyl) ethene **12** (1 μM), and 125 μM $CoCl_2$.

the nuclear extracts (Figures 62 and 63) with the exception of the fluorinated Oxi8006 indole **55** (Figure 63, p). The effectiveness of every compound tested was unexpected because tubulin IC_{50} values of the compounds varied greatly. Some compounds, such as 2ME2 and the diamino stilbene **106**, are very effective at inhibiting tubulin polymerization with tubulin IC_{50} values of < 3 μM. Other compounds like **16**, **17**, **18**, and **96** all have tubulin IC_{50} values of >40 μM, but were all effective at decreasing the amount of HIF-1α detected in the nuclear extracts. Of the 16 compounds tested the benzosuberene **96** (Figure 63, l) was the most effective at reducing the amount of HIF-1α.[115] The effectiveness of compound **96** is an important find, because its tubulin polymerization inhibition IC_{50} > 40 μM, yet it was the most effective compound tested. Based on the findings from the ELISA assay, two possibilities were considered. 1) there is not a direct relationship between microtubule disruption, and HIF-1α preservation, or 2) all compounds tested that were poor inhibitors of tubulin polymerization decreased HIF-1α by an alternative method. The validity of the ELISA kit was tested using a western blot analysis (Figures 62 and 63 A). In each western blot, Control 1 had less HIF-1α than Control 2, though the difference was less dramatic in Figure 64 A. There were inconsistencies found between the ELISA assay and the western blot analysis. Compounds **12**, **35**, **47**, and **112** were much more active in the ELISA assay than in the western blot. Benzophenone **37** showed more activity in the western blot analysis than in the ELISA assay. Benzosuberene analogue **96** was the most effective at decreasing HIF-1α extracted in both the ELISA assay and the western blot.

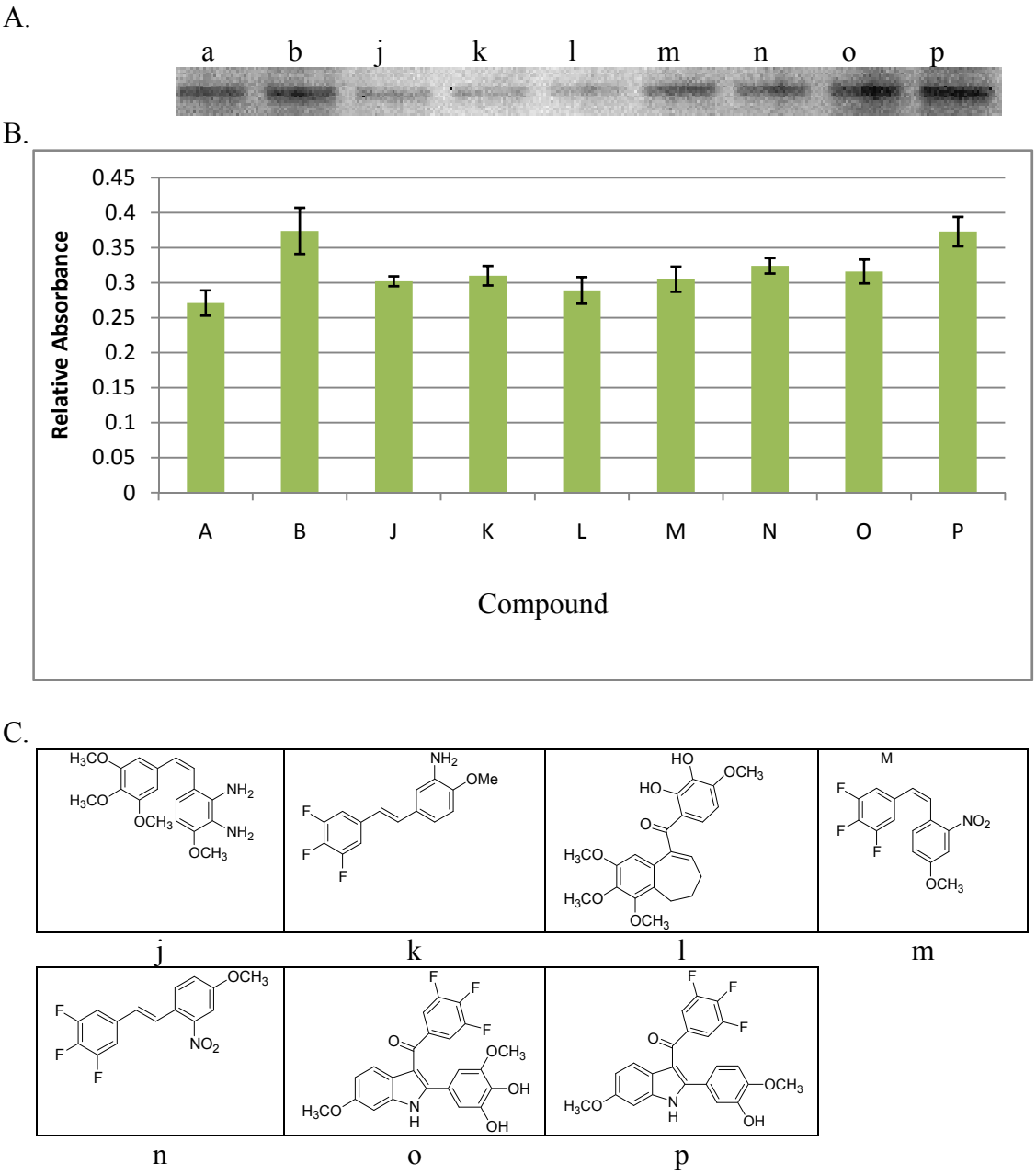

Figure 63. A) Western Blot and B) ELISA immunoassay for HIF-1α detection in HeLa cells treated with (C) compounds: (a) no compound no $CoCl_2$; (b) no compound 125 μM $CoCl_2$; (j) (Z)-2-(2′,3′-diamino-4′-methoxyphenyl)-1-(3,4,5-trimethoxyphenyl) ethene **106** (1 μM), and 125 μM $CoCl_2$; (k) E)-2-(4′-methoxy-3′-aminophenyl)-1-(3,4,5-trifluorophenyl) ethene **16** (1 μM), and 125 μM $CoCl_2$; (l) (2,3-dihydroxy-4-methoxy-phenyl)-(1,2,3-trimethoxy-8,9-dihydro-7H-benzocyclohepten-5-yl)-methanone **96** (1 μM), and 125 μM $CoCl_2$; (m) (Z)-2-(4′-methoxy-2′-nitrophenyl)-1-(3,4,5-trifluorophenyl) ethene **17** (1 μM), and 125 μM $CoCl_2$; (n) (Z)-2-(4′-methoxy-2′-nitrophenyl)-1-(3,4,5-trifluorophenyl) ethene **18** (1 μM), and 125 μM $CoCl_2$; (o) [2-(3,4-Dihydroxy-5-methoxy-phenyl)-5-methoxy-1H-indol-3-yl]-(3,4,5-fluoro-phenyl)-methanone **47** (1 μM), and 125 μM $CoCl_2$; (p) 2-[(3′-Hydroxy-4′-methoxy)-phenyl]-3-[(3″,4″,5″-trifluoro)-benzoyl]-6-methoxyindole **55** (1 μM), and 125 μM $CoCl_2$.

From the HIF-1α analysis benzosuberene **96** was very effective as was the benzophenone **37**. The Panomics ELISA assay is an appropriate agent for screening many compounds for their ability to inhibit HIF-1α preservation; however, the results should be confirmed by western blot. Western blots with actin controls should be performed to confirm an equal amount of protein was analyzed from each sample.

CHAPTER FOUR

Conclusions and Future Directions

Conclusions

Twenty potential VDA analogues were successfully synthesized, as were eleven bioreductive analogues of CA1 and CA4, and five NOS inhibiting CA4P and Oxi8007 analogues. Tubulin was purified and used to determine a compounds ability to inhibit tubulin polymerization, as well as determine the thermodynamic binding parameters of CA1 and phenstatin analogue **37** using isothermal titration calorimetry. A SRB cytotoxicity assay was successfully established for rapid screening of compounds to arrest cell growth against DU-145 and NCI H460 cell lines. Twenty compounds were also analyzed for their ability to inhibit the preservation of HIF-1α using an ELISA method as well as western blot analysis.

Several analogues of CA1 and CA4 were synthesized. It seemed that combretastatin analogues that contained a trimethoxy motif on the A-ring were more effective inhibitors of tubulin polymerization than were stilbene analogues that contained a trifluoro connectivity. Comparison of *E*-stilbene analogues **8** and **10** suggests that replacement of the trimethoxy ring with a trifluoro substituent increases a *trans*-stilbenes ability to inhibit tubulin polymerization. In comparison of the fluorinated *Z*-isomers, in only the case, analogue **15**, was a derivative active at in inhibiting tubulin polymerization having a tubulin IC_{50} value of 2.9 μg/mL. Nitro groups on the B-ring seemed to be less desirable than phenols or amines as evidenced by comparing stilbenes **13** and **15**.

For the indole derivatives synthesized, replacement of the trimethoxy substituents with a trifluorinated moiety was less effective at both inhibiting tubulin polymerization, and increasing cancer cell cytotoxicity. The reason for the decreased effectiveness of the fluorinated indoles most likely results from the hydrophobic nature of the compounds. Rather than dispersing evenly in solution they may aggregate which may lower interaction with the tubulin. Placement of a phenol in the 4′-position and a methoxy in the 5′-position of the indoles, as in compound **47**, decreased the ability of the compound to inhibit tubulin polymerization when compared to Oxi8006.

Considering the benzosuberene analogues synthesized by Madhavi Sriram, compound **107** was the most effective at inhibiting tubulin polymerization with an IC_{50} value of 1.7 μM. Of the compounds tested for cell line cytotoxicity **114** was the most effective with GI_{50} values of 0.14 μg/mL and 0.16 μg/mL for DU-145 and NCI H460 cell lines respectively. Also, benzosuberene **96** was the most effective of all compounds screened at inhibiting HIF-1α. For SAR relationships, placement of the trimethoxy moiety on the C-ring was beneficial over placement on the A-ring. Perhaps the preferred spacial alignment of the benzosuberene analogues within the tubulin colchicine binding site requires the C-ring to lie in plane A so that a methoxy substituent may hydrogen bond with Cys239. The phenol moiety is preferred on the A-ring such that it may H-bond with the backbone amide of Val 179. Also a direct linkage between the B and C rings is preferred to having a methylene or methanone bridge (Figure 64).

An examination of a library of compounds suggested that benzophenone **37** was superior to other compounds in tubulin polymerization inhibition, cancer cell cytotoxicity, and HIF-1α degradation assays. Compound **37** was a very effective

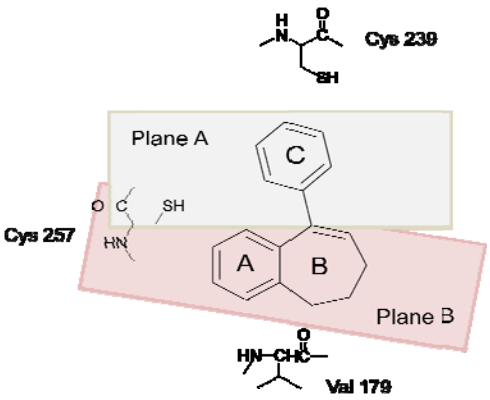

Figure 64. SAR study for Benzosuberenes

binder of tubulin with $K_b = 5.3 * 10^5$ (mol^{-1}) and a ΔH of -73.4 (kJ mol^{-1}) which was significantly more exothermic than CA1 (ΔH = -35.2 kJ mol^{-1}). Benzophenone **37** can form H-bonds with the backbone amide of Val 177, Cys 239, and backbone nitrogens of Ala 248, Asp 249, and Leu 250, which explains its highly exothermic binding. Of more interest is that the binding of **37** is entropically unfavorable indicating a shift in conformation within the protein. Benzophenone **37** had an IC_{50} value of 2-4 μM, and showed better cell line toxicity than CA1 and is a prime candidate for further testing.

Future Directions

Tubulin inhibition studies and cell line toxicity should be continued for compounds synthesized within the Pinney Group so SAR studies can be expanded. ITC for compound **37** needs to be verified with two more ITC experiments. A-ring indoles synthesis should be continued as they were not successfully synthesized in this study. Bioreductive drugs should also be screened for cell line cytotoxicity in hypoxic conditions.

APPENDICES

APPENDIX A

Selected NMR Spectra

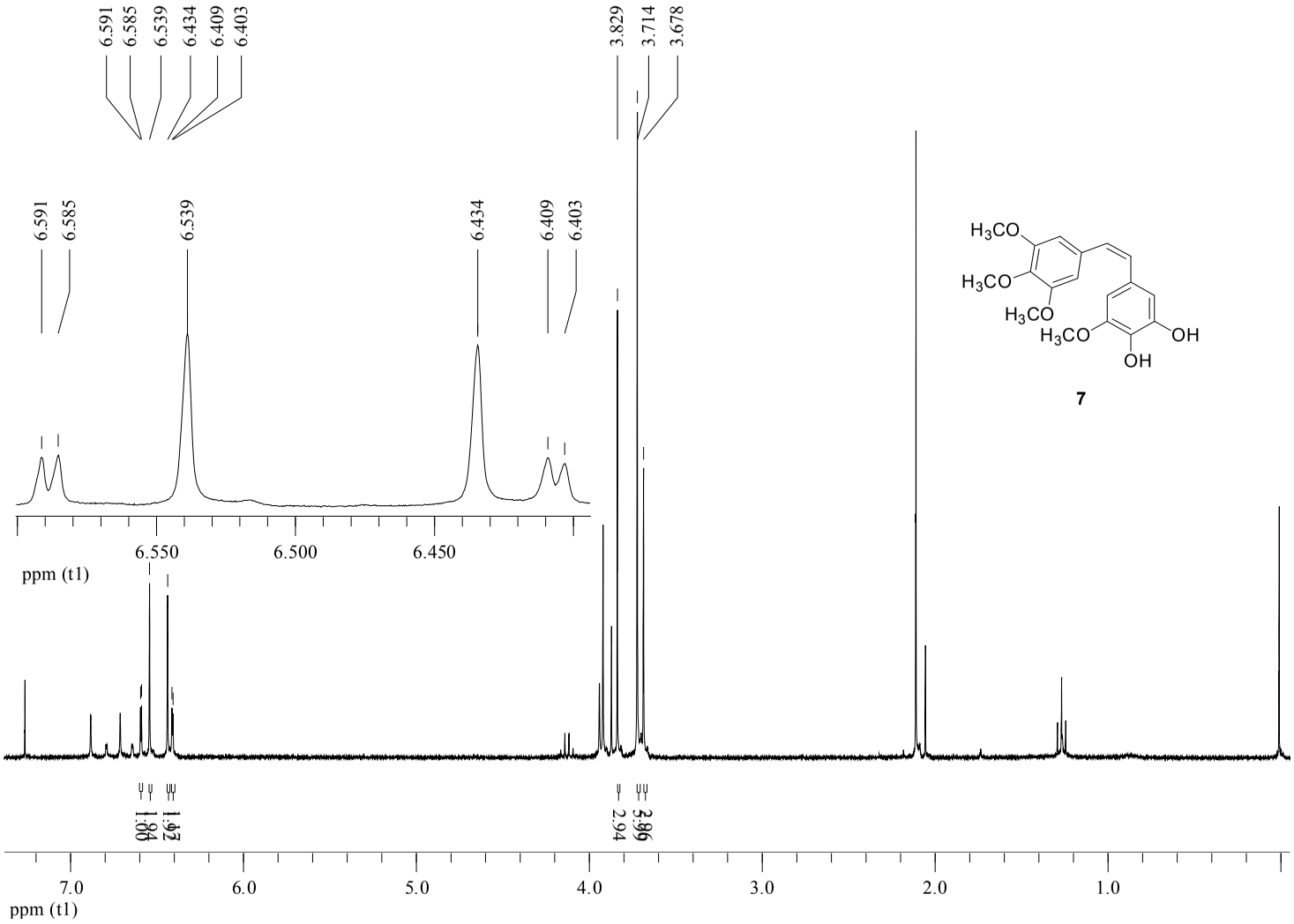

A.1. ^{1}H NMR ($CDCl_3$, 300 MHz) of Compound **7**

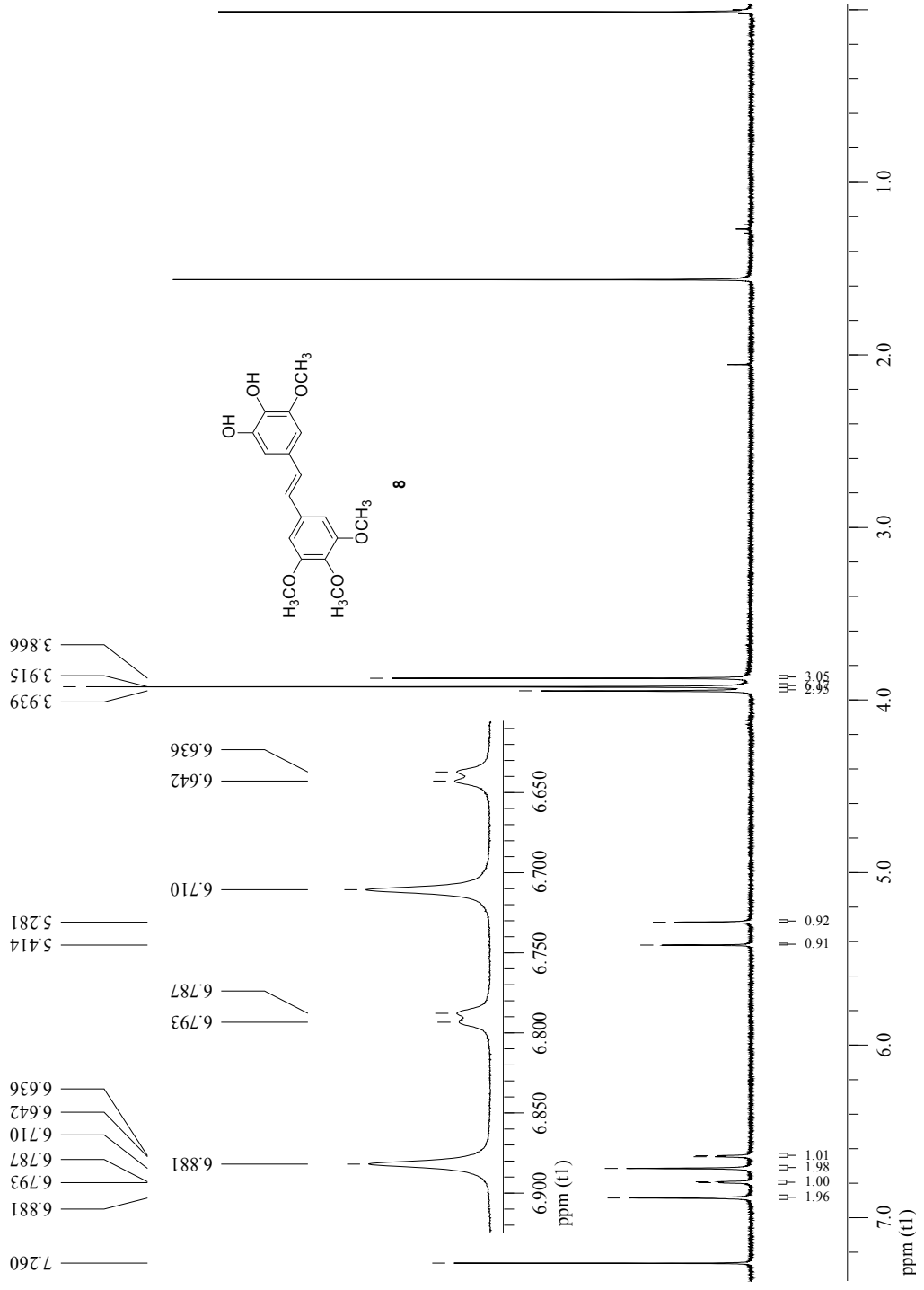

A.2. ^{1}H NMR ($CDCl_3$, 300 MHz) of Compound **8**

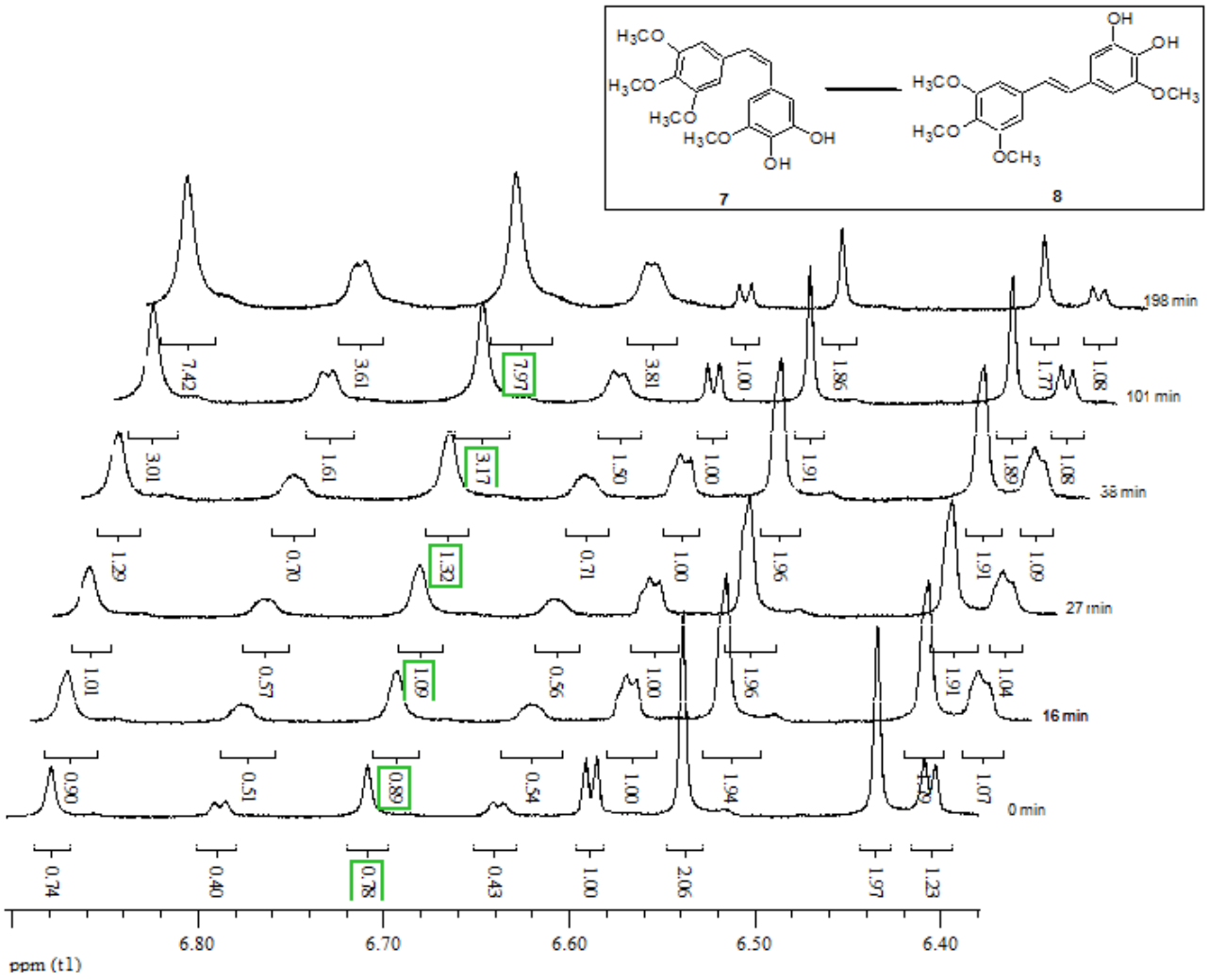

A.3. ^{1}H NMR ($CDCl_3$, 300 MHz) of Compound **7** Isomerizing to Compound **8**.

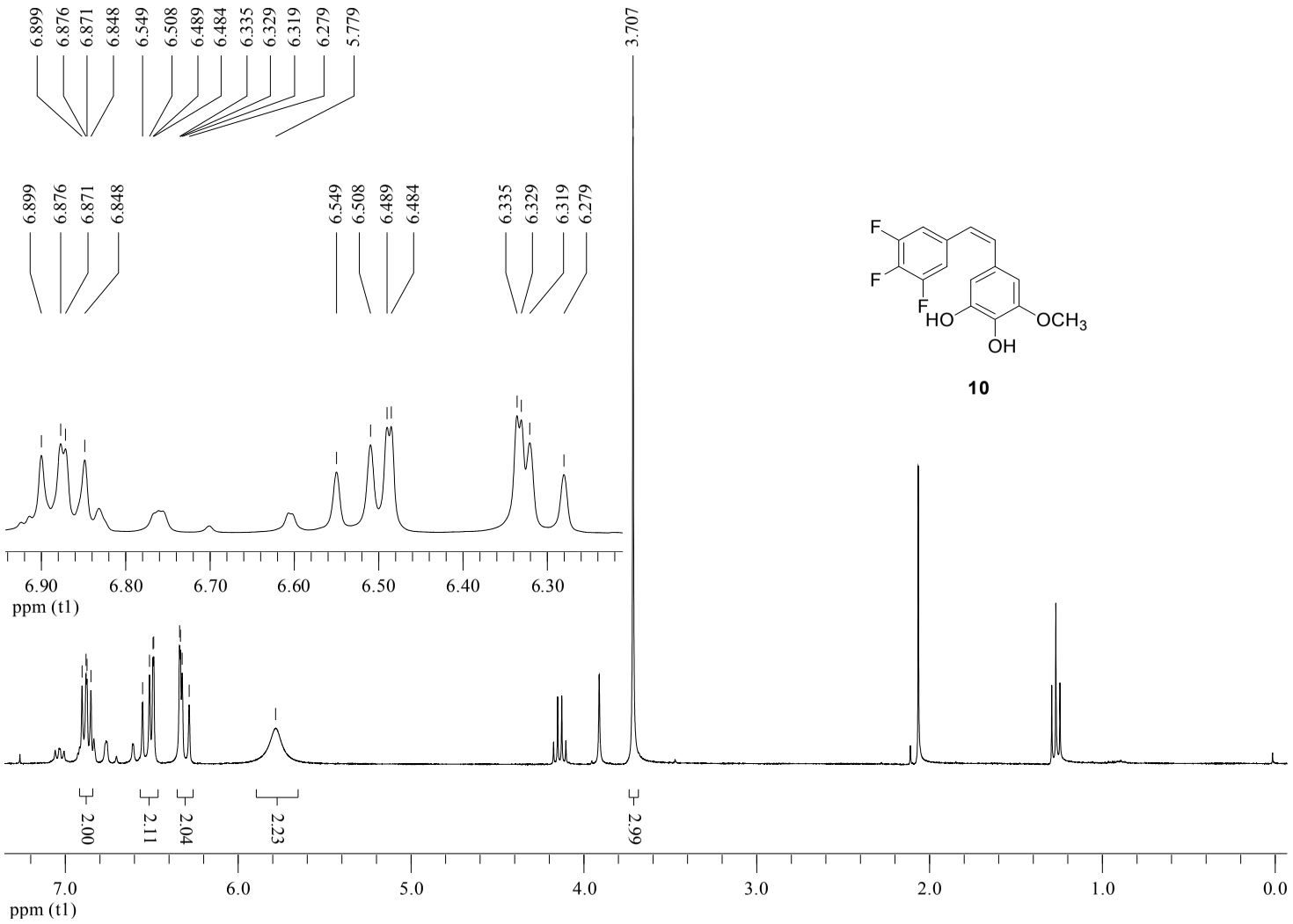

A.4. ^{1}H NMR ($CDCl_3$, 300 MHz) of Compound **10**

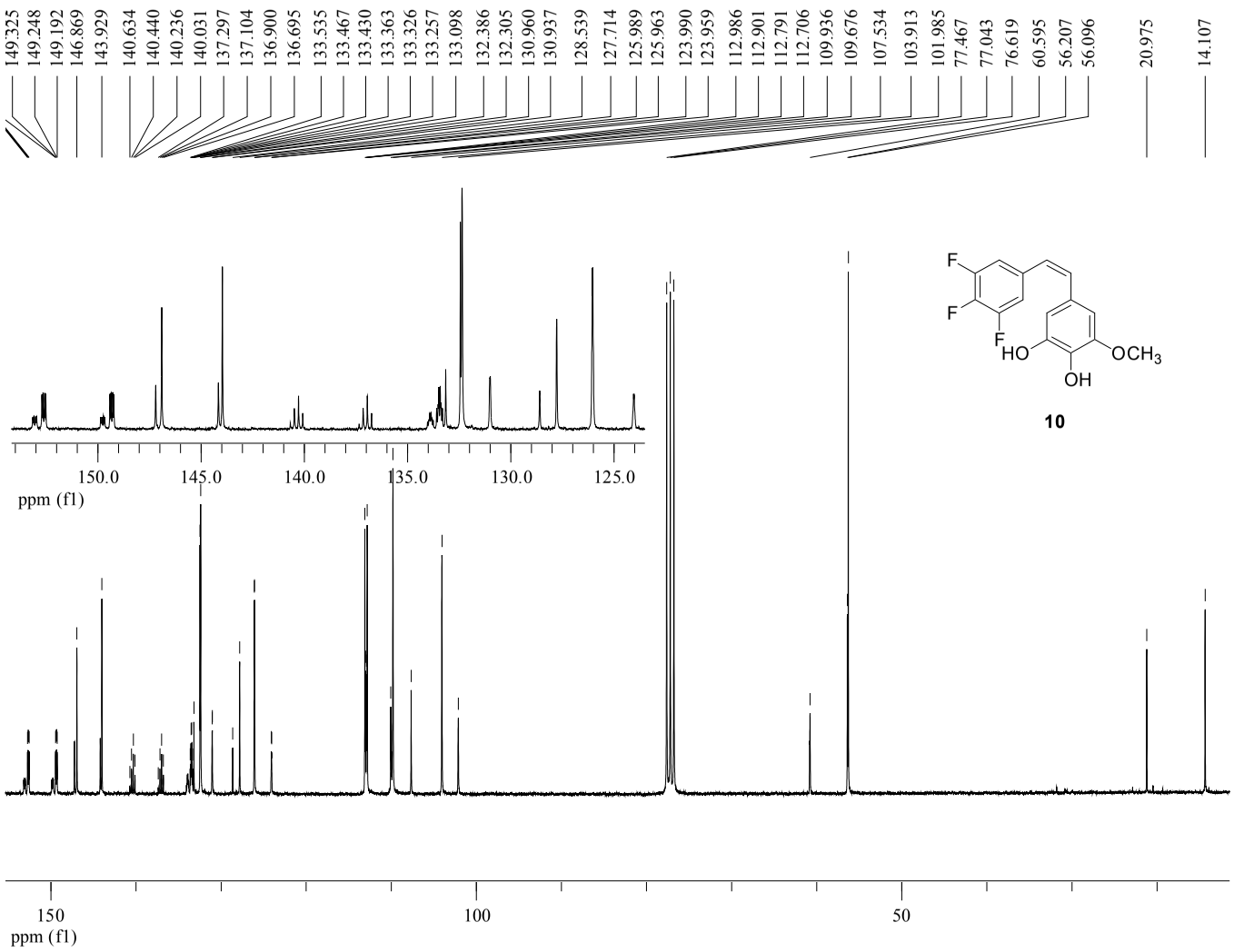

A.5. ^{13}C NMR ($CDCl_3$, 75 MHz) of Compound **10**

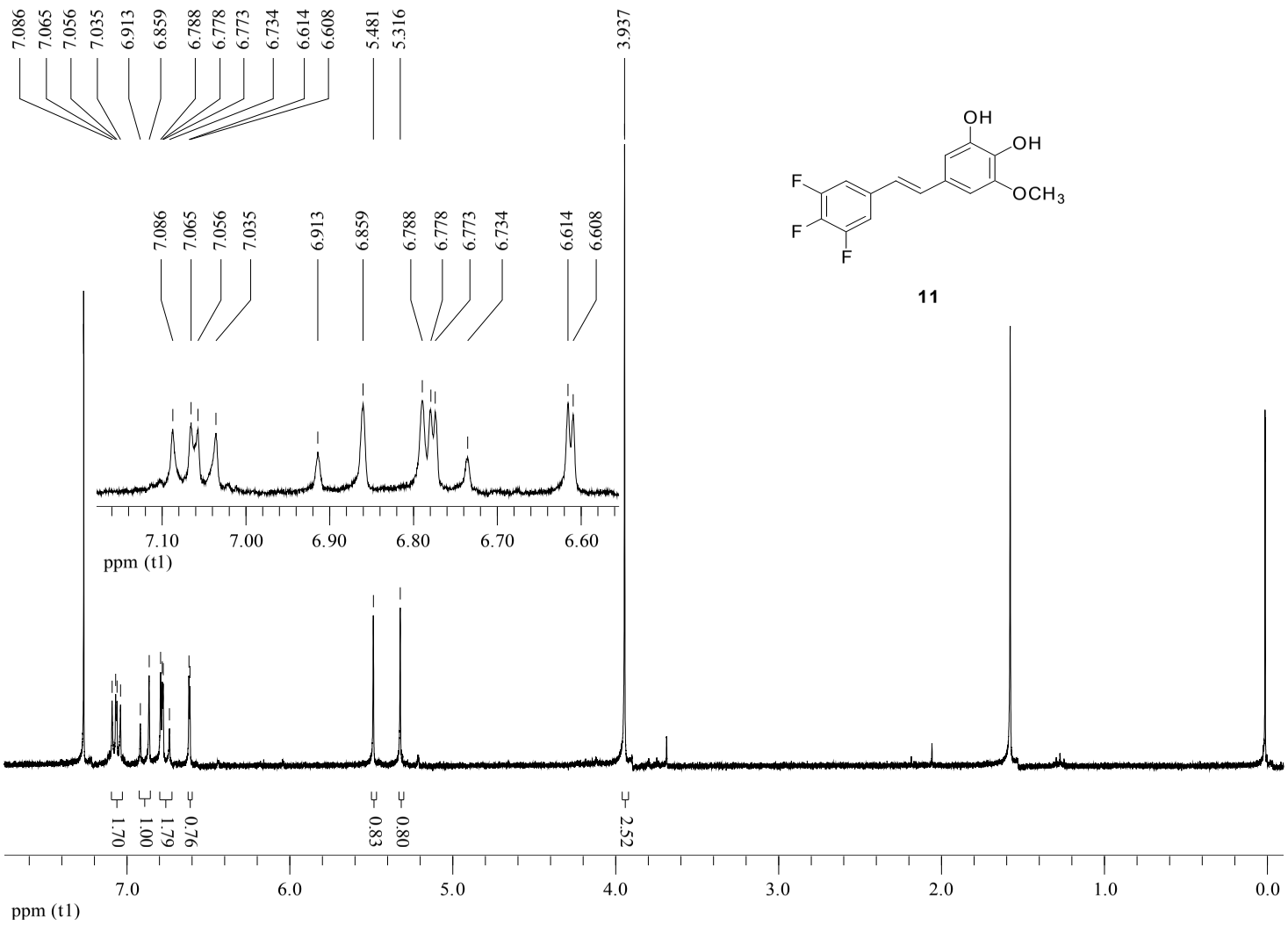

A.6. ^{1}H NMR ($CDCl_3$, 300 MHz) of Compound **11**

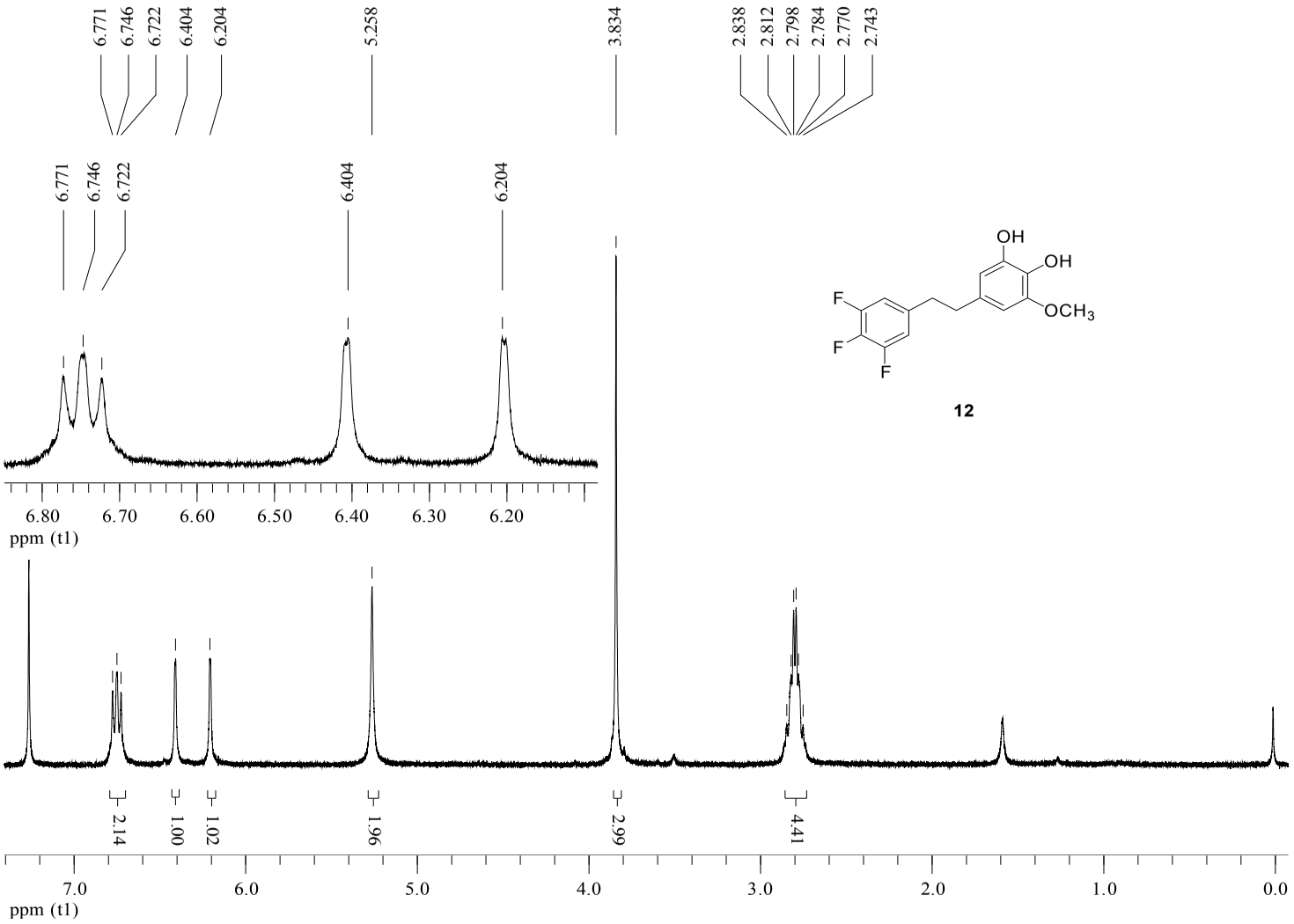

A.7. ^{1}H NMR ($CDCl_3$, 300 MHz) of Compound **12**

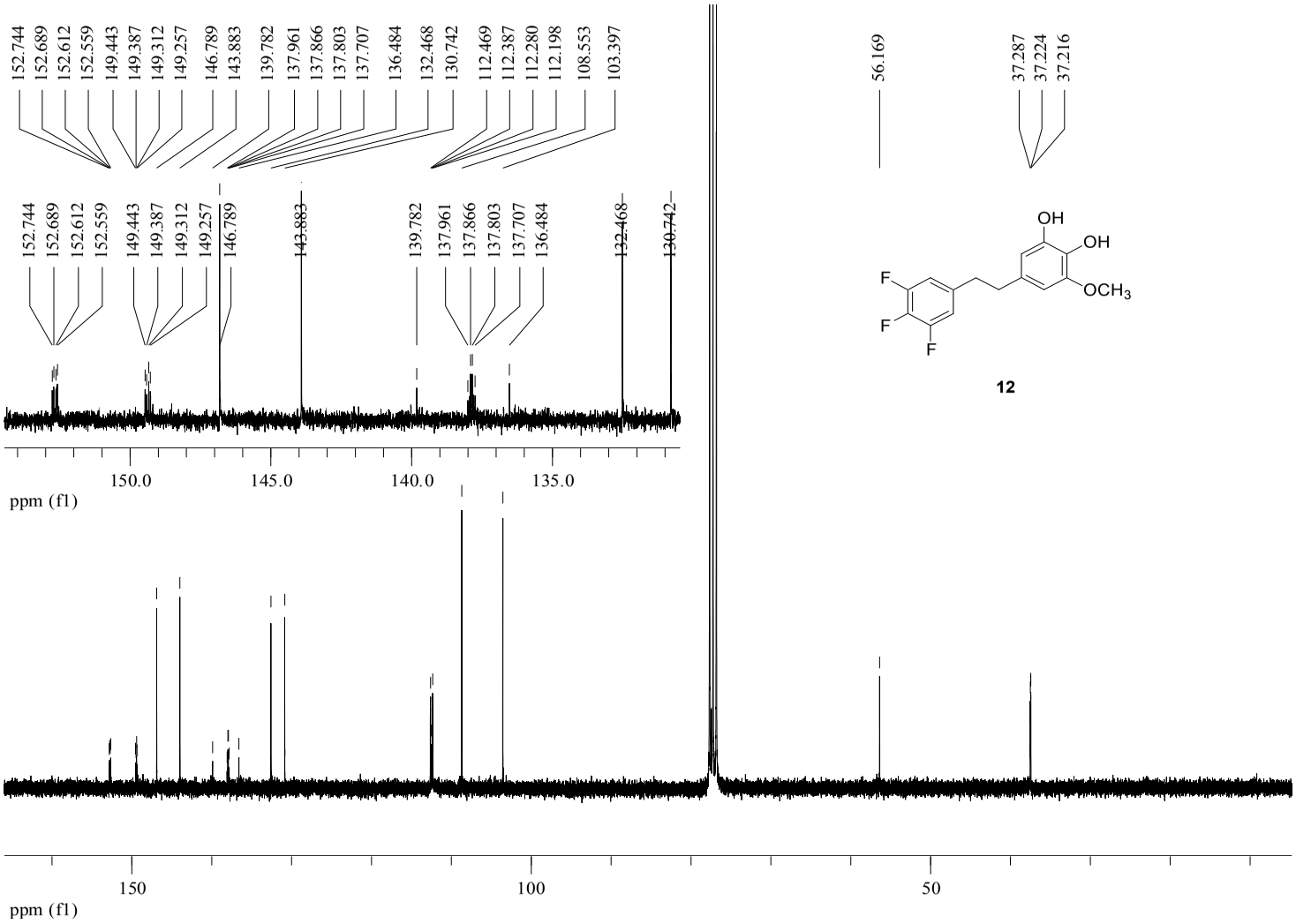

A.8. ^{13}C NMR ($CDCl_3$, 75 MHz) of Compound **12**

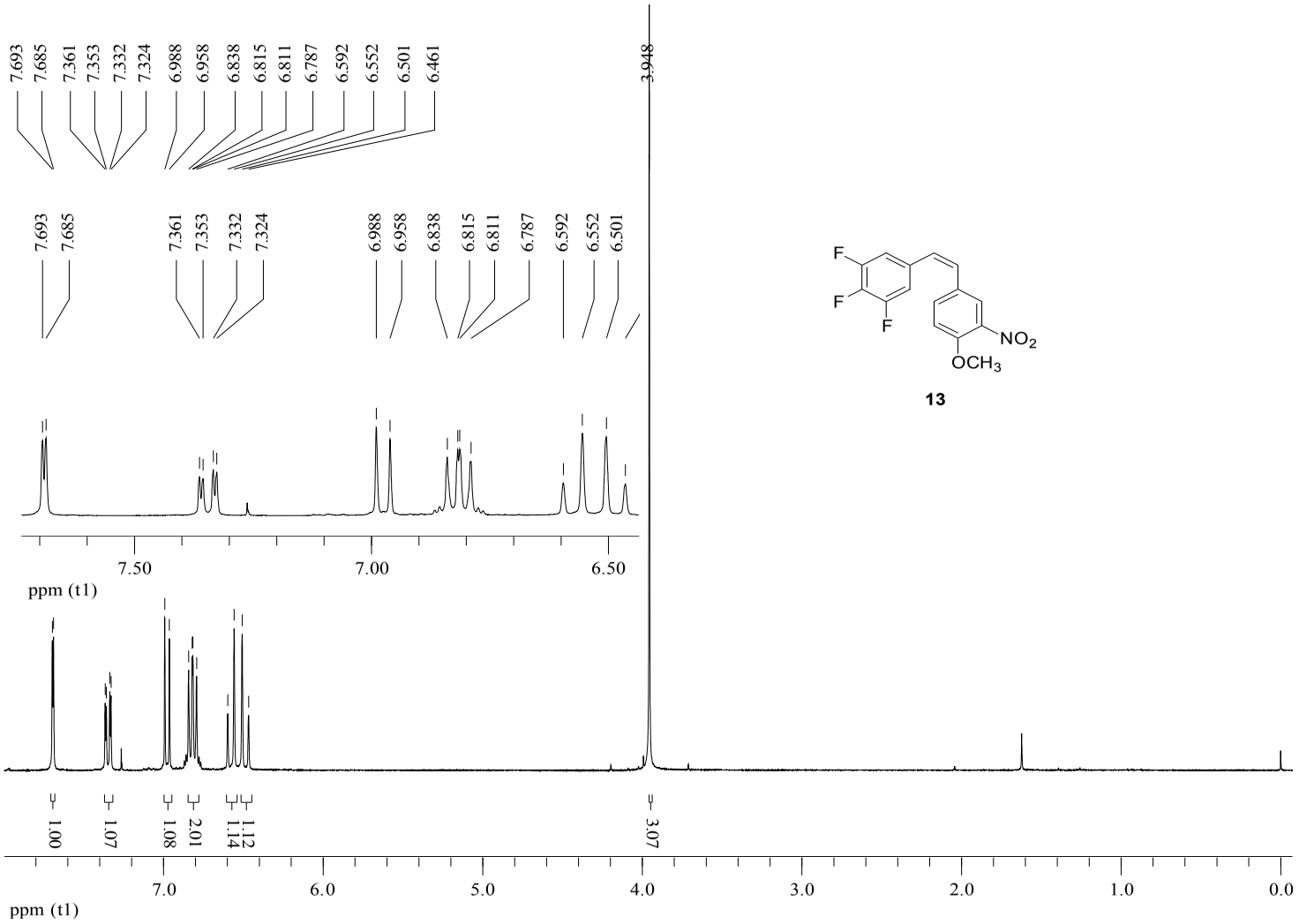

A.9. ^{1}H NMR ($CDCl_3$, 300 MHz) of Compound **13**

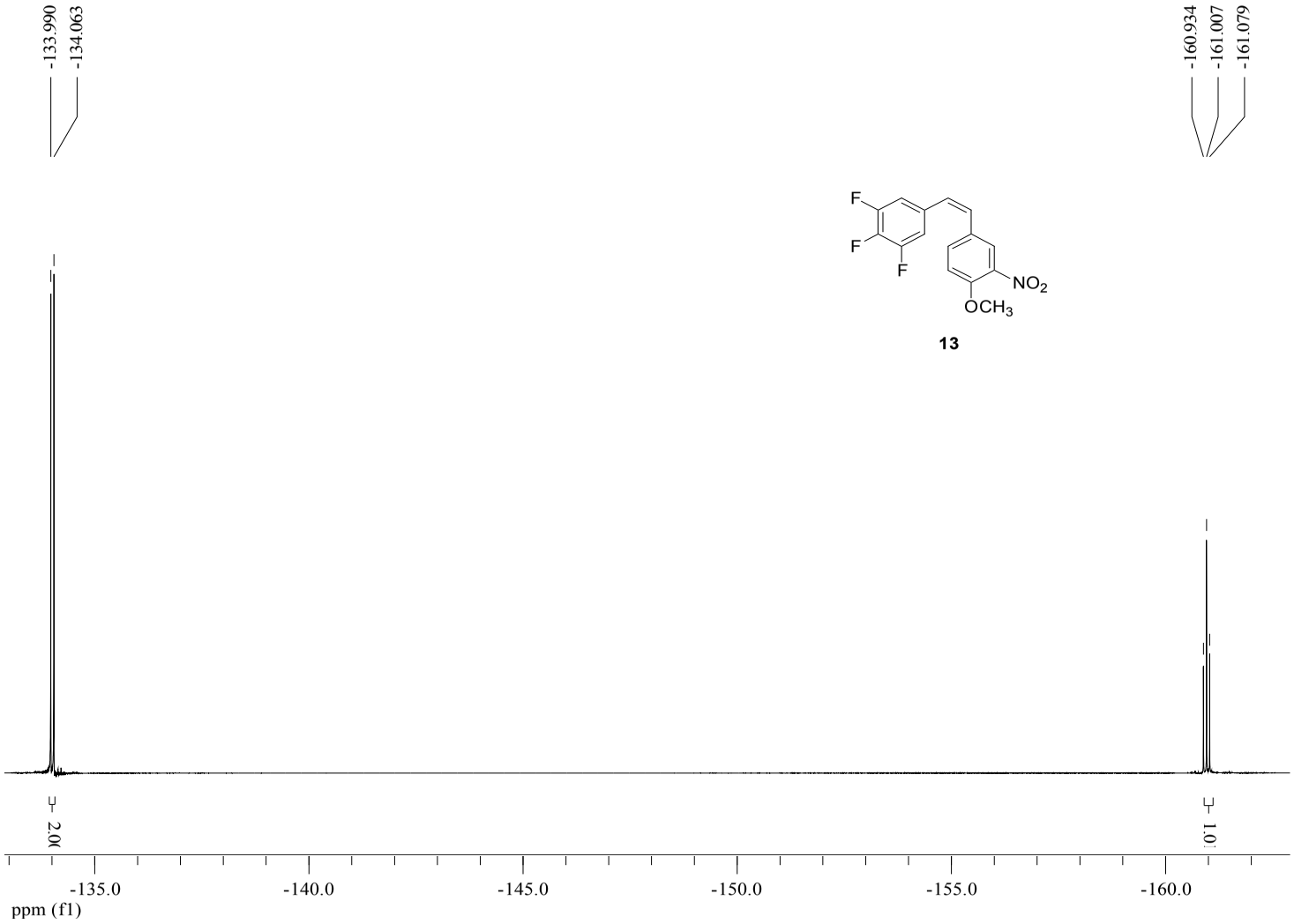

A.10. ^{19}F NMR ($CDCl_3$, 282 MHz) of Compound **13**

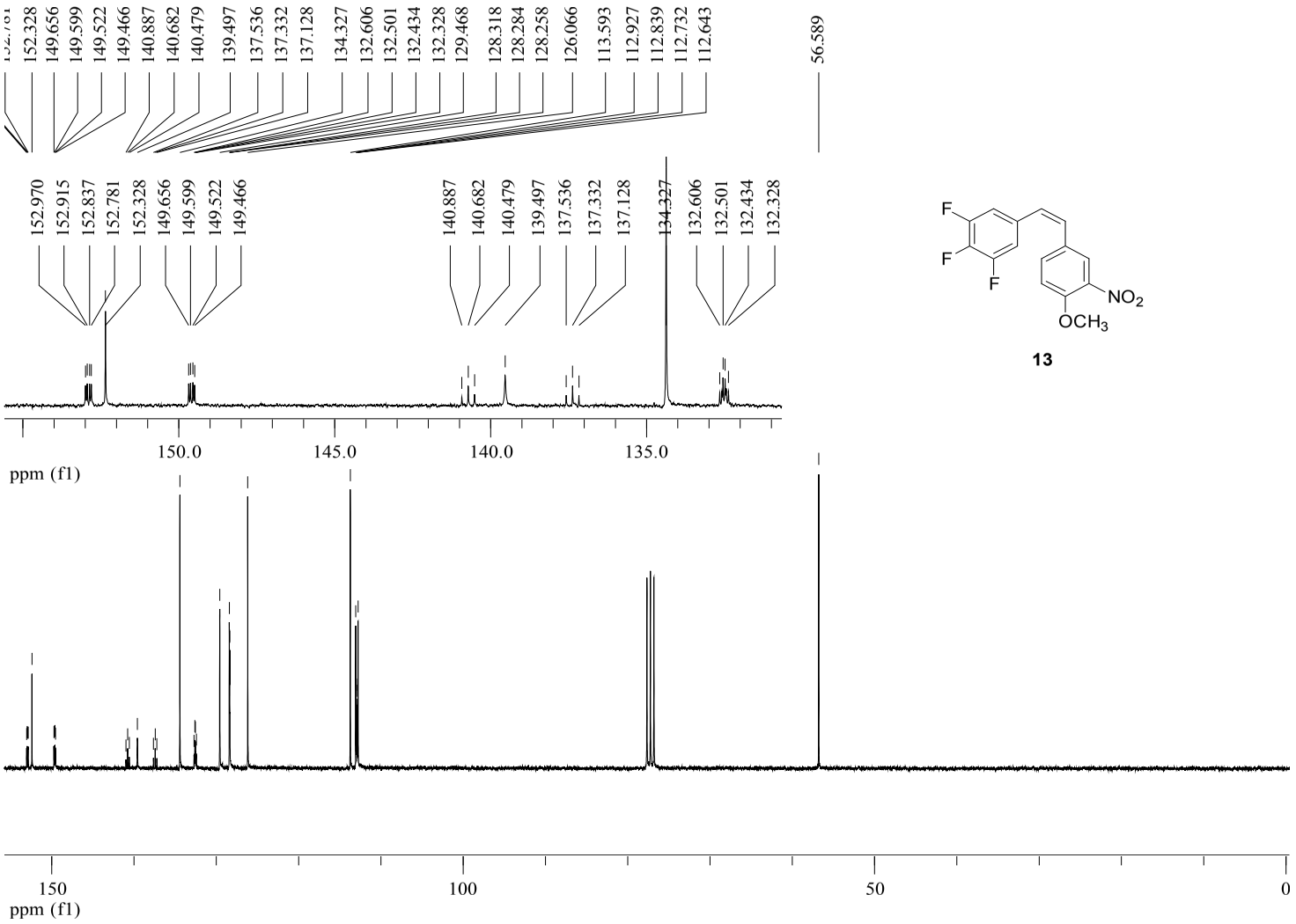

A.11. ^{13}C NMR ($CDCl_3$, 75 MHz) of Compound **13**

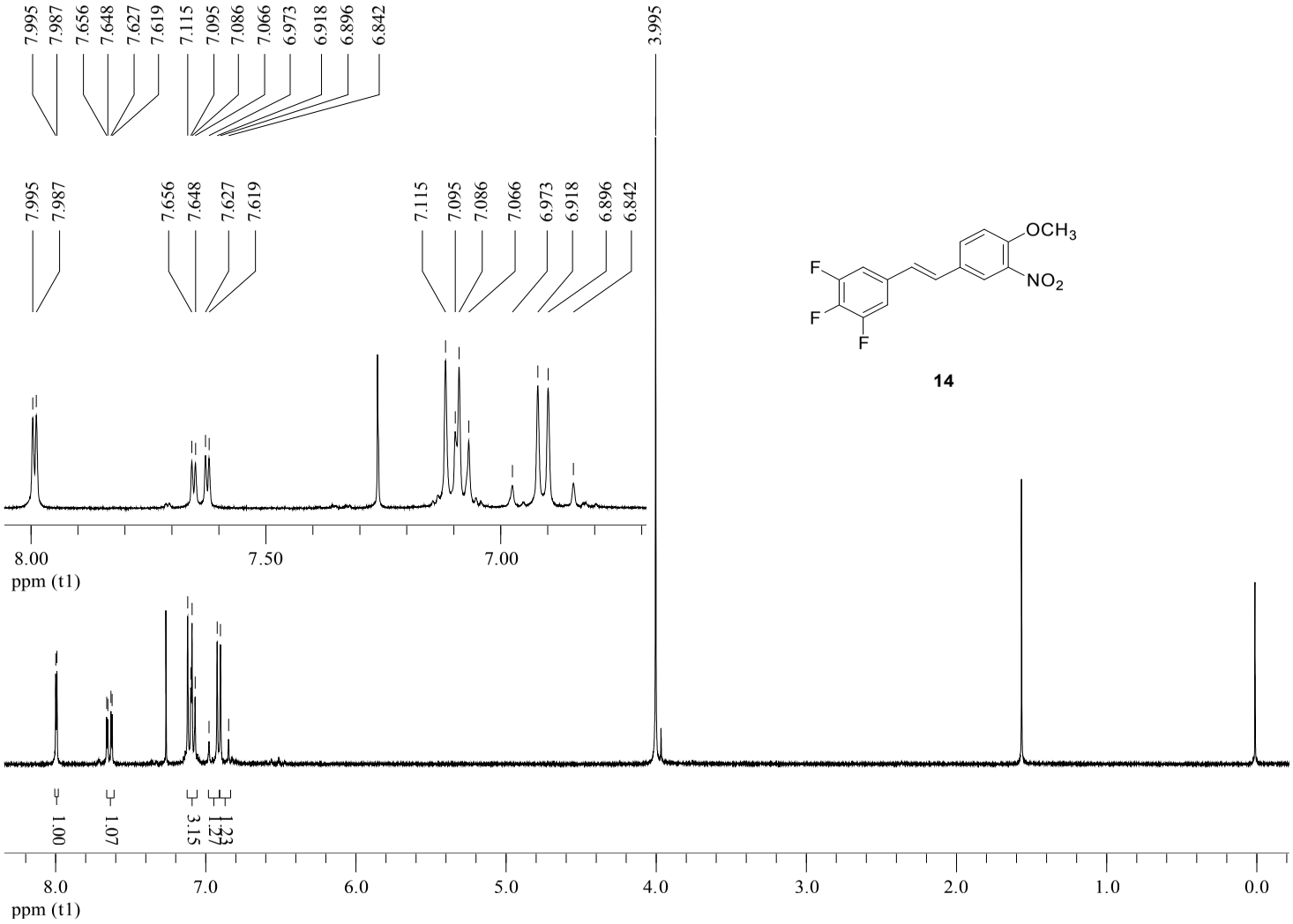

A.12. ^{1}H NMR ($CDCl_3$, 300 MHz) for Compound **14**

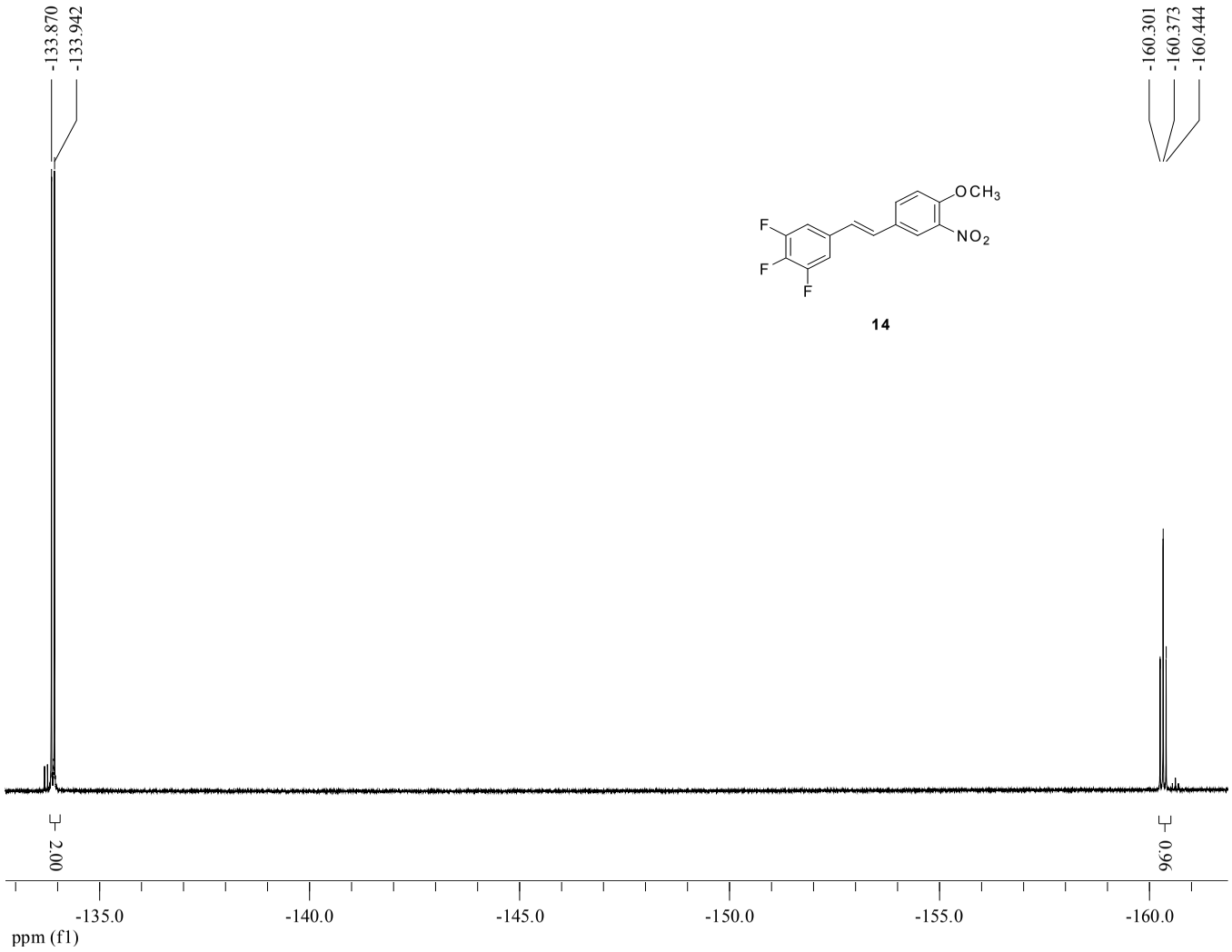

A.13. ^{19}F NMR ($CDCl_3$, 300 MHz) of Compound **14**

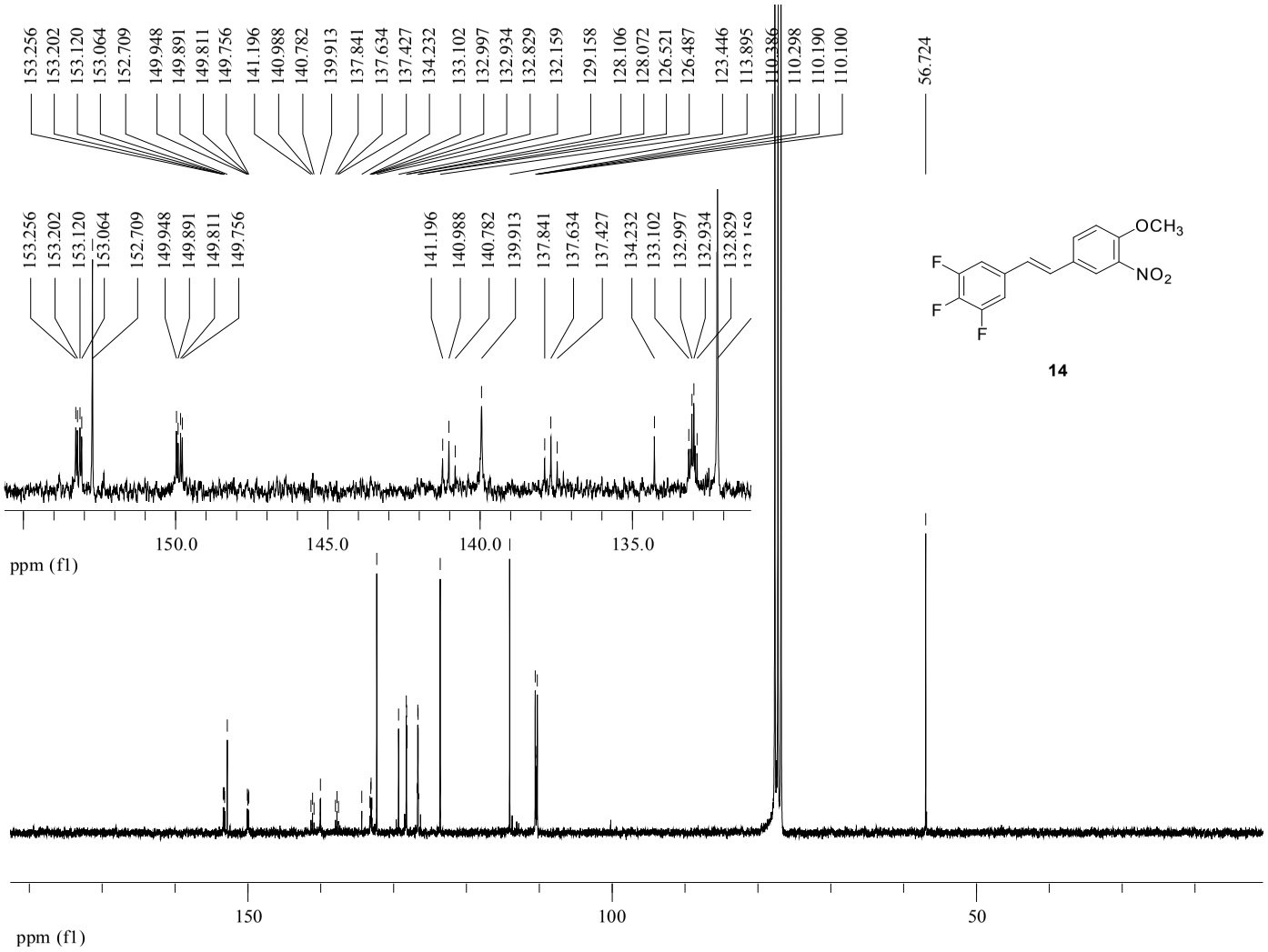

A.14. ^{13}C NMR ($CDCl_3$, 75 MHz) of Compound **14**

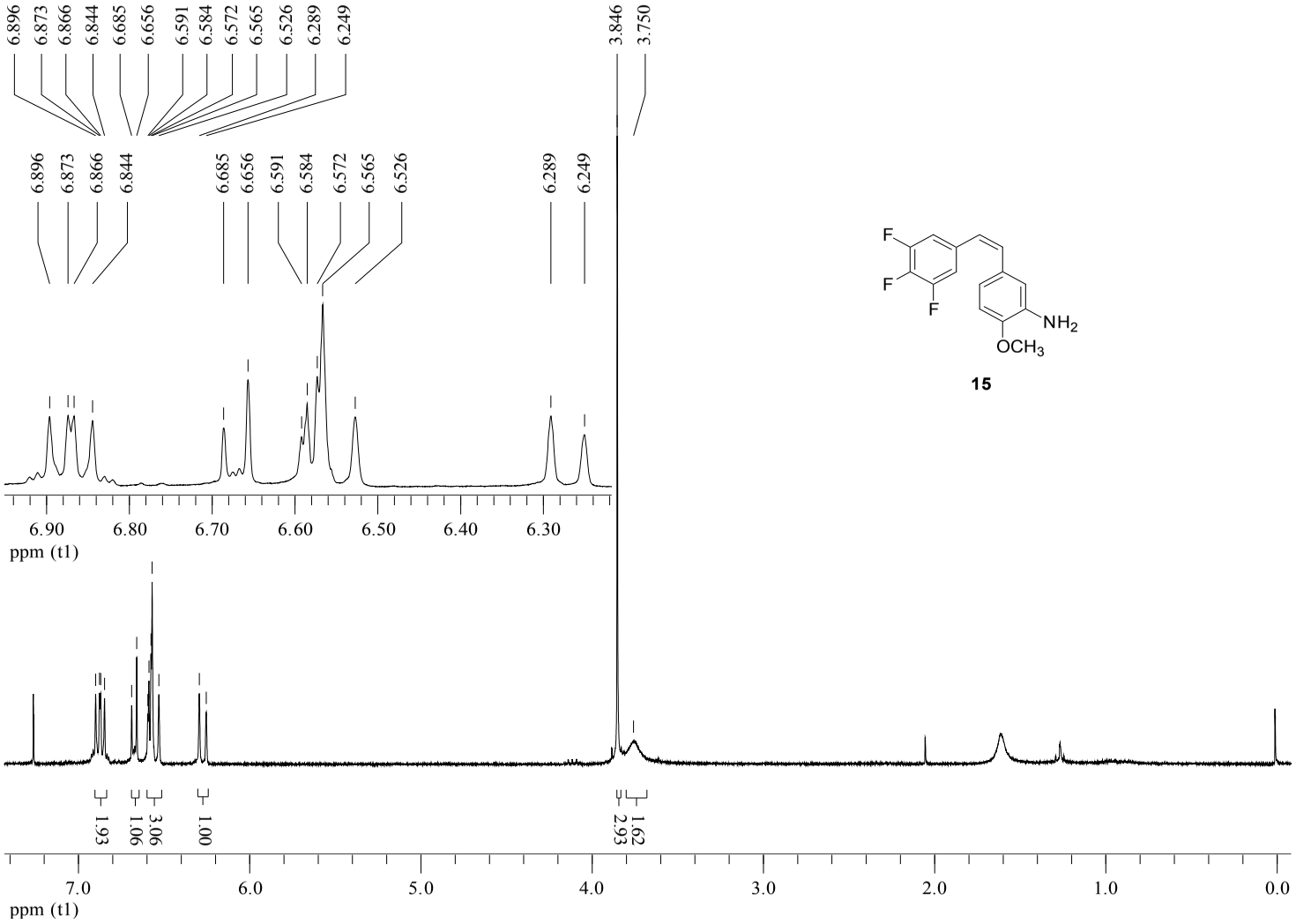

A.15. ^{1}H NMR ($CDCl_3$, 300 MHz) of Compound **15**

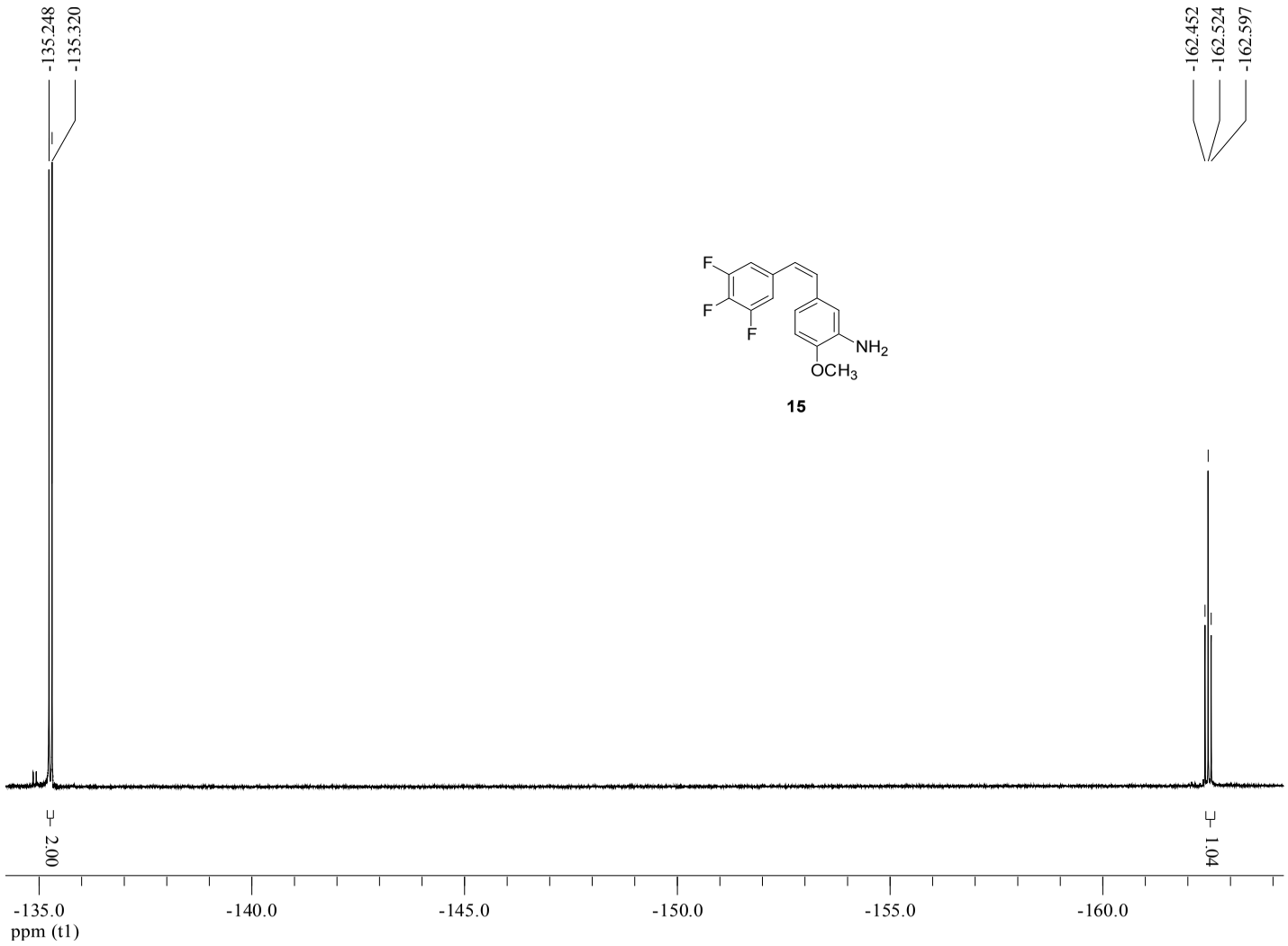

A.16. ^{19}F ($CDCl_3$, 282 MHz) of Compound **15**

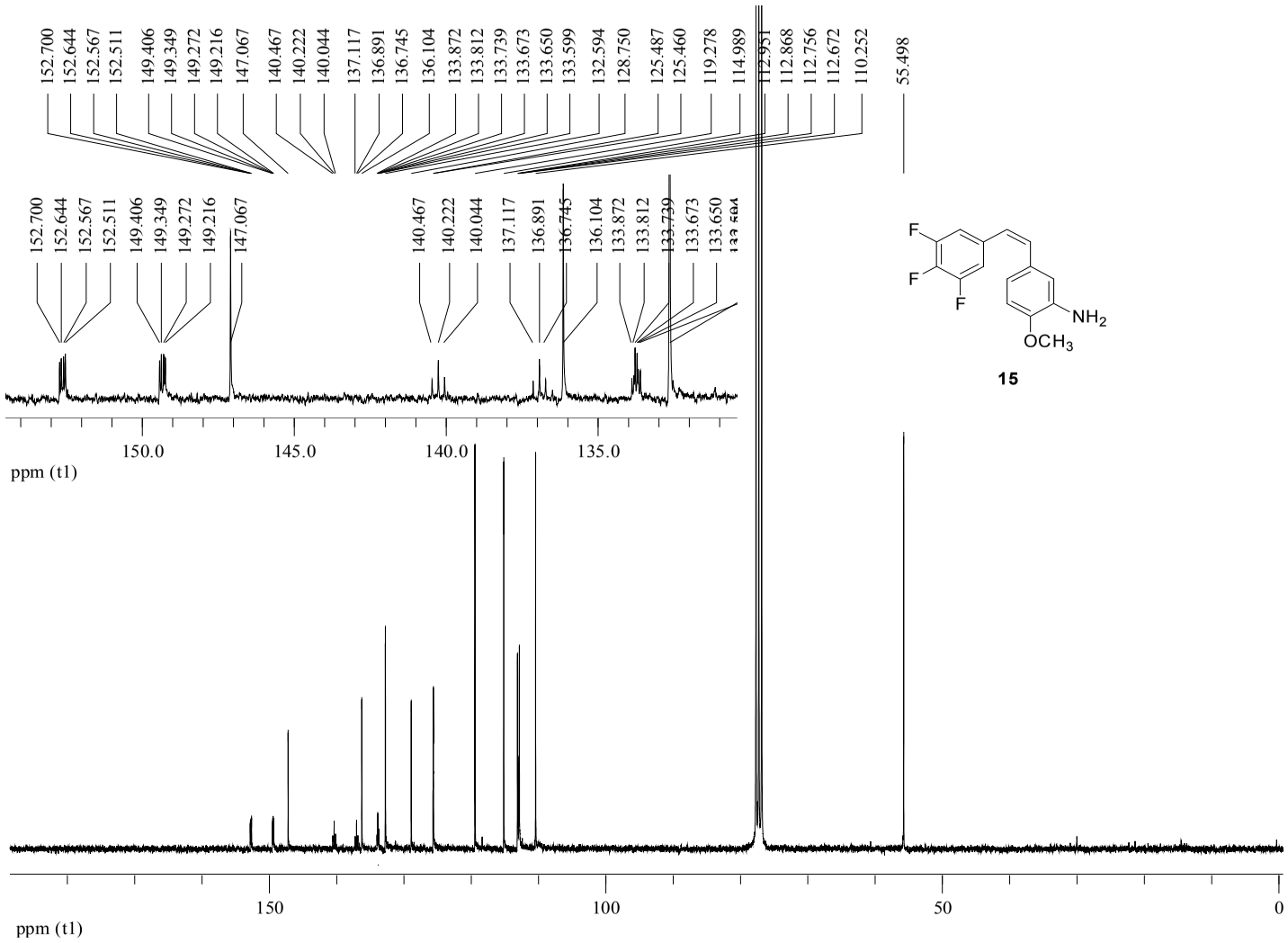

A.17. ^{13}C NMR ($CDCl_3$, 75 MHz) of Compound **15**

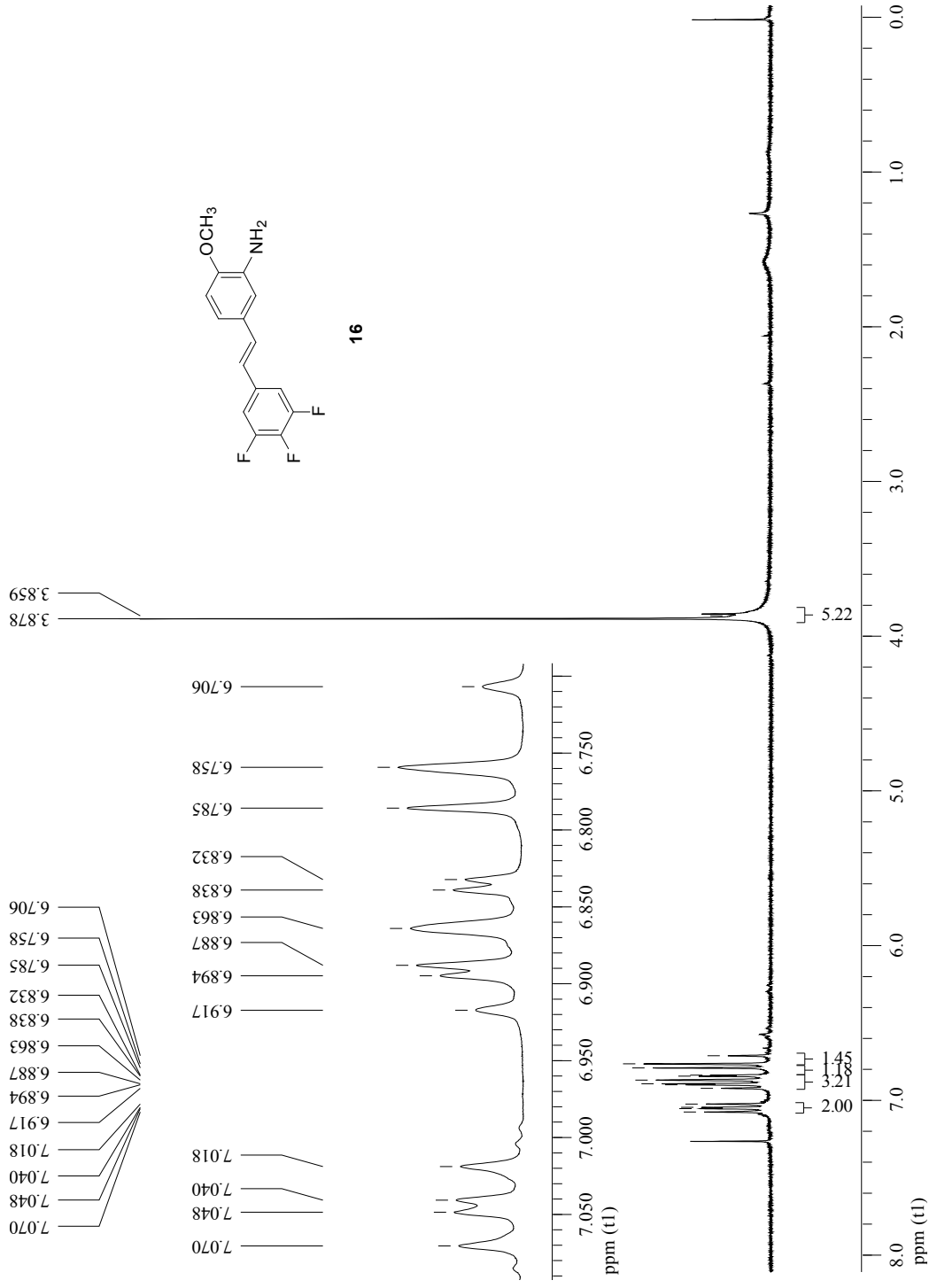

A.18. ^{1}H NMR ($CDCl_3$, 300 MHz) of Compound **16**

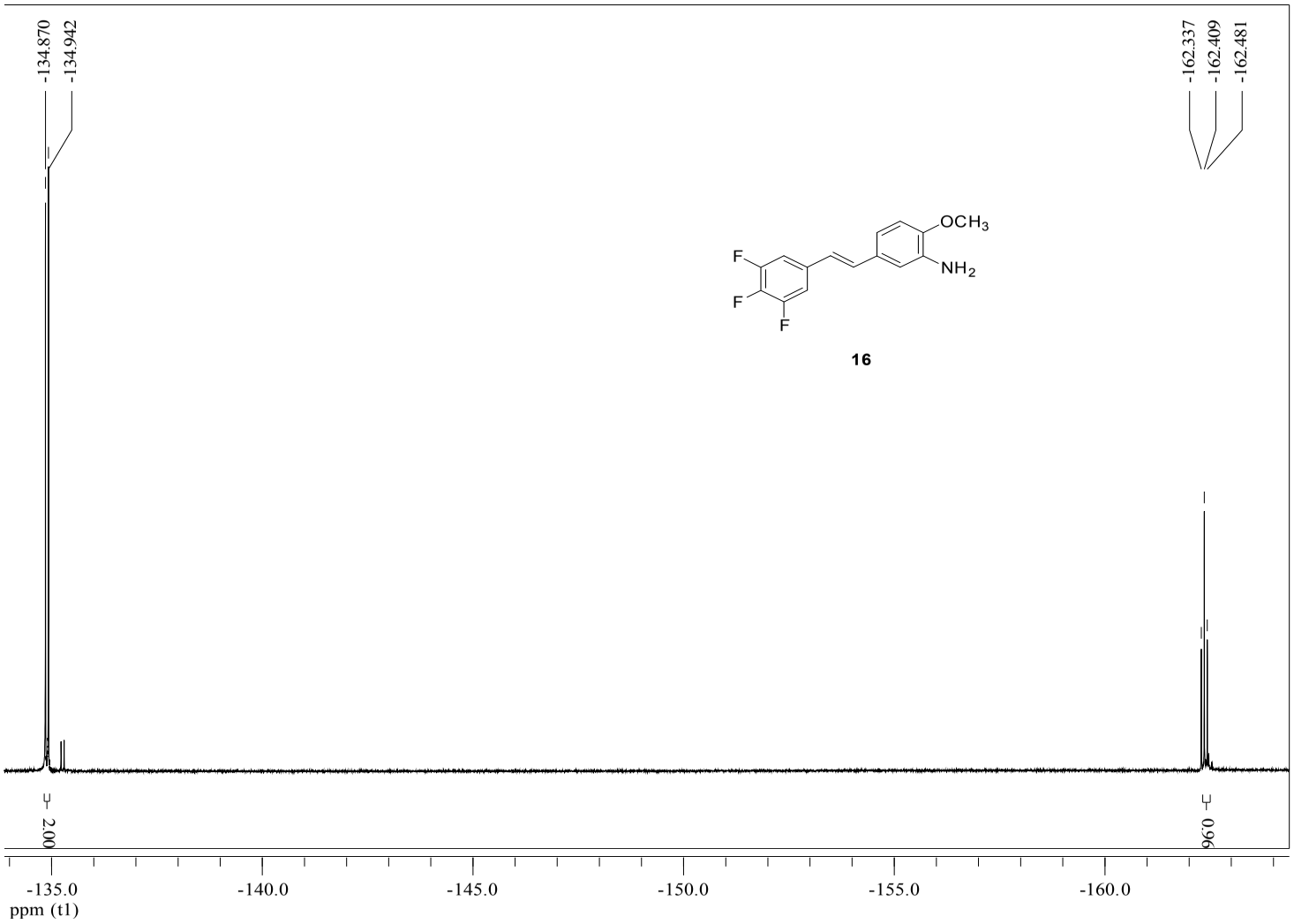

A.19. ^{19}F NMR ($CDCl_3$, 282 MHz) of Compound **16**

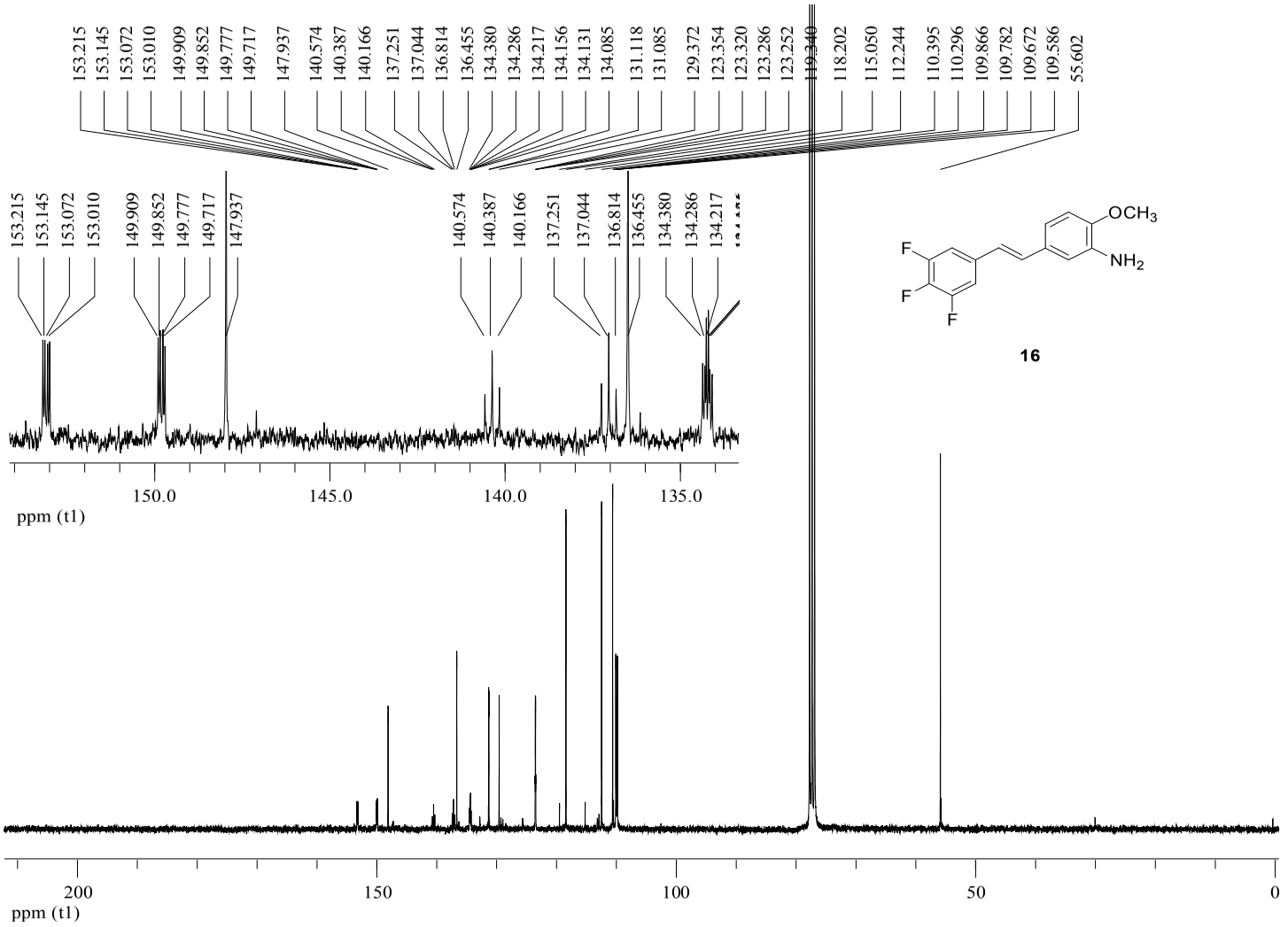

A.20. ^{13}C NMR ($CDCl_3$, 300 MHz) of Compound **16**

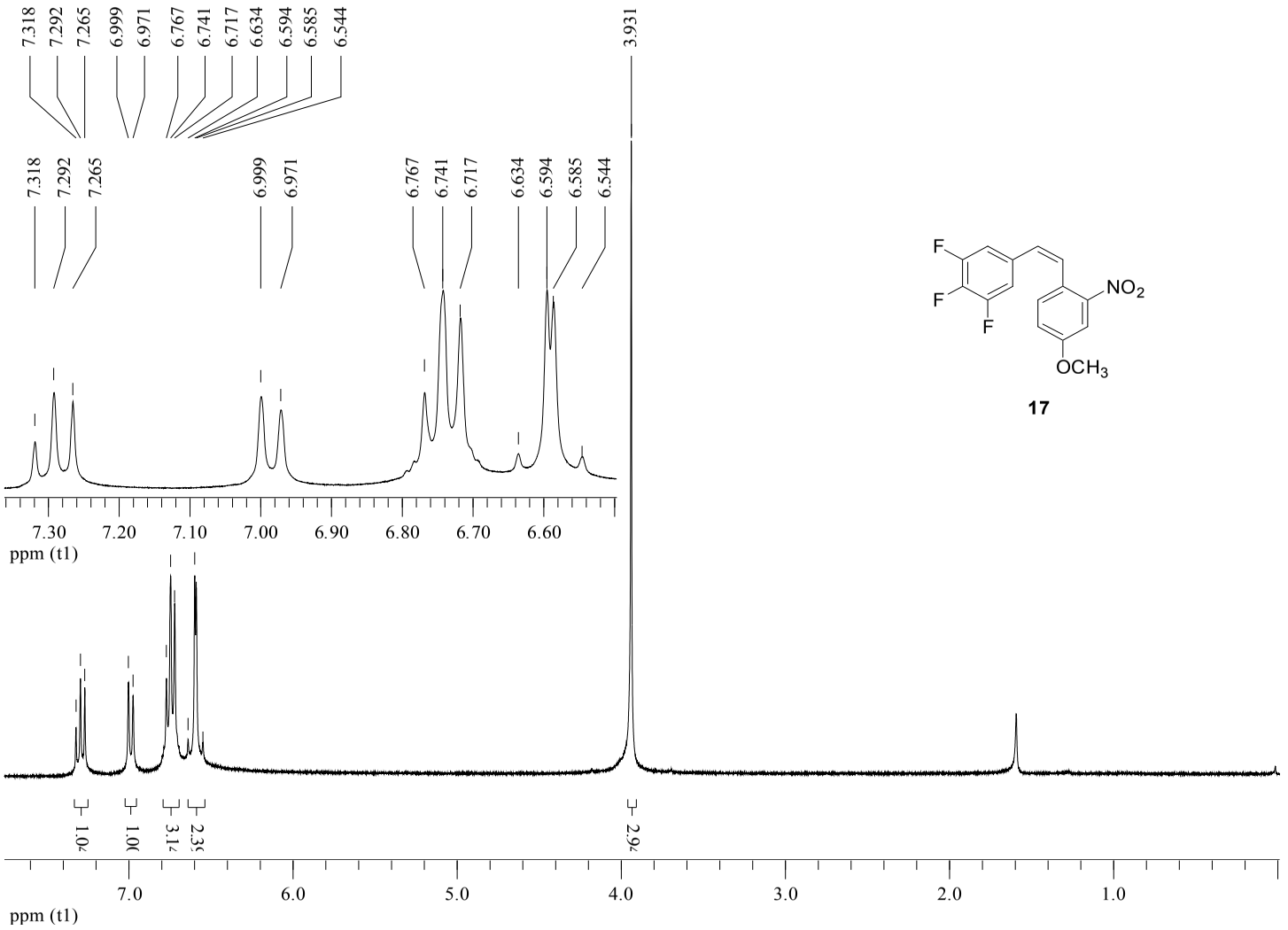

A.21. ^{1}H NMR ($CDCl_3$, 300 MHz) of Compound **17**

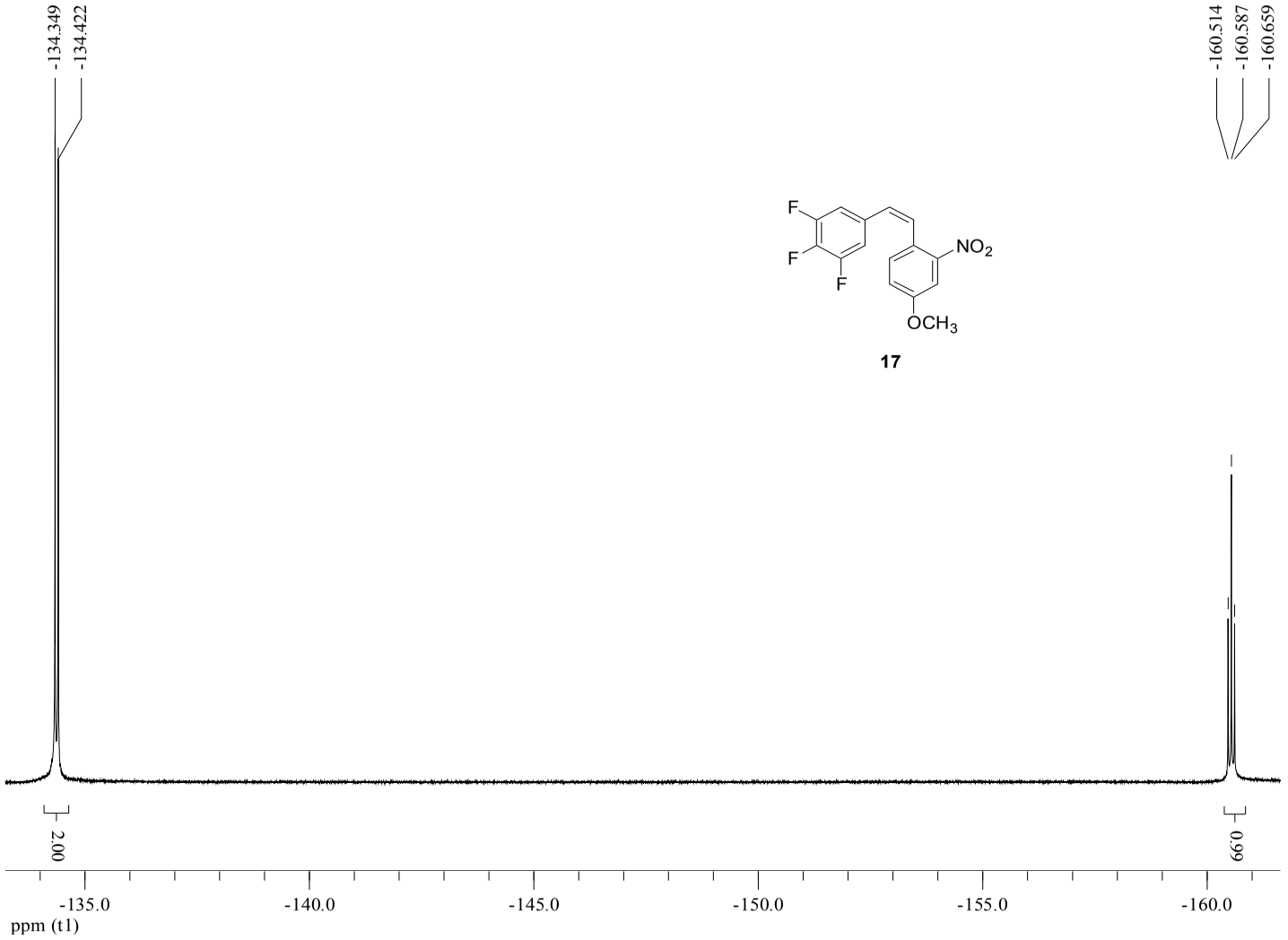

A.22. ^{19}F NMR ($CDCl_3$, 282 MHz) of Compound **17**

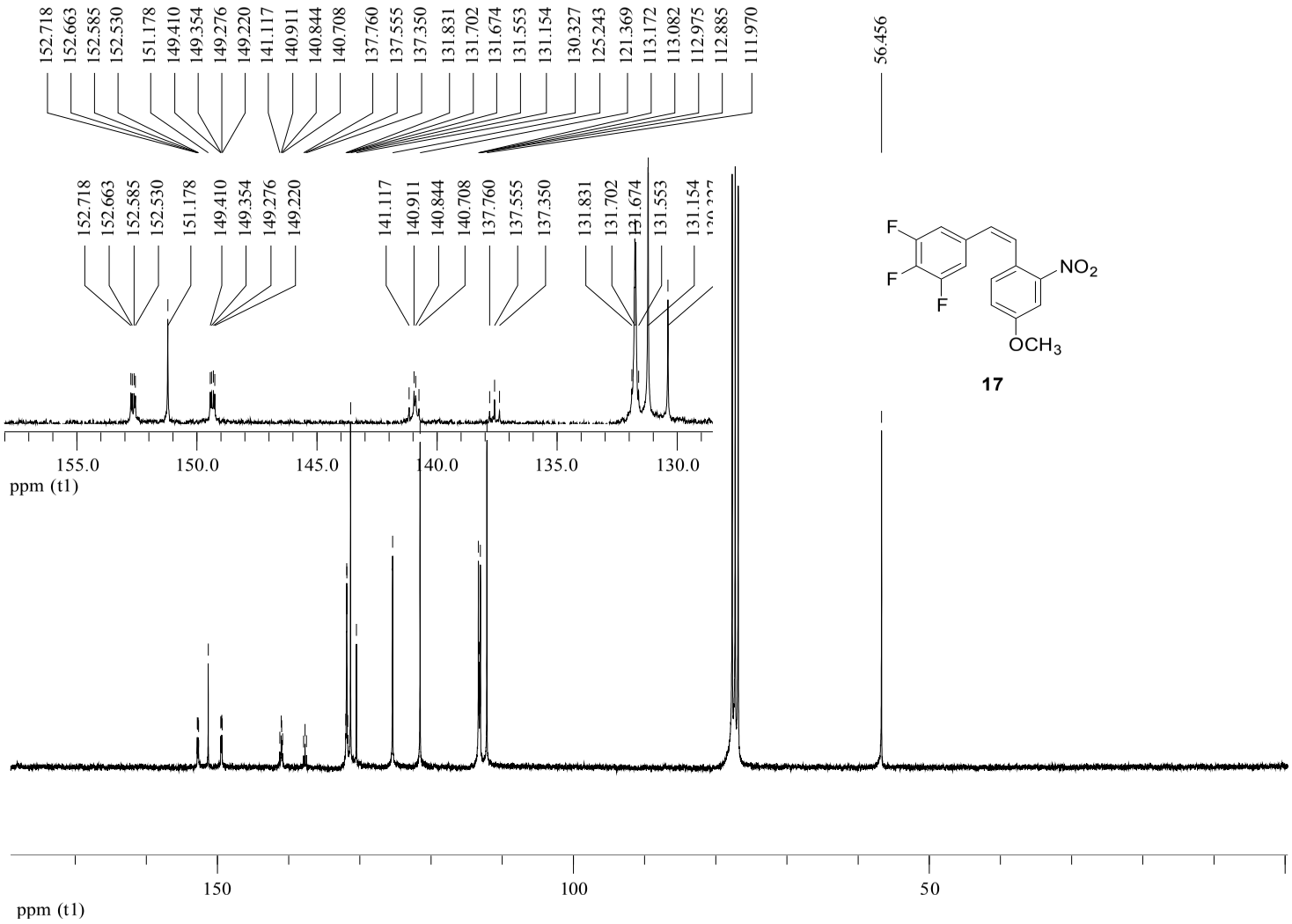

A.23. ^{13}C NMR ($CDCl_3$, 75 MHz) of Compound **17**

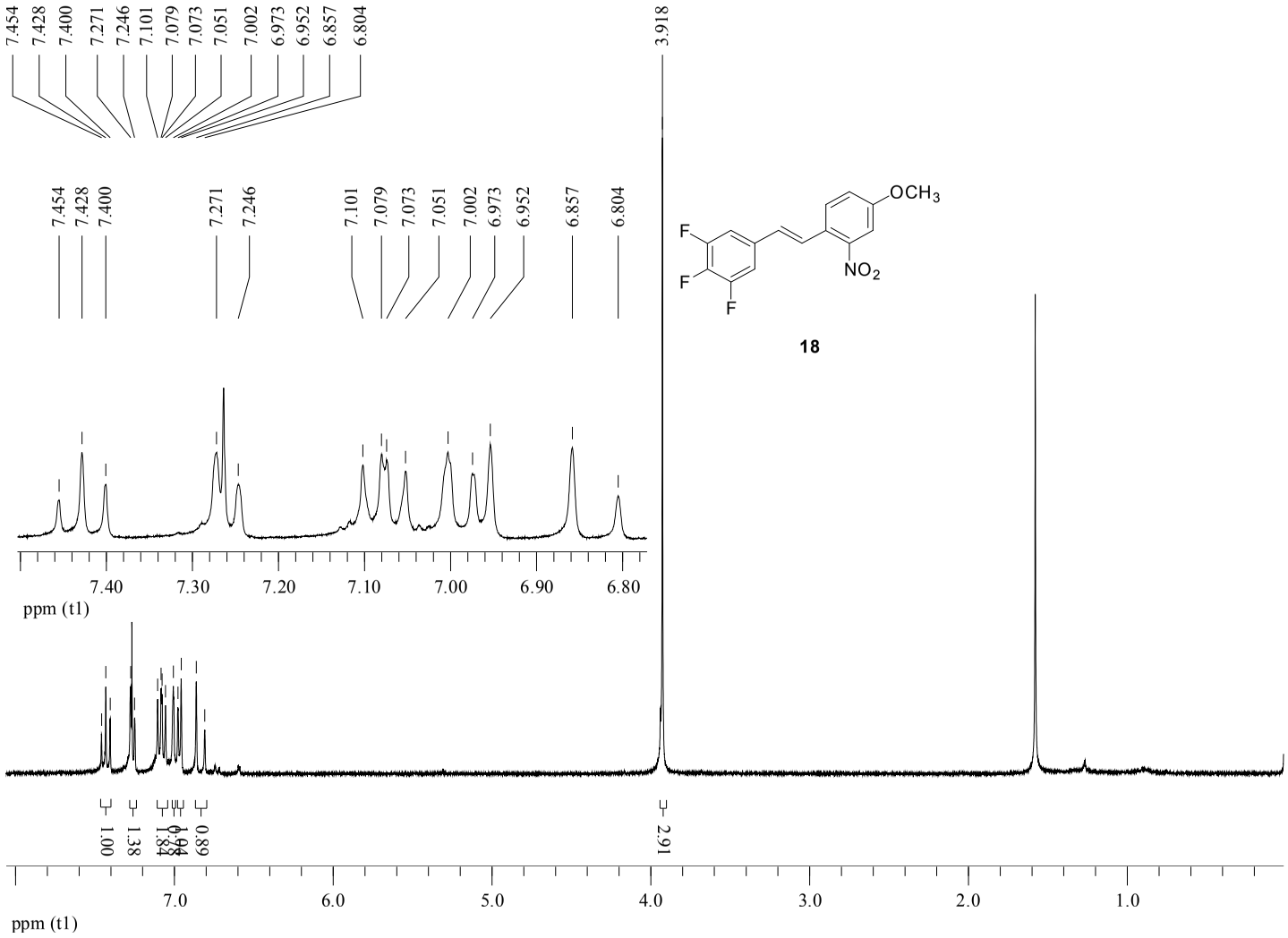

A.24. ^{1}H NMR ($CDCl_3$, 300 MHz) of Compound **18**

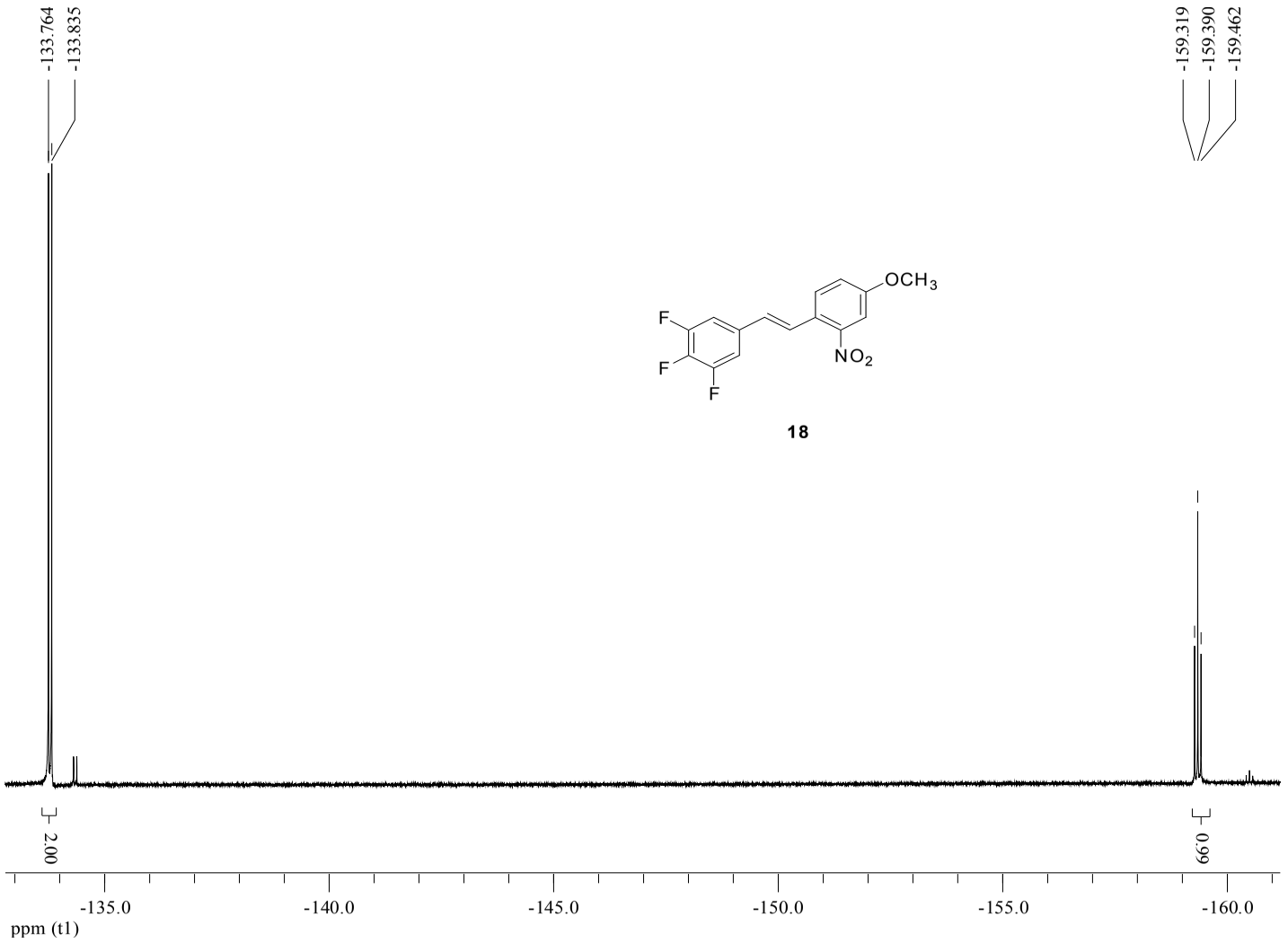

A.25. ^{19}F NMR ($CDCl_3$, 282 MHz) of Compound **18**

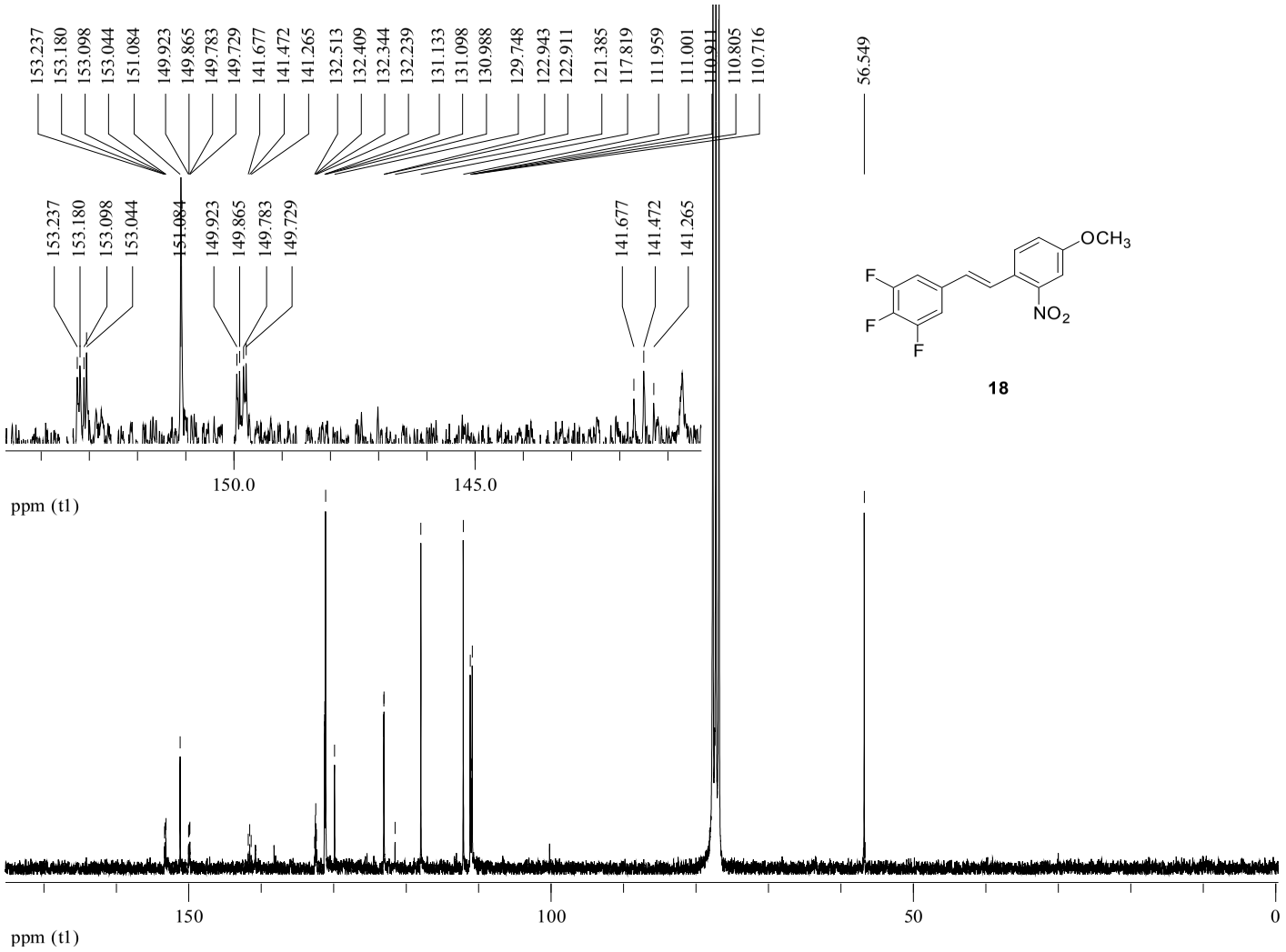

A.26. ^{13}C NMR ($CDCl_3$, 75 MHz) of Compound **18**

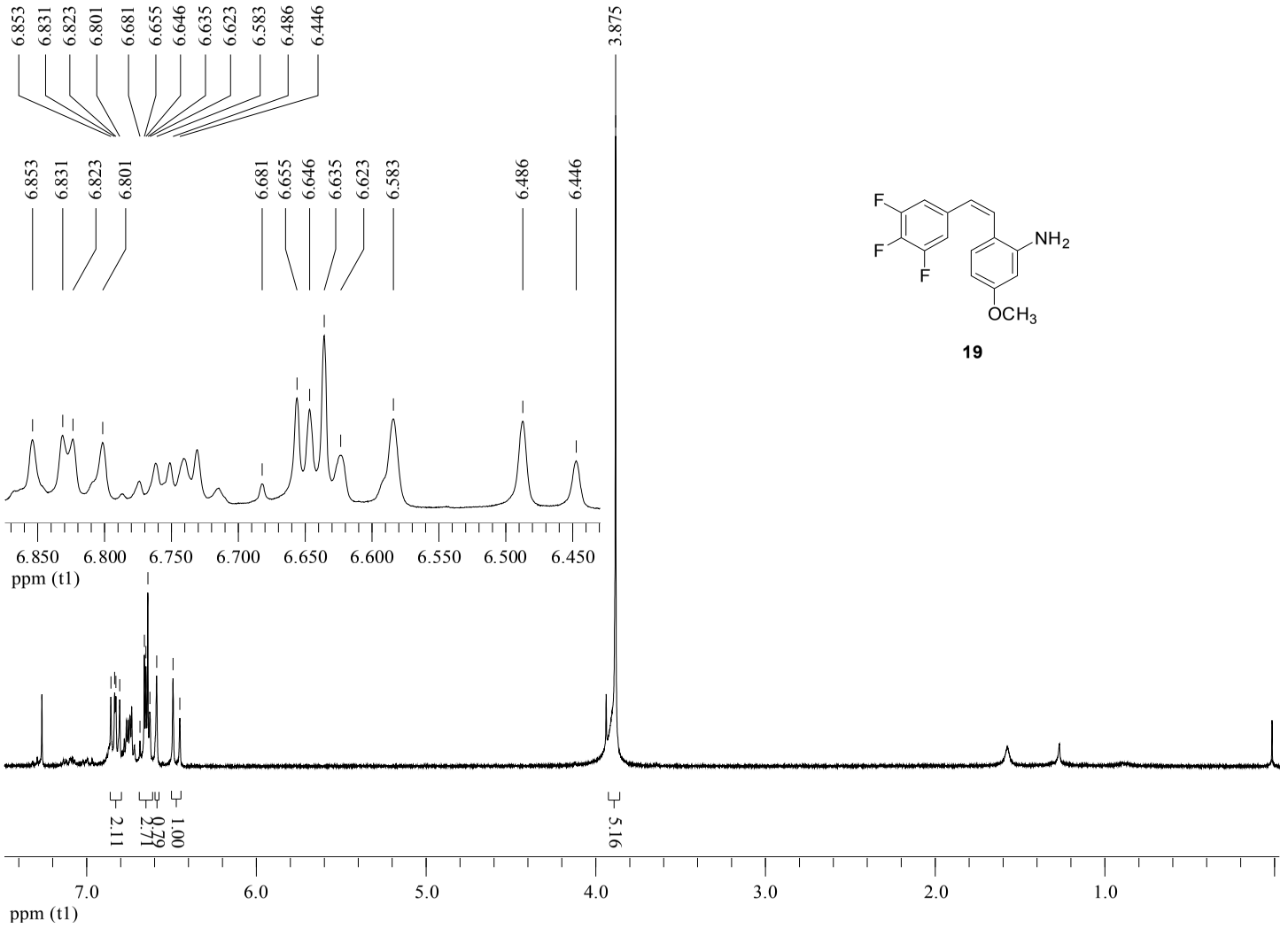

A.27. ^{1}H NMR ($CDCl_3$, 300 MHz) of Compound **19**

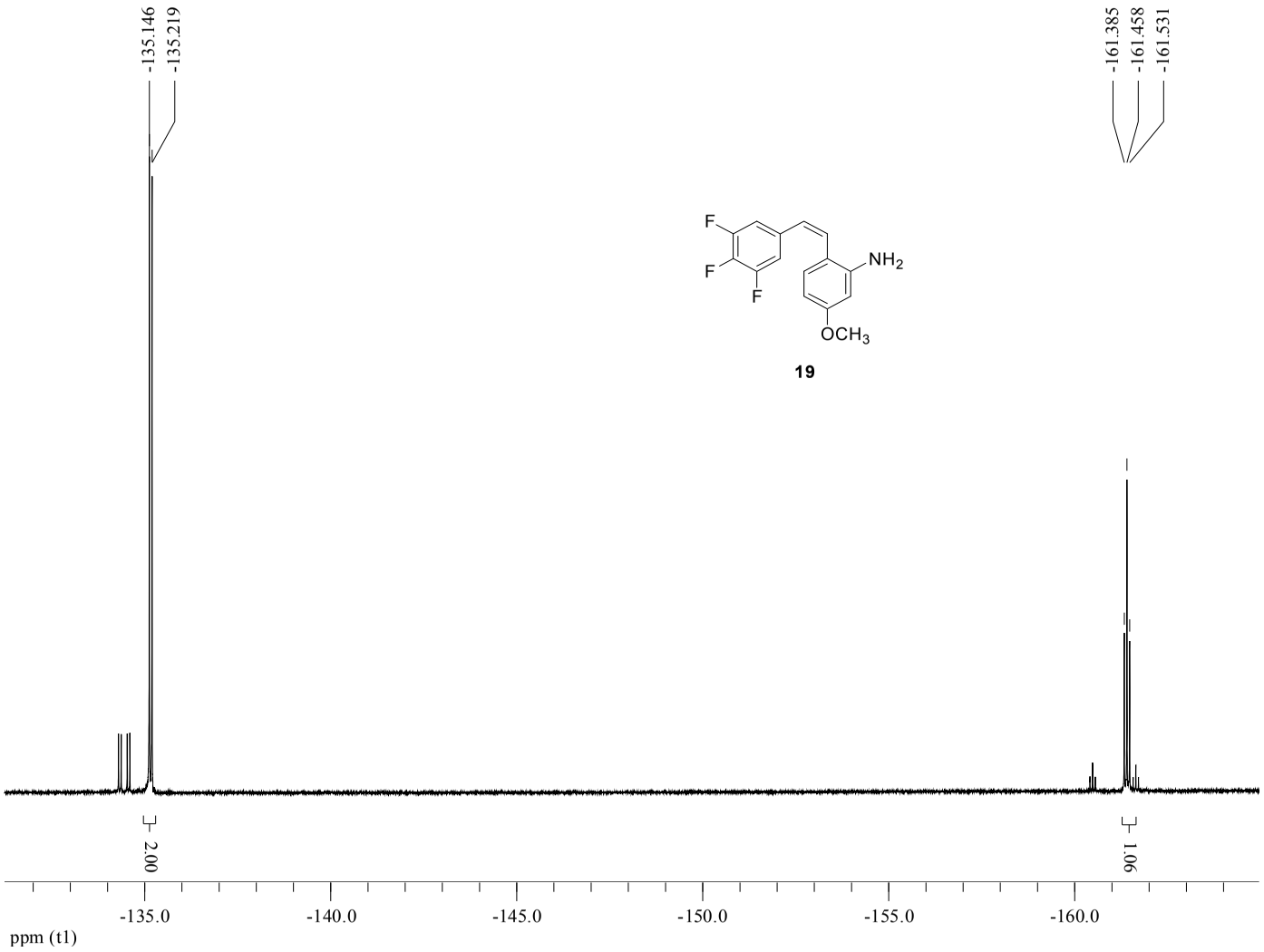

A.28. ^{19}F NMR ($CDCl_3$, 282 MHz) of Compound **19**

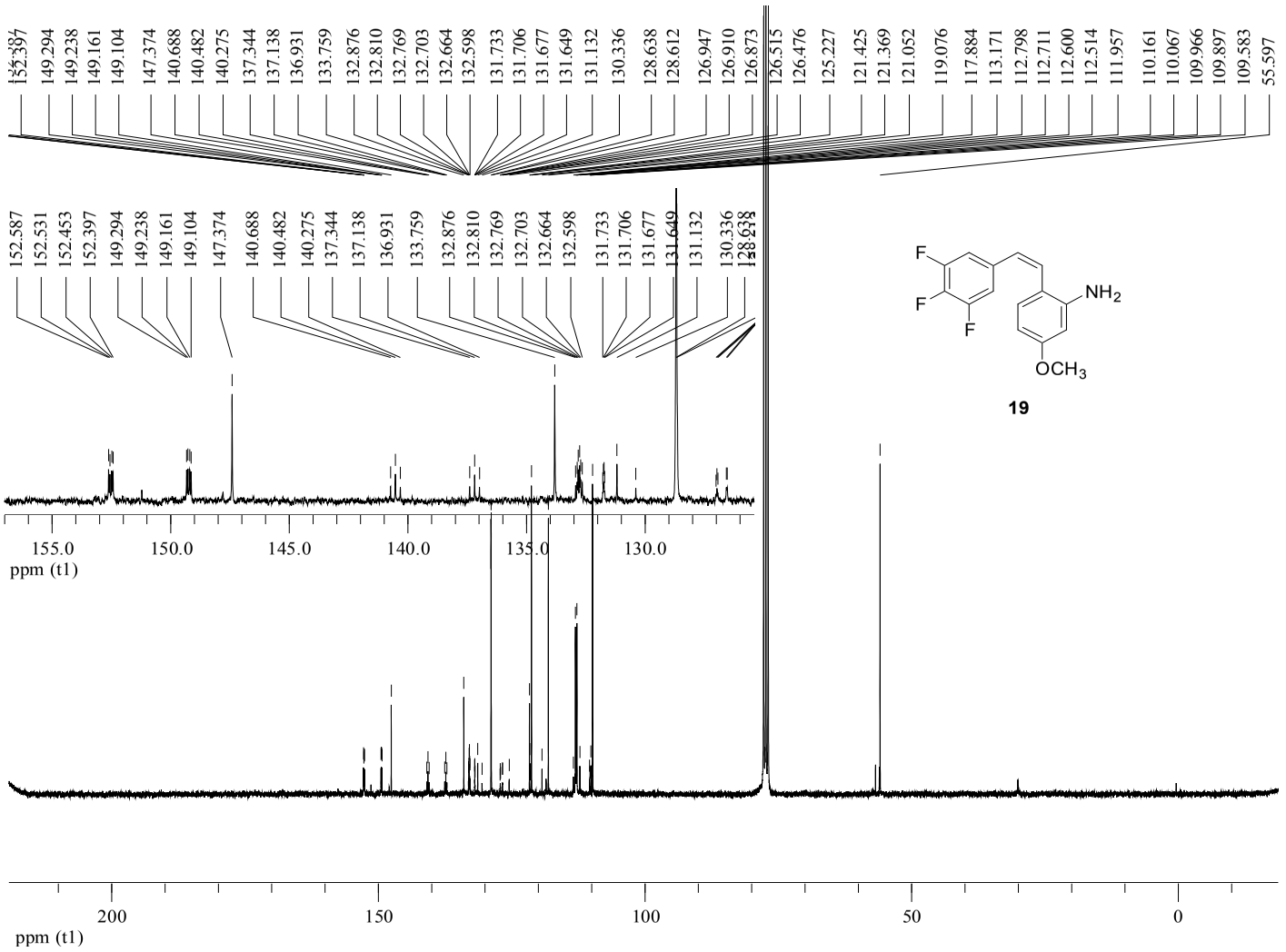

A.29. ^{13}C NMR ($CDCl_3$, 75 MHz) of Compound **19**

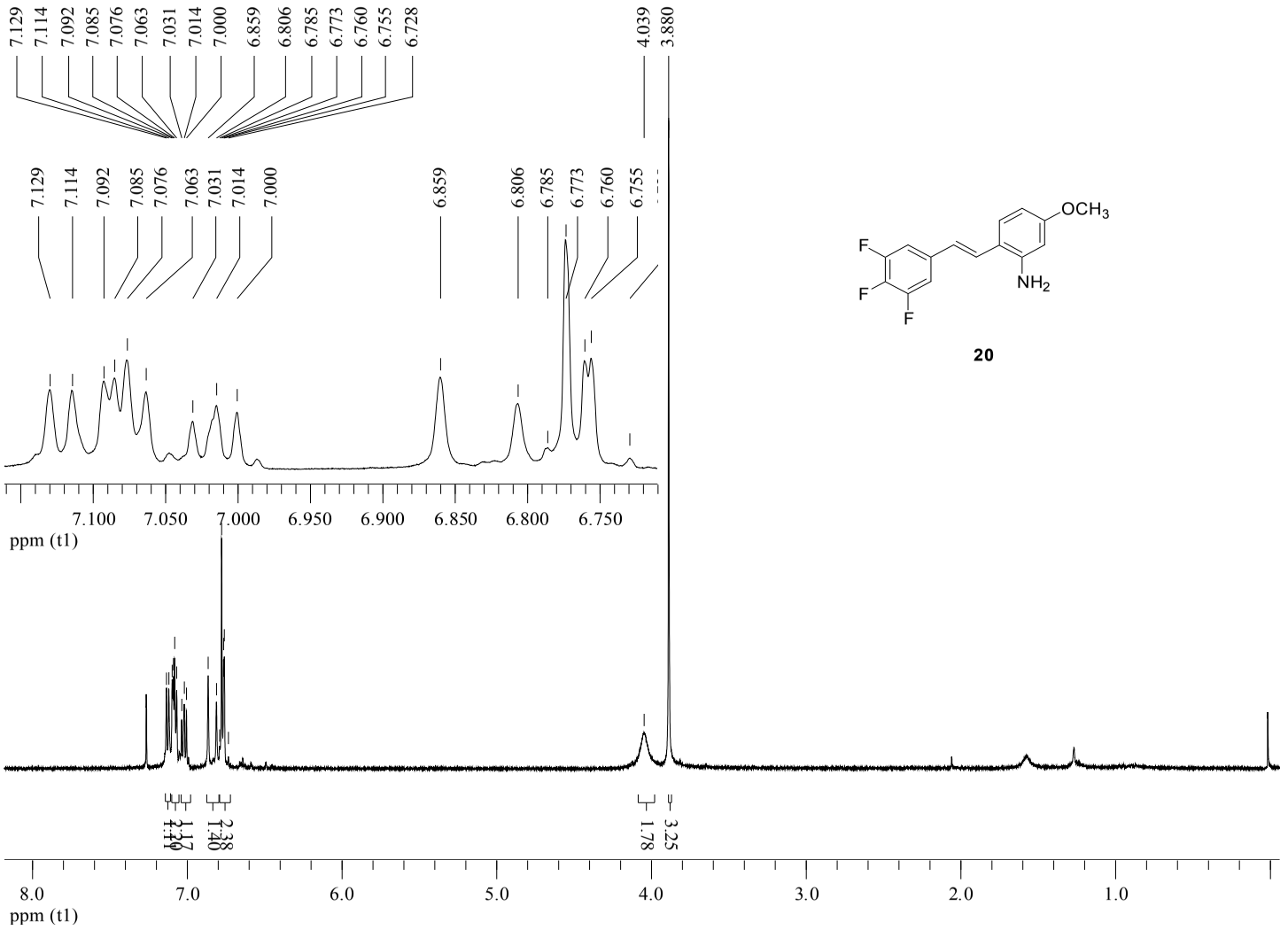

A.30. ^{1}H NMR ($CDCl_3$, 300 MHz) of Compound **20**

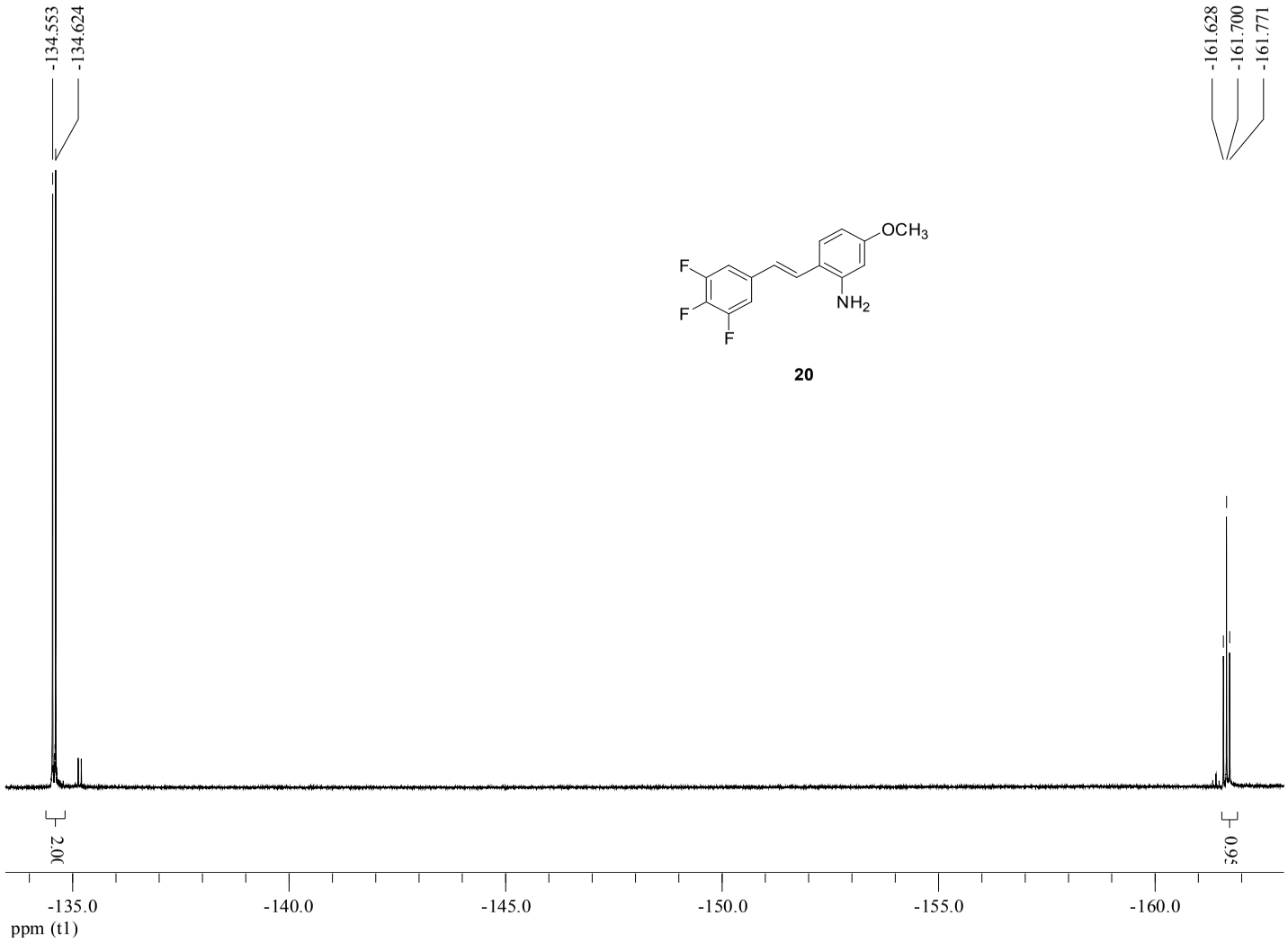

A.31. ^{19}F NMR ($CDCl_3$, 282 MHz) of Compound **20**

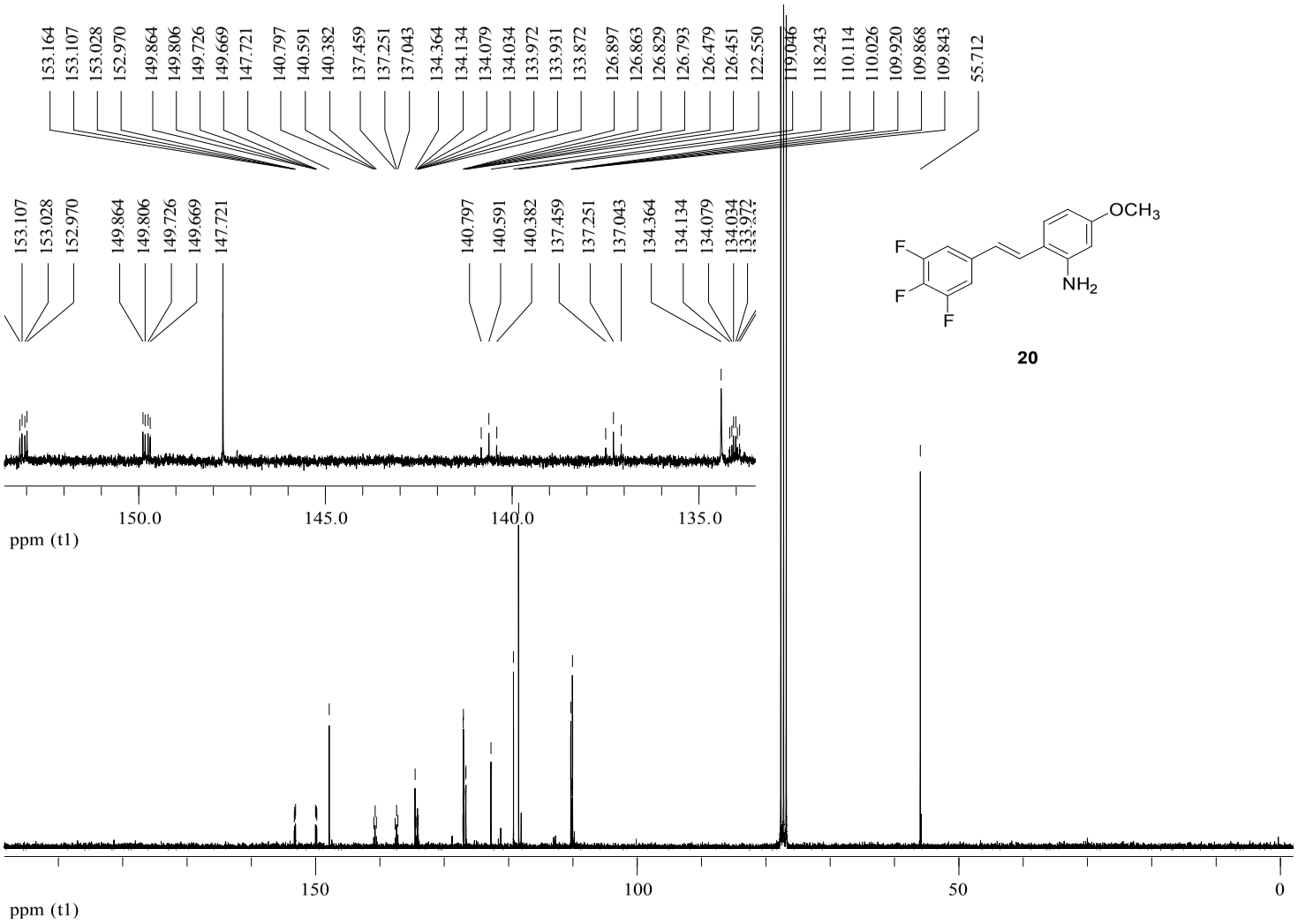

A.32. ^{13}C NMR ($CDCl_3$, 75 MHz) of Compound **20**

A.33. ^{1}H NMR ($CDCl_3$, 300 MHz) of Compound **37**

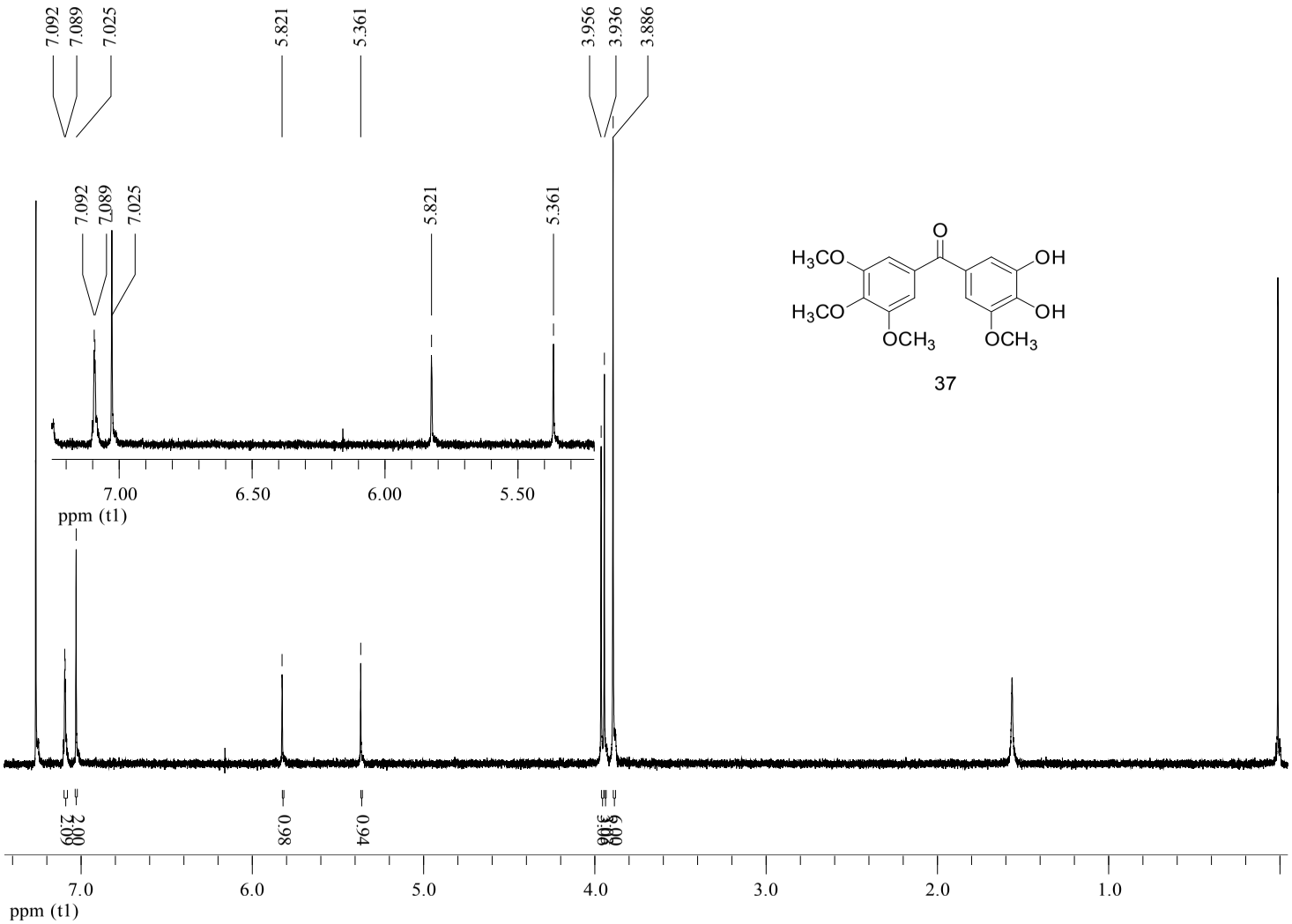

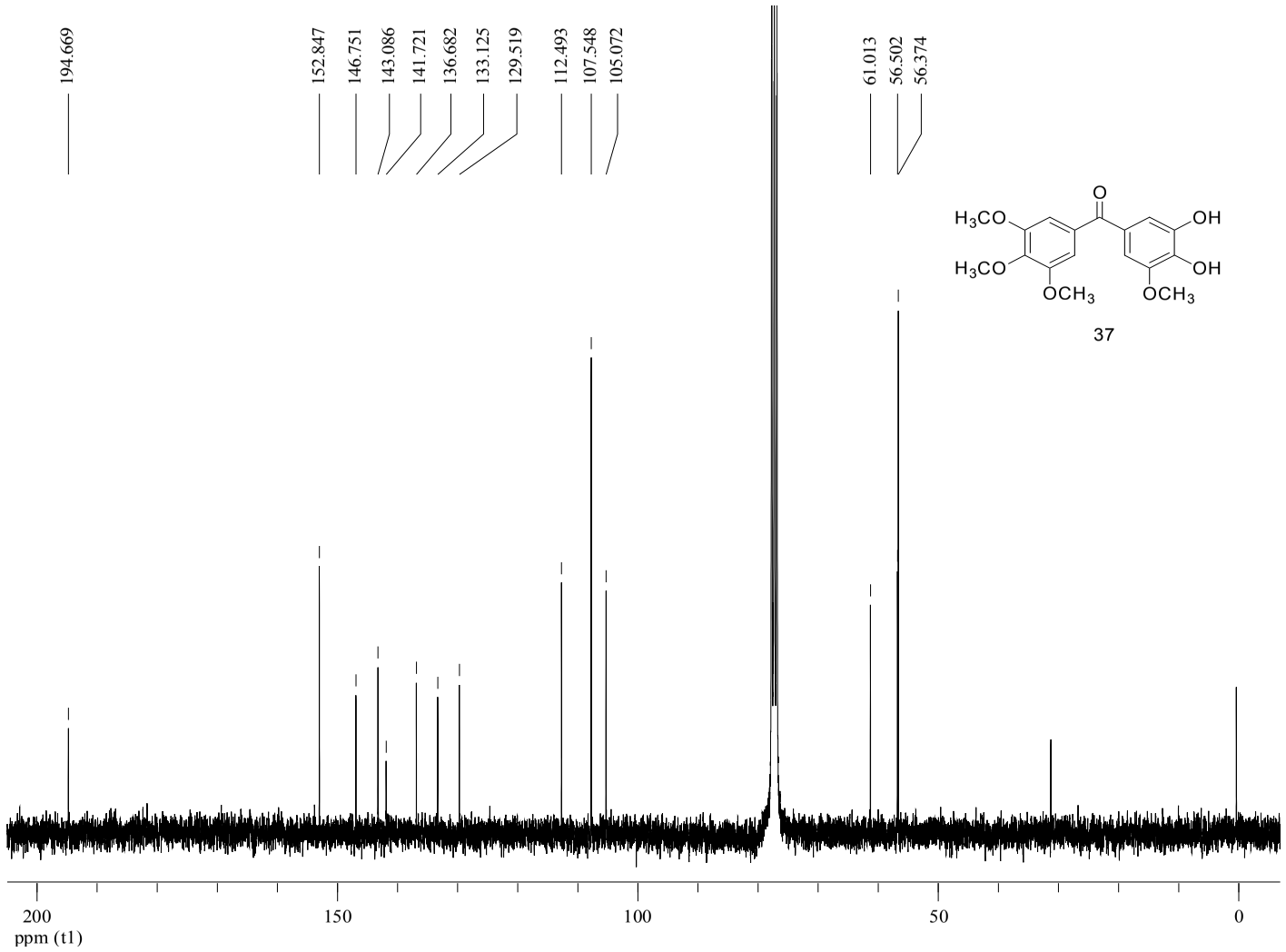

A.34. ^{13}C NMR ($CDCl_3$, 75 MHz) of Compound **37**

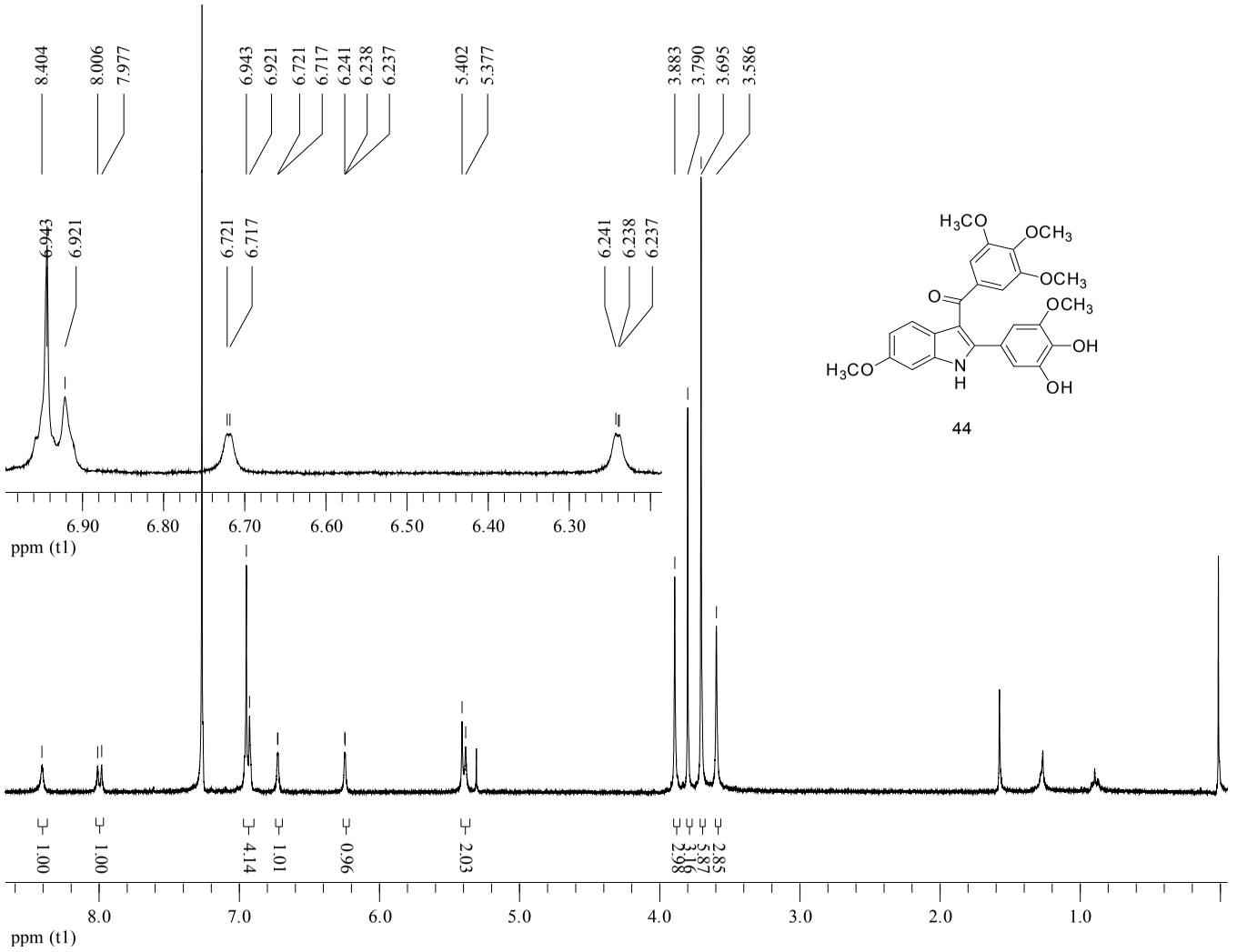

A.35. ^{1}H NMR ($CDCl_3$, 300 MHz) of Compound **44**

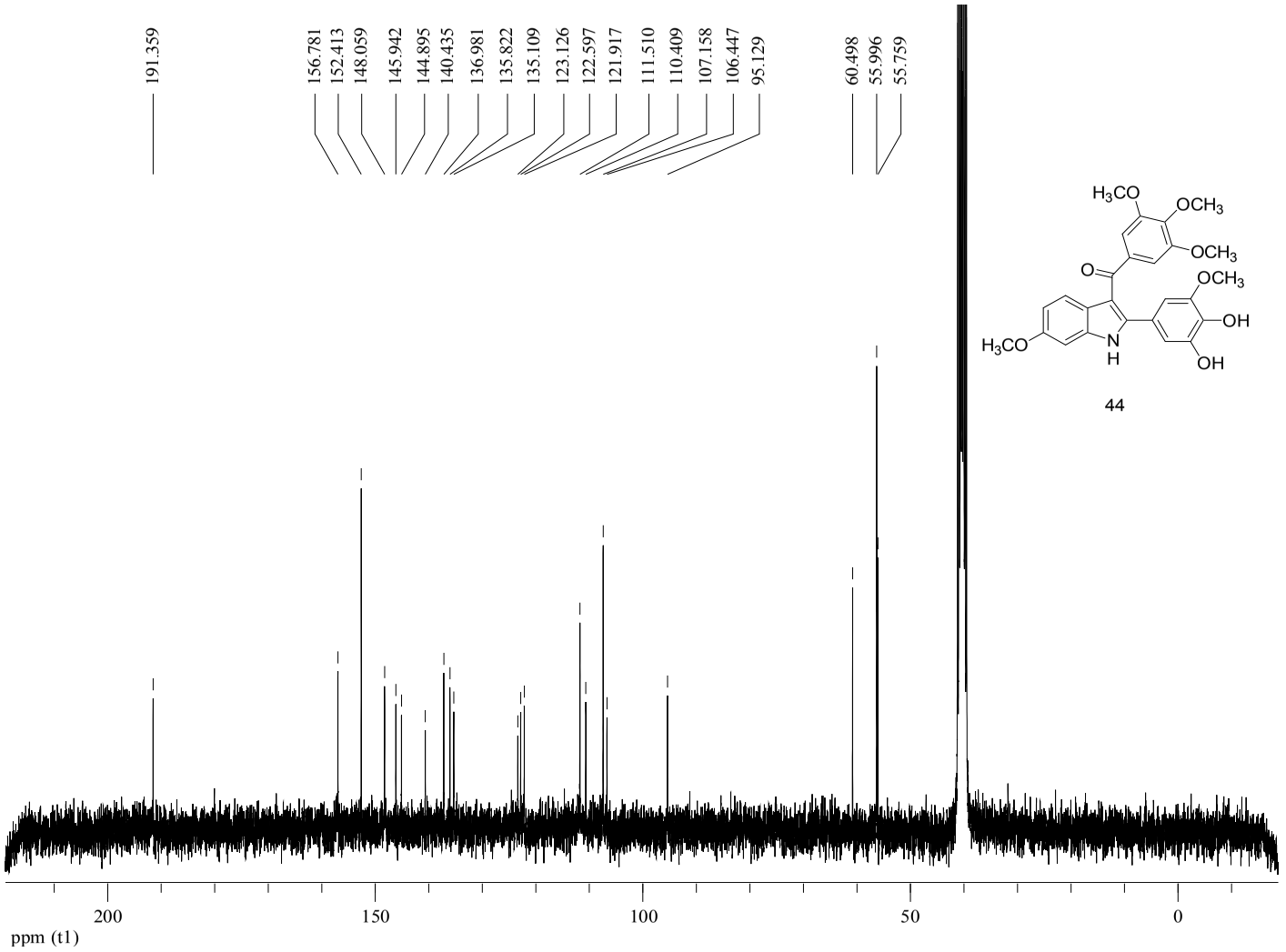

A.36. ^{13}C NMR ($CDCl_3$, 75 MHz) of Compound **44**

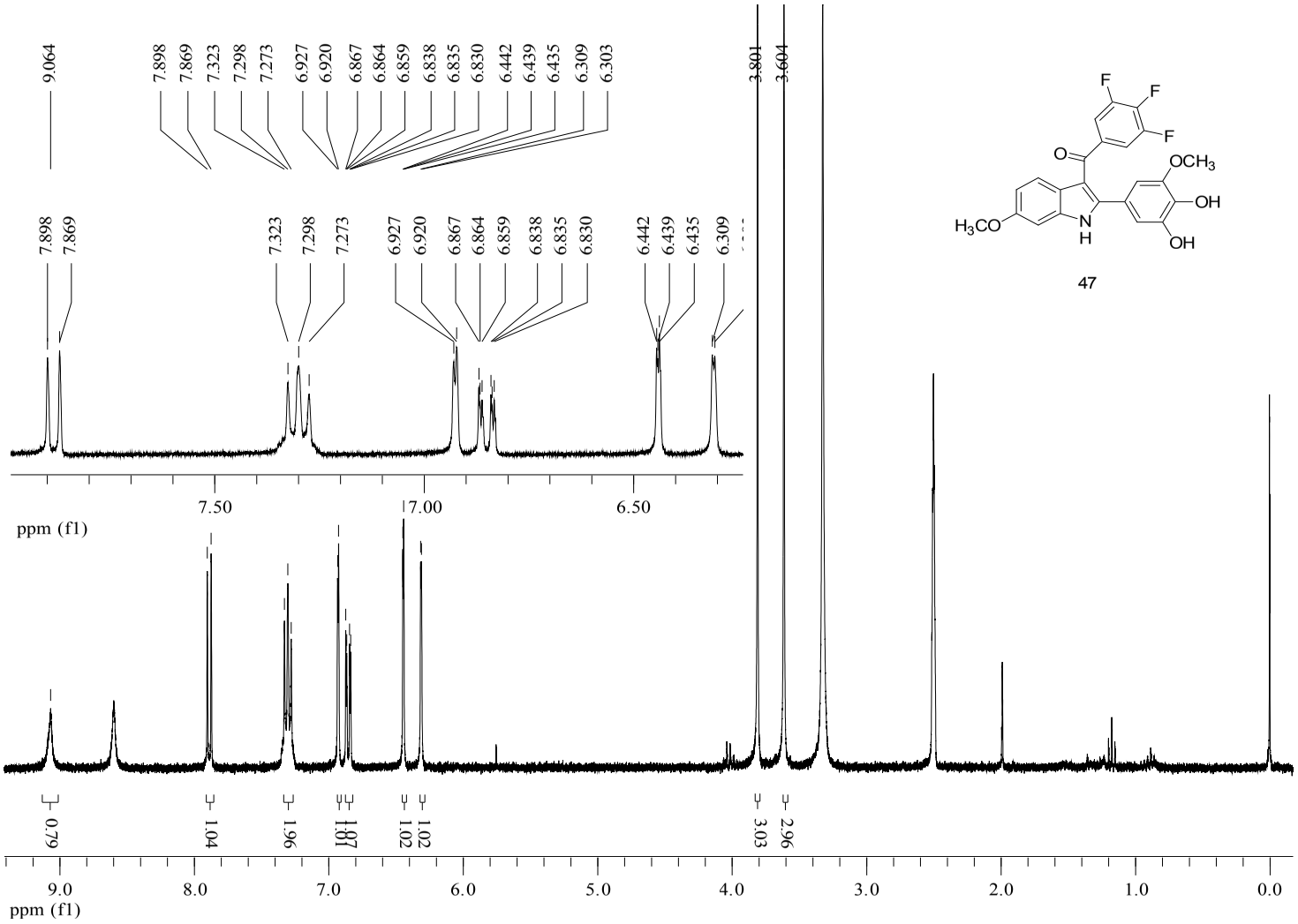

A.37. ^{1}H NMR (DMSO-d_6, 300 MHz) of Compound **47**

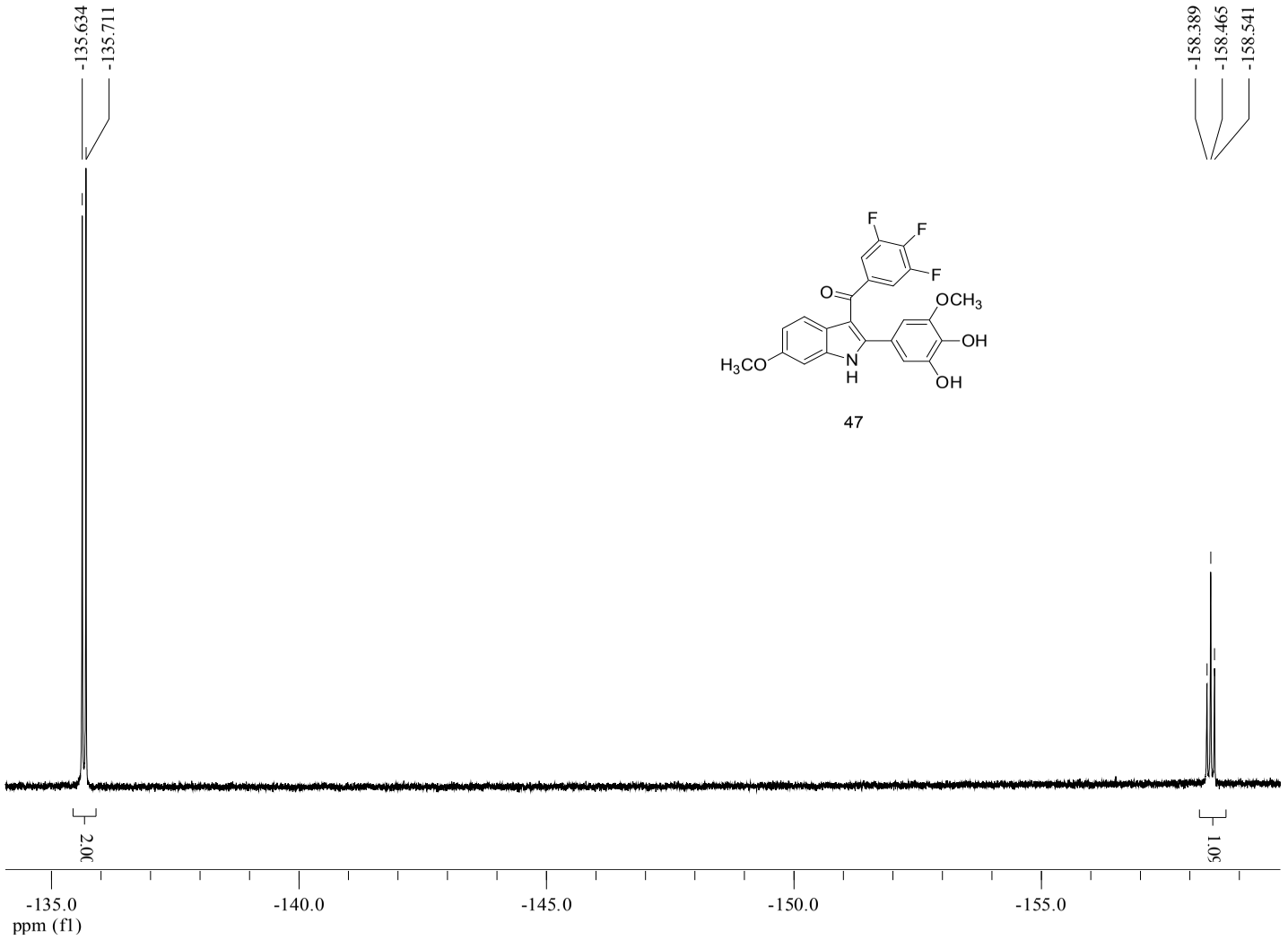

A.38. ^{19}F NMR (DMSO-d_6, 282 MHz) of Compound **47**

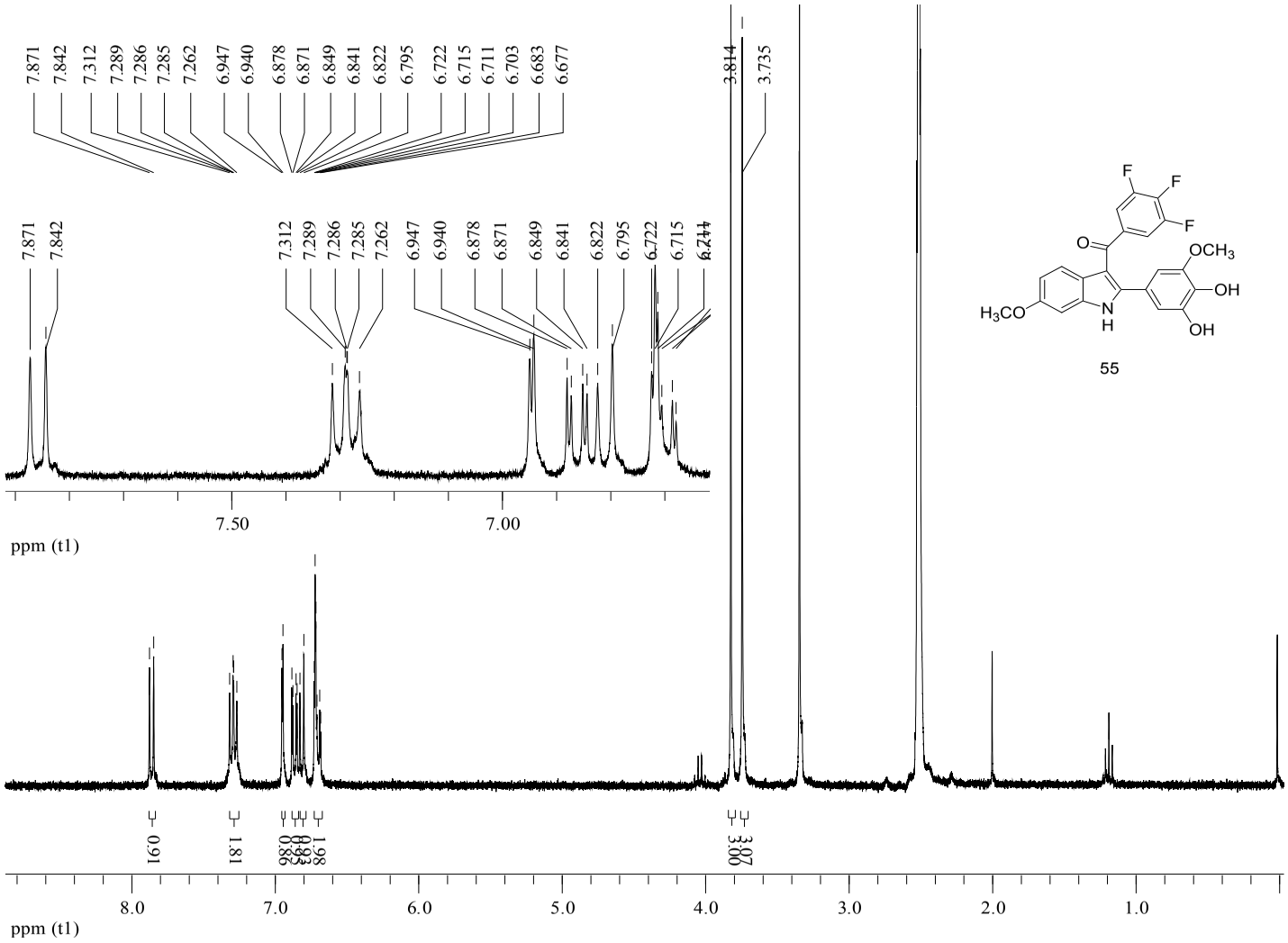

A.39. ^{1}H NMR (DMSO-d_6, 300 MHz) of Compound **55**

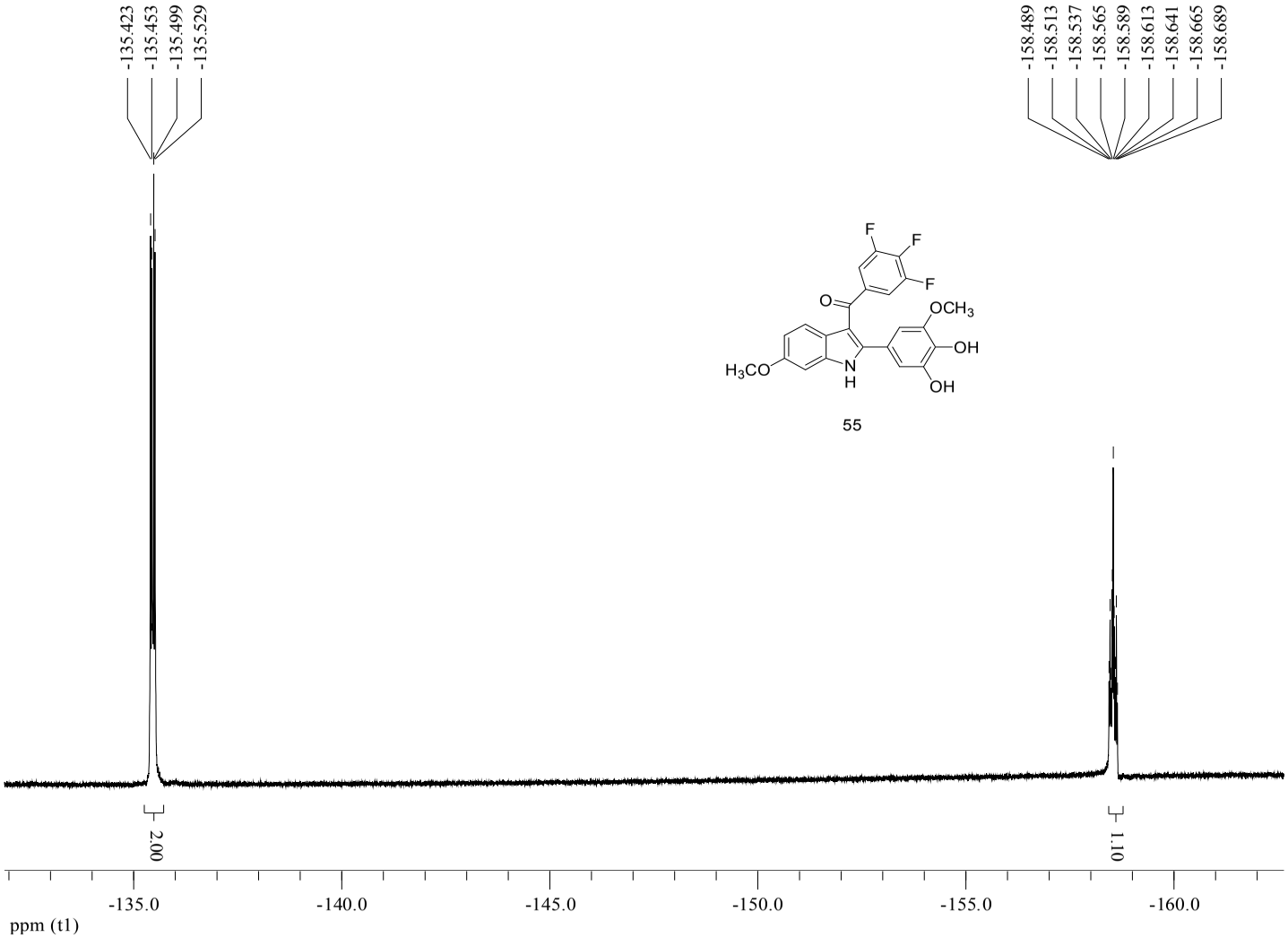

A.40. ^{19}F NMR (DMSO-d_6, 282 MHz) of Compound **55**

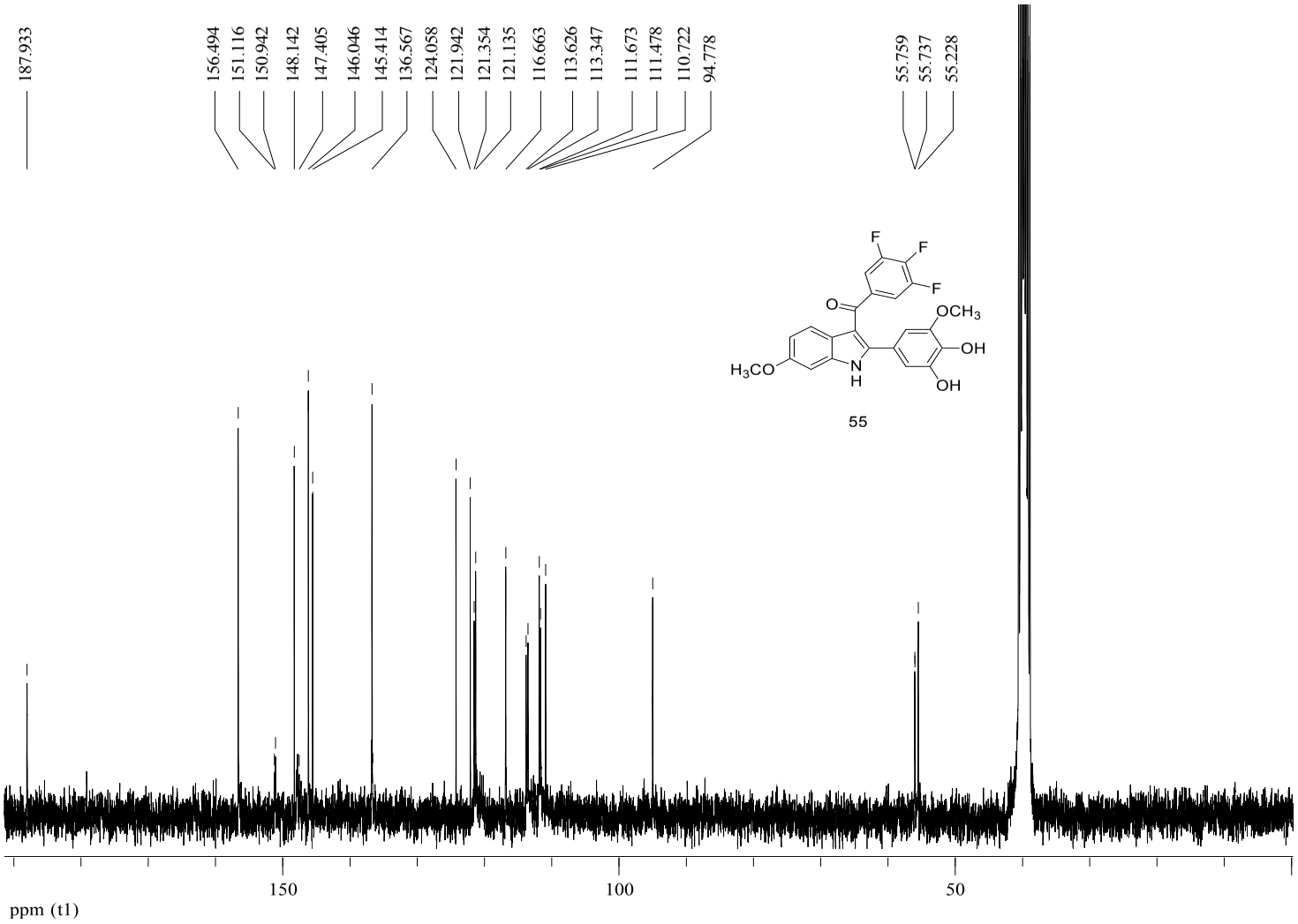

A.41. ^{13}C NMR (DMSO-d_6, 75 MHz) of Compound **55**

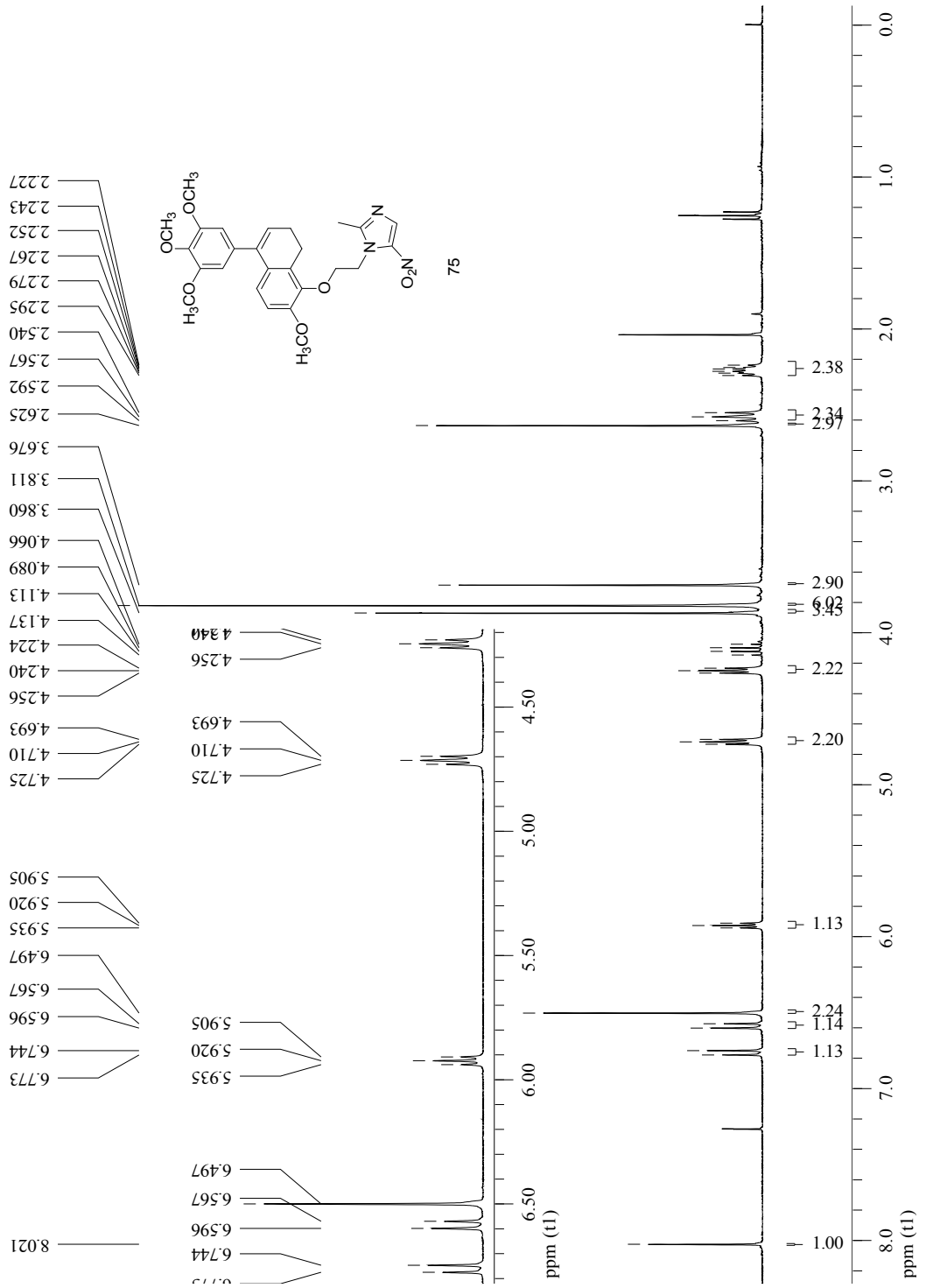

A.42. ^{1}H NMR ($CDCl_3$, 300 MHz) of Compound **75**

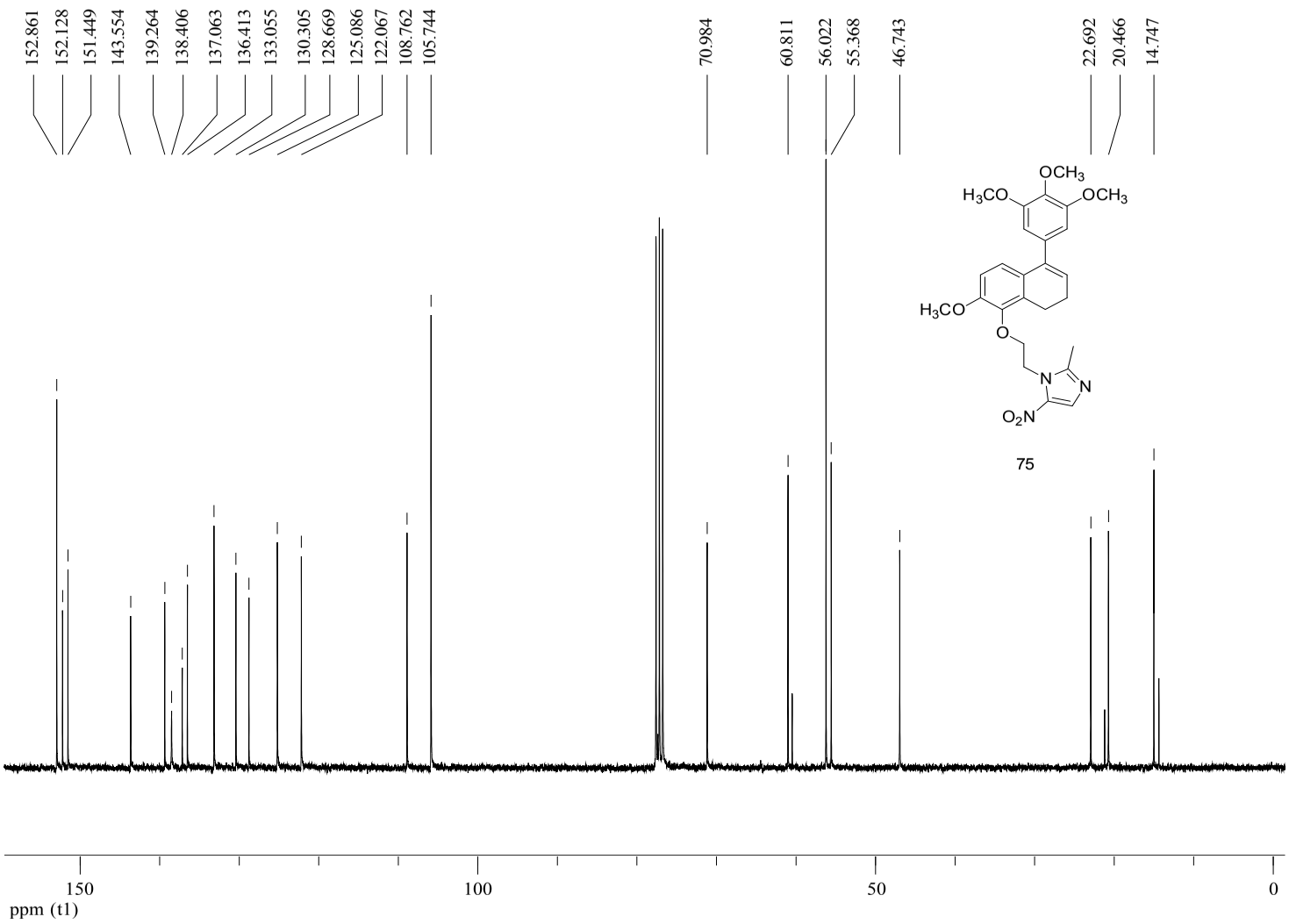

A.43. ^{13}C NMR ($CDCl_3$, 75 MHz) of Compound **75**

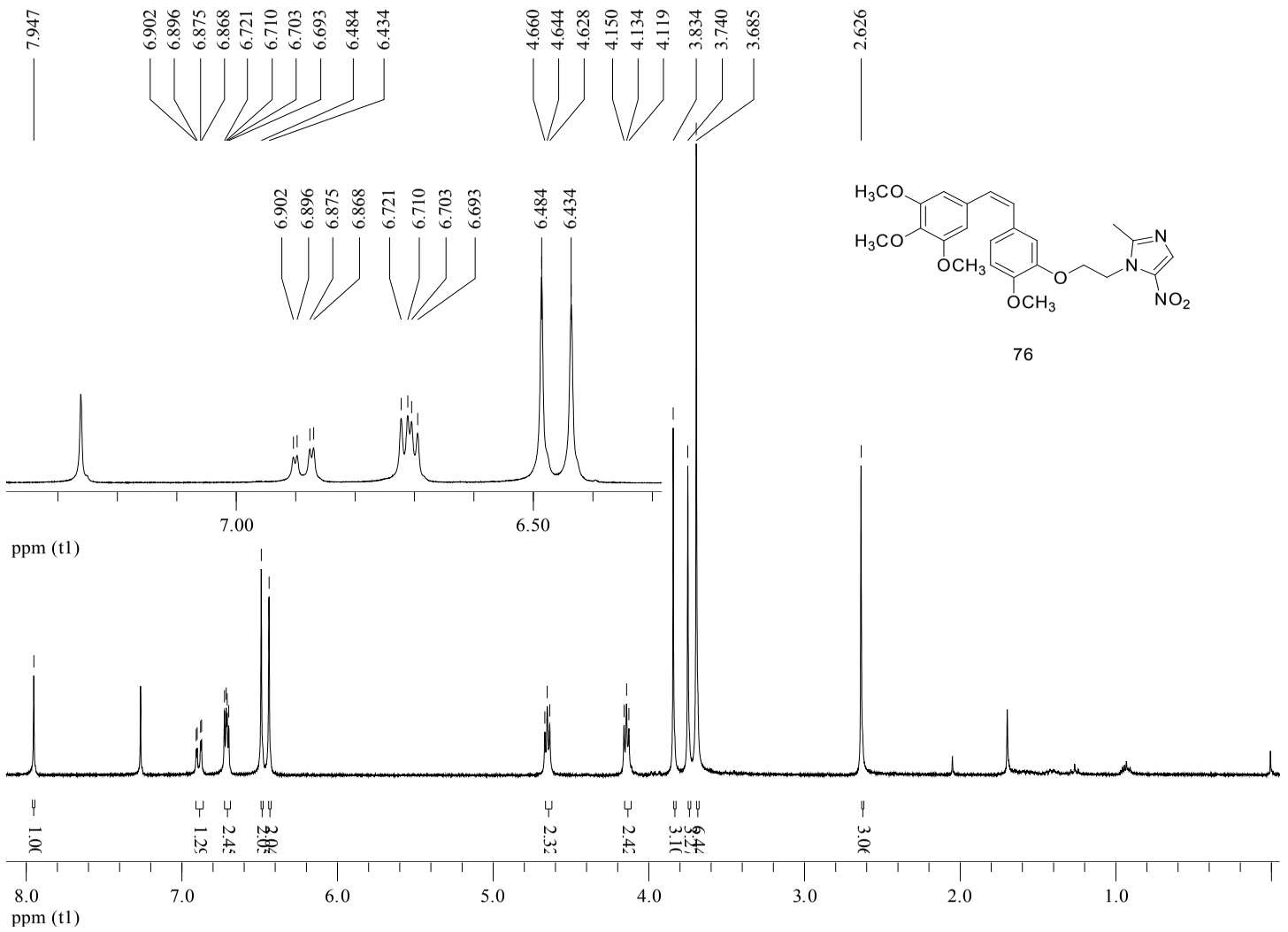

A.44. ^{1}H NMR ($CDCl_3$, 300 MHz) of Compound **76**

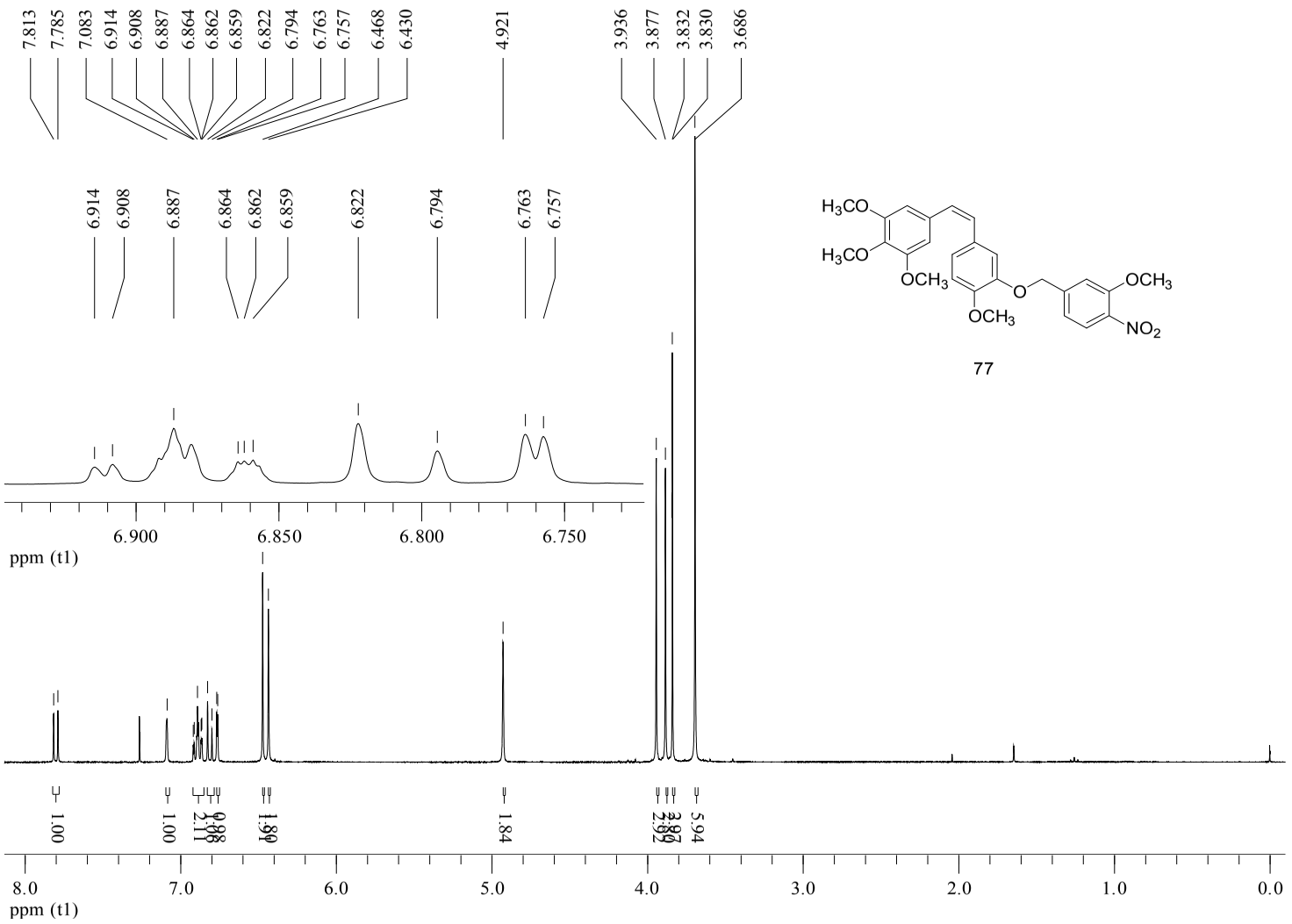

A.45. ^{1}H NMR ($CDCl_3$, 300 MHz) of Compound **77**

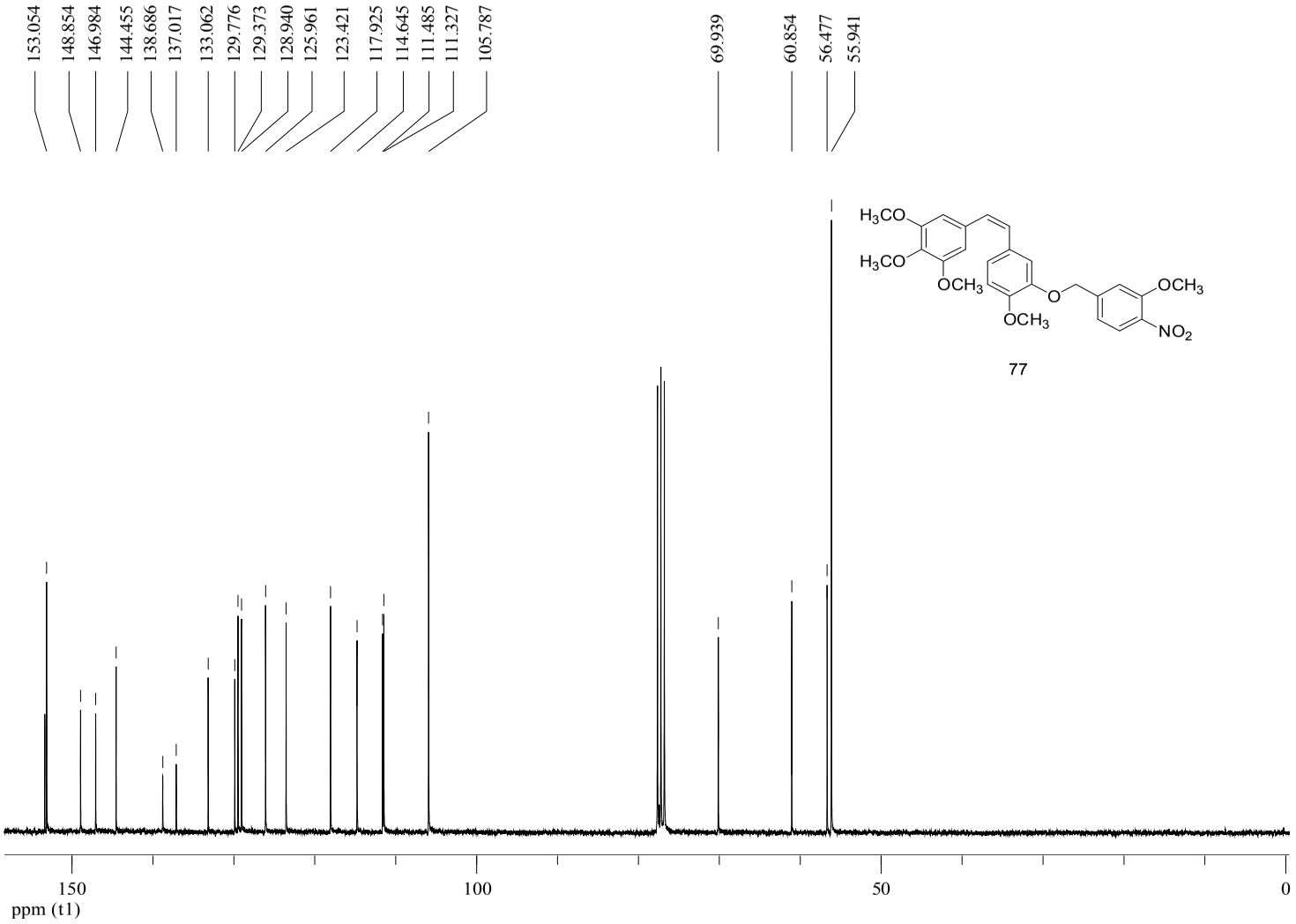

A.46. ^{13}C NMR ($CDCl_3$, 75 MHz) of Compound **77**

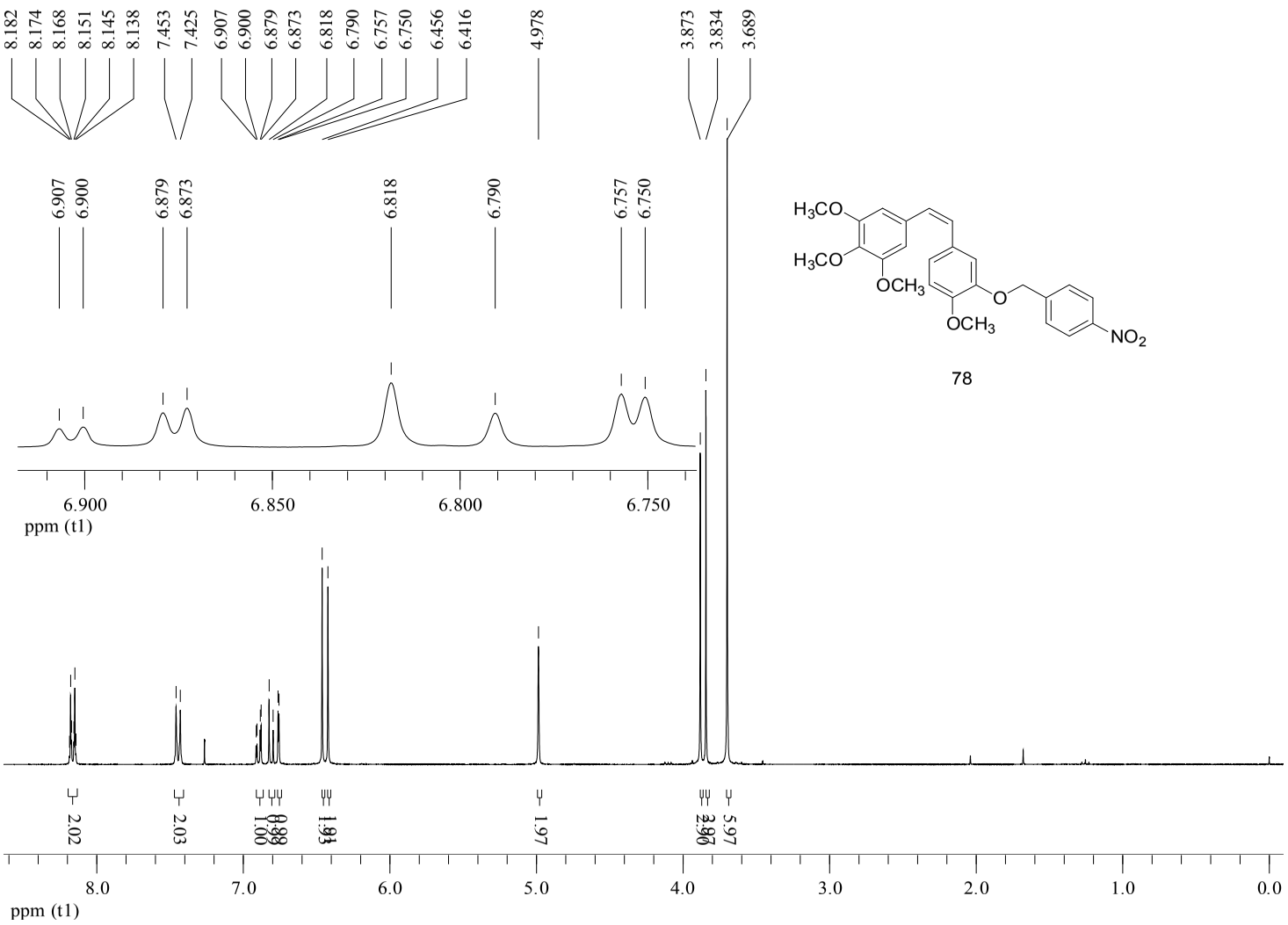

A.47. ^{1}H NMR ($CDCl_3$, 300 MHz) of Compound **78**

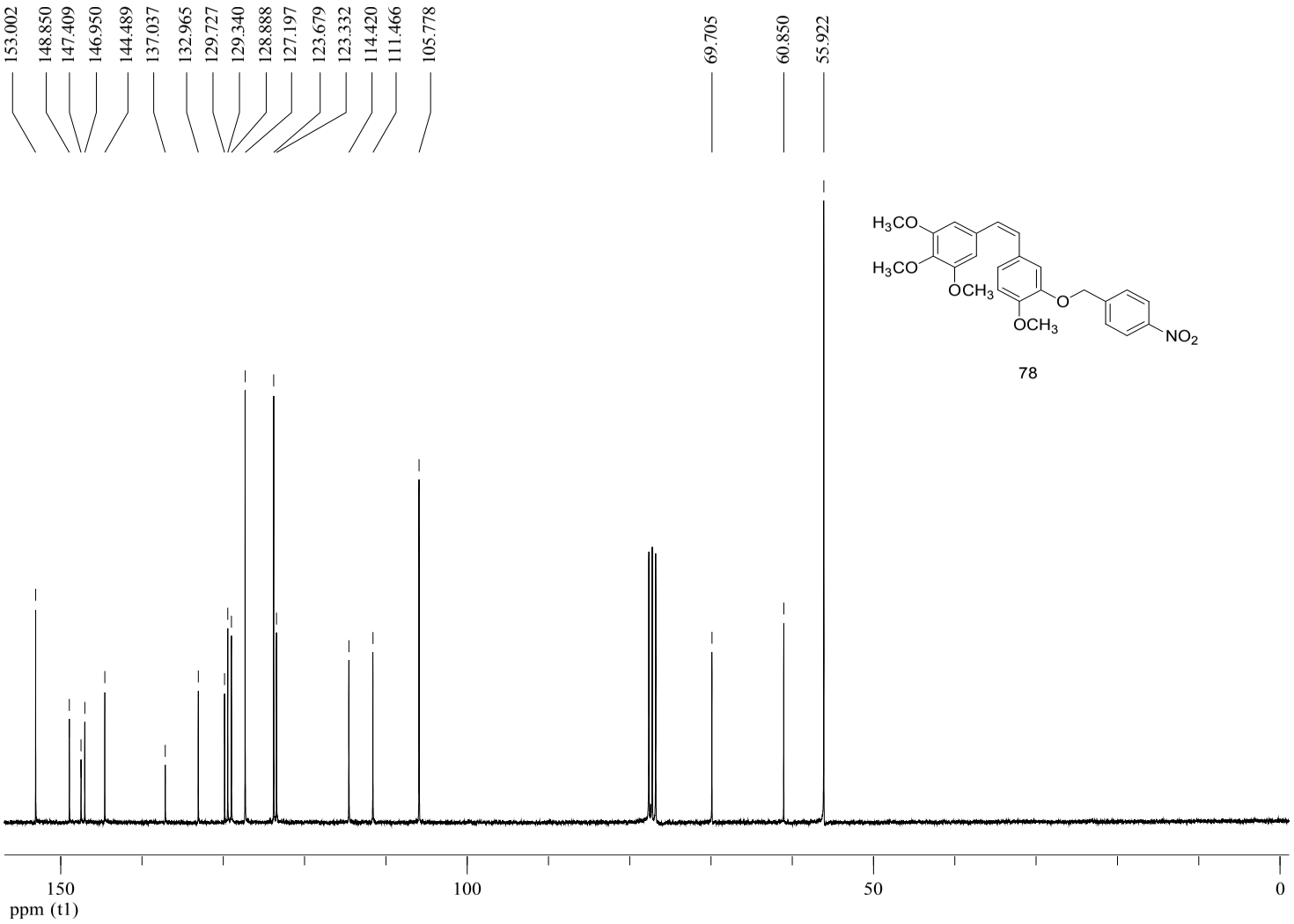

A.48. ^{13}C NMR ($CDCl_3$, 75 MHz) of Compound **78**

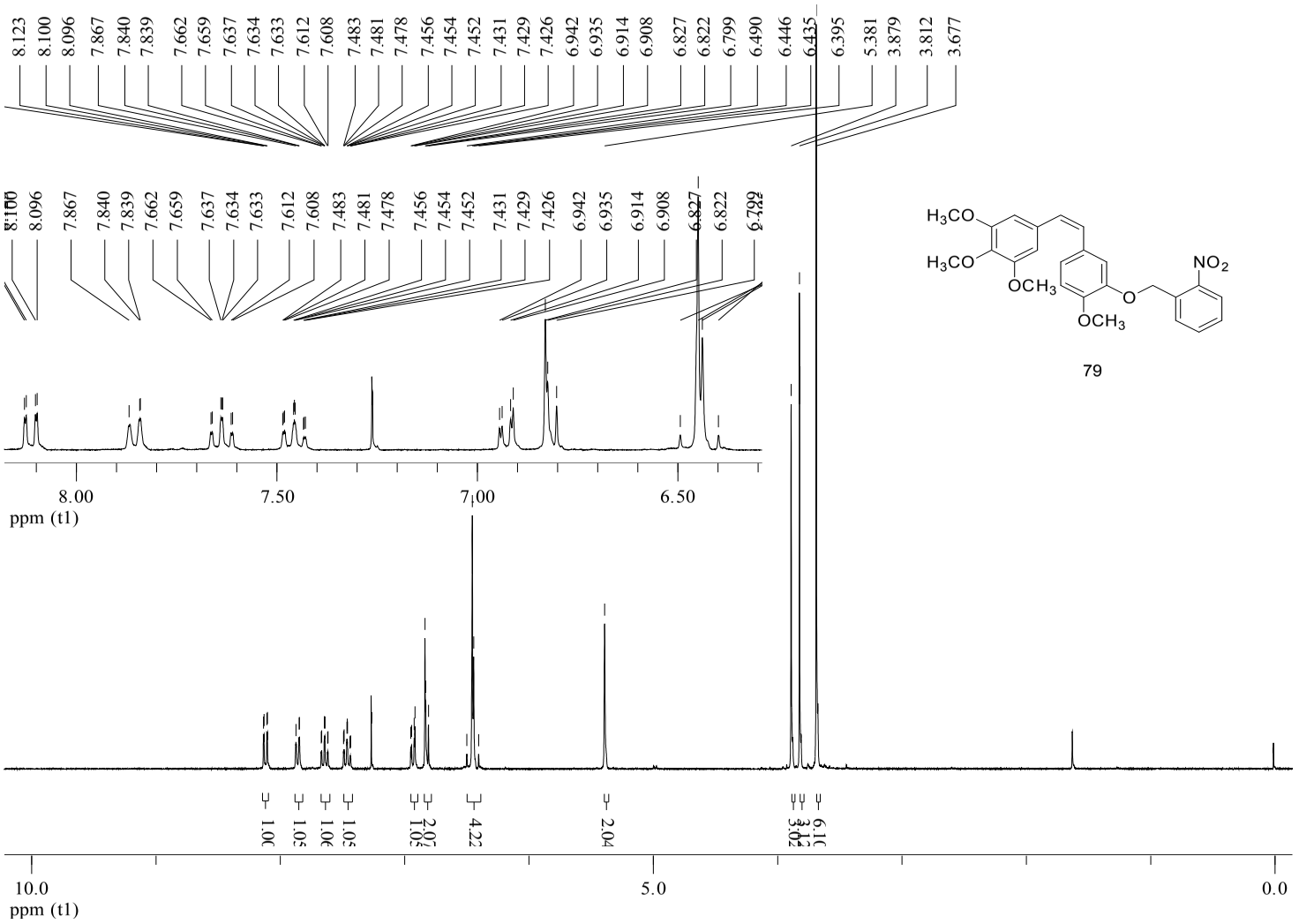

A.49. ^{1}H NMR ($CDCl_3$, 300 MHz) of Compound **79**

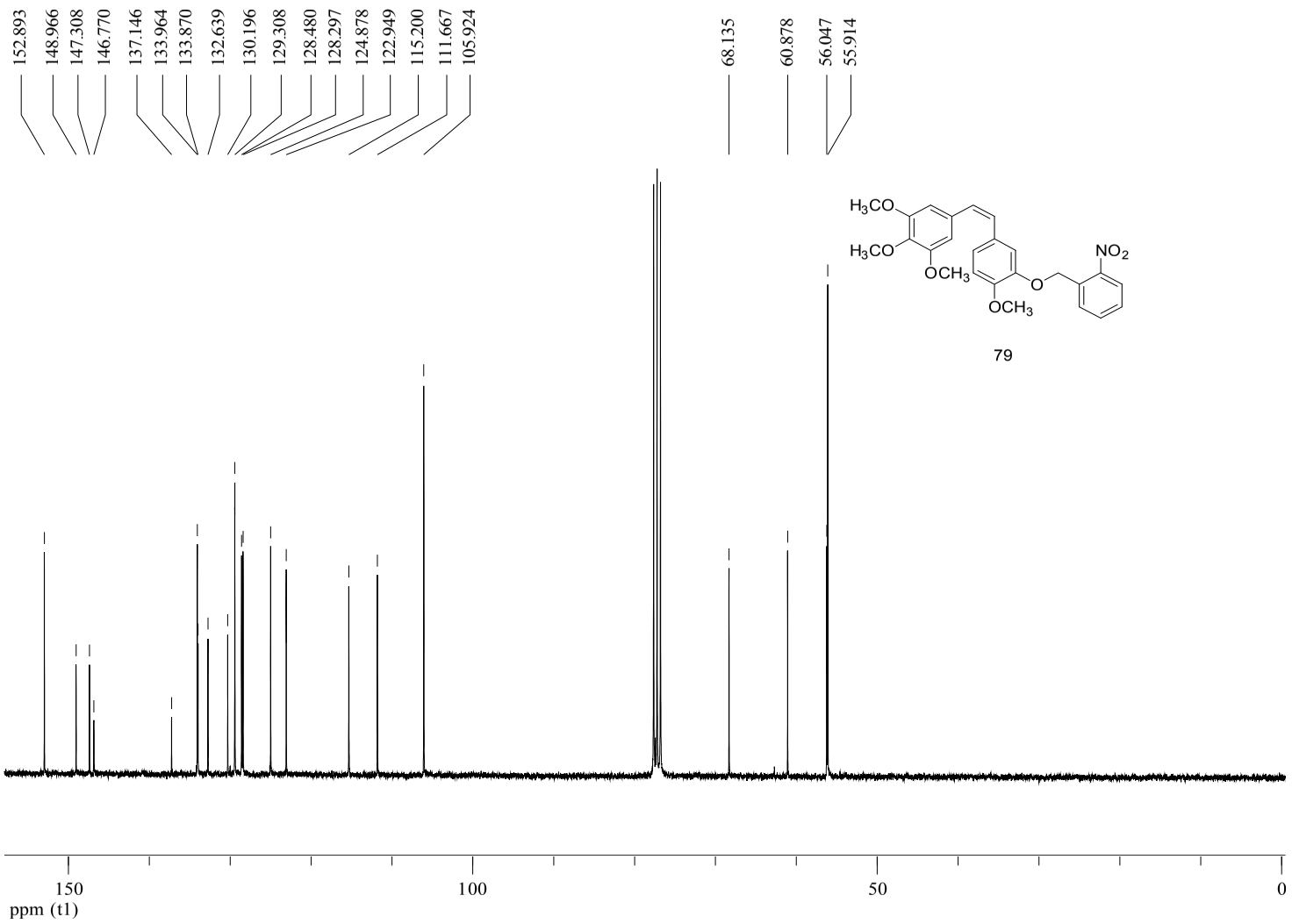

A.50. ^{13}C NMR ($CDCl_3$, 75 MHz) of Compound **79**

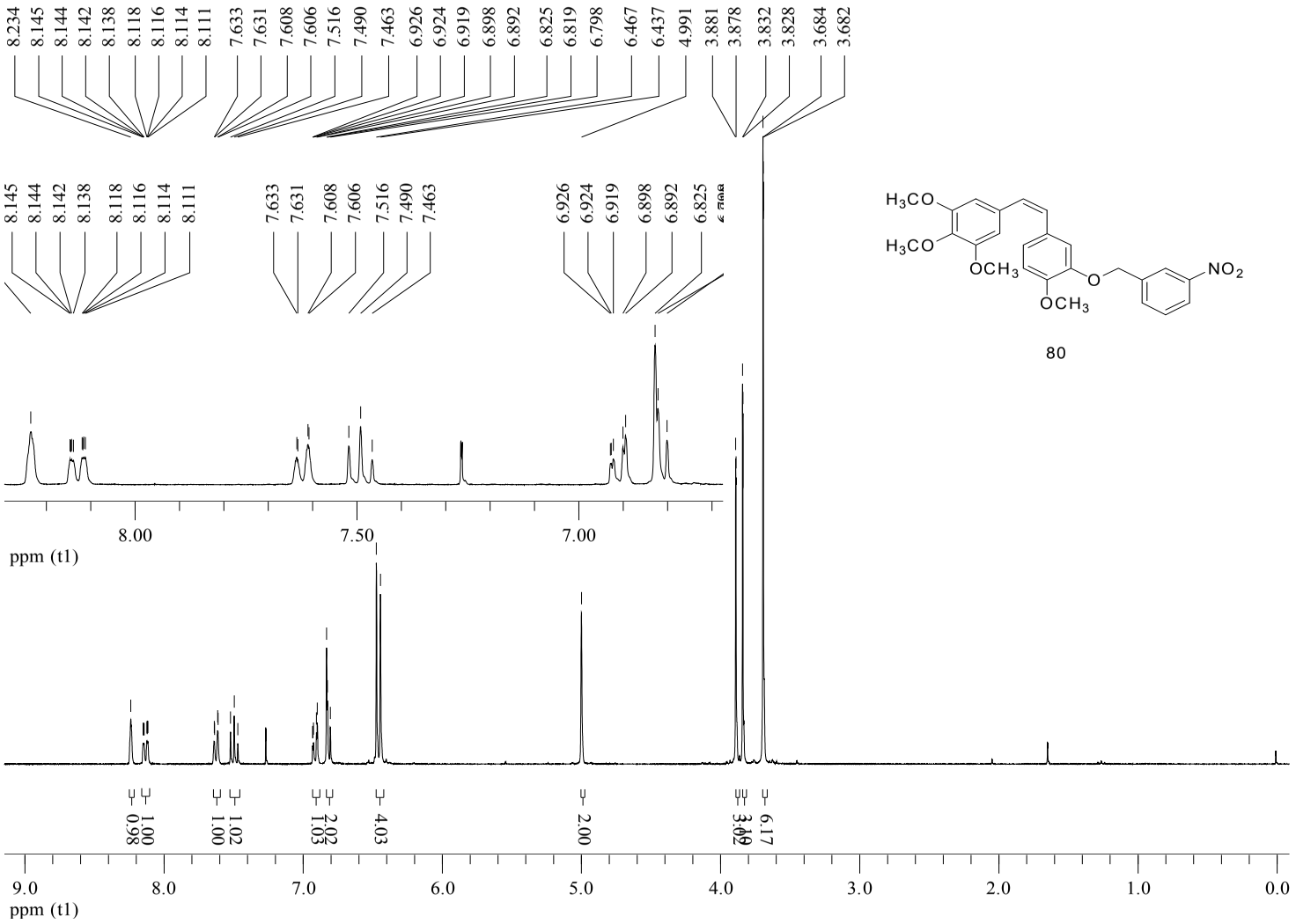

A.51. ^{1}H NMR ($CDCl_3$, 300 MHz) of Compound **80**

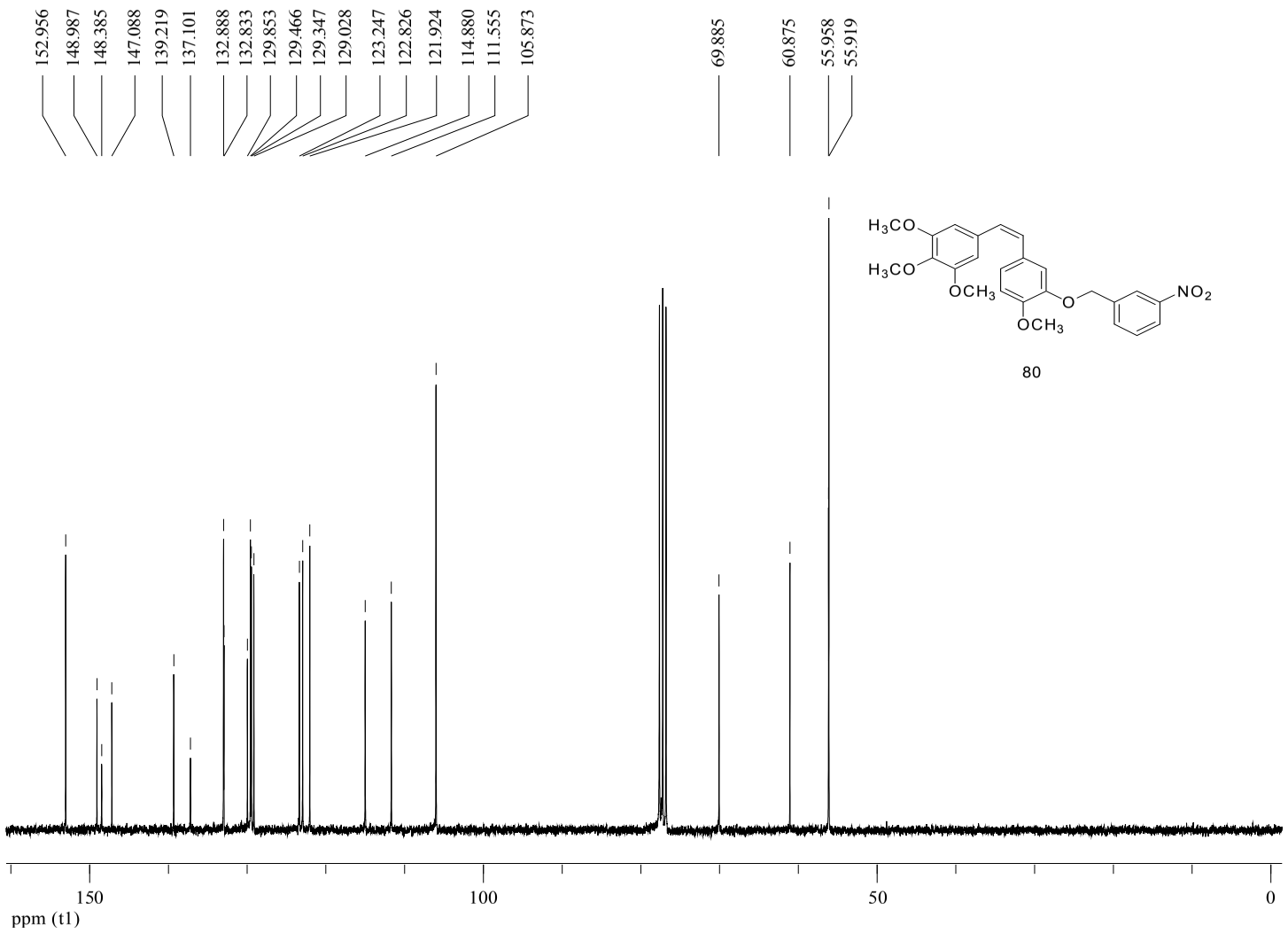

A.52. ^{13}C NMR ($CDCl_3$, 75 MHz) of Compound **80**

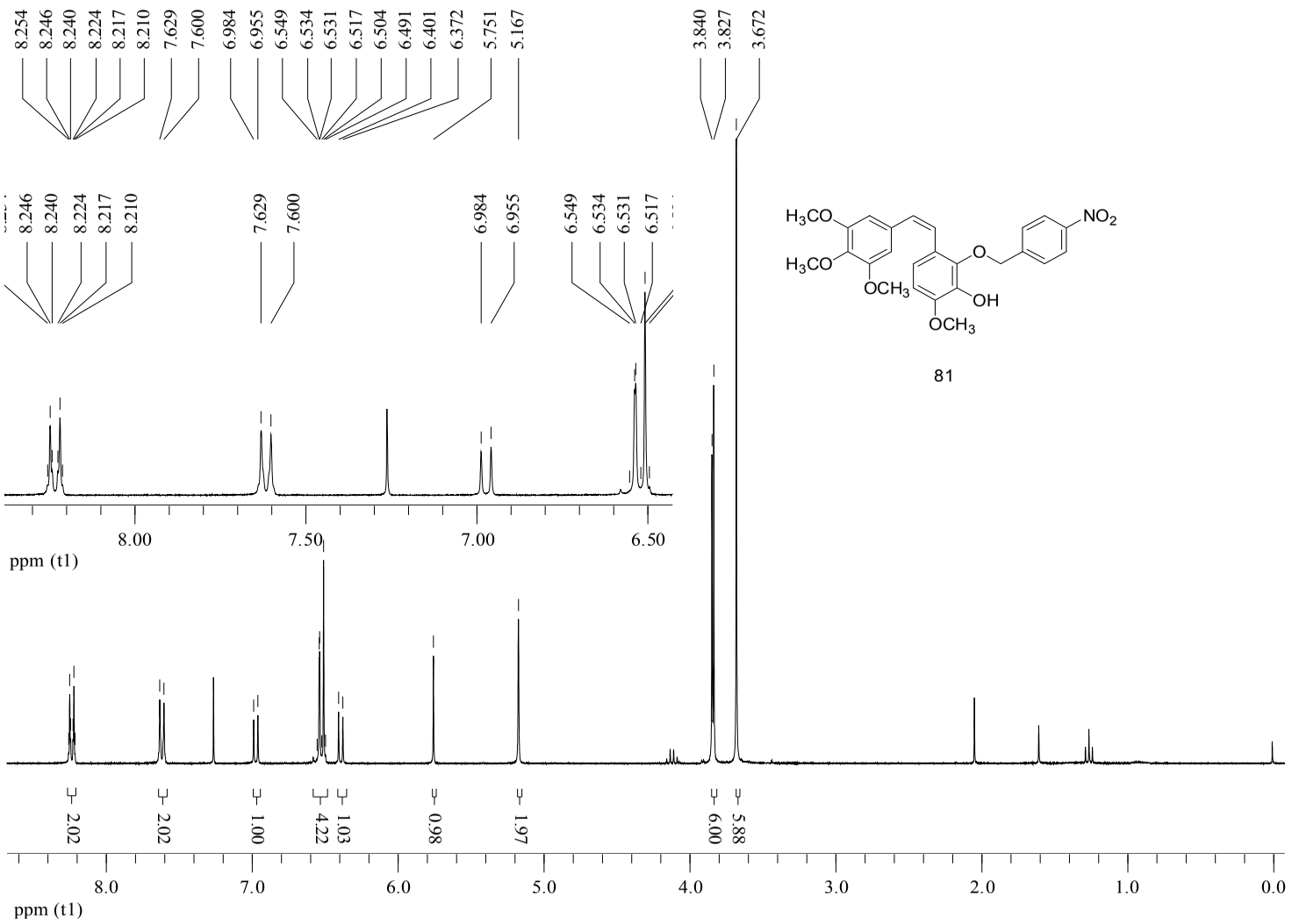

A.53. ^{1}H NMR ($CDCl_3$, 300 MHz) of Compound **81**

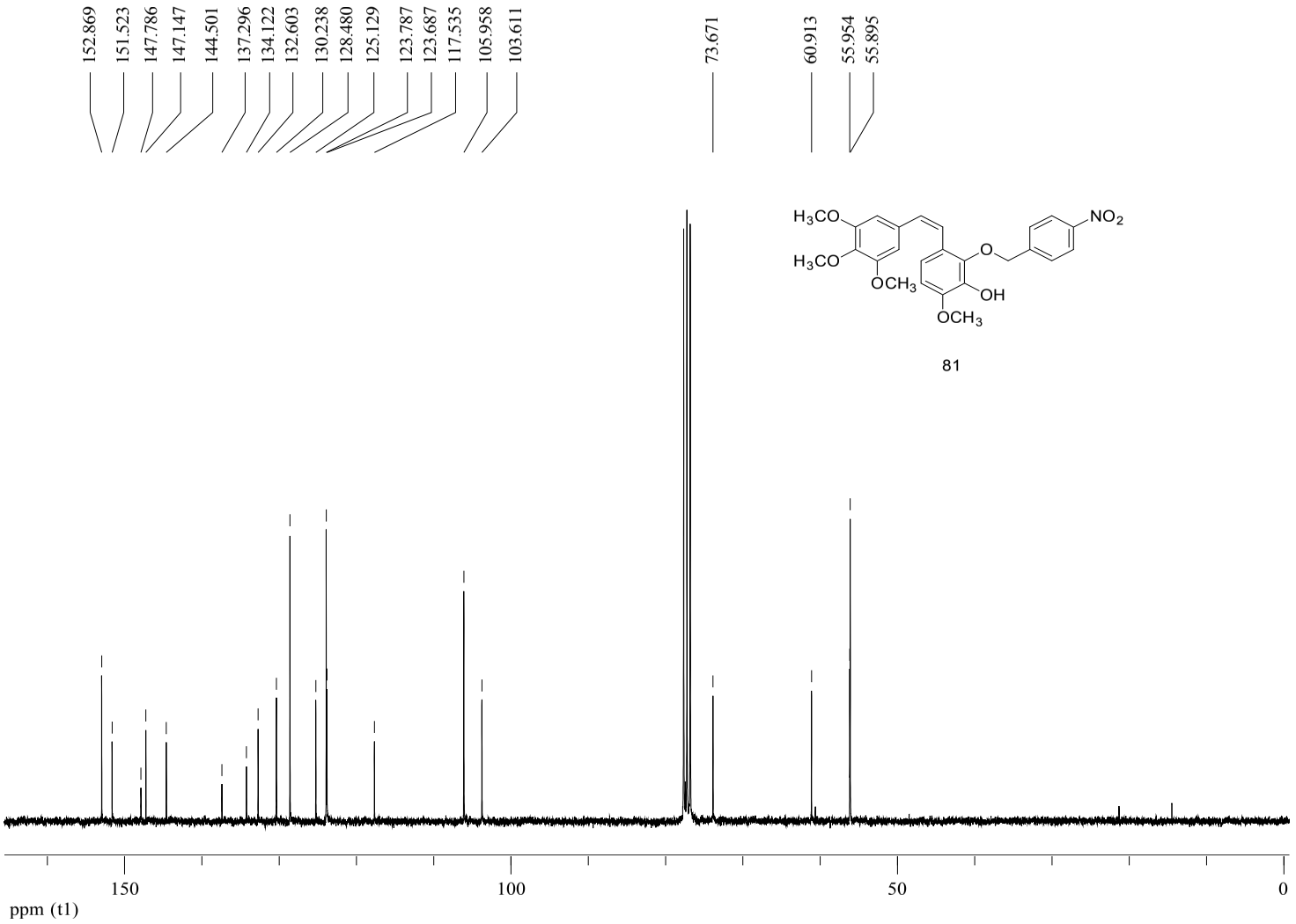

A.54. ^{13}C NMR ($CDCl_3$, 75 MHz) of Compound **81**

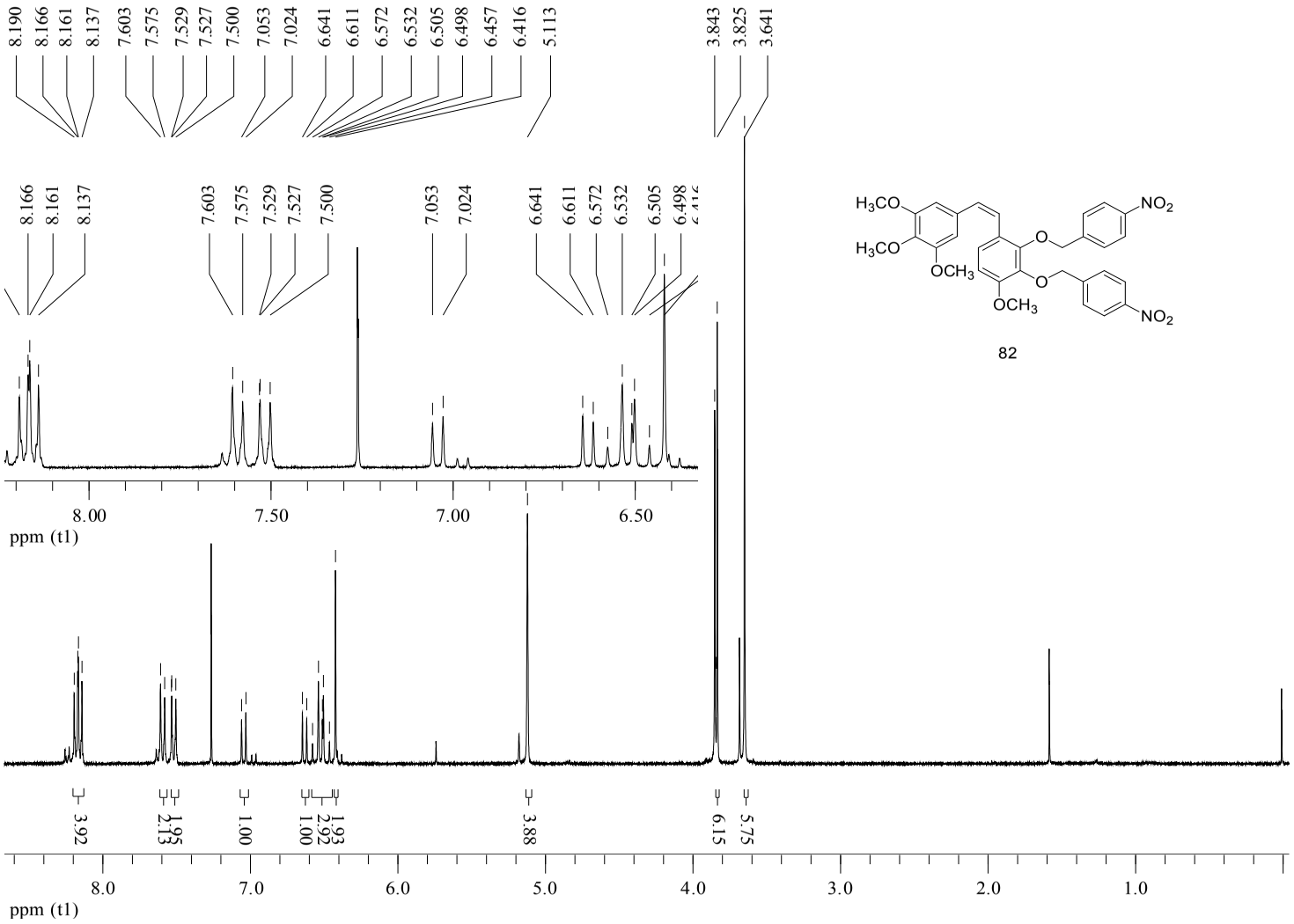

A.55. ^{1}H NMR ($CDCl_3$, 300 MHz) of Compound **82**

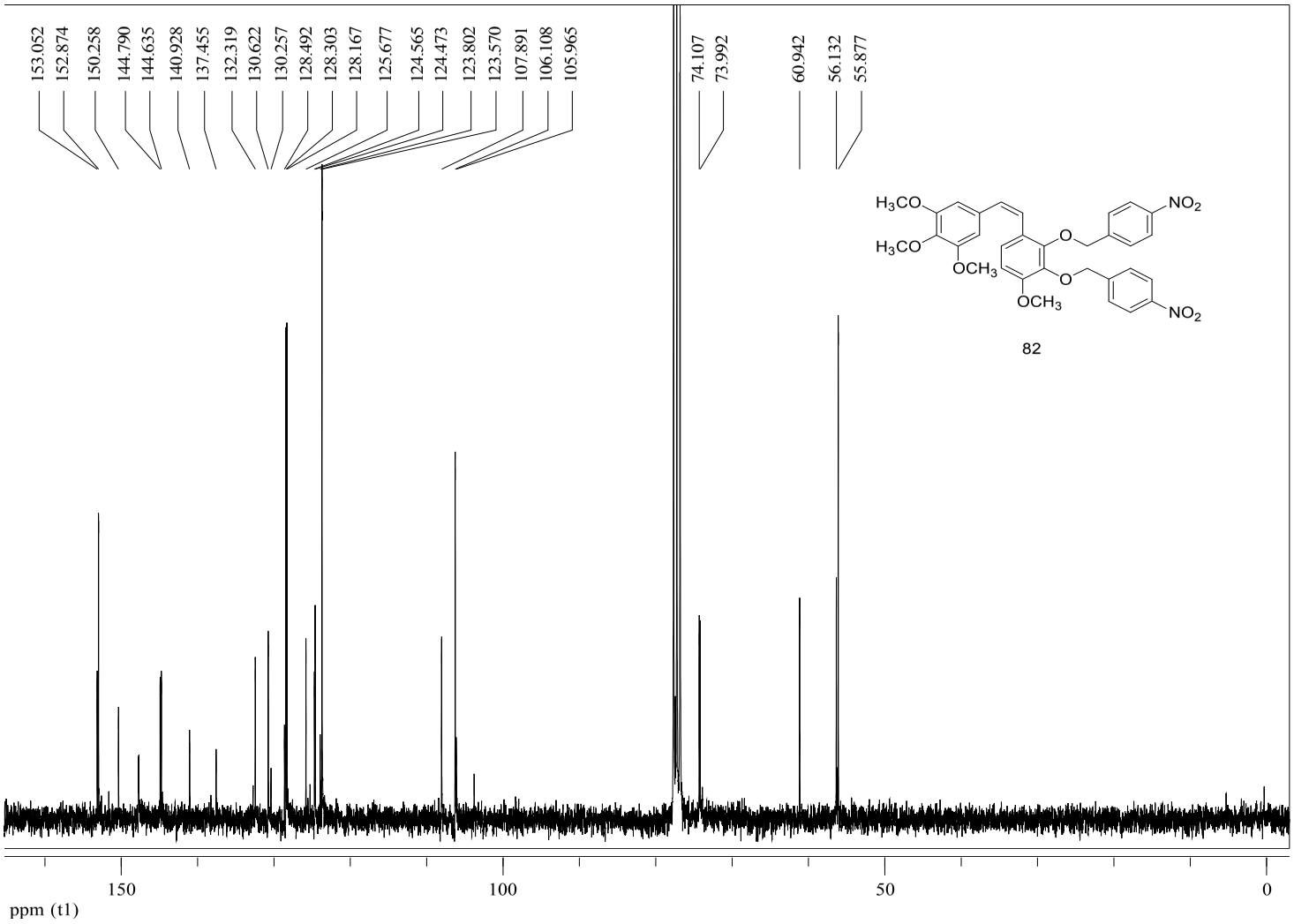

A.56. ^{13}C NMR ($CDCl_3$, 75 MHz) of Compound **82**

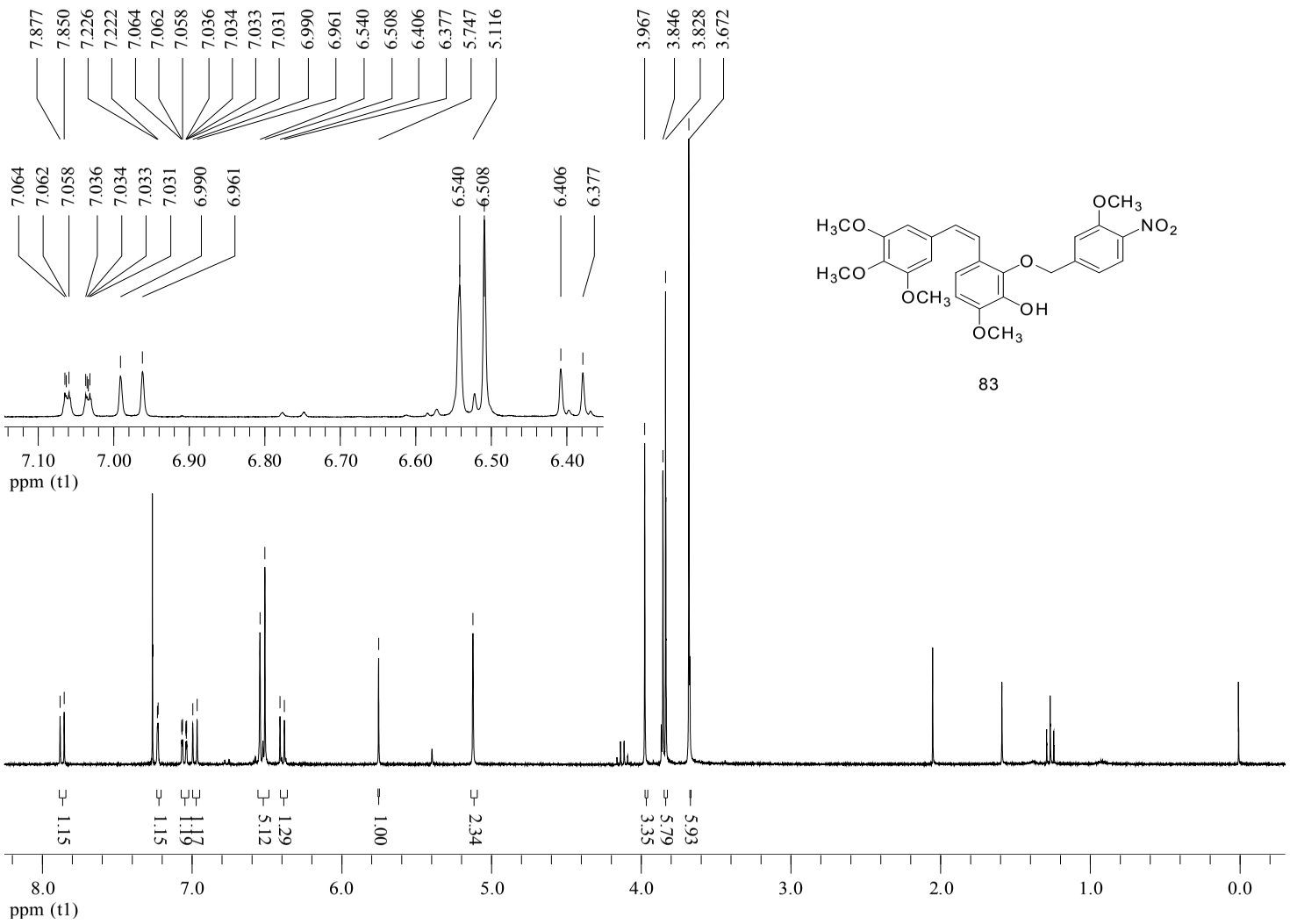

A.57. ^{1}H NMR ($CDCl_3$, 300 MHz) of Compound **83**

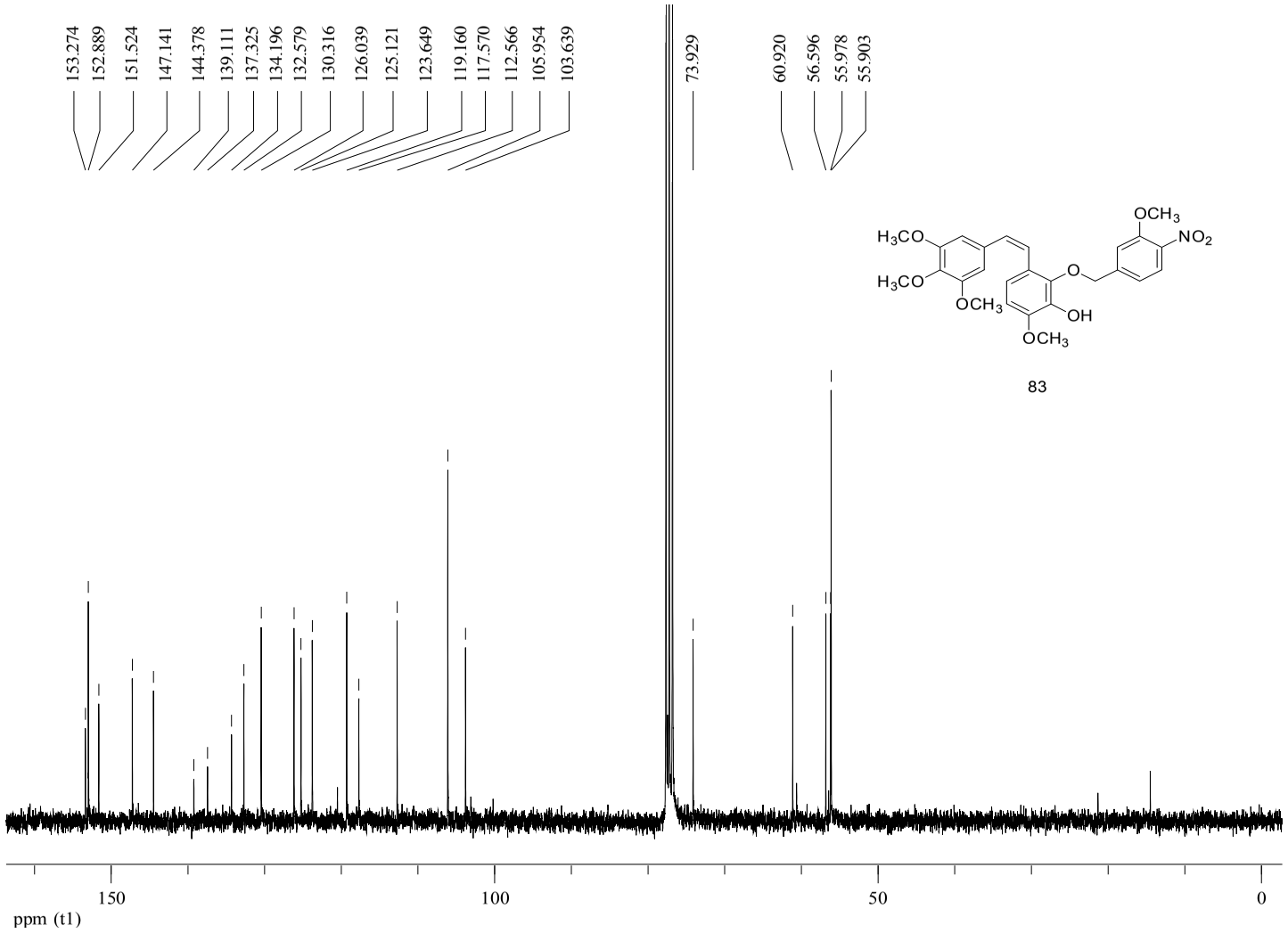

A.58. ^{13}C NMR ($CDCl_3$, 75 MHz) of Compound **83**

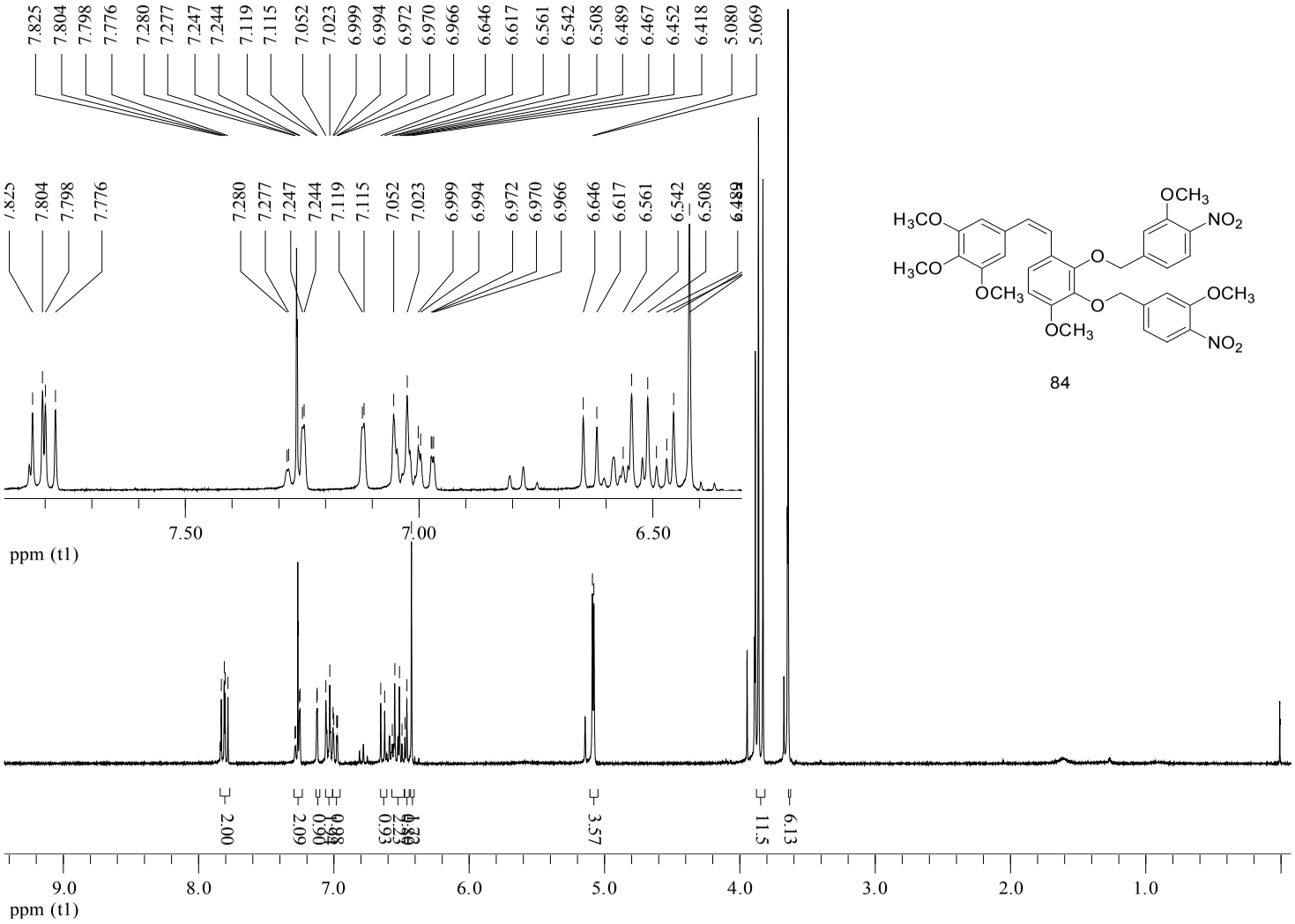

84

A.59. ^{1}H NMR ($CDCl_3$, 300 MHz) of Compound **84**

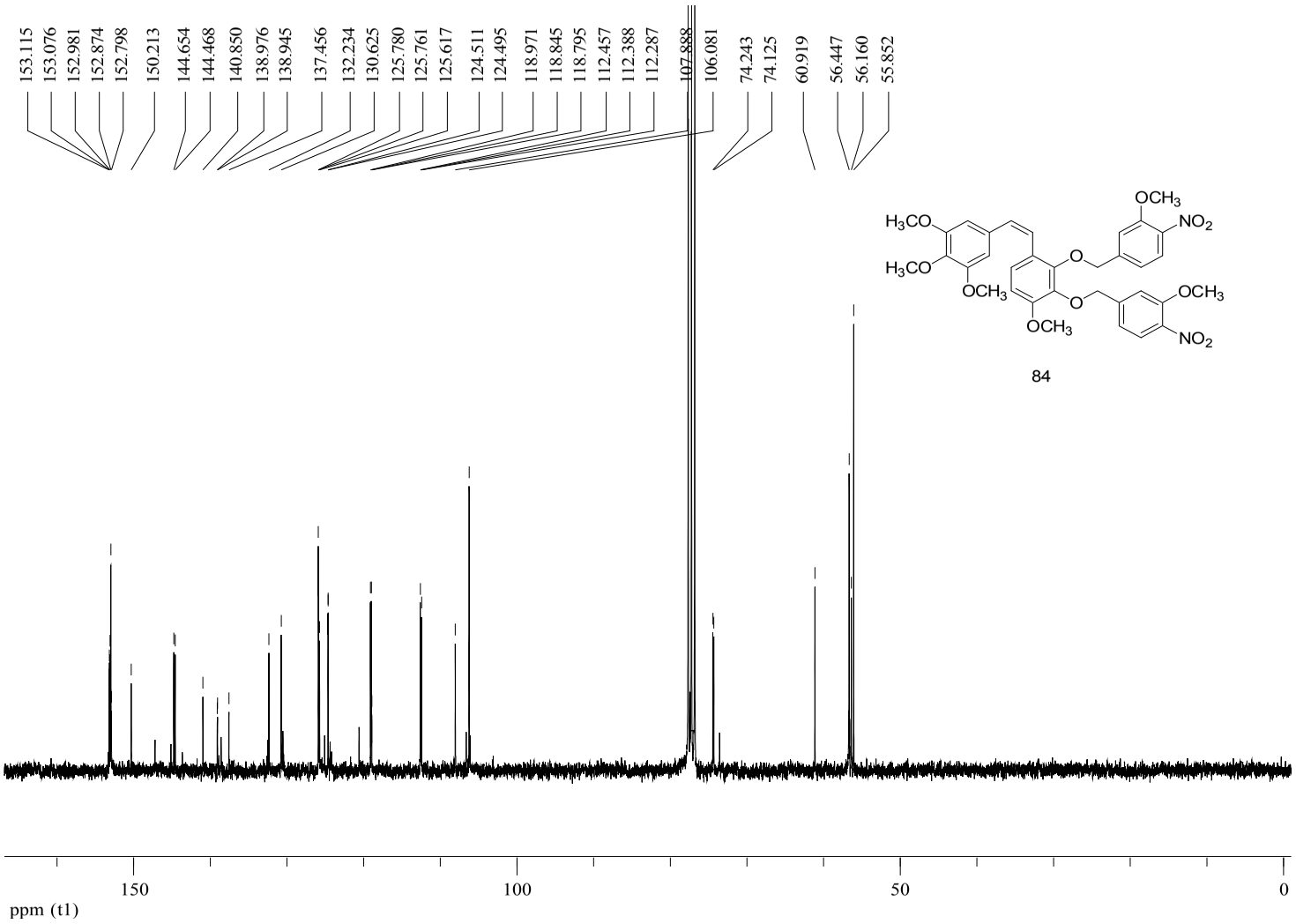

A.60. ^{13}C NMR ($CDCl_3$, 75 MHz) of Compound **84**

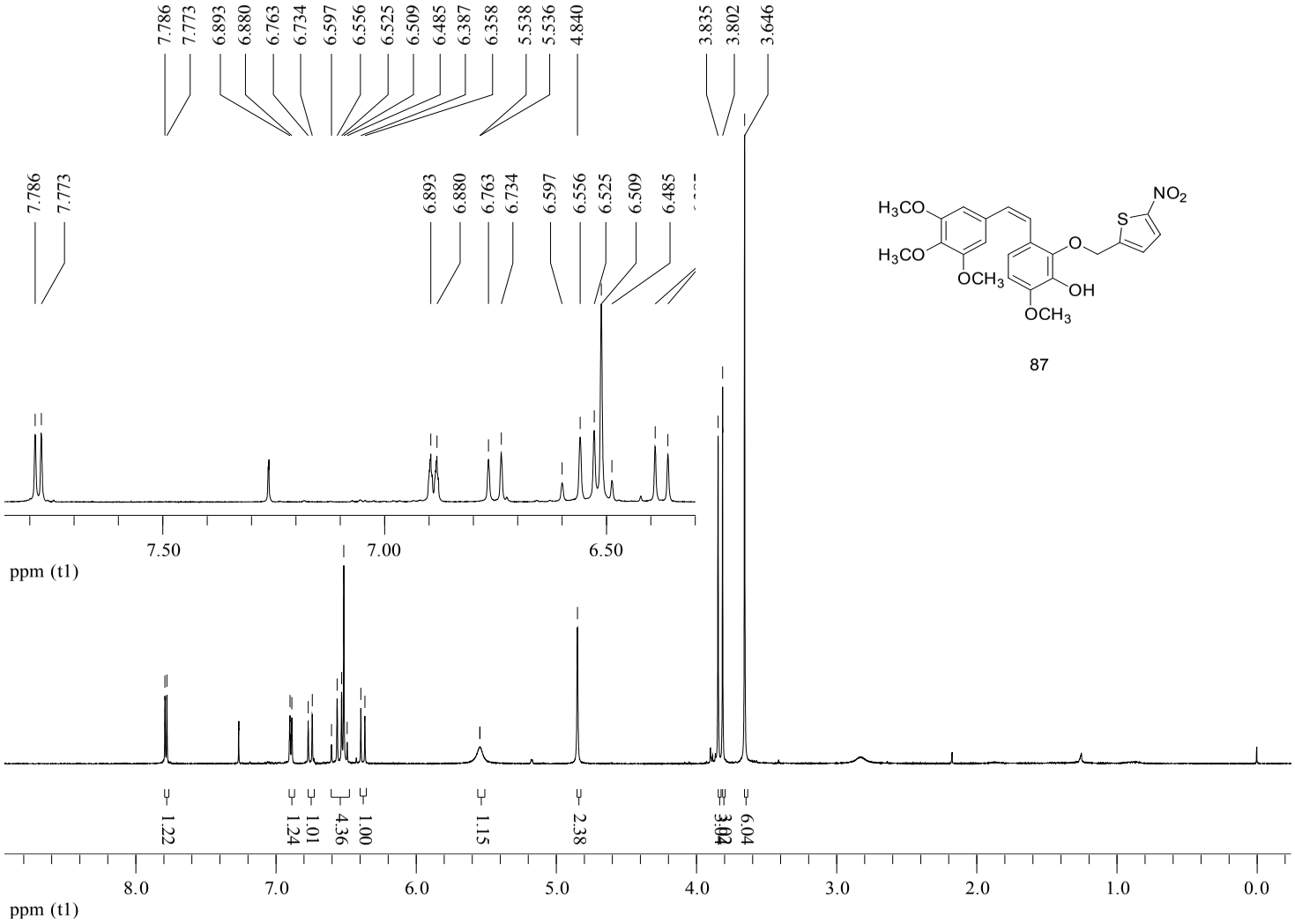

87

A.61. ^{1}H NMR ($CDCl_3$, 300 MHz) of Compound **87**

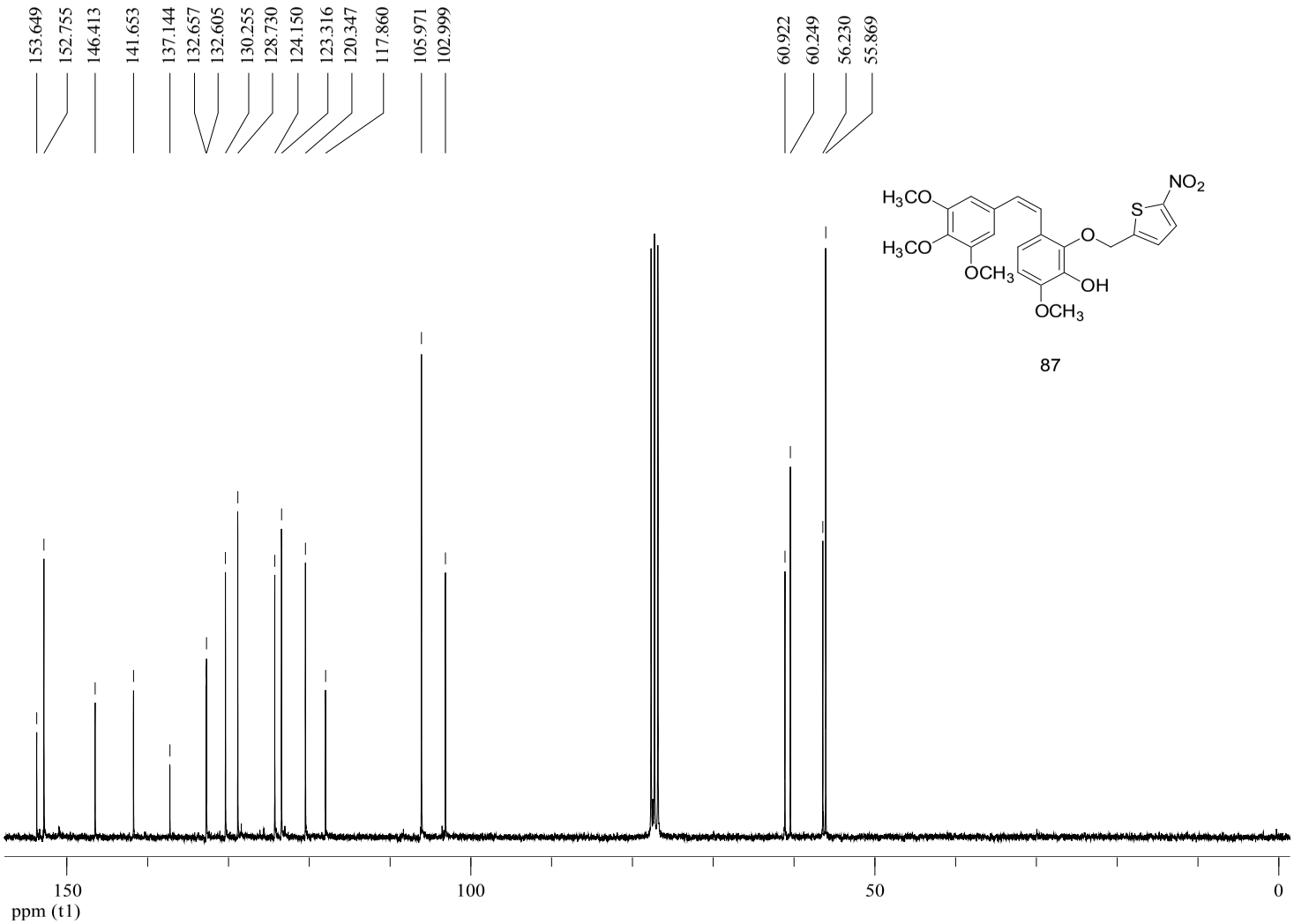

A.62. ^{13}C NMR ($CDCl_3$, 75 MHz) of Compound **87**

APPENDIX B

Tubulin Assay Spectra

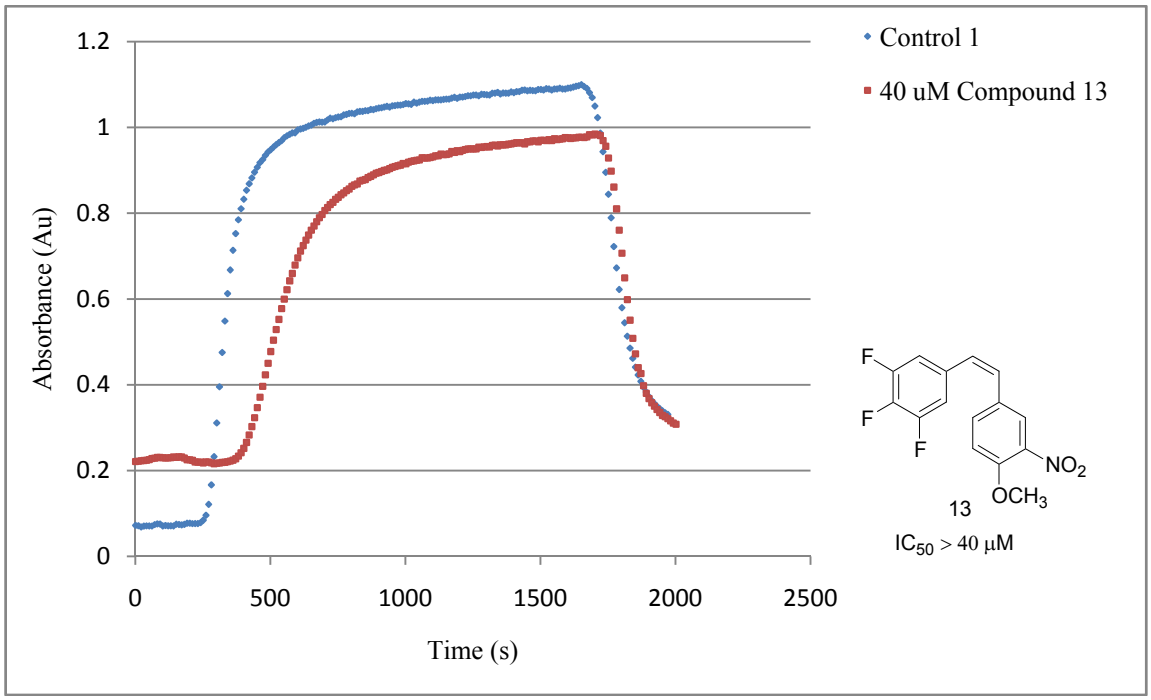

B.1. Tubulin Assay of Compound **13**

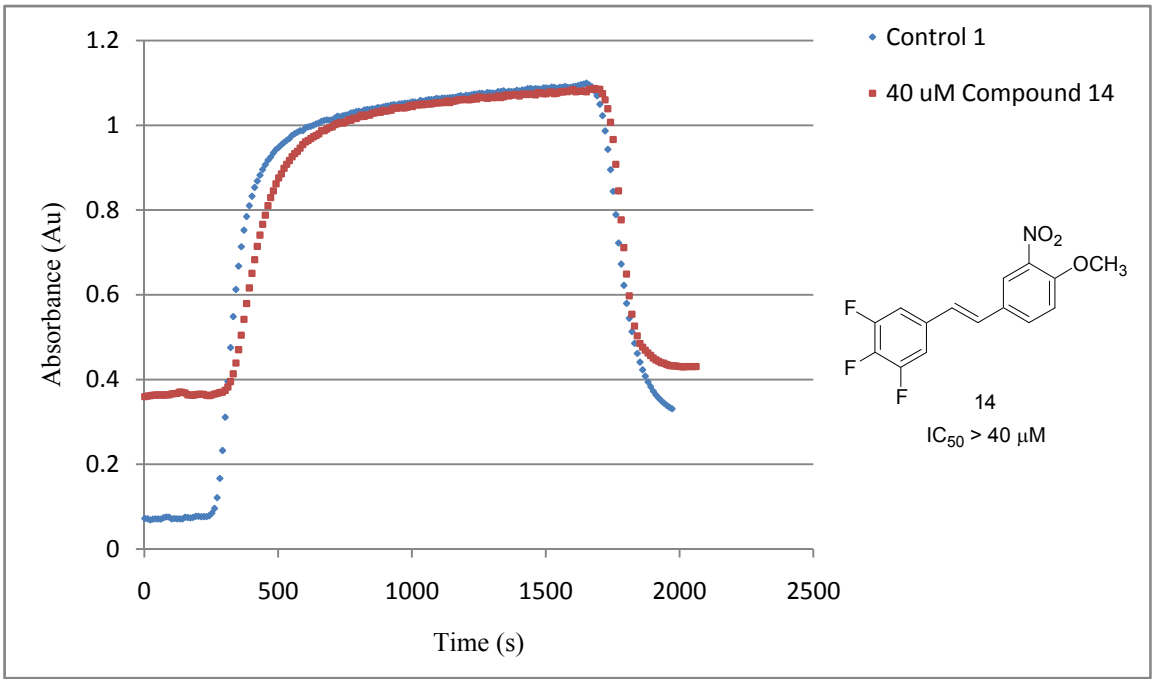

B.2. Tubulin Assay of Compound **14**

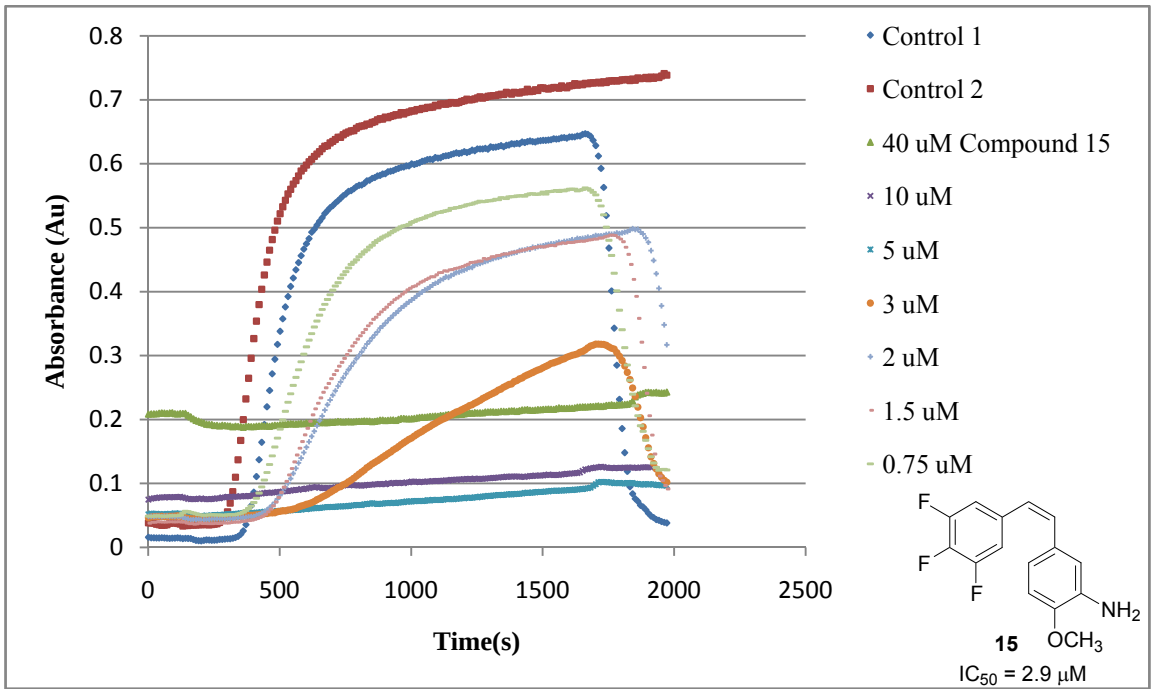

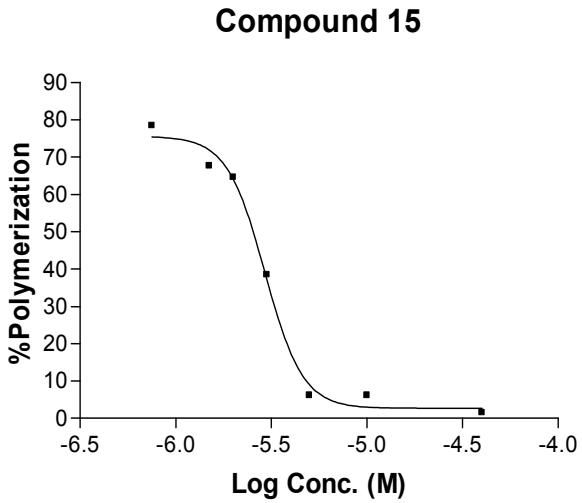

Sigmoidal dose-response (variable slope)	
Best-fit values	
BOTTOM	2.675
TOP	75.57
LOGEC50	-5.534
HILLSLOPE	-4.387
EC50	2.927e-006
Std. Error	
BOTTOM	2.820
TOP	3.641
LOGEC50	0.02475
HILLSLOPE	1.026
95% Confidence Intervals	
BOTTOM	-6.299 to 11.65
TOP	63.98 to 87.15
LOGEC50	-5.612 to -5.455
HILLSLOPE	-7.651 to -1.123
EC50	2.442e-006 to 3.509e-006
Goodness of Fit	
Degrees of Freedom	3
R^2	0.9926
Absolute Sum of Squares	48.88
Sy.x	4.037
Data	
Number of X values	7
Number of Y replicates	1
Total number of values	7
Number of missing values	0

B.3. Tubulin Assay of Compound **15**

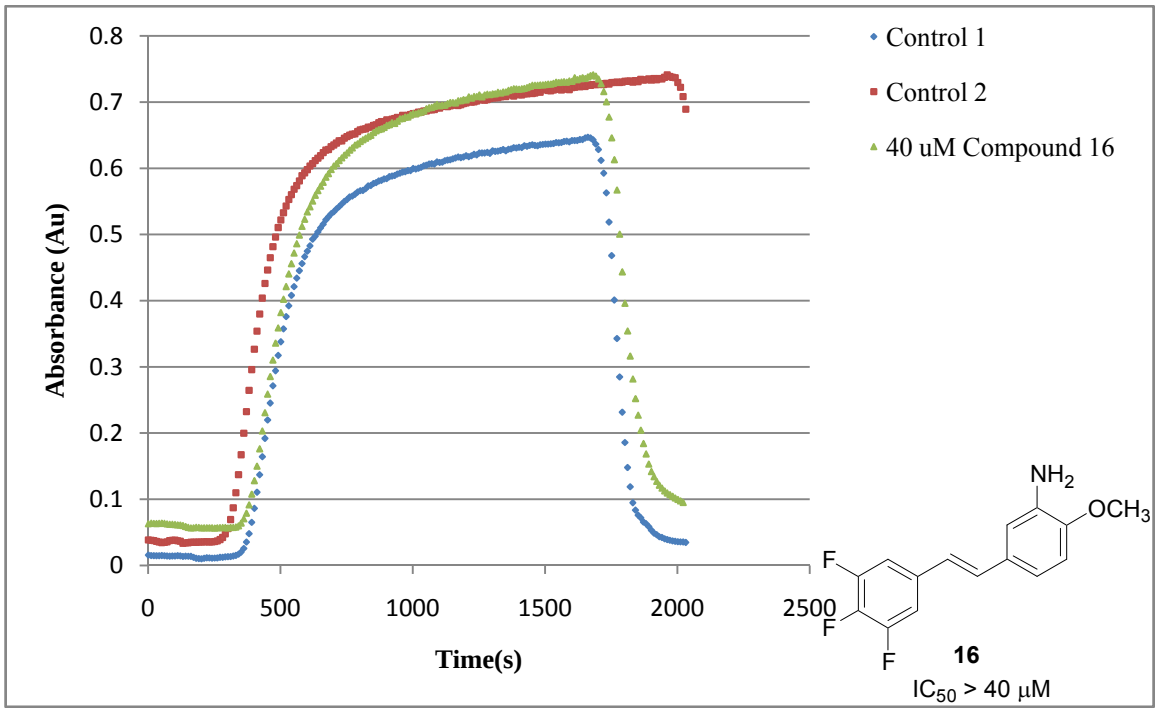

B.4. Tubulin Assay of Compound **16**

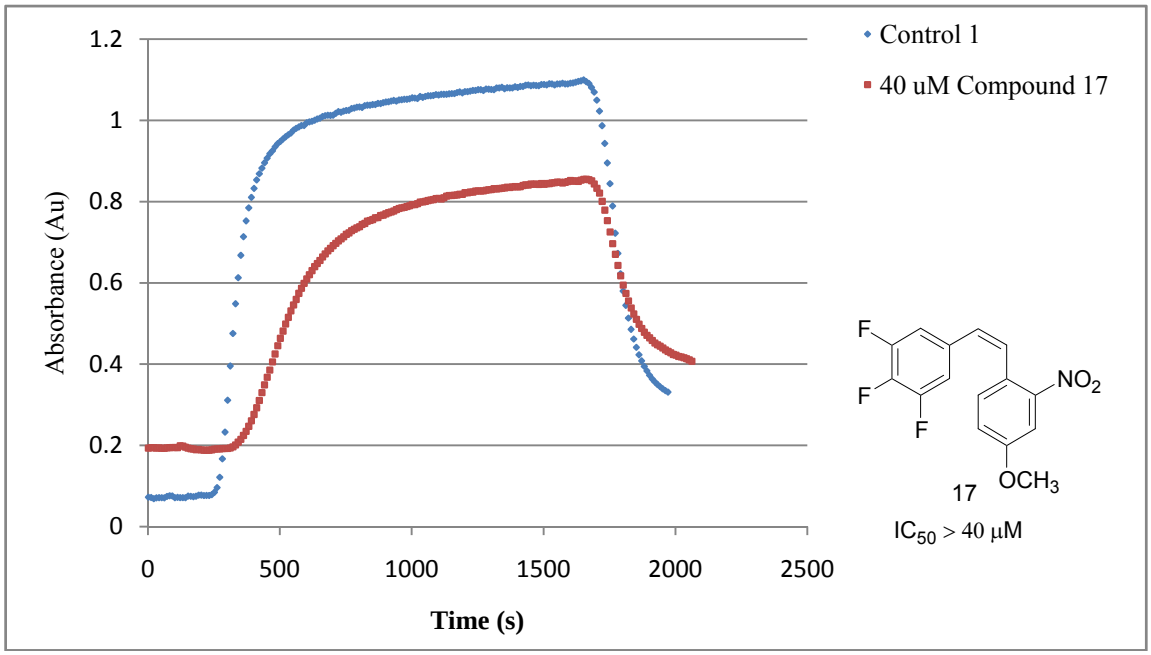

B.5. Tubulin Assay of Compound **17**

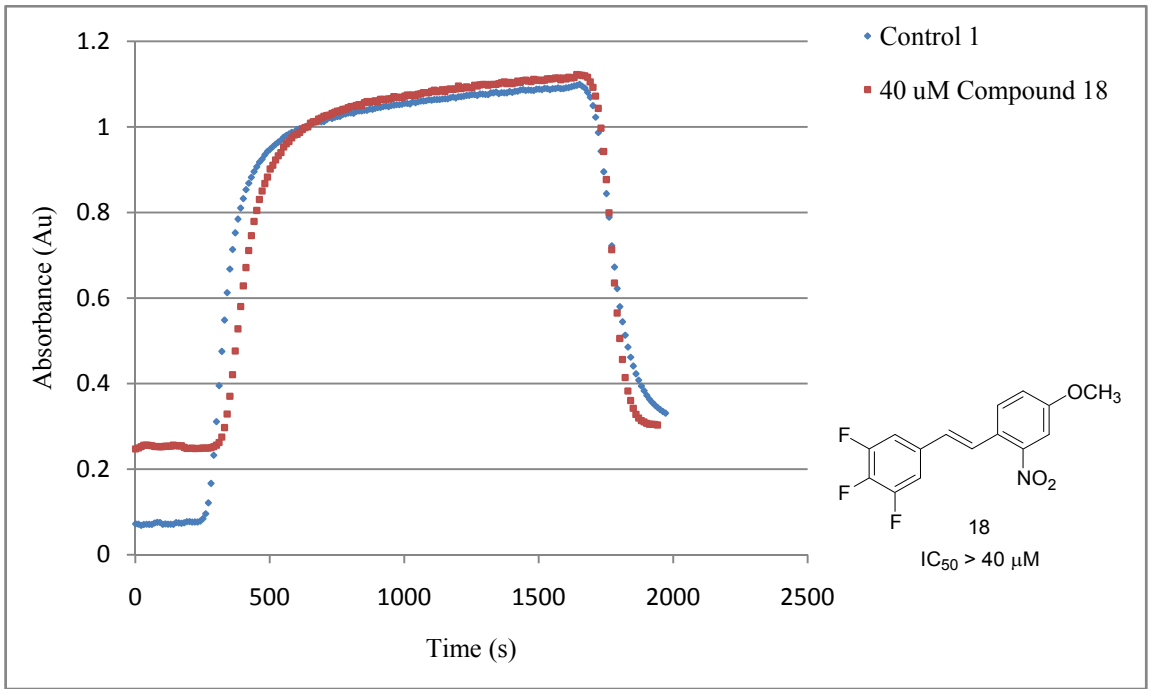

B.6. Tubulin Assay of Compound **18**

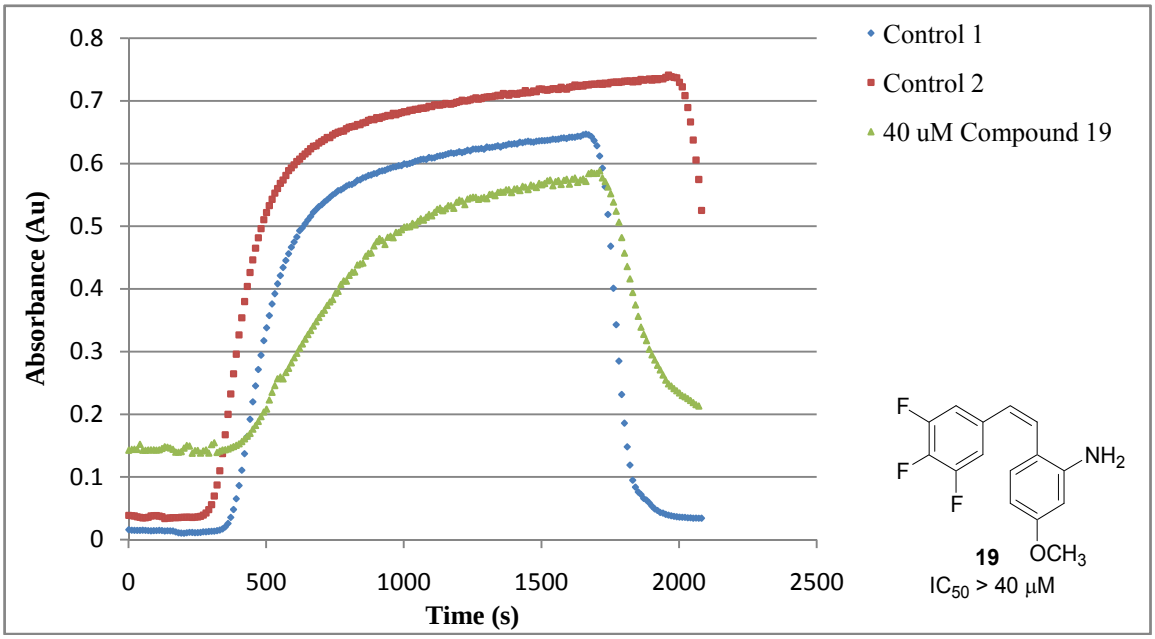

B.7. Tubulin Assay of Compound **19**

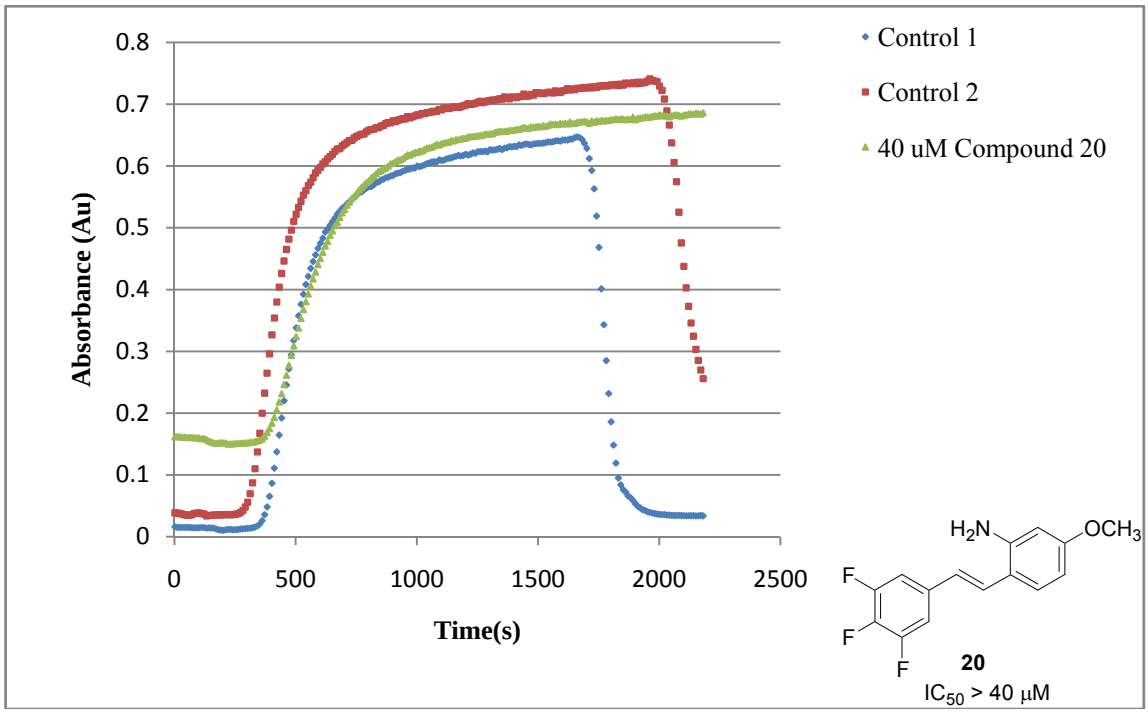

B.8. Tubulin Assay of Compound **20**

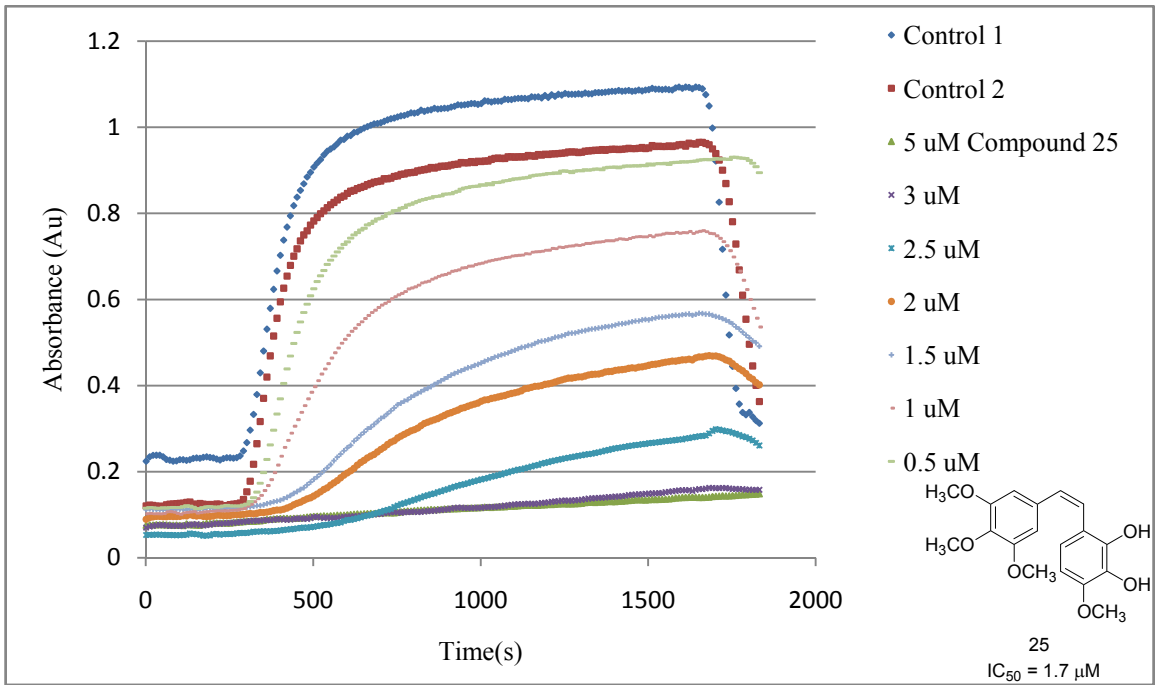

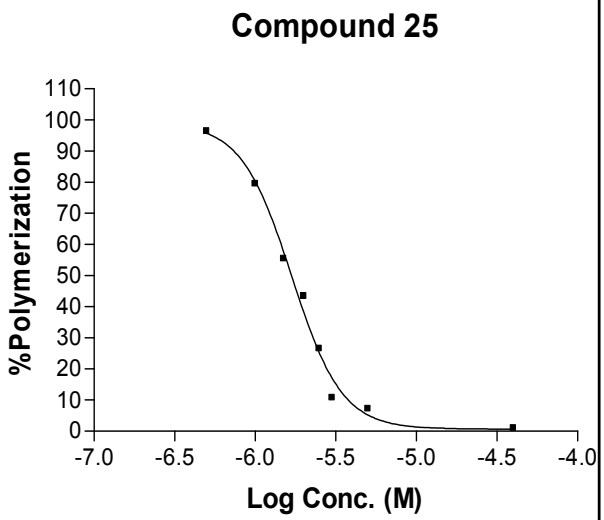

Sigmoidal dose-response (variable slope)	
Best-fit values	
BOTTOM	0.6939
TOP	98.90
LOGEC50	-5.773
HILLSLOPE	-2.790
EC50	1.685e-006
Std. Error	
BOTTOM	3.745
TOP	5.865
LOGEC50	0.03076
HILLSLOPE	0.4762
95% Confidence Intervals	
BOTTOM	-9.703 to 11.09
TOP	82.61 to 115.2
LOGEC50	-5.859 to -5.688
HILLSLOPE	-4.112 to -1.468
EC50	1.384e-006 to 2.051e-006
Goodness of Fit	
Degrees of Freedom	4
R^2	0.9910
Absolute Sum of Squares	77.84
Sy.x	4.411
Data	
Number of X values	8
Number of Y replicates	1
Total number of values	8
Number of missing values	0

B.9. Tubulin Assay of Compound **25**

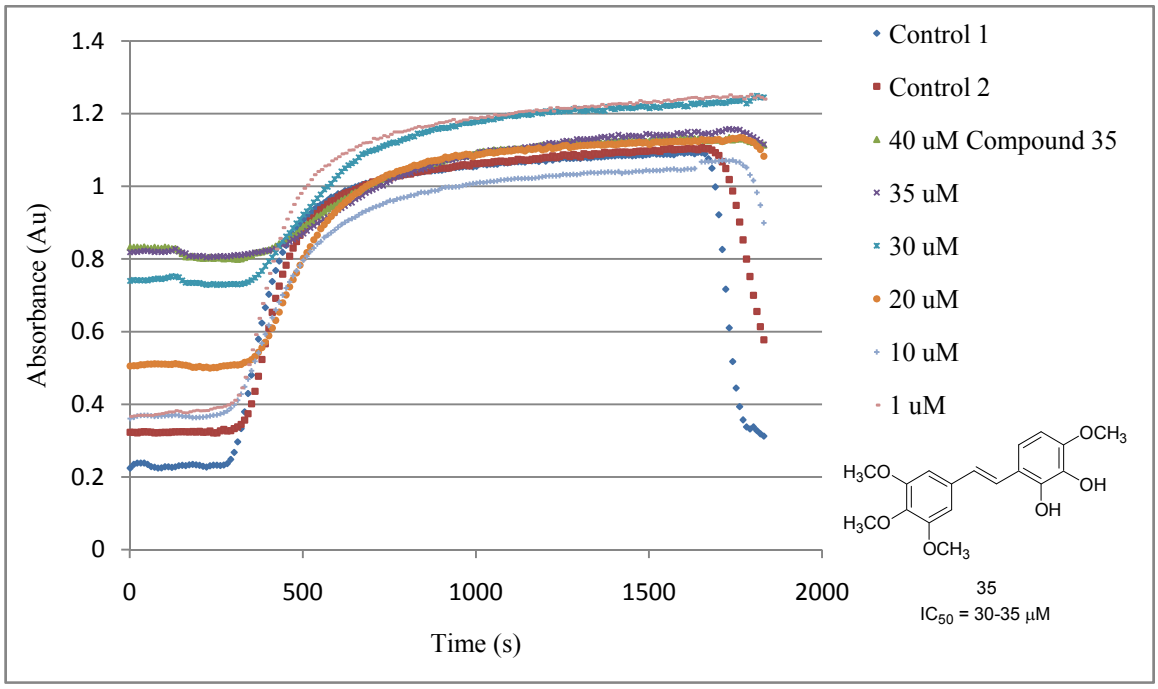

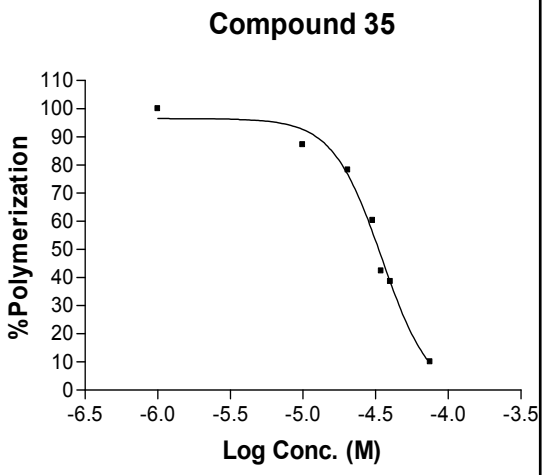

Sigmoidal dose-response (variable slope)	
Best-fit values	
BOTTOM	-2.598
TOP	96.45
LOGEC50	-4.458
HILLSLOPE	-2.569
EC50	3.486e-005
Std. Error	
BOTTOM	14.89
TOP	4.761
LOGEC50	0.06002
HILLSLOPE	0.8366
95% Confidence Intervals	
BOTTOM	-49.97 to 44.77
TOP	81.30 to 111.6
LOGEC50	-4.649 to -4.267
HILLSLOPE	-5.231 to 0.09322
EC50	2.245e-005 to 5.411e-005
Goodness of Fit	
Degrees of Freedom	3
R^2	0.9851
Absolute Sum of Squares	88.73
Sy.x	5.438
Data	
Number of X values	7
Number of Y replicates	1
Total number of values	7
Number of missing values	0

B.10. Tubulin Assay of Compound **35**

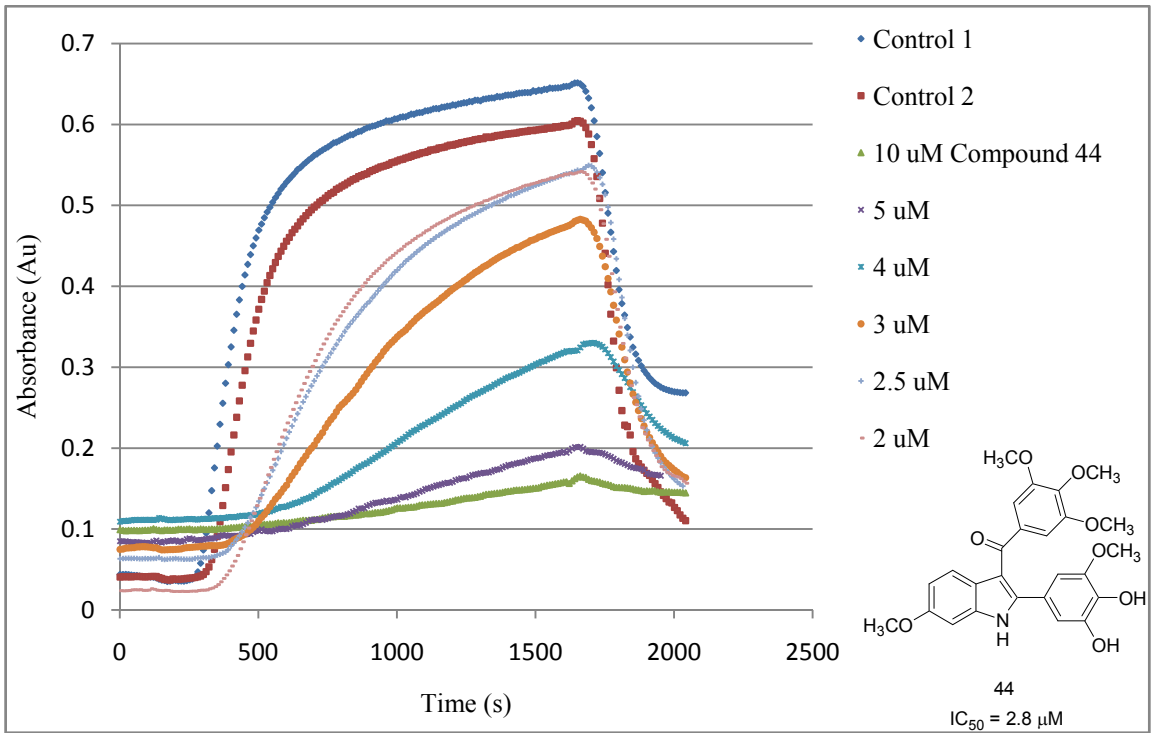

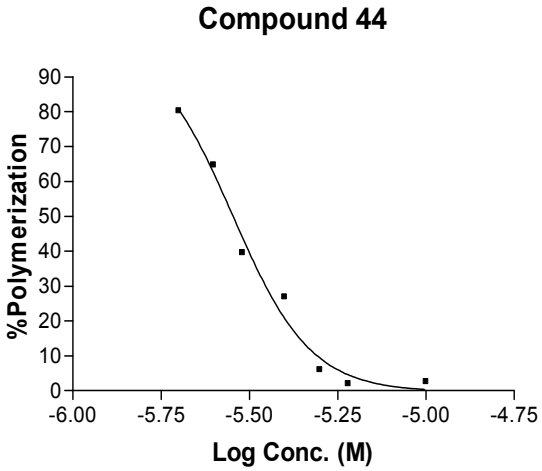

Sigmoidal dose-response (variable slope)	
Best-fit values	
BOTTOM	-0.3715
TOP	100.7
LOGEC50	-5.547
HILLSLOPE	-3.944
EC50	2.838e-006
Std. Error	
BOTTOM	5.597
TOP	25.09
LOGEC50	0.06173
HILLSLOPE	1.477
95% Confidence Intervals	
BOTTOM	-18.18 to 17.44
TOP	20.89 to 180.5
LOGEC50	-5.743 to -5.351
HILLSLOPE	-8.644 to 0.7571
EC50	1.805e-006 to 4.461e-006
Goodness of Fit	
Degrees of Freedom	3
R^2	0.9855
Absolute Sum of Squares	85.59
Sy.x	5.341
Data	
Number of X values	7
Number of Y replicates	1
Total number of values	7
Number of missing values	0

B.11. Tubulin Assay of Compound **44**

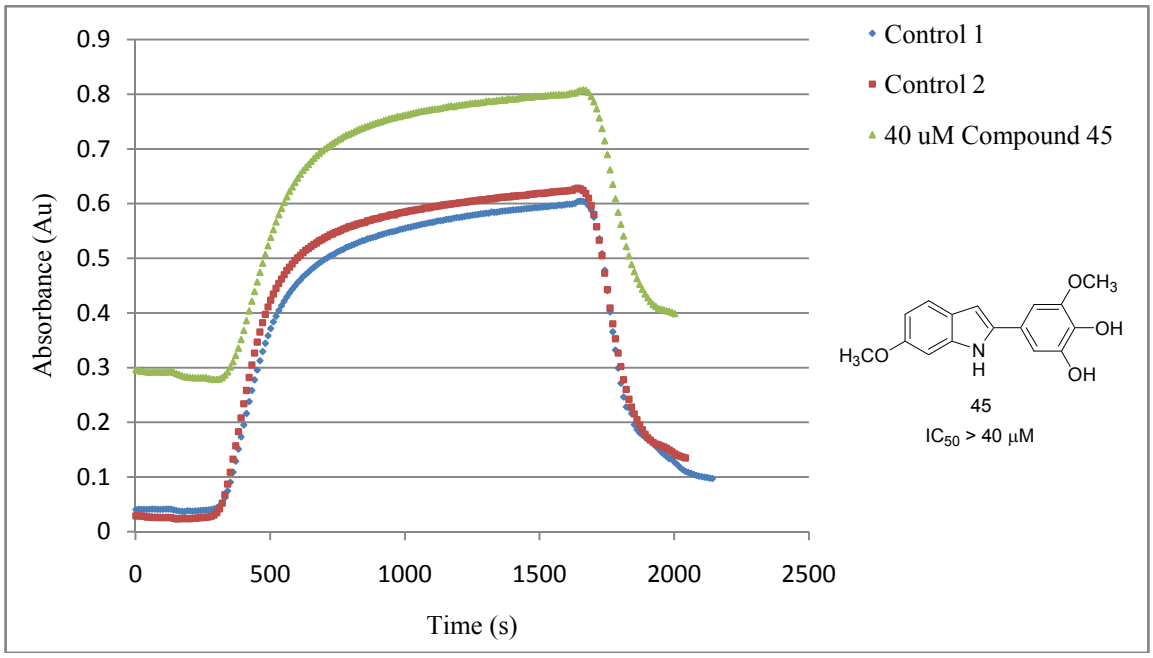

B.12. Tubulin Assay of Compound **45**

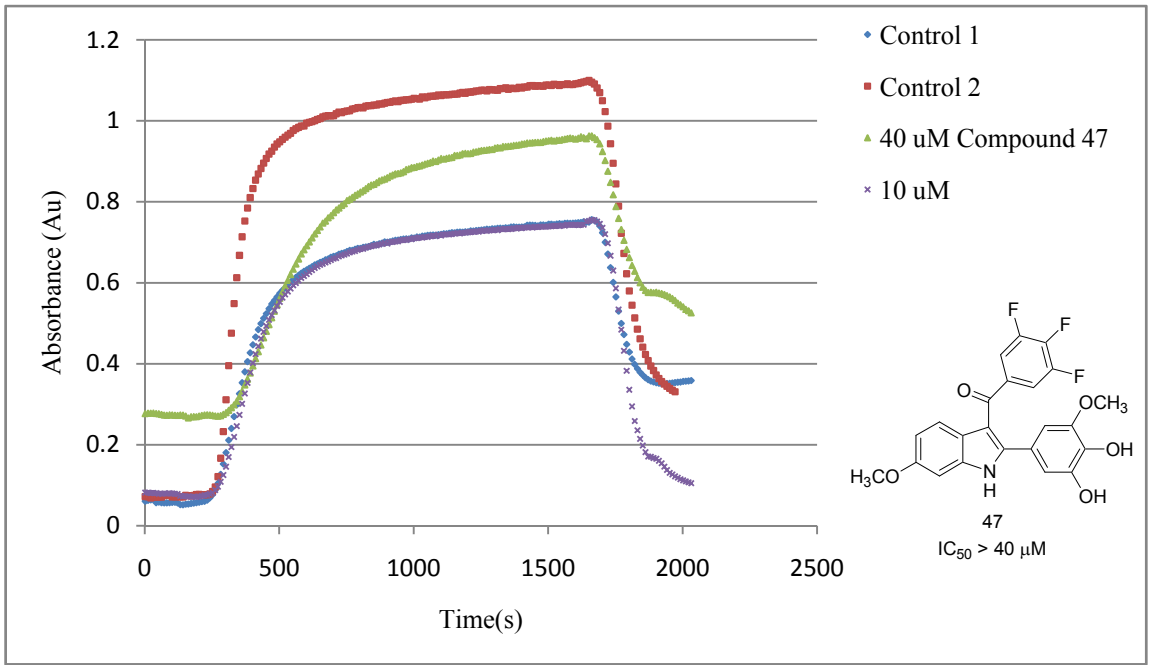

B.13. Tubulin Assay of Compound **47**

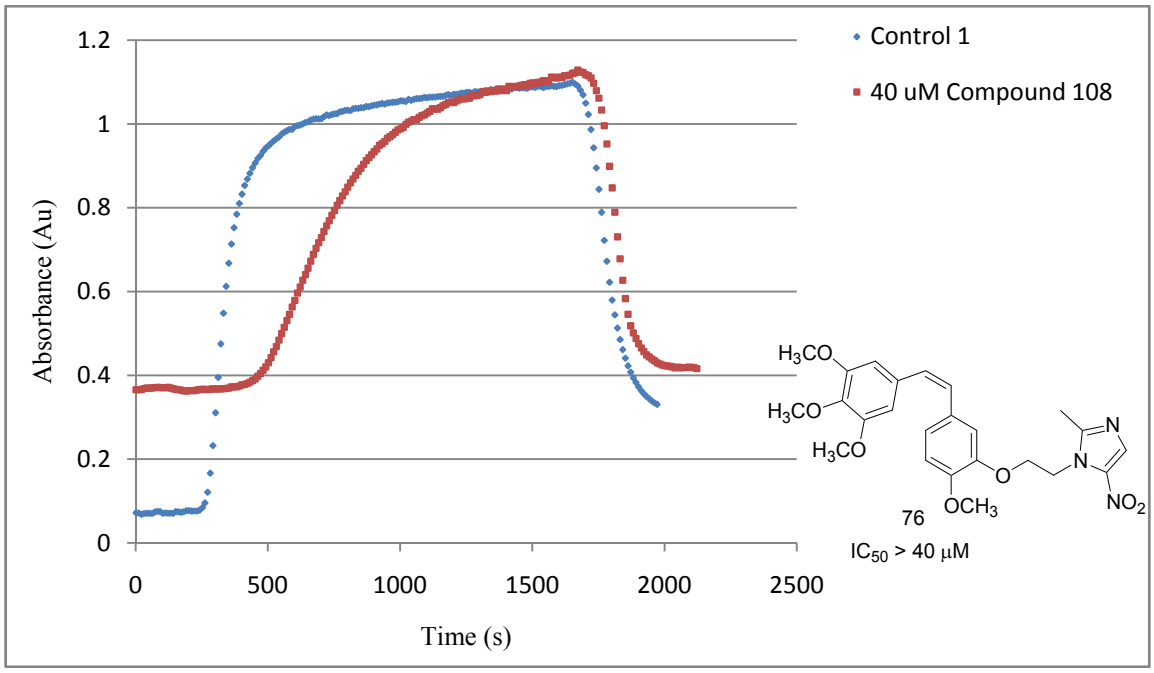

B.14. Tubulin Assay of Compound **76**

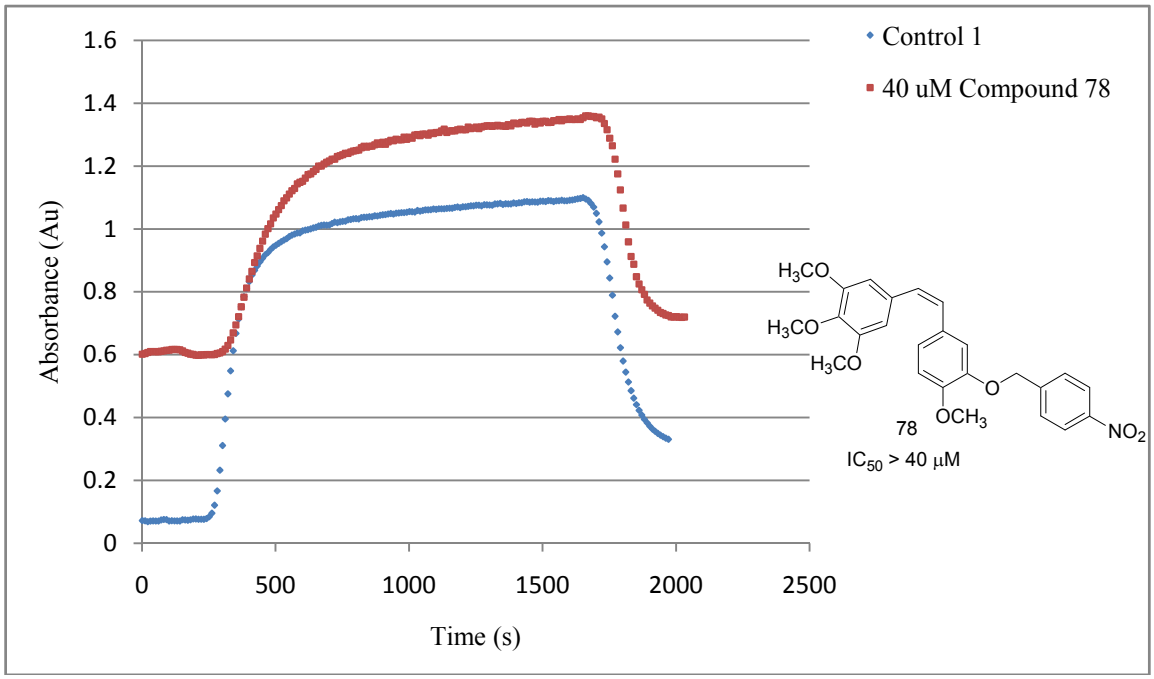

B.15. Tubulin Assay of Compound **78**

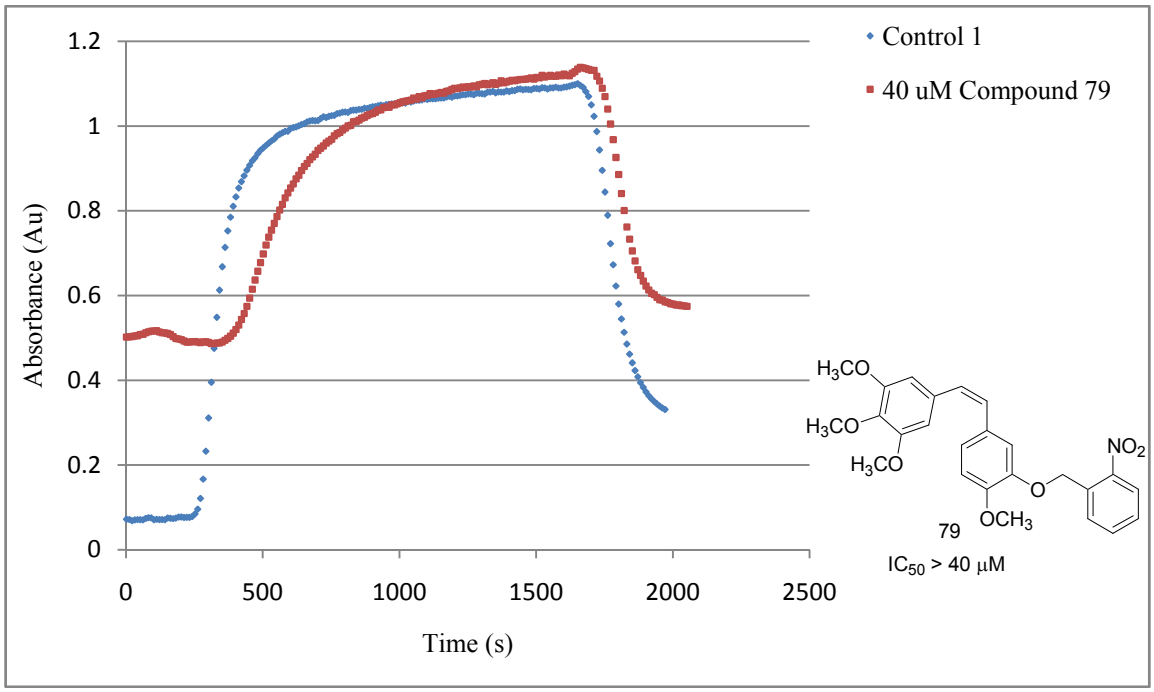

B.16. Tubulin Assay of Compound **79**

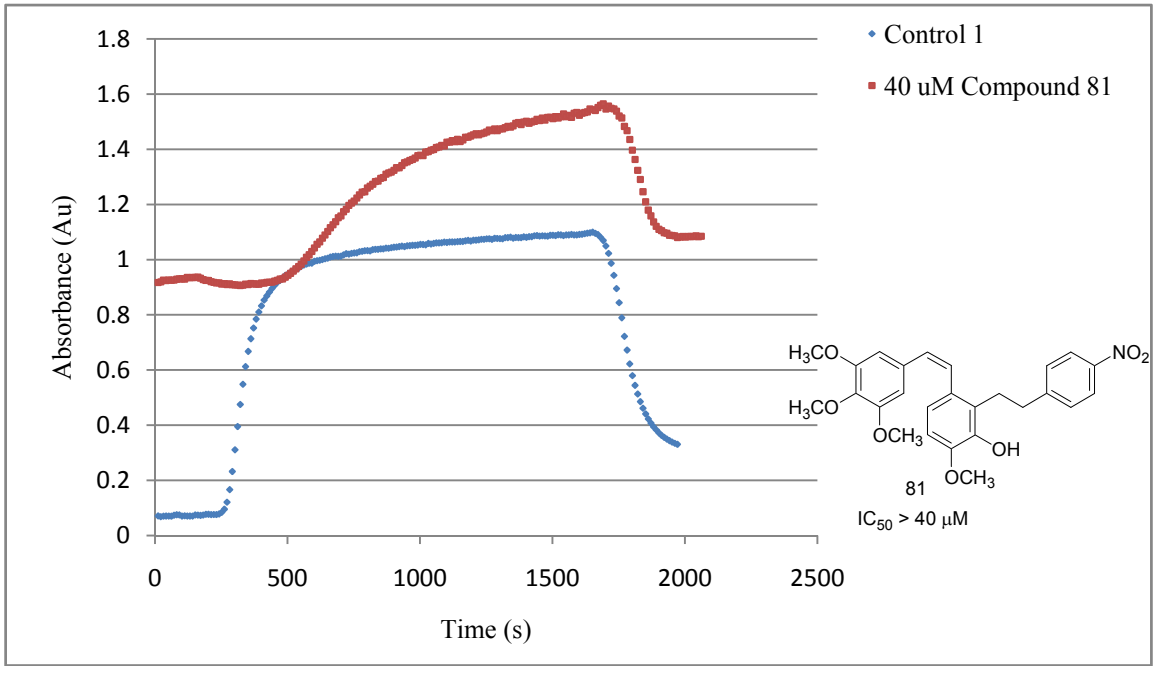

B.17. Tubulin Assay of Compound **81**

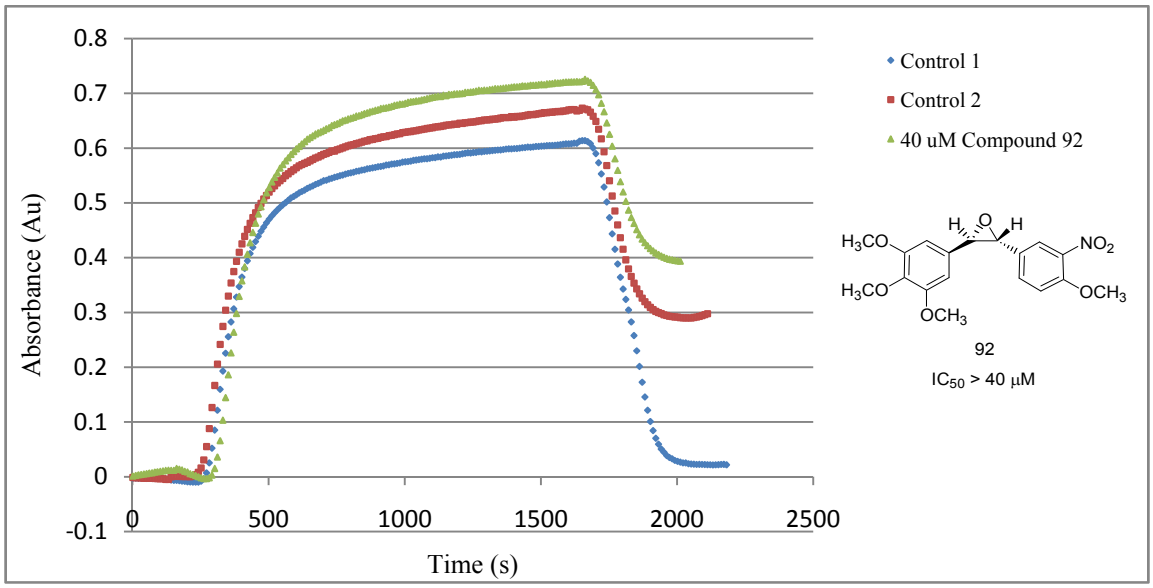

B.18. Tubulin Assay of Compound **92**

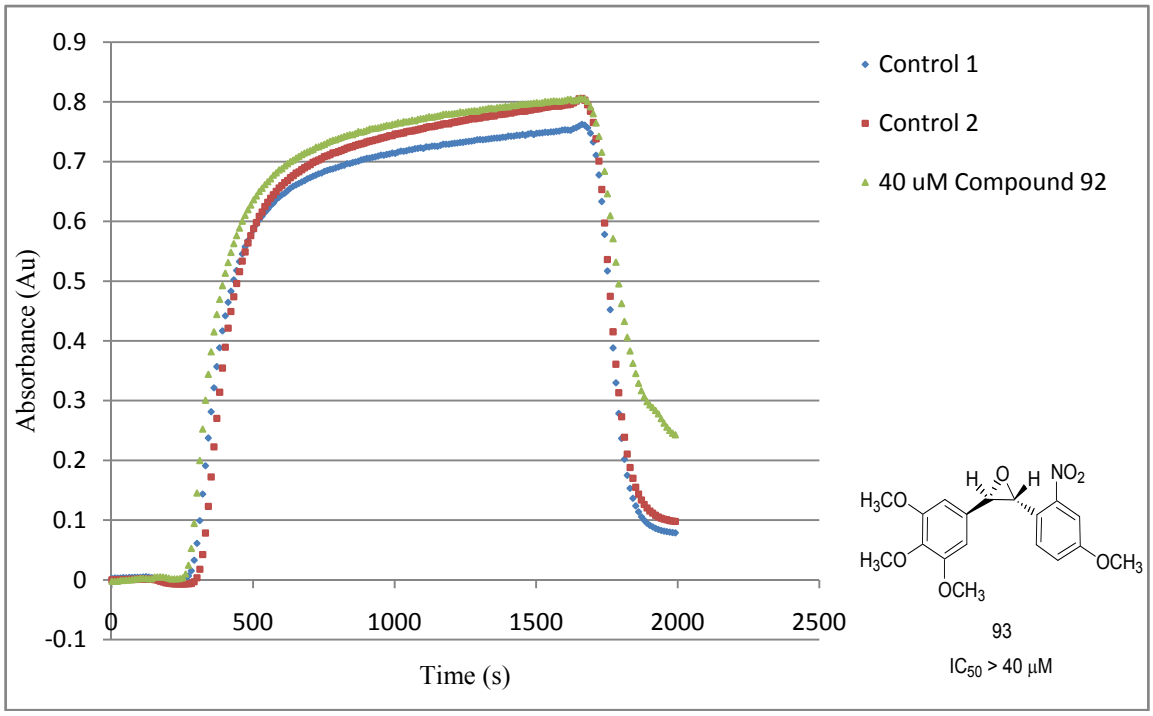

B.19. Tubulin Assay of Compound **93**

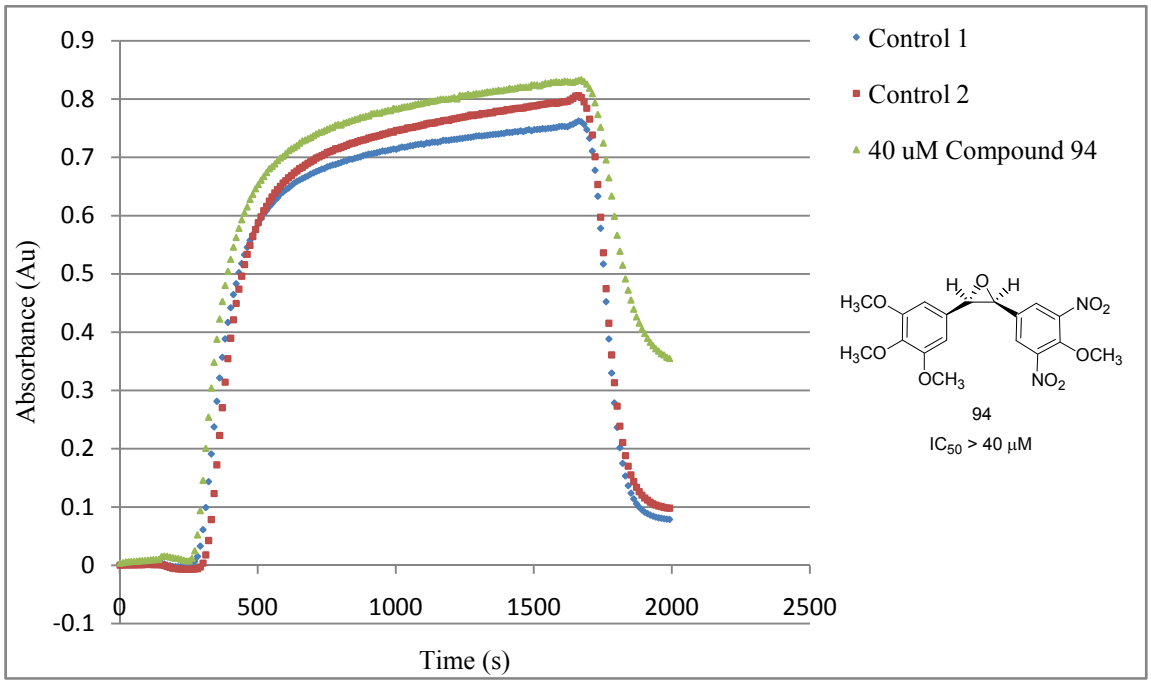

B.20. Tubulin Assay of Compound **94**

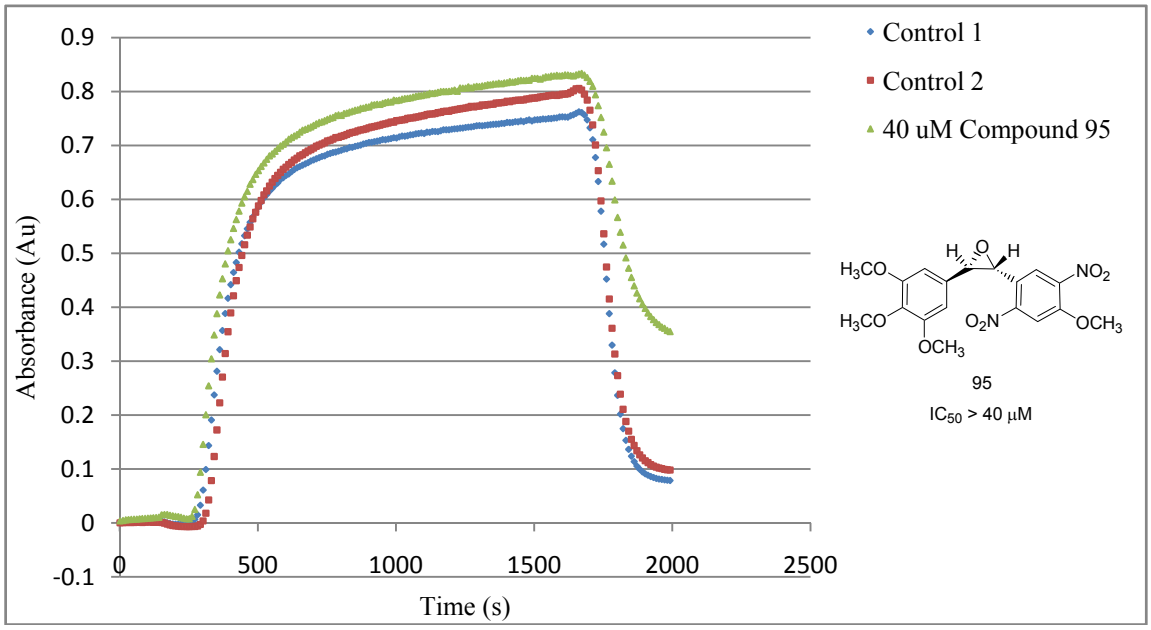

B.21. Tubulin Assay of Compound **95**

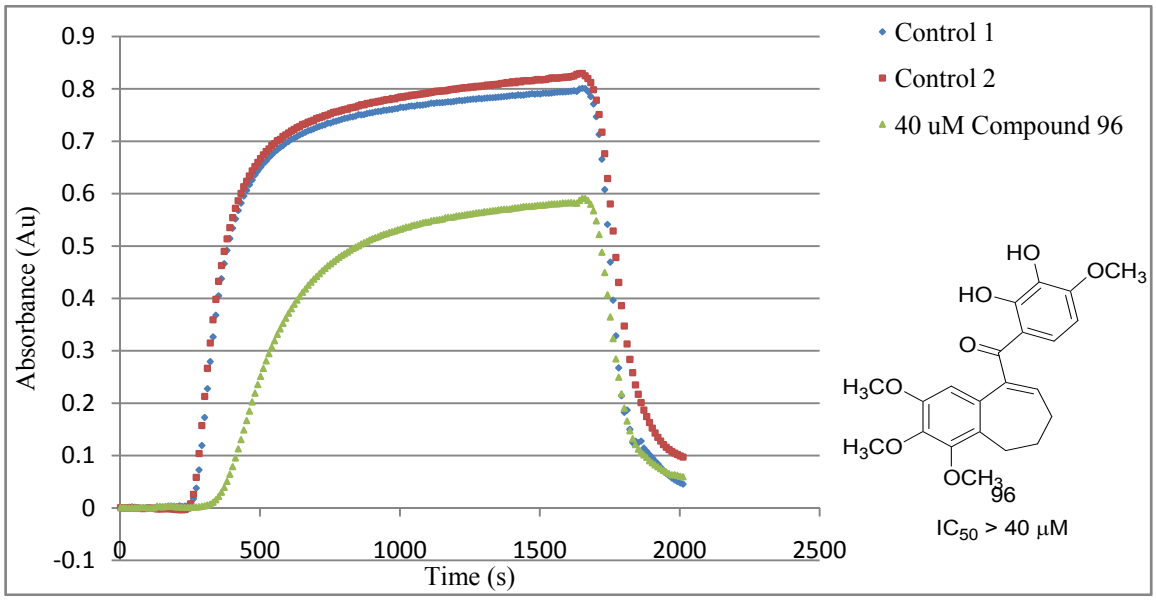

B.22. Tubulin Assay of Compound **96**

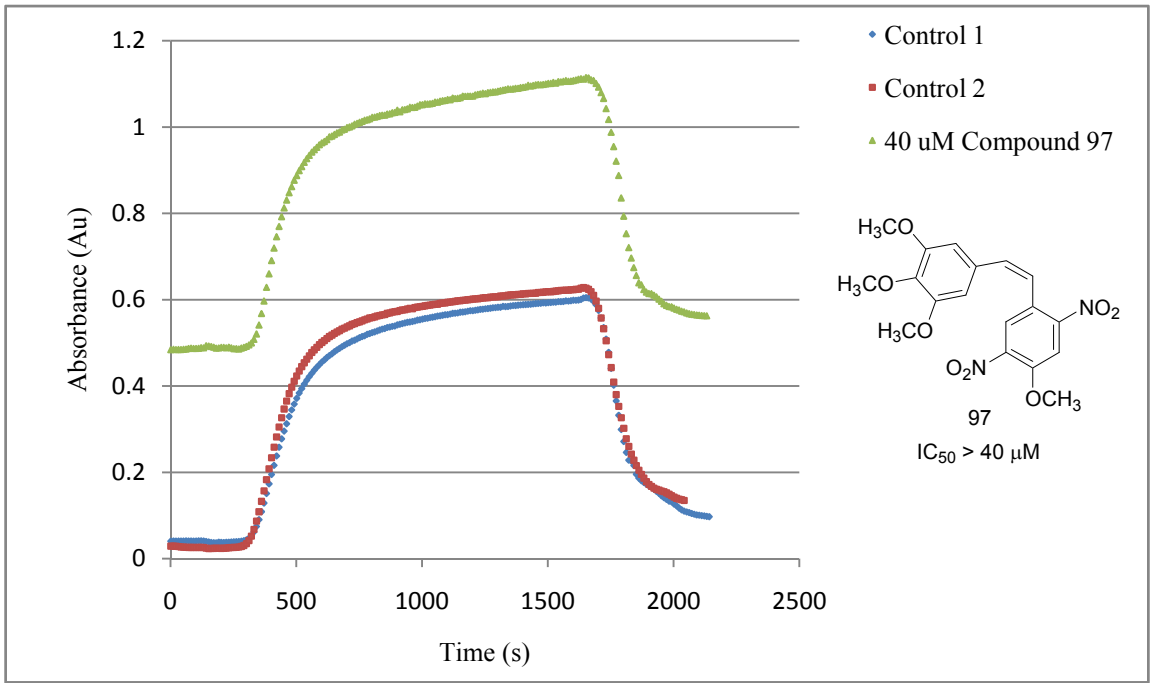

B.23. Tubulin Assay of Compound **97**

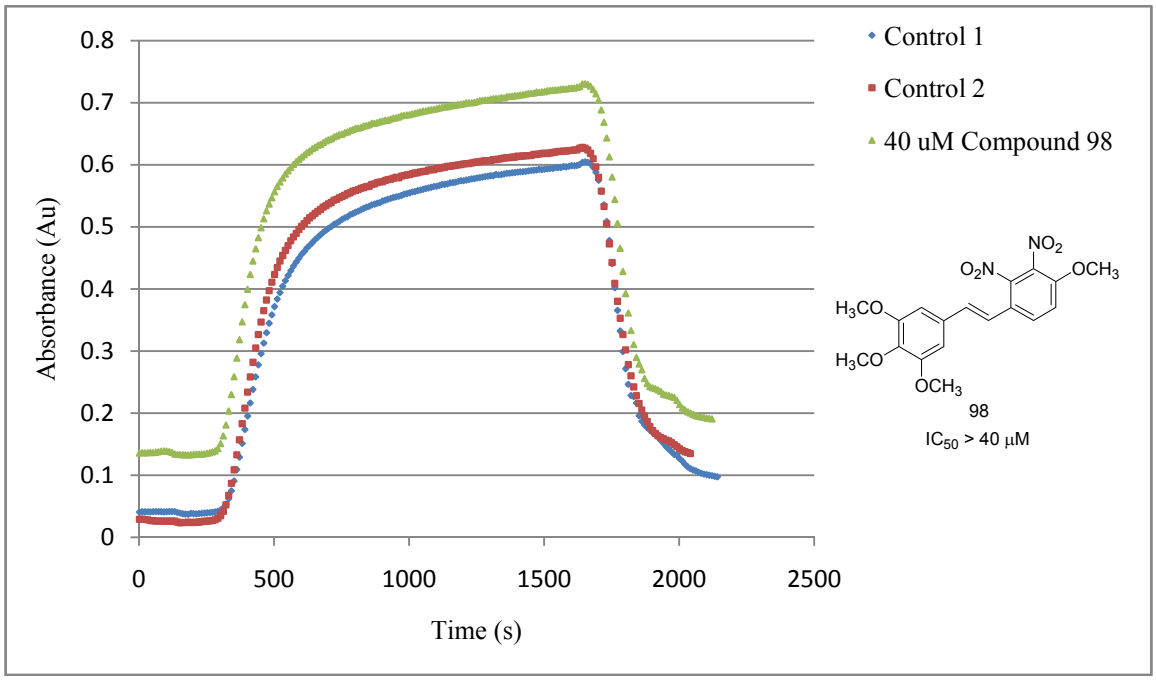

B.24. Tubulin Assay of Compound **98**

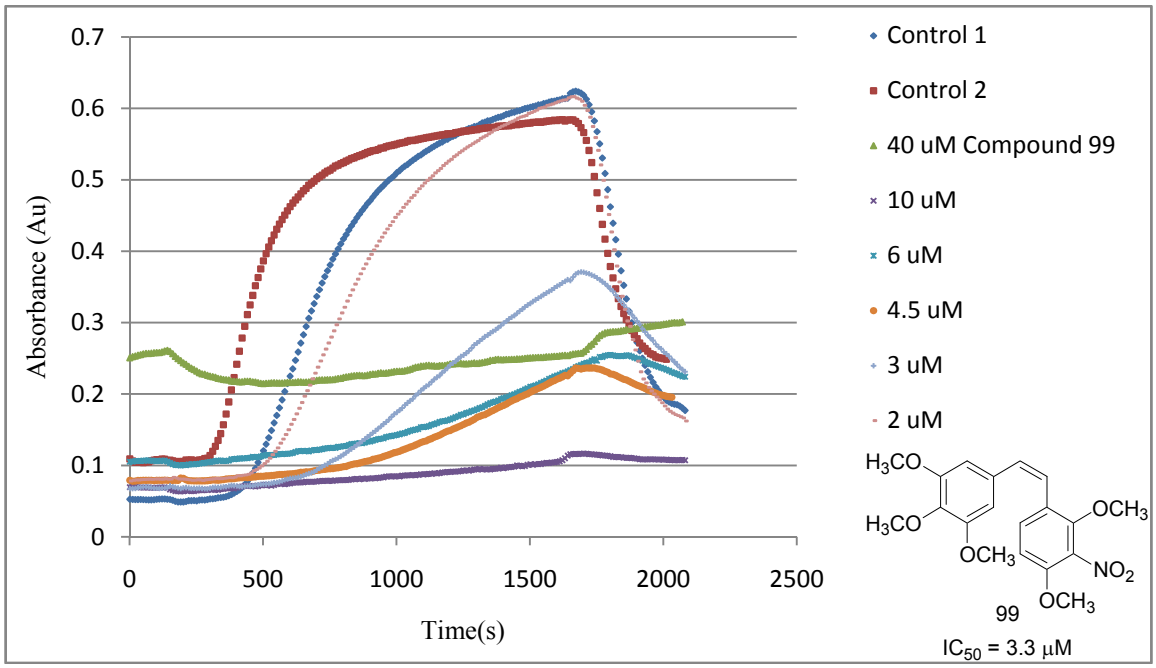

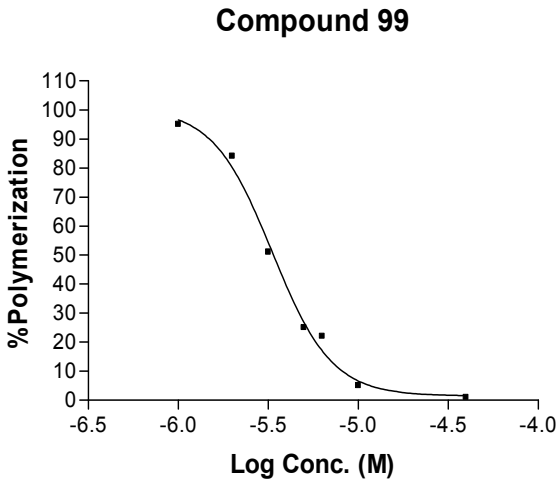

Sigmoidal dose-response (variable slope)	
Best-fit values	
BOTTOM	1.463
TOP	100.6
LOGEC50	-5.478
HILLSLOPE	-2.633
EC50	3.328e-006
Std. Error	
BOTTOM	3.982
TOP	6.441
LOGEC50	0.03658
HILLSLOPE	0.4854
95% Confidence Intervals	
BOTTOM	-11.21 to 14.14
TOP	80.13 to 121.1
LOGEC50	-5.594 to -5.361
HILLSLOPE	-4.177 to -1.088
EC50	2.545e-006 to 4.350e-006
Goodness of Fit	
Degrees of Freedom	3
R^2	0.9929
Absolute Sum of Squares	59.63
Sy.x	4.458
Data	
Number of X values	7
Number of Y replicates	1
Total number of values	7
Number of missing values	0

B.25. Tubulin Assay of Compound **99**

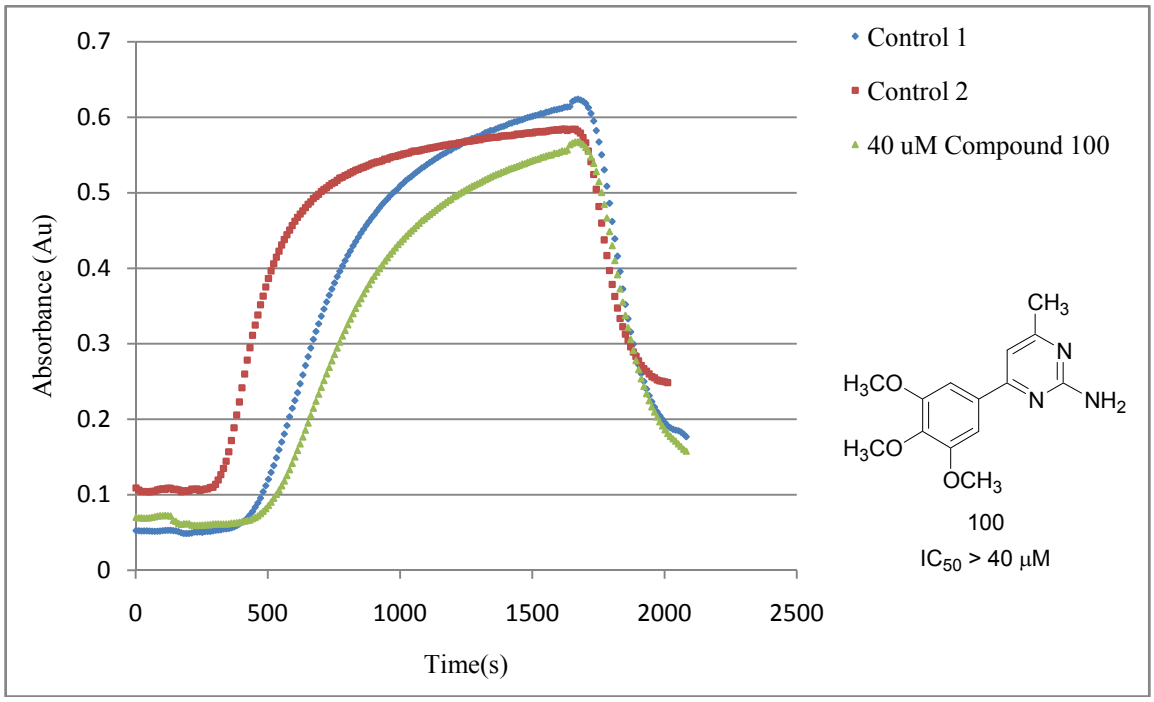

B.26. Tubulin Assay of Compound **100**

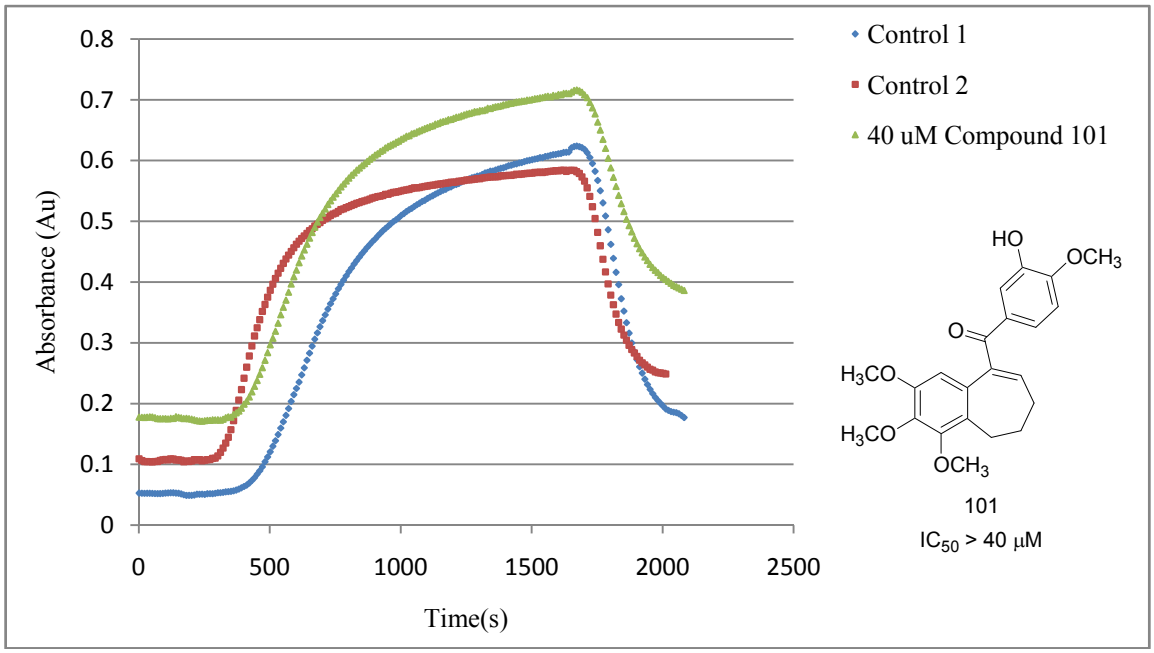

B.27. Tubulin Assay for Compound **101**

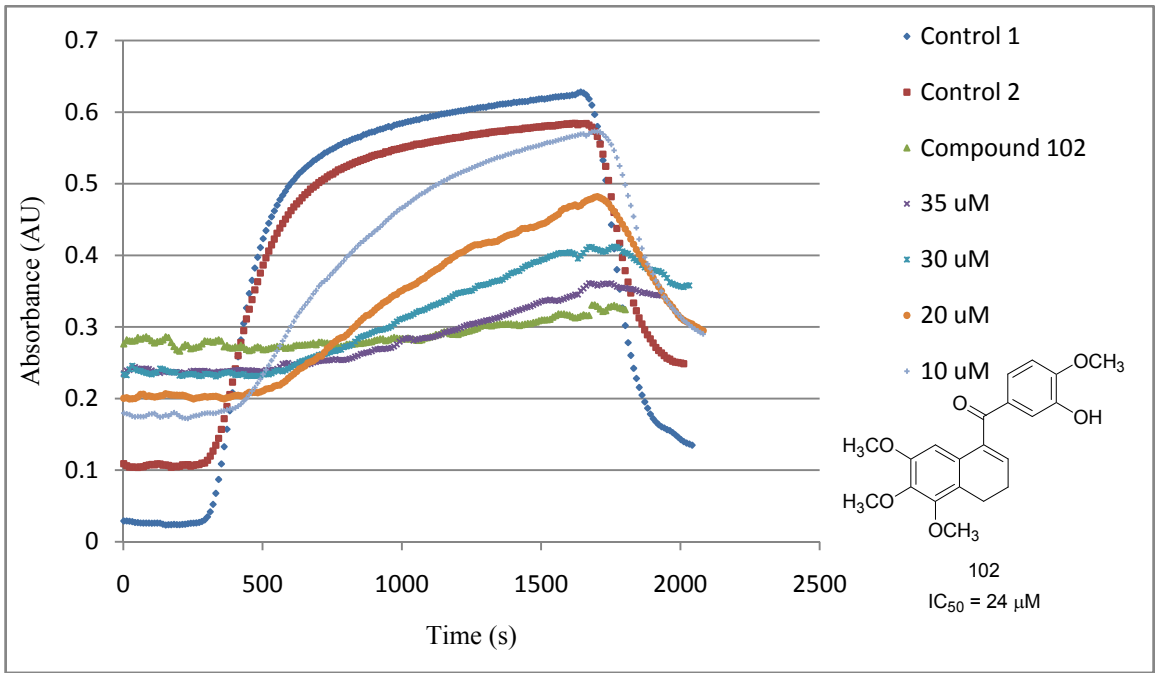

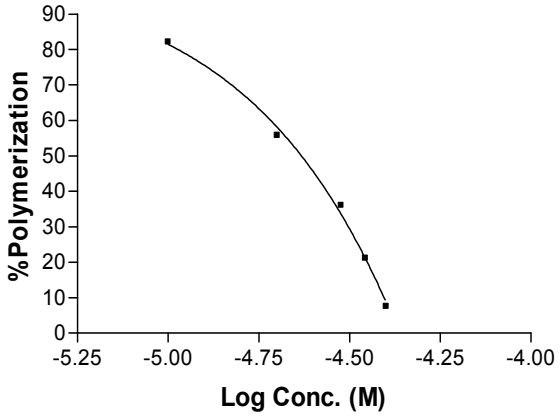

Sigmoidal dose-response (variable slope)	
Best-fit values	
BOTTOM	-4259
TOP	102.0
LOGEC50	-2.897
HILLSLOPE	-1.105
EC50	0.001268
Std. Error	
BOTTOM	452866
TOP	57.63
LOGEC50	45.36
HILLSLOPE	2.802
95% Confidence Intervals	
BOTTOM	-5758000 to 5.750e+006
TOP	-630.2 to 834.2
LOGEC50	-579.2 to 573.4
HILLSLOPE	-36.71 to 34.50
EC50	
Goodness of Fit	
Degrees of Freedom	1
R^2	0.9964
Absolute Sum of Squares	12.33
Sy.x	3.511
Data	
Number of X values	5
Number of Y replicates	1
Total number of values	5
Number of missing values	0

B.28. Tubulin Assay of Compound **102**

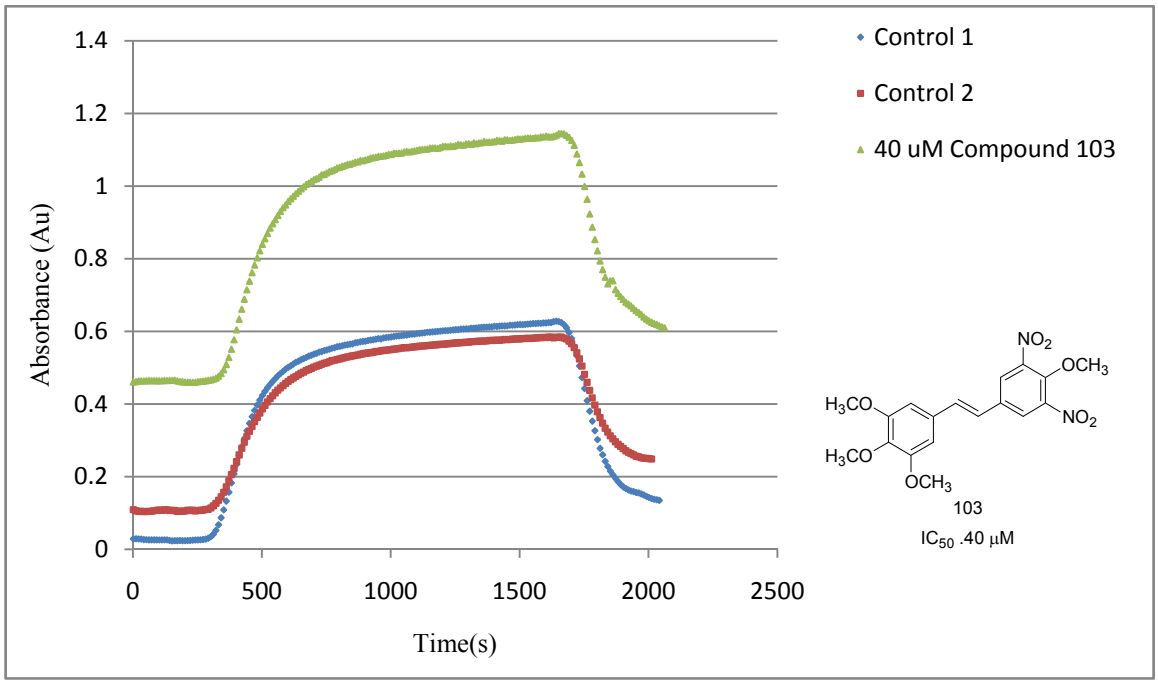

B.29. Tubulin Assay of Compound **103**

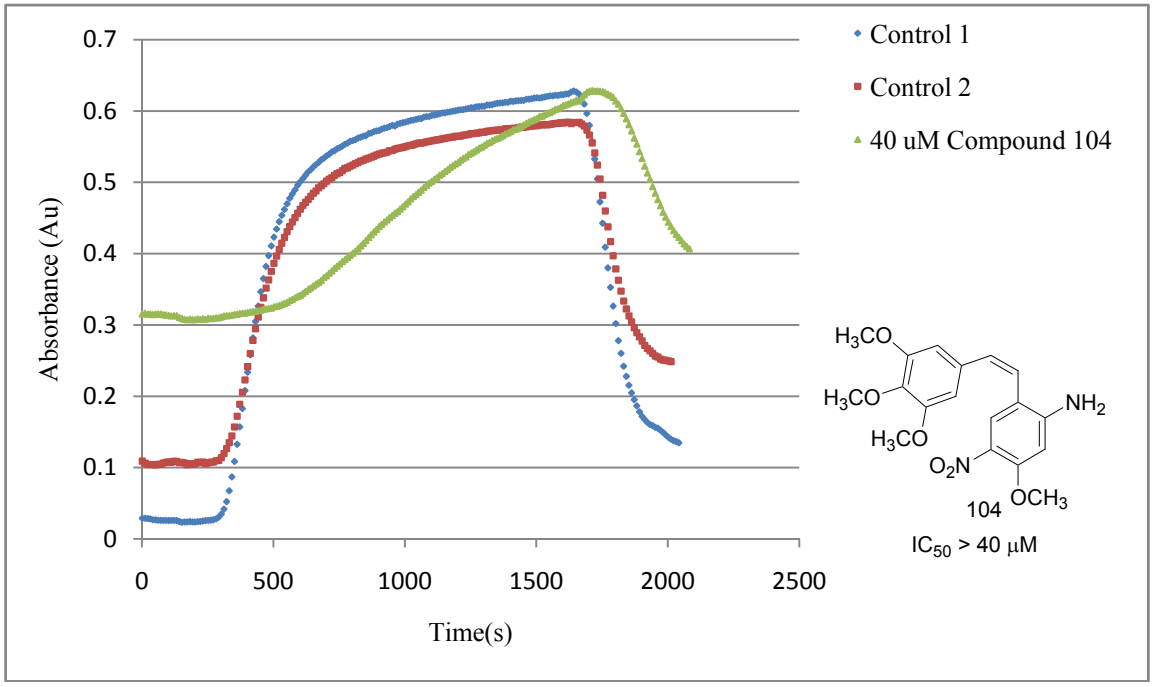

B.30. Tubulin Assay of Compound **104**

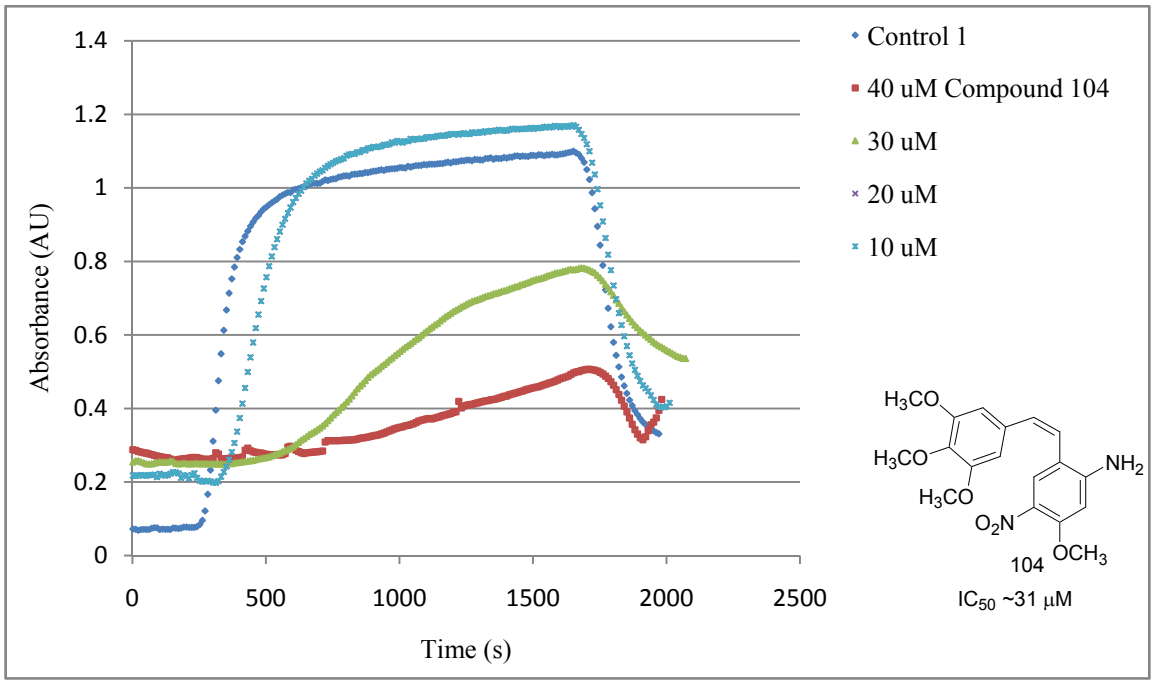

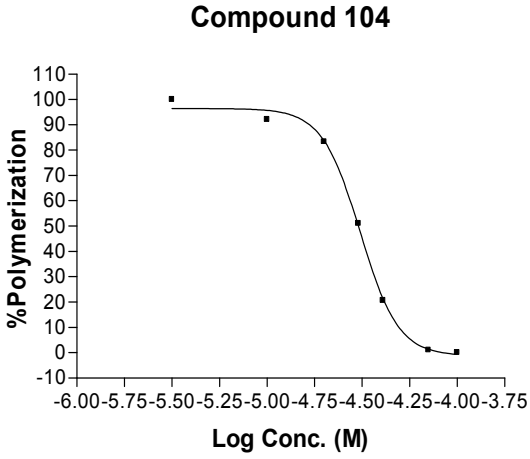

Sigmoidal dose-response (variable slope)	
Best-fit values	
BOTTOM	-1.248
TOP	96.44
LOGEC50	-4.510
HILLSLOPE	-4.337
EC50	3.092e-005
Std. Error	
BOTTOM	2.527
TOP	2.202
LOGEC50	0.01275
HILLSLOPE	0.5348
95% Confidence Intervals	
BOTTOM	-9.289 to 6.793
TOP	89.43 to 103.4
LOGEC50	-4.550 to -4.469
HILLSLOPE	-6.038 to -2.635
EC50	2.816e-005 to 3.395e-005
Goodness of Fit	
Degrees of Freedom	3
R^2	0.9976
Absolute Sum of Squares	27.33
Sy.x	3.018
Data	
Number of X values	7
Number of Y replicates	1
Total number of values	7
Number of missing values	0

B.31. Tubulin Assay of Compound **104**

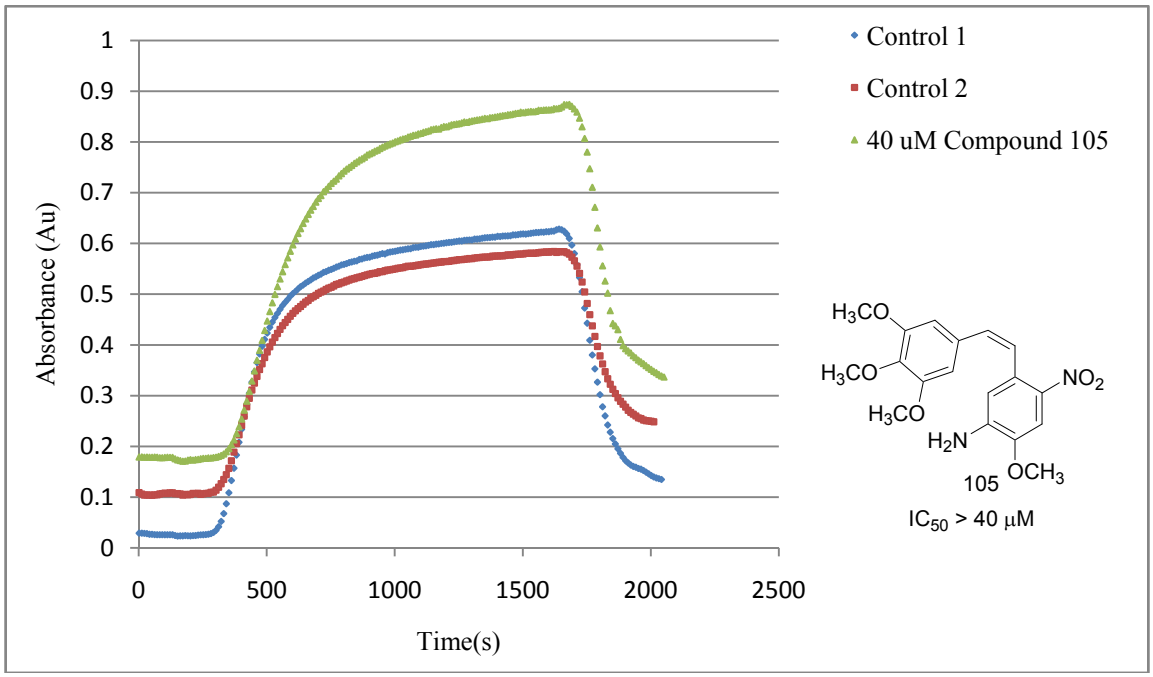

B.32. Tubulin Assay of Compound **105**

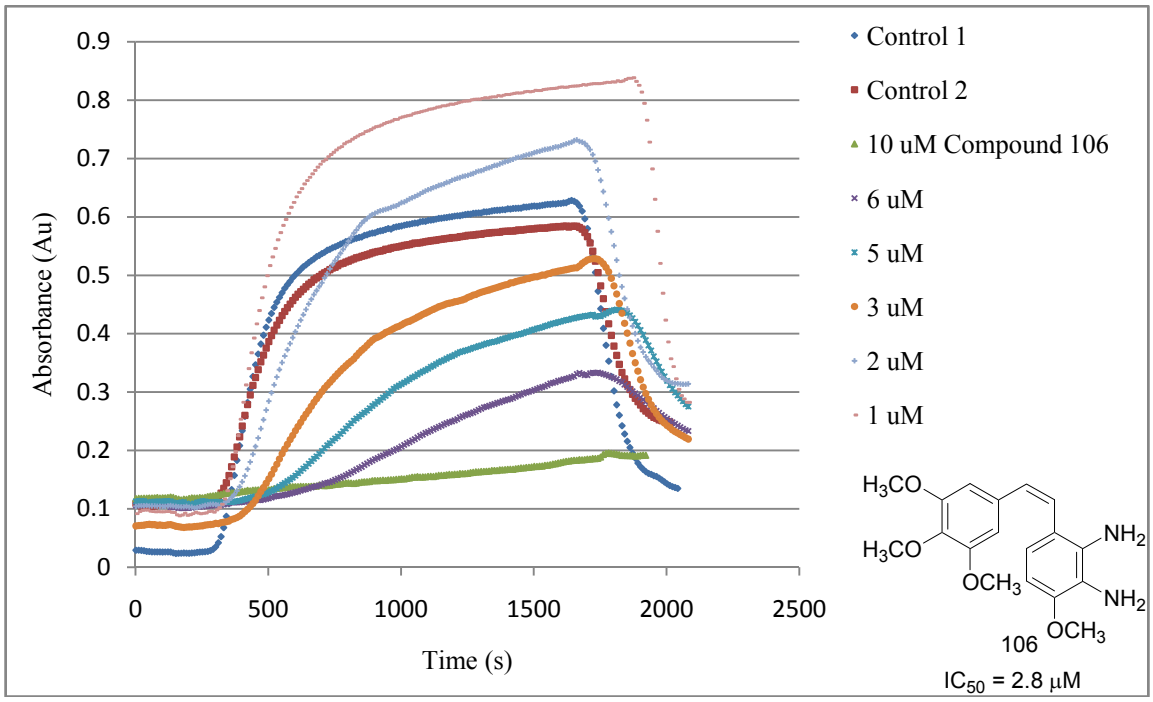

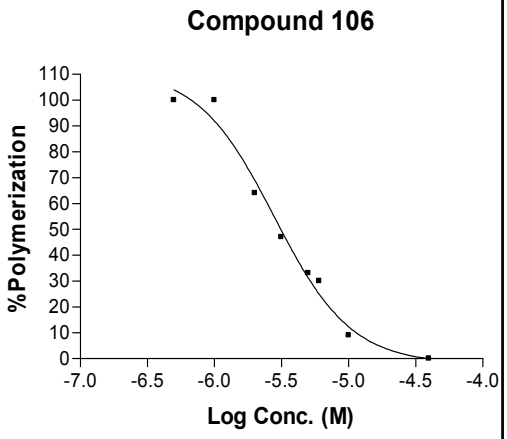

Sigmoidal dose-response (variable slope)	
Best-fit values	
BOTTOM	-2.000
TOP	111.7
LOGEC50	-5.554
HILLSLOPE	-1.516
EC50	2.793e-006
Std. Error	
BOTTOM	7.403
TOP	11.52
LOGEC50	0.07989
HILLSLOPE	0.4012
95% Confidence Intervals	
BOTTOM	-22.55 to 18.55
TOP	79.77 to 143.7
LOGEC50	-5.776 to -5.332
HILLSLOPE	-2.630 to -0.4025
EC50	1.676e-006 to 4.654e-006
Goodness of Fit	
Degrees of Freedom	4
R^2	0.9849
Absolute Sum of Squares	151.6
Sy.x	6.156
Data	
Number of X values	8
Number of Y replicates	1
Total number of values	8
Number of missing values	0

B.33. Tubulin Assay of Compound **106**

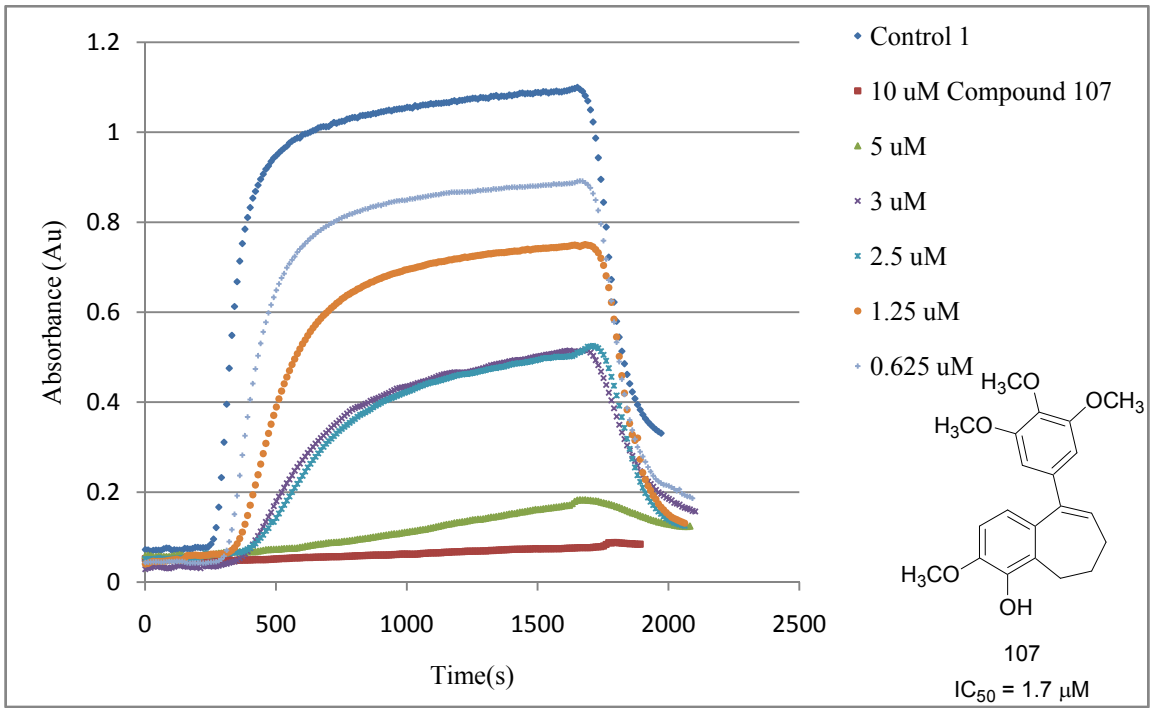

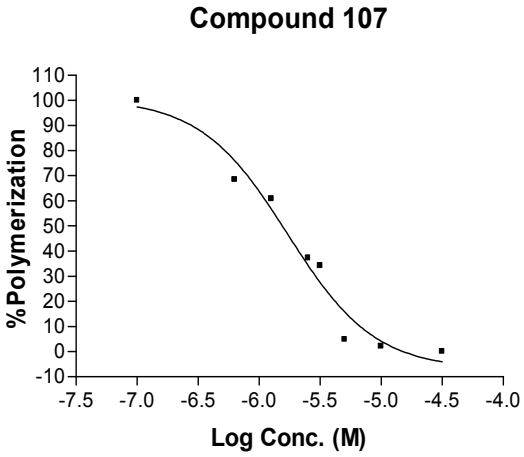

Sigmoidal dose-response (variable slope)	
Best-fit values	
BOTTOM	-7.070
TOP	100.8
LOGEC50	-5.768
HILLSLOPE	-1.218
EC50	1.708e-006
Std. Error	
BOTTOM	10.35
TOP	11.15
LOGEC50	0.1178
HILLSLOPE	0.4075
95% Confidence Intervals	
BOTTOM	-35.79 to 21.65
TOP	69.81 to 131.7
LOGEC50	-6.095 to -5.440
HILLSLOPE	-2.349 to -0.08624
EC50	8.042e-007 to 3.627e-006
Goodness of Fit	
Degrees of Freedom	4
R^2	0.9702
Absolute Sum of Squares	272.4
Sy.x	8.252
Data	
Number of X values	8
Number of Y replicates	1
Total number of values	8
Number of missing values	0

B.34. Tubulin Assay of Compound **107**

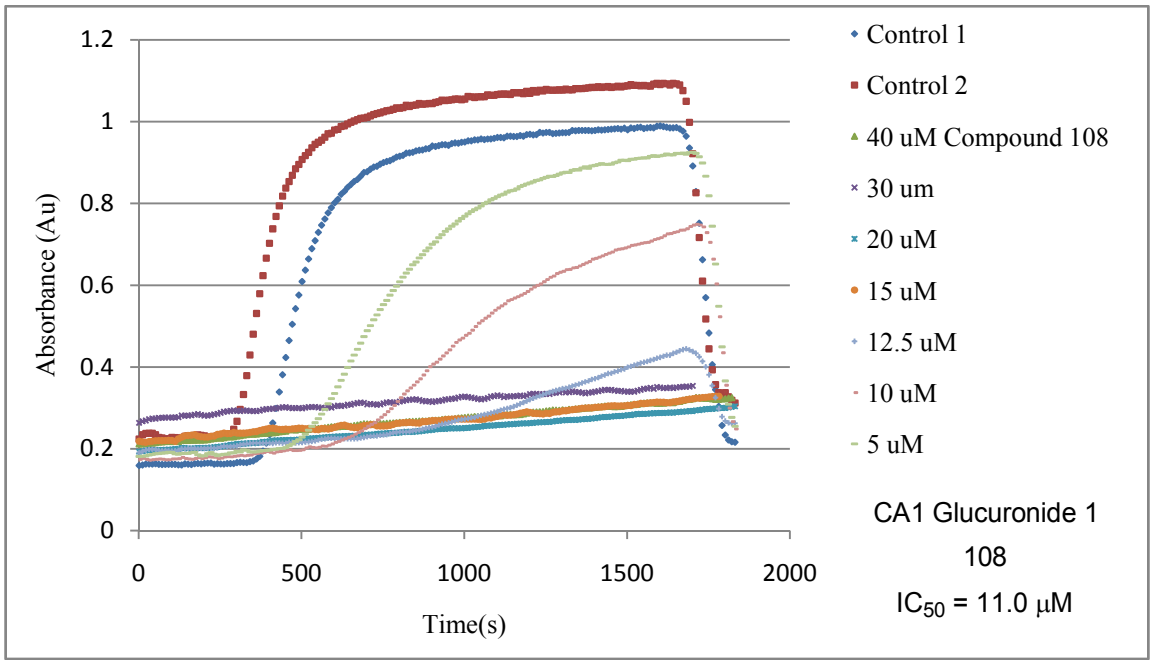

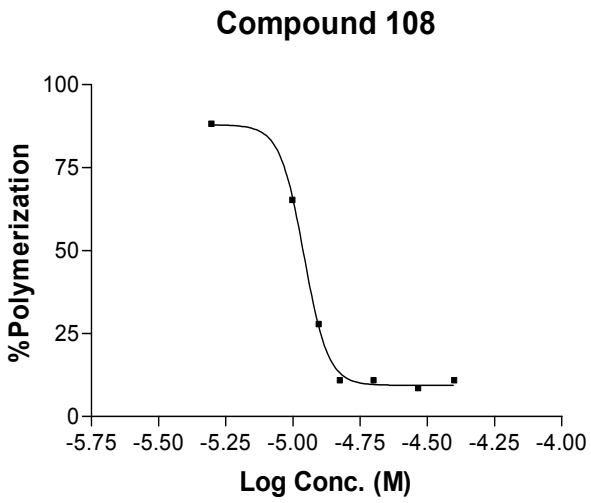

Sigmoidal dose-response (variable slope)	
Best-fit values	
BOTTOM	9.432
TOP	87.90
LOGEC50	-4.959
HILLSLOPE	-9.751
EC50	1.098e-005
Std. Error	
BOTTOM	1.031
TOP	1.858
LOGEC50	0.005067
HILLSLOPE	0.8268
95% Confidence Intervals	
BOTTOM	6.152 to 12.71
TOP	81.98 to 93.81
LOGEC50	-4.975 to -4.943
HILLSLOPE	-12.38 to -7.120
EC50	1.058e-005 to 1.140e-005
Goodness of Fit	
Degrees of Freedom	3
R^2	0.9983
Absolute Sum of Squares	10.29
Sy.x	1.852
Data	
Number of X values	7
Number of Y replicates	1
Total number of values	7
Number of missing values	0

B.35. Tubulin Binding Assay of Compound **108**

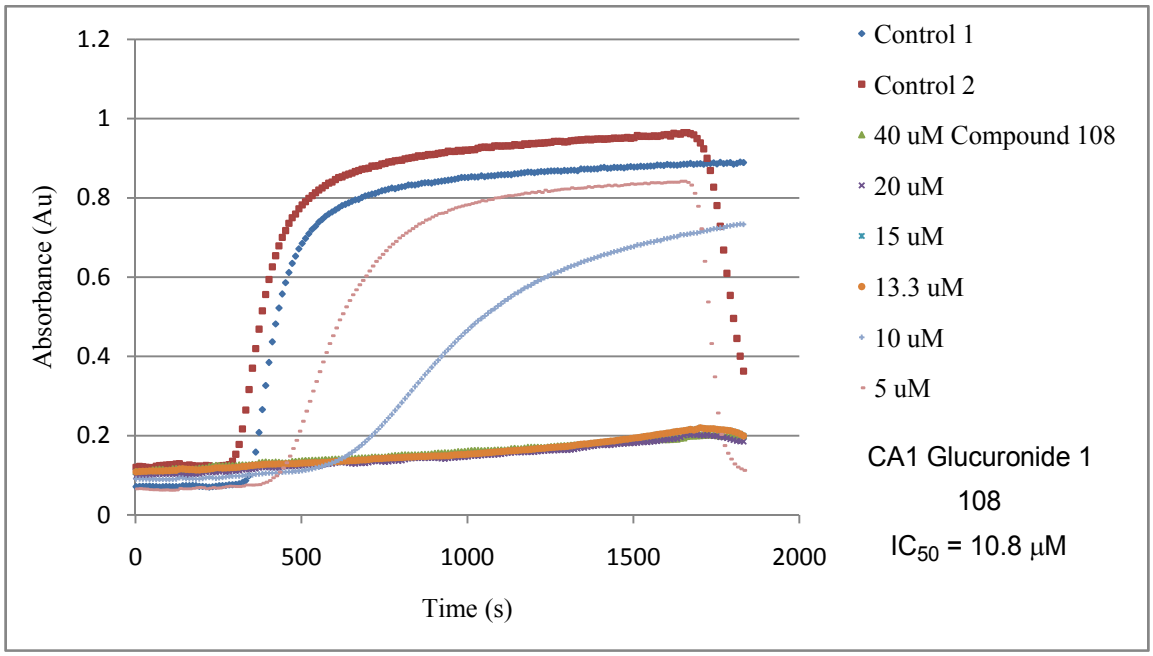

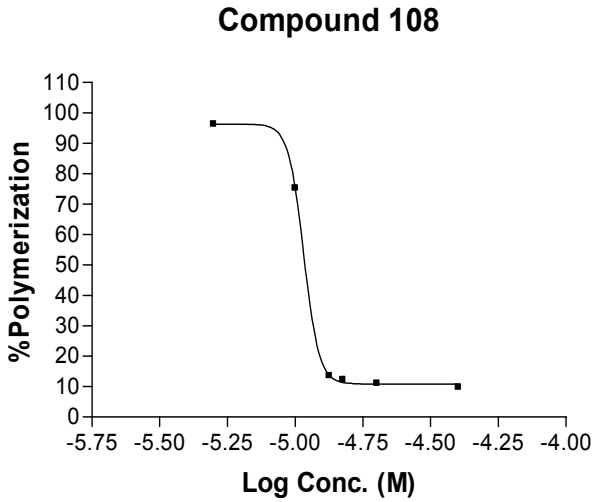

Sigmoidal dose-response (variable slope)	
Best-fit values	
BOTTOM	10.86
TOP	96.31
LOGEC50	-4.968
HILLSLOPE	-15.43
EC50	1.075e-005
Std. Error	
BOTTOM	0.6144
TOP	0.9786
LOGEC50	0.003475
HILLSLOPE	1.433
95% Confidence Intervals	
BOTTOM	8.212 to 13.50
TOP	92.10 to 100.5
LOGEC50	-4.983 to -4.954
HILLSLOPE	-21.60 to -9.268
EC50	1.039e-005 to 1.113e-005
Goodness of Fit	
Degrees of Freedom	2
R^2	0.9997
Absolute Sum of Squares	1.915
Sy.x	0.9785
Data	
Number of X values	6
Number of Y replicates	1
Total number of values	6
Number of missing values	0

B.36. Tubulin Assay of Compound **108**

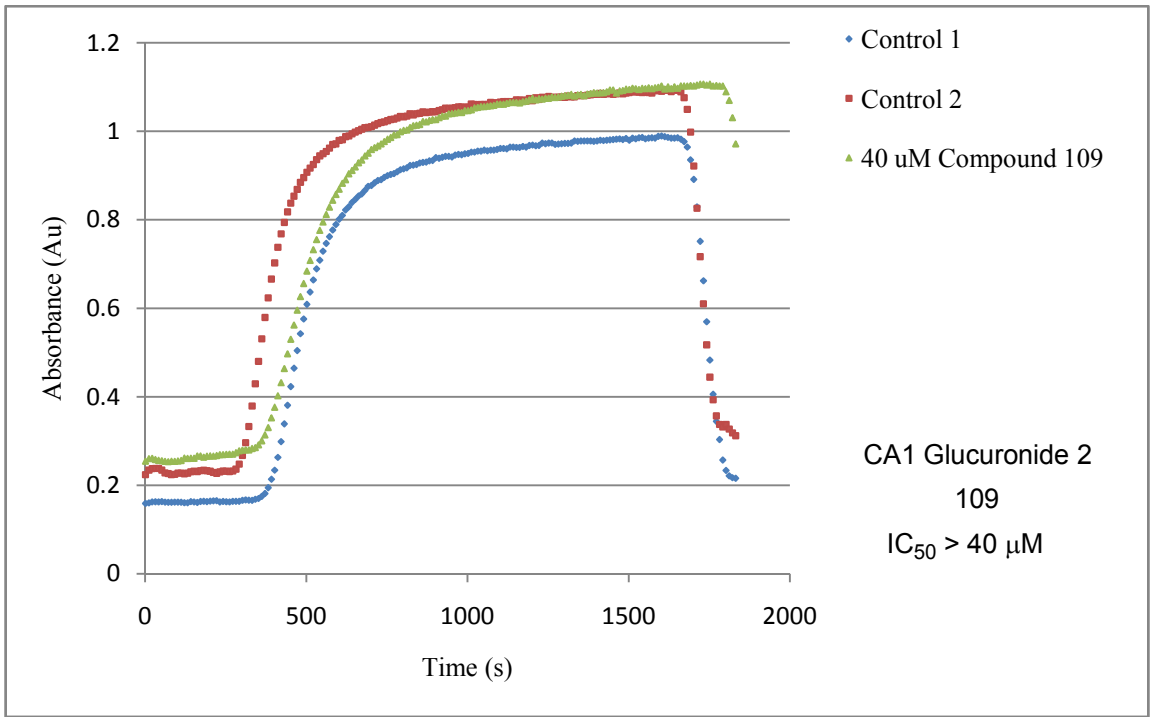

B.37. Tubulin Assay of Compound **109**

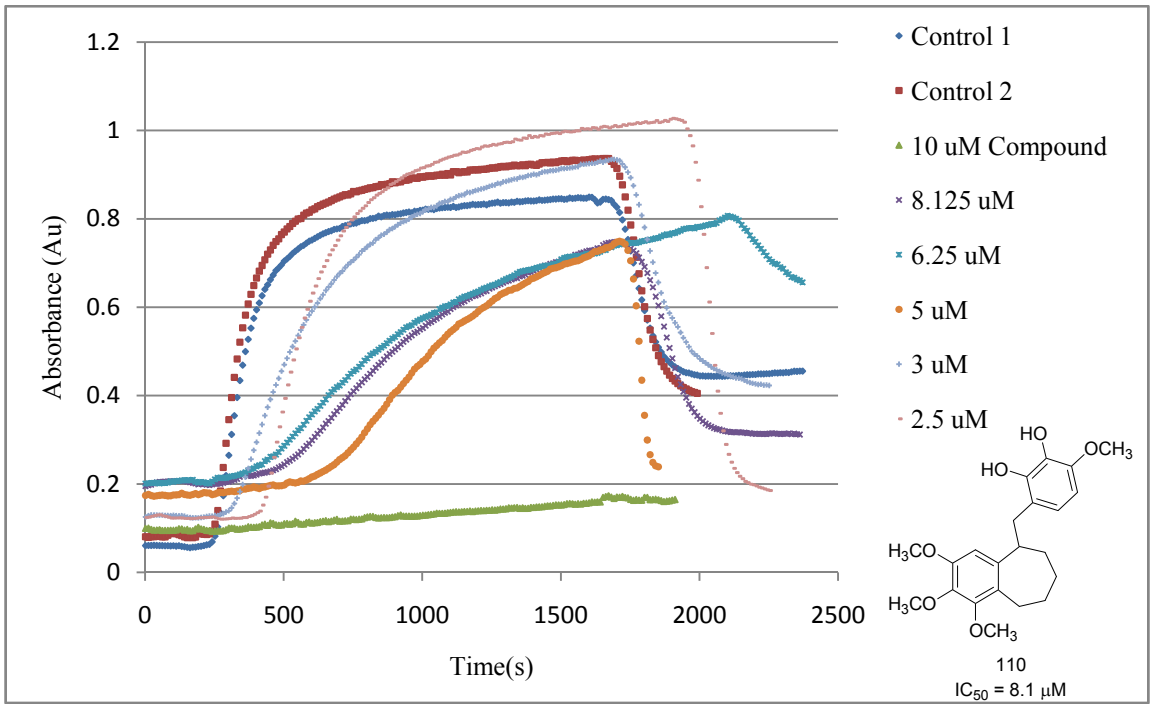

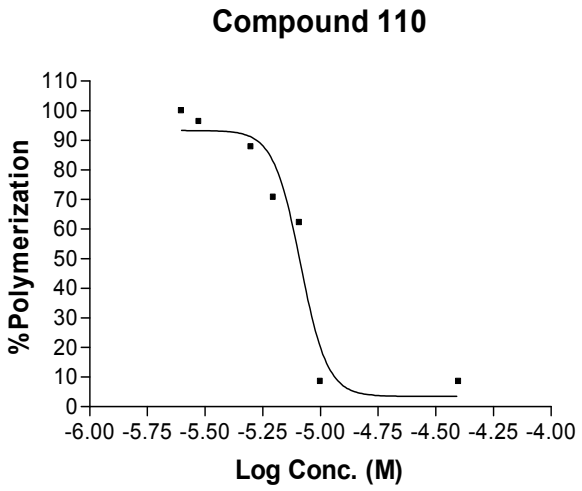

Sigmoidal dose-response (variable slope)	
Best-fit values	
BOTTOM	3.498
TOP	93.33
LOGEC50	-5.086
HILLSLOPE	-7.445
EC50	8.197e-006
Std. Error	
BOTTOM	12.91
TOP	8.240
LOGEC50	0.03781
HILLSLOPE	4.155
95% Confidence Intervals	
BOTTOM	-37.57 to 44.56
TOP	67.12 to 119.6
LOGEC50	-5.207 to -4.966
HILLSLOPE	-20.67 to 5.777
EC50	6.214e-006 to 1.081e-005
Goodness of Fit	
Degrees of Freedom	3
R^2	0.9422
Absolute Sum of Squares	524.8
Sy.x	13.23
Data	
Number of X values	7
Number of Y replicates	1
Total number of values	7
Number of missing values	0

B.38. Tubulin Assay of Compound **110**

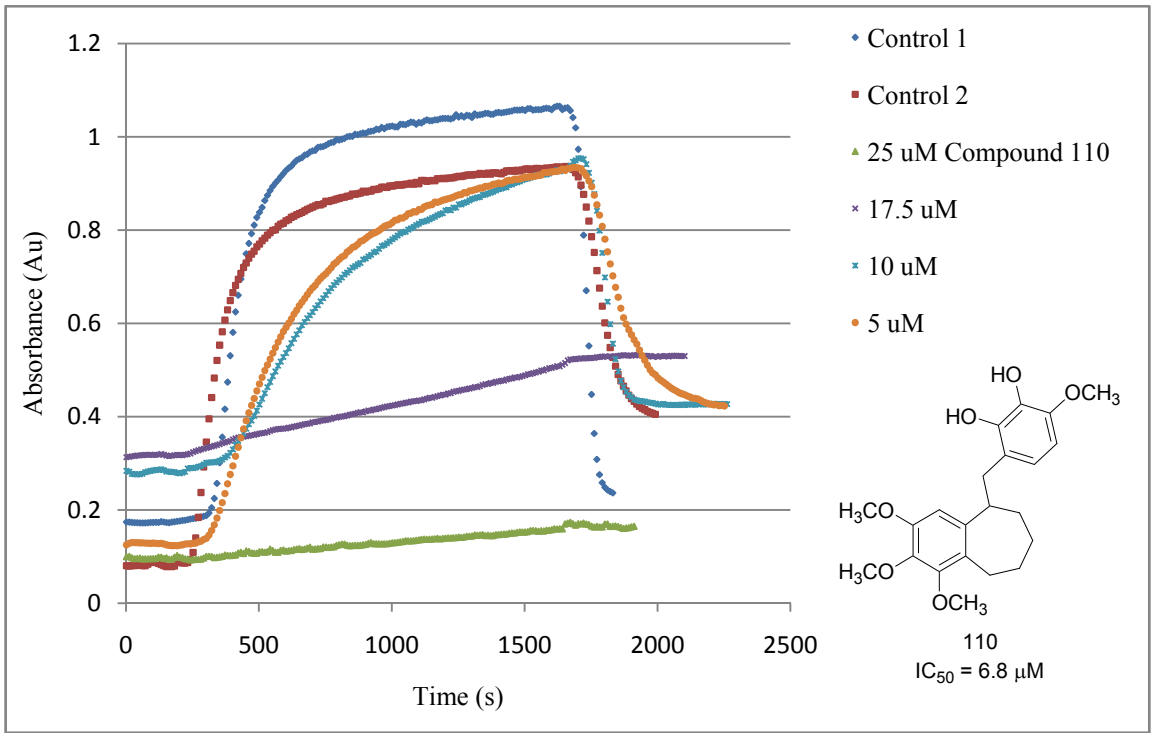

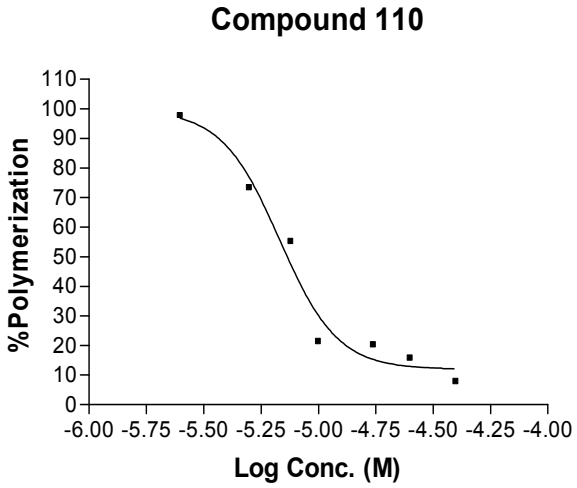

Sigmoidal dose-response (variable slope)	
Best-fit values	
BOTTOM	11.97
TOP	99.45
LOGEC50	-5.169
HILLSLOPE	-3.443
EC50	6.781e-006
Std. Error	
BOTTOM	5.717
TOP	11.15
LOGEC50	0.05570
HILLSLOPE	1.391
95% Confidence Intervals	
BOTTOM	-6.221 to 30.16
TOP	63.98 to 134.9
LOGEC50	-5.346 to -4.991
HILLSLOPE	-7.869 to 0.9829
EC50	4.509e-006 to 1.020e-005
Goodness of Fit	
Degrees of Freedom	3
R^2	0.9714
Absolute Sum of Squares	200.2
Sy.x	8.168
Data	
Number of X values	7
Number of Y replicates	1
Total number of values	7
Number of missing values	0

B.39. Tubulin Assay of Compound **110**

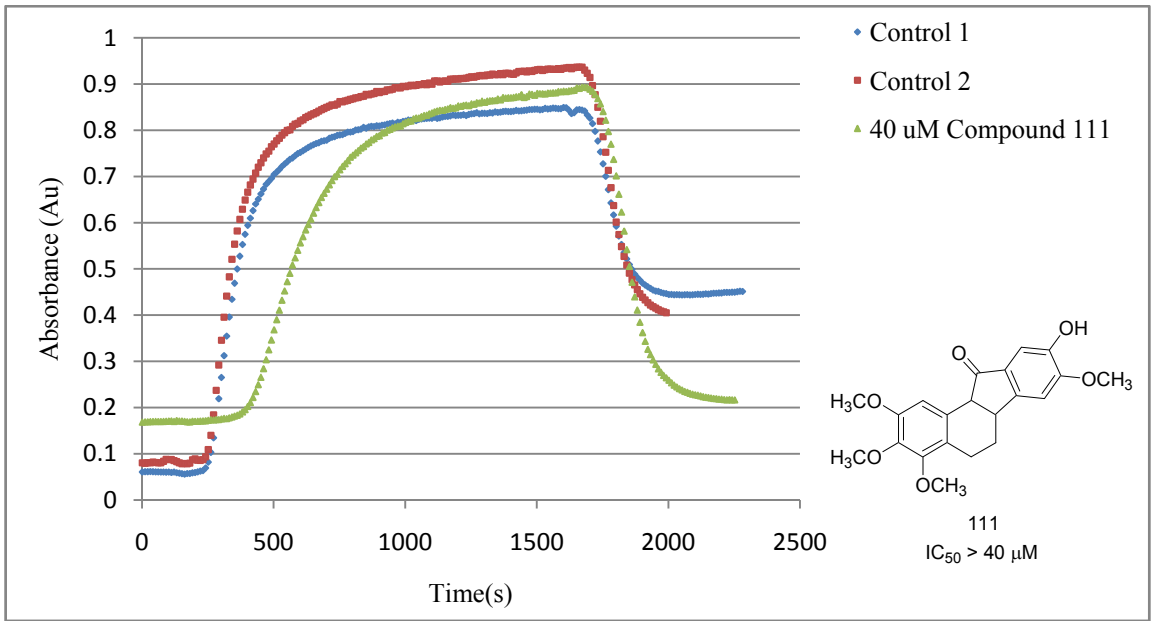

B.40. Tubulin Assay of Compound **111**

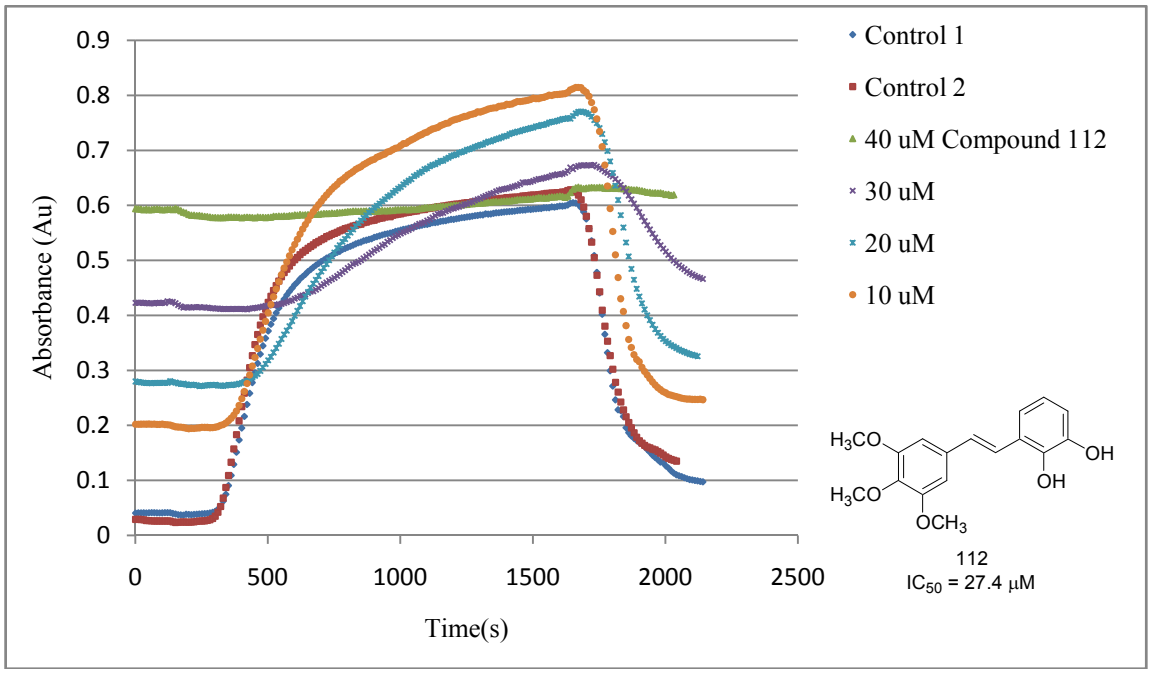

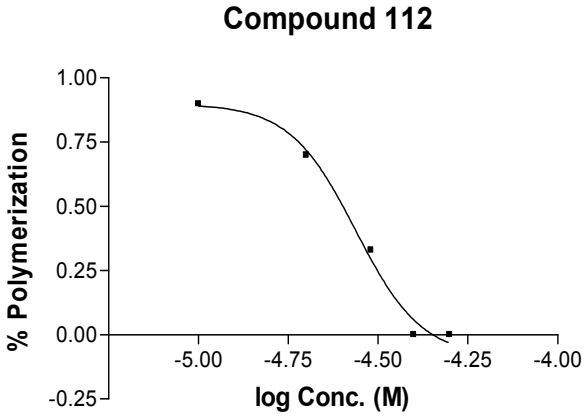

Sigmoidal dose-response (variable slope)	
Best-fit values	
BOTTOM	-0.08645
TOP	0.8992
LOGEC50	-4.562
HILLSLOPE	-4.730
EC50	2.740e-005
Std. Error	
BOTTOM	0.1322
TOP	0.08772
LOGEC50	0.04292
HILLSLOPE	1.970
95% Confidence Intervals	
BOTTOM	-1.766 to 1.593
TOP	-0.2153 to 2.014
LOGEC50	-5.108 to -4.017
HILLSLOPE	-29.76 to 20.30
EC50	7.807e-006 to 9.618e-005
Goodness of Fit	
Degrees of Freedom	1
R^2	0.9909
Absolute Sum of Squares	0.006060
Sy.x	0.07784
Data	
Number of X values	5
Number of Y replicates	1
Total number of values	5
Number of missing values	0

B.41. Tubulin Assay of Compound **112**

APPENDIX C

SRB Data

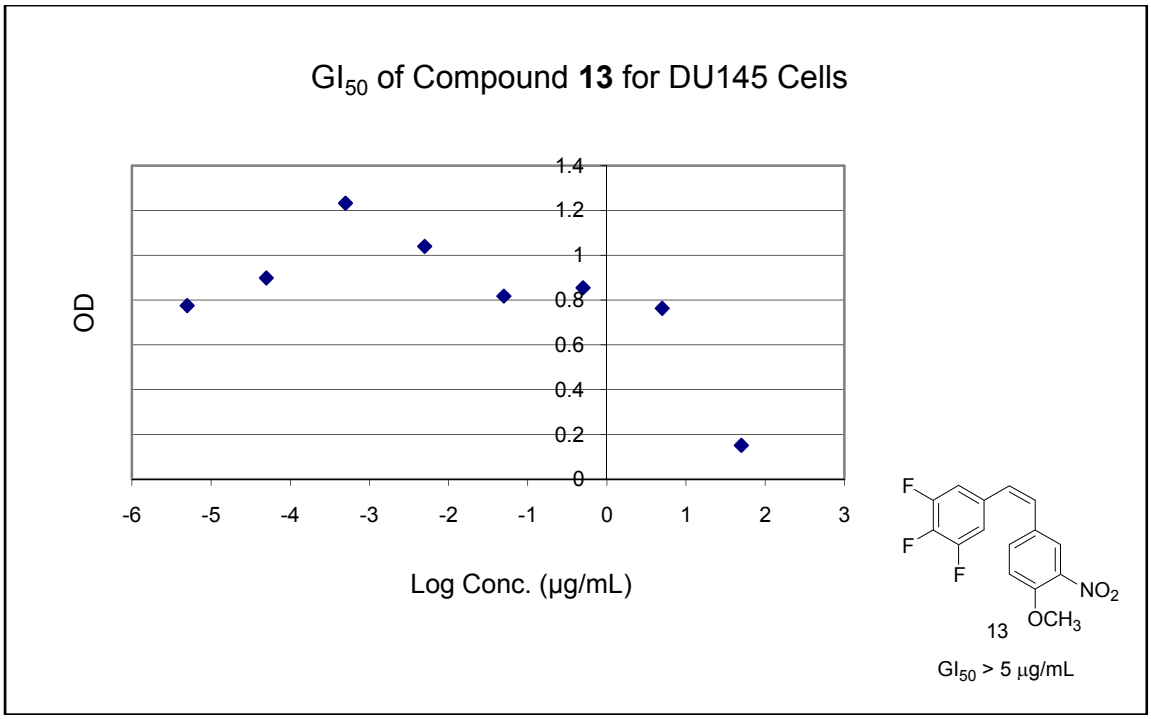

C.1. GI_{50} of Compound **13** for DU145 Prostate Cancer Cells

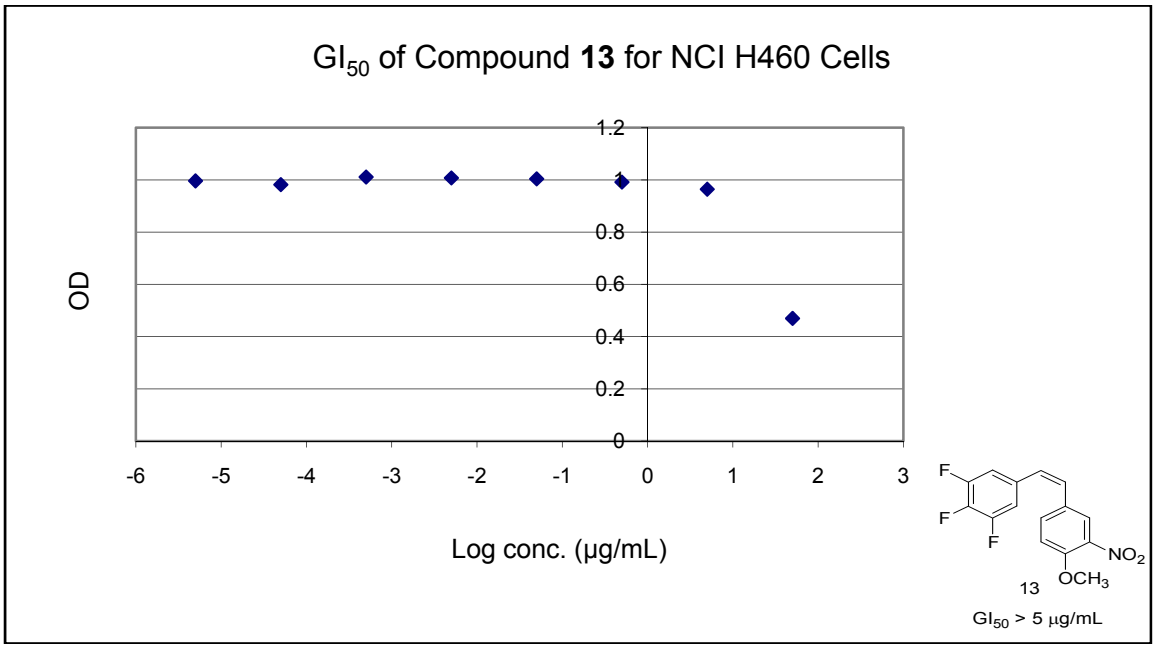

C.2. GI_{50} of Compound **13** for NCI H460 Lung Cancer Carcinoma Cells

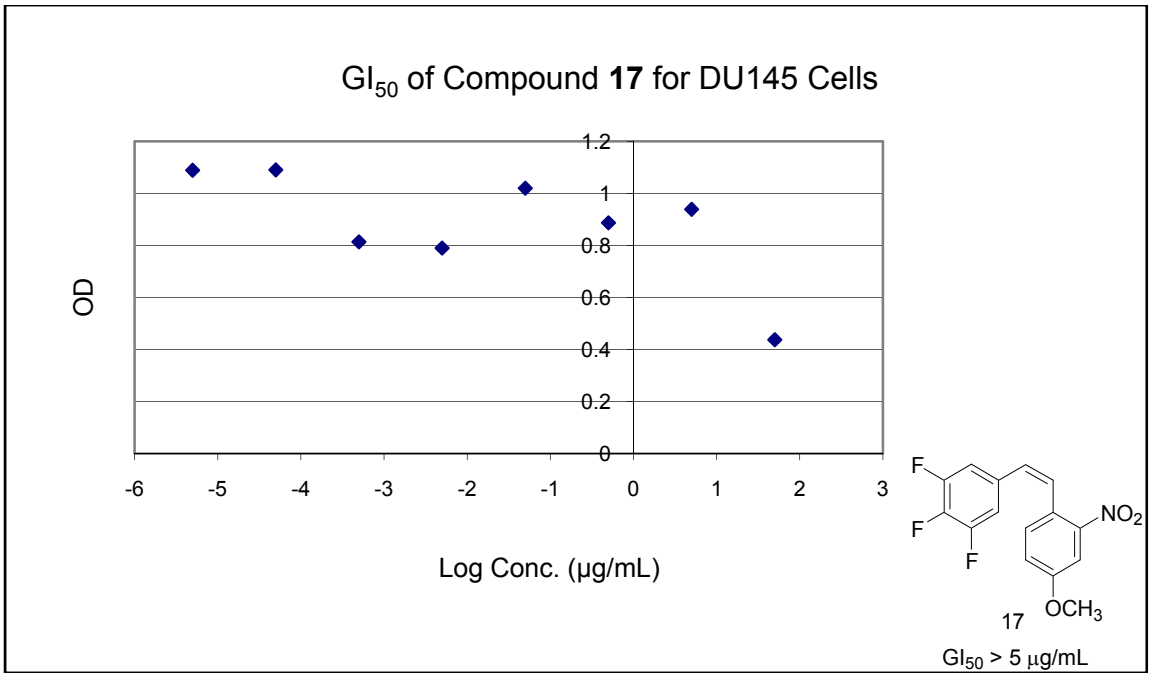

C.3. GI_{50} of Compound **17** for DU145 Prostate Cancer Cells

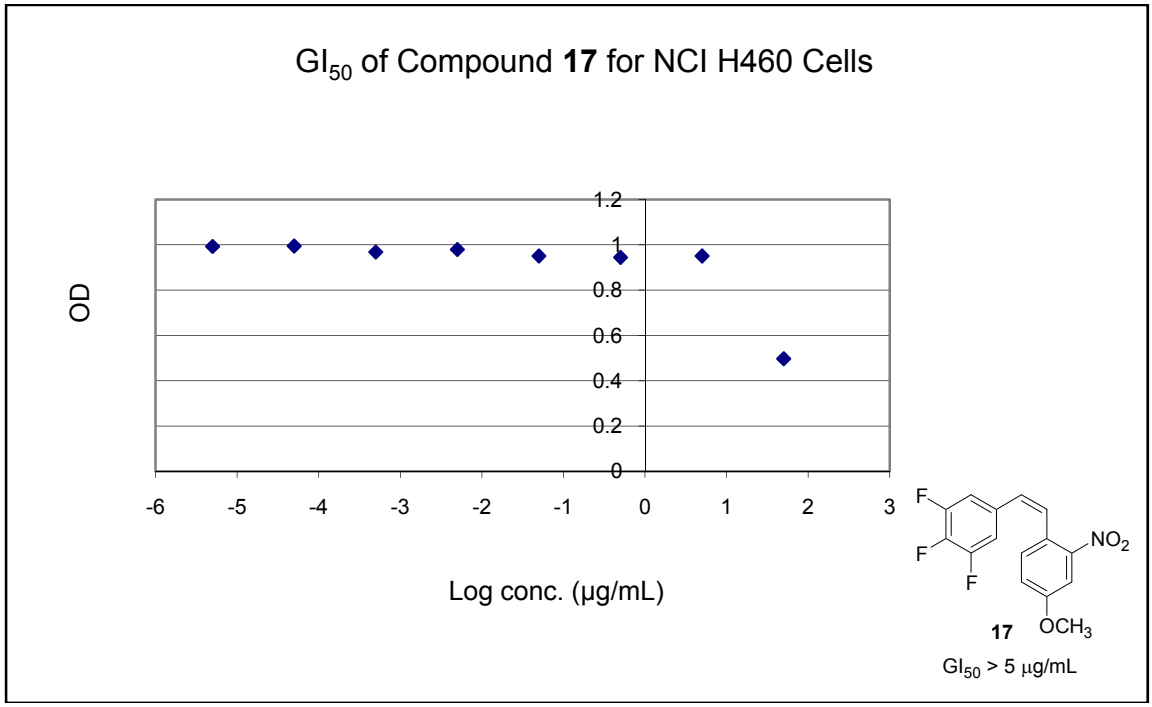

C.4. GI_{50} of Compound **17** for NCI H460 Lung Cancer Carcinoma Cells

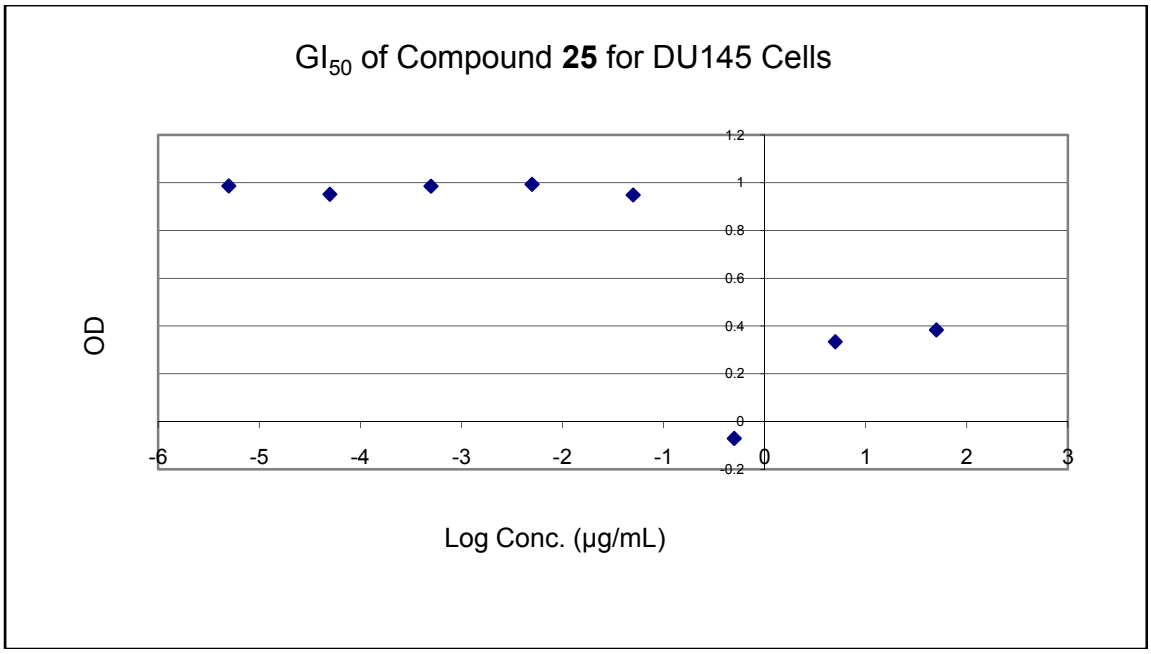

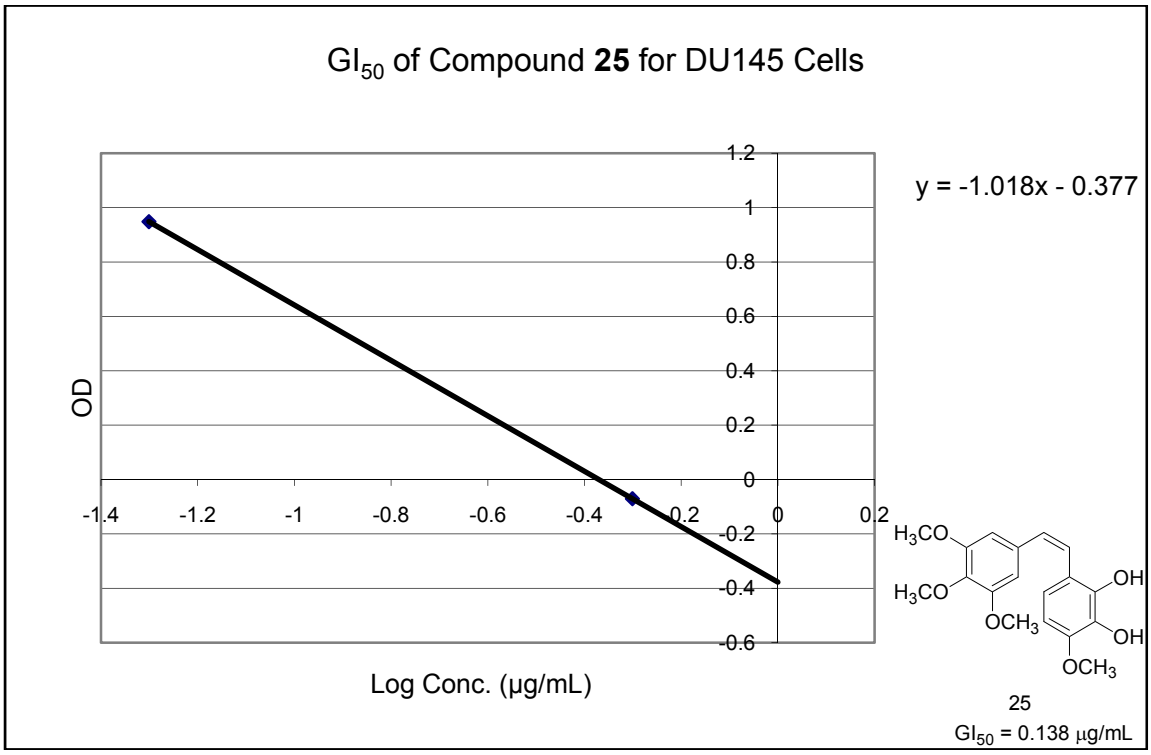

C.5. GI_{50} of Compound **25** for DU-145 Prostate Cancer Cells

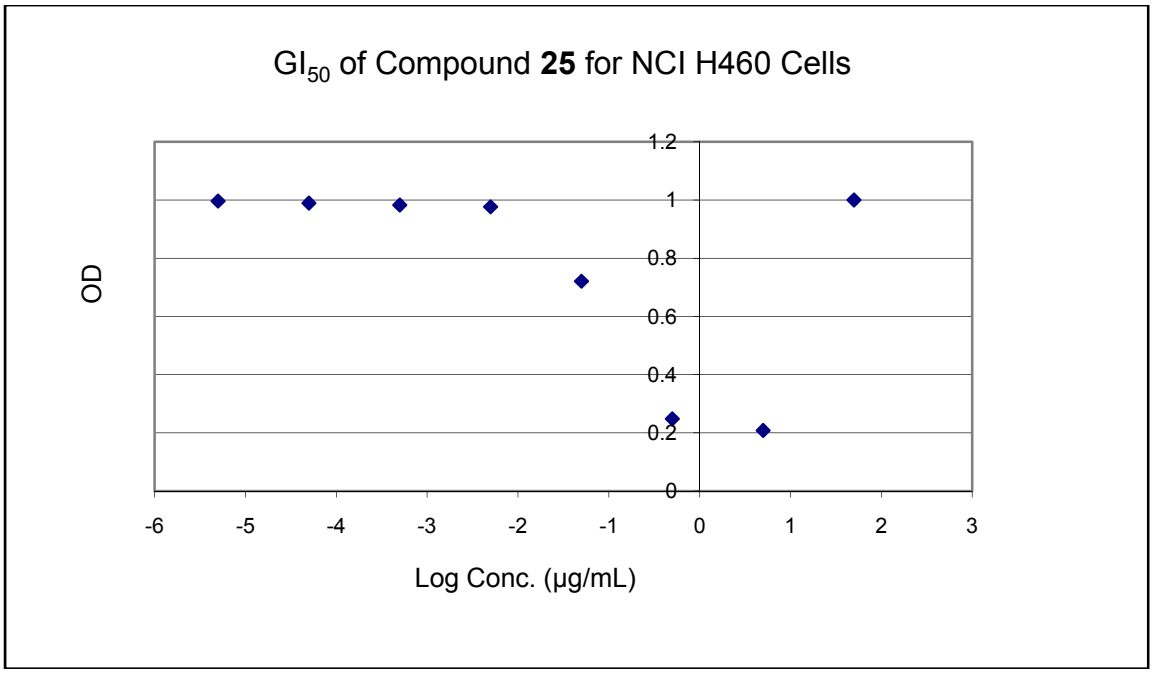

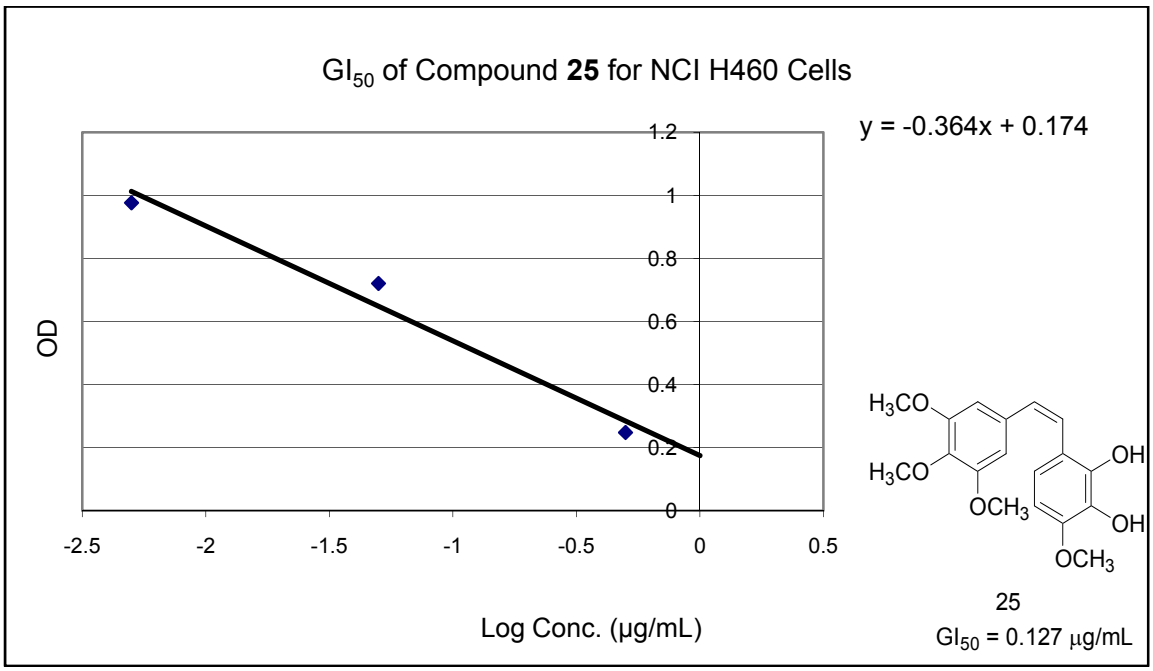

C.6. GI_{50} of Compound **25** for NCI H460 Lung Cancer Carcinoma Cells

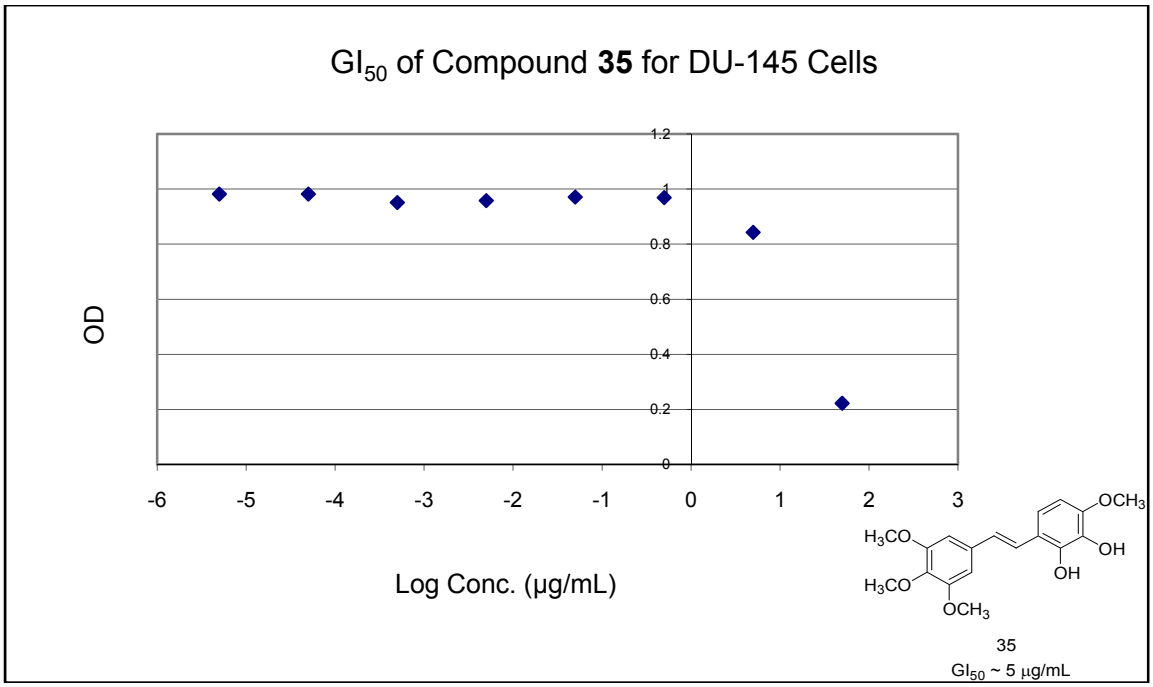

C.7. GI_{50} of Compound **35** for DU-145 Prostate Cancer Cells

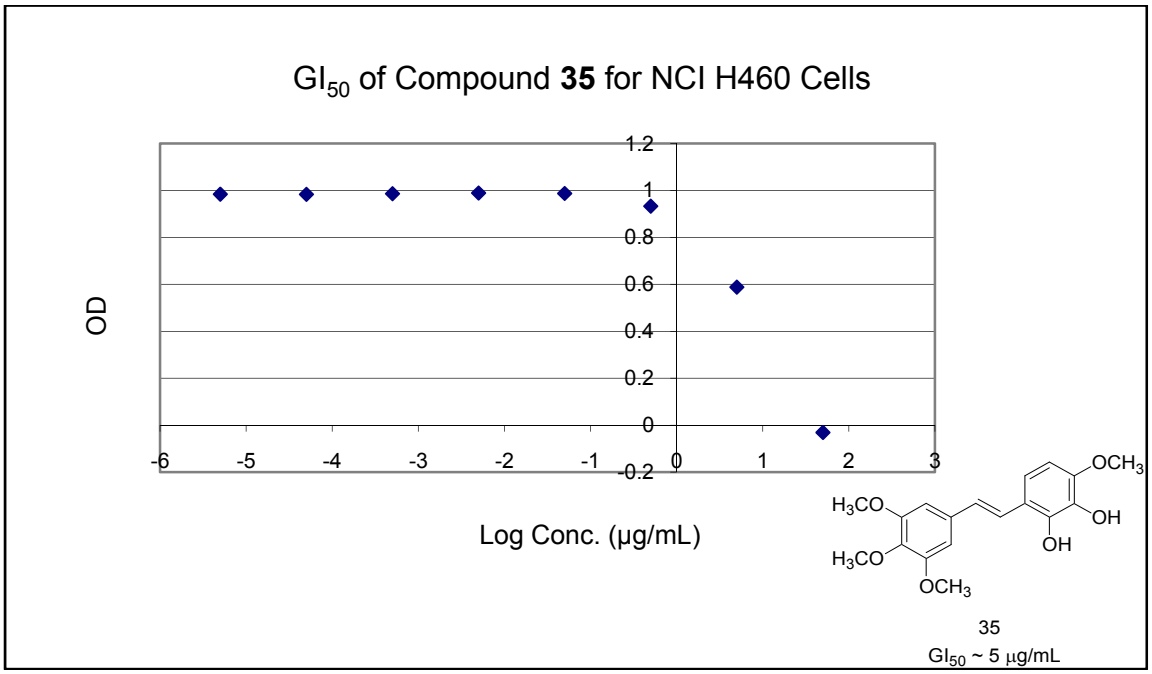

C.8. GI_{50} of Compound **35** for NCI H460 Lung Cancer Carcinoma Cells

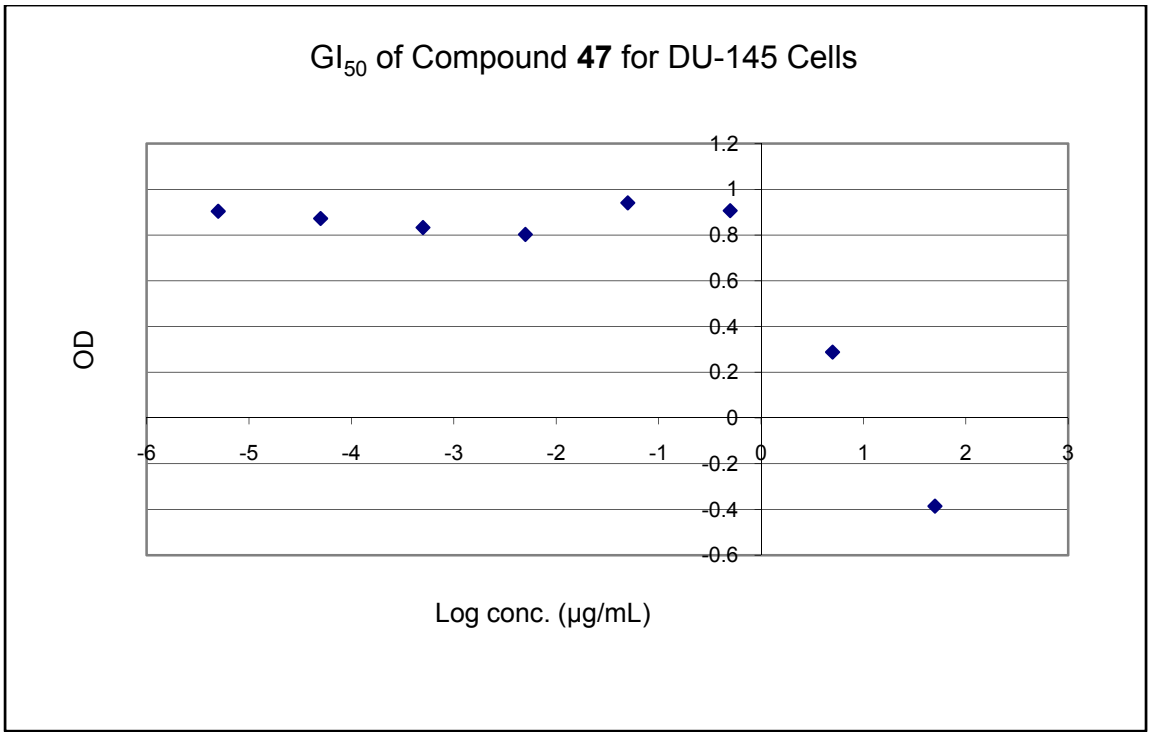

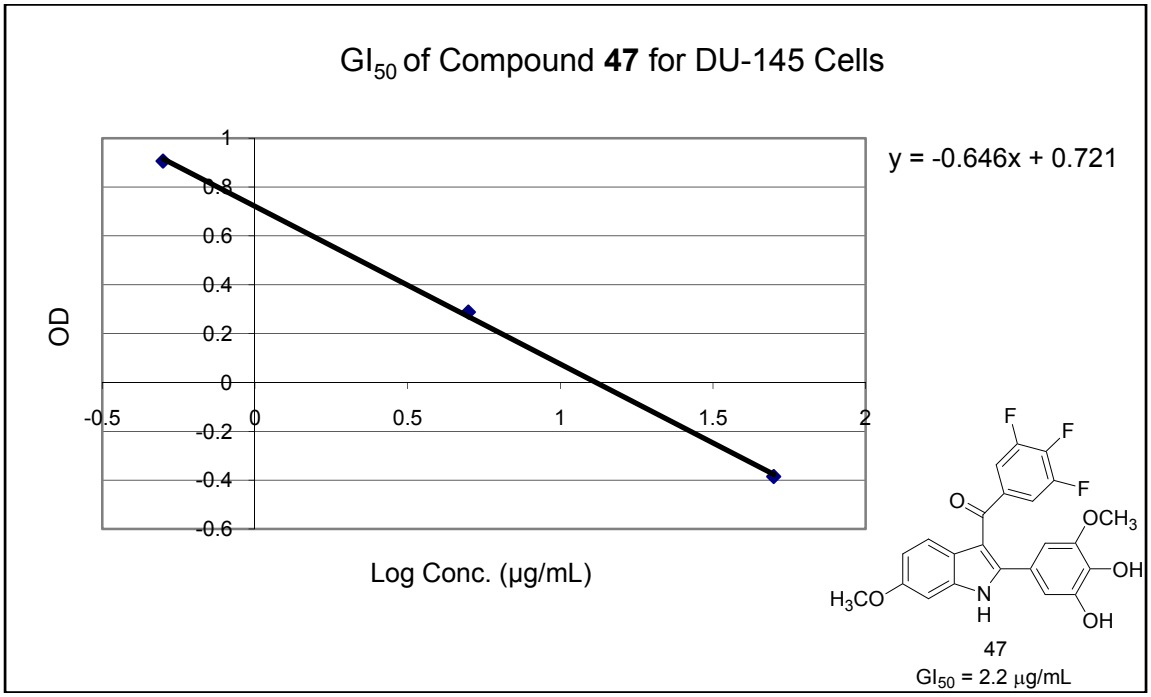

C.9. GI_{50} of Compound **47** for DU-145 Prostate Cancer Cells

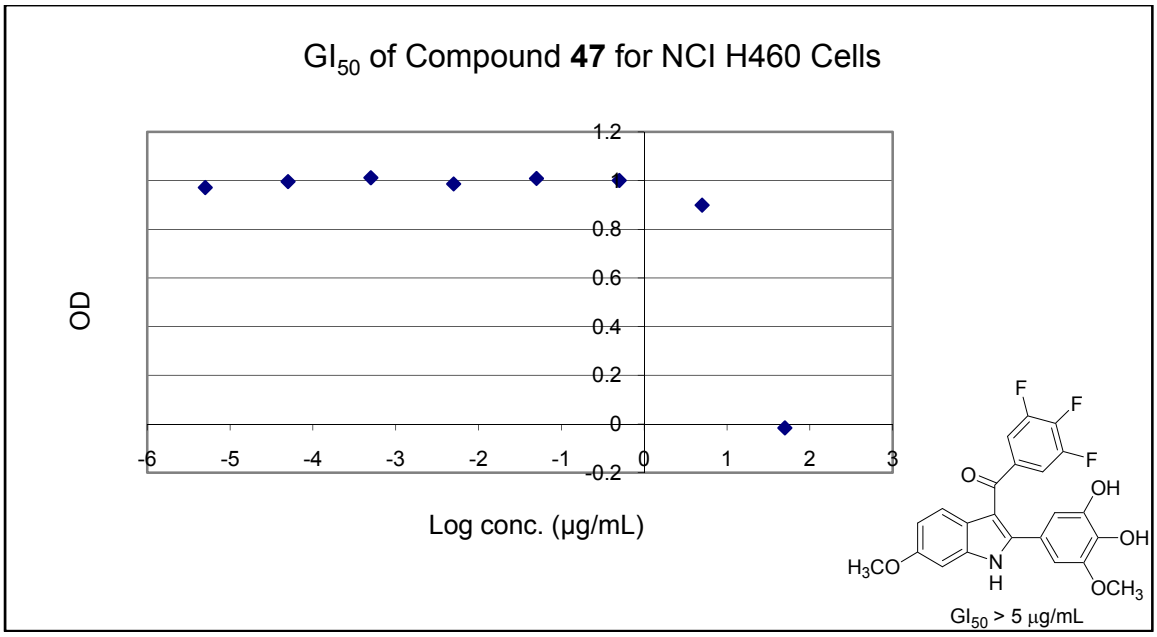

C.10. GI_{50} of Compound **47** for NCI H460 Lung Cancer Carcinoma Cells

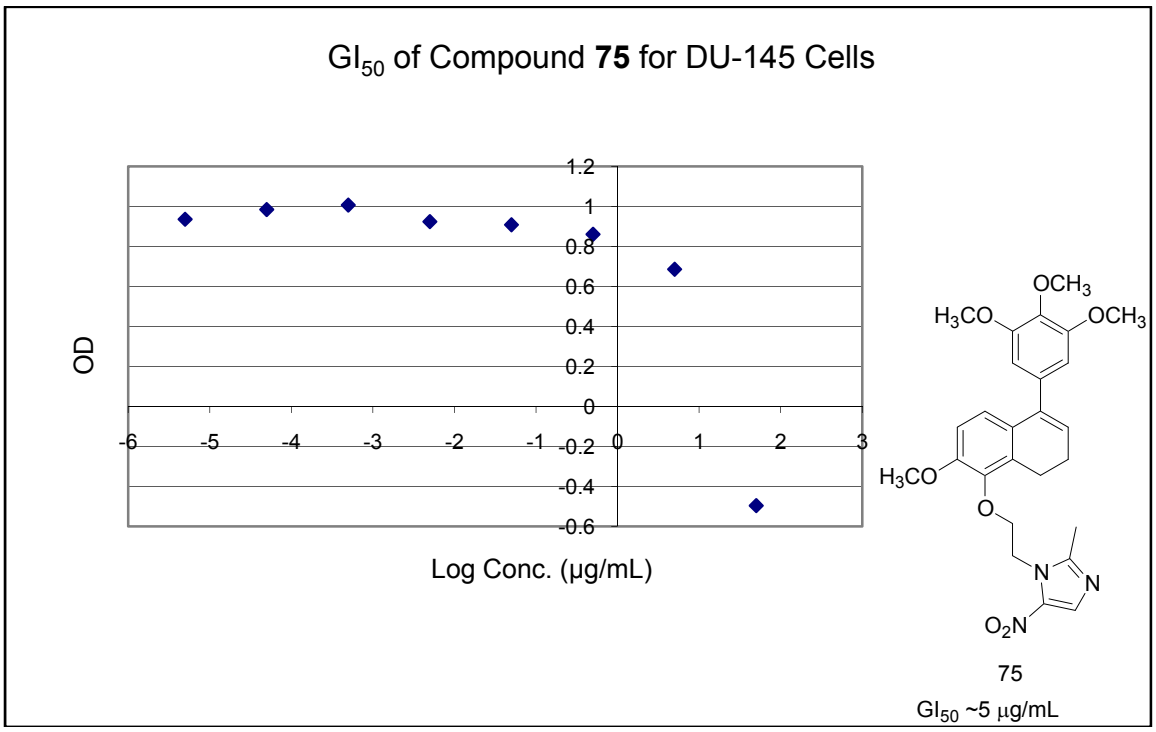

C.11. GI_{50} of Compound **75** for DU-145 Prostate Cancer Cells

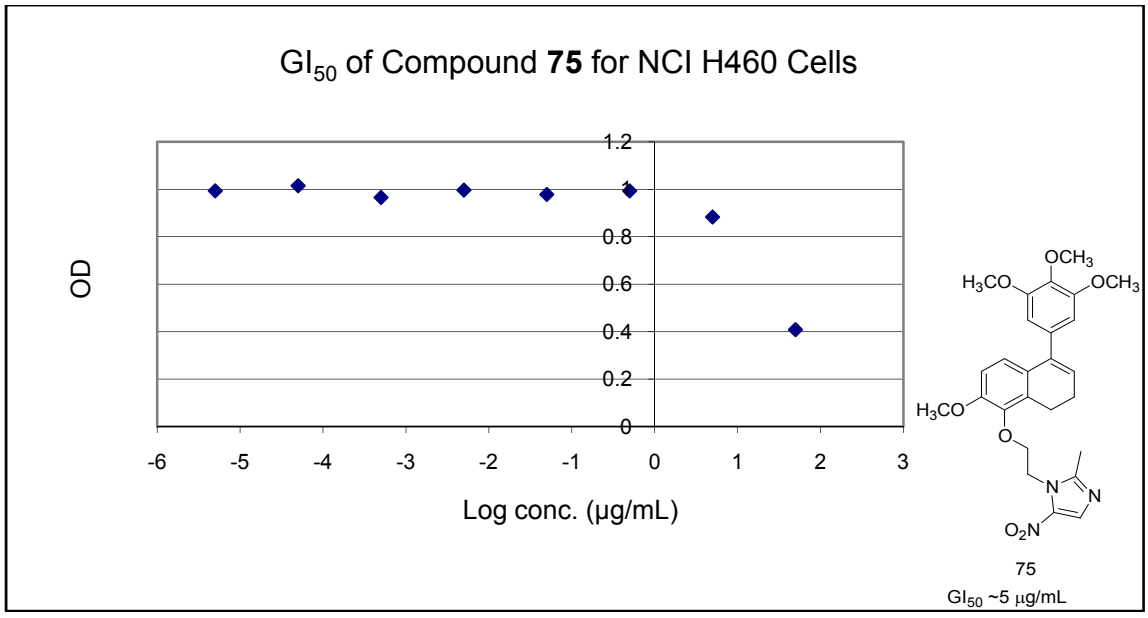

C.12. GI_{50} of Compound **75** for NCI H460 Lung Cancer Carcinoma Cells

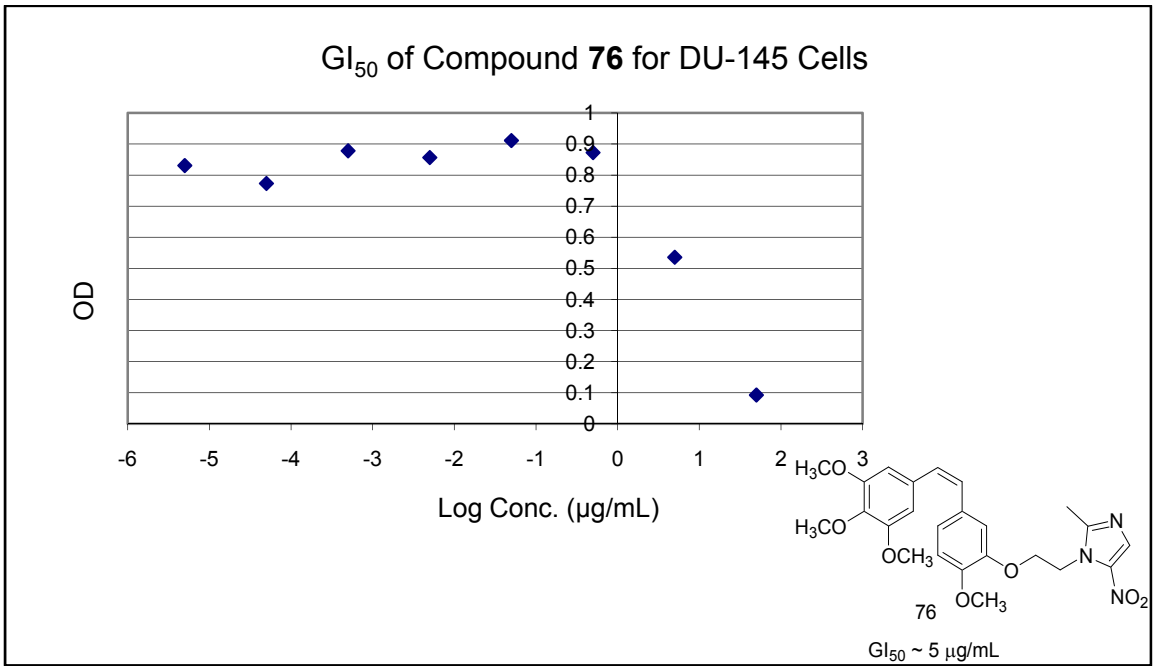

C.13. GI_{50} of Compound **76** for DU-145 Prostate Cancer Cells

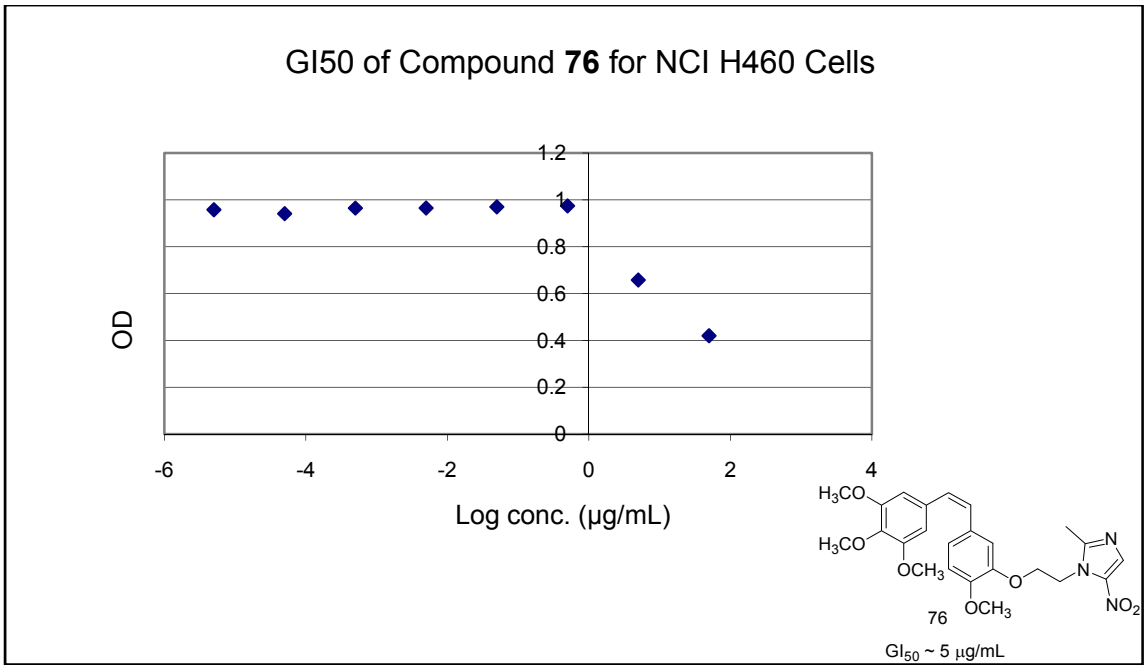

C.14. GI_{50} of Compound **76** for NCI H460 Lung Cancer Carcinoma Cells

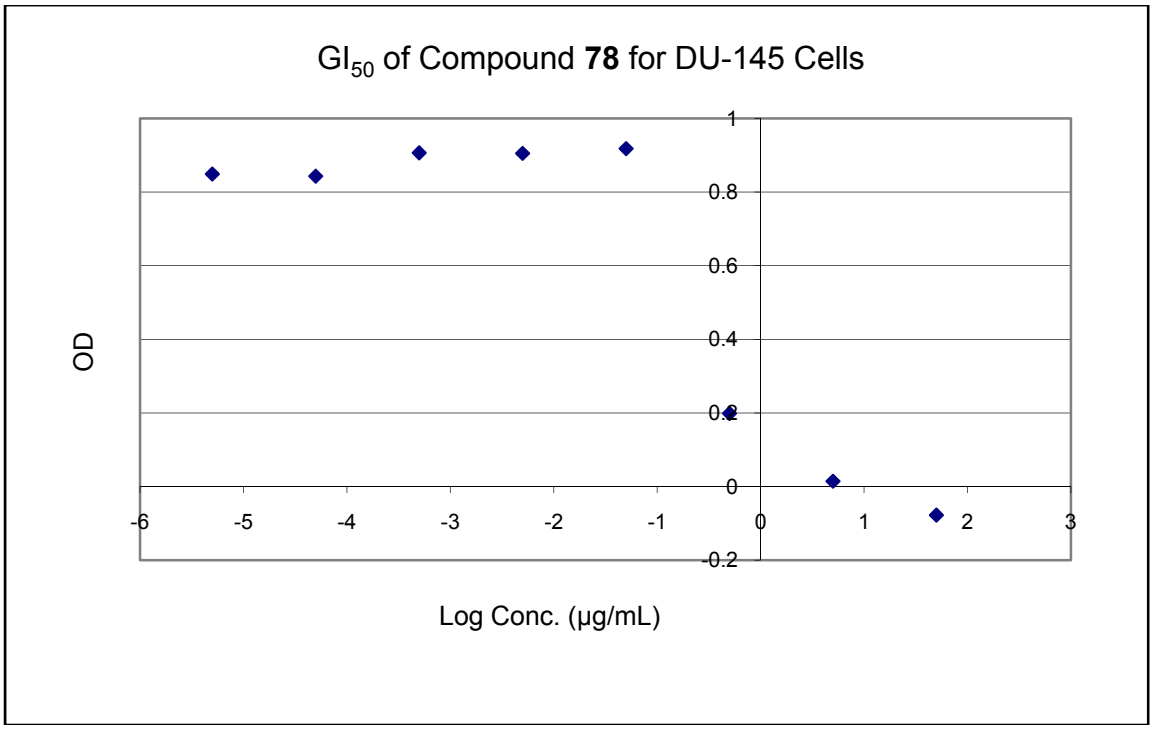

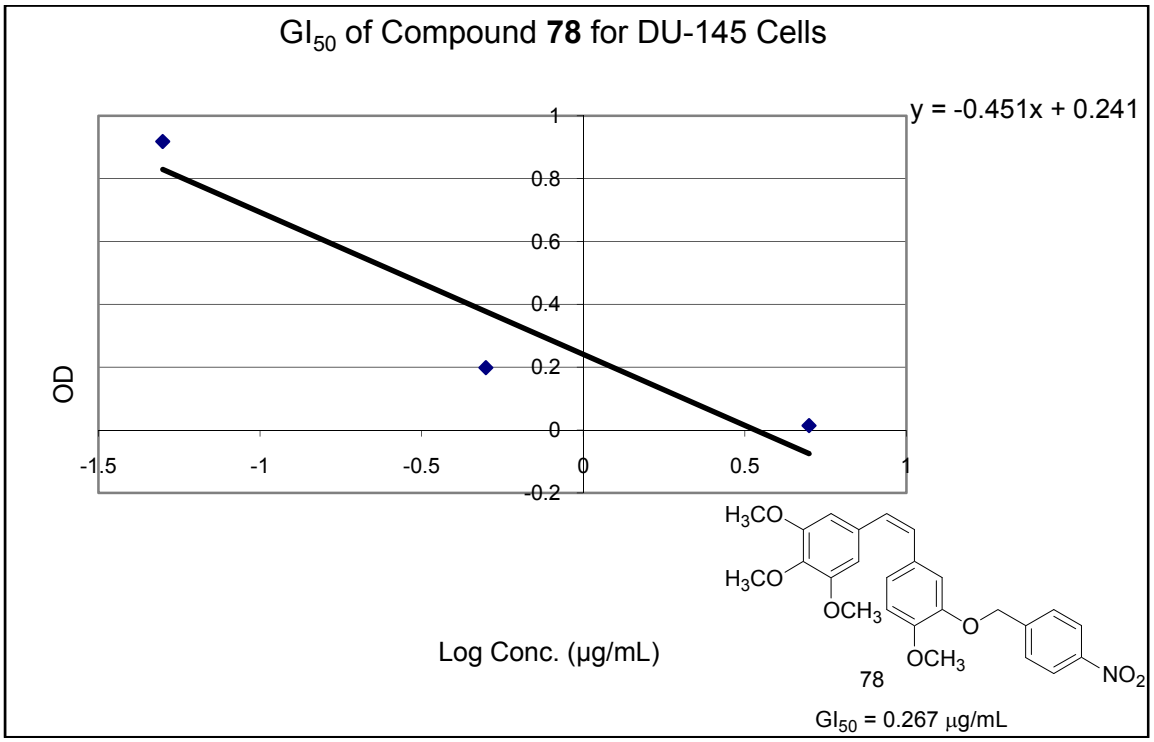

C.15. GI_{50} of Compound **78** for DU-145 Prostate Cancer Cells

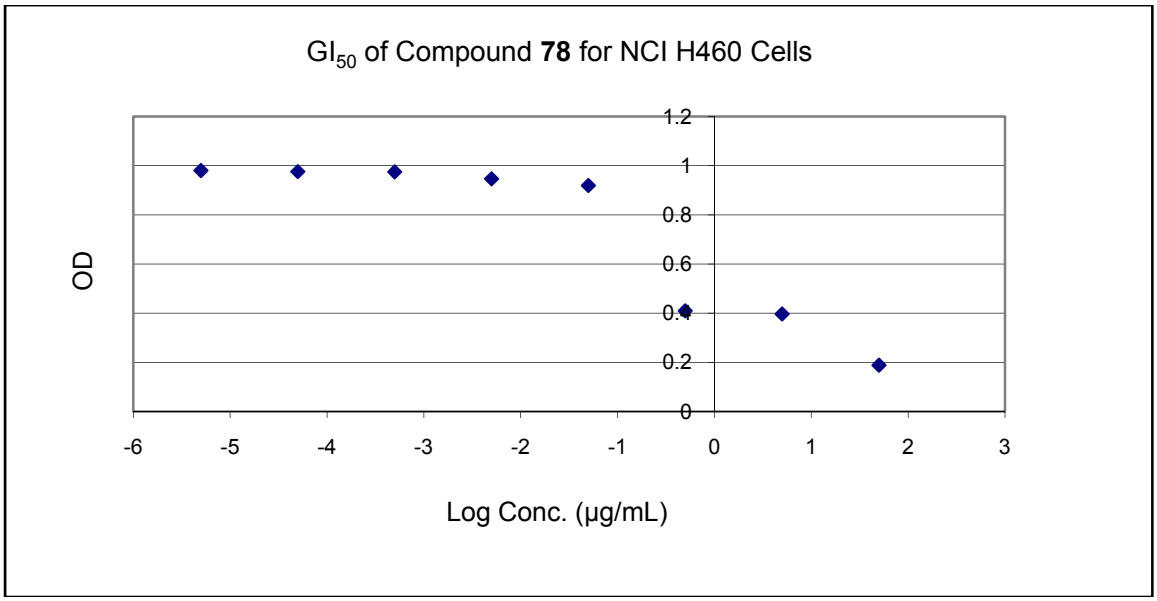

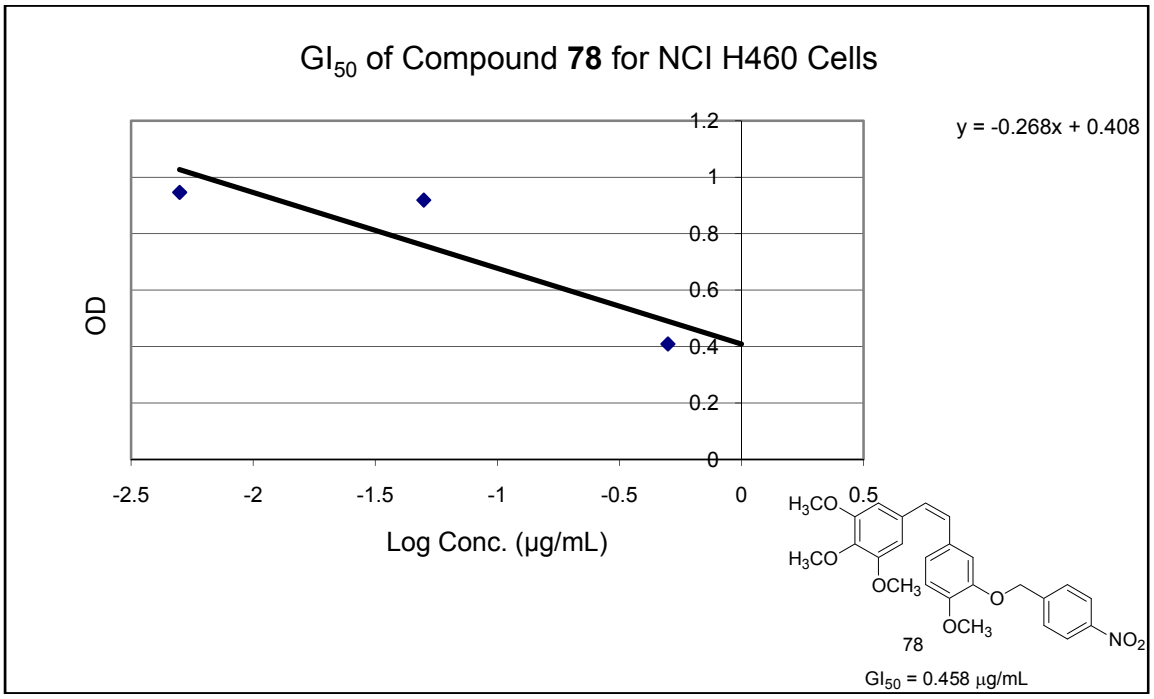

C.16. GI_{50} of Compound **78** for NCI H460 Lung Cancer Carcinoma Cells

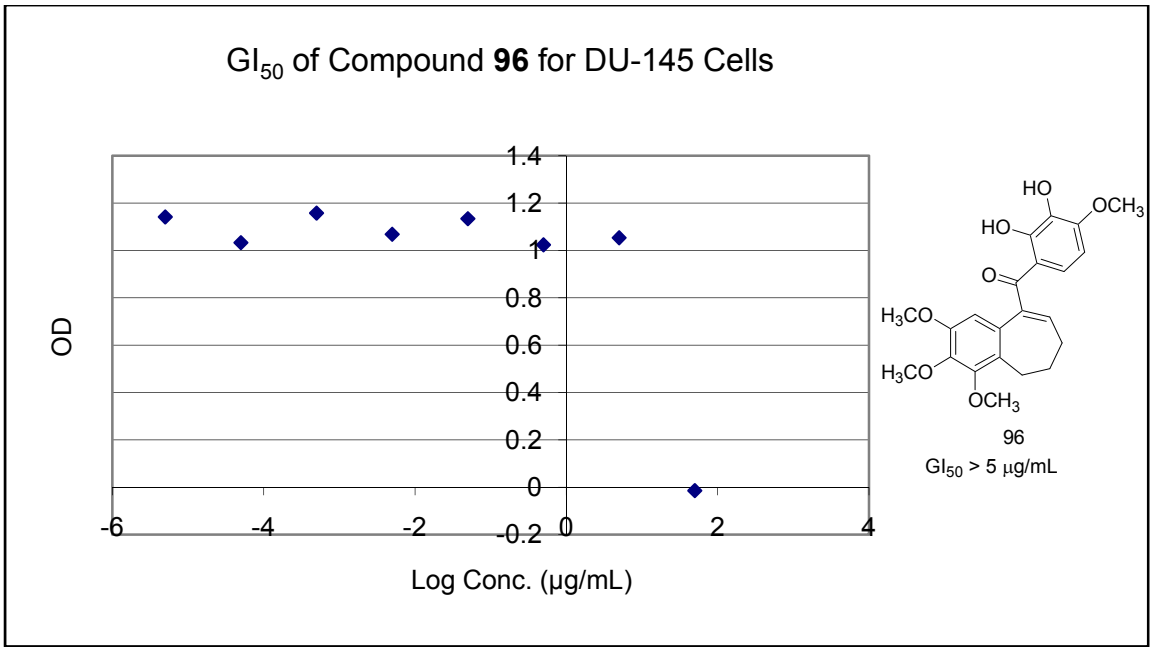

C.17. GI_{50} of Compound **96** for DU-145 Prostate Cancer Cells

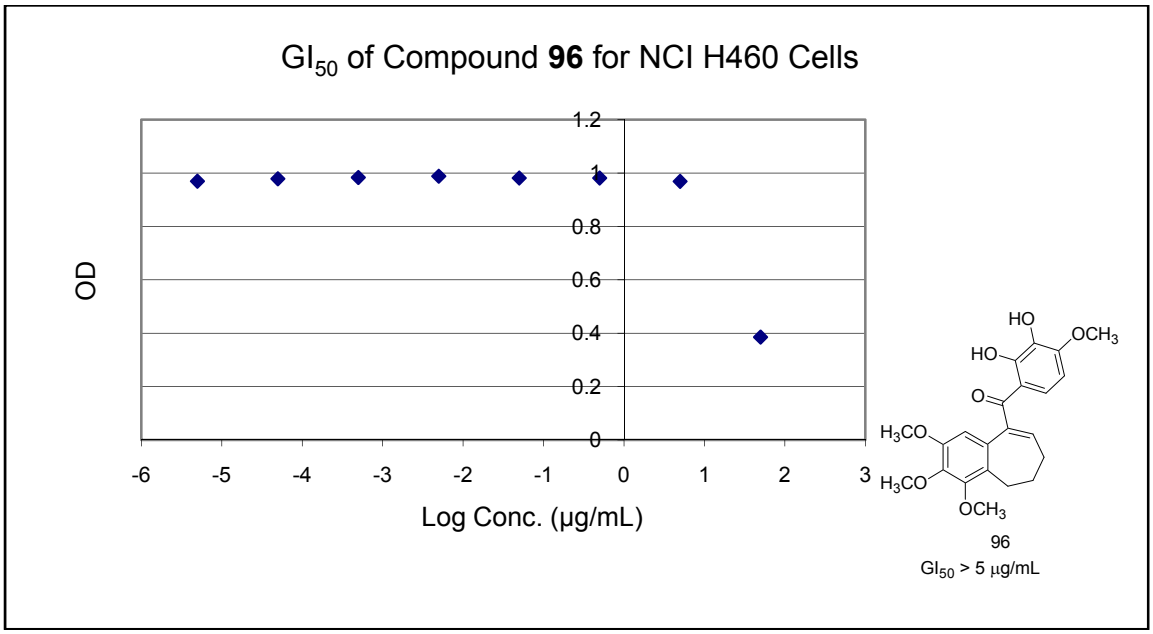

C.18. GI_{50} of Compound **96** for NCI H460 Lung Cancer Carcinoma Cells

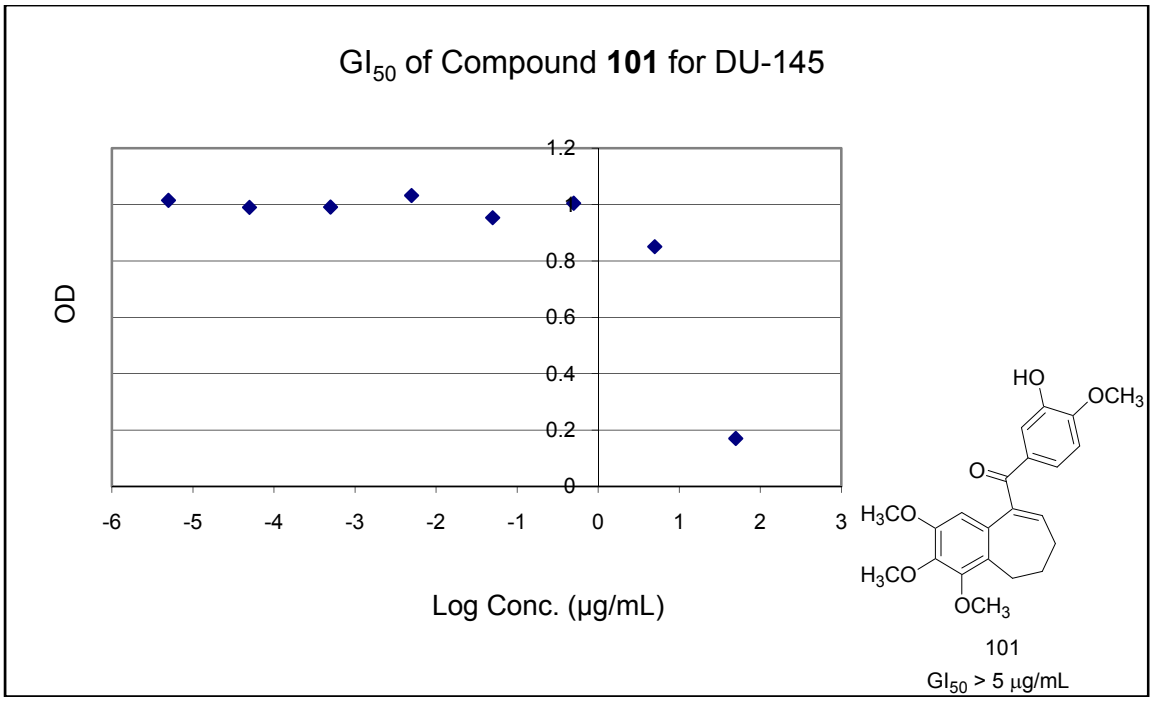

C.19. GI_{50} of Compound **101** for DU-145 Prostate Cancer Cells

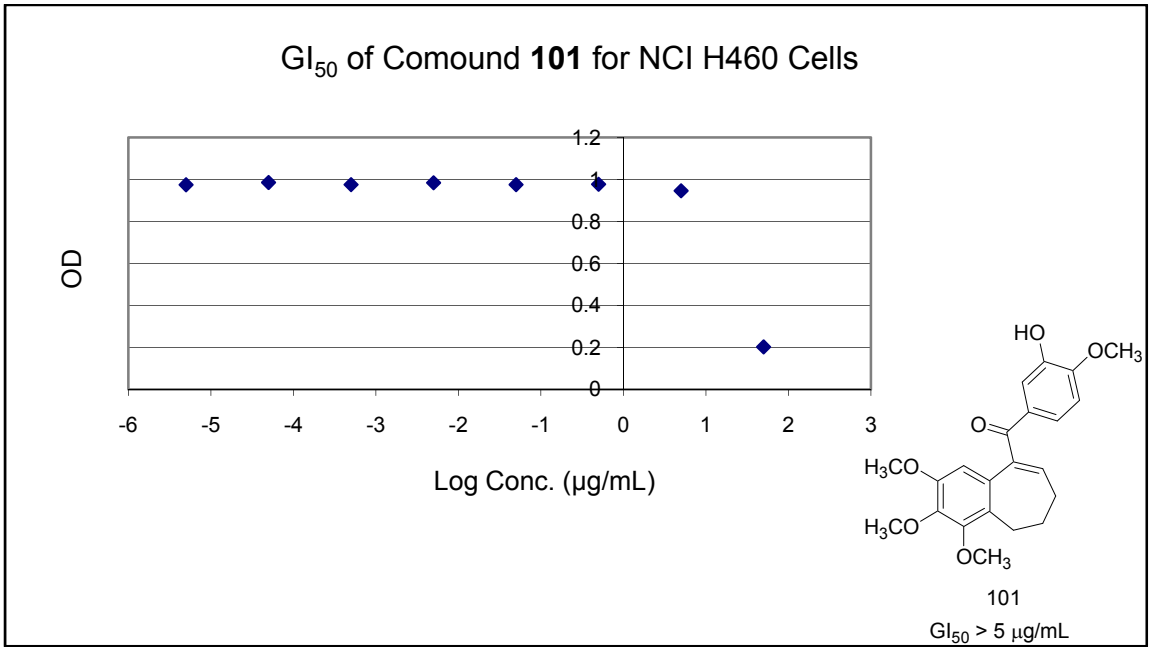

C.20. GI_{50} of Compound **101** for NCI H460 Lung Cancer Carcinoma Cells

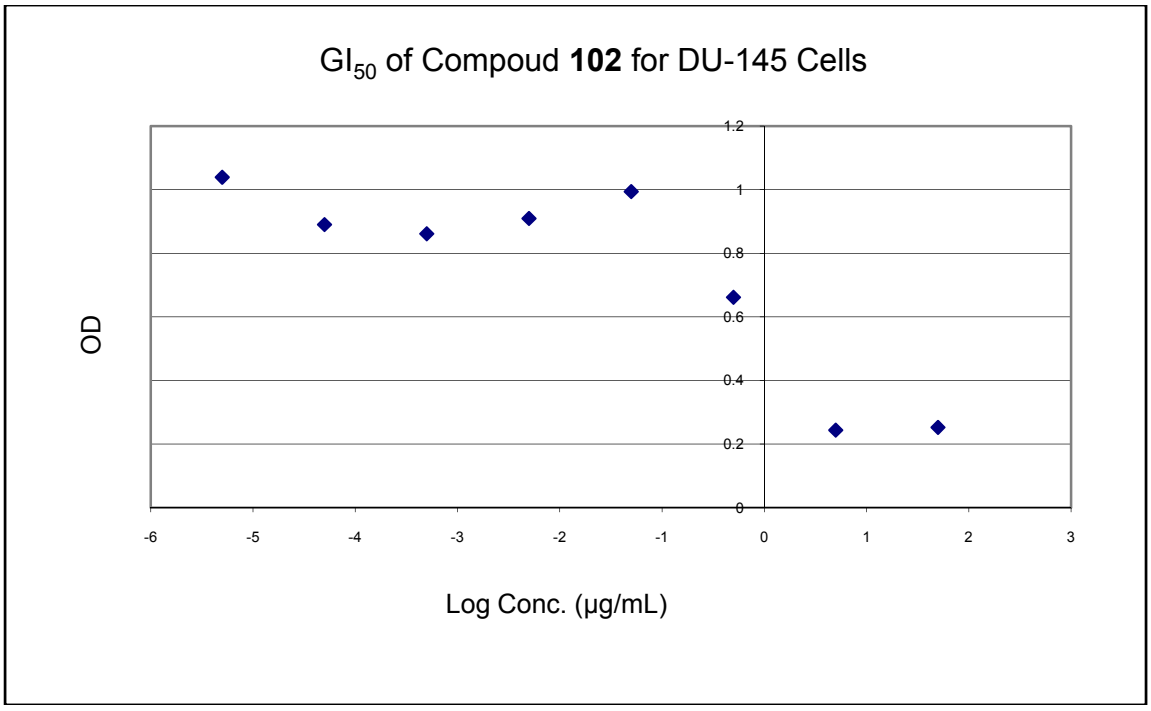

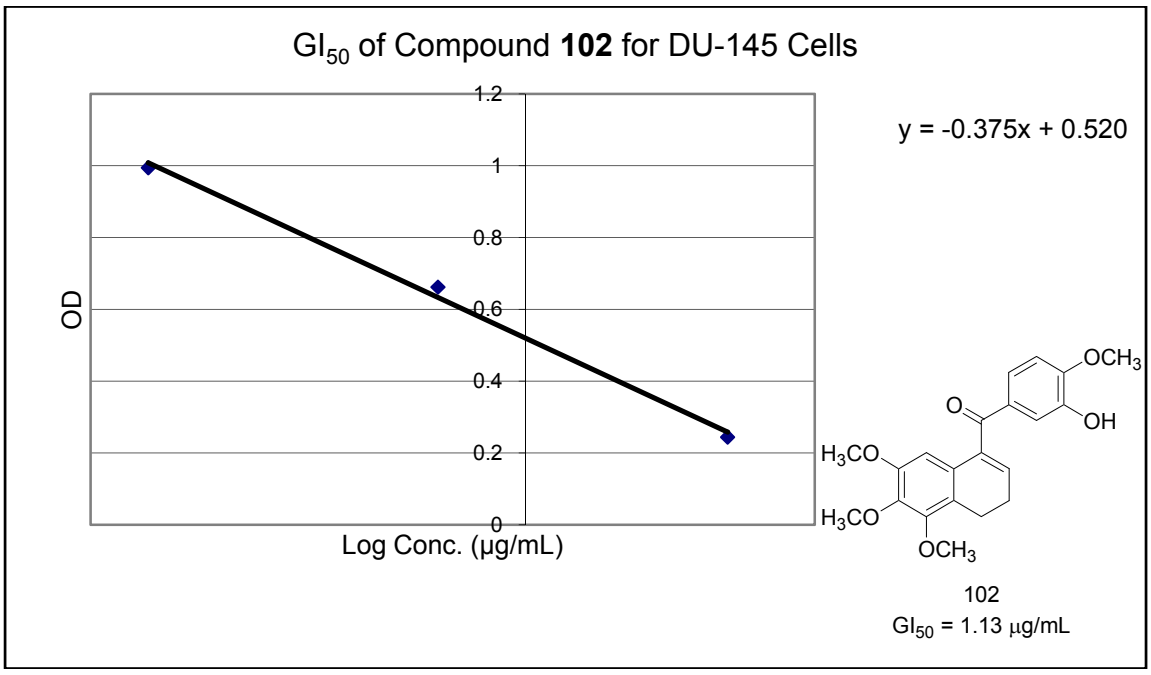

C.21. GI_{50} of Compound **102** for DU-145 Prostate Cancer Cells

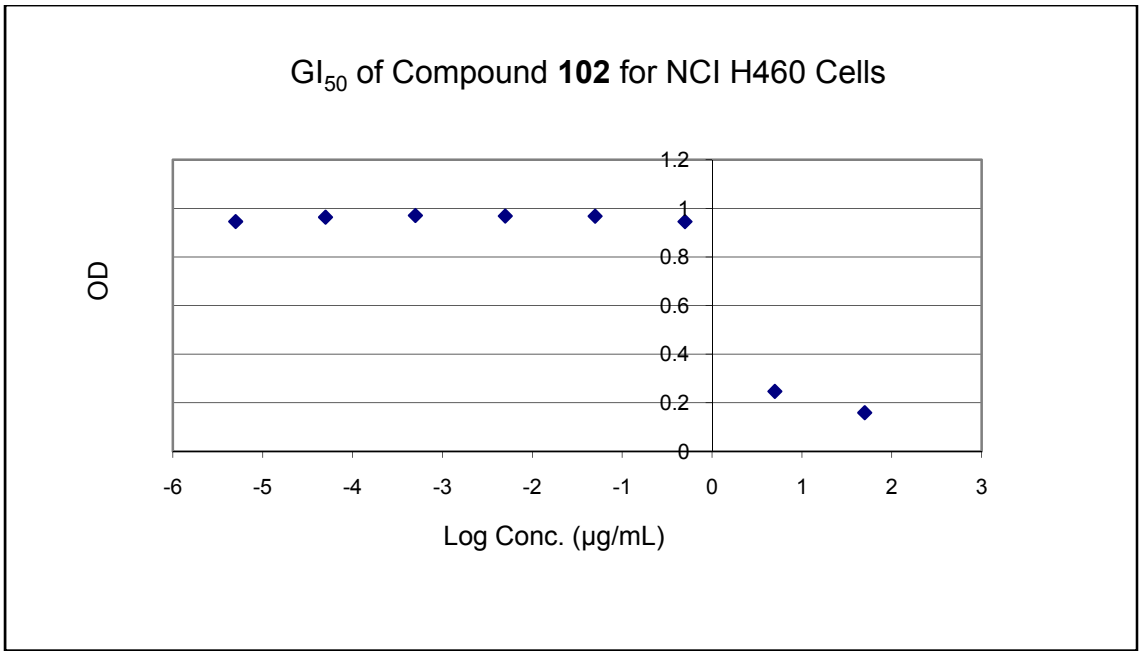

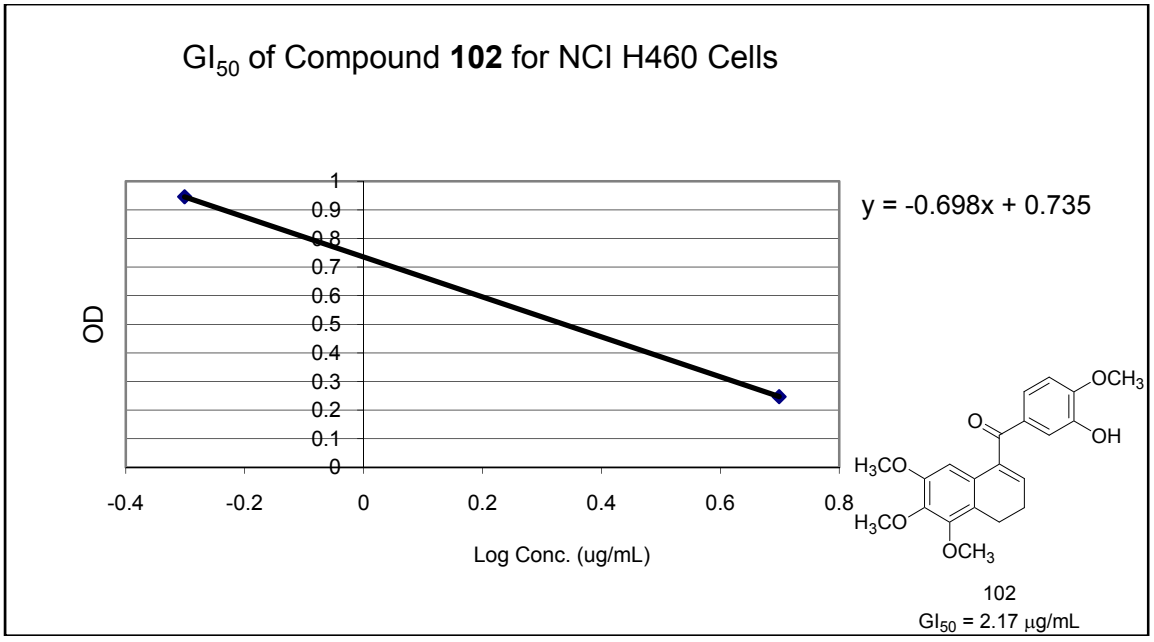

C.22. GI_{50} of Compound **102** for NCI H460 Lung Cancer Carcinoma Cells

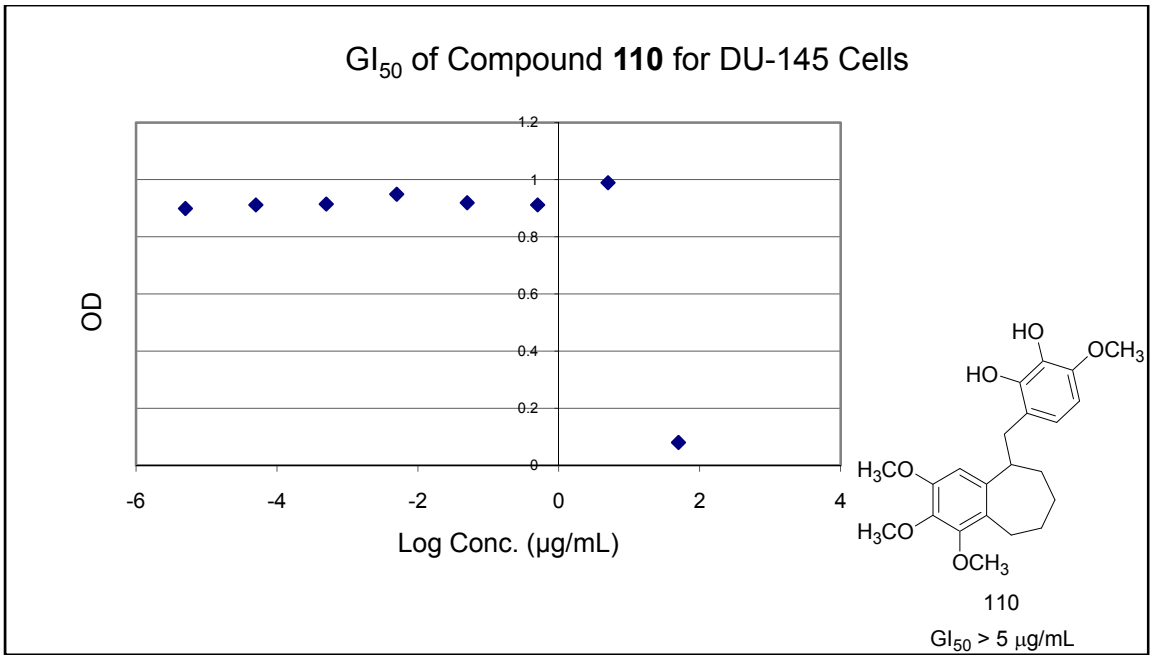

C.23. GI_{50} of Compound **110** for DU-145 Prostate Cancer Cells

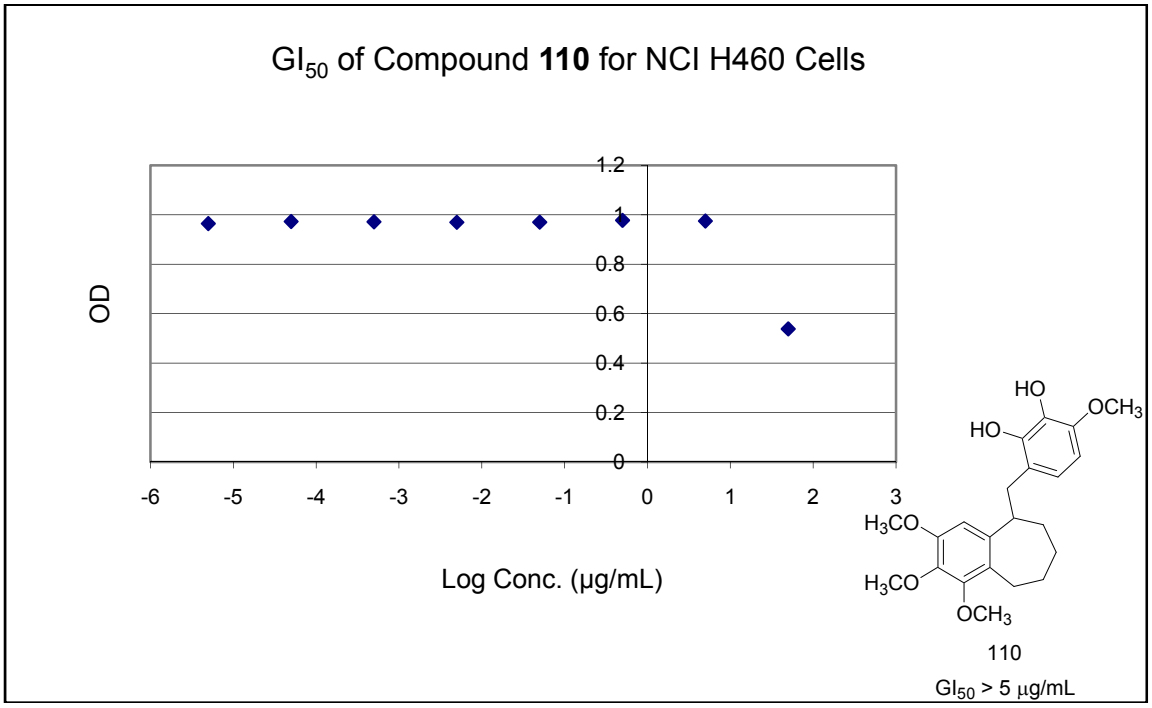

C.24. GI_{50} of Compound **110** for NCI H460 Lung Cancer Carcinoma Cells

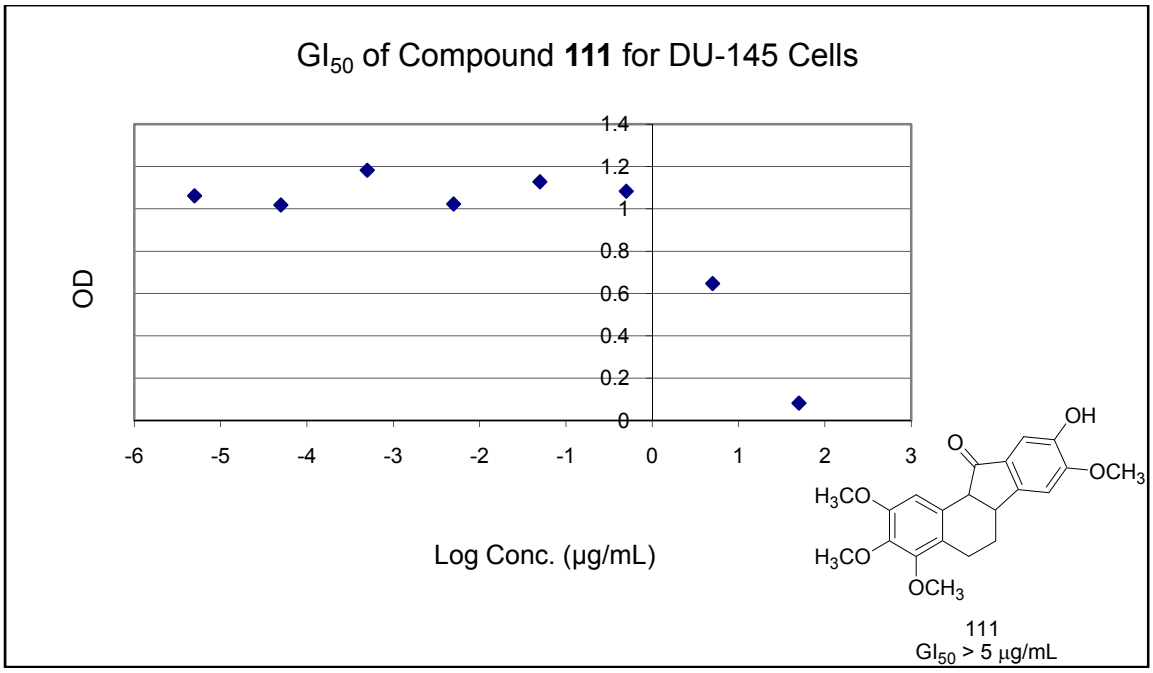

C.25. GI_{50} of Compound **111** for DU-145 Prostate Cancer Cells

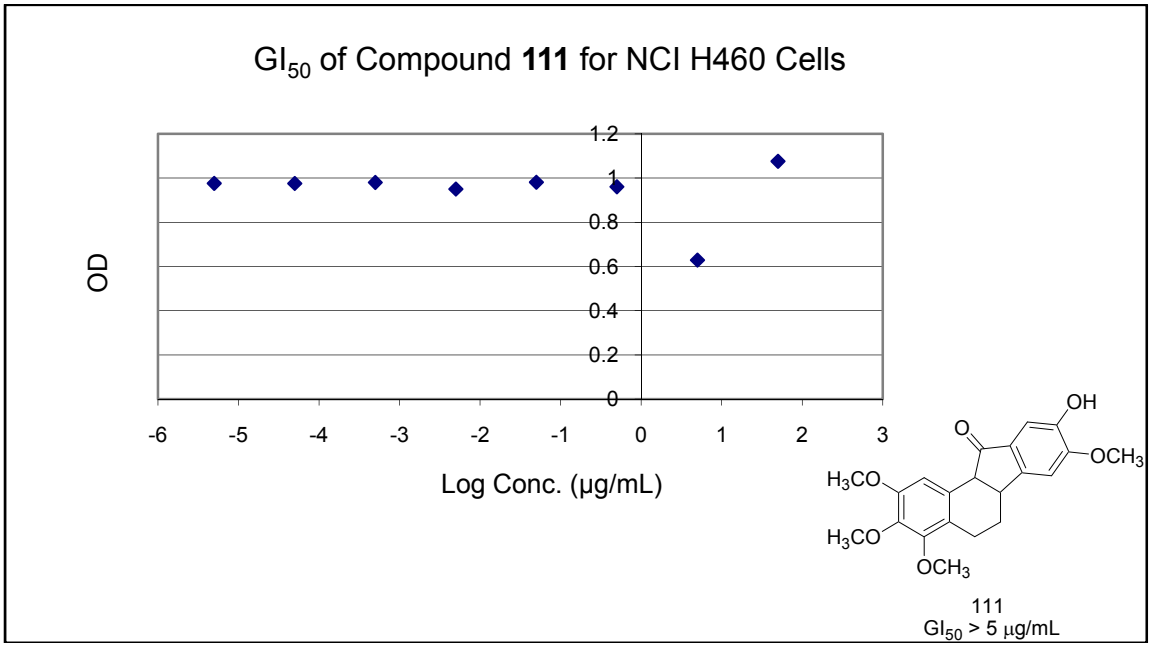

C.26. GI_{50} of Compound **111** for NCI H460 Lung Cancer Carcinoma Cells

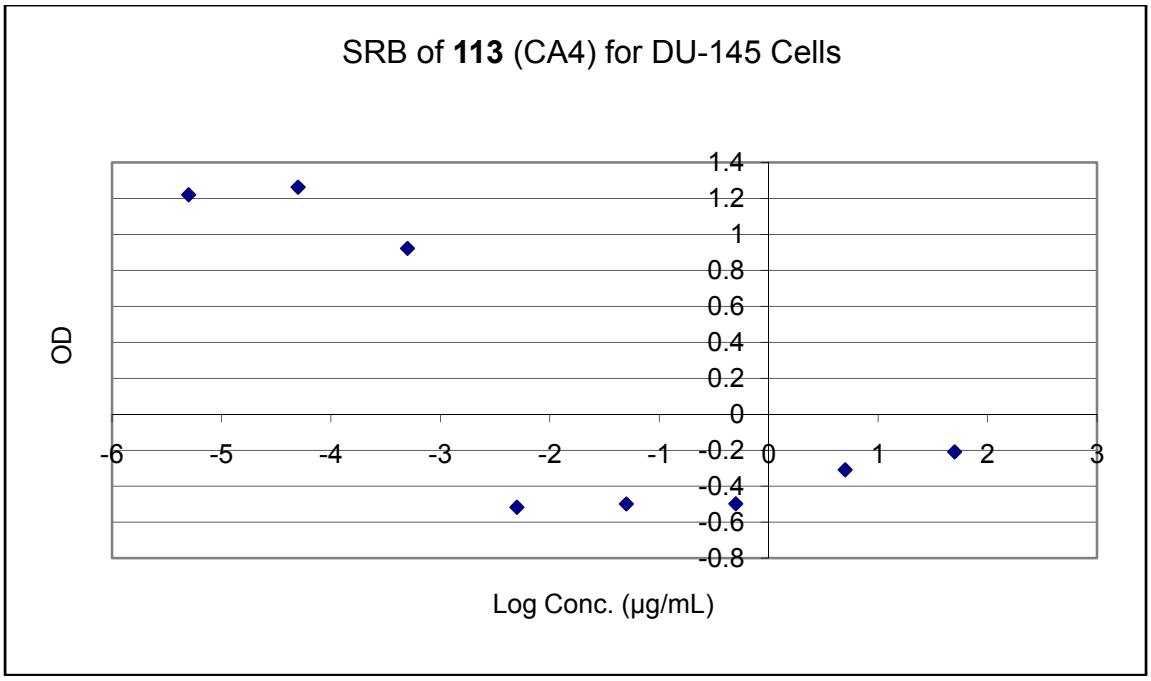

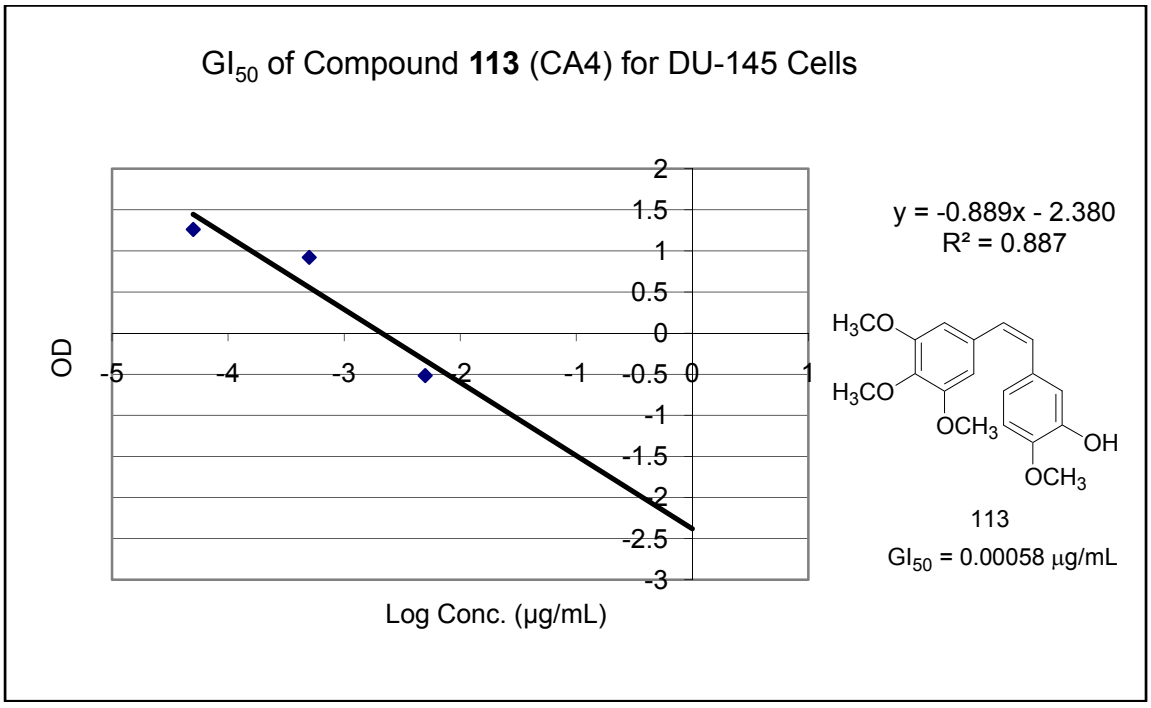

C.27. GI_{50} of Compound **113** for DU145 Prostate Cancer Cells

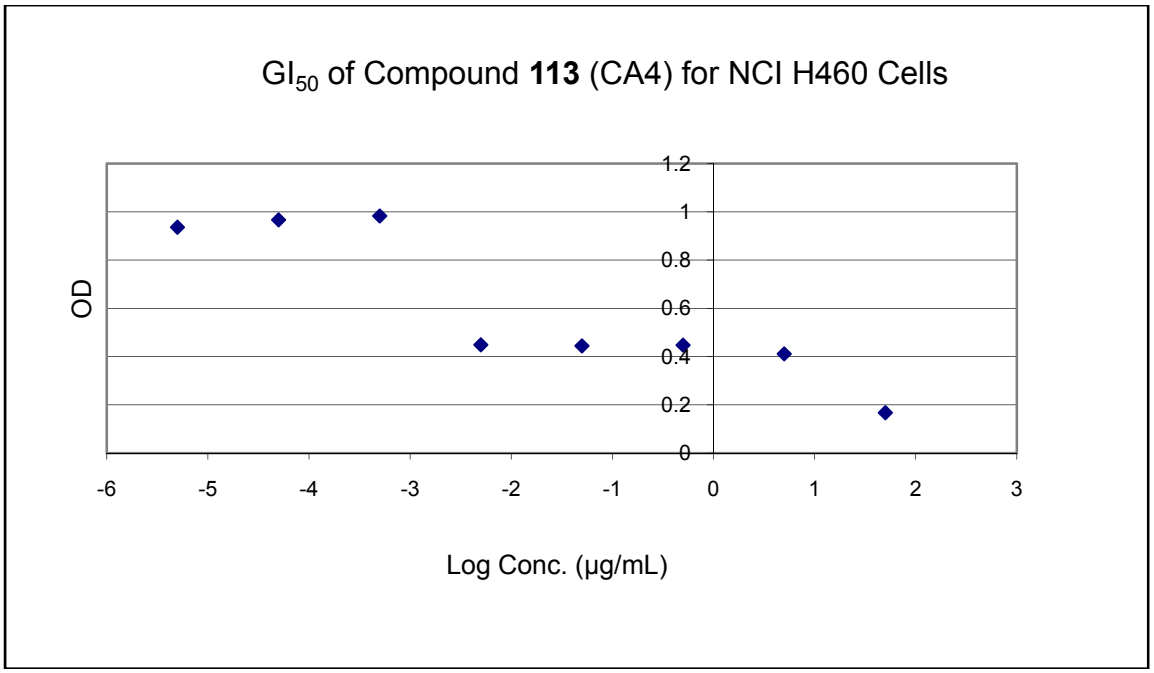

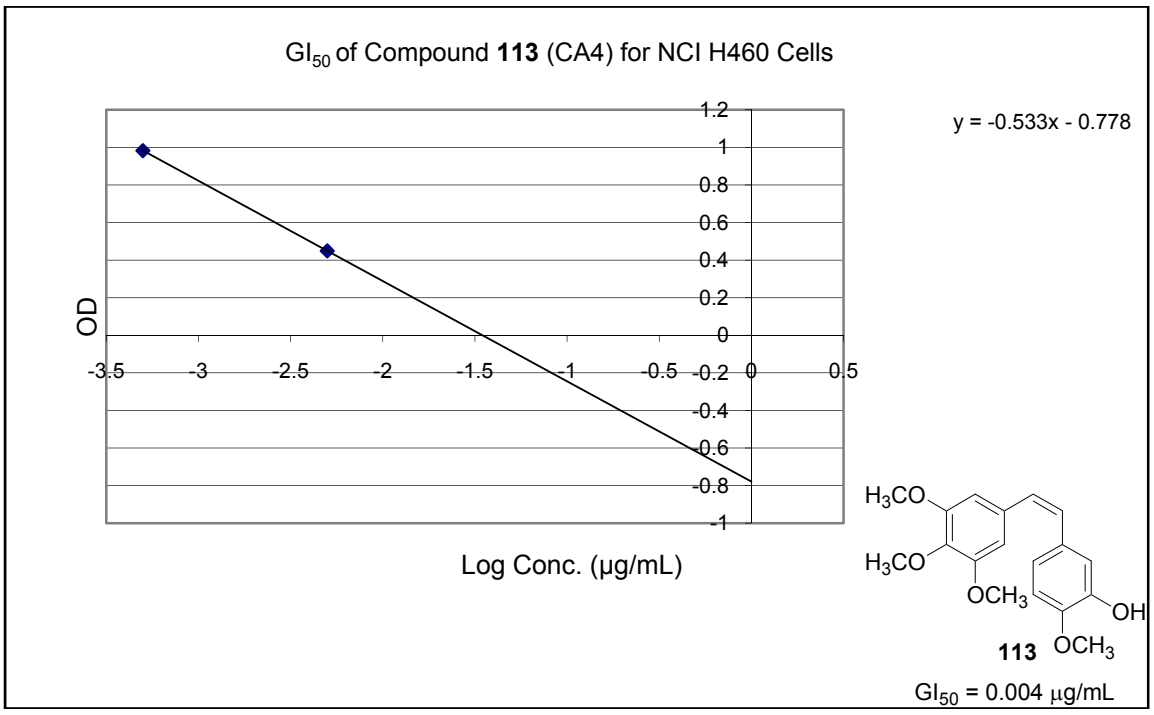

C.28. GI_{50} of Compound **113** for NCI H460 Lung Cancer Carcinoma Cells

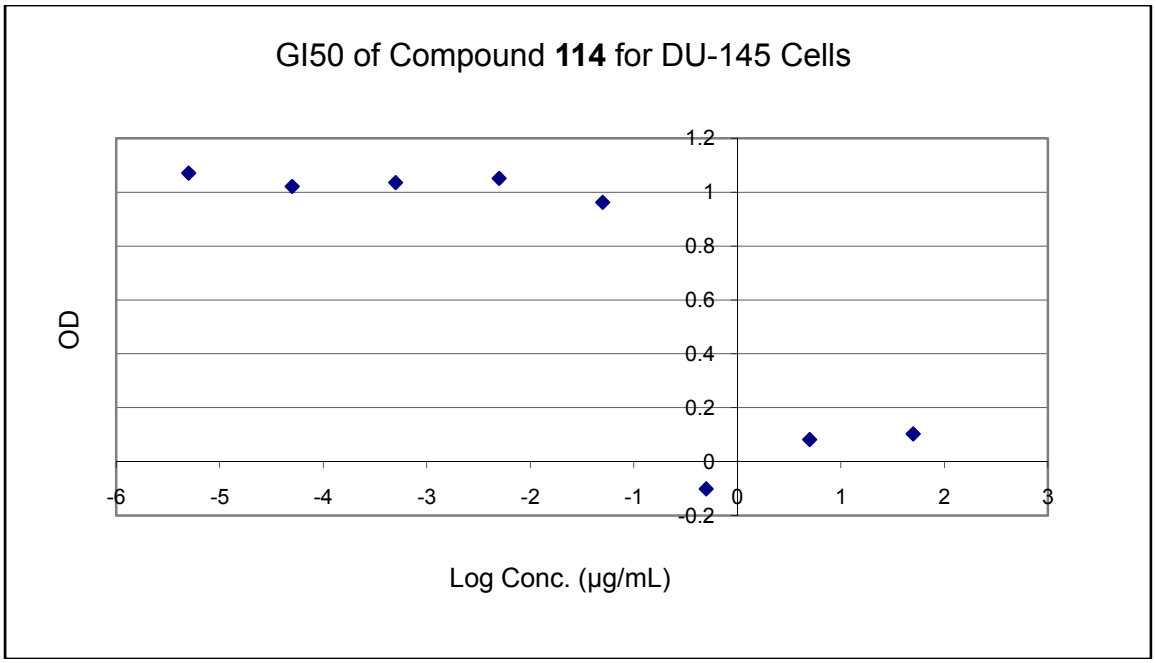

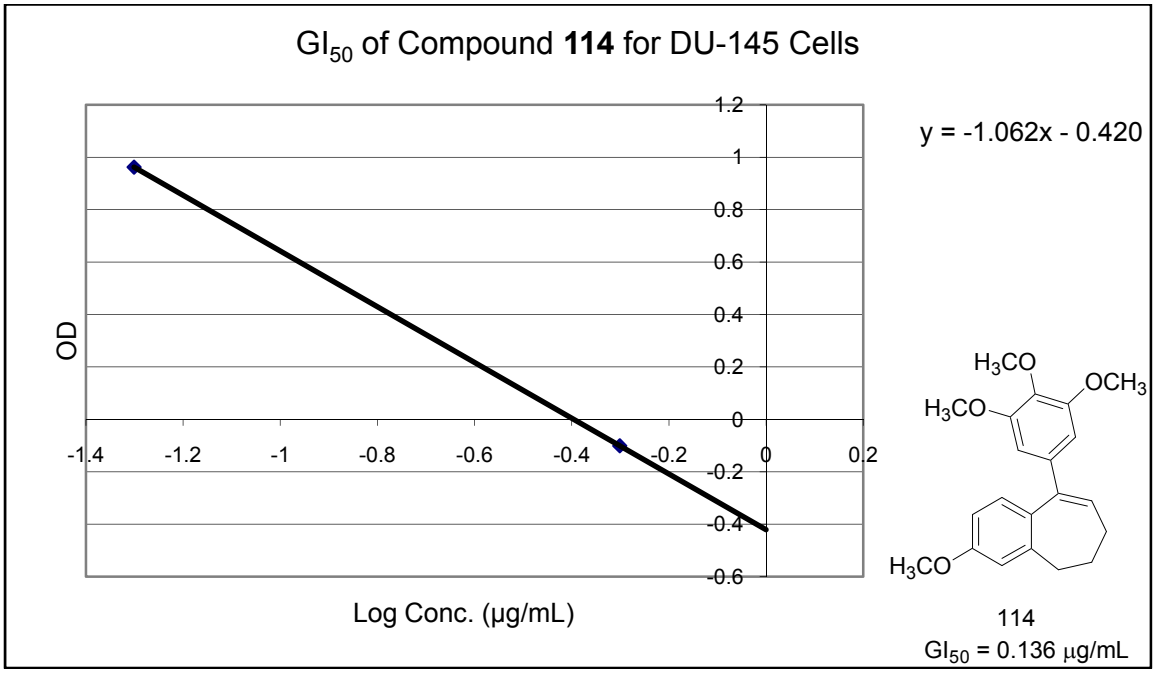

C.29. GI_{50} of Compound **114** for DU-145 Prostate Cancer Cells

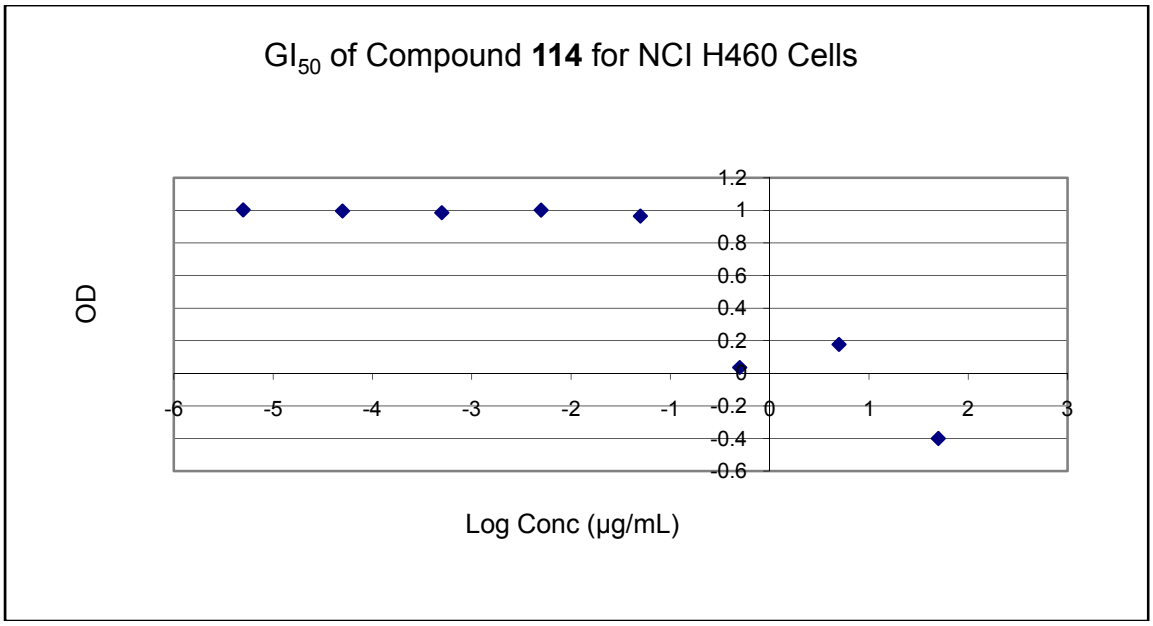

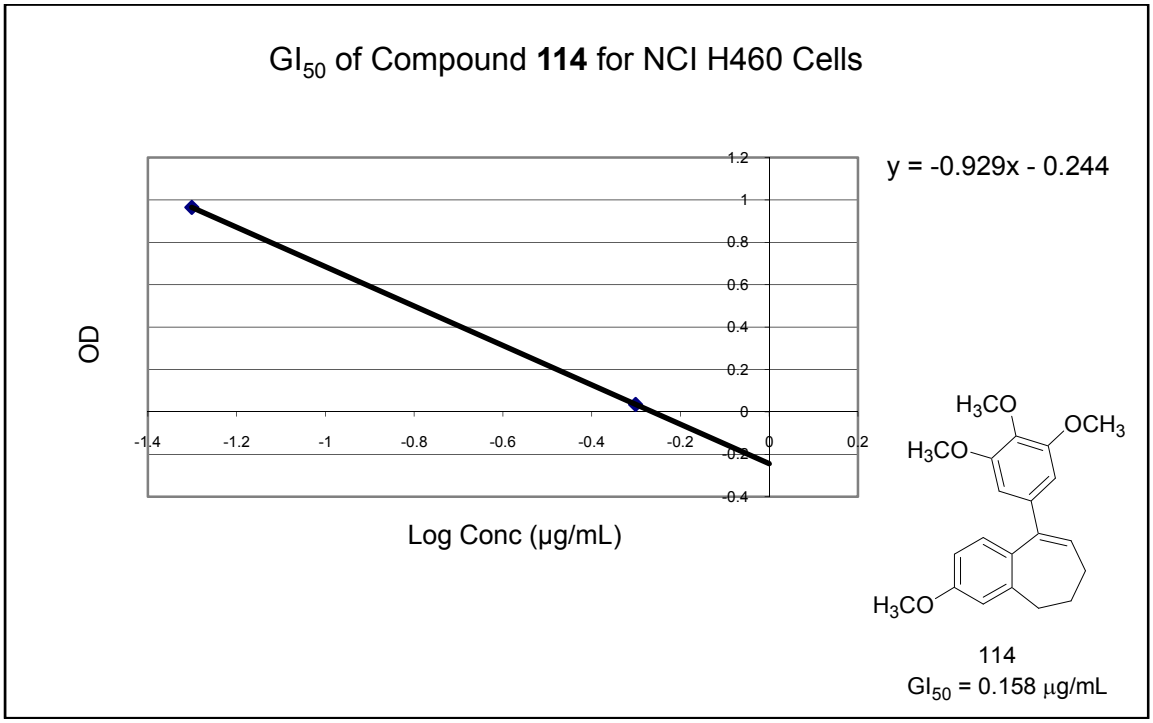

C.30. GI_{50} of Compound **114** for NCI H460 Lung Cancer Carcinoma Cells

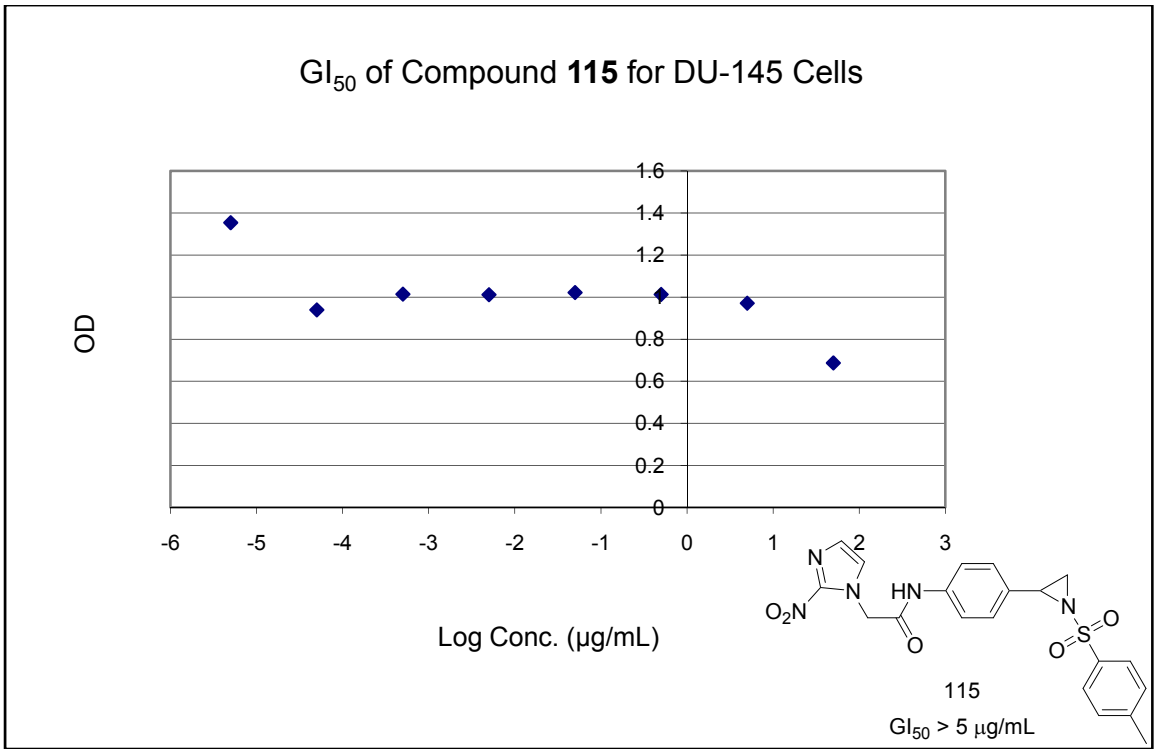

C.31. GI_{50} of Compound **115** for DU-145 Prostate Cancer Cells

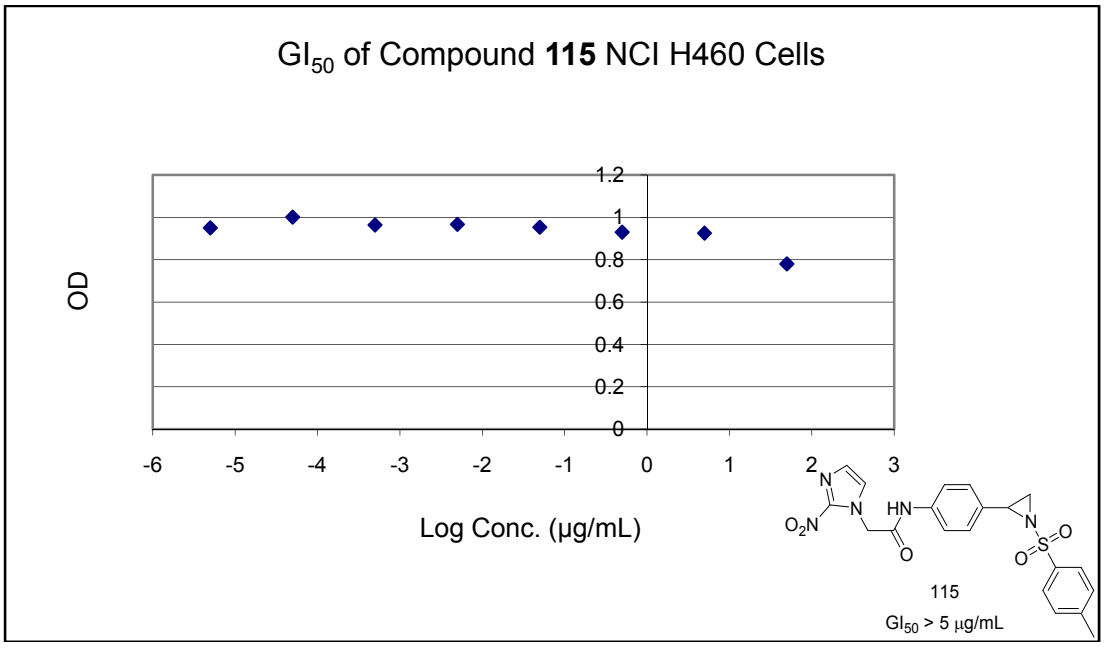

C.32. GI_{50} of Compound **115** for NCI H460 Lung Cancer Carcinoma Cells

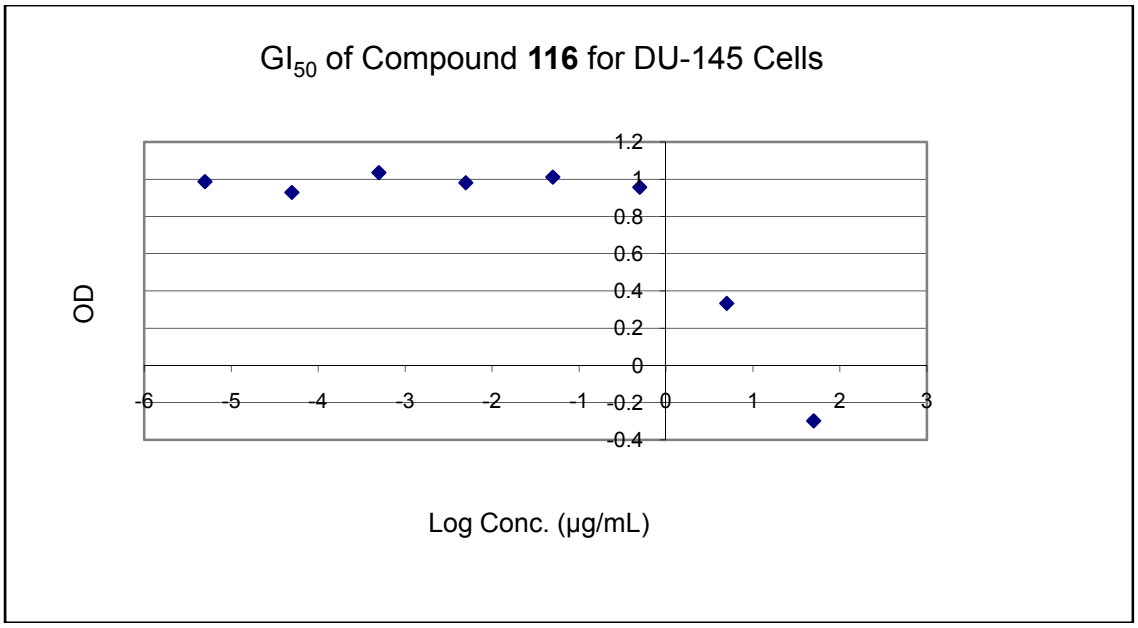

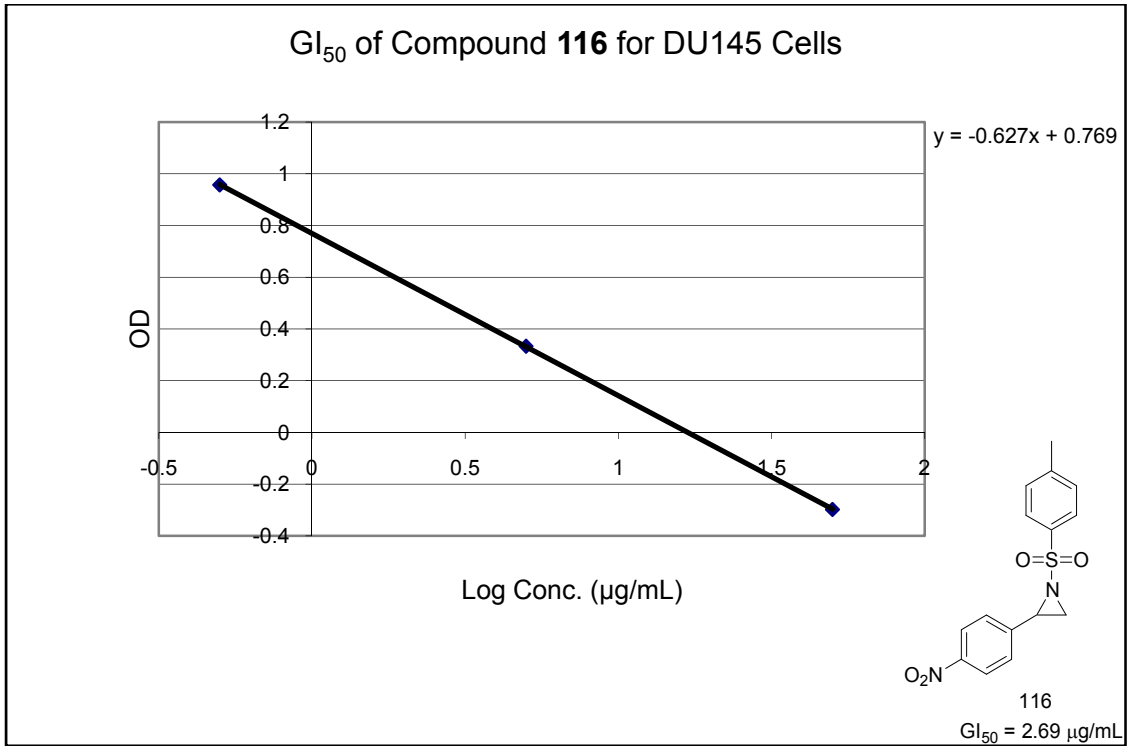

C.33. GI_{50} of Compound **116** for DU-145 Prostate Cancer Cells

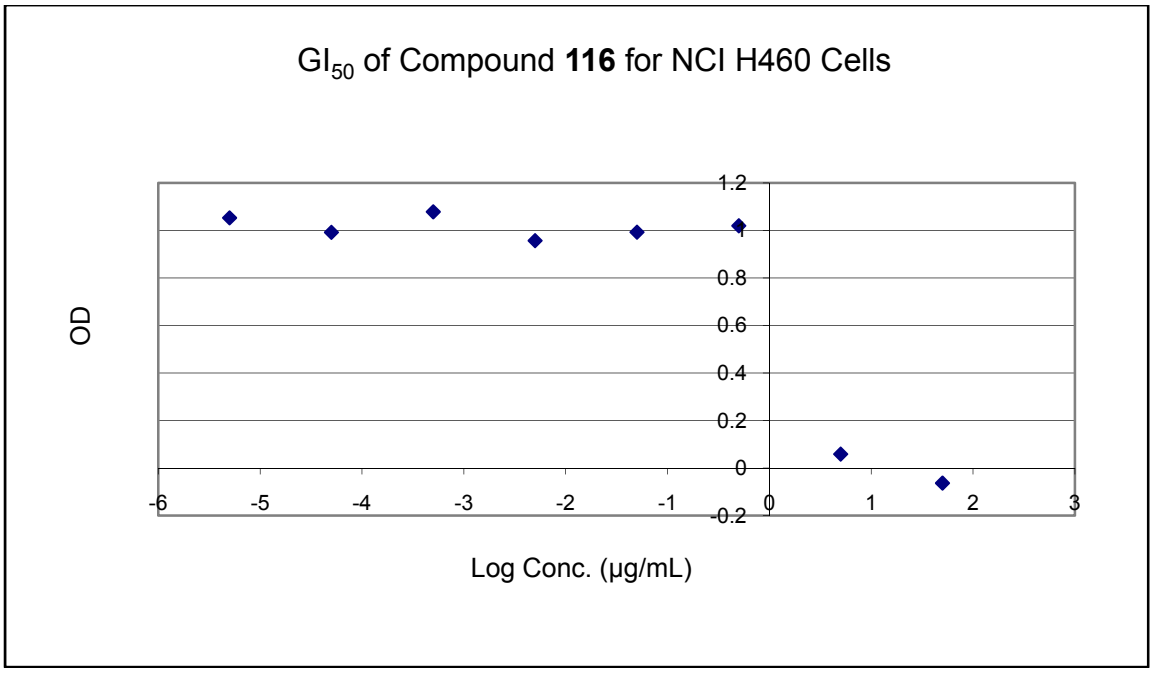

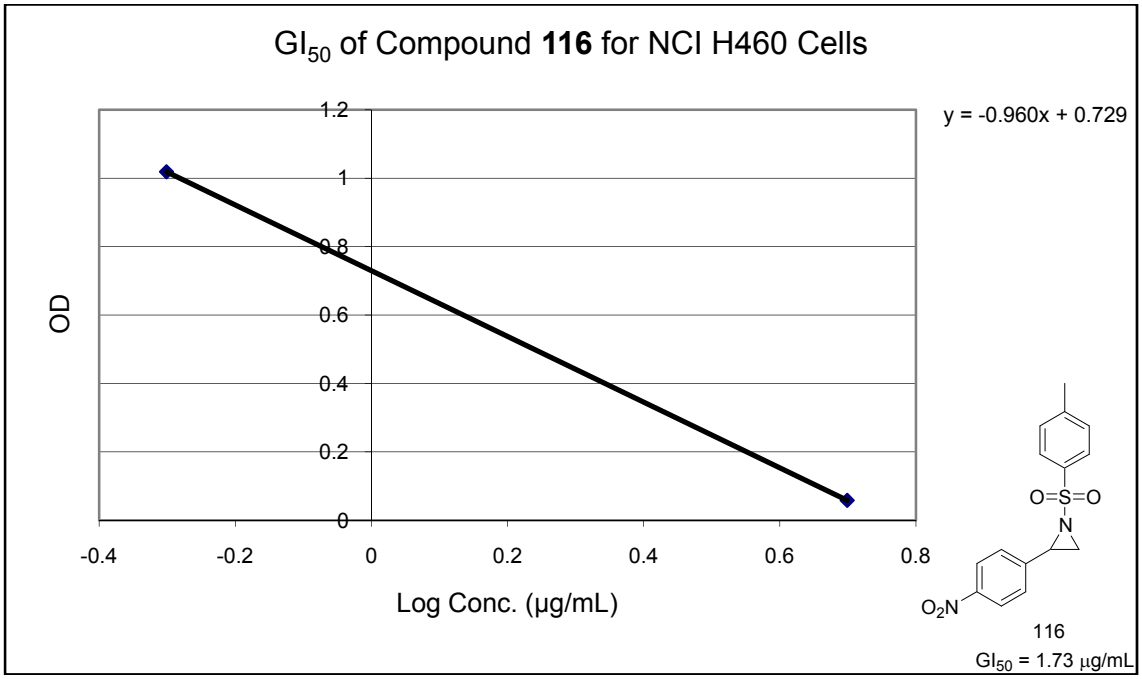

C.34. GI_{50} of Compound **116** for NCI H460 Lung Cancer Carcinoma Cells

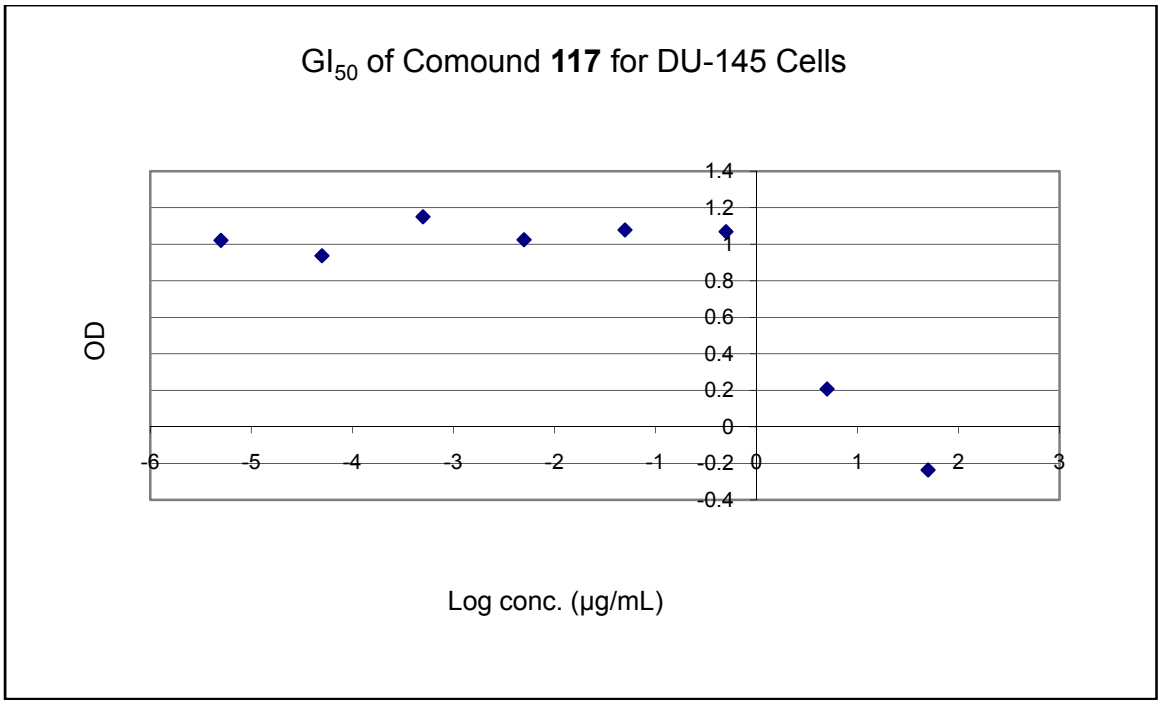

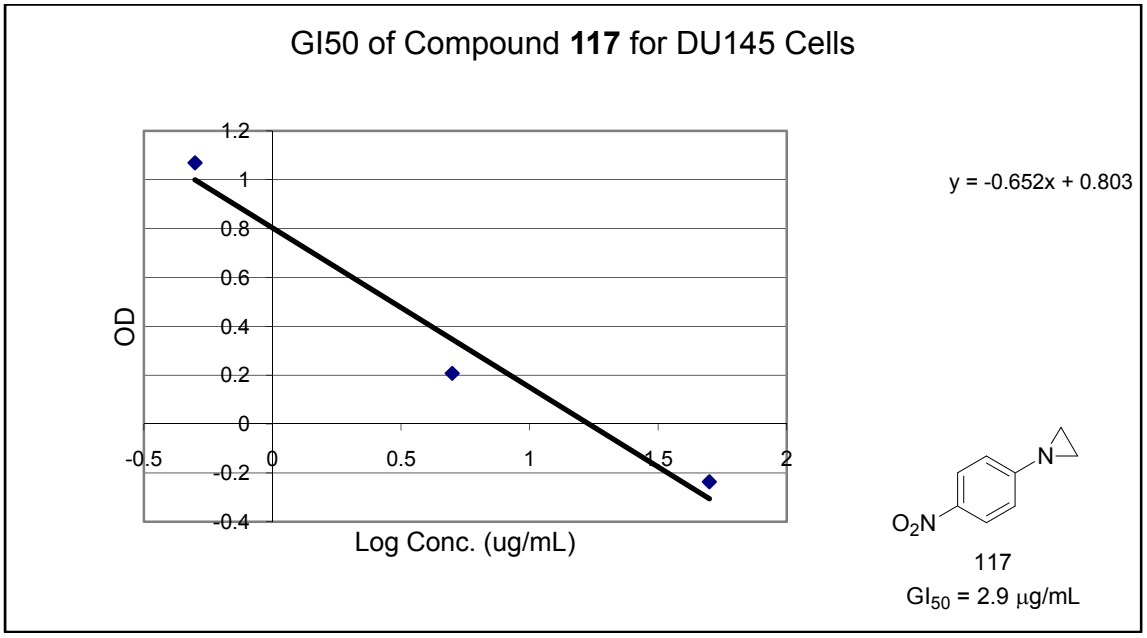

C.35. GI_{50} of Compound **117** for DU-145 Prostate Cancer Cells

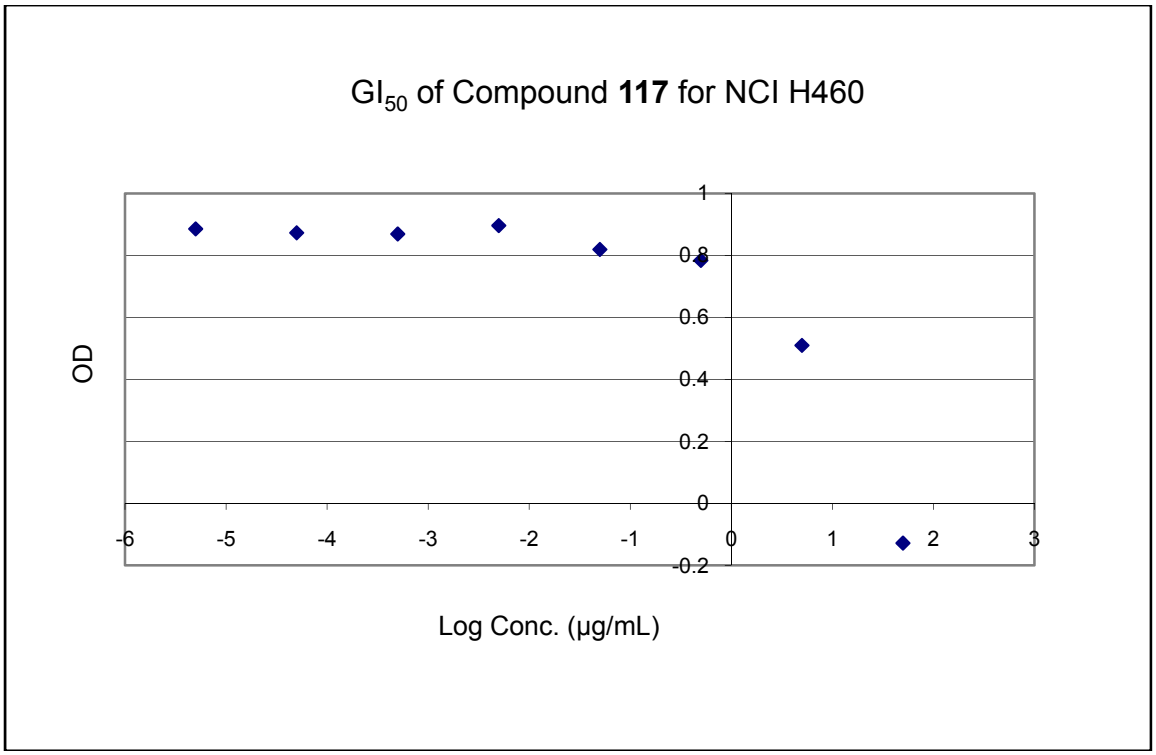

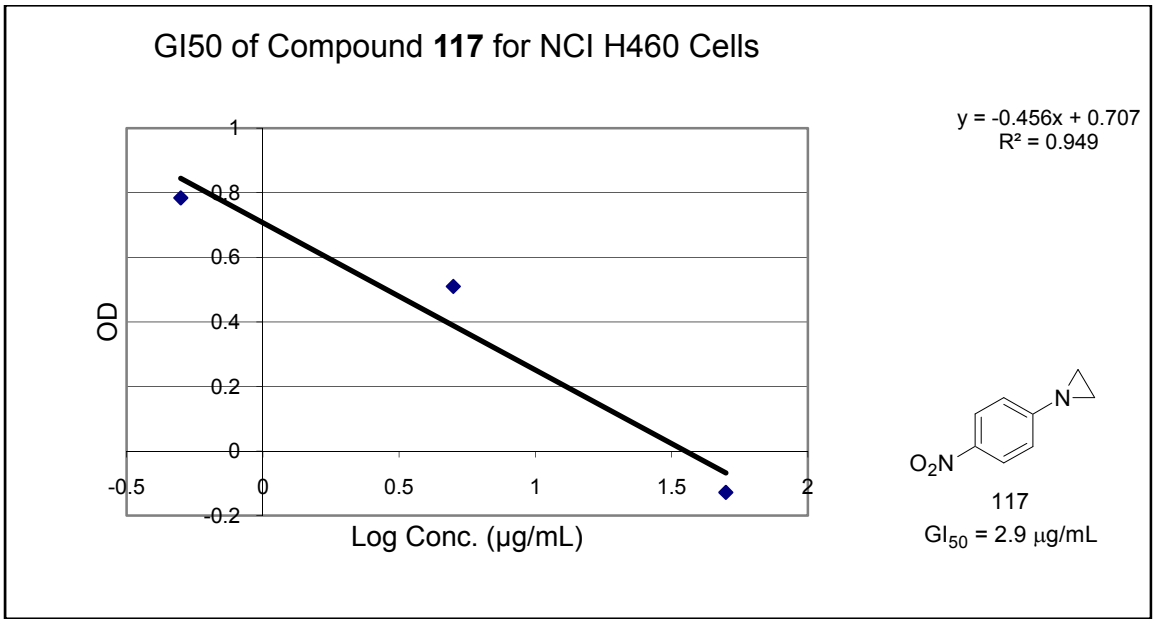

C.36. GI_{50} of Compound **117** for NCI H460 Lung Cancer Carcinoma Cells

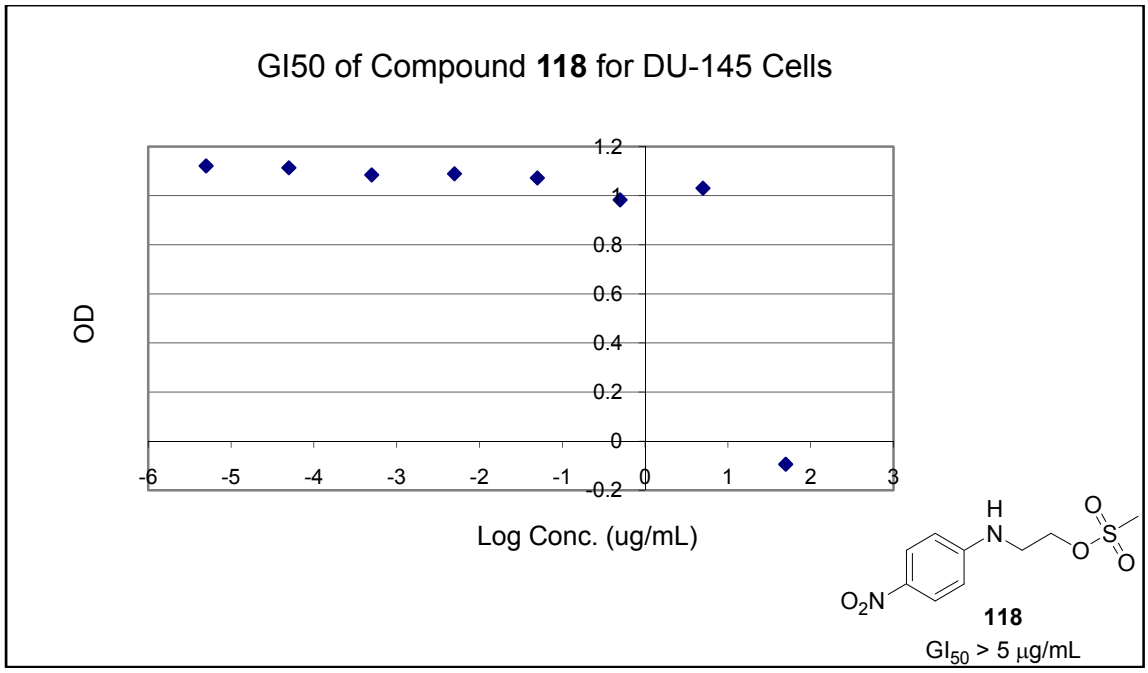

C.37. GI_{50} of Compound **118** for DU-145 Prostate Cancer Cells

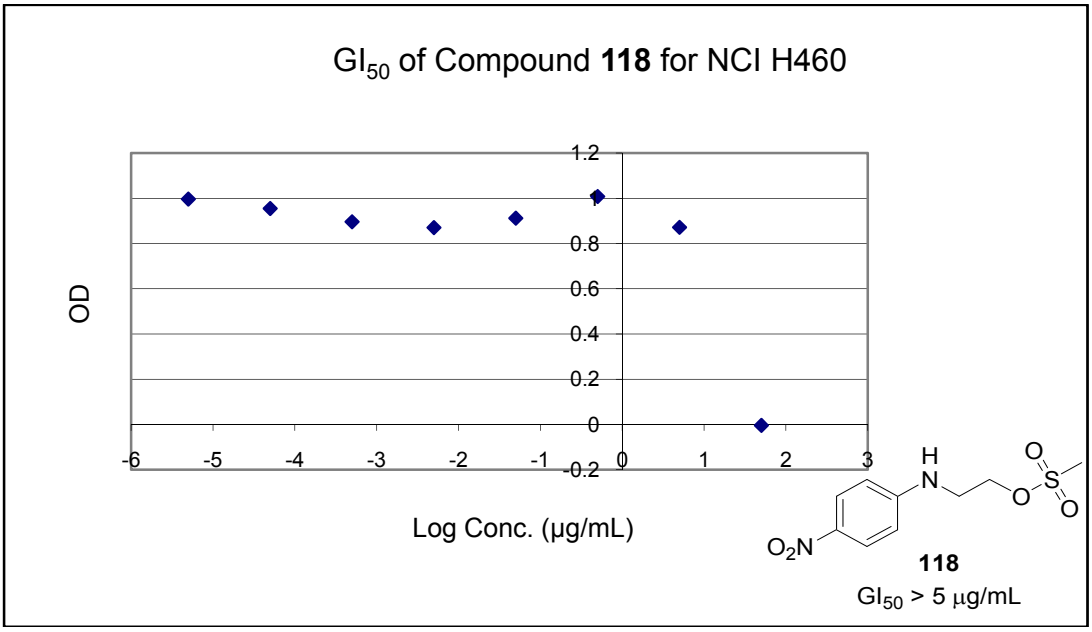

C.38. GI_{50} of Compound **118** for NCI H460 Lung Cancer Carcinoma Cells

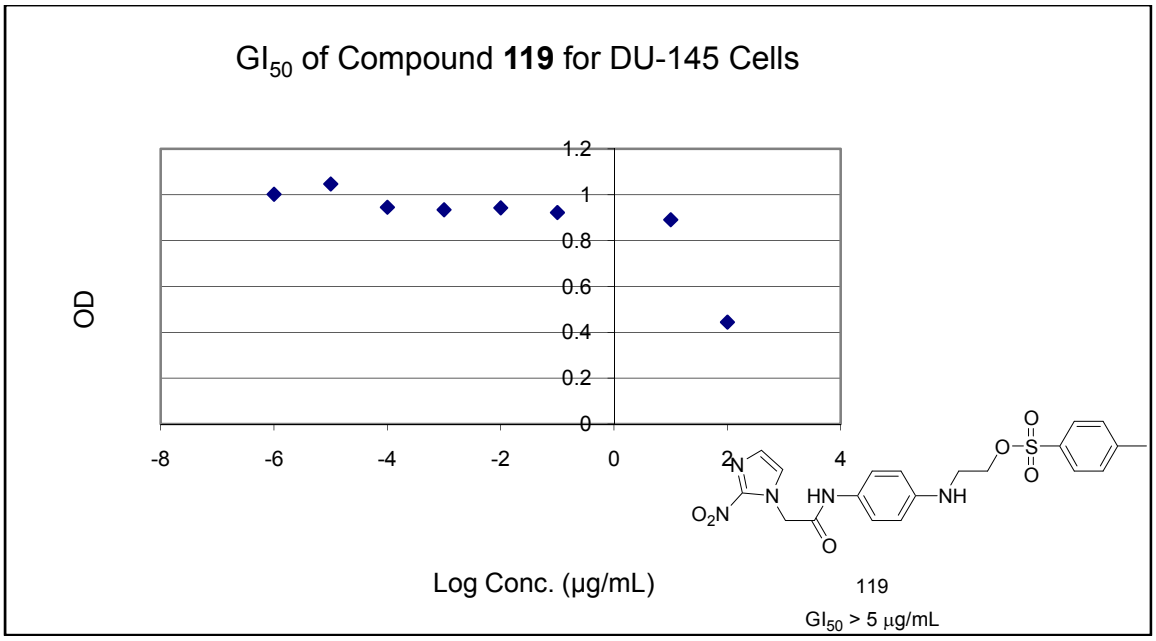

C.39. GI_{50} of Compound **119** for DU-145 Prostate Cancer Cells

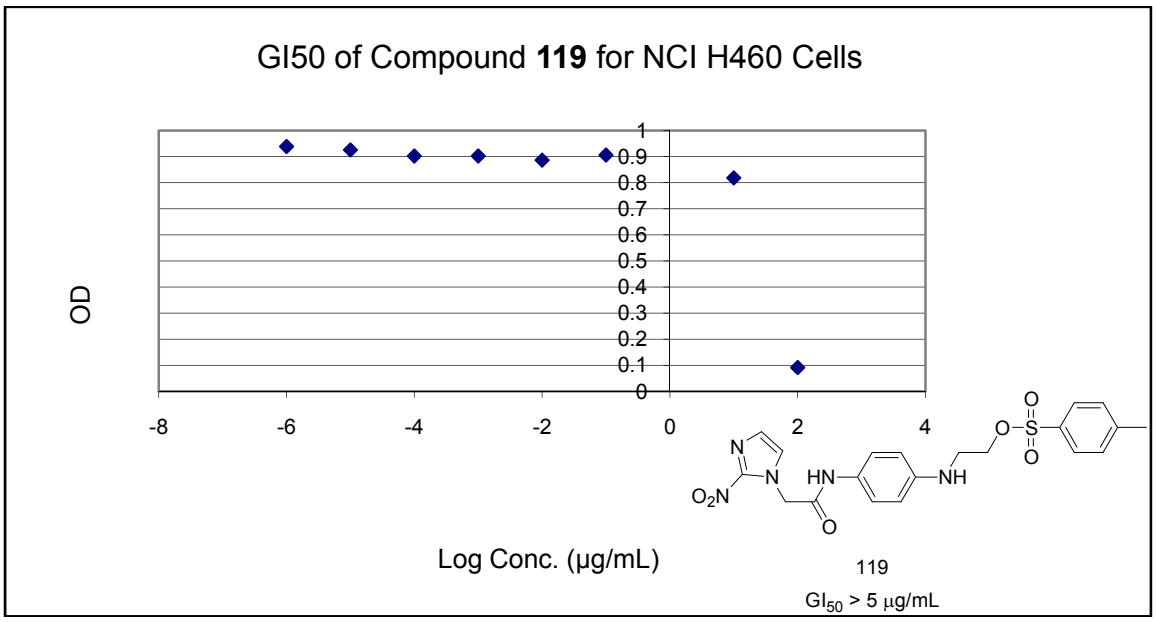

C.40. GI_{50} of Compound **119** for NCI H460 Lung Cancer Carcinoma Cells

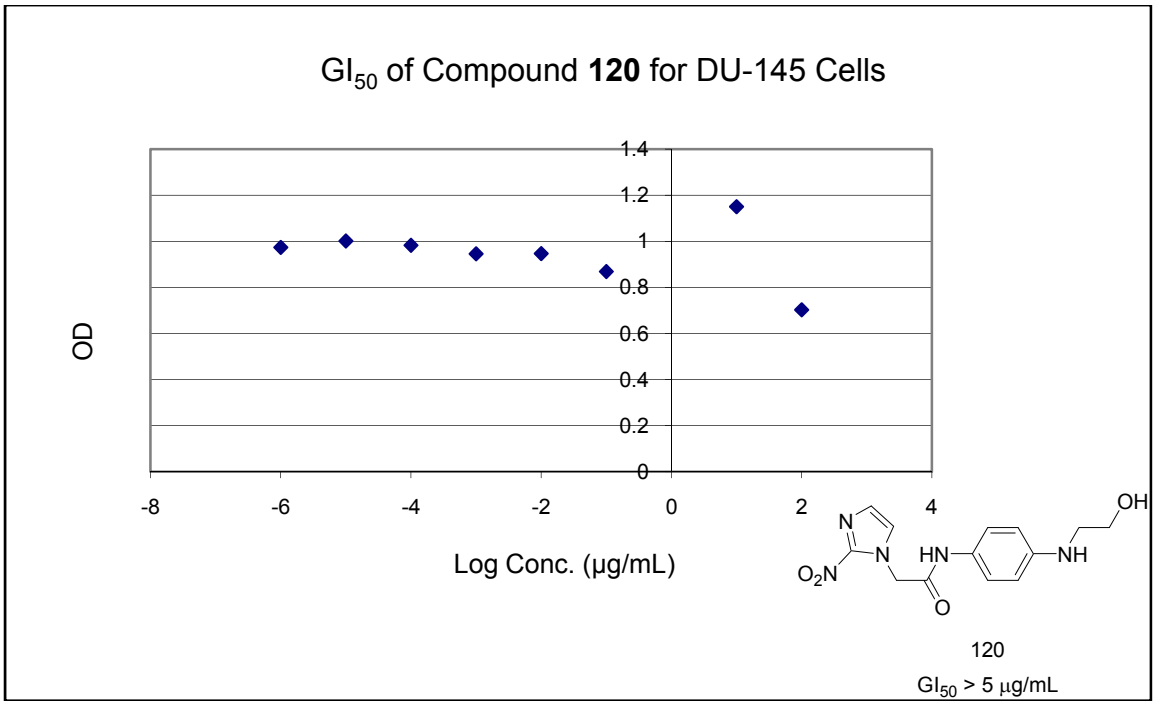

C.41. GI_{50} of Compound **120** for DU-145 Prostate Cancer Cells

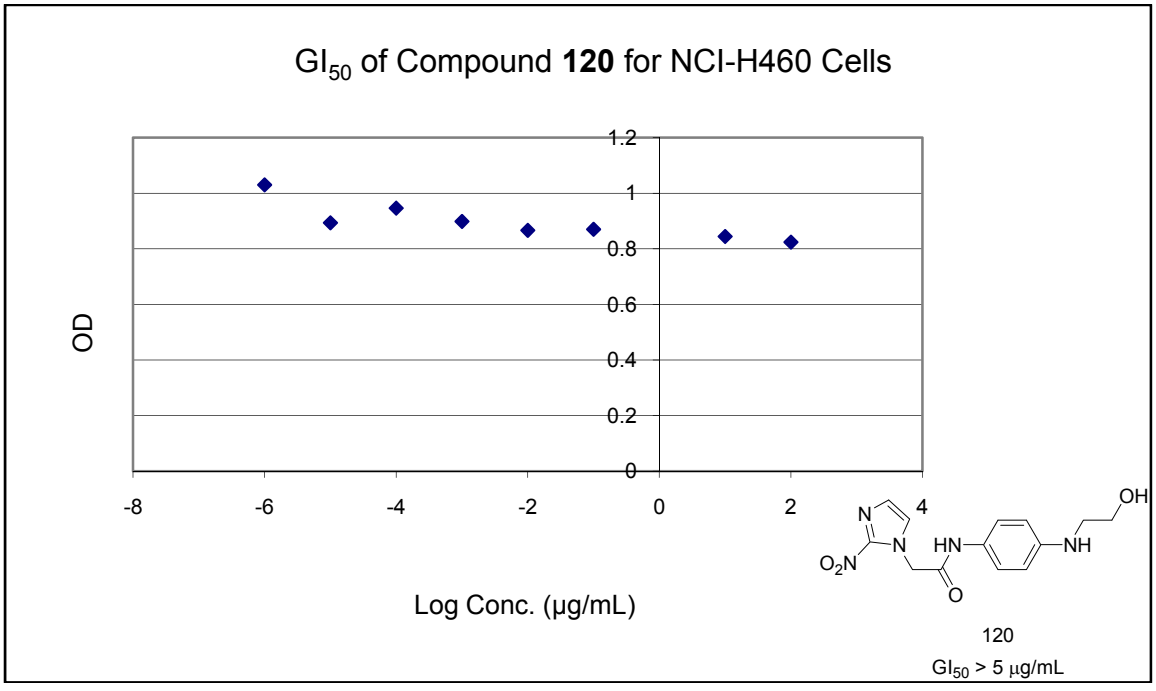

C.42. GI_{50} of Compound **120** for NCI H460 Lung Cancer Carcinoma Cells

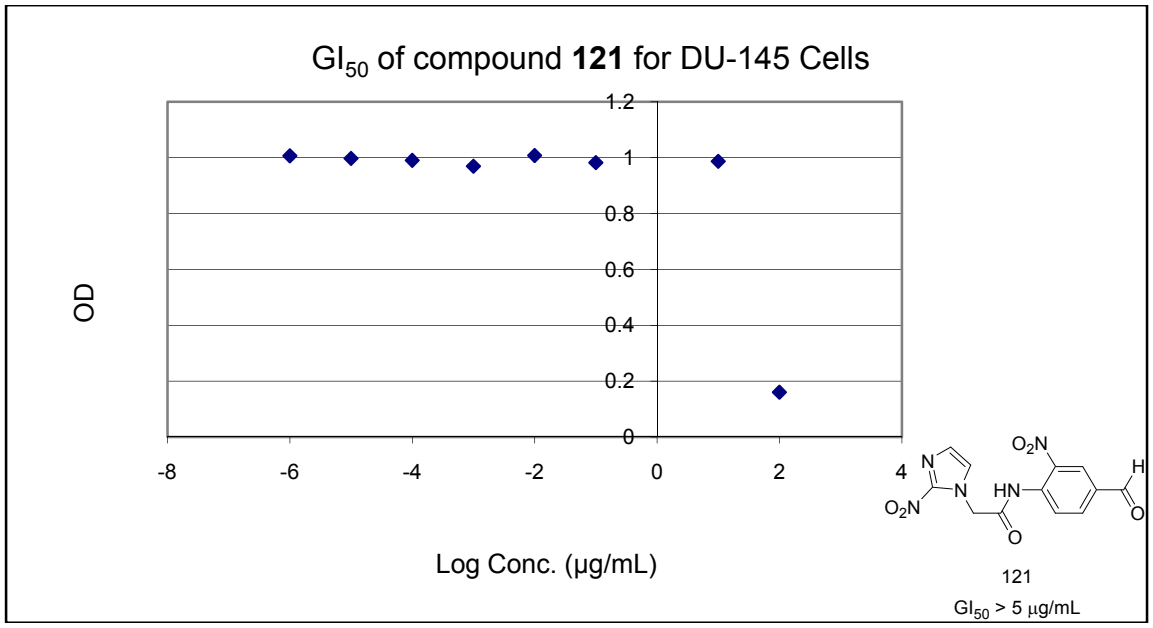

C.43. GI_{50} of Compound **121** for DU-145 Prostate Cancer Cells

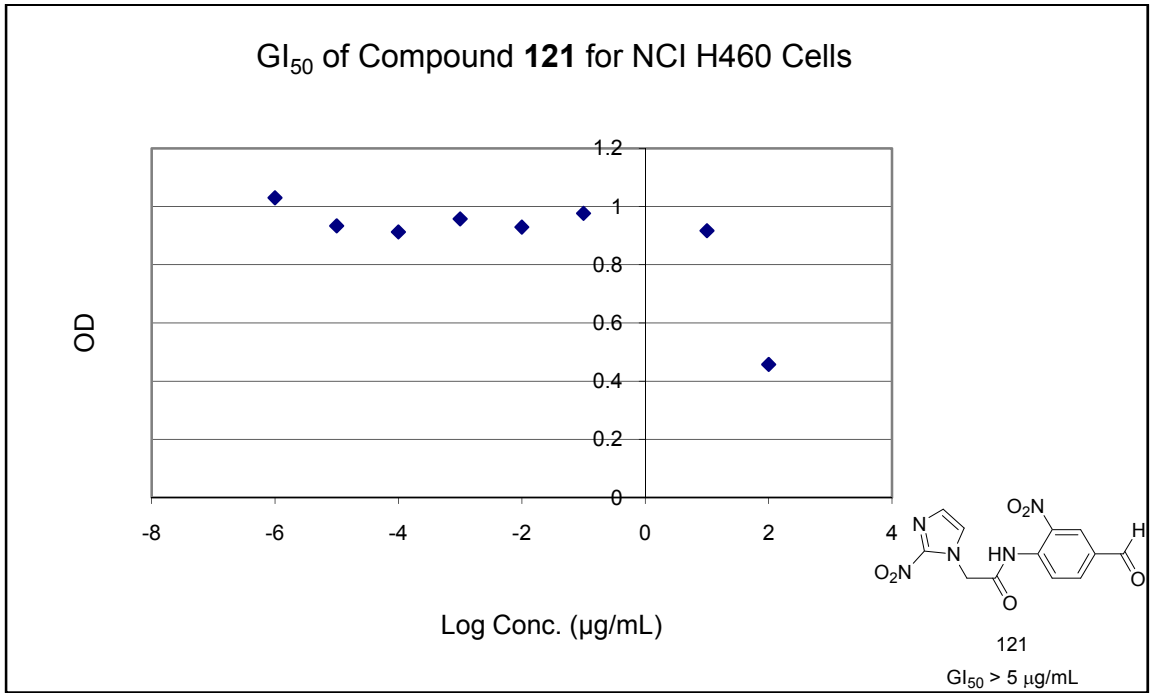

C.44. GI_{50} of Compound **121** for NCI H460 Lung Cancer Carcinoma Cells

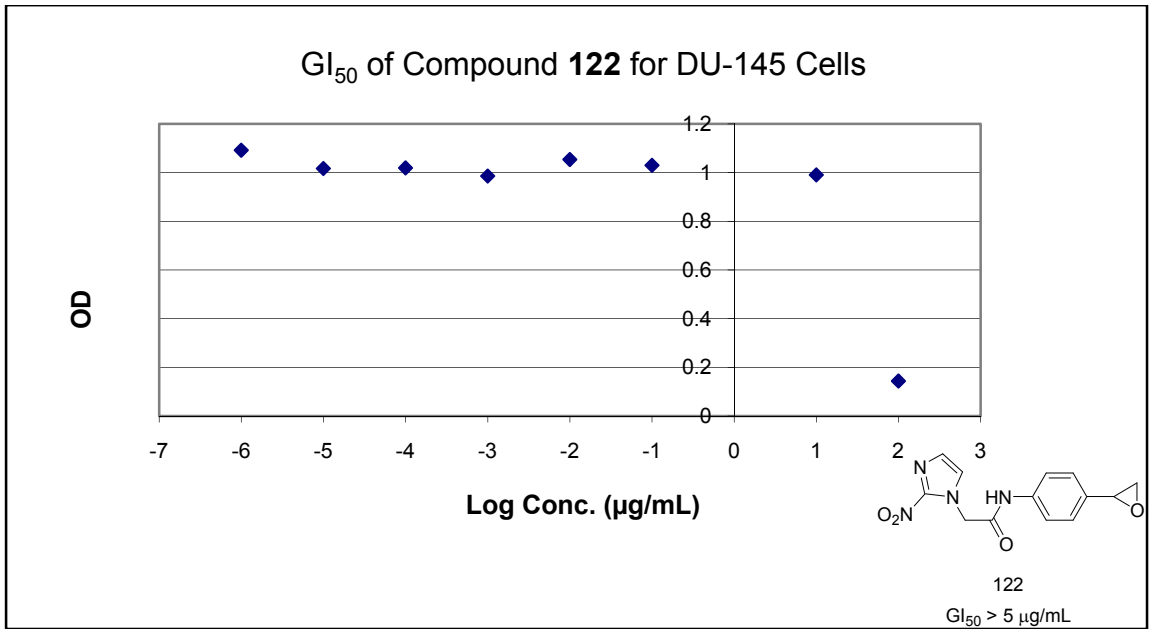

C.45. GI_{50} of Compound **122** for DU-145 Prostate Cancer Cells

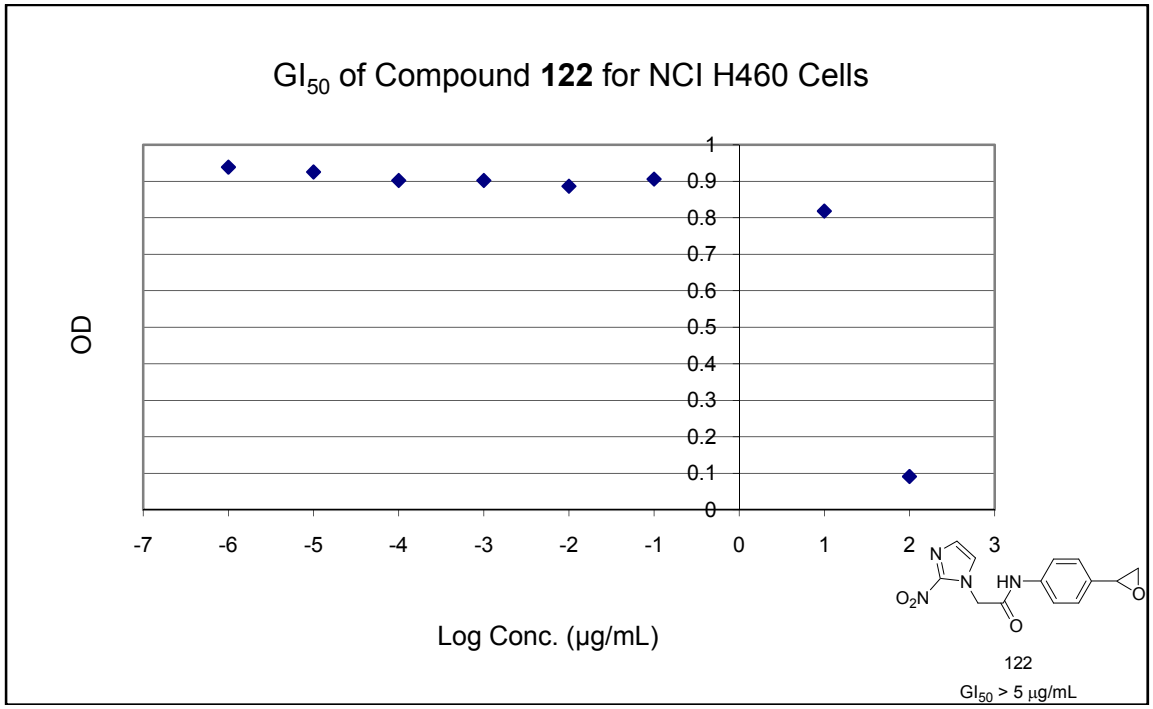

C.46. GI_{50} of Compound **122** for NCI H460 Lung Cancer Carcinoma Cells

Appendix D

Permissions For Figures

License Number	1885590701134
License date	Feb 10, 2008
Licensed content publisher	Elsevier Limited
Licensed content publication	Drug Resistance Updates
Licensed content title	Anti-vascular tumor therapy: recent advances, pitfalls and clinical perspectives
Licensed content author	Eichhorn Martin E., Strieth Sebastian and Dellian Marc
Licensed content date	April 2004
Volume number	7
Issue number	2
Pages	14
Type of Use	Thesis / Dissertation
Portion	Figures/table/illustration/abstracts
Quantity	1
Format	Print
You are the author of this Elsevier article	No
Are you translating?	No
Purchase order number	
Expected publication date	May 2009
Elsevier VAT number	GB 494 6272 12
Permissions price	0.00 USD
Value added tax 0.0%	0.00 USD
Total	0.00 USD

D.1. Permission for Figure 3

License Number	1885581354166
License date	Feb 10, 2008
Licensed content publisher	Nature Publishing Group
Licensed content publication	Nature Reviews Cancer
Licensed content title	Exploiting tumour hypoxia in cancer treatment
Licensed content author	J. Martin Brown and William R. Wilson
Volume number	
Issue number	
Pages	
Year of publication	2004
Portion used	Figures / tables
Requestor type	Student
Type of Use	Thesis / Dissertation
PO Number	
Total	0.00 USD

D.2. Permission for Figure 4

Hi John,

Good to hear from you. Looks like you are closing in on your work. Of course, it is fine with me. You may use as much as you want. I have no problem with that. Hopefully you have consulted with Dr. Trawick and it is fine with her. Wish you success as you write your dissertation.

Regards to everyone,

****
Benon E. Mugabe, Ph.D.

Postdoctoral Research Fellow
University of Tennessee,
Health Science Center,
College of Medicine,
Department of Pharmacology,
874 Union Ave, # 209 Crowe Research Bldg,
Memphis, TN 38163
Phone: 901-448-6010
Fax: 901-448-7300
Email: bmugabe@utmem.edu

D.3. Permission for Figure 8 and 21

License Number	1885600933038
License date	Feb 10, 2008
Licensed content publisher	Elsevier Limited
Licensed content publication	Current Opinion in Cell Biology
Licensed content title	Structural intermediates in microtubule assembly and disassembly: how and why?
Licensed content author	Nogales Eva and Wang Hong-Wei
Licensed content date	April 2006
Volume number	18
Issue number	2
Pages	6
Type of Use	Thesis / Dissertation
Portion	Figures/table/illustration/abstracts
Quantity	1
Format	Print
You are the author of this Elsevier article	No
Are you translating?	No
Purchase order number	
Expected publication date	May 2009
Elsevier VAT number	GB 494 6272 12
Permissions price	0.00 USD
Value added tax 0.0%	0.00 USD
Total	0.00 USD

D.4. Permission for Figure 15

Dear Mr. Hall:

Thank you for your request for permission to reprint the figures cited in your e-mail below. We are happy to grant you permission to use this material in your doctoral dissertation. Please use the following acknowledgment: "Reprinted, with permission, from the Annual Review of Biochemistry, Volume 69 (c)2000 by Annual Reviews www.annualreviews.org"

This permission to reprint is for a one-time usage only and any subsequent use of this material requires submission of a new permission request. Fees for this noncommercial usage have been waived for you. If I can be of further assistance, please do not hesitate to contact me.

Sincerely,
Laura Folkner
Permissions Department
ANNUAL REVIEWS
A Nonprofit Scientific Publisher
4139 El Camino Way
Palo Alto, CA 94306
Ph: 650.843.6636
Fax: 650.855.9815
lfolkner@annualreviews.org

D.5. Permission for Figure 16 and 17

License Number	1885600933038
License date	Feb 10, 2008
Licensed content publisher	Elsevier Limited
Licensed content publication	Current Opinion in Cell Biology
Licensed content title	Structural intermediates in microtubule assembly and disassembly: how and why?
Licensed content author	Nogales Eva and Wang Hong-Wei
Licensed content date	April 2006
Volume number	18
Issue number	2
Pages	6
Type of Use	Thesis / Dissertation
Portion	Figures/table/illustration/abstracts
Quantity	1
Format	Print
You are the author of this Elsevier article	No
Are you translating?	No
Purchase order number	
Expected publication date	May 2009
Elsevier VAT number	GB 494 6272 12
Permissions price	0.00 USD
Value added tax 0.0%	0.00 USD
Total	0.00 USD

D.6. Permission for Figures 20 and 21

License Number	1885620266024
License date	Feb 10, 2008
Licensed content publisher	Elsevier Limited
Licensed content publication	Bioorganic & Medicinal Chemistry
Licensed content title	Design, synthesis, and biological evaluation of combretastatin nitrogen-containing derivatives as inhibitors of tubulin assembly and vascular disrupting agents
Licensed content author	Monk Keith A., Siles Rogelio, Hadimani Mallinath B., Mugabe Benon E., Ackley J. Freeland, Studerus Scott W., Edvardsen Klaus, Trawick Mary Lynn, Garner Charles M., Rhodes Monte R., Pettit George R. and Pinney Kevin G.
Licensed content date	1 May 2006
Volume number	14
Issue number	9
Pages	14
Type of Use	Thesis / Dissertation
Portion	Figures/table/illustration/abstracts
Quantity	1
Format	Print
You are the author of this Elsevier article	No
Are you translating?	No
Purchase order number	
Expected publication date	Jun 2009
Elsevier VAT number	GB 494 6272 12
Permissions price	0.00 USD
Value added tax 0.0%	0.00 USD
Total	0.00 USD

D.7. Permission for Figure 23

License Number	1885620852966
License date	Feb 10, 2008
Licensed content publisher	Elsevier Limited
Licensed content publication	International Journal of Radiation Oncology*Biology*Physics
Licensed content title	Enhancement of vascular targeting by inhibitors of nitric oxide synthase
Licensed content author	Davis Peter D., Tozer Gillian M., Naylor Matthew A., Thomson Peter, Lewis Gemma and Hill Sally A.
Licensed content date	1 December 2002
Volume number	54
Issue number	5
Pages	5
Type of Use	Thesis / Dissertation
Portion	Figures/table/illustration/abstracts
Quantity	2
Format	Print
You are the author of this Elsevier article	No
Are you translating?	No
Purchase order number	
Expected publication date	May 2009
Elsevier VAT number	GB 494 6272 12
Permissions price	0.00 USD
Value added tax 0.0%	0.00 USD
Total	0.00 USD

D.8. Permission for Figures 28 and 29

License Number	1885630077561
License date	Feb 10, 2008
Licensed content publisher	Elsevier Limited
Licensed content publication	Cancer Cell
Licensed content title	2ME2 inhibits tumor growth and angiogenesis by disrupting microtubules and dysregulating HIF
Licensed content author	Mabjeesh Nicola J., Escuin Daniel, LaVallee Theresa M., Pribluda Victor S., Swartz Glenn M., Johnson Michelle S., Willard Margaret T., Zhong Hua, Simons Jonathan W. and Giannakakou Paraskevi
Licensed content date	April 2003
Volume number	3
Issue number	4
Pages	13
Type of Use	Thesis / Dissertation
Portion	Figures/table/illustration/abstracts
Quantity	2
Format	Print
You are the author of this Elsevier article	No
Are you translating?	No
Purchase order number	
Expected publication date	May 2009
Elsevier VAT number	GB 494 6272 12
Permissions price	0.00 USD
Value added tax 0.0%	0.00 USD
Total	0.00 USD

D.9. Permissions for Figures 35 and 36

License Number	1885631166931
License date	Feb 10, 2008
Licensed content publisher	Elsevier Limited
Licensed content publication	European Journal of Cancer
Licensed content title	Evaluations of vascular disrupting agents CA4P and OXi4503 in renal cell carcinoma (Caki-1) using a silicon based microvascular casting technique
Licensed content author	Salmon Howard W., Mladinich Christopher and Siemann Dietmar W.
Licensed content date	November 2006
Volume number	42
Issue number	17
Pages	6
Type of Use	Thesis / Dissertation
Portion	Figures/table/illustration/abstracts
Quantity	1
Format	Print
You are the author of this Elsevier article	No
Are you translating?	No
Purchase order number	
Expected publication date	May 2009
Elsevier VAT number	GB 494 6272 12
Permissions price	0.00 USD
Value added tax 0.0%	0.00 USD
Total	0.00 USD

D.10. Permissions for Figure 37

REFERENCES

1. American Cancer Society. www.cancer.org/downloads/STT/CAFF2007PWSecured.pdf.

2. Karpozilos, A.; Pavlidis, N. *Eur. J. Cancer.* **2004**, 40, 2033-2040.

3. Grange, J. M.; Stanford, J. L.; Stranford, C. A. *J. Royal Soc. Med.* **2002**, 95, 296-299.

4. National Cancer Institute www.cancer.gov/cancertopics/what-is-cancer/print?page=&keyword=.

5. McKinnell, R. G.; Parchment, R. E.; Perantoni, A. O.; Pierce, G. B. *The Biological Basis of Cancer*. Cambridge University Press. 1998.

6. Voet, D.; Voet, J. *Biochemistry*. John Wiley & Sons. **2004**. 529.

7. Pilat, M. J.; LoRusso, P. M. *J. Cellular Biochem.* **2006**, 99, 1021-1039.

8. Pettit, G. R.; Minardi, M. D.; Rosenberg, H. J.; Hamel, E.; Bibby, M. C.; Martin, S. W.; Jung, M. K.; Pettit, R. K.; Cuthbertson, T. J.; Chapuis, J. *J. Nat. Prod.* **1987**, 50, 1, 119-131.

9. Tozer, G. M.; Kanthou, C.; Parkins, C. S.; Hill, S. A. *Int. J Exp. Path.* **2002**, 83, 21-38.

10. Monk, K. A.; Siles, R.; Hadimani, M. B.; Mugabe, B. E.; Ackley, J. F.; Studerus, S. W.; Edvarsen, K.; Trawick, M. L.; Garner, C. M.; Rhodes, M. R.; Pettit, G. R.; Pinney, K. G. *Bioorg. Med. Chem*. **2006**. 14, 3231-3244.

11. Salmon, H. W.; Siemann, D. W. *Clin. Cancer. Res.* **2006**, 12, 13, 4090.

12. Shi, Q.; Chen, K.; Morris-Natschke, S. L.; Lee, K. *Curr. Pharm. Des.* **1998**, 4, 219-248.

13. Nguyen, T. L.; McGrath, C.; Hermone, A. R.; Burnett, J. C.; Zaharevitz, D. W.; Day, B. W.; Wipf, P.; Hamel, E.; Gussio, R. *J. Med. Chem.* **2005**, 48, 19, 6107-6116.

14. Hadimani, M. B. Studies toward the discovery of new classes of privileged molecules as colchicine-site binding ligands for tubulin: structure-based design,

15. synthesis, and bioactivity of small ligands targeted at tumor vasculature. Baylor University, **2005**.

16. Mocharla, V. P. Design, synthesis, and biological evaluation of diverse small molecular frameworks as tubulin binding agents. Doctoral dissertation, Baylor University, **1999**.

17. Shirali, A. R. Inhibitors of tubulin assembly: Design ligands featuring benz[*b*]thiophene molecular frameworks and preparation of their corresponding phosphorous containing prodrugs as tumor specific vascular targeting agents. Master's thesis, Baylor Univeristy, **2000**.

18. Jelinek, C. J. Discovery and development of dihydronapthalene-based vascular disrupting agents and combretastatin-related analogs. Master's thesis, Baylor Univeristy, **2005**.

19. Leavitt, R. W. *Principles of Genetics*. 3rd ed. WCB Publishers, **1991**, 48-50.

20. Downing, K. H. *Annu. Rev. Cell Dev. Biol.* **2000**, 16, 89-111.

21. Desai, A; Mitchison T. J. *Annu. Rev. Cell Dev. Biol*. **1997**. 13, 83-117.

22. Nogales, E; Wang, H. *Curr. Opin. Cell Biol.* **2006**, 18, 179-184.

23. Nogales, E. *Annu. Rev. Biochem*. **2000**, 69, 277-302.

24. Ravelli, R. B; Gigant, B.; Curmi, P. A.; Jourdain, I.; Lachkar, S.; Sobel, A.; Knossow, M. *Nature*. **2004**, 428, 198-202.

25. Hamel, E.; Lin, C. M. *Biochemistry*, **1984**, 23, 4173-4184.

26. Barbier, P.; Peyrot, V.; Dumortier, C.; D'Hoore, A.; Rener, G. A.; Engelborghs, Y. *Biochemistry*. **1996**, 35, 2008-2015.

27. Hamel, E. *Cell Biochem. and Biophys*. **2003**, 38, 1-21.

28. Berne, B. J. *J. Mol. Biol.*, **1974**, 89, 755.

29. Gaskin, F. *Methods Enzymol*. **1982**, 85, 433-439.

30. Arakawa, T.; Timasheff, S. *J. of Biol. Chem.* **1984**. 259, 8, 4979-4986.

31. Monk, K. A.; Siles, R.; Hadimani, M. B.; Mugabe, B. E.; Ackley, J. F.; Studerus, S. W.; Edvarsen, K.; Trawick, M. L.; Garner, C. M.; Rhodes, M. R.; Pettit, G. R.; Pinney, K. G. *Bioorg. Med. Chem*. **2006**. 14, 3231-3244.

32. Cliff M.J.; Gutierrez, A.; Ladybury, E. J. *J. Mol. Recognition.* **2004**, 17, 513-523.

33. Holdgate, G. A. *Bio Techniques*. Vol. 31, 2001, pp. 164-184.
34. Atkins, P. Physical Chemistry, 6th ed. W.H. Freeman and Company, New York, 2000.

35. Perez-Ramirez, B.; Andreu, M. J.; Gorbunoff, J. M.; Timasheff, S. N.. *Biochemistry*, **1996**, 35, 3277-3285.

36. Menendez, M.; Laynez, J.; Medrano, J.; Andreu, J. M. *J. Biol. Chem.* **1989**, 264, 16367-16371.

37. Garland, D.L. *Biochemistry*. **1978**, 178, 4266-4272.

38. Lamberir, A.; Engelborghs, Y. *J. Biol. Chem.* **1981**, 256, 3279-3282.

39. Owa, T.; Yoshino, H.; Okauchi, T.; Yoshimatsu, K.; Ozawa, Y.; Sugi, N. H.; Nagasu, T.; Koyanagi, N.; Kitoh, K. *J. Med. Chem.*, **1999**, 42, 3789-3799.

40. Owa, T.; Yoshimatsu, K.; Sugi, N. H.; Ozawa, Y.; Nagasu, T.; Koyanagi, N.; Okabe, T.; Kitoh, K.; Yoshino, H. *Bioorg. Med. Chem. Lett.*, **2000**, 10, 1223-1226.

41. Owa, T.; Yokoi, A.; Yamazaki, K.; Yamori, T.; Nagasu, T. *J. Med. Chem.*, **2002**, 45, 4913-4922.

42. Banerjee, M; Poddar, A.; Mitra, G.; Surolia, A.; Owa, T.; Bhattacharyya, B. *J. Med. Chem.* **2005**, 48, 547-555.

43. Rappl, C.; Barbier, P.; Bourgarel-Rey, V.; Gregoire, C.; Gilli, R.; Carre, M.; Combes, S.; Finet, J.; Peyrot, V. *Biochemistry*, **2006**, 45, 9210-9218.

44. Morbidelli, L.; Donnini, S.; Ziche, M. *Curr. Pharm. Des.* **2003**, 9, 521-530.

45. McKee, T.; McKee, J. R. *Biochemistry: The Molecular Basis of Life*. **2003**. 308.

46. Tungtan, B.; Altug, S.; *Curr. Med. Chem*. **2004**, 3, 271-301.

47. Parkins, C.S.; Holder, A.L.; Hill, S.A.; Chaplin, D.J.; Tozer, G.M. *Br. J. Cancer*. **2000**, 83, 6, 811-816.

48. Davis, P. D.; Tozer, G. M.; Naylor, M. A.; Thomson, P.; Lewis, G.; Hill, S. A. *Int. J. Radiat. Oncol.* **2002**, 54, 5, 1532-1536.

49. Powis, G.; Kirkpatrick, L. *Mol. Cancer Ther.* **2004**, 647-654.

50. Ke, Q.; Costa, M. *Mol. Pharmacol.* **2006**, 70, 1469-1480.

51. Escuin, D.; Kline, E. R.; Giannakakou, P. *Cancer Res.* **2005**, 65, 9021-9028.

52. Wang, G. L; Semenza, G. L. *J. Biol. Chem*. **1995**, 270, 3, 1230-1237.
53. Giaccia, A.; Siim, B. G.; Johnson, R. S. *Nature Reviews*. **2003**, 2, 1-9.

54. Huang, L. E.; Bunn, F., B. *J. Biol. Chem.* **2003**, 278, 2, 19575-19578.

55. Semenza, G. L. *Nature Reviews Cancer*. **2003**, 3, 721-732.

56. Mabjeesh, N.J; et. al. *Cancer Cell*. **2003**, 3, 363-375.

57. Triantafyllou, A.; Liakos, P.; Tsakalof, A.; Georgatsou, E.; Simos, G.; Bonanou, S. *Free Radical Res*. **2006**, 40, 847-856.

58. Olenyuk, B.; Zhang, G.; Klco, J. M.; Kickols, N. G.; Kaelin, W. G.; Dervan, P. B. *Proc. Natl. Acad. Sci. USA*. **2004**, 101, 48, 16768-16773.

59. Wang, G. L.; Jiang, B.; Rue, E. A.; Semenza, G. L. *Proc. Natl. Acad. Sci. USA*. **1995**, 92, 5510-5514.

60. Wang, G. L.; Jiang, B.; Rue, E. A.; Semenza, G. L. *Proc. Natl. Acad. Sci. USA*. **1995**, 92, 5510-5514.

61. Ljungkvist, A. S. E. *Radiation Research*. **2007**. 167, 127-145.

62. Silverman, R. B. *The Organic Chemistry of Enzyme-Catalyzed Reactions*. Academic Press, 2000.

63. www.Panomics.com. **2007**.

64. Thompson. P.; Naylor, M. A.; Everett, S. A.; Stratford, M. R. L.; Lewis, G.; Hill, S.; Patel, K. B.; Wardman, P.; Davis, P. D. *Mol. Cancer. Ther*. **2006**, 5, 11, 2886-2894.

65. Mckeown, S. R.; Cowen, R. L.; Williams, K. L. *Clin*. *Onc.* **2007**, 19, 427-442

66. .Aiub, C. A.; Mazzei, J. L.; Pinto, L. F. R.; Felzenszwalb, I. *Chem.-Biol. Interact.* **2006**, 161, 427-442.-

67. Hay, M. P.; Sykes, B. M.; Denny, W. A.; O'Conner, C. J. *J. Chem. Soc., Perkin Trans. 1*. **1999**, 19, 2759-2770.

68. Davis, P. D.; Naylor, M. A.; Thomson, P.; Everett, S. A.; Stratford, M. R. L.; Wardman, P. PCT. Int. App. 2004085421, 2004.

69. Thompson. P.; Naylor, M. A.; Stratford, M. R. L.; Lewis, G.; Hill, S.; Patel, K. B.; Wardman, P.; Davis, P. D. *Bioorg. Med. Chem. Lett.* **2007**, 17, 4320-4322.

70. http://dtp.nci.nih.gov/branches/btb/ivclsp.html

71. Vichai, V.; Kirtikara, K. *Nature Protocols.* **2006,** 1, 3, 1112-1116.

72. Papazisis, K. T.; Geromichalos, G. D.; Dimitriadis, K. A.; Kortsaris, A. H. *J. Immunol. Meth*. **1997**, 208, 151-158

73. Prescott, L. M.; Harley, J.P.; Klein, D. A. *Microbiology*. 3rd ed. Wm. C. Brown Publishers. **1996**. 25.

74. Papetti, M.; Herman, I. M. *Am. J. Physiol. Cell Physiol.* **2002**, 282, C947-C970.

75. Brown, J. M; Wilson, W. R. *Nature Reviews Cancer*. **2004**, 4, 437-44**7.**

76. Eichhorn, M. E; Strieth, S.; Dellina, M. *Drug Resistance Updates*. **2004**, 7, 125-138.

77. Pettit, G. R.; Minardi, M. D.; Rosenberg, H. J.; Hamel, E.; Bibby, M. C.; Martin, S. W.; Jung, M. K.; Pettit, R. K.; Cuthbertson, T. J.; Chapuis, J. *J. Nat. Prod.*, **2005**, 68, 1450-1458.

78. Salmon, H. W.; Mladinich, C.; Siemann, D. M. *Eur. J. Cancer*. **2006**, 42, 3073-3078.

79. Marletta, M. A. *J. Biol. Chem.* **1993**, 268, 17, 12331-12334.

80. Wang, C.; Cormeir, A.; Gigant, B.; Knossow, M. *Biochemistry*. **2007**, 46, 10595-10602.

81. Mugabe, B. E. Structure-activity Relationships and Thermodynamicss of Combretastatin A-4 and A-1 Derivatives as Potential Inhibitors of Tubulin Polymerization. Ph.D. Dissertation, Baylor Univeristy, **2005**.

82. Skloot, R. "Cells That Save Lives Are a Mother's Legacy." *The New York Times*. Nov. 17, 2001. www.nytimes.com/2001/11/17/arts/17HELA.html.

83. Jung, Y.; Isaacs, J. S; Lee, S.; Trepel, J.; Neckers, L. *J. Biological Chem.* **2003**, 278, 9, 7445-7452.

84. Ohta, A.; Tonomura, Y.; Sawaki, J.; Sato, N.; Akiike, H.; Ikuta, M.; Shimazaki, M. *Heterocycles*, **1991**, 32, 5, 965-973.

85. Pettit, G. R; Singh, S, B; Niven, M. L; Hamel, E; Schmidt, J. M. *J. Nat. Prod.* **1987**, 50, 1, 119-131.

86. Ellis, J. E; Lenger, S. R. *Syn. Comm.* **1998**, 28, 9, 1517-1524.

87. Shirali, A. R. Inhibitors of tubulin assembly: Desinged ligands featuring Benzo[b]thiophene, Dihydronaphthalene and Aroylchromene molecular core structures, Doctoral dissertation, Baylor University, **2002**.

88. Griffin, R. J.; Calvert, A. H.; Newell, D. R.; Golding, B. T.; Curtman, J. N. (Newcastle University Ventures Limited). US patent **2000**/ 20006156739.

89. Chaplin, D. J..; Edvardsen, K.; Pinney, K. G.; Prezioso, J. A.; Wood, M. (Oxigene, Inc., USA). WO 2004078126, **2004**.

90. Ishii, H.; Chen, I. S; Ishikawa, T. *J. Chem. Soc. Perkin Trans. 1: Org. and Bioorg. Chem*. **1987**, 3, 671-676.

91. Fukuyama, Y; Iwatsuki, C; Kodama, M. *Tetrahedron*, **1998**, 54, 10007-10016.

92. Ferrario, F.; Levi, S.; Trupiano, F. *Syn Comm*. **1991**, 21, 1, 99-105.

93. Davis. P. D; Tozer, G. M; Naylor, M. A; Thomson, P; Lewis, G; Hill, S. A. *Int. J. Rad. Oncol. Biol. Phys*, **2002**, 54, 95, 1532-1536.

94. Hadfield, J. A.; McGown, A. T.; Mayalarp, S. P.; Land, E. J.; Hamblett, I.; Gaukroger, K.; Lawrence, N. J.; Hepworth, L. A.; Butler, J. PCT WO 2002050007, **2002**.

95. Ghatak, A; Dorsey, J. M; Garner, C. M; Pinney, K. G. *Tet. Lett.* **2003**, 44, 4145-4148

96. Pinney, K. G; Mocharla, V. M; Chen, Z; Garner, C. M; Ghatak, A; Dorsey, J. M. US patent **2004**/ 20040044059 A1

97. Invitrogen quick reference card. www.invitrogen.com

98. *Protein Blotting Handbook*. Millipore Corp. **2005**.

99. Siles, R; Ackley, J. F; Hadimani, M. B; Hall, J.J; Mugabe, B; Guddneppanavar, R; Monk, K. A; Chapuis, J; Pettit, G. R; Chaplin, D. J; Edvardsen, K; Trawick, M. L; Garner, C. M; Pinney, K.G. *J. Nat. Prod*. **2008** (Article in press)

100. Pettit. G. R; Toki, B; Hrald, D. L; Pascal Verdier-Pinard, H; Boyd, M. R; Hamel, E; Pettit, R. K. *J. Med. Chem*, **1998**, 41 (10), 1688-1695

101. Pettit, G. R; Grealish, M. P; Herald, D. L; Boyd, M. R; Hamel, E; Pettit, R. K. *J. Med. Chem.* **2000**, 43, 2731-2737

102. Pinney, K. G; Wang, F; Hadimani, M; Mejia, M. D. P. US patent 2007/0082872 A1, **2007**

103. Cullis, E. R; Kalber, T. L; Ashton, S. E; Cartwright, J. E; Griffiths, J. R; Ryan, A. J; Robinson, S. P. *Microvascular. Research*, **2006**, 71, 76-84

104. Pillips. R. M. *Exp. Opin. Invest. Drugs*. **1998**, 7 (5), 905-928

105. Lepore, S. D; He, Y. *J. Org. Chem*, **2003**, 68, 8261-8263

106. Dembinski, R. Eur. J. Org. Chem. 2004, 2763-2772

107. Thomson, P; Naylor, M. A; Everett, S. A; Stratford, M. R. L; Lewis, G; Hill, S; Patel, K. B; Wardman, P; Davis. P. D, Mol. *Bioorg. Med. Chem. Lett*. **2007**, 17, 4320-4322.

108. Pettit. G.R.; Rhodes, M. R.; Herald, D. L.; Hamel, E.; Schmidt, J. M.; Pettit, R. K. *J. Med. Chem.* **2005**. 48, 12, 4087-4099.

109. Kamath, K.; Okouneva, T.; Larson, G.; Panda, D.; Wilson, L.; Jordan, M. A. *Mol. Canc. Ther.* **2006**, 5, 9, 2225-2233.

110. Pinney, K. G.; Mejia, M. P.; Villalobos, V. M.; Rosenquist, B. E.; Pettit, G. R.; Verdier-Pinard, P.; Hamel, E. *Bio-org. Med. Chem*. **2000**, 8, 10, 2417-2425.

111. Miranda, M. G. Design, Synthesis, and Biological Evaluation of Novel Serotonin Reuptake Inhibitors and Novel Derivatives of a Nitrogen-Containing Combretastatin Analog. 2006.

112. Liou, J.; Chang, Y.; Kuo, F.; Chang, C.; Tseng, H.; Wang, C.; Yang, Y.; Chang, J.; Lee, S.; Hsieh, H. *J. Med. Chem.* **2004**, 47, 17, 4247-4257.

113. Chaplin, D. J.; Garner, C. M.; Kane, R. R.; Pinney, K. G.; Prezioso, J. A. (Oxigene, Inc., USA) WO 2003035008.

114. Siles, Rogelio. Design, Synthesis, and Biological Evaluation of New Anti-cancer Nitrogen-Containing Combretastatins and Novel Cysteine Protease Inhibitors for the Treatment of Chagas. Baylor University, 2006.

115. Pinney, K. G.; Sriram, M. PCT Int. Appl WO 2006138427

116. Sriram, M. Design, Synthesis, Biochemical and Biological Evaluation of Benzocyclic and Enediyne Analogs of Combretastatins as Potential Tubulin Binding Ligands in the Treatment of Cancer. Baylor University. 2007.

117. Pinney, K. G.; Mocharla, V. P.; Chen, Z.; Garner, C. M.; Ghatak, A.; Hadimani, M.; Kessler, J.; Dorsey, J. M.; Edvardsen, K.; Chaplin, D. J.; Prezioso, J.; Ghatak, U. R. US 2004043969.

118. Pinney, K. G.; Mocharla, V. P.; Chen, Z.; Garner, C. M.; Ghatak, A.; Hadimani, M.; Kessler, J.; Dorsey, J. M. WO 2001068654.

119. Ricker, J. L.; Chen, Z.; Yang, X; Pribluda, V. S.; Swartz, G. M.; Van Waes, C. *Clinical Cancer Research.* **2004**, 10, 24, 8665-8673.

120. Josephy, P.D.; Eling, T.; Mason, R. P. *J. Biol. Chem.* **1982**, 257, 7, 3669-3675.

121. Boyer, R. *Modern Experimental Biochemistry*. 3rd ed. Addison Wesley Longman. 2000, 43-45.

122. Jayaweera, P.M.; Jayarathne, T. A.U. *Surface Science*. **2006**, 600, L297-L300.

123. Pettit, G. R.; Singh, S. B.; Cragg, G. M. *J. Org. Chem.* **1985**, 50, 18, 3404-3406

124. Pettit, G. R.; Cragg, G. M.; Herald, D. L.; Schmidt, J. M.; Lohavanijava, P. *Canadian J. Chem.* **1982**, 60, 11, 1374-1376.

125. Pettit, G. R.; Singh, S. B. *Canadian J. Chem.* **1987**, 65, 10, 2390-2396.

126. Pettit, G. R.; Singh, S. B.; Schmidt, J. M.; Niven, M. L.; Hamel, E.t; Lin, C. M. *J. Nat. Prod.* **1988**, 51, 3, 517-527.

127. Pettit, G. R.; Singh, S. B.; Niven, M. L *J. Am. Chem. Soc*. **1988**, 110, 25, 8539-8540.

128. Pettit, G. R.; Singh, S. B.; Hamel, E.; Lin, C. M.; Alberts, D. S.; Garcia-Kendall, D. *Experientia*, **1989**, 45, 2, 209-211.

129. Singh, S. B.; Pettit, G. R. *J. Org. Chem*. 1989, 54, 17, 4105-4114.

130. El-Zayat, A. A. E.; Degen, D.; D., Sonya; C., Gary M.; Pettit, G. R.; Von Hoff, D. D *Anti-Cancer Drugs*. **1993**, 4, 1, 19-25.

131. Pinney, K. G.; Jelinek, C.; Edvardsen, K.; Chaplin, D. J.; Pettit, G. R. Anticancer Agents from Natural Products. 2005, 23-46.

132. Kanthou, C.; Tozer, G. *Blood*. 99, 6, 2060-2069.

133. Jackson, J.R.; Patrick, D.R.; Dar, M.M.; Huang, P.S. *Nat. Rev. Cancer.* **2007**, 7, 107-117.

134. Dr. Diane Wycuff. Director of the Molecular Bioscience Center at Baylor University.

135. http://dctd.cancer.gov/ProgramPages/DTP_Resources_Drug_Discovery.htm

136. http://dtp.nci.nih.gov/branches/btb/ivclsp.html

137. A list of Pinney group members that have been involved in the development of a method for radiolabeling OX16C: Ackley, F. J.; Arthasery, P.; Hadimani, M. B.; Hall, J. J.; Jelinek, C. J.; Nguyen, B.; Pinney, K. G.; Sriram, M.; Guddneppanavar, R.; Shirali, A. R.; Siles, R.

138. A list of Pinney group members that have been involved in the development of a method for synthesizing OXi6196: Chen, Z.; Dogra, A.; Dorsey, J. M.; Garner, C. M.; Ghatak, A.; Hall, J. J.; Jelinek, C. J.; Mocharla, V.; Nguyen, B.; Pinney, K. G.; Sriram, M.

139. Hadimani M. B; Kessler R. J.; Kautz J. A.; Ghatak A.; Shirali A. R. O'Dell H.; Garner C. M.; Pinney K. G. *Acta crystallographica. Section C, Crystal struct. Comm.* **2002**, 58 330-332.

140. Personal communication with Dr. Kevin G. Pinney.